DANMARKS OG GRØNLANDS GEOLOGISKE UNDERSØGELSE RAPPORT 2010/100

Rødryggen-1 Core Well, GGU 517101, Wollaston Forland, Northeast Greenland – Final Well Report

Contribution to Petroleum Geological Studies, Services and Data in East and Northeast Greenland

Volume 1(2)

Jussi Hovikoski, Peter Alsen,
Jørgen Bojesen-Koefoed, John Boserup,
Claus Kjøller, Peter Nytoft, Mette Olivarius,
Dan Olsen, Henrik Ingermann Petersen,
Stefan Piasecki, Emma Sheldon
& Henrik Vosgerau

GEOLOGICAL SURVEY OF DENMARK AND GREENLAND
MINISTRY OF ENVIRONMENT AND ENERGY

G E U S

DANMARKS OG GRØNLANDS GEOLOGISKE UNDERSØGELSE RAPPORT 2010/100

Rødryggen-1 Core Well, GGU 517101, Wollaston Forland, Northeast Greenland – Final Well Report

Contribution to Petroleum Geological Studies, Services and Data in East and Northeast Greenland

Volume 1(2)

Jussi Hovikoski, Peter Alsen,
Jørgen Bojesen-Koefoed, John Boserup,
Claus Kjøller, Peter Nytoft, Mette Olivarius,
Dan Olsen, Henrik Ingermann Petersen,
Stefan Piasecki, Emma Sheldon
& Henrik Vosgerau

Confidential report

Copy No.

Released 01-07-2025

GEOLOGICAL SURVEY OF DENMARK AND GREENLAND
MINISTRY OF CLIMATE END ENERGY

GEUS

1. Executive summary

This report presents the core data package of the Rødryggen-1 core drilled in northern Wollaston Forland, NE Greenland in 2009. The report is delivered to the participating sponsoring companies of the specific analytical programme of the Rødryggen-1 core as described in appendix B2 in the collaboration agreement between GEUS and sponsoring oil companies regarding petroleum geological studies, services and data in East and Northeast Greenland.

The primary objective of the drilling was to core the Upper Jurassic Bernbjerg Formation of the Hall Bredning Group to obtain fresh, unweathered and continuous samples for investigations of source rock potential and detailed stratigraphic extent of this mudstone succession. The core reached a total depth of 234.5 m with 99% recovery.

The coring was followed by an extensive analytical programme that included total GR-logging, detailed sedimentological description of the core, erecting biostratigraphic and lithostratigraphic divisions, chemostratigraphy, determination of mineralogy and diagenesis patterns, porosity, permeability and sonic velocity measurements, analysis of petroleum potential, thermal maturity, biomarker and stable carbon isotope analyses, and a sandstone provenance study.

The results indicate that the core penetrates three major lithostratigraphic units: 1) the Kimmeridgian – Lower Volgian Bernbjerg Formation (234.5–97 m), 2) the Middle Volgian – Upper Ryazanian Lindemans Bugt Formation (97–24.4 m), and 3) the Upper Ryazanian – Upper Valanginian Palnatokes Bjerg Formation (Albrechts Bugt Member, 24.4–0 m). All the observed formation boundaries are conformable. This observation differs from the results of previous outcrop-based studies, which have suggested that the Albrechts Bugt Member erosionally overlies the Bernbjerg Formation in the area.

Both the Bernbjerg Formation and the Lindemans Bugt Formation comprise organic-rich black shales that are classified as gas/oil-prone petroleum source rocks. The uppermost unit, the Albrechts Bugt Member, shows no source rock potential.

Facies analysis demonstrates that the studied black shale succession reflects an overall transgressive setting from a wave-influenced, shallow muddy shelf (the Bernbjerg Formation) to a restricted basinal environment below maximum storm wave base (the Lindemans

Bugt Formation). The change from the Bernbjerg Formation to the Lindemans Bugt Formation is gradational and probably corresponds to increased tectonic activity in the Wollaston Forland area during the Middle Volgian (Surlyk, 2003). This rift climax resulted in accelerated tilted fault block development and basin segmentation and lasted until the Early Ryazanian. As a result, the basin geometry allegedly changed from the Kimmeridgian – Early Volgian regionally continuous, tectonically-influenced shallow shelfal setting (i.e. the Bernbjerg Formation) to narrow, 10–30 km wide, S-N oriented basins that were strongly tilted westwards (i.e. the Lindemans Bugt Formation).

The change from the Lindemans Bugt Formation to the Albrechts Bugt Member (Palnatokes Bjerg Formation) is also conformable and associated with progressively less clastic sediment input into the basin. The dominant facies consists of fossiliferous marly mudstone that is intensively burrowed with a *Zoophycos* dominated low-diversity trace fossil assemblage. The Albrechts Bugt Member accumulation coincides with the latest synrift – early post rift phase, where the basin was fully segmented and influenced by an eustatic sea-level rise (Surlyk, 1978); sedimentation took place in a sediment-starved basin in a tilted fault block.

In addition to facies analysis, the chemostratigraphy efficiently differentiates between the various lithologies and formations of the Rødryggen-1 core. The mud component of the recurrent cemented intervals has the same composition as that of the uncemented mudstone. Periodic enhanced deposition of bioclasts, possibly associated with transgressive events, is thus considered the cause of the locally occurring cemented intervals in the core.

The poroperm and diagenesis analyses confirm that the reservoir properties of the sedimentary succession of the Rødryggen-1 core are poor. The sand content is low to nil, and the creation of secondary porosity has been minor.

The clay mineralogy distinguishes each formation and reveals changes in the depositional environment. The heavy mineral assemblage of the outcrop samples from the Bernbjerg Formation used for provenance analysis is dominated by ankerite and muscovite. The ankerite is correlated to the cemented intervals of the Rødryggen-1 core, whereas the muscovite indicates a short transport distance. The zircon age distributions point to source areas along the immediate coast of NE Greenland.

The observed paleoenvironmental change at the Bernbjerg Formation – Lindemans Bugt Formation boundary is clearly reflected in source rock characteristics: The Lindemans Bugt Formation contains predominantly marine Type II kerogen, whereas the Bernbjerg Formation shows higher proportions of terrestrial organic matter and contains mixed Type II/III kerogen. This change is consistently indicated by data from a number of independant types of analyses such TC/TOC/TC/Rock-Eval screening, organic petrology, biological marker analysis (e.g., relative C_{30} content), stable Carbon isotope analysis, and palynology.

The Lindemans Bugt Formation shales show an average TOC of 3.50% and an average S2 yield of app. 12.7 mg/g. The Hydrogen Index ranges between 9 and 445 with an average of 333. The Bernbjerg Formation shales, on the other hand, show an average TOC of 4.84% and an average S2 yield of app. 11.5 mg/g. The Hydrogen Index ranges between 136 and 342 with an average of 235.

The succession as a whole is immature to marginally mature with respect to petroleum generation, but a clearly increasing trend in the level of thermal maturity with depth is consistently indicated by a number of different independent analysis types.

Assessment of the uplift history of the drilled succession is difficult based on the available data. Maturity modelling (Petromod) using a very simplified approach yields approximately 1.5 kilometres of uplift, which is consistent with earlier outcrop-based estimations from the area. Considering the uncertainties involved in the modelling, this estimate may serve only as a rough guide to the order of magnitude of uplift in the area.

1.1 Main conclusions

- The Rødryggen-1 core penetrates three major lithostratigraphic units: 1) Bernbjerg Formation (234.5–97.0 m), 2) Lindemans Bugt Formation (97.0–24.4 m), and 3) Palnatokes Bjerg Formation (Albrechts Bugt Member, 24.4–0 m). The lower boundary of the Bernbjerg Formation was not reached.
- The drilled succession is dated Kimmeridgian – Late Valanginian on the basis of dinoflagellate, ammonite and nannofossil stratigraphy. The Bernbjerg Formation is Kimmeridgian – Lower Volgian, the Lindemans Bugt Formation is Middle Volgian – Upper Ryazanian and the Albrechts Bugt Formation is Upper Ryazanian – Upper Valanginian pars.
- Both the Bernbjerg Formation and the Lindemans Bugt Formation comprise organic-rich black shales that are classified as gas/oil-prone petroleum source rocks. The uppermost unit, the Albrechts Bugt Member, shows no source rock potential.
- Facies analysis demonstrates that the studied black shale succession reflects an overall transgressive setting from a wave-influenced, shallow muddy shelf (the Bernbjerg

Formation) to a restricted basinal environment below maximum storm wave base (the Lindemans Bugt Formation).

- The poroperm and diagenesis analyses indicate that the reservoir properties of the sedimentary succession of the Rødryggen-1 core are poor.
- Sonic velocity measurements tentatively suggest that the mudstones of Bernbjerg and Lindemans Bugt Formations most commonly have velocities between 2900 and 4000 m/s. The calcite-cemented mudstones of the Albrechts Bugt member have high velocities (~3800–~4600 m/s).
- The heavy mineral assemblage of the outcrop samples from the Bernbjerg Formation used for provenance analysis indicates a short transport distance. The zircon age distributions point to source areas along the immediate coast of NE Greenland.
- TC/TOC/TC/Rock-Eval screening, organic petrology and biomarker analyses reveal a marked shift in source rock characteristics between the Bernbjerg Formation and the Lindemans Bugt Formation.
- The Lindemans Bugt Formation shales show an average TOC of 3.50% and an average S2 yield of app. 12.7 mg/g. The Hydrogen Index ranges between 9 and 445 with an average of 333.
- The Bernbjerg Formation shales show an average TOC of 4.84% and an average S2 yield of app. 11.5 mg/g. The Hydrogen Index ranges between 136 and 342 with an average of 235.
- The Lindemans Bugt Formation contains predominantly marine Type II kerogen, whereas the Bernbjerg Formation shows higher proportions of terrestrial organic matter and contains mixed Type II/III kerogen.
- Biomarker data show typical characteristics of a marine source rock but with an increasing proportion of terrestrially-influenced kerogen in the Bernbjerg Formation. The relative proportion of C_{30} steranes (24-n-propylcholestanes) – indicator of marine organic matter in the source rock – is high (8-13 %) in the Lindemans Bugt Formation and generally below 8 % in the Bernbjerg Formation.
- The change in source rock character and paleoenvironment at the Bernbjerg-Lindemans Bugt Formation boundary is interpreted to reflect increased tectonic activity during the Middle Volgian, which resulted in accelerated tilted fault block development and basin segmentation.
- The succession as a whole is immature to marginally mature with respect to petroleum generation, but a clearly increasing trend in the level of thermal maturity with depth is consistently indicated by a number of different independent analysis types.
- Preliminary assessment of the uplift history of the cored succession based on maturity modelling (Petromod) tentatively suggests an uplift of ~1.5 kilometres.

1.2 Implications for exploration

The Rødryggen-1 core contains more than 200 m of organic-rich mudrocks classified as gas/oilprone petroleum source rocks. These upper Jurassic shales form the local equivalent of the Kimmeridge Clay Formation *s.l.* that in the North Atlantic region is known under a variety of names including the Hareelv, Kap Leslie, Farsund, Mandal, Draupne, Spekk and Bazhenov Formations.

The Upper Jurassic source rocks spans two lithostratigraphic formations, the Bernbjerg and Lindemans Bugt Formations, which also represent different tectonostratigraphic units: the Kimmeridgian - Lower Volgian Bernbjerg Formation was deposited in a regionally continuous, tectonically influenced shallow shelfal setting, whereas the deposition of the Middle Volgian – Upper Ryazanian Lindemans Bugt Formation assumably took place in narrow, 10–30 km wide, S-N oriented basins that were strongly tilted westwards (Surlyk, 2003). Therefore, in addition to the change in source characteristics and maturity recorded in these units, any estimations of source rock volumes should take account the probable change in basin geometry during the deposition of these strata. In this regard, the future correlation with the Brorson Halvø core drilled in 2010, situated at the uplifted seaward block crest of the studied Permpas block, is expected to give a further insight into tectonostratigraphic evolution of the area and geometry of these units.

The Rødryggen-1 core is throughout of low permeability and porosity and consequently lacks potential reservoir intervals. One of the nearest reservoir units are the Middle Volgian – Valanginian coarse-grained fan delta deposits (Rigi and Yound Sund Members of the Lindemans Bugt and Palnatokes Bjerg Formations, respectively), occurring in the westernmost tilted fault block. Moreover, the lowermost part of the Bernbjerg Formation (the Ugpik Ravine Member), which was not reached by the Rødryggen-1 core, reportedly bears thin sandy layers, which may be of limited reservoir significance. Moreover, the Bernbjerg Formation overlies either the Pelion Formation, the Payer Dal Formation or the Jakobsstigen Formation of the Vardekløft Group (Surlyk, 2003), all of which contain sandstone-dominated intervals. Finally, in offshore basins, the Upper Jurassic source rocks may be overlain by Cretaceous sandstone units.

The petroleum potential of the studied upper Jurassic shales as indicated by the analyses carried out on samples collected from the Rødryggen corewell is significantly higher than expected from analyses of outcrop samples collected in the nearby area. Essentially, the petroleum potential as given by the average Hydrogen Index of the core samples is two to three times higher than that seen in outcrop samples. This is very similar to observations made in the Blokelv corewell (Jameson Land). The phenomenon may probably be attributed to the very high proportions of pyritic sulphur present in the samples. Upon weathering, pyrite will generate sulphuric acid that will destroy organic matter in the rock and reduce the apparent petroleum potential. This effect is prominent in outcrop samples, whereas it is not present in core samples.

1.3 References

Surlyk, F. 1978: Submanrine fan sedimentation along fault scarps on tilted fault blocks (Jurassic–Cretaceous boundary, East Greenland). Grønlands Geologiske Undersøgelse Bulletin, **128**, 108 pp.

Surlyk, F. 2003: The Jurassic of East Greenland: a sedimentary record of thermal subsidence, onset and culmination of rifting. In: Ineson, J.R. & Surlyk, F. (eds): The Jurassic of Denmark and Greenland. Geological Survey of Denmark and Greenland Bulletin, **1**, 659–722

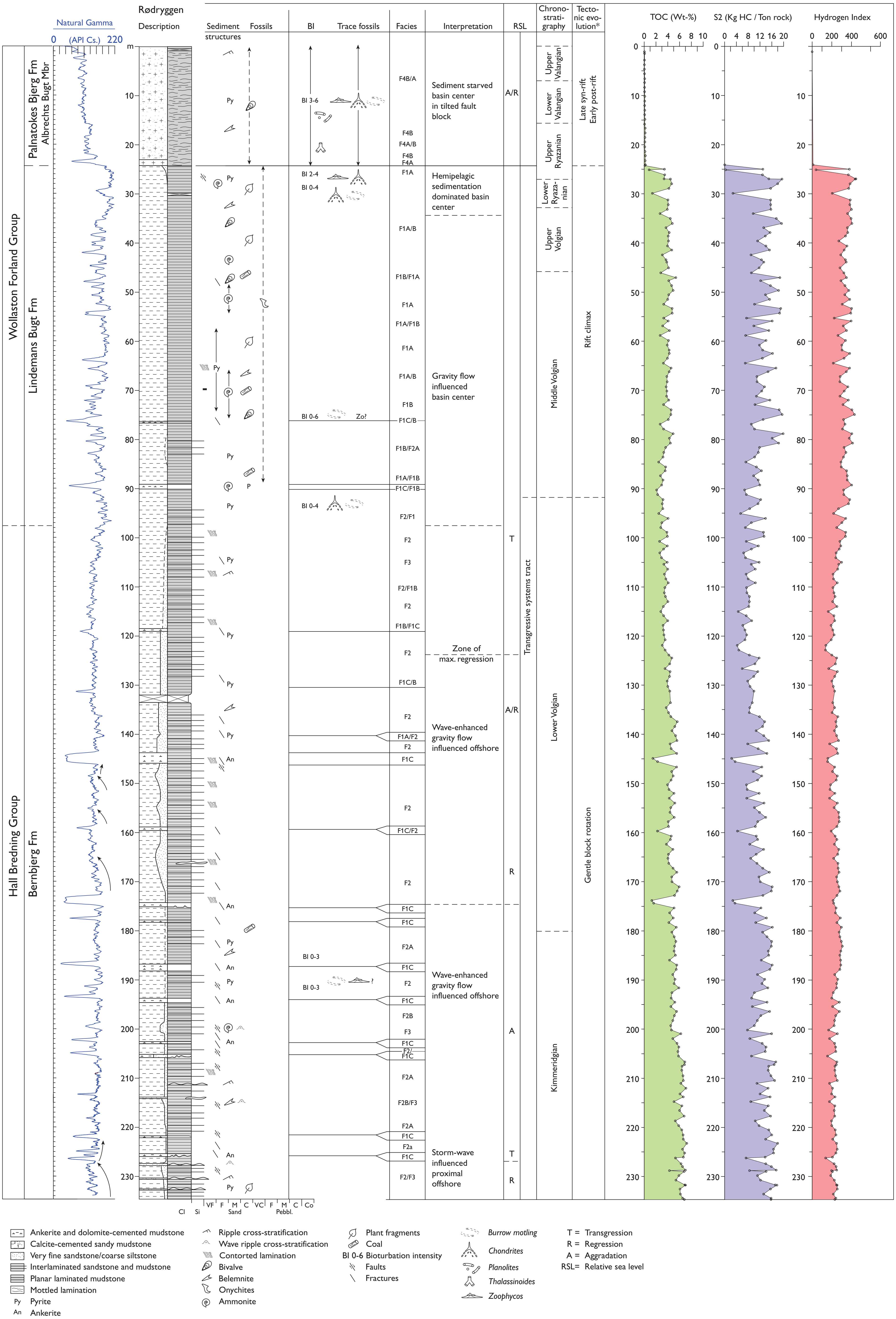

Figure 1.1 Core summary chart showing main source rock variables. Tectonic evolution after Surlyk (2003)

2. Introduction

This report presents the core data package of the Rødryggen-1 core drilled in northern Wollaston Forland, NE Greenland. The report is delivered to the participating sponsoring companies of the specific analytical programme of the Rødryggen-1 core as described in appendix B2 in the collaboration agreement between GEUS and sponsoring oil companies regarding petroleum geological studies, services and data in East and Northeast Greenland.

The Rødryggen-1 core, GGU 517101, was drilled during the summer of 2009 in northern Wollaston Forland approximately 30 km northeast of the Daneborg military station (Fig. 2.1). Rødryggen-1 is the second core in an onshore drilling program in East and North-East Greenland that started in 2008 with the drilling of the Blokelv core in central Jameson Land.

The primary objective was to core the Upper Jurassic Bernbjerg Formation of the Hall Bredning Group to obtain fresh, unweathered and continuous samples for investigations of source rock potential and detailed stratigraphic extent on this mudstone succession.

The borehole was spudded on August 3th 2008 and completed on August 14th 2009 at a total depth of 234.5 m. The core recovery was 99%. The core diameter is 42 mm.

The borehole is located on the western side of Rødryggen ("red ridge") which is an elongated hill or ridge conspicuously situated at the eastern margin of Storsletten, Wollaston Forland. Previous studies in the area have suggested that the Rødryggen consists of dark mudstones of the Upper Jurassic–Lower Cretaceous Bernbjerg Formation overlain by light grey or yellowish mudstones of the Lower Cretaceous Albrechts Bugt Member followed by red mudstones of the Lower Cretaceous Rødryggen Member which in turn is overlain by the "Mid Cretaceous sandy shale sequence" *sensu* Nøhr-Hansen (1993). The drill camp was situated at a small plateau formed by the uppermost part of the Albrechts Bugt Member.

The coring revealed that the upper Jurassic stratigraphy in the area is more complex than previously thought. The dark mudstone succession consisted of two lithostratigraphic units: 1) Kimmeridgian – Lower Volgian Bernbjerg Formation (234.5–97 m) and 2) Middle Volgian – Upper Ryazanian Lindemans Bugt Formation (97–24.4 m). In the top of the core, the Lindemans Bugt Formation further grades into Upper Ryazanian – Upper Valanginian Palnatokes Bjerg Formation (Albrechts Bugt Member, (24.4–0 m). Both the Bernbjerg and Lindemans Bugt Formations consist of black mudstones of good source rock quality.

2.1 Objectives

The target of the drilling was the Upper Jurassic Bernbjerg Formation. The thickness of the formation is unknown at the drill site and nowhere is the formation exposed in its full original thickness, which is estimated to have been approximately 600 m (Maync 1947, Surlyk 1977). The purpose of the drilling was to acquire fresh unweathered and continuous samples for investigations of the source rock potential of the mudstones by applying modern source rock analysis and to obtain samples for detailed stratigraphic information on the mudstones.

2.2 Well data, general information

Country	Greenland / Denmark
Borehole number	GGU 517101
Borehole name	Rødryggen-1
Area	North-East Greenland, Wollaston Forland
Operator	GEUS
Drilling operator	GEUS

Borehole Location	
Altitude:	110 m above mean sea level.
Coordinates WGS 84:	Latitude: 74°32.561´ N, Longitude: 19°50.924´ W
UTM Zone:	27W 0401666 N - 7852249 E

Drill rig	Sandvik DE 130
Drilling contractor	GEUS
Casing diameter	64/57 mm
Casing depth	15.8 m
Borehole diameter	56 mm
Core diameter	42 mm
Total depth	234.5 m
Core recovery	99%
Status	Abandoned open hole, top of casing closed with a steel cap.

Logistic history:	
Drilling crew arriving in East Greenland, Daneborg	July 24th 2009
Transportation of rig and crew to drillsite at Rødryggen	July 27th – July 29th 2009
Establishment of field camp and drilling rig	July 27th - August 2th 2009
Spud	August 3th 2009
Drilling completed	August 14th 2009
Drill rig back at Constable Pynt	August 16th 2009
Effective drilling	11 days
Total days on drill location	22 days

2.3 Sampling and logging programme at drill site

A total of 70 whole core samples for gas analyses were collected immediately from the base of the recovered core for every 3 m in average. Samples have lengths up to about 10 cm and they were stored in sealed metal cans.

Samples, collected for preliminary Rock-Eval/TOC screening and biostratigraphic age identification based on dinoflagellates, include mudstone samples from the upper and lower part of the cored Albrechts Bugt Member at 1.1 m (517101-1) and 24.1 m (517101-3), respec-tively; and mudstone samples from the uppermost and lowermost part of the cored black shale succession at 25.0 m (517101-5), 27.0 m (517101-7) and 234.4 m (517101-75), respectively.

One surface sample of weathered mudstone (Albrechts Bugt Member) was collected at the drill site (0 m drilling / 110 m a.s.l.).

An extensive sampling programme was later conducted at GEUS laboratories.

Logging in the field included a total gamma log from terrain surface and down to 209 m. This was later supplemented with a total gamma log and a density log from 193 – 234.5 m measured in the core-lab at GEUS.

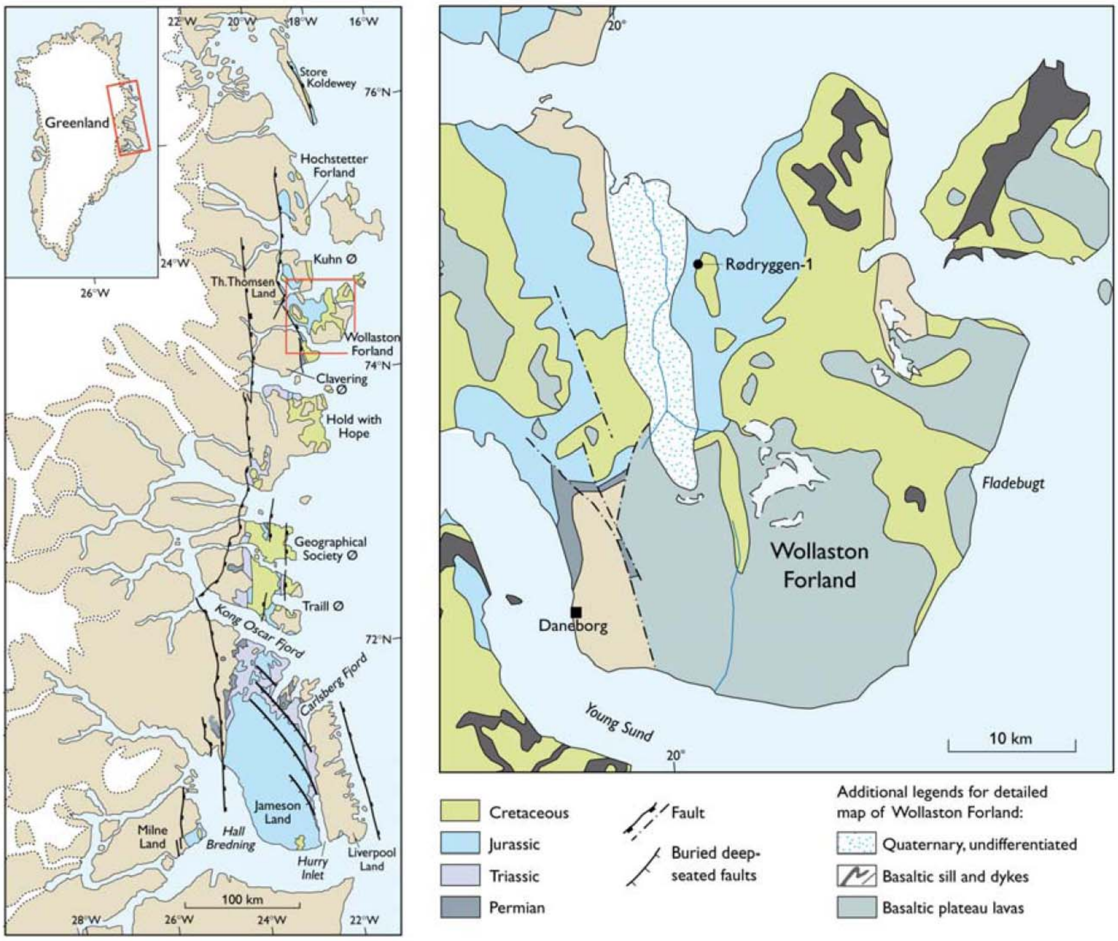

Figure. 2.1 Geological map of northeast Greenland showing the Rødryggen-1 borehole site.

3. Stratigraphy

3.1 Lithostratigraphy

The Rødryggen core penetrates three major lithostratigraphic units: 1) Kimmeridgian – Lower Volgian Bernbjerg Formation (234.5–97 m), 2) Middle Volgian – Upper Ryazanian Lindemans Bugt Formation (97–24.4 m), and 3) Upper Ryazanian – Upper Valanginian Palnatokes Bjerg Formation (Albrechts Bugt Member, (24.4–0 m) (Figs. 3.1.1 and 3.1.2) The assignment of the interval 97-24.4 m to the Lindemans Bugt Formation is tentative and it may require modifications in the future. The reason for this is that Middle Volgian – Upper Ryazanian deposits do not crop out in the studied Permpas tilted fault block (see Chapter 4 for discussion) and consequently they have never been described in the field. Sedimentologically the most similar deposits to these strata are the contemporaneous fine-grained members (the Laugites Ravine Member and particularly the Niesen Member) of the Lindemans Bugt Formation. These units have been originally described in the westernmost tilted fault blocks (the Kuppel and Kuhn Ø Blocks, Surlyk, 1978) and are related to distal parts of fan deltas. Future work will be needed to decide whether the studied deposits can be assigned to these members (requires amended description) or a new member needs to be erected.

3.1.1 Bernbjerg Formation (Hall Bredning Group)

The Upper Oxfordian – Lower Volgian Bernbjerg Formation is a widespread depositional unit in NE Greenland cropping out from Store Koldewey in North to Traill Ø in South (Surlyk, 2003 and references therein). Its type and reference sections are located in Wollaston Forland and South-Western Kuhn Ø (Surlyk, 1977), where the formation reaches a maximum thickness of 500–600 m (Surlyk 1977; Surlyk & Clemmensen 1983; Alsgaard et al., 2004). The Bernbjerg Formation sharply overlies either the Pelion Formation, the Payer Dal Formation or the Jakobsstigen Formation of the Vardekløft Group (Surlyk, 2003). In the Rødryggen core, the lower boundary of the Bernbjerg Formation was not reached. The formation is overlain by the Upper Jurassic – Lower Cretaceous Wollaston Forland Group. The nature of the upper contact depends on location within a tilted fault block; in the down faulted part of a fault block the boundary is conformable, whereas in the elevated fault block crests the contact is an angular unconformity (Surlyk 1977, 1978b, 1991).

Lithologically the formation is mainly characterized by dark grey to black mudstone and interlaminated sandstone and mudstone. Sand beds, 5-50 cm-thick may locally show current and/or wave-ripple cross stratification (Surlyk, 1977). Surlyk (2003) referred a heterolithic lower unit to as the Ugpik Ravine Member. The Rødryggen core penetrates only the mud-dominated upper part of the Bernbjerg Formation.

3.1.2 Lindemans Bugt Formation (Wollaston Forland Group)

Lower boundary in the Rødryggen-1 core: The boundary between Bernbjerg Formation and Lindemans Bugt Formation is strongly transitional and occurs between 125–76 m. The exact formation boundary is placed in ~97 m, where the GR increases to ~200 API for the first time. The formation change is also recognizable as gradational facies change from heterolithic interlamination (Facies 2AB) to clayey mudstone (Facies 1AB), increasing pyrite and fossil content and locally increasing bioturbation degree. Moreover, the formation change is well expressed in variety of source rock characteristics such as increasing Hydrogen Index, TS, S_1 and S_2 (Chapter 8.1), and biomarker data (e.g., increasing C_{30} content; Chapter 8.2).

The Middle Volgian – Upper Ryazanian Lindemans Bugt Formation consists of syntectonic breccias, conglomerates, sandstone and mudstone units. Its areal distribution is limited to the northeastern Clavering Ø, northwestern Wollaston Forland, eastern Th. Thomsen Land and south west Kuhn Ø (Surlyk, 1978). In the field, the formation unconformably overlies the Bernbjerg or Pelion Formations, or rests directly on the Caledonian basement (Surlyk, 1978). The type area is exposed in northwest Wollaston Forland on the slopes of Niesen and Palnatokes Bjerg mountains. The formation is wedge-shaped in West-East direction and is estimated to reach a maximum thickness of 2 km. It is divided into three members: coarse-grained Rigi Member, heterolithic Laugites Ravine Member, and mud-dominated Niesen Member. The Niesen Member is lithologically most similar to the studied Rødryggen-1 interval consisting of dark mudstones, interlaminated mudstones and fine grained sandstones, and thin beds of fine grained sandstone. Scattered calcareous concretions and nodules and calcite cemented beds occur locally (Surlyk, 1978). Finally, the member locally contains abundant *Buchia*-bivalves, ammonites, belemnites and plant fragments (Surlyk, 1978). The maximum thickness of the Niesen Member is ~200 m.

3.1.3 Albrechts Bugt Member (Palnatokes Bjerg Formation, Wollaston Forland Group)

Lower boundary in the Rødryggen-1 core: The contact between Lindemans Bugt Formation and Albrechts Bugt Member of the Palnatokes Bjerg Formation is gradational and occurs within ca. 1 m (~25.5–24.4 m). The boundary is readily recognizable by an abrupt decrease in GR-values, increasing matrix carbonate- and sand-content, decreasing clay-content, change in matrix colour from black to light grey, increasing bioturbation intensity, and change in fossil content with nannofossils, foraminifera and *Buchia* shells becoming abundant.

The Lower Cretaceous Palnatokes Bjerg Formation crops out in Wollaston Forland, Kuhn Ø, Hochstetter Forland and Traill Ø (Surlyk, 1978). The formation consists of the coarse grained Young Sund and Falskebugt Members, and the fine-grained Albrechts Bugt and Rødryggen Members. The cored interval penetrates only the Albrechts Bugt Member. The type locality of the member is situated at Rødryggen, Wollaston Forland, and reference sections are located in eastern Kuhn Ø, Mt Niesen and Rødryggen (Wollaston Forland; Surlyk, 1978). The thickness of the unit is laterally variable: it reaches a maximum thickness of ~ 300 m at Mt. Niesen (Wollaston Forland), where it interfingers with the fine-grained facies of the Young Sund Member. Towards East the member rapidly pinches out to ~30 m (Surlyk, 1978). In the field, the lower boundary of the Albrechts Bugt Member is typically gradational when the deposits overlie the Lindemans Bugt Formation (the Niesen or Rigi Members), interlayered when the Albrechts Bugt co-occur with the coarse grained Young Sund (West) or Falske Bugt (East) Members of the Palnatokes Bjerg Formation, or conformable/ angular unconformity when it overlies the Bernbjerg Formation (Surlyk, 1978). The upper boundary is transitional when overlain by the red mudstones of Rødryggen Member. Alternatively, the upper contact of the Albrechts Bugt can be an erosional or angular unconformity when the deposits are overlain by Aptian-Albian dark mudstones.

Lithologically the Albrechts Bugt Member consists of calcareous sandy, light grey to yellowish mudstone with abundant calcareous concretions (Surlyk, 1978). In the field, the Albrechts Bugt Member shows a conspicuous bright yellow weathering-colour that contrasts strongly with the essentially grey colour of the fresh and unweathered rock. The deposits are typically highly bioturbated and rich in *Buchia* bivalves, belemnite and ammonite fossils (see also Alsen, 2006).

3.1.4 References

Alsen, P. 2006: The Early Cretaceous (Late Ryazanian – Early Hauterivian) ammonite fauna of North-East Greenland: taxonomy, biostratigraphy, and biogeography. Fossils & Strata, **53**, 229 pp.

Alsgaard, p., Felt, V., Vosgerau, H., and Surlyk, F., 2003: The Jurassic of Kuhn Ø, North-East Greenland. In: Ineson, J.R. & Surlyk, F. (eds): The Jurassic of Denmark and Greenland. Geological Survey of Denmark and Greenland Bulletin, **1**, 865–892.

Surlyk, F. 1977: Stratigraphy, tectonics and palaeogeography of the Jurassic sediments of the areas north of Kong Oscars Fjord, East Greenland. Grønlands Geologiske Undersøgelse Bulletin, **123**, 56 pp.

Surlyk, F. 1978: Submanrine fan sedimentation along fault scarps on tilted fault blocks (Jurassic–Cretaceous boundary, East Greenland). Grønlands Geologiske Undersøgelse Bulletin, **128**, 108 pp.

Surlyk, F. 2003: The Jurassic of East Greenland: a sedimentary record of thermal subsidence, onset and culmination of rifting. In: Ineson, J.R. & Surlyk, F. (eds): The Jurassic of Denmark and Greenland. Geological Survey of Denmark and Greenland Bulletin, **1**, 659–722.

Surlyk, F. & Clemmensen, L.B. 1983: Rift propagation and eustacy as controlling factors during Jurassic inshore and shelf sedimentation in northern East Greenland. Sedimentary Geology, **34**, 119–143.

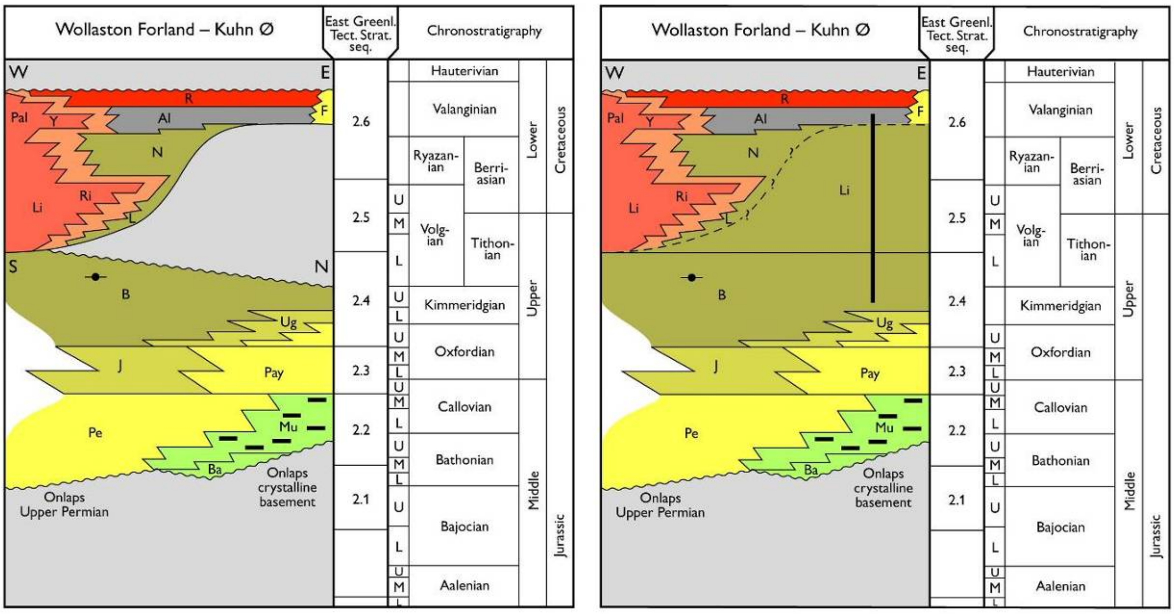

Figure 3.1.1 A) A general Jurassic – Early Cretaceous stratigraphical scheme in Wollaston Forland and Kuhn Ø areas (Surlyk, 2003). B) The stratigraphic scheme in the Rødryggen-1 core (vertical black line). Note the presence of Middle Volgian–Upper Ryazanian mudstones, and that the boundaries between lithostratigraphic units are gradational in the Rødryggen-1 core. The nature of these contacts is different in other parts of the tilted fault blocks and a major late Jurassic –Early Cretaceous unconformity is developed locally (e.g., Stratumbjerg, Wollaston Forland).

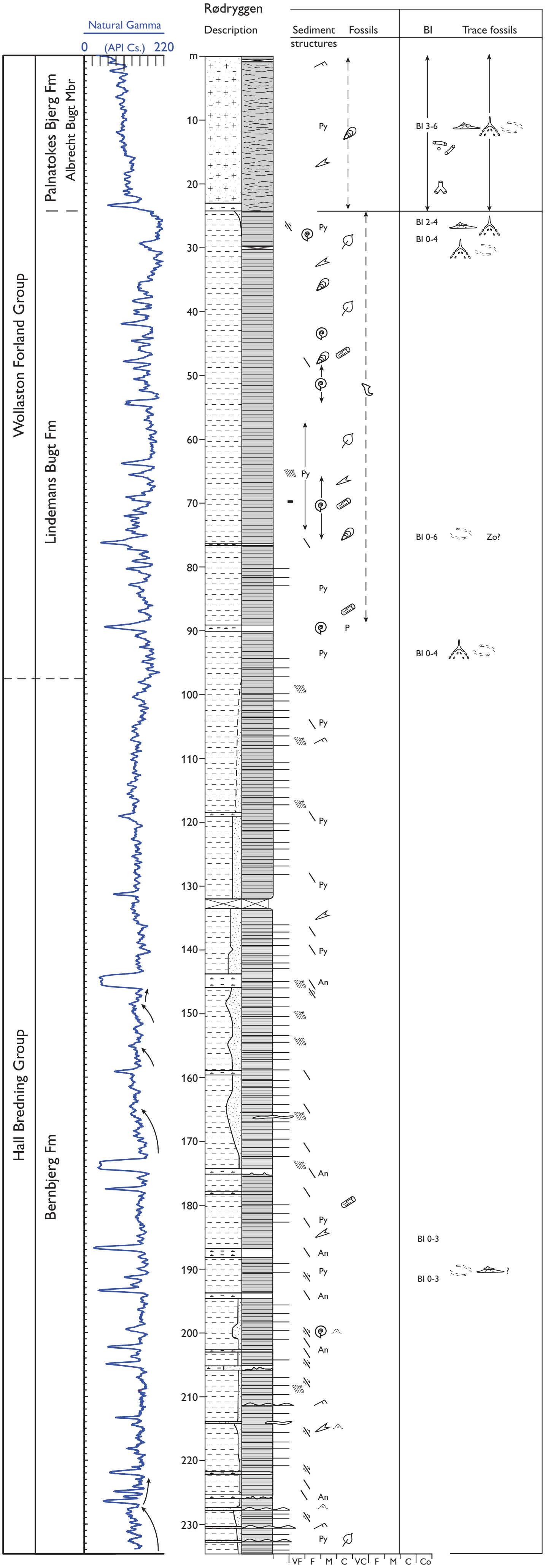

Figure 3.1.2 Lithostratigraphic division of the Rødryggen core. See Figure 4.1 for legend and facies division.

3.2 Biostratigraphy

3.2.1 Introduction

The Jurassic system is subdivided in great detail by means of ammonite zones which form a standard biostratigraphic and chronostratigraphic framework. Ammonite provincialism in some intervals hampers direct correlation to the standard ammonite zonation (established in Northwest Europe), and secondary standards are then established locally. Difficulties in ammonite correlation are particularly pronounced around the Jurassic–Cretaceous boundary leading to various separate chronostratigraphic divisions even at stage level. The ammonite zonation for most of the Upper Jurassic in East Greenland is mainly based on the ammonite successions in Milne Land and Jameson Land (Callomon & Birkelund 1982; Birkelund and Callomon 1985; Birkelund *et al*. 1984). The Oxfordian ammonite zonation used in East Greenland belongs to the Boreal and Subboreal faunal provinces (Sykes & Callomon 1979; Birkelund *et al.* 1984; Zeiss 2003). Less provincialism during the Kimmeridgian allows the ammonite succession in Greenland to be referred to the standard ammonite zonation of NW Europe (Birkelund & Callomon 1985; Zeiss 2003). Provincialism increased progressively during the latest Jurassic. The Lower Volgian ammonite zonation in Greenland is adopted from England, whereas a separate Boreal zonation was established for the Middle Volgian in Greenland allowing only few correlation levels to the Subboreal zonation of England (Callomon & Birkelund 1982; Zeiss 2003).

The Milne Land area is characterised by a gap in the sedimentary succession between the Middle Volgian to the lowermost Cretaceous, whereas the Upper Volgian in southern Jameson Land is documented by scattered biostratigraphic data. Further to the North a more complete Jurassic–Cretaceous boundary succession exists in the Wollaston Forland - Kuhn Ø area. The succession represents thick, coarse-grained synrift deposition containing sporadic levels with ammonites. The ammonite succession was documented by Maync (1949), Donovan (1964) and Surlyk (1978) providing a zonation that covers the Middle Volgian – Ryazanian. Only one zone (*Praechaetaites tenuicostatus* Zone) has been assigned to the Upper Volgian. However, the presence of *Subcraspedites* (*Swinnertonia*) from Kuhn Ø (Casey 1973) and a record in the present study indicate the presence of the Subboreal *Subcraspedites primitivus* Zone in Greenland providing a correlation of the base Upper Volgian from Greenland to NW Europe.

The ammonite zonation of the Upper Jurassic – Lower Cretaceous interval of relevance to the present study is shown in Figure 3.2.1. Note the usage of Boreal stage names and the position of the Boreal Upper Jurassic – Lower Cretaceous at the Volgian–Ryazanian boundary. The Jurassic–Cretaceous boundary in the standard chronostratigraphy established in the Tethyan Realm is placed at the Tithonian–Berriasian boundary. There is increasing agreement that that level corresponds to the Middle–Upper Volgian boundary, implying that the uppermost Boreal Jurassic actually is to be considered lowermost Cretaceous in a Tethyan sense.

3.2.2 Macrofossils and ammonite stratigraphy in the Rødryggen-1 core

Introduction

The Rødryggen-1 core was drilled through the lower part of the Albrechts Bugt Member and into the underlying dark mudstone succession of the Lindemans Bugt and Bernbjerg Formations. The Albrechts Bugt Member and the overlying Rødryggen Member (both units of the Palnatokesbjerg Formation) are well-exposed in the flanks of the Rødryggen ridge. Their vivid yellowish and reddish colours stand out in the landscape, and have attracted attention since the earliest geological mapping of the area. The locality chosen for drilling site has thus previously been subject to various macrofossil studies, ammonites in particular, by various workers since the 1940´ies. Collections by W. Maync and D.T. Donovan in the 1940-50'ies and S. Piasecki and F. Surlyk in the 1980–90'ies were recently supplemented by large bed-by-bed collections by P. Alsen. The collections form the basis for a monograph of the late Ryazanian to Hauterivian ammonite fauna which included material from three sections through Albrechts Bugt – Rødryggen Members on the flanks of the Rødryggen ridge (Alsen 2006). Alsen & Rawson (2005) presented a specific study on the age diagnostic base-Valanginian ammonite genus *Delphinites*. The ammonite succession provides a chronostratigraphic framework in which other disciplines can be studied. Brachiopods were investigated by Harper *et al*. (2005) and belemnites by Alsen & Mutterlose (2009). Ongoing integrated stratigraphic studies are undertaken in collaboration with Ruhr University, Bochum and deal with belemnites (Alsen & Mutterlose *in prep.*), calcareous nannofossil stratigraphy (Pauly *et al.* 2010) and stable isotope stratigraphy. The dark mudstone succession underlying the Palnatokes Bjerg Formation weathers into a badland landscape in the surroundings of the Rødryggen ridge. Maync (1947) referred the mudstones to the Kimmeridgian, which were described as black, sandy shales with ammonites and *Aucella* (=*Buchia*-bivalves). The mudstones have been considered Kimmeridgian and belonging to the Bernbjerg Formation until the present study.

Material and methods

A study of ammonites in the recently drilled Blokelv-core in Jameson Land provided an accurate ammonite stratigraphy which, integrated with palynostratigraphy, provided a powerful, rigid chronostratigraphic framework for the study of the core (Bjerager *et al.* 2009). This encouraged a similar search for ammonites in the present Rødryggen-1 core. The uppermost part of the core belongs to the Albrechts Bugt Member and contains numerous shells, mostly bivalves of the genus *Buchia* which is a useful biostratigraphic taxon for the Volgian–Hauterivian (Surlyk & Zakharov 1982). Outcrop studies show that also belemnites are common (Alsen & Mutterlose 2009), whereas ammonites are relatively rare (Alsen 2006). Only *Buchia* specimens from the Albrechts Bugt Member were extracted from the Rødryggen-1 core. Since the stratigraphy of that member is described in detail from outcrop studies, the present study focussed on the dark mudstones below the Albrechts Bugt Member.

A core tends to preferably split along bedding planes and particularly along planes with fossils. Hence, the end faces of every core piece were examined for ammonites and other macrofossils. The search for ammonites was carried out top-down in the core. The upper 65 m of the black mudstone succession contain relatively many ammonites (level c. 26–90 metre) whereas no ammonites were found the interval between 90 to almost 200 m. The latter interval is characterized by finely laminated dark mudstones, which theoretically has a good preservation potential for fossils. Ammonites are thus probably present. However, a large proportion of the mentioned interval was heavily fractured hampering the examination for fossils. The distribution of ammonite levels in the core is almost exclusively confined to the Lindemans Bugt Formation, whereas the Bernbjerg Formation appears barren. It is possible that lack of ammonite finds in the Bernbjerg Formation is not only due to difficult sampling conditions (fractured core). Lack of ammonite finds may also reflect a more fossil poor unit, since the Bernbjerg Formation was deposited during times of higher sedimentation rate (Chapter 4). The confinement of fractures to the Bernbjerg Formation compared to the overlying Lindemans bugt Formation may reflect the post Bernbjerg Formation and syn Lindemans Bugt Formation tilting and movement during the Latest Jurassic maximum rifting. At c. 197 m ammonite fragments again appeared, and relatively close to the total depth an ammonite was recovered from level c. 228 m.

The search resulted in a total of 27 sampled macrofossil specimens. Most are fragmented. Identification also suffers from the relatively small diameter of the core (compared to the Blokelv-core) usually allowing only small portions, and thus less diagnostic characters, of a fossil to be examined.

Data

Level 227.72 m: GGU 517101-426 (Fig. 3.2.2A); ammonite, crushed fragment, dense, fine, slightly prorsiradiate (forward-leaning) and concave ribbing; coiling involute; probably *Amoeboceras* suggesting pre-latest occurrence of that genus. i.e. a Middle Kimmeridgian age or older.

Level 199.42 m: GGU 517101-425; ammonite?, indeterminate fragment

Level 90.85 m: GGU 517101-424 (Fig. 3.2.2B), ammonite, crushed fragment, medium sized; ribbing subdued with straight primaries and intercalated secondaries that begin on midflank, gently sloping umbilical wall; possibly a *Dorsoplanites* sp.

Level 89.30 m: GGU 517101-423 (Fig. 3.2.2.C), ammonite, small part of a large specimen, only the crushed part of upper flank visible; straight, blunt distant ribs that bifurcate very high. Identification difficult, but tentatively referred to as *Dorsoplanites primus*, an identification which is supported by palynostratigraphic dating of the level to Lower–Middle Volgian boundary interval. *D. primus* indicates M31 and is index for the *D. primus* Zone

Level 89.26 m: GGU 517101-422, Onychites, large (hook from belemnite)

Level 75.43 m: GGU 517101-421(Fig. 3.2.2.D), ammonite, extraction showing coarse, biplicate rursiradiate ribbing from a large specimen, resembling various species within the genus *Pavlovia* but appears closest to *P. variocostata* Callomon & Birkelund characterised by a modification to subdued, irregular widely-spaced and extremely coarse biplicate ribs in adult stage. The taxon indicates the M35 of the *P. communis* Zone.

Level 74.20 m: GGU 517101-420 (Fig. 3.2.2.E), ammonite, the part visible in this core piece shows dense, subdued ribbing in a large form, with blunt, primaries that divide in an almost fasciculate manner into 3-4 secondaries and intercalatories. The subdued ribbing somewhat resembles but does not exactly match the one of *Dorsoplanites liostracus* Callomon & Birkelund. A closer match is found in a specimen figured by Rogov & Zakharov (2009) and referred to as *D. sachsi* Michailov. However that find was referred to the *D. maximus* Zone corresponding to the *E. pseudapertum* Zone (M41–M44) in Greenland conflicting with the identifications and biostratigraphic ages made on material above in the core. The present specimen is thus conservatively referred to as *Dorsoplanites* sp.

Level 74.03 m: GGU 517101-419 (Fig. 3.2.2.F), ammonite, crushed fragment showing slightly flexuous relatively strong, blunt primary ribs and weak intercalating secondaries. This ribbing style resembles the one of the, however, much larger *Pavlovia corona* Call. & Birk. (1982, pl. 3, fig. 1). That species suggests faunal horizon M37 (*D. liostracus* Zone, Middle Volgian).

Level 70.06 m: GGU 517101-418 (Fig. 3.2.2.G), ammonite, fragment, apparently from open whorled (evolute) form with relatively distant ribbing, primaries that are blunt, gently prorsiradiate and forward concave. Secondaries mostly intercalate and develop at midflank. Considering the identification of the ammonite in subsample -414 and by comparison, in descending order, of taxa from faunal horisons of Callomon & Birkelund (1982) and figured material in Spath (1936) referred to those horizons a probable match is not found until faunal horizons M34-42 (*Pavlovia communis – E. pseudapertum* Zone; Middle Volgian), since the ribbing of the present specimen resembles the 'indistinct' one of *Dorsoplanites gracilis* Spath (pl. 29, fig. 3). *D. gracilis* was subdivided into a succession of transients α to η by Callomon & Birkelund (1982) which occur in a rather thick interval between M34–42. The preservation of the present specimen does not allow an accurate designation/identification on transient level and thus neither identification of a faunal horizon, although delimited by the underlying M37 specimen at 74.03 m.

Level 66.84 m: GGU 517101-417, ammonite, crushed fragment, densely and finely ribbed venter, indeterminate.

Level 66.54 m: GGU 517101-416, belemnite, recrystalized rostrum, indeterminate.

Level 62.43 m: GGU 517101-415 (Fig. 3.2.2.H), Onychites; hooks from belemnites are common in the core, those sampled at this level are well-preserved and serve as an example for photographing.

Level 55.98 m: GGU 517101-414 (Fig. 3.2.2.I), ammonite, small, with well-preserved, relatively distant ribbing with strong, straight, prorsiradiate primaries that divide into two secondaries rather high on the flank. Close to *Epipalliceras pseudapertum* Spath (1936, pl. 9 fig. 4) indicating M42 faunal horizon and index of the middle Middle Volgian *E. pseudapertum* Zone.

Level 55.25 m: GGU 517101-413, ammonite, poorly preserved, indeterminate specimen.

Level 54.53 m: GGU 517101-412, ammonite fragment, crushed, ?*Laugeites* sp.

Level 53.67 m: GGU 517101-411 (Fig. 3.2.2.J), ammonite fragment from apparently very large ammonite with straight, strong, and distant primary ribs, which begin sharp but appear to become blunt and flatten on/towards the (mid?-)flank. Resembles *Laugeites biplicatus* Mesezhnikov as figured by Repin *et al.* 2006 (Atlas of molluscs from Jurassic of Pechora, Russia). The Russian taxon indicates the *Epivirgatites nikitini* Zone in Russia, which is equivalent to the *Laugeites groenlandicus – Epilaugeites vogulicus* Zones, i.e. M47–higher zones. However, the present specimen is delimited to the M47 due to the M47-identification above at level 51.55 m.

Level 52.82 m: GGU 517101-410, ammonite fragment, poorly preserved and indeterminate.

Level 51.55 m: GGU 517101-409 (Fig. 3.2.2.K), ammonite, complete; small ?juvenile with relatively high whorl sides and narrow umbilicus, very dense fine and delicate ribbing (>31 per whorl) with primaries that divide/bifurcate almost immediately or low on flank into dense and fine secondaries. Ribbing is almost straight, slightly forward leaning concave. By comparison with Donovan (1964) and Surlyk *et al*.1973 the specimen is referred to the genus *Laugeites,* which is characterised as being smaller, more compressed and more delicately ribbed than its predecessor *Dorsoplanites* (see discussion in description of *Dorsoplanites intermissus* Callomon & Birkelund 1982 appendix). The relatively closely resembling *L. parvus* and other Greenland *Laugeites* have more forward leaning ribs, whereas the ribbing on the present specimen is almost radiate. Closest resemblance appears to be found in *Laugeites planus* Mesezhnikov (in Zakharov & Mesezhnikov 1974) described from Russia. It indicates the M47, upper Middle Volgian *L. groenlandicus* Zone.

Level 48.54 m: GGU 517001-427: ammonite fragment

Level 48.37 m: GGU 517101-408, ammonite fragment

Level 47.52 m: GGU 517101-407 (Fig. 3.2.2.L), *Buchia*-bivalve

Level 47.20 m: GGU 517101-406 (Fig. 3.2.2.M), Aptychus (ammonite jaw apparatus)

Level 45.73 m: GGU 517101-405, *Buchia*-bivalve, complete

Level 45.37 m: GGU 517101-404 (Fig. 3.2.2.N), ammonite, fragment showing strong, distant, bullate primaries that divide into somewhat weak secondaries. Set of secondaries are intercalated with weak ribs that start at a level equal to the furcation level of the primaries, together it gets an appearance of distant primaries and dense secondaries and intercalatories. Closest resemblance is found outside Greenland in the taxon *Subcraspedites (Swinnertonia) subundulatus* occurring in the Upper Volgian *Subcraspedites (Swinnertonia) primitivus* Zone in England (Casey 1973 pl. 4 fig.1). That zone is now adopted to the East Greenland zonation.

Level 43.21 m: GGU 517101-403, ammonite, fragment showing dense, fine, delicate parallel ribbing from a small specimen. Considering the identification of 517001-404 below (as *S.* (*Sw.*) cf. *subundulatus*) the specimen is compared with and found considered to resemble the likewise finely ribbed juvenile *Subcraspedites* (*Swinnertonia*) sp. juv. figured in Casey (1973 pl. 4) also of the *S. primitivus* Zone.

Level 43.18 m: ammonite fragment, not sampled

Level 35.80 m: GGU 517101-402, *Buchia*-bivalve, well-preserved

Level 27.73 m: GGU 517101-401(Fig. 3.2.2.O), ammonite, ribbing that covers all of the bedding surface of the core piece; ribs radiate from a very narrow umbilicus indicating pronounced involuteness; primaries divide into two secondaries, and bend forwards from the level of furcation. Resembles *Hectoroceras* indicating the upper Lower Ryazanian *Hectoroceras kochi* Zone*.*

The data are summarized in Table 3.2.1.

Ammonite stratigraphy (Fig. 3.2.3)

***D. primus* Zone**

This zone and M 31 is indicated by the index species at 89.30 m.

***P. communis* Zone**

The presence of *P. variocostata* in level 75.43 m indicates the M 35 faunal horizon that lies in the upper part of the *P. communis* Zone.

***D. liostracus* Zone**

This zone is the lower of two zones characterized by mainly containing species of *Dorsoplanites* but it also includes *Pavlovia* (Callomon & Birkelund 1982). It is subdivided into two faunal horizons, M36–37. The zone and M37 is indicated at 74.03 m by the presence of *Pavlovia corona* Callomon & Birkelund and possible *D. liostracus* at level 74.20 m.

D. liostracus – E. pseudapertum Zones

An ammonite at level 70.06 m is identified as *Dorsoplanites gracilis* Spath. The species originally described and figured by Spath (1935) was later demonstrated to include a succession of evolutionary transients designated α to η by Callomon & Birkelund (1982). The species with transients are stratigraphically widely distributed from M34 – M42 corresponding to the *P. communis – E. pseudapertum* Zones. The preservation of the present material does not allow a specific identification of the specimen to a certain transient, hampering a more exact stratigraphic position within the mentioned interval. The interval is however delimited by the presence of *D. liostracus* Zone ammonite below. The index of the *E. pseudapertum* Zone was identified at level 55.98 m.

L. groenlandicus Zone

Ammonites belonging to *Laugeites* including the species *L. biplícatus* at 53.67 m and *L.* cf. *planus* 51.55 m indicate the *Laugeites groenlandicus* Zone. This leaves only very little room for the Anguinus Zone, which occurs between the Pseudapertum and the Groenlandicus Zones (Fig. 3.2.1). The presence in the core of a thin Anguinus Zone is, however, indicated by palynostratigraphy which records the Pseudapertum-Anguinus Zone boundary.

S. primitivus Zone

The presence of *Subcraspedites* (*Swinnertonia*) *subundulatus?* at 45.37 m and a specimen that is tentatively referred to the same subgenus at 43.21 m indicate the *Subcraspedites primitivus* Zone. The subgenus *Swinnertonia*, which in England is confined to the *S. primitivus* Zone, has previously been recorded in Greenland in one of the upper conglomerates of the Laugeites Ravine Member on Kuhn Ø (Casey 1973 revision of Spath 1952 identifications; see also Surlyk 1978), but the zone has not previously been used in North-East Greenland. The upper Middle – Upper Volgian is generally not well subdivided by means of ammonite zones, due to a lack of ammonite data in Greenland. The presence of the *S. primitivus* Zone in Greenland as suggested by the present limited material is tentative but likely, since it is supported by palynostratigraphic data obtained from same core interval (see elsewhere in this chapter). The *S. primitivus* Zone was established in the North Sea area where it is used to mark the base of the Upper Volgian. The recognition of the zone thus provides a link from the North Sea area to North-East Greenland.

H. kochi Zone

The uppermost ammonite find in the Rødryggen-1 core, at 27.73 m is referred to the genus *Hectoroceras* which is a taxon confined to the *H. kochi* Zone. This zone was established in Greenland but is recognized widely and forms an excellent means for correlation.

Ammonite zones recorded from outcrop

No ammonites were recovered from the Albrechts Bugt Member interval in the core. However, recent outcrop studies of the Albrechts Bugt Member resulted in the recognition of 5 Valanginian ammonite zones at the drillsite (incl. the upper part of the member not drilled). With the inclusion of ammonite stratigraphic data of the Albrechts Bugt Member from elsewhere in the Wollaston Forland area the member is referred to the uppermost Ryazanian and six Valanginian ammonite zones (Alsen 2006). Those datings are supported by calcareous nannofossil studies by Pauly *et al.* 2010 and are also supported by the present study. The unit overlying overlying the Albrechts Bugt Member, also not drilled, is the Rødryggen Member which contains *Simbirskites*-ammonites and is thus referred to as *Simbirskites* beds indicating the Hauterivian (Alsen 2006). This age assessment was also subsequently supported by calcareous nannofossil studies (Pauly *et al.* 2010).

Biostratigraphic studies of ammonites, belemnites and calcareous nannofossils suggest that the lithostratigraphic boundary between the Albrechts Bugt and Rødryggen Members is essentially isochronous within the Wollaston Forland – Kuhn Ø Area (Alsen 2006; Alsen & Mutterlose 2009; Pauly *et al.* 2010). This contrasts to data from the Traill Ø area to the south, where the two members are known from two separate localities, respectively, but contain essentially similar ammonite faunas (Alsen 2006). This demonstrates a similar age of the two units inferring a strongly diachronous lithostratigraphic boundary. Note however, that the two members are not known to occur together in that area. The Rødryggen Member is unconformably overlain by dark mudstones, which have so far only yielded ammonites without age significance. The dark mudstones are referred to the Barremian in the Wollaston Forland area (Nøhr-Hansen 1993; Pauly *et al.* 2010).

3.2.3 Palynostratigraphy

Material and methods

Samples were collected from the Rødryggen-1 core by splitting the core in two and crushing 4 to 6 cm of the half-core for analysis. The core is characterised by GGU nr. 517001 and the samples are characterised by a sub-number and a depth below surface (in the range-chart). The depth is the medium point of the length of the sample.

A total of 37 samples from the Rødryggen-1 core were processed by palynological preparation methods, including treatment with HCl, HF, oxidation with HNO_3 and heavy liquid separation. The samples from Bernbjerg and Lindemans Bugt Formations comprise black shale with abundance of marine and terrestrial organic matter which demands repeated oxidation and ultrasonic treatment to release identifiable dinoflagellates. Each preparation step is represented by a slide to follow the process. Finally, the organic residue was sieved on 21 µm filter, was sometimes swirled and was finally mounted on glass slides using a glycerine jelly medium.

The dinoflagellate (dinoflagellate cyst) content was analysed using a normal light microscope. All dinoflagellates in one slide from each sample were counted to perform a semi-quantitative analysis in relation to the content of organic matter (dinoflagellates/slide = dinoflagellates/organic matter). This works well within the black shales but the diversity/abundance in Albrecht Bugt Member with very low organic content cannot be compared with data from the shales by this method. Other algae, acritarchs, phrasinophycean and freshwater algae in the slide were counted as well. Further dinoflagellate species occurring in other slides were recorded as present but not included in the counting. The depositional environment is interpreted, the organic content is briefly described and the thermal maturity is estimated on the basis of sporomorph colours (Thermal Alteration Index; TAI). The taxonomy used herein follows that in the Lentin and Williams Index of Fossil Dinoflagellates 2004 Edition unless otherwise indicated by author references (Fensome & Williams 2004).

The result of the palynological study is presented in a range-chart. The dinoflagellate species are sorted after their highest occurrence and presented with their relative proportion of the dinoflagellate assemblage (Fig. 3.2.4). The stratigraphic results are illustrated in a stratigraphic summary-chart (Fig. 3.2.5). No recorded occurrence of dinoflagellate taxa is interpreted as a result of caving due to all analysed material is from cores. Reworked dinoflagellate taxa are shown in a separate panel. The spore and pollen flora is not recorded systematically but reworked spores and pollen are mentioned occasionally in the text. Occurrences marked with a "?" indicate uncertainty of the identification.

Stratigraphic methods

Based on first- and last occurrence of stratigraphic important species (events) the studied succession has been correlated to ammonite zones of the local Boreal ammonite zonation (Callomon & Birkelund 1982; Birkelund, Callomon & Fürsich 1984; Birkelund & Callomon 1985; Surlyk 1973, 1977, 1978; Alsen 2006). Especially in the upper part of the succession, the dinoflagellate events have been correlated to North-West Europe or Russian, Subboreal ammonite zones because correlation to local ammonite zonation has not been established yet. Altered or new correlations of dinoflagellate event with local ammonite stratigraphy have been established in this work. The ammonite biozonation correlates with ammonite chronozones and the succession is dated on the basis of these chronostratigraphic units.

Ammonite zonations vary with geographically separate fauna provinces and at many stratigraphic levels, these diverging zonations are not precisely correlated. However, stratigraphic schemes generally ignore this fact. Correlating dinoflagellate events with ammonite zones in different fauna provinces, and then comparing these ammonite zones across biogeographic boundaries to obtain a relevant age, is hazardous. However, in some cases this is the only possibility.

In this chapter, ammonite biozones are indentified only by species name (e.g. Elegans Zone), ammonite faunal horizons from Milne Land are identified by M numbers (e.g. M 24) and dinoflagellate events by the full name in italics (e.g. top of abundant *Oligosphaeridium patulum*).

In general, dinoflagellate stratigraphy based on events of selected species, appears relatively robust across palaeogeographic and palaeoclimatic barriers. However, in the Jurassic, the flora varies significantly in composition, diversity and abundance from Subboreal to Boreal and Arctic regions (e.g. Brideaux 1977; Brideaux & Fisher 1976; Lebedeva & Nikitenko 1999; Riding, Federova & Ilyina 1999; Smelror & Dypvik 2005) and consequently the age of stratigraphic events may vary as well. Examples are documented in this work based on the common ammonite and dinoflagellate stratigraphy presented herein.

Dinoflagellate stratigraphy

234.40 m (TD) – 220.51 m

This is the succession from the terminal core depth to the top of abundant *Perisseiasphaeridium pannosum* (220.51 m) and the appearance of *Oligosphaeridium patulum* (220.51 m).

Dinoflagellate assemblage

Perisseiasphaeridium pannosum, *Paragonyaulacysta capillosa* and *Cribroperidinium* spp. dominate the assemblage and *Epiplosphaera reticulospinosa* and *Paragonyaulacysta bo-*

realis is locally common. *P. borealis* appears for the first time in the top of this assemblage (220.51 m) but is known to occur from the Baylei Zone on Milne Land (Piasecki 1981, 1996).
The assemblage is relatively diverse and abundant.

Biostratigraphy

P. pannosum appears abundantly from ammonite fauna horizon M 20 on Milne Land (Piasecki 1981, 1996; Bjerager *et al*. 2009) in basal Eudoxus Zone and the top of abundant *P. pannosum* occurs between M 22 and 23 at the top of Eudoxus Zone on Milne Land. A similar stratigraphic range occurs on Jameson Land (Piasecki 1981, 1996; Bjerager *et al*. 2009) and is followed in both places by appearance and abundance of *Oligosphaeridium patulum* in the overlying Autissiodorensis Zone. In Rødryggen-1, *O. patulum* occurs in low numbers in the next higher sample and becomes abundant in higher samples. Therefore, this succession correlates with the Eudoxus Zone on Milne Land and Jameson Land, East Greenland (Piasecki 1981, 1996).

Age

Kimmeridgian, Late Jurassic

Depositional environment

Offshore, shallow marine environment with oxygenated to dysoxic bottom conditions and with high influx of terrestrial organic material from higher plants; sporomorphs and woody material. Comparable with a delta front environment.

Organic matter and maturity

Terrestrial organic material dominates totally, especially black and brown woody material with some sporomophs. Finely dispersed, amorphous material is present together with some dinoflagellates. The content of marine organic matter varies but is constantly low in these samples, Type III–IV OM. The TAI Index is 2^+, dark orange i.e. in the earliest catagenetic stage, the beginning of the oil window.

220.51 m – 150.25 m

The succession is from the first appearance of *Oligosphaeridium patulum* (210.44 m) to the first appearance of *Trichodinium piaseckii* (140.25 m).

Dinoflagellate assemblage

The dinoflagellate assemblage is characterised by abundant *Oligosphaeridium patulum*, *Cribroperidinium* spp. and *Cyclonephelium distinctum sensu* Ioanides *et al.* 1976. *Paragonyaulacysta capillosa* is common but less frequent upwards. The assemblage is mostly recorded of low diversity and low abundance, probably due to the abundance other organic material.

Biostratigraphy
O. patulum appears in the basal Autissiodorensis Zone between ammonite fauna horizon M 22–23 on Milne Land (Piasecki 1981, 1996; Bjerager *et al*. 2009). *T. piaseckii* appears below ammonite fauna horizon M 25, Wheatlyensis Zone (Piasecki 1981, 1996). The succession is therefore correlated with Autissiodorensis and Elegans Zones,

Age
Kimmeridgian – Early Volgian, Late Jurassic

Depositional environment
Offshore marine environment with oxygenated to dysoxic bottom conditions and with high influx of terrestrial organic material from higher plants; sporomorphs and woody material. Comparable to a delta front to upper delta slope environment.

Organic matter and maturity
Terrestrial organic material dominates especially black and brown woody material with some sporomophs. Amorphous material is present together with dinoflagellates, Type III OM. The TAI Index is 2^+, dominantly dark orange.

150.25 m – 130.26 m
The interval is from the first appearance of *Trichodinium piaseckii* (150.25 m) followed by *Senoniasphaera clavelli* (140.25 m) to the top of abundant *Oligosphaeridium patulum* (130.26 m).

Dinoflagellate assemblage
The dinoflagellate assemblage is dominated of *Oligosphaeridium patulum* and *Cribroperidinium* spp. and *Sirmiodinium grossii*, *Circulodinium* spp. and *Cyclonephelium distinctum sensu* Ioanides *et al.* 1976 are common locally. The assemblage is recorded as relatively diverse and abundant.

Biostratigraphy

S. clavelli and *T. piaseckii* appear below ammonite fauna horizon M 25, Wheatlyensis Zone on Milne Land (Piasecki 1981, 1996). The top of abundant *O. patulum* occurs at ammonite fauna horizon M 25 (Piasecki 1981, 1996). This succession therefore correlates with the (Scitilus ?) and Wheatlyensis Zone.

Age

Early Volgian, Late Jurassic

Depositional environment

Offshore marine environment with anoxic bottom conditions and with influx of terrestrial organic material degraded from higher plants; sporomorphs and woody material. Comparable with a delta slope environment.

Organic matter and maturity

Terrestrial organic material dominates especially black and brown woody material with some sporomophs. Amorphous material is present together with some dinoflagellates, Type III OM. The content of woody material is high in the lowest sample and decreases upwards to be low in the uppermost sample. The TAI Index is 2^{+}, dark orange.

130.26 m – 110.15 m

The interval from the top of abundant *Oligosphaeridium patulum* (130.26 m) to the last occurrence of *Trichodinium piaseckii* in 110.15 m.

Dinoflagellate assemblage

The dinoflagellate assemblage is dominated of *Cribroperidinium* spp. and *Sirmiodinium grossii*. *Apteodinium* spp., *Cassiculosphaeridium magna*, *Paragonyaulacysta capillosa* and *P. borealis* are locally common. The assemblage is recorded as moderately diverse and abundant.

Biostratigraphy

The top of abundant *O. patulum* occurs at ammonite fauna horizon M 25, Wheatlyensis Zone (Piasecki 1981, 1996). *Trichodinium piaseckii* occurs for the last time between ammonite fauna M 25 and 29 on Milne Land, Wheatlyensis and Pectinatus Zones respectively (Piasecki 1981, 1996). This event is therefore correlated to the Wheatlyensis – Pectinatus Zones in accordance with the highest occurrence of the type-material from UK, the North Sea region (Bailey, Miller Varney 1997).

Age

Early Volgian, Late Jurassic

Depositional environment

Offshore marine environment with anoxic bottom conditions and with influx of terrestrial organic material degraded from higher plants; sporomorphs and woody material. Comparable to a delta slope environment.

Organic matter and maturity

The organic content comprises marine amorphous material with abundant terrestrial organic matter of black and brown woody material and sporomorphs, Type II–III OM. The TAI Index is 2, orange, i.e. the diagenetic stage before the oil window. The gradual transition from the diagenetic to the catagenetic stage of thermal maturation of organic matter is then estimated approximately at 130–140 meters depth, i.e. the entrance to the oil window.

110.15 m – 99.72 m

The succession from the last occurrence of *Trichodinium piaseckii* in 110.15 m to the last occurrence of common *Operculodinium patulum* in 99.72 m.

Dinoflagellate assemblage

Evansia sp. E Wiggins 1975, *Oligosphaeridium patulum*, *Paragonyaulacysta capillosa*, *P. borealis* and *Sirmiodinium grossii* are common in this succession. The assemblage is considered moderately diverse and abundant.

Biostratigraphy

The uppermost occurrence of *Trichodinium piaseckii* is between ammonite fauna M 25 and 29 on Milne Land, Wheatlyensis to Pectinatus Zones respectively (Piasecki 1981, 1996). The last common occurrence of *O. patulum* occurs between ammonite fauna M 25 and 29 on Milne Land, Wheatlyensis to Pectinatus Zones respectively (Piasecki 1981, 1996). In North-West Europe, common *O. patulum* occurs up to the Pectinatus Zone (e.g. Riding & Thomas 1992). In Rødryggen-1 core, the Wheatlyensis Zone is identified below this interval and this event is referred to the Pectinatus Zone.

Age

Early Volgian, Late Jurassic

Depositional environment

Offshore marine environment with anoxic bottom conditions and with some influx of terrestrial organic material degraded from higher plants; sporomorphs and woody material. Comparable with a lower delta slope environment.

Organic content and maturity

Marine organic amorphous material mixed with terrestrial material of spores and pollen and woody material, Type II OM. The content of woody material is high in the lowest sample and decreasing upwards to be low in the uppermost sample. The TAI Index is 2, orange.

99.72 m – 79.74 m

The interval between the top of common *Oligosphaeridium patulum* (99.72 m) and the lowest appearance of *Muderongia* spp. (79.74 m).

Dinoflagellate assemblage

This interval is represented by one sample. *Cassiculosphaeridium magna* is abundant and *Sirmiodinium grossii* is common. Some very characteristic dinoflagellates occur in this sample and are preliminary identified as *Cribroperidinium jubaris* and *Rhynchodiniopsis aff. fimbriata*. These species may mark the transition from Upper to Middle Volgian. The assemblage is recorded as relatively diverse and abundant.

Biostratigraphy

The top of common *O. patulum* occurs in the Pectinatus Zone and is discussed above. This is supported by the ammonite *Dorsoplanites primus* Callomon & Birkelund (89.39 m) which occurs above this event and indicates ammonite faunal horizon M 31, Primus Zone. In the Rødryggen-1 core, the first occurrence of common *Muderongia* spp. in the shape of *Muderongia* sp. A Davey 1979, is below the ammonite *Pavlovia variocostata* (75.43 m), ammonite fauna horizon M 35, Communis Zone (this report).

In North-West Europe, the appearance of common *Muderongia* spp. (in the shape of *Muderongia* sp. A Davey 1979) is well established in the Rotunda Zone (e.g. Riding & Thomas 1992). The Rotunda Zone is correlated with the Communis Zone (M 34–35) in East Greenland (Birkelund and Callomon 1984). The *Muderongia* spp. event is hereby correlated with the Communis Zone of the East Greenland biostratigraphy on the basis of this study.

On Milne Land, the appearance of *Muderongia* sp. A occurs remarkably higher in the succession, i.e. in the Anguinus Zone, M 46, Middle Volgian (Piasecki 1981, 1996) and this is now considered a delayed appearance. The present succession correlates with Pectinatus to Communis Zones.

Age

Early Volgian – Middle Volgian, Late Jurassic

Depositional environment

Offshore marine environment with anoxic bottom conditions and with limited influx of terrestrial organic material. Comparable with a basin floor environment.

Organic content and maturity

Marine organic amorphous material mixed with terrestrial material of spores and pollen and woody material, Type II OM. The content of woody material is high in the lowest sample and decreases upwards to be low in the uppermost sample. The TAI Index is 2, orange.

79.74 m – 70.15 m

The succession from the first appearance of *Muderongia* spp. (*M.* sp. A Davey 1979) in 79.4 m to the first appearance of *Lagenorhytis delicatula* in 70.15 m.

Dinoflagellate assemblage

Apteodinium spp., *Cribroperidinium* spp., *Lagenorhytis delicatula*, *Sirmiodinium grossii*, *Paragonyaulacysta borealis* and *P. capillosa* are locally common to dominating. Diversity of the assemblage is relatively high whereas the abundance is low.

Biostratigraphy

The lowest occurrence of common *Muderongia* spp., in the shape of *Muderongia* sp. A Davey 1979, is correlated with the Communis Zone (see above). Two identified ammonites occur in this succession; *Pavlovia corona* Callomon & Birkelund in 74.03 m and *Dorsoplanites gracilis* Spath in 70.06 m indicating Liostracus Zone (M 37) and Liostracus to Pseudaperum Zones (M 37–42) respectively (Birkelund, Callomon & Fürsich 1984; this report). The appearance of *Lagenorhytis delicatula* is just below the occurrence of the ammonite *Dorsoplanites gracilis* in 70.06 m. *L. delicatula* is generally assigned a Lower Cretaceous range so this low appearance in the Middle Volgian, Upper Jurassic, is surprising and must be studied further. It forms a potentially excellent local marker and is here dated within three ammonite zones, Liostracus to Pseudapertum Zones.

Age

Middle Volgian, Late Jurassic

Depositional environment

Offshore marine environment with anoxic bottom conditions and limited influx of terrestrial organic material mainly as spores and pollen. Comparable with a basin floor environment.

Organic content and maturity

Marine organic amorphous material associated with spores and pollen and little woody material of varying abundance, Type II OM. The TAI Index is 2, orange.

70.15 m – 59.85 m

The succession from the first appearance of *Lagenorhytis delicatula* (70.15 m) to the top of *Leptodinium subtile* (59.85 m).

Dinoflagellate assemblage

Cribroperidinium spp. dominates the assemblage and *Rhynchodiniopsis pennata* is common.

The assemblage is relatively diverse and abundant.

Biostratigraphy

The unusual appearance of *Lagenorhytis delicatula* as low as in Middle Volgian strata is discussed above. In contrast, the top of *Leptodinium subtile* is a well known marker from the North-West Europe, which has highest occurrence in the Albani Zone (Riding & Thomas 1992). The upper Albani Zone is correlated with the Pseudapertum Zone in the East Greenland ammonite stratigraphy (Birkelund, Callomon & Fürsich 1984). As discussed above, the Liostracus to Pseudoapertum Zone is indicated for the lower part of the interval. The ammonite *Epipalliceras pseudapertum* occurs in 55.98 m (this report) just above this interval and supports the correlation to M 42, Pseudapertum Zone for the uppermost part.

Age

Middle Volgian, Late Jurassic

Depositional environment

Offshore marine environment with anoxic bottom conditions and with limited influx of terrestrial organic material mainly as spores and pollen. Comparable with a basin floor environment.

Organic matter and maturity

Marine amorphous material associated with terrestrial organic matter mainly of spores and pollen but with a small but varying content woody material, Type II OM. The TAI Index is 2, orange.

59.85 m – 35.02 m

The interval from the last appearance of *Leptodinium subtile* (59.85 m) to the first occurrence of *Gochteodinia villosa* (35.02 m).

Dinoflagellate assemblage

Cribroperidinium spp. dominates the assemblage. *Canningia* spp., *Circulodinium* spp. and *Sentusidinium* spp. dominate one sample. The assemblage is mostly of low diversity and low abundance probably due to abundance of organic matter

Biostratigraphy

The *Leptodinium subtile* event is discussed above; the event is correlated with the Pseudapertum Zone. The stratigraphic range of *Gochteodinia villosa* is used for dinoflagellate zonation in western Europe, Russia and Siberia. The first occurrence is correlated with the Portlandian Opressus Zone in UK (Riding & Thomas 1992) and with the Upper Volgian, Fulgens Zone on the Russian platform (Riding, Fedorova & Ilyina 1999). The Upper Volgian, Primitivus Zone (Subboreal, UK zonation) is indentified in this core by ammonites from 45.37 – 43.21 m (this report). *G. villosa* appears above these ammonites i.e. in the Primitivus or higher ammonite zones. The Fulgens Zone of the Russian zonation is not correlated with the western Subboreal zonation in North-West Europe but correlation with the Upper Volgian, Primitivus Zone is suggested (e.g. in Riding, Fedorova & Ilyina 1999).

Age

Middle to Late Volgian, Boreal Late Jurassic

Depositional environment

Offshore marine environment with anoxic bottom conditions and with limited but varying influx of terrestrial organic material. Comparable with a basin floor environment.

Organic matter

Dominated of marine amorphous material and terrestrial material, especially spores and pollen. The limited content of woody material varies slightly in abundance from sample to sample.

The TAI Index is 2, orange.

35.02 m – 27.00 m

The succession from the first appearance of *Gochteodinia villosa* (35.02 m) to the last occurrence of *Rotosphaeropsis thulae* (27.00 m).

Dinoflagellate assemblage

Sirmiodinium grossii and *Circulodinium* spp. are dominating in the lower part and *Systematophora palmula* and *Tanyosphaeridium isocalamus* are dominating the upper part of the unit. Locally *Adnathosphaeridium* spp., *Cribroperidinum* spp. and *Sentusidinium* cf. *rioulty* occur abundantly. *Pterospermella* spp. is locally common. The assemblage is diverse and abundant.

Biostratigraphy

First appearance of *G. villosa* in the Primitivus Zone (Upper Volgian) is discussed above. *R. thulae* disappears at the top of the Kochi Zone and *Systematophora palmula* appears (27.00 m) above the Kochi Zone of North-West Europe Subboreal ammonite stratigraphy (Riding & Thomas 1992). An ammonite in the core at 27.73 m, is referred to the Kochi Zone and supports this correlation (this report). The Kochi Zone occurs both in Subboreal and Boreal fauna-provinces.

Age

Late Volgian – Early Ryazanian, Boreal Late Jurassic to Boreal Early Cretaceous

Depositional environment

Offshore marine environment with anoxic bottom conditions and with limited but varying influx of terrestrial organic material. Comparable with a basin floor environment.

Organic content and maturity

Marine organic amorphous material associated with limited terrestrial organic matter of varying abundance, Type II OM. The TAI Index is 2, orange.

27.00 m –15.85 m

The succession from the last occurrence of *R. thulae* and first appearance of *S. palmula* in 27.00 m to the first appearance of *Oligosphaeridium complex* in 15.85 m.

Dinoflagellate assemblage

Epiplosphaera spp., *Heterosphaeridium*? spp., *Sirmiodinium grossii*, *Systematophora palmula*, *Systematophora daveyi* locally dominate this unit. The assemblage is relatively diverse and abundant in the lower part but becomes poor in the upper part. This change is associated with a significant shift in depositional environment from black shale to calcareous mudstone.

Biostratigraphy

R. thulae occur for the last time and *S. palmula* appears for the first time at the top of the Kochi Zone of the Subboreal ammonite stratigraphy in North-West Europe. An ammonite in the core at 27.73 m is referred to the Kochi Zone and supports this correlation (Riding & Thomas 1992). *O. complex* appears for the first time at the Ryazanian – Valanginian boundary in North-West Europe (Riding & Thomas 1992).

The Kochi Zone is the highest ammonite zone identified and correlated with the dinoflagellate stratigraphy in this core. Alsen (2006) identified ammonites and ammonite zones in the Albrects Bugt Member in sections near the Rødryggen-1 core. Due to solifluction in the outcrop sections, precise correlation with the core and the core-samples is not possible. Correlation of the dinoflagellate stratigraphy with local ammonite stratigraphy in the Upper Ryazanian – Valanginian is therefore considered a separate study. The Ryazanian fauna is strictly Boreal, whereas the Valanginian fauna comprises Tethyan, Subboreal and Boreal elements (Alsen, 2006).

Age

Late Ryazanian, Early Cretaceous

Depositional environment

Offshore marine environment with a major environmental turn over approximately at 24.4–25.5 m, where a changes from limited influx of terrestrial organic material, prolific production of marine algae and anoxic bottom conditions to no supply of terrestrial material, limited algal growth and strongly oxidised bottom condition at the basin floor.

Organic content and maturity

Transition from organic rich samples with abundance of amorphous organic matter (marine) with little terrestrial material (Type II OM in Lindemans Bugt Formation) to low organic content of rounded black coal grains and abundance of dinoflagellates and spores and pollen (Transitional Beds) followed by very poor organic content of rounded coal grains, orange-brown dinoflagellate cysts and very rare to non spores and pollen (Type IV OM in Albrechts Bugt Member). The TAI Index is 2 (orange) in the Lindemans Bugt Formation but 2+, dark orange, in the Albrechts Bugt Member. This suggests an upwards increase in maturity from the shale to the overlying silt – fine-grained sand of Albrechts Bugt Member. This may reflect several different local processes and do not necessary reflect overall basin subsidence or geometry.

15.85 m – 6.59 m

The succession from the first appearance of *Oligosphaeridium complex* (15.85 m) to the last occurrence of *Gochteodinia villosa* (6.59 m).

Dinoflagellate assemblage

Oligosphaeridium complex, *Oligosphaeridium* spp. and *Epiplosphaera* spp. dominates the assemblage. The assemblage is relatively diverse and abundant in the lower part but becomes poorer upwards.

Biostratigraphy

O. complex appears for the first time at the Ryazanian–Valanginian boundary in North-Western Europe (Riding & Thomas 1992). The highest occurrence of *Gochteodinia villosa* and *Systemtophora palmula* is in the Lower Valanginian (Davey 1982; Riding & Thomas 1992).

Age

Early Valanginian, Early Cretaceous

Depositional environment

The organic content indicates deposition with no supply of terrestrial material, limited algal growth and possibly strongly oxidised bottom condition in a basin floor environment.

Organic content and maturity

Poor, organic content of rounded to angular coal grains and dark dinoflagellate cysts; spores and pollen are very rare, Type IV OM. The TAI Index is 2+, dark orange.

6.59 m – 1.10 m

The succession from the highest occurrence of *Gochteodinia villosa* (6.59 m) to the highest recorded *Lagenorhytis delicatula* (1.10 m).

Dinoflagellate assemblage

Oligosphaeridium complex dominates the assemblage and *Cassiculosphaeridium magnum*, *Circulodinium distinctum*, *Epiplosphaera* spp. and *Downiesphaeridium tribuliferum* are locally abundant. The assemblage is relatively poor.

Biostratigraphy

The absence of *Gochteodinia villosa* and *Systematophora palmula* and the presence of *Lagenorhytis delicatula* in the uppermost core suggest Upper Valanginian strata in comparison with the North-West European stratigraphy (Davey 1982; Riding & Thomas 1992).

Age

Late Valanginian *pars.*, Early Cretaceous

Depositional environment

The organic content indicates deposition with no supply of terrestrial material, limited algal growth and possibly strongly oxidised bottom condition in a basin floor environment.

Organic content and maturity

Poor, organic content of rounded coal grains and orange-brown dinoflagellate cysts; spores and pollen are very rare Type IV OM. The TAI Index is 2+, dark orange.

Discussion

The importance of composite dinoflagellate and ammonite stratigraphy is demonstrated in this report. Both fossil groups have strengths and weaknesses but in combination the stratigraphy is strong. The recovery of ammonites from lower part of the core is low, possibly due to diagenesis and shale movement whereas the dinoflagelates are recovered in fairly good preservation although they are shrouded in amorphous organic matter. In the upper core, ammonites are recovered from many levels and confirm or correct the dinoflagellate stratigraphy. In the highest core, the dinoflagellates stratigraphy correlate across ammonite fauna provinces e.g. with North-West Europe whereas the East Greenland ammonites correlate with faunas from Tethys as well as Russia and Siberia. Both ammonite- and dinoflagellate stratigraphy of Upper Jurassic – Lower Cretaceous in East Greenland need further studies to reach the full potential.

The present study of the dinoflagellates in the Rødryggen-1 core demonstrates clearly that many species recorded in North-West Europe are present in very low numbers or absent in North-East Greenland. This may partly reflect the depositional environment. Studies in other part of the basin may reveal some of these taxa. However, studies in palaeoboreal and palaeoartic region support this trend of flora depletion towards the North (e.g. Brideaux, 1977; Brideaus & Fisher 1976; Århus 1988; Smelror & Dypvik,2005).

The abundance of *Paragonyaulacysta capillosa* and *P. borealis* in the East Greenland basins shows another trend of northern species migrating towards the south. The first occurrence of *Gochteodinia villosa* in the Primitivus Zone rather than in the underlying "Opressus Zone" shows palaeogeographic changes of the stratigraphy probably reflecting oceanographic changes introducing both subboreal ammonites and dinoflagellate to the Boreal North-East Greenland.

Results

The succession in the Rødryggen-1 core is dated Kimmeridian – Late Valanginian, Late Jurassic –Early Cretaceous on the basis of dinoflagellate stratigraphy.

The Bernbjerg Formation is Kimmeridgian – Lower Volgian, the Lindemans Bugt Formation is Middle Volgian – Upper Ryazanian and the Albrechts Bugt Member is Upper Ryazanian – Upper Valanginian *pars.*

The dinoflagellate stratigraphy is correlated at seven levels with ammonite zones identified in the core.

The Boreal Upper Jurassic includes the Upper Volgian and the Boreal Lower Cretaceous begins with the Ryazanian, so the Boreal Jurassic – Cretaceous boundary is located in the Lindemans Bugt Formation.

Transitions between lithostratigraphic units are gradual suggested by the gradual changes in composition of organic matter across lithostratigraphic boundaries, and suggesting continuous sedimentation throughout the core.

The age of the upper Bernbjerg Formation is limited to Early Volgian but the sedimentation of proliferous black shale continues into the Late Ryazanian in the frame of Lindemans Bugt Formation.

The organic material suggests a depositional environment dominated by terrestrial material and low oxygene, bottom conditions, which become more anoxic and more rich in marine organic material upwards in the Bernbjerg Formation; OM type III–IV to Type III . Terrestrial material becomes subordinate in relation to marine organic material in the Lindemans Bugt Formation (OM Type II) and the anoxia terminates in the Albrechts Bugt Member where marine algal blooming also ceases or/and the organic remains are oxidised totally away from the bottom sediments (OM Type IV) . Absence of terrestrial organic matter in Albrechts Bugt Member (except for rounded coaly grains) indicates a starved sedimentation or/and severe oxidation of the bottom sediments.

The organic material is immature in the upper core, TAI 2, except for the Albrechts Bugt Member where darker colours of the dinoflagellates suggest TAI 2^+ probably reflecting local processes e.g. migration of hot water in the sandy unit, heavy primary oxidation or heating by intrusive rocks now removed by erosion. Downwards in the core, a shift to darker sporomorph colours and consequently to higher thermal maturity occurs approximately at 130 – 140 m, where TAI 2^+ indicates the beginning of the oil window. No higher maturity is recorded in the lower core.

3.2.4 Nannofossils

Materials and methods

Ten samples from the Rødryggen-1 core (4 from the Bernbjerg Formation, 3 from the Lindemans Bugt Formation and 3 from the Albrechts Bugt Member) were examined for nannofossil content. The Bernbjerg and Lindemans Bugt Formation samples were almost barren with respect to calcareous nannofossils. Samples from ~16.6 m, ~13.82 m and ~3.6 m from the Albrechts Bugt Member yielded relatively good nannofossil recovery.

Nannofossil slides were prepared using the simple smear slide technique of Bown & Young (1998). Where samples appeared to be barren with respect to calcareous nannofossils, 3 length traverses of the smear slide were examined. Where a particular species of nannofossil dominated the slide, 1 length traverse was counted, then 2 further lengths were checked for rare forms. Biostratigraphic ranges of nannofossils are found in Burnett (1998) and Bown *et al.* 1998.

Results

The only calcareous fossils in the nannofossil-size fraction of the Bernbjerg Formation samples and one sample from the Lindemans Bugt Formation, were rare specimens of *Thoracosphaera* spp., a long-ranging calcareous dinoflagellate cyst. The remaining two Lindemans Bugt Formation samples were barren with respect to calcareous nannofossils.

The three samples from the Albrechts Bugt Member, in comparison, contained calcareous nannofossils which are useful regarding biostratigraphy and palaeoenvironmental interpretation.

Bernbjerg Formation

214 m:
Assemblage: Barren with respect to calcareous nannofossils, *Thoracosphaera* spp. present.

Age: Not assigned.

184 m:
Assemblage: Barren with respect to calcareous nannofossils, *Thoracosphaera* spp. present.

Age: Not assigned.

178.26 m:
Assemblage: Barren with respect to calcareous nannofossils, *Thoracosphaera* spp. present.

Age: Not assigned.

144.8 m:
Assemblage: Barren with respect to calcareous nannofossils.

Age: Not assigned.

Lindemans Bugt Formation

76.9 m:
Assemblage: Barren with respect to calcareous nannofossils, 2 specimens of *Thoracosphaera* spp., organic material present.

Age: Not assigned.

65.2 m:

Assemblage: Barren with respect to calcareous nannofossils, organic material present.

Age: Not assigned.

33 m:
Assemblage: Barren with respect to calcareous nannofossils, organic material present.

Age: Not assigned.

Palnatokes Bjerg Formation, Albrechts Bugt Member

16.6 m:
Assemblage: The low diversity nannofossil assemblage is domainted by *Watznaueria barnesiae*. *Watznaueria fossacincta* and *Crucibiscutum salebrosum* are also common. In addition, *Watznaueria britannica*, *Retecapsa crenulata*, *Sollasites horticus*, *Tegumentum stradneri, Rhagodiscus asper* and the long-ranging calcareous dinoflagellate cyst *Thoracosphaera* spp. are present.

Remarks: High abundances of *C. salesbrosum* and *Watznaueria* spp. co-occur with present *S. horticus* in the North Sea in the Late Ryazanian - Early Valanginian (Jeremiah, 2001) and off mid Norway (Mutterlose & Kessels 2000). *R. crenulata* has its FO (First Occurrence) in the late Late Ryazanian (Jakubowski 1987). Pauly *et al.* (2010) documented the FO of *C. salesbrosum*, *R. asper* and *Watznaueria* spp. in the Late Ryazanian of North-East Greenland (Perisphinctes Ravine, Kuhn Ø and the Rødryggen RR2/09 section, Wollaston Forland).

Age: Late Ryazanian – Early Valanginian, Early Cretaceous

13.82 m:
Assemblage: A nannofossil assemblage dominated by *Crucibiscutum salebrosum* and *Watznaueria barnesiae*. Also present are *Rhagodiscus asper*, *Watznaueria fossacincta*, *Watznaueria britannica*, *Watznaueria manivitiae*, *Retecapsa angustiforata, Zeugrhabdotus embergeri*, *Cyclagelosphaera margerelii*, *Tegumentum stradneri, Zeugrhabdotus erectus* and *Thoracosphaera* spp.

Remarks: High abundances of *C. salesbrosum* and *Watznaueria* spp. co-occur with present *S. horticus* in the North Sea in the Late Ryazanian - Early Valanginian (Jeremiah, 2001) and off mid Norway (Mutterlose & Kessels 2000). *R. crenulata* has its FO in the late Late

Ryazanian (Jakubowski 1987). Pauly *et al.* (2010) documented the FO of *C. salesbrosum*, *R. asper, R. angustiforata* and *Watznaueria* spp. in the Late Ryazanian of North-East Greenland (Perisphinctes Ravine, Kuhn Ø and the Rødryggen RR2/09 section, Wollaston Forland).

Age: Late Ryazanian – Early Valanginian, Early Cretaceous

3.6 m:

Assemblage: The low diversity nannofossil assemblage is domainted by *Watznaueria barnesiae*. Also present are *Watznaueria fossacincta*, *Calculites* ? sp.1, *Tranolithus gabalus*, *Rhagodiscus asper*, *Watznaueria britannica* and *Thoracosphaera* spp. *C. salesbrosum* is absent.

Remarks: *T. gabalus*, *R. asper* and *Watznaueria* spp. range from the Late Ryazanian in the North Sea (Jakubowski 1987, Jeremiah 2001), NE Greenland (Pauly *et al.* 2010) and off mid Norway (Mutterlose & Kessels 2000). *Calculites* ? sp.1 was described in Bown *et al.* (1998) as ranging from the Early Hauterivian? – ?Early Barremian, albeit in Tunisia and Bulgaria. Of note is the absence of *C. salesbrosum*. In NE Greenland, this species has its LAD (Last Appearancec Datum) in the Late Hauterivian (Pauly *et al.* 2010) and a little later in the North Sea (Jakubowski 1987). However the absence of this species from this sample could be an artefact of preservation (note the corresponding microfossil sample yielded a poor calcareous assemblage).

Age: early Hauterivian?–?early Barremian, Early Cretaceous or older.

The results are displayed as a nannofossil distribution chart (Fig. 3.2.6) using the following abundance values. Rare = 1, Few = 5, Common = 50, Abundant = 75, Dominant = 100.

Discussion

The samples from the Bernbjerg Formation yielded only rare specimens of the long-ranging species *Thoracosphaera* spp. The calcareous samples at ~16.6 m and ~13.82 m from the Albrechts Bugt Member yielded low diversity but high abundance nannofossil assemblages. Sample ~ 3.6 m from the same unit yielded an assemblage dominated by only few species. These three samples were useful for biostratigraphic and palaeoenvironmental interpretation.

Palaeoenvironment

Thoracosphaera spp. was the only calcareous ‘nannofossil’ found in the Bernbjerg Formation. *Thoracosphaera* has been interpreted as an indicator of stressed environments (Perch-Nielsen, 1985). The presence of pyrite noted in the microfossil samples (Chapter3.2.5) infers that most calcareous material that may have originally been present would have been subject to dissolution. A shift in sedimentation from the Lindemans Bugt Formation to the Albrechts Bugt Member is documented in the Rødryggen-1 core by a change in the nannofloral content, from samples almost barren of calcareous material, to assemblages with abundant nannofossils.

The calcareous samples from the Albrechts Bugt Member yield low diversity, high abundance nannofossil assemblages. The three samples were dominated by *Crucibiscutum salebrosum* and / or *Watznaueria* species, with present *S. horticus*. This assemblage is typical of the high latitudes (cool – cold water) in the Early Valanginian to Early Barremian (e.g. Mutterlose & Kessels 2000; Mutterlose *et al.* 2003). Mutterlose & Kessels (2003) attribute high latitude, low diversity assemblages to unstable conditions at this time. Pauly *et al.* (2010) adds that the NE Greenland nannofossil assemblages indicate nutrient enrichment.

3.2.5 Microfossils

Materials and methods

Ten samples from the Rødryggen-1 core (4 from the Bernberg Member, 3 from the Lindemans Bugt Formation and 3 from the Albrechts Bugt Member) were examined for microfossil content. Only the samples from ~16.6 m and ~13.82 m from the Albrechts Bugt Member yielded good calcareous microfossil recovery.

20 g of crushed dry sample was prepared for microfossil analysis, by placing the sample in a 1000 ml pyrex beaker and adding 3% hydrogen peroxide solution. The sample was gently agitated and let soak for ca. 5 hours at room temperature. The sample was stirred occasionally and kept covered to prevent contamination. It was then washed over a 63 µm sieve and dried in the oven at 45°C. The dried material was sieved and picked for microfossils. Foraminiferal classification and stratigraphic ranges are based on a variety of references

e.g. Bartenstein & Brand, 1951; Sliter, 1980; Caron, 1985; Nagy & Basov, 1998 and Weidich, 1990.

Results

The samples from the Bernbjerg Formation contained a very low abundance and diversity microfauna, characterised by deformed agglutinating Foraminifera which were so poorly preserved that identification was not usually possible. The Bernbjerg Formation samples also comprised coal fragments, siliceous and pyritised sponge spicules and pyritised Radiolaria. It was not possible to apply a microfossil stratigraphy to the Bernbjerg Formation due to the scarcity of well-preserved microfossils. In comparison, the samples from the Albrechts Bugt Member of the Palnatokes Bjerg Formation comprised a rich and diverse calcareous microfauna which was more useful regarding the stratigraphy.

Bernbjerg Formation

214 m:

Assemblage: 1 siliceous ?Radiolaria (very badly preserved), coal fragments.

Age: Not assigned.

184 m:

Assemblage: Coal fragments, framboidal pyrite, 1?*Globuligerina hoterivica* (planktonic foraminifera with orange preservation).

Age: According to Caron (1985) *G. hoterivica* (now *Favusella hoterivica*) represents a link between Middle and Late Jurassic *Globuligerina* species and early forms of *Favusella* which appeared in the Barremian. The conspicuous orange colour of the specimen (no sediments are reported with this coluoration) and the fact that it is the only planktonic Foraminifera specimen recorded from these samples questions its validity as an *in-situ* species.

178.26 m:

Assemblage: Common coal fragments.

Age: Not assigned.

144.8 m:

Assemblage: Some coal fragments, coarse grained spherules (unidentified), 1 broken piece of unidentifiable benthic foraminifera, 1 deformed, unidentifiable brown, agglutinating foraminifera.

Age: Not assigned.

Lindemans Bugt Formation

76.9 m:
Assemblage: Common coal fragments, 1 broken *Ammobaculites* spp. and 1 ?*Recurvoides obskiensis*. The remaining deformed, brown agglutinating foraminifera are unidentifiable, but they are more abundant than in sample -144.8 m. Some siliceous sponge spicules and rare pyritised Nasselarian Radiolaria were recorded.

Age: According to Nagy & Basov (1998) *R. obskiensis* ranges throughout Central Spitzbergen Foraminiferal Zones F7 and into upper Zone F8: equivalent to the uppermost Volgian to the lower Late Ryazanian.

65.2 m:
Assemblage: Abundant coal fragments, rare *Inoceramus* spp.
Age: Not assigned.

33 m:
Assemblage: Abundant 'blocky' coal fragments and pyritised sponge spicules, also siliceous sponge spicules, rare deformed, brown, unidentifiable agglutinating foraminifera and rare pyritised Nasselarian Radiolarian (?*Dictyomitra* spp.).

Age: Not assigned.

Palnatokes Bjerg Formation, Albrechts Bugt Member

16.6 m:
Assemblage: Calcareous shell debris comprises the main component of this sample. *Inoceramus* spp. (bivalve) and Echinoderm fragments are common and siliceous sponge spicules are present.

The foraminiferal assemblage is dominated by glassy preserved, benthic Foraminifera, comprising *Astacolus gratus*, *Citharina intumescens*, *Dentalina nana*, *Dentalina soluta*, *Dentalina torta*, *Dentalina* spp., *Frondicularia rehburgensis*, *Frondicularia simplicissima*, *Globulina exserta*, *Globulina prisca*, *Glomospirella* spp., *Lagena globulosa*, *Lagena hauteriviensis hauteriviensis*, *Lagena oxystoma*, *Lenticulina cultrata*, *Lenticulina* spp., *Marginulinopsis cephalotes*, *Patelina subcretacea*, *Pseudoglandulina* cf *humilis*, *Pyrulina cylinroides*, *Pyrulina* spp., *Saracenaria cushmanii*, *Spirrilina elongata*, *Spirrilina minima*, *Spirrilina tenuissima*, *Trocholina conica*, *Trocholina valdensis* and *Vaginulina recta*.

Agglutinating Foraminifera (white preservation) are also present and include *Ammobaculites* spp., *Ammodiscus* spp., *Bathysiphon* spp., *Bigenerina* spp., *Rhabdammina* spp., and *Rhizammina* spp.

Age: *T. conica*, *T. valdensis*, *L. hauteriviana hauteriviana*, *L. oxystoma*, *P. cylindroides*, *L. cultrata, G. prisca* and *P. subcretacea* are present in the Ryazanian, e.g. Sliter (1980); Sliter & Premoli-Silva (1984); Weidich (1990). However, several of these and other species in the assemblage range up into the Valanginian according to these authors, albeit in Africa, Mexico and Austria respectively.

13.82 m:

Assemblage: A rich and diverse agglutinating and calcareous benthic foraminiferal assemblage.

Benthic foraminifera (glassy preservation) include *Astacolus scitula*, *Dentalina* spp., *Epistomina tenuicostata*, *Globulina prisca*, *Glomospirella* spp., *Lenticulina cultrata*, *Lenticulina* spp., *Pyrulina* spp., *Pseudoglandulina humilis, Trocholina conica* and *Trocholina valdensis*.

Agglutinating foraminifera (white preservation) include *Ammobaculites agglutinans*, *Bathysiphon* spp., *Reophax minutissima*, *Rhizammina* spp., *Textularia bettenstaedti, Triplasia emslandensis emslandensis* and *Triplasia ?pseudoromeri*. Note: this sample contains more agglutinating foraminifera than the sample at ~16.6 m.

Shell debris and *Inoceramus* fragments are common and Ostracod species are present.

Age: In the Valanginian, *T. pseudoromeri*, *T. emslandensis emslandensis*, *R. minutissima* and *A. agglutinans* co-occur in northwest Germany (Bartenstein & Brand, 1951) and *Epistomina tenuicostata* first occurs in the lower Valanginian (but ranges into the Hauterivian) in Germany and Ryazanian to the Hauterivian.

3.6 m:

Assemblage: Rare deformed, white unidentifiable agglutinating foraminifera, 1 *Lenticulina* spp. (glassy preservation), rare *Inoceramus* spp. and rare shell debris.

Age: Not assigned.

The results are displayed as a microfossil distribution chart (Fig. 3.2.7) using the following abundance values. Present = 1, Rare = 2, Common = 5, Abundant = 15, Dominant = 50.

Discussion

The samples from the Bernbjerg and Lindemans Bugt Formations mostly yielded coal fragments, extremely poorly preserved and deformed agglutinating foraminifera (many altered beyond recognition) and pyritised sponge spicules and rare Radiolaria. These elements allow limited palaeoenvironmental interpretation. One planktonic foraminifera was found in sample -146 but may not be *in-situ*. The calcareous samples at ~16.6 m and ~13.82 m from the Albrechts Bugt Member yielded high diversity microfossil assemblages. Sample ~ 3.6 m from the same formation yielded a very poor assemblage. The rich benthic faunas will be useful for biostratigraphic dating and allow palaeoenvironmental interpretation.

Palaeoenvironment

A shift in sedimentation from the Lindemans Bugt Formation to the Albrechts Bugt Member is documented in the Rødryggen-1 core by a change in the microfaunal content, from low diversity, poorly preserved, agglutinating foraminiferal assemblages with some Radiolaria, to assemblages rich in calcareous benthic species (e.g. *Dentalina* spp., *Globulina* spp., *Lagena* spp., *Lenticulina* spp.).

Mutterlose *et al.* (2003) documented that dark, organic, carbon-rich mudstones of the Greenland-Norwegian Sea were dominated by agglutinating foraminifera (e.g. *Haplophragmoides* spp., *Recurvoides* spp.) in the Volgian–Berriasian (Ryazanian) and suggested that their presence in this type of sediment attested to their high tolerance of unfavourable environmental conditions. A change in sedimentation to grey, carbonate-rich marls of the Valanginian to Hauterivian brought about an increase in diversity of foraminiferal assemblages with calcareous benthic species (e.g. *Lenticulina* spp., *Globulina* spp.) proliferating. According to Mutterlose *et al.* (2003), this change in sedimentation and increase in diversification was a result of sea-level rise in the Valanginian and the calcareous benthic foraminiferal assemblages are indicative of open-marine, aerobic, bathyal conditions. Similar conditions were reported from the Valanginian of the North Sea, England and Germany. It is not unreasonable to suggest that these conditions were also applicable to the Rødryggen area.

3.2.6 References

Alsen, P. 2006: The Early Cretaceous (Late Ryazanian – Early Hauterivian) ammonite fauna of North-East Greenland: taxonomy, biostratigraphy, and biogeography. Fossils & Strata, **53**, 229 pp.

Alsen, P. & Mutterlose, J. 2009: The early Cretaceous of North-East Greenland: A cross-roads of belemnite migration. Palaeogeography, Palaeoclimatology, Palaeoecology, **280**, 168–182.

Alsen, P. & Rawson, P.F. 2005: The Early Valanginian (Early Cretaceous) ammonite genus *Delphinites* (*Pseudogarnieria*) from East Greenland. Bulletin of the Geological Society of Denmark, **52**, 201–212.

Bailey, D., Miller, P. & Varney, T. 1997: Some dinoflagellate cysts from The Kimmeridge Clay Formation in North Yorkshire and Dorset, UK. Proceedings of the Yorkshire Geological Society, **51**, 235–245.

Bartenstein, H. & Brand, E. 1951: Mikropaläontologische Untersuchungen zur Stratigraphie des nordwestdeutschen Valendis. Abh. Senckenberg. Natur. Ges. **485**, 239–336.

Birkelund, T & Callomon, J.H. 1985: The Kimmeridgian ammonite faunas of Milne Land, central East Greenland. Grønlands Geologiske Undersøgelse Bulletin, **153**, 56 pp. + 23 plates

Birkelund, T., Callomon, J.H. & Fürsich, F.T 1984: The stratigraphy of the Upper Jurassic and Lower Cretaceous sediments of Milne Land, central East Greenland. Grønlands Geologiske Undersøgelse Bulletin, **147**, 56 pp.

Bjerager, M., Alsen, P., Bojesen-Koefoed, J., Japsen, P., Kjøller, C., Larsen, L.M., Nytoft, P., Olivarius, M., Olsen, D., Petersen H.I., Piasecki, S. & Schovsbo, N. 2009: Blokelv Core Well, GGU 511101, Upper Jurassic Hareelv Formation in Jameson Land, East Greenland - Final Well Report. Contribution to Petroleum Geological Studies, Services and Data in East and Northeast Greenland. Stratigraphic analyses. Danmarks og Grønlands Geologiske Undersøgelse Rapport 2009/86, Volumes 1–3, 223 pp., + 8 Enclosures.

Bown, P. R. 1998: Lower Cretaceous. In: Bown, P. R. (ed.): Calcareous Nannofossil Biostratigraphy. British Micropalaeontological Society Series. Chapman & Hall/Kluwer Academic, 86–131.

Bown, P. and Young, J. 1998: Techniques. In: Bown, P. R. (ed.): Calcareous Nannofossil Biostratigraphy. British Micropalaeontological Society Series. Chapman & Hall/Kluwer Academic, 16–28.

Brideaux, W.W. 1977: Taxonomy of Upper Jurassic – Lower Cretaceous microplankton from the Richardson Mountains, District of Mackenzie, Canada. Geological Survey of Canada Bulletin 281, 89 pp.

Brideaux, W.W. & Fisher, M.J. 1976: Upper Jurassic – Lower Cretaceous dinoflagellate assemblages from Arctic Canada. Geological Survey of Canada Bulletin, **259**, 53 pp.

Burnett, J. A. 1998: Upper Cretaceous. In: Bown, P. R. (ed.): Calcareous Nannofossil Biostratigraphy. British Micropalaeontological Society Series. Chapman & Hall/Kluwer Academic, 132–199.

Callomon, J.H. 1993: The ammonite succession in the Middle Jurassic of East Greenland. Bulletin of the Geological Society of Denmark, **40**, 83–113.

Callomon, J.H. & Birkelund, T. 1982: The ammonite zones of the Boreal Volgian (Upper Jurassic) in East Greenland. In Embry, A.F. & Balkwill, H.R. (eds.): Arctic Geology and Geophysics. Canadian Society of Petroleum Geologists Memoir 8, 349–369.

Caron, M. 1985: Cretaceous planktic Foramininfera. In: Bolli, H. M., Saunders J. B. & Perch-Nielsen, K. (eds): Plankton Stratigraphy. Cambridge University Press, 17–86.

Casey, R. 1973: The ammonite succession at the Jurassic–Cretaceous boundary in eastern England in Casey, R. & Rawson, P.F. (eds.): The Boreal Lower Cretaceous. Geological Journal Special Issue 5, Seel House Press, Liverpool, 193–266.

Davey, R.J. 1979: The stratigraphic distribution of dinocysts in the Portlandian (latest Jurassic) to Barremian (Early Cretaceous) of North-West Europe. AASP Contribution Series 5B, 49–81.

Davey, R.J. 1982: Dinocyst stratigraphy of the latest Jurassic to Early Cretaceous of the Haldager No. 1 borehole, Denmark. Danmarks Geologiske Undersøgelse, Serie B, **6**, 57 pp.

Donovan, D.T. 1964: Stratigraphy and ammonite fauna of the Volgian and Berriasian rocks of East Greenland. Meddelelser om Grønland 154 (4), 34 pp.

Fensome, R.A. & Williams, G.L. 2004: Lentin and Williams Index of Fossil Dinoflagellates 2004 Edition. AASP Contribution Series Number 42, 909 pp.

Harper, D.A.T., Alsen, P., Owen, E., Sandy, M.R., 2005. Early Cretaceous brachiopods from North-East Greenland: biofacies and biogeography. Bulletin of the Geological Society of Denmark, **52**, 213–225.

Jakubowski, M. 1987: A proposed Lower Cretaceous Calcareous Nannofossil Zonation Scheme for the Moray Firth Area of the North Sea. Abhandlungen der Geologischen Bundesanstalt, A 39, 99–119.

Jeremiah, J. 2001: A Lower Cretaceous nannofossil zonation for the North Sea Basin. Journal of Micropalaeontology, **20**, 1, 45–80.

Lebedeva, N.K. & Nikitenko, B.L. 1999: Dinoflagellate cysts and microforaminifera of the Lower Cretaceous Yatria River section, Subarctic Ural, NW Siberia (Russia). Grana 38, 134–143.

Milner, P.S. & Piasecki, S. 1996: Boreal Middle Jurassic dinoflagellate cyst stratigraphy of Jameson Land, East Greenland. In: Piasecki, S. et al. (eds) Formation of Source and Reservoir Rocks in a Sequence Stratigraphic Framework, Jameson Land, East Greenland. Energy Research Programme EFP-93, Projects 1313/93 & /0017, Vol. I & II. Danmarks og Grønlands Geologiske Undersøgelse Rapport 1996/30, 46 pp., + 13 Appendices.

Mutterlose, J. and Kessels, K. 2000: Early Cretaceous calcareous nannofossils from high latitudes: implications for palaeobiogeography and palaeoclimate. Palaeogeography, Palaeoclimatology, Palaeoecology, **160**, 347–372.

Mutterlose, J., Brumsack, H., Flögel, S., Hay, W., Klein, C., Langrock, U., Lipinski, M., Ricken, W., Söding, E., Stein, R. & Swientek, O. 2003: The Greenland-Norwegian Seaway:

A key area for understanding Late Jurassic to Early Cretaceous paleoenvironments. Paleoceanography, **18**, 1, 1010.

Nagy, J. & Basov, V.A. 1998: Revised foraminiferal taxa and biostratigraphy of Bathonian to Ryazanian deposits in Spitsbergen. Micropaleontology, **44**, 3, 217–255.

Nøhr-Hansen, H. 1993: Dinoflagellate cyst stratigraphy of the Barremian to Albian, Lower Cretaceous, North-East Greenland. Grønlands Geologiske Undersøgelse Bulletin, **166**, 171 pp.

Pauly, S., Mutterlose, J. & Alsen, P. 2010: Early Cretaceous calcareous nannofossils from northeast Greenland (poster). 13th International Nannoplankton Association Conference, Yamagata, Japan, Abstract Volume, p. 88.

Perch-Nielsen K. 1985: Cenozoic calcareous nannofossils. In: Bolli, H. M., Saunders J. B. & Perch-Nielsen, K. (eds): Plankton Stratigraphy. Cambridge University Press, 427–554.

Piasecki, S. 1981: Middle to Late Jurassic dinoflagellate cyst stratigraphy from Milne Land and Jameson Land (East Greenland) correlated with ammonite stratigraphy, 167 pp. Unpublished Licentiat (Ph.D.) thesis, University of Copenhagen.

Piasecki, S. 1996: Boreal dinoflagellate cyst stratigraphy of Middle to Upper Jurassic sediments of Milne Land, East Greenland. In: Piasecki, S. *et al.* (eds): Formation of Source and Reservoir Rocks in a Sequence Stratigraphic Framework, Jameson Land, East Greenland. Energy Research Programme EFP-93, Projects 1313/93 & 00171996/30, Vol. I & II. Danmarks og Grønlands Geologiske Undersøgelse Rapport, 100 pp.

Repin, Yu.S., Zakharov, V..A., Meledina, S.V. & Nalnyaeva, T.I. 2006: Atlas of the molluscs of the Pechora Jurassic. Bulletin of the VNIGRI, **3**, 262 pp.

Riding, J.B. & Thomas, J.E. 1992: Dinoflagellate cysts of the Jurassic System. In: Powell, A.J. (ed.): A stratigraphic index of dinoflagellate cysts Chapman and Hall, 7–97.

Rogov, M. & Zakharov, V.A. 2009: Ammonite- and bivalve-based biostratigraphy and Panboreal correlation of the Volgian Stage. Science in China Series D: Earth Sciences **52,** 1890–1909.

Sliter, W.V. 1980: Mesozoic Foraminifers and deep-sea Benthic environments from deep-sea drilling projects sites 415 and 416, Eastern North Atlantic. In: Lancelot, Y., Winterer, E. L. and Scientific Party: Initial Reports of the Deep Sea Drilling Project, **50**, 353–415.

Sliter, W.V. & Premoli-Silva, I. 1984: Autochthonous and displaced (allochthonous) Cretaceous benthic foraminifers from Deep Sea Drilling Project Leg 77, sites 535, 536, 537, 538 and 540, Gulf of Mexixo. In: Buffler, R.T., Schlager, W. and Scientific Party: Initial Reports of the Deep Sea Drilling Project, **77**, 593–627.

Smelror, M. 1988: Late Bathonian to Early Oxfordian dinoflagellate cyst stratigraphy of Jameson Land and Milne Land, East Greenland. Rapport Grønlands Geologiske Undersøgelse, **137**, 135–159.

Smelror, M. & Dypvik, H. 2005: Marine microplankton biostratigraphy of the Volgian–Ryazanian boundary strata, western Barents Shelf. Norges geologiske Undersøkelser Bulletin, **443**, 61–69.

Spath, L.F. 1936: The Upper Jurassic invertebrate faunas of Cape Leslie, Milne Land. II. Upper Kimmeridgian and Portlandian. Meddelelser om Grønland, **99**, 3, 180 pp.

Surlyk, F. 1973: The Jurassic–Cretaceous boundary in Jameson Land, East Greenland in Casey, R. & Rawson, P.F. (eds.): The Boreal Lower Cretaceous. Geological Journal Special Issue 5, Seel House Press, Liverpool, 81–100,

Surlyk, F. 1977: Stratigraphy, tectonics and palaeogeography of the Jurassic sediments of the areas north of Kong Oscars Fjord, East Greenland. Grønlands Geologiske Undersøgelse Bulletin, **123**, 56 pp.

Surlyk, F. 1978: Submanrine fan sedimentation along fault scarps on tilted fault blocks (Jurassic–Cretaceous boundary, East Greenland). Grønlands Geologiske Undersøgelse Bulletin, **128**, 108 pp.

Surlyk, F., Callomon, J.H., Bromley, R.G. & Birkelund, T. 1973: Stratigraphy of the Jurassic–Lower Cretaceous sediments of Jameson Land and Scoresby Land, East Greenland. Grønlands Geologiske Undersøgelse Bulletin, **105**, 76 pp.

Surlyk, F. & Zakharov, V.A. 1982: Buchiid bivalves from the Upper Jurassic and Lower Cretaceous of East Greenland. Palaeontology, **25**, 4, 727–753.

Weidich, K.F. 1990: Die kalkalpine Unterkreide und ihre Foraminiferenfauna. Zitteliana 17, München, 3–312.

Williamson, M.A. & Stam, B. 1988: Jurassic/Cretaceous Epistominidae from Canada and Europe. Micropaleontology, **34**, 136–158.

Woollam, R. & Riding, J.B. 1983: Dinoflagellate cyst stratigraphy of the English Jurassic. Institute of Geological Sciences, Report 83/2, 41 pp.

Zakharov, V.A. & Mesezhnikov, M.S. 1974: The Volgian Stage of the Subarctic Ural (ed. Sachs, V.N.). Academy of Sciences of the USSR, Siberian Branch, Transactions of the Institute of Geology and Geophysics, **196**, 214 pp.

Zeiss, A. 2003: The Upper Jurassic of Europe: its subdivision and correlation. In Ineson, J.R. & Surlyk, F.(eds.): The Jurassic of Denmark and Greenland. Geological Survey of Denmark and Greenland Bulletin, **1**, 75–114.

Århus, N. 1988: Palynostratigraphy of some Bathonian–Hauterivian sections in the Arctic with emphasis on the Janusfjellet Formation type-section, Spitsbergen. Institutt for Kontinentalsokkelundersøkelser og Petroleumteknologi AS, Report 23.1252.11/01/88, 139 pp.

Chronostratigraphy				Ammonite stratigraphy		
System	Series	Stage	Sub-stage	Zone/Subzone	Faunal horizons	
Cretaceous (pars.)	Lower Cretaceous (pars.)	Valanginian	Upper			
				Dichotomites bidichotomoides Zone		
				Dichotomites crassus Zone		
			Lower	*Dichotomites hollwedensis* Zone		
				Polyptychites michalskii Zone		
				Nikitinoceras hoplitoides Zone		
				Delphinites undulatoplicatilis Zone		
		Ryazanian	Upper	*Peregrinus albidum* Zone		
				Surites tzikwinianus Zone		
				Surites analogus Zone		
			Lower	*Hectoroceras kochi* Zone		
				Praetollia maynci Zone		
Jurassic (pars)	Upper Jurassic (pars)	Volgian	Upper	*Praechetaites tenuicostatus* Zone		
				Subcraspedites primitivus Zone		
			Middle	*Epilaugeites vogulicus* Zone		
				Laugeites groenlandicus Zone	M 47	***Laugeites groenlandicus*** Spath, 1935, *Crendonites* cf./aff. *subgorei* Spath elegans Spath, 1936
				Crenodites anguinus Zone	M 46	***Crenodites anguinus*** Spath, 1936, *Crendonites euglyptus* Spath, 1936, *Crendonites lesliei* Spath, 1936, *Crendonites subregularis* Spath,1936, *Dorsoplanites* sp.
					M 45	***Pavlovia aff. subgorei*** (Spath, 1936)
				Epipallasiceras pseudoapertum Zone	M 44	***Dorsoplanites intermissus*** Callomon & Birkelund, 1982
					M 43	***Pavlovia groenlandica* (Spath, 1936),** *Pavlovia* sp., *Dorsoplanites* aff. *gracilis* Spath, 1936
					M 42	***Epipallasiceras pseudoapertum*** Spath, 1936, *Epipallasiceras praecox* incl. *E. tumidum* Spath, 1936, *Dorsoplanites maximus* Spath, 1936, *Dorsoplanites gracilis* Spath, 1936
					M 41	***Epipallasiceras acutifurcatum*** Callomon & Birkelund, 1982
				Dorsoplanites gracilis Zone	M 40	***Epipallasiceras rotundiforme*** Spath, 1936, *Dorsoplanites gracilis* Spath, 1936, *Dorsoplanites aldingeri* Spath, 1936, *Dorsoplanites crassus* Spath, 1936, *Dorsoplanites triplex* var. *mutabilis* Spath, 1936, *Pavlovia* sp.
					M 39	***Dorsoplanites gracilis δ*** Spath, 1936, *Pavlovia* sp.
					M 38	***Dorsoplanites antiquus*** Spath ***/ transitorius*** Spath, 1936
				Dorsoplanites liostracus Zone	M 37	***Dorsoplanites liostracus*** Callomon & Birkelund, 1982, *Pavlovia corona* Callomon & Birkelund, 1982, *Dorsoplanites gracilis* γ Spath, 1936, *Pavlovia* sp.
					M 36	***Dorsoplanites gracilis β*** Spath, 1936
				Pavlovia communis Zone	M 35	***Pavlovia variocostata*** Callomon & Birkelund, 1982
					M 34	***Pavlovia communis*** Spath, 1936, *Pavlovia regularis* Spath, 1936, *Pavlovia subaperta* Spath, 1936, *Pavlovia perinflata* Spath, 1936, *Dorsoplanites* α *gracilis* Spath, 1936
				Pavlovia rugosa Zone	M 33	***Pavlovia rugosa*** Spath, 1936, *Pavlovia alternaplicata* Spath / *kochi* Spath, 1936, *Pavlovia inflata* Spath, 1936, *Pavlovia allovirgatoides* Spath / *similis* Spath, 1936, *Pavlovia variabilis* Spath, 1936, *Dorsoplanites* sp.
				Pavlovia iatriensis Zone	M 32	***Pavlovia iatriensis*** Ilovaisky, 1917, *Dorsoplanites* cf. and aff. *dorsoplanus* (Vishniakov, 1882)
				Dorsoplanites primus Zone	M 31	***Dorsoplanites primus*** Callomon & Birkelund, 1982, *Pavlovia* sp.
			Lower	*Pectinatites pectinatus* Zone – *P. paravirgatus* Subzone	M 30	***Paravirgatites* sp. B**
					M 29	***Paravirgatites* sp. A,** *P.* aff. *devillei* Spath, 1936, *P.* cf. *boidini* Spath, 1936
				Pectinatites pectinatus Zone – *P. eastcottensis* Subzone	M 28	***Pectinatites eastlecottensis*** Salfeld, 1913, *Pectinatites (Pectinatites)* cf. *pectinatus* (Phillips, 1871), *Pectinatites (Pectinatites)* cf. *cornutifer* (Buckman, 1925)
					M 27	***Pectitanites groenlandicus*** Spath, 1936, *Pectinatites (Pectinatites)* aff. *eastlecottensis* Salfeld, 1913, *Pectinatites (Pectinatites)* cf. *cornutifer* (Buckman, 1925), *Pectinatites (Wheatleyites) rarescens* Buckman, 1925
				Pectinatites hudlestoni Zone	M 26	***Pectinatites* cf. abbreviatus** Cope, 1967
				Pectinatites wheatleyensis Zone	M 25	***Sphinctoceras* spp.,** *Pectinatites (Virgatosphinctoides) smedmorensis* Cope, 1967 and *laticostatus* Cope, 1967, *Sphinctoceras (Eosphinctoceras)* cf. or. aff. *magnum* Mesezhnikov, 1974 or *distans* Neaverson, 1925
				Pectinatites elegans Zone	M 24	***Pectinatites elegans*** Cope, 1967, *Pectinatites (Virgatosphinctoides) major* Cope, 1967, *Pectinatites (Virgatosphinctoides)* spp.
		Kimmeridgian	Upper	*Aulacostephanus autissiodorensis* Zone	M 23	***Aulacostephanus* sp. cf. or aff. *Au. kirghisensis*** (d'Orbigny, 1845)
			Middle	*Aulacostephanus eudoxus* Zone	M 22	***Amoeboceras elegans*** Spath, 1935
					M 21	***Amoeboceras (Hoplocardioceras) decipiens*** Spath, 1935, *Aulacostephanus eudoxus* (d'Orbigny, 1850)
					M 20	***Amoeboceras (Euprionodoceras) kochi*** Spath, 1935
				Aulacostephanus mutabilis Zone	M 19	***Rasenia borealis*** Spath, 1935, *Aulacostephanus mutabilis* (Sowerby, 1823), *Aulacostephanus (Aulacostephanites)* cf. *Au. (Au.) eulepidus* (Schneid), *Amoeboceras (Amoebites)* cf. *A. (A.) beaugrandi* (Sauvage 1871), *Streblites*? cf. *S. taimyrensis* Mesezhnikov, 1976
			Lower	*Rasenia cymodoce* Zone	M 18	***Rasenia evoluta*** Spath, 1935
					M 17	***Rasenia cymodoce*** (d'Orbigny, 1850), *Amoeboceras (Amoebites)* aff. *A. (A.). subkitchini* Spath, 1935, *Amoeboceras (Amoebites)* aff. *A. (A.) rasenense* Spath, 1935
					M 16	***Rasenia inconstans*** Spath, 1935, *Pachypictonia*? Sp. nov. C Birkelund & Callomon, *Amoeboceras (Amoebites)* aff. *A. (A.) subkitchini* Spath, 1935, *Amoeboceras (Amoebites)* aff. *A. rasenense* Spath, 1935
					M 15	***Rasenia inconstans*** Spath, 1935, *Amoeboceras (Amoebites) subkitchini* Spath, 1935, *Amoeboceras (Amoebites)* aff. *A. (A.) rasenense* Spath, 1935
				Pictonia baylei Zone	M 14	***Pictonia* sp. nov. A** Birkelund & Callomon, 1985 aff. *normandiana* Tornquist, *Amoeboceras (Amoebites) bayli* Birkelund & Callomon, 1985, *A. (Amoebites)* sp. aff. *A. (A.) schulginae* Mesezhnikov, 1967, *A. (Amoebites)* cf. *A. (A.) ernesti* (Fischer, 1913)

Fig. 3.2.1. Upper Jurassic – Lower Cretaceous ammonite stratigraphy. Column with zones and subzones: Upper Jurassic after Surlyk 1978a, 1991, Sykes & Callomon 1979, Callomon & Birkelund 1980, 1982, Birkelund *et al.* 1984, Birkelund & Callomon 1985; Lower Cretaceous after Surlyk 1978 (Ryazanian), Alsen 2006 (Ryazanian–Hauterivian); this study. Column with faunal horizons: Index species in bold. Upper Jurassic numbering from Milne Land (M14–M47) after Callomon & Birkelund 1982, Birkelund *et al.* 1984, Birkelund & Callomon 1985.

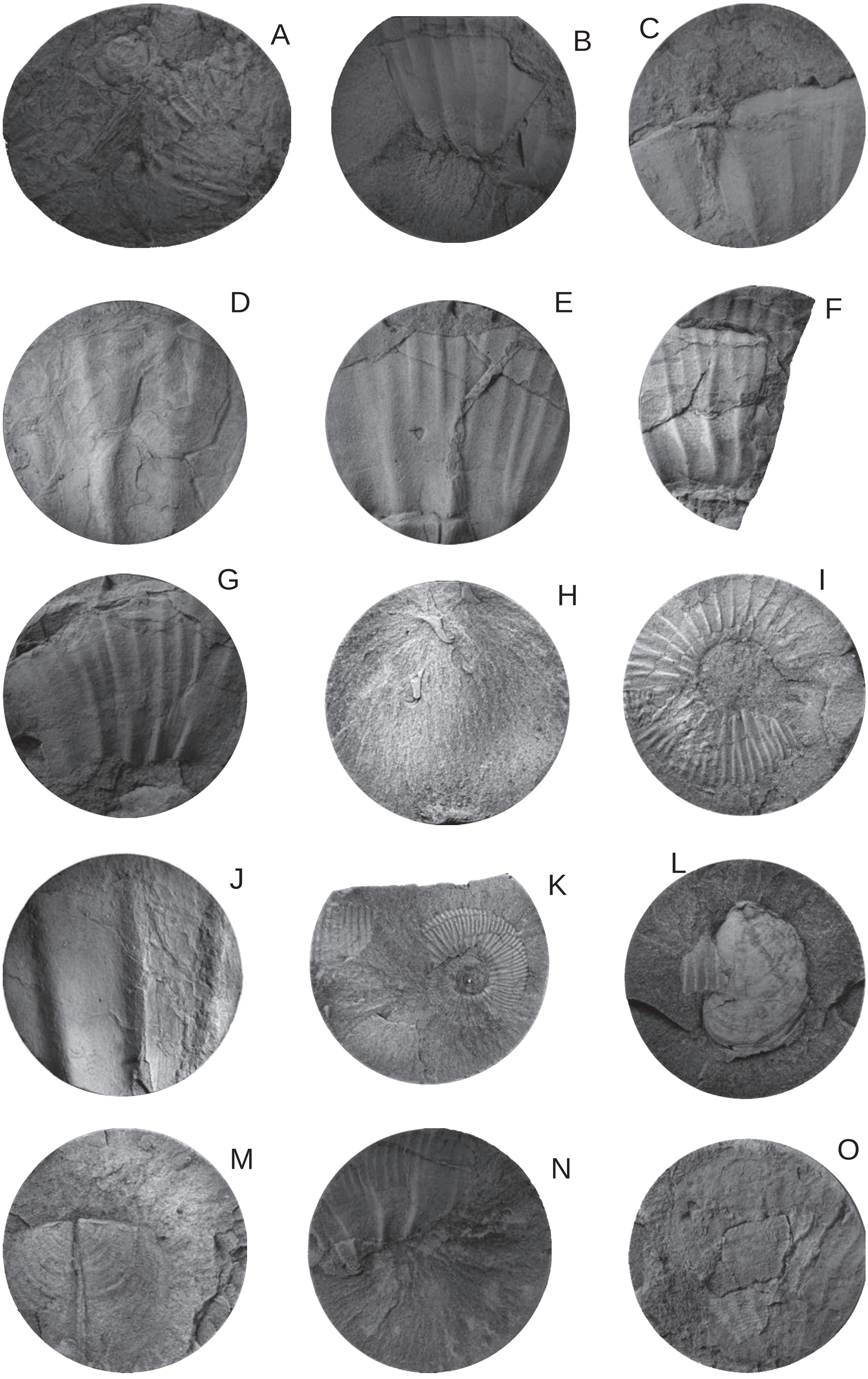

Figure 3.2.2. Photos of selected macrofossils sampled from the Rødryggen-1 core. A: *Amoeboceras* sp. at level 227.72 m (GGU 517101-426). B: *Dorsoplanites* at level 90.85 m (GGU 517101-424). C: *Dorsoplanites primus* at level 89.30 m (GGU 517101-423). D: *Pavlovia variocostata* at level 75.43 m (GGU 517101-421). E: *Dorsoplanites* sp. at level 74.20 m (GGU 517101-420). F: *Pavlovia corona* at level 74.03 m (GGU 517101-419). G: *Dorsoplanites gracilis* at level 70.06 m (GGU 517101-418). H: *Onychites* at level 62.43 m (GGU 517101-415). I: *Epipalliceras pseudapertum* at level 55.98 m (GGU 517101-414). J: *Laugeites biplicatus* at level 53.67 m (GGU 517101-411). K: *Laugeites* cf. *planus* at level 51.55 m (GGU 517101-409). L: Bivalve and small ammonite fragment at level 47.52 m (GGU 517101-407). M: Aptychus, ammonite jaw apparatus at level 47.20 m (GGU 517101-406). N: *Subcraspedites (Swinnertonia) subundulatus* at level 45.37 m (GGU 517101-404). O: *Hectoroceras* sp. at level 27.73 m (GGU 517101-401).

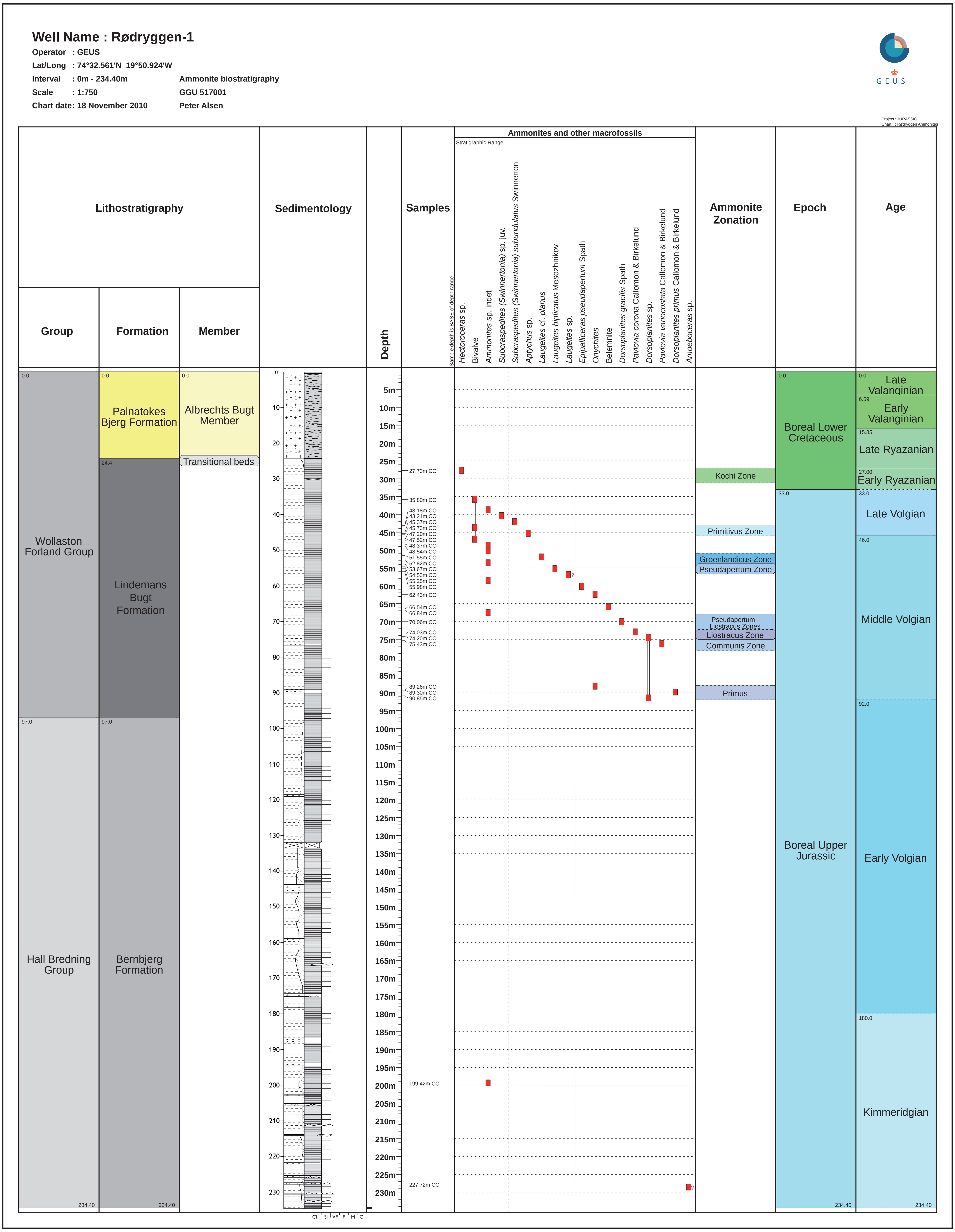

Figure 3.2.3. Chart summarising ammonite taxa recorded, the ammonite ranges and the biostratigraphic subdivision of the Rødryggen-1 core and shown against a sedimentological/lithological log.

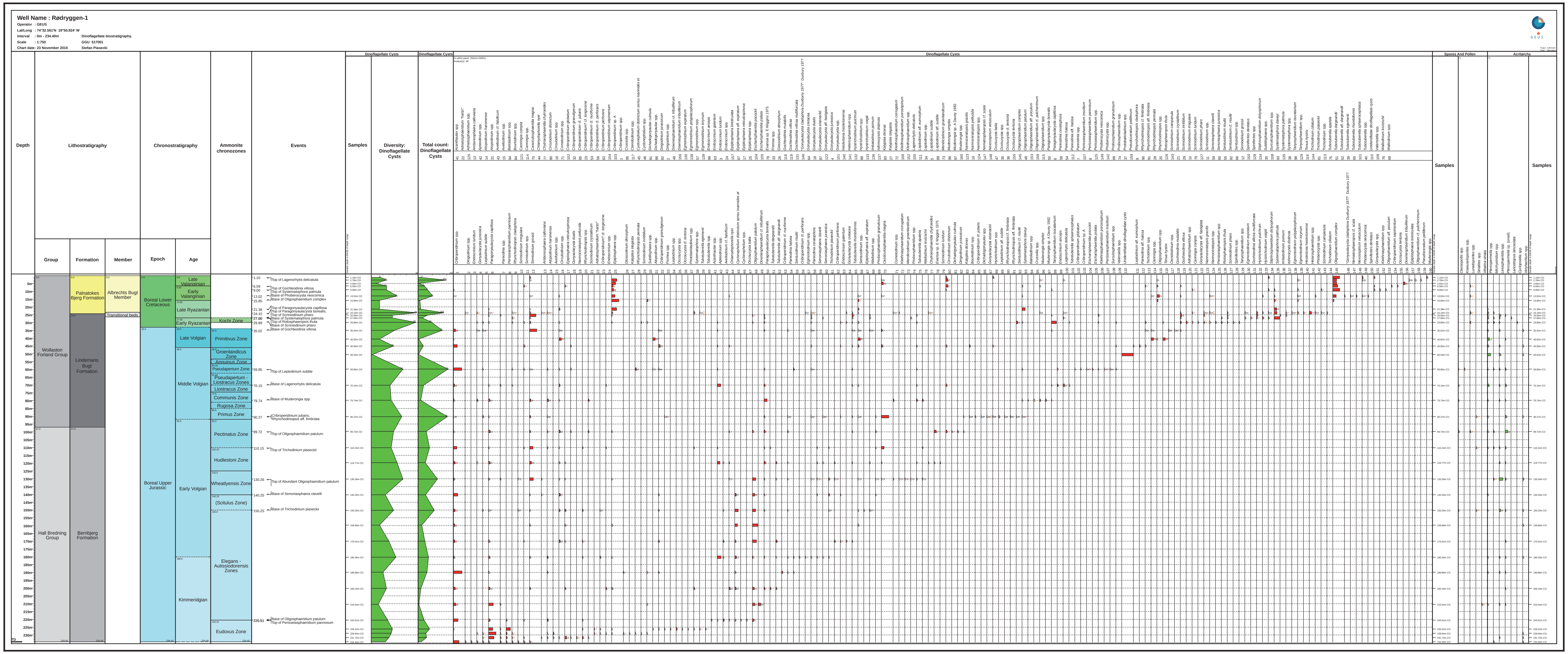

Figure 3.2.4. Range-chart showing the distribution of dinoflagellate cysts in Rødryggen-1 core and the stratigraphic events used for dating the core in combination with ammonite occurrences.

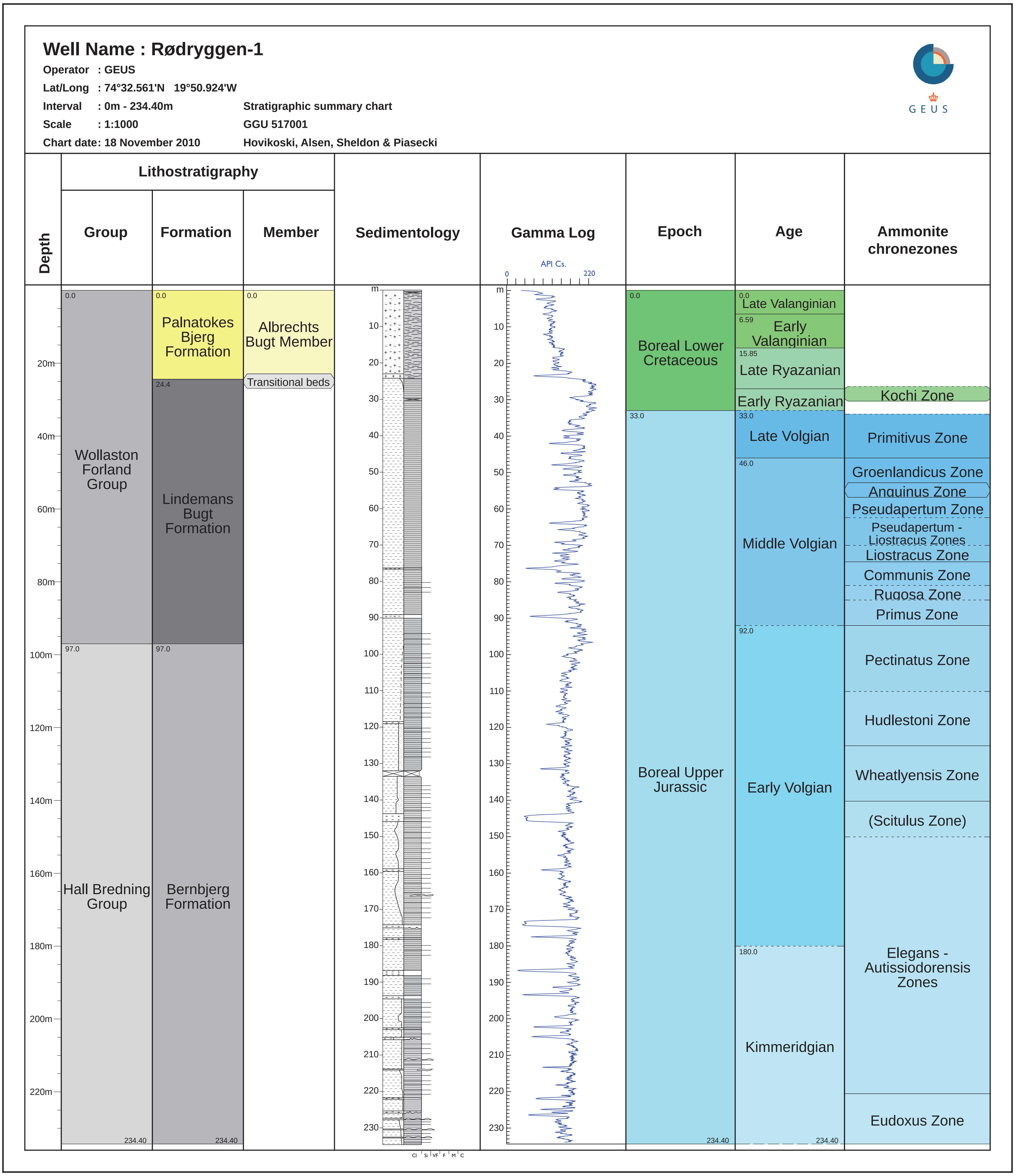

Fig. 3.2.5. Stratigraphic summary chart of integrated sedimentology, gamma log, foraminifer-, nannofossil-, ammonite- and dinoflagellate-stratigraphy.

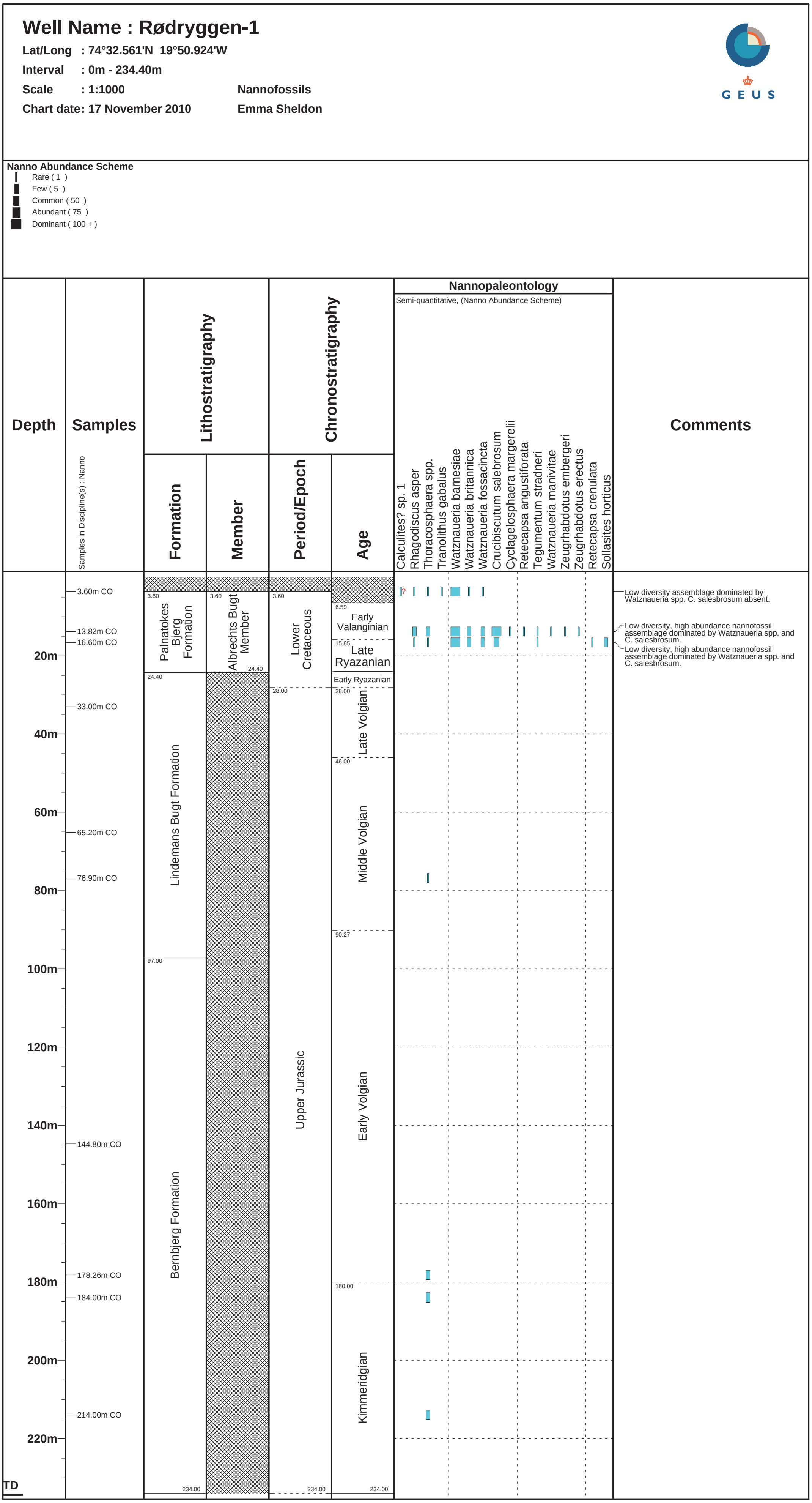

Figure 3.2.6. Nannofossil distribution chart.

Figure 3.2.7. Microfossils distribution chart.

Depth	GGU sub-sample number	Description / taxononomy	Faunal horizon	Ammonite stratigraphy
27.73 m	-401	*Hectoroceras* sp.		*H. kochi* Zone
35.80 m	-402	bivalve		
43.18 m	not sampled	*Ammonites* sp. indet.		
43.21 m	-403	*Subcraspedites* (*Swinnertonia*) sp. juv.		*S.* (*Sw.*) *primitivus* Zone
45.37 m	-404	*S.* (*Swinnertonia*) cf. *subundulatus* Swinnerton		*S.* (*Sw.*) *primitivus* Zone
45.73 m	-405	bivalve		
47.20 m	-406	Aptychus		
47.52 m	-407	bivalve		
48.37 m	-408	*Ammonites* sp. indet.		
48.54 m	-427	*Ammonites* sp. indet.		
51.55 m	-409	*Laugeites* cf. *planus* Mesezhnikov	M47	*L. groenlandicus* Zone
52.82 m	-410	*Ammonites* sp. indet.		
53.67 m	-411	*Laugeites biplicatus* Mesezhnikov	M47	*L. groenlandicus* Zone
54.53 m	-412	?*Laugeites* sp.		
55.25 m	-413	*Ammonites* sp. indet.		
55.98 m	-414	*Epipalliceras pseudapertum* Spath	M42	*E. pseudapertum* Zone
62.43 m	-415	Onychites		
66.54 m	-416	belemnite		
66.84 m	-417	*Ammonites* sp. indet.		
70.06 m	-418	*Dorsoplanites gracilis* Spath	M37-42	*D. liostracus* - *E. pseudapertum* Zones
74.03 m	-419	*Pavlovia corona* Callomon & Birkelund	M37	*D. liostracus* Zone
74.20 m	-420	*Dorsoplanites* sp.		
75.43 m	-421	*Pavlovia variocostata* Callomon & Birkelund	M35	*P. communis* Zone
89.26 m	-422	Onychites		
89.30 m	-423	*Dorsoplanites primus* Callomon & Birkelund	M31	*D. primus* Zone
90.85 m	-424	*Dorsoplanites* sp.		
199.42 m	-425	*Ammonites* sp. indet.		
227.72 m	-426	*Amoeboceras*?		

Table 3.2.1 Summary of macrofossil samples from the Rødryggen-1 core with GGU no. 517001 and with each macrofossil sample subnumbered -401–427. Identifications of taxa and their biostratigraphic implications indicated where possible.

3.3 Chemostratigraphy

The chemostratigraphy of the sediments in the Rødryggen-1 core has been used to uncover trends that cannot readily be distinguished in the mineralogical characterization. For instance, the geochemistry was used to differentiate between some minerals with quite similar X-Ray Diffraction (XRD) peaks which were difficult to separate on the diffractograms, and abnormal contents of some elements in single samples were used to discover intervals of deviant mineral occurrences. The different lithologies of the core have efficiently been characterized by their specific chemistry, and also the formations are distinguishable on the basis of their chemistry.

3.3.1 Methods

Bulk geochemical analyses have been carried out on 25 samples from the Rødryggen-1 core by AcmeLabs, Canada. The selected intervals of the core include 14 mudstones, 9 cemented mudstones, 1 cemented fracture and 1 sandstone. The intervals were chosen to overlap with the sampling depths of other types of analyses, and only one sandstone interval was chosen because of the scarcity of this lithology. The surface of the core was removed to avoid contamination. The samples were then crushed and 5 gram of each sample was used for the analyses. Major oxides and several minor elements were found by Inductively Coupled Plasma Emission Spectroscopy (ICP-ES), whereas trace elements were identified by Inductively Coupled Plasma Mass Spectroscopy (ICP-MS). The Rare Earth Elements (REE) were included in the measurements and comprise the Light REE (LREE, La-Sm) and the Heavy REE (HREE, Eu-Lu). They are normalized to the chondrite composition of Boynton (1984). Total carbon (TOT/C) and total sulphur (TOT/S) were measured by Leco analysers. Loss On Ignition (LOI) was measured after heating to 1000ºC. The content of oxides is addressed as elements in the text.

3.3.2 Chemical trends

The full list of bulk geochemical data is registered in (Appendix 10.3). An overview of the chemostratigraphy up through the core is provided in Fig. 3.3.1 for selected elements. The same variables are shown in Fig. 3.3.2, where they are normalized to the average value of all samples in order to demonstrate the trends in data. The mudstone samples have larger contents of Si (average: 53.3 wt%) and Al (average: 15.3 wt%) than the cemented mudstone (average: Si 19.0 wt%, Al 5.6 wt%). In contrast, the cemented intervals have larger contents of Ca (average: 21.8 wt%), Mg (average: 8.1 wt%), Fe (average: 11.4 wt%), Mn (average: 0.6 wt%) and LOI (average: 30.8 wt%) than the mudstone (average: Ca 2.8 wt%, Mg 1.5 wt%, Fe 6.8 wt%, Mn 0.1 wt%, LOI 14.9 wt%). TOT/C is about twice as high in the cemented intervals (average: 9.6 wt%) than in the mudstones (average: 4.7 wt%), whereas TOT/S is about twice as high in the mudstones (average: 3.4 wt%) as in the cemented mudstones (average: 1.7 wt%). Ti and Zr are more abundant in the mudstone (average: Ti 0.7 wt%, Zr 169.2 ppm) than in the cemented mudstone (average: Ti 0.3 wt%, Zr 89.0 ppm). The mudstone contains the largest amount of all trace elements except for Y.

3.3.3 Chemostratigraphical trends

The relatively small Al content indicates that the sediments do not have as large a content of clay minerals as would be expected for a mudstone. The Al content is especially small in the cemented intervals (Fig. 3.3.3). The silica content is on the other hand larger than expected for a mudstone, but is also markedly smaller in the cemented mudstone. The positive correlation between Si and Al with quite constant Si/Al ratio shows that the proportion between quartz and clay minerals are rather constant for all the lithologies, but the large variation in absolute values shows that especially the cemented intervals are diluted by other mineral phases. The Si/Al ratio has some cluster tendencies for the mudstones, showing that the initial mudstone composition was not completely homogeneous for all formations. Moreover, the presumed presence of feldspars also has an impact on the Al content.

The fine Fe to S correlation reveals pyrite to be present in all samples (Fig. 3.3.4). The mudstone and cemented intervals have different trends, where the cemented trend is more Fe rich indicating that Fe is also abundantly present in another mineral phase than pyrite in the cemented parts of the Bernbjerg and Lindemans Bugt Formations. The largest amounts of pyrite are found in the Lindemans Bugt Formation. The very high Fe content in one of the cemented intervals in the Lindemans Bugt Formation (Fig. 3.3.1) must be caused by a local siderite concretion, which also explains the high Mn content.

The elements dominating the cemented mudstones (Fig. 3.3.2) are all associated with carbonate minerals, which explain the low amount of quartz and clay minerals. The large LOI of the cemented intervals (Fig. 3.3.1) stems primarily from inorganic C in the carbonate minerals, but organic C and dehydration of clay minerals must also contribute as the LOI of the mudstone is not as low as would otherwise be expected from the relatively low amount of carbonate minerals. The similar trends of Ca, Mg, Fe and Mn in the Bernbjerg and Lindemans Bugt Formations (Fig. 3.3.1) reveal ankerite to be present in large amounts in the cemented intervals. Some of the fairly high Mg content must be present in dolomite, as also indicated by the association of some of the Fe with pyrite (Fig. 3.3.4). The fracture-fill sample has the most extreme Mg value, so the fracture must be filled by dolomite. The content of Ca and Mg decreases up through the cemented parts of the Bernbjerg and Lindemans Bugt Formations (Fig. 3.3.5). This is also true for the Fe content when the large amount of pyrite in the Lindemans Bugt Formation is taken into consideration. The amount of ankerite and dolomite is thus decreasing upwards through the core. The large amount of Ca in the Palnatokes Bjerg Formation shows that calcite is present in large amounts in the cemented intervals and in smaller amounts in the mudstones.

The Bernbjerg Formation and the Palnatokes Bjerg Formation each have a specific constant ratio between Ca and C that is equal for all lithologies, where the absolute values are highest in the cemented mudstone (Fig. 3.3.6). The trend is the same for both formations, but the Bernbjerg Formation is richer in C, and the Palnatokes Bjerg Formation has a higher content of Ca. The Ca:C ratio is 1.1 for the Bernbjerg Formation and 4.0 for the Palnatokes Bjerg Formation. This shows that the cemented intervals are enriched in carbonate minerals, and that the cemented intervals contain a mud component with the same composition as the mudstone in the uncemented intervals. The different Ca:C ratios of the formations reveal that this mudstone component is formation specific. The Lindemans Bugt Formation lies in-between the trends of the two other formations, but the trend in this formation is not as clear as it is masked by pyrite, apatite and feldspar in different intervals. The C content of the mudstone component decreases upwards (Fig. 3.3.1), which shows that each formation has a lower content of organic matter than the preceding (Fig. 3.3.6). The decrease is not caused by decreasing carbonate content, as evident in the mudstone intervals by the lack of cations required for carbonate minerals (Fig. 3.3.1).

The trace element content is highest in the mudstone, as it is diluted by carbonate minerals in the cemented intervals. The trace elements are also controlled by grain size and drops in the coarser-grained intervals like the sandstone in Fig. 3.3.1, because the trace elements largely are associated with clay minerals and organic matter. A few cemented intervals have higher REE content than the rest (Fig. 3.3.7) and they are therefore interpreted as having an initially smaller grain size. All samples are LREE-enriched and have rather flat HREE chondrite-normalized patterns. This is a typical crustal composition along with the negative Eu-anomaly. It is obvious from the fracture-fill sample that high content of carbonate minerals results in low content of REE. However, the trends of the cemented intervals are generally enriched in HREE in proportion to the uncemented mudstones.

Ti and Zr are heavy mineral indicators, as they are primarily present in quite stable heavy minerals (Friis et al., 2007). Zr is almost exclusively found in zircon, whereas Ti chiefly occurs in Ti-oxides. The sandstone has a higher heavy mineral content than the mudstone (Fig. 3.3.2), because of the characteristically silt and sand-sized nature of the heavy minerals. The cemented intervals of the mudstone have the lowest content of heavy minerals, as they are diluted by carbonate minerals. The presence of P in Ca rich intervals (Fig. 3.3.1) mainly found at the bottom of the Lindemans Bugt Formation indicates that apatite is present.

3.3.4 Conclusions

The chemostratigraphy has been used to discriminate between different lithologies and formations of the Rødryggen-1 core. Cemented intervals in the mudstone succession can in this way be appointed directly from the geochemistry. The positive correlation between Ca and C in the cemented intervals is due to carbonate cementation. The Ca to C ratio is efficient in separating sediments from the Bernbjerg Formation and the Palnatokes Bjerg Formation, whereas the Lindemans Bugt Formation has too large scatter to be reliable. The Si to Al positive correlation with low values in the cemented intervals shows that the mudstone component of the cemented intervals equals that of the rest of each formation.

3.3.5 References

Boynton, W.V., 1984: Geochemistry of the rare earth elements: meteorite studies. In: Henderson, P. (ed.): Rare earth element geochemistry. Elsevier, 63–114.

Friis, H., Poulsen, M.L.K., Svendsen, J.B. & Hamberg, L., 2007: Discrimination of density flow deposits using elemental geochemistry – Implications for subtle provenance differentiation in a narrow submarine canyon, Palaeogene, Danish North Sea. Mar. Petrol. Geol., **24**, 221-235.

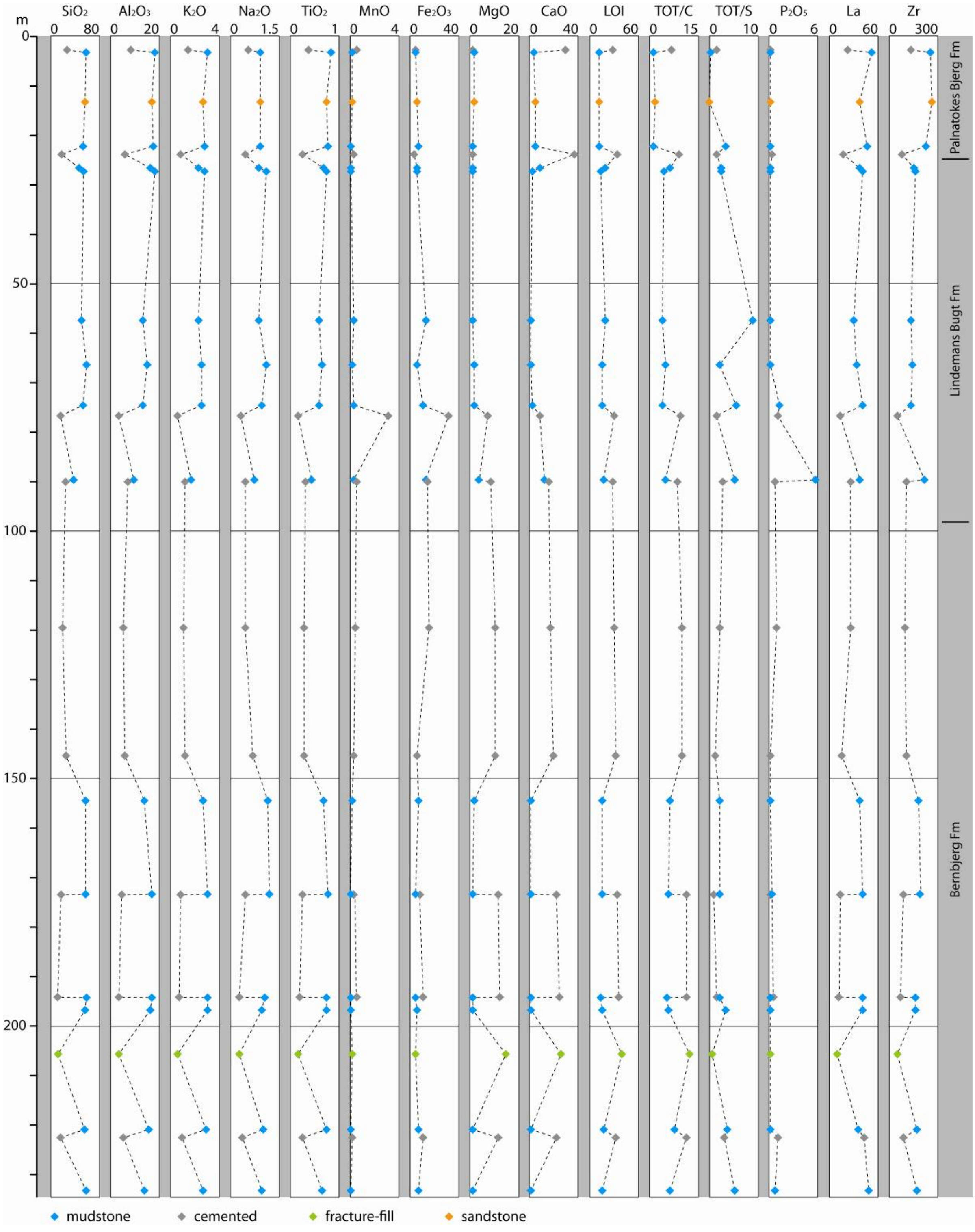

Figure 3.3.1. Chemostratigraphy of 14 mudstones, 9 cemented mudstones, 1 cemented fracture and 1 sandstone from the Rødryggen-1 core. Major elements are in wt% and trace elements in ppm.

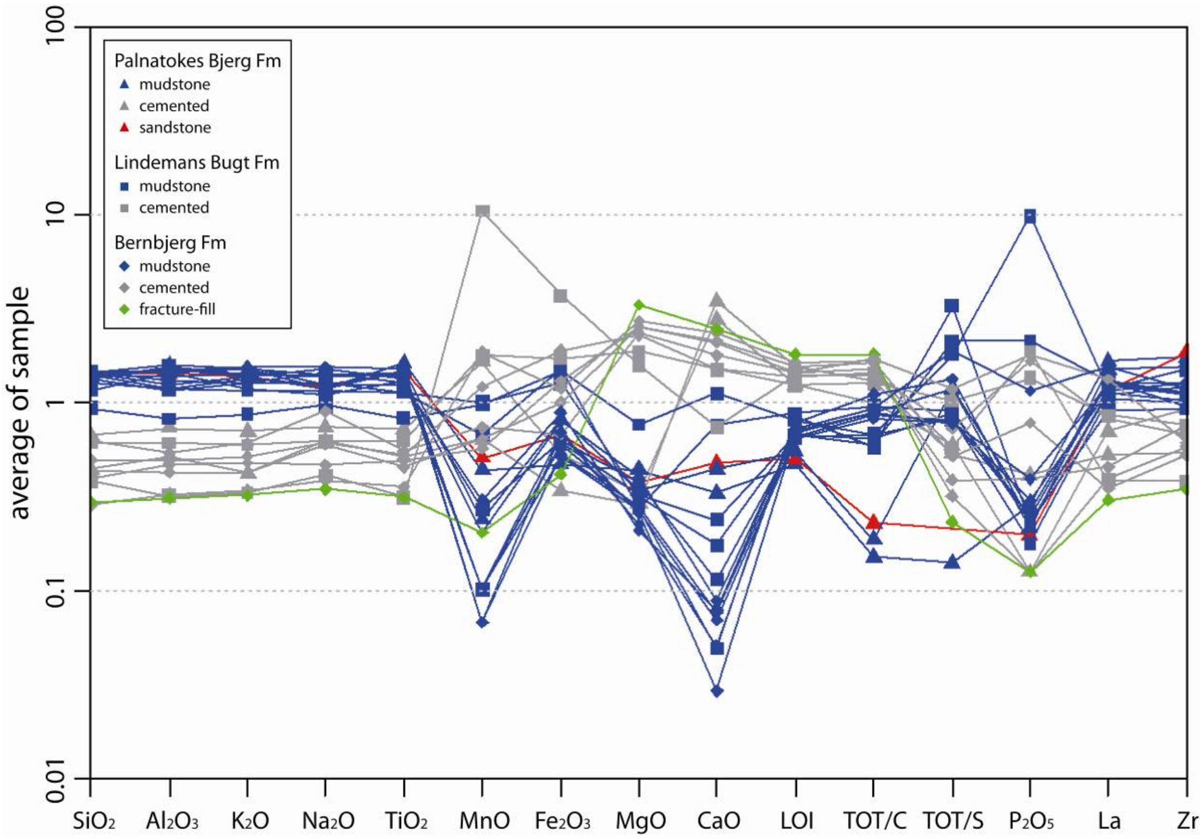

Figure 3.3.2. The same variables as in figure 3.3.1, but with the average values of all samples used as normalization value. This helps identify trends and outliers.

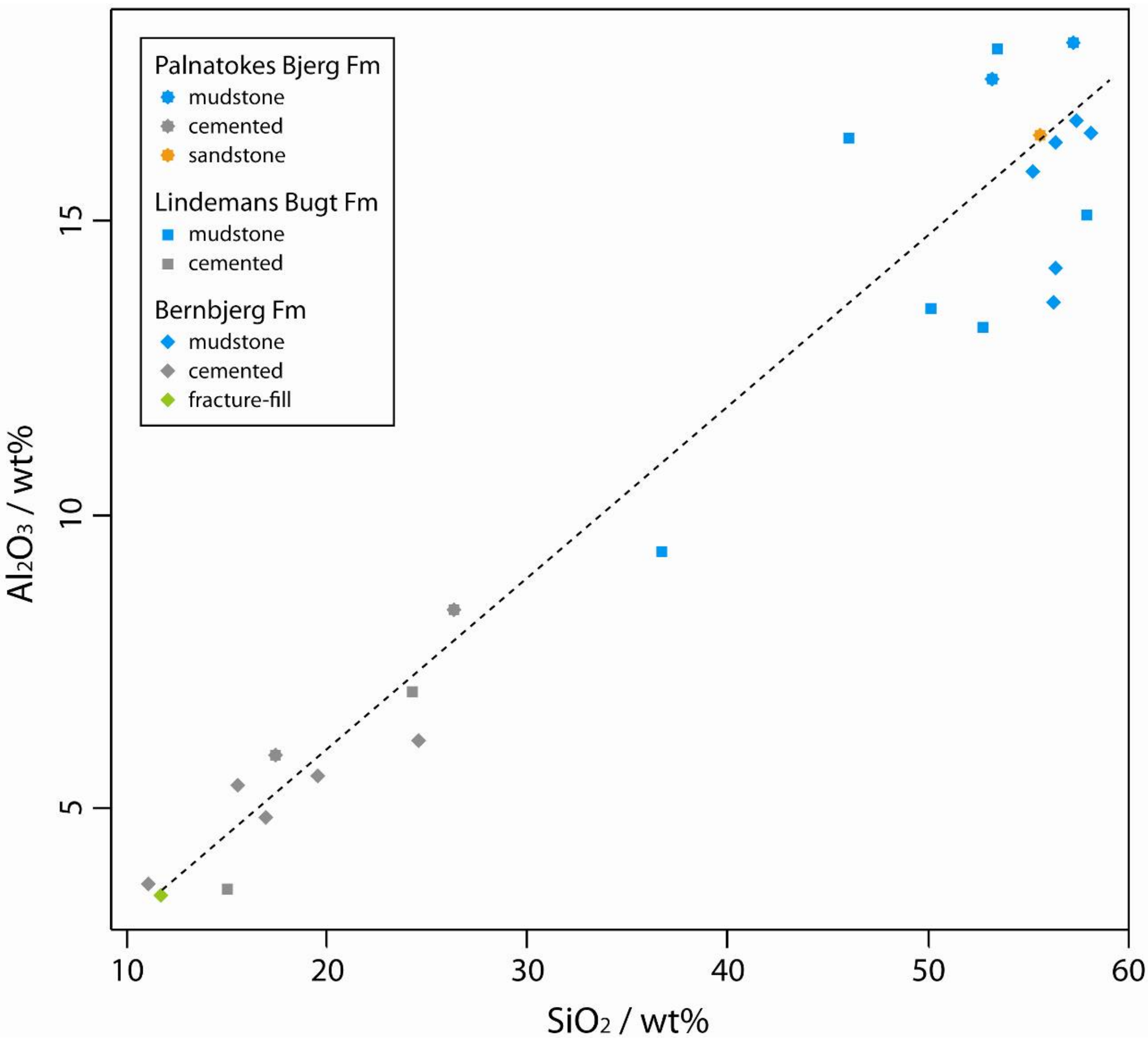

Figure 3.3.3. The Si/Al ratio is partly proportional to quartz versus clay minerals, showing that both are present in larger amounts in the mudstones, whereas the cemented intervals contain a large amount of carbonate minerals.

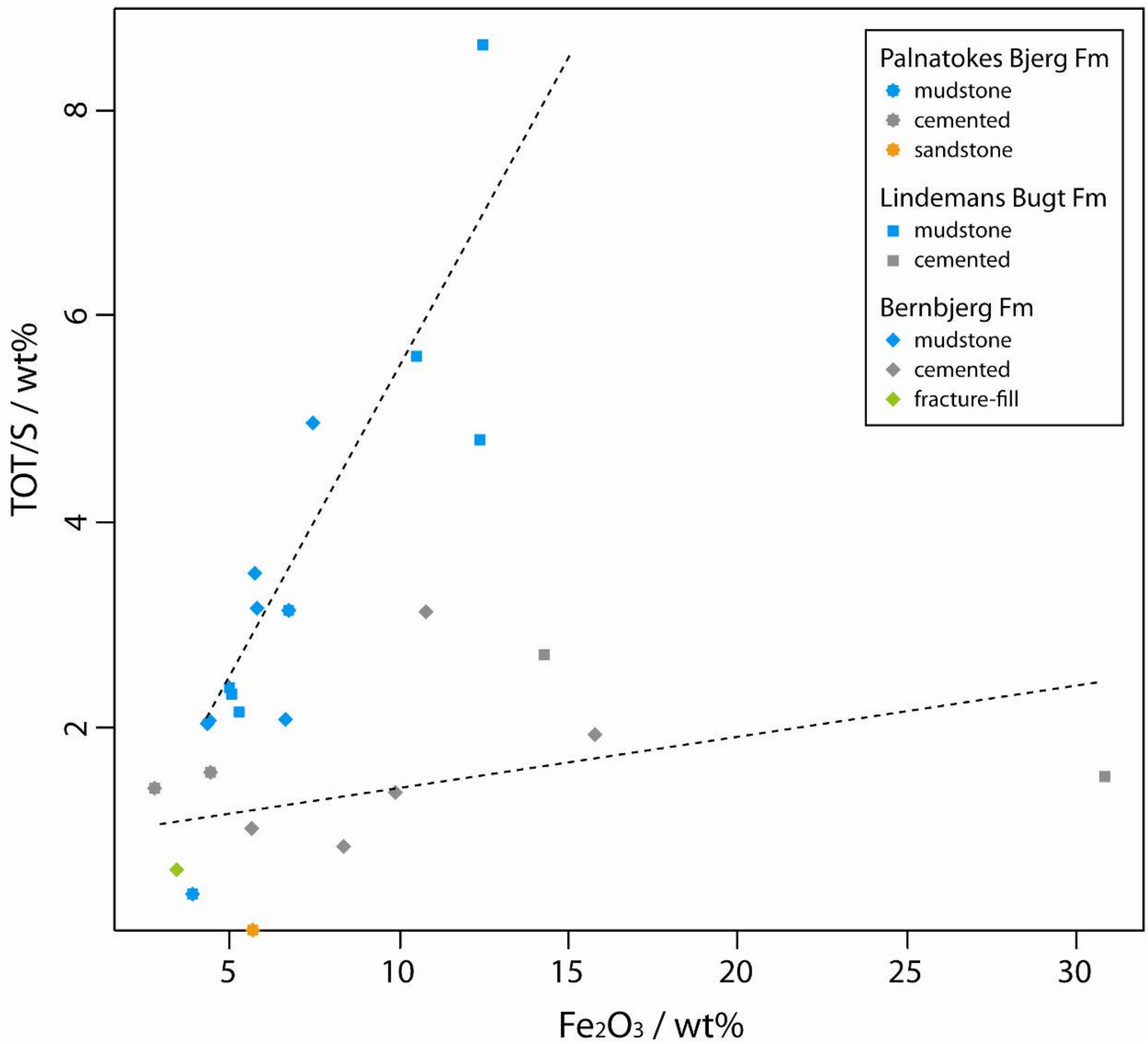

Figure 3.3.4. All samples contain pyrite, but the cemented intervals in the Bernbjerg and Lindemans Bugt Fms must also include another Fe mineral to account for the large Fe content.

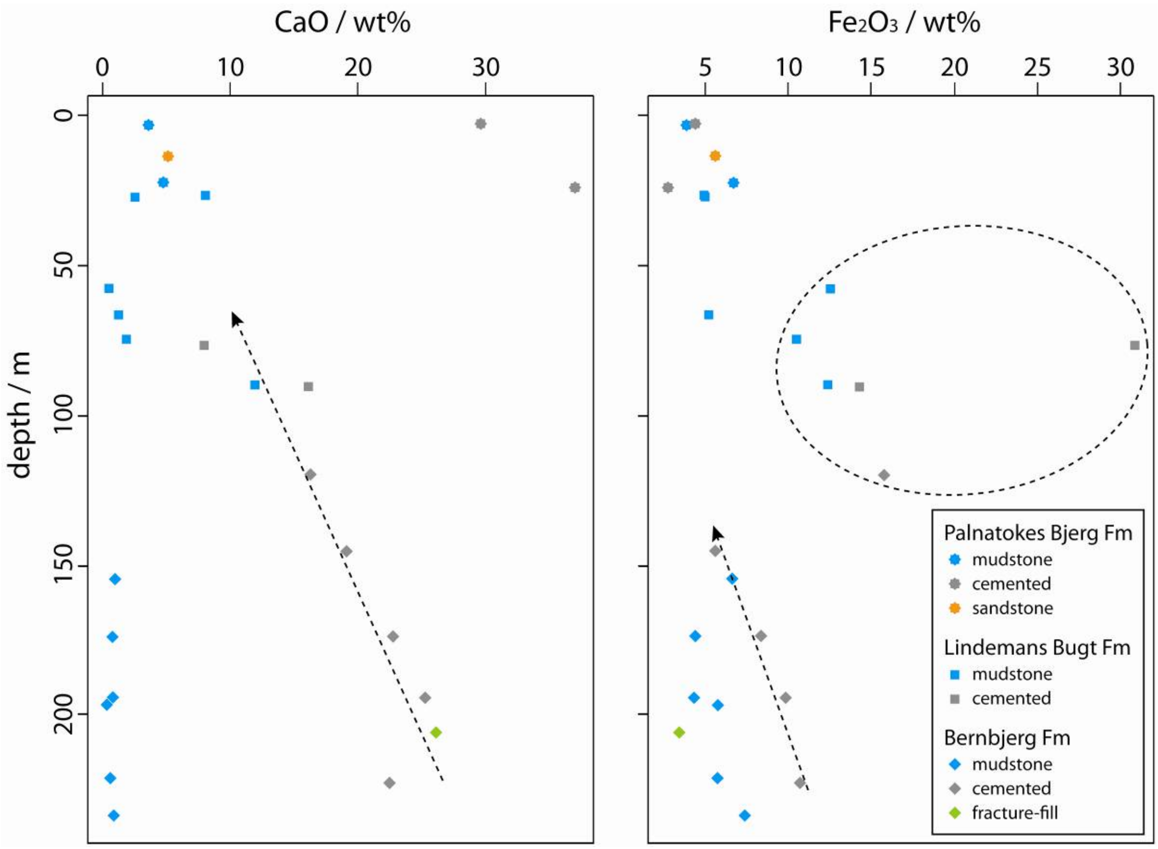

Figure 3.3.5. The content of Ca and Mg decreases simultaneously up through Bernbjerg and Lindemans Bugt Formations in the cemented intervals. The same is true for Fe, although the trend is masked by pyrite in the upper part of the Bernbjerg Fm and in the Lindemans Bugt Fm.

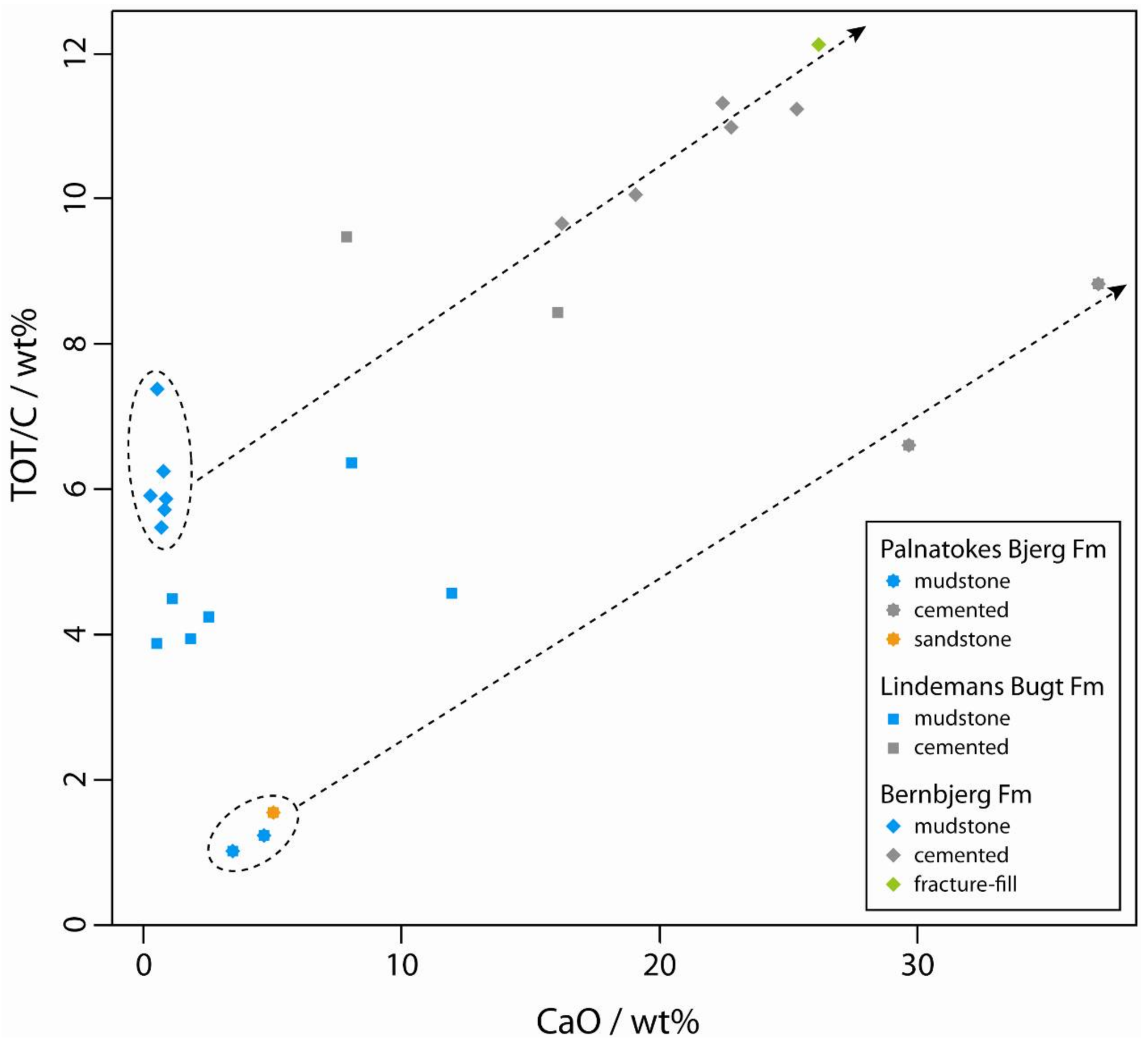

Figure 3.3.6. The Ca/C ratio is quite similar for all lithologies in each formation. This indicates that the mudstone component is always the same, but diluted by other phases in the cemented intervals. The trend is not so pronounced for the Lindemans Bugt Fm.

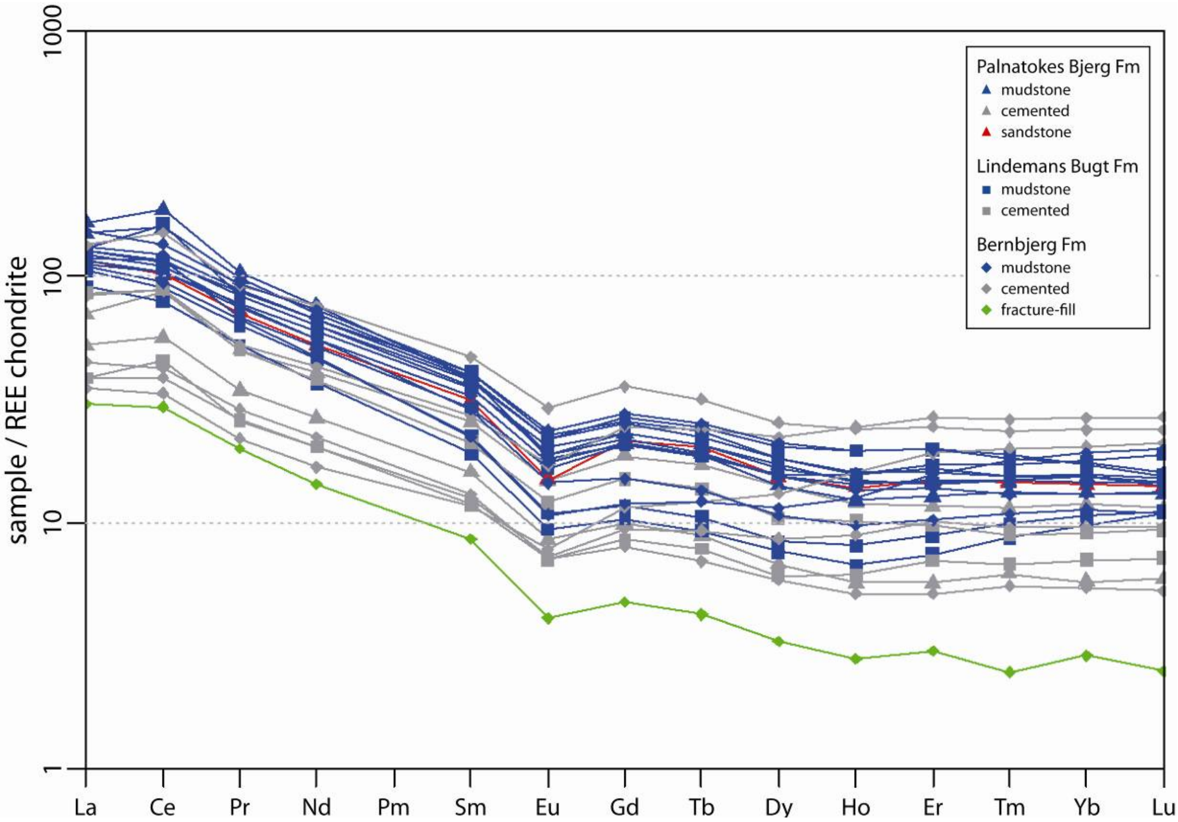

Figure 3.3.7. REE normalized to the chondrite composition of Boynton (1984). The cemented intervals have generally lower contents of all REE with the fracture-fill as the extreme example.

3.4 Petrophysical core log stratigraphy

Petrophysical logs recorded in the Rødryggen core well include a total gamma log from interval 0-209 m, which was logged in the open drill hole. Logging of the Rødryggen-1 borehole was initiated immediately after the drilling was completed. A total gamma ray log and conductivity log was planned. However, due to problems with the winch only a total gamma ray log down to 209 m was obtained. Later, total gamma ray logging supplemented by density logging was carried out in the core-lab at GEUS on the lower part of the core (190 – TD) in order to obtain a complete gamma ray log, representative for the entire drilled succession. The merged gamma ray log and the log measured in the field are shown in Figure 3.4.1 together with the gamma ray log and density log measured in the core-lab.

Together with sedimentological description the gamma log proved to provide valuable information about depositional trends and stratigraphic contacts. Moreover, most of the described sedimentary facies (Chapter 4) displayed characteristic GR readings, which may help in preliminary extrapolation of these data to not yet drilled offshore wells in NE Greenland in the future. Limitations in the data included that individual sandstone layers of the Bernbjerg Formation were typically too thin to be visible in the GR log. This is commonly the case in the heterolithic lower part of the Bernbjerg Formation Moreover, the recurring presence of carbonate (ankerite) rich intervals in the Bernbjerg Formation mimics sandstone rich intervals. Finally, interpretation of depositional trends in mud-dominated depositional systems may be complicated by various processes such as flocculation of clays. Especially in high-energy mud-dominated settings, mud commonly forms floccules, which develop into dense bottom hugging sediment suspensions (i.e. fluid muds; Schieber, 2007; Macquaker et al., 2010). Therefore, distinction of prograding/retrograding trends from well logs may be complicated by the fact that higher energy sedimentary facies may demonstrate increasing clay content. For instance, a transgressive trend observed in sedimentary facies between ~227–174 m is not readily visible on the GR log.

3.4.1 Methods

Analytical procedure in the laboratory

The Rødryggen-1 core was received at the GEUS core-lab as 1 meter sections wrapped in alumina foil. With intervals of approximately 3 meters in the depth direction, the core contained a depth marking that indicated the depth at that point in meters. The core diameter was measured at several places along the core to be 4.05 cm ± 0.02 cm. The 1 meter core sections were packed in flat plastic boxes, each holding 7 core sections. The core boxes were marked with top depth and bottom depth.

The core section from 192.56 m to 234.54 m was scanned, i.e. a total of 42 meters. A majority of the core length presented a full diameter, cylindrical core to the scanner. The fundamental requirement of the scanning procedure, that the scanned material be cylindrical, was therefore fulfilled for a majority of the cores. The raw bulk density log trace gives a good indication of the quality of the core: core sections where significant parts of the core are missing have raw bulk density traces with large amplitude variations and minimum bulk density readings below 2.2 g/ml.

The core sections were scanned with the spectral gamma and bulk density scanner of GEUS Core Laboratory. The core sections were scanned sequentially with the core sections being fitted together to present the scanner to a continuous core slowly passing the detectors of the scanner. Most core sections were scanned without the alumina foil, but disintegrating sections were scanned within the alumina foil to prevent the core from falling apart.

Scanning was performed with a speed of 1 cm/min with read-out of the collected gamma and density data every 60 seconds. Total gamma activity and bulk density were measured.

Filtering of the density data was done in order to remove the large amplitude variations caused by missing or crushed core or from gaps between the termination of one core section and the beginning of the next. The filtering was performed in a way that the original high signal-to-noise ratio and depth resolution of approximately 1 cm was preserved.

Analytical methods

Total core gamma scanning

The natural gamma radiation of a core is recorded within an energy window of 0.5 - 3.0 MeV, using Tl activated NaI scintillation detectors, connected to a multichannel analyzer. The core passes through a lead shielded tunnel at constant speed while the gamma activity is continuously recorded. For the Rødryggen scanning a speed of 1 cm/min was used throughout the scanning, with data read-out every 1 minute, resulting in data points with 1 cm spacing. Nominally, each data point represents the mean gamma activity over a 1 cm depth interval, the assigned depth being the middle of the interval. Actually, the scintillation detectors record the gamma activity in a broader section of the core. The sensitivity profile in the depth direction of the core has approximately the shape of a gauss-function with a

Full Width at Half Maximum (FWHM) of approximately 17 cm. The measured gamma activity is corrected for background gamma activity.

To improve the readability of the logs, the raw data were filtered with a box-car filter with a bandwidth of 10 cm. The smoothing causes a slight deterioration of the sensitivity profile in the depth direction to approximately 19 cm FWHM, still with an approximate gauss-shape. The processing of the total core gamma data assumes that the core has a constant diameter. Core sections where this assumption does not hold have gamma activities that are systematically biased. If core material is missing, the calculated gamma activity is too low.

Bulk density scanning

The measurement of core bulk density is based on the attenuation of gamma rays passing through the core. The gamma rays come from a 30 mCi ^{137}Cs radioactive source emitting photons of energy 662 keV. A collimated beam of gamma rays with a diameter of 0.8 cm passes through the core and is recorded by a NaI scintillation detector.

At the scanning, the core passes the gamma ray source and detector assembly at a constant speed while the gamma ray attenuation is continuously recorded. The density scanning was conducted contemporaneously with the gamma scanning and therefore the scanning speed of 1 cm/min that applies for this operation also applies for the density scanning. Similarly, a read-out interval of 1 cm was used for the density scanning. However, the density data were not box-car filtered because the reproducibility of the density data was so good that smoothing was not necessary.

The processing of the bulk density data assumes that the core has a constant diameter. Core sections where this assumption does not hold have densities that are systematically biased. If core material is missing, the resulting density values are too low.

Filtering of the density data was done in order to remove the large amplitude variations caused by missing core, crushed core or from gaps between the termination of one core section and the beginning of the next. The filtering was performed in a way that the original high signal-to-noise ratio and the depth resolution of approximately 1 cm are preserved.

Depth assignment

The Rødryggen-1 core was scanned with a constant speed of 1 cm/min. The actual length of every core section in its scanning position was recorded, as well as the position of the section top and section bottom relative to the detectors of the scanner. Using this information every data point were assigned a laboratory depth relative to the top of the core. Because the lengths of core sections during scanning were not necessarily equal to the nominal lengths of the sections, the laboratory depth relative to the top of the core could not be converted to true core depth by simple translation. For every core section a rubber-band depth conversion were applied according to

$$CoreDepth(I,J) = Top(J) + (I - 0.5) * Increment * \frac{Bottom(J) - Top(J)}{Length(J)}$$

where *CoreDepth(I,J)* is the depth assigned to data point no. *I* in core section no. *J*, *Top(J)* and *Bottom(J)* are the nominal depth of top and bottom, *Increment* is the depth interval between data points, and *Length(J)* is the length of section *J* during scanning. Additional minor corrections were applied to data point where the data collection had occurred across sections borders.

3.4.2 Results

The three lithostratigraphic units – the Bernbjerg Formation (234.5–97 m), the Lindemans Bugt Formation (97–24.4 m), and the Palnatokes Bjerg Formation (Albrechts Bugt Member, (24.4–0 m) –are expressed on the total GR log in the following way:

The lower part of the Bernbjerg Formation interval shows serrated log pattern which shows a locally subtle, few m-thick funnel shaped intervals. The funnel shaped successions reflect upward coarsening parasequences (marked by arrows in Fig. 4.1). The serrated pattern is mainly due to alternating heterolithic interlamination (F2, F3) and ankerite cemented mudstone intervals (F1C). The anomalously low GR peaks (20-50 API), which typically occurs within an interval of overall high GR readings, reflect high carbonate (ankerite) matrix content (F1C).

The overall relatively high GR signature of the Bernbjerg Formation reflects silty, mud-dominated lithology. In addition, between 175-125 m, present is a prograding to aggrading sedimentary interval superimposed on the general retrograding trend. This interval has increased amount of silt (common F2B), which is expressed as a slight decrease in GR baseline values.

The transitional formation boundary between the Bernbjerg Formation and the Lindemans Bugt Formation is expressed on the GR log as gradationally increasing GR values between 125-97 m. The exact formation boundary is placed at ~97 m were GR approaches 200 API for the first time. Above that, the GR ray pattern turns to more serrated. The Lindemans Bugt Formation interval has no sandstone, and the serrated GR pattern is probably due to clay content variation: The highest API values (>160 API) corresponds to laminated - massive mudstone (F1A), whereas the interbedded lower values (90-150 API) are due to presence of F1B, which contains abundant pyrite and ankerite, which decrease the clay content in this sub-facies.

The interval 35-25 m records a further sudden increase in the GR values. This interval corresponds with the Late Volgian - Late Ryazanian interval that consists dominantly of F1A. This zone appears to be stratigraphically most condensed, and records the first appearance of well-developed trace fossil *Zoophycos.*

The change from the Lindemans Bugt to the Palnatokes Bjerg Formation is also transitional and occurs within c. 1 m (~25.5–24.4 m). The boundary is readily recognizable from GR as an abrupt decrease in GR values. This reflects increase in matrix carbonate- and sand-content, and decreasing clay-content. The main lithology of the Albrechts Bugt Member interval is calcareous (sandy) mudstone and consequently the GR base line in Albrechts Bugt (~100 API) is typically lower than in the Bernbjerg Formation. The locally occurring low GR peaks (40-65 API; e.g., at ~24 m and ~2.5 m) reflect marly mudstone intervals (F4A). Overall, the relatively constant GR readings are in line with the observed aggradational depositional pattern and limited facies variability in the studied Albrechts Bugt Member interval.

3.4.3 References

Macquaker, J., Bentley, S., and Bohacs, K., 2010: Wave-enhanced sediment-gravity flows and mud dispersal across continental shelves: Reappraising sediment transport processes operating in ancient mudstone successions. Geology, **38**, 947–950.

Schieber, J., Southard, J., and Thaisen, K., 2007: Accretion of mudstone beds from migrating floccule ripples. Science, **318**, 1760–1763.

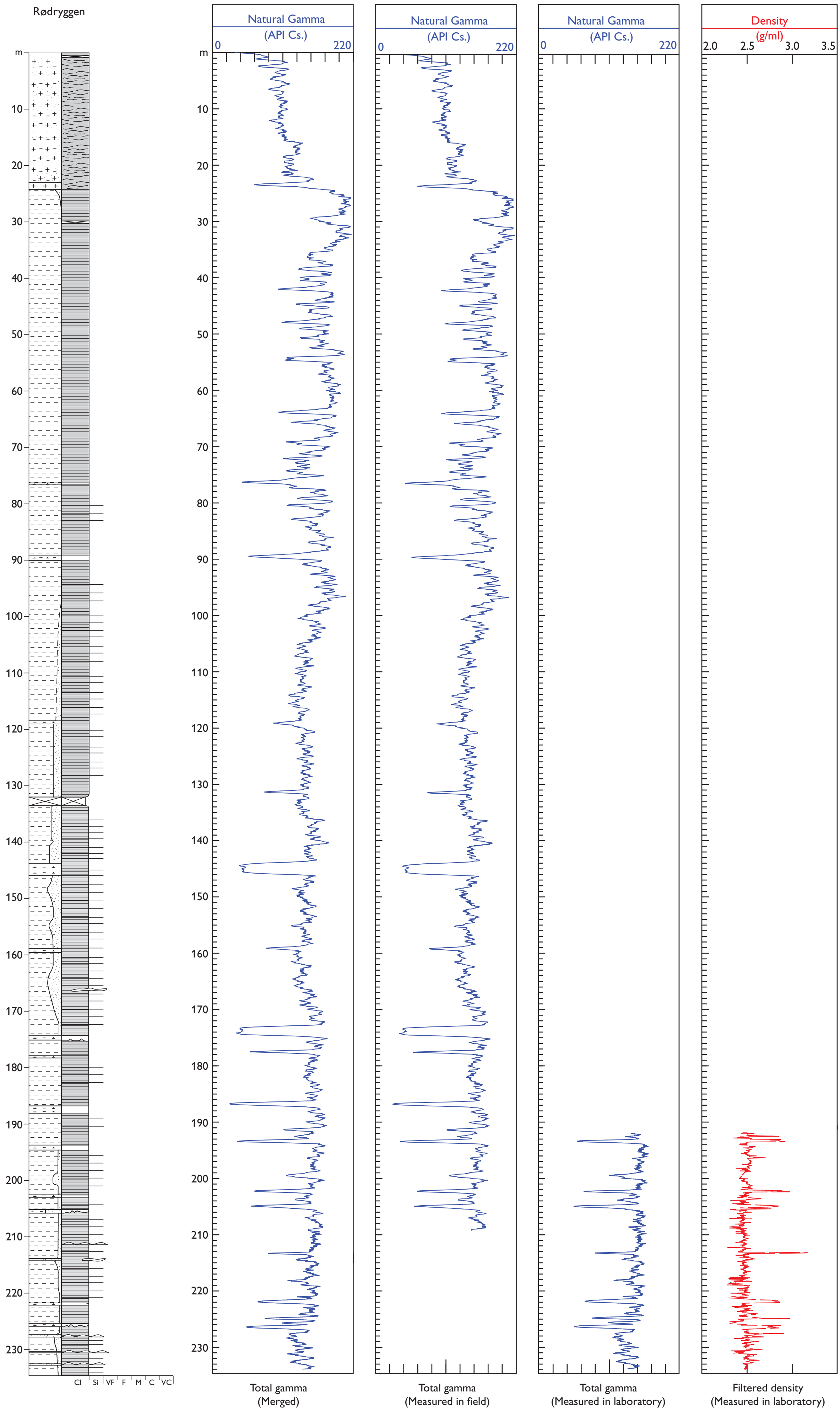

Figure 3.4.1 Gamma Ray logs (composite, measured in the field and in the laboratory) and density log together with the lithological column of the Rødryggen-1 well

3.5 Stratigraphic conclusions

The Rødryggen-1 core penetrates three major lithostratigraphic units: 1) Bernbjerg Formation (234.5–97.0 m), 2) Lindemans Bugt Formation (97.0–24.4 m), and 3) Palnatokes Bjerg Formation (Albrechts Bugt Member, 24.4–0 m). The lower boundary of the Bernbjerg Formation was not reached.

The boundary between the Bernbjerg Formation and the Lindemans Bugt Formation is transitional and occurs between 125–76 m. The formation boundary is herein placed at ~97 m, defined by the level where the GR increases to ~200 API for the first time. That level coincides more or less with biostratigraphic dating of the Middle Volgian, which is also the age of the base of the Lindemans Bugt Formation in outcrop elsewhere in Wollaston Forland. The formation transition is characterized by a gradational change in sedimentary facies, a change in dominance from terristrial to marine organic matter, increasing pyrite and fossil content. Moreover, the formation transition is well expressed in a variety of source rock characteristics such as increasing HI index, TS, S_1 and S_2 content (Chapter 8.1), and biomarker data (e.g., increasing C_{30} content; Chapter 8.2). Confinement of fractures to the Bernbjerg Formation compared to the overlying Lindemans Bugt Formation may reflect the post- Bernbjerg Formation and syn- Lindemans Bugt Formation tilting and movement during the Latest Jurassic maximum rifting and adds support to a subdivision into Bernbjerg and Lindemans Bugt Formations.

The contact between the Lindemans Bugt Formation and the Albrechts Bugt Member of the Palnatokes Bjerg Formation is gradational occuring within ca. 1 m (~25.5–24.4 m). The boundary is easily recognized as an abrupt decrease in GR values, increase in matrix carbonate- and sand-content, decreasing clay-content, change in matrix colour from black to light grey, increasing bioturbation intensity, change towards minimal organic content, and change in fossil content with nanofossils, foraminifers and *Buchia* shells becoming abundant.

The Rødryggen-1 core is succesfully subdivided into detailed biostratigraphic units that are referred to ammonite chronozones.

The ammonite zone, *S. primitivus* Zone known from NW-Europe, is now recognised in East Greenland providing the first direct correlation from Greenland to NW Europe.

Dinoflagellate events are correlated with the Boreal ammonite zonation. Some events are revised and their specific stratigraphic occurrences documented in East Greenland.

The drilled succession is dated Kimmeridgian – Late Valanginian on the basis of dinoflagellate, ammonite and nanofossil stratigraphy. The Bernbjerg Formation is Kimmeridgian – Lower Volgian, the Lindemans Bugt Formation is Middle Volgian – Upper Ryazanian and the Albrechts Bugt Formation is Upper Ryazanian – Upper Valanginian *pars.* Consequently, the source rock interval spans from Kimmeridgian to – Upper Ryazanian.

The stratigraphy of the drill site is more complex than was previously thought. The presence of Middle Volgian – Lower Ryazanian mudstones is demonstrated, and reflects that deposition was continuous from the Kimmeridgian to the late Valanginian (Fig. 3.1.1). The stratigraphic interval (97.0–24.4 m) is referred to the Lindemans Bugt Formation. Closest resemblances to that unit are found in the contemporaneous fine-grained Laugites Ravine Member and particularly the Niesen Member of the Lindemans Bugt Formation. However, these units are related to distal parts of fan deltas and are only known from the westernmost tilted fault blocks (the Kuppel and Kuhn Ø Blocks, Surlyk, 1978). Future work may support the present lithostratigraphic subdivision, but may also call for the establisment of a new member within the Lindemans Bugt Formation.

3.5.1 References

Surlyk, F. 1978: Submanrine fan sedimentation along fault scarps on tilted fault blocks (Jurassic–Cretaceous boundary, East Greenland). Grønlands Geologiske Undersøgelse Bulletin, **128**, 108 pp.

4. Sedimentology

The Rødryggen-1 core was sedimentologically and ichnologically described at a scale of 1:20. The sedimentological description included descriptions of lithology, grain size (visual estimation) and its trend, primary and secondary sedimentary structures, bedding contacts, soft-sediment deformation structures, mineralogical accessories and the identification of important stratigraphic surfaces. Ichnological data comprises description of ichnogenera, trace-fossil assemblage, cross-cutting relationship and bioturbation index (BI of Taylor and Goldring, 1993). BI provides a description of the degree to which original sedimentary fabric has been destroyed as a result of biogenic processes. This classification scheme allocates a numerical value ranging from 0 to 6 – the values corresponding to a percentage of bioturbation (cf. Taylor and Goldring, 1993). Undisturbed or non-bioturbated sedimentary fabrics are classified as BI 0 (0 percent reworked), while pervasively bioturbated media (100 percent reworked) are classified as BI 6. Intermediate levels of bioturbation are characterized using BI 1–5 and are defined as follows: BI 1, 1–4 percent reworked; BI 2, 5–30 percent reworked; BI 3, 31–60 percent reworked; BI 4, 61–90 percent reworked; and, BI 5, 91–99 percent reworked (Taylor and Goldring, 1993). Locally, lack of lithological contrast hindered exact delineation of the bioturbation degree.

4.1 Sedimentary facies

4.1.1 Bernbjerg and Lindemans Bugt Formations (234.55–24.4 m)

The studied deposits of the Bernbjerg Formation and Lindemans Bugt Formation interval are divided into 3 facies (F1-F3) and 5 sub-facies (F1A-F1C, F2A and F2B) based on their sedimentological and ichnological properties.

F1: Mudstone

F1A: Massive to laminated clayey mudstone (Figs. 4.2AB)

Description: F1A is a common facies type in the Lindemans Bugt Formation (core depth 24.4– ~97 m; Fig. 4.1), where it forms typically dm- to m-scale successions. It has the finest grain size of the described facies and shows typically the highest GR values of the succession (>180 API). The facies is typically interbedded gradationally with F1B, which leads to a serrated GR pattern (e.g., at depth 30–70 m). F1A consists of dark grey to black, massive-appearing or faintly laminated clayey mudstone. Bioturbation intensity fluctuates, ranging from unbioturbated to thin, completely bioturbated intervals (BI 0-6). Recognized trace fossils include diminutive *Zoophycos* and *Chondrites.* Most commonly, however, bioturbated intervals show indistinct, sub-mm to mm-scale burrow mottling (Fig. 4.2). The estimation of BI and recognition of trace fossils was locally hampered by lack of lithological contrast. Lithological accessories include common pyrite and marine organic matter; coal fragments are seen locally. F1A is fossil-rich, bearing ammonites, belemnites and molluscs.

Interpretation: The fine-grain size, locally high bioturbation intensity and the nature of the ichnofauna are all consistent with an overall low-energy marine setting. This interpretation is also supported by the sediment structures (local parallel-laminated clayey mud) and the lack of soft sedimentary deformation structures (which could otherwise be indicative of rapidly aggraded flocculated clay with a high water content). The trace fossil assemblage reflects a stressed, probably oxygen restricted setting (e.g., Martin, 2004). This interpretation is in line with the common occurrence of pyrite and well-preserved organic matter.

Considering the above mentioned sedimentological and ichnological properties coupled with the stratigraphic occurrence of the facies (see below), F1A is interpreted to represent an oxygen-deficient basinal environment.

F1B: Colour-banded mudstone (Figs. 4.2CD)

Description: F1B is a common sub-facies type in the Lindemans Bugt Formation (core depth 90–30 m). It alternates gradationally with F1C and F1A, being an intermediate facies type between these two sub-facies. On the GR log, F1B shows intermediate values commonly ranging between 120–150 API. The facies consists of interlaminated clayey mud, pyrite, and ankerite-rich mud, which leads to the colour-banding that is characteristic of the facies. The biogenic component, both terrestrial (e.g., disseminated coal fragments) and marine (e.g., *Onychites* (belemnite fragments), ammonites, molluscs and other bioclasts), is typically very high. Pyrite can locally form up to 30% of the volume of the facies. F1B typically appears to be unbioturbated (BI 0) and shows small-scale soft-sedimentary deformation structures (micro-slumps consisting of contorted lamination and micro-scale loading structures). Lack of lithological contrast hinders determination of bioturbation intensity locally in black mudstone-dominated intervals.

Interpretation: Abundant small-scale soft sedimentary deformation, up to a few mm-thick mud-drapes rich in terrestrial organic matter, and local lenticular lamina suggest that deposition was probably from muddy gravity flows rather than being solely a result of hemipelagic suspension fall-out. The gravity flows were probably facilitated by the increasing depositional gradient due to Middle Volgian – Early Ryazanian fault block development (Surlyk, 1978; 2003). The localised ankeritic laminae probably reflect rare primary laminae rich in bioclasts (e.g., calcispheres; see F1C description).

Considering the above-mentioned sedimentological and ichnological properties coupled with the stratigraphic occurrence of the facies (see below), F1B is interpreted to represent the accumulation of oxygen-deficient, basinal mudstone in a tilted fault block setting (see discussion) occasionally sourced by muddy gravity flows.

F1C: Ankerite- and dolomite-cemented mudstone (Figs. 4.3A-C)

Description: F1C is a recurring facies type between 230–70 m in the core. It occurs most commonly as dm-scale intervals. On the GR log, F1C is readily identified as an anomalously low GR peaks (20-50 API) that typically occur within an interval of overall high GR readings (base of upward coarsening interval), or at the very top of coarsening-upward successions. F1C consists of ankerite- and dolomite-cemented mudstone (Chapter 5 and 3.3), which characteristically shows interlaminated laminated mudstone and bioclasts. The bioclasts are replaced by pyrite and ankerite. Although poorly preserved, their typical circular cross-section is suggestive of calcispheres, some vase-shaped cross-sections resemble calpionellids (Fig. 4.3C). Locally, F1C shows soft sedimentary deformation and changes in lamina angle in comparison to bounding facies. Accessory minerals include common pyrite and phosphate (at ~89.8 m; Chapter 5).

F1C is mainly unbioturbated (BI 0), but particularly in the Lindemans Bugt Formation, it may include thin burrow mottled intervals (BI 0-6).

Interpretation: The enrichment in bioclastic material and authigenic minerals (phosphate) are best explained by reduced sedimentation rates (condensation) during transgression. This interpretation is supported by locally increasing bioturbation intensity and the stratigraphic occurrence of F1C at the very top/base of parasequences. Soft sedimentary deformation features and locally occurring rapid changes in lamina angle suggest that some of the F1C layers are probably reworked.

F2: Interlaminated clay, silt and sand (Figs. 4.4A-G)

*Description**:*** F2 is a dominant facies type in the Kimmeridgian – Lower Volgian-Bernbjerg Formation (234.5 –~97 m; Fig. 4.1), where it typically forms several meters-thick aggradational (i.e. trendless facies successions) successions. It is a transitional facies type with F3 (see below) and can be gradationally or erosionally interbedded with this facies. In addition, F2 is locally intercalated with F1C. On the GR log, F2 forms aggradational successions displaying relatively uniform GR values (~140-160 API). Locally, intervals dominated by F2 show stacked funnel-shaped GR-patterns, a few meters-thick (e.g., 175–148 m).

F2 can be divided into two sub-facies: F2A consists of parallel laminated silt and clay; and F2B comprises interlaminated very fine grained sand/ coarse silt and clay. F2B forms erosionally based a few mm-thick, upward fining lamina sets that may grade into F2A. Ideally, the lamina set consist of the following components (Figs. 4.4CD): 1) a basal micro-scoured contact below mm-scale very fine grained sandstone or coarse silt lamina (unit A). This basal lamina shows lateral thickness variability, pinch-outs and may contain inclined sub-mm-thick mud-drapes. The basal unit A is abruptly overlain by mm-thick parallel laminated clay and silt (unit B), which further grade into a (unit C) massive mud-drape that may contain patches of pyrite. Finally, in rare instances, diminutive sub-mm scale burrow mottling descends from the uppermost mud-drape.

In addition to the upward fining lamina couplet, F2B shows locally subtle changes in lamina angle, lamina truncations, and on-lapping lamina contacts, particularly where the facies is interbedded with F3 (Figs. 4.4EF). Soft sedimentary deformation is also very common and occurs as mm- to cm-scale micro-slump units (contorted Z-shaped lamina (Fig. 4.4G).

F2A differs from F2B in that it lacks internal erosional contacts, sand, clear normal grading, and high-frequency changes in lamina angle. Moreover, it contains more common pyrite and displays rare burrow mottled intervals. F2 is most commonly unbioturbated, but locally sporadic diminutive burrow mottling is recorded (BI 0-2).

Interpretation: The tripartite lamina sets are identical to wave-enhanced gravity flow deposits recently described by Macquaker et al. (2010; Figs. 4.4BCD). They proposed a three-phased flow model to explain the formation of these structures (summarized in Fig. 4.4D): 1) wave-induced turbulence and resuspension forms an erosionally-based sand or coarse silt lamina (unit A); 2) The increasing sediment concentration in the wave boundary layer damps turbulence, a pressure gradient develops and gravity flow begins. Shear mixing at the base of the laminar flow and mixing with sediment already in suspension results in the deposition of interlaminated silt and clay (unit B). 3) As the flow energy wanes, the lutocline collapses (i.e., suspended fluid mud cloud), flow stops, and the deposits grade into a mud drape (Unit C). The wave-enhanced gravity flow interpretation is further supported by the fact that F2B grades into wave-ripples (F3). The distribution of F2B suggests that much of the Bernbjerg Formation was deposited in a shallow basin above storm wave base. Moreover, the data show that despite the mud-dominated lithology, the bulk of the sediment volume was probably deposited as thin event laminae. This interpretation is further supported by lamina pinch-outs, lamina truncations and onlapping lamina contacts, which also suggest a traction component in sedimentation (Schieber et al., 2007). The thinness of the F2B occurrences (only up to a few mm) and the very subtle, low relief erosional contacts at the base of the event lamina suggest that the events were of low energy. Rarity of bioturbation, however, suggests that the event frequency was high.

F2A occurrences lack signs of erosive oscillation currents and traction deposition. However, it locally appears to display the units BC above described, which may indicate that this sub-facies was influenced by distal wave-initiated gravity flow currents that extended below storm wave base due to a high bottom gradient. This interpretation is indirectly supported by very common presence of micro-slumps, which indicate the presence of a slope and a gravity flow prone depositional setting. F2A is locally bioturbated suggesting lower event frequency and more protracted colonization window than in F2B.

In summary, considering the above mentioned sedimentological and ichnological properties, as well as the stratigraphic occurrence of the facies, F2B is interpreted to reflect wave-enhanced gravity flow deposition on a relatively high-gradient shelf. These flows possibly extended some distance below storm wave base as slope maintained gravity flow currents (F2A).

F3: Ripple cross-stratified sand (Figs. 4.5A-C)

Description: F3 is a recurring facies type near the base of the core (ca. 200-234 m; Fig. 4.1). It consists of cm-scale layers of ripple cross-stratified very fine-grained sandstone that are typically interbedded with F2. Together these facies form m-scale upward coarsening or fining successions (Fig. 4.1.). On the GR log, F3 is not always clearly expressed (due thinness of the layers) and shows variable values ranging between ~80-120 API. The ripples are locally symmetrical and are characterized by irregular lower bounding surfaces and bipolar foresets. Locally, anomalously thick massive mud-laminae are associated with the sand lenses. F3 is unbioturbated (BI 0). Soft sedimentary deformation and terrestrial organic matter are common.

Interpretation: Irregular lower bounding surfaces, locally bipolar foresets and symmetrical ripple forms indicate that the ripples were wave-influenced. The thickest structureless mud-drapes are associated with ripples, which probably points to the formation of flocculated clay (wave-generated fluid mud). Considering the stratigraphic occurrence of the facies, F3 is interpreted to represent storm-influenced proximal offshore deposits on a muddy shelf.

4.1.2 Albrechts Bugt Member (24.4–0 m)

The studied Albrechts Bugt Member interval consists of one facies (F4), which can be further divided into two sub-facies (F4A and F4B). Most commonly, however, the deposits represent intermediate facies occurrences.

F4: Bioturbated mudstone

F4A: Bioturbated limestone or marly mudstone (Figs. 4.6AB)

Description: Facies 4A is a subordinate facies type occurring sporadically throughout the studied Albrechts Bugt interval. On the GR log, the facies is recognizable by displaying the lowest API values (~ 60 API). It typically forms cm- to dm-scale successions and consists of fully bioturbated (BI 6) limestone or marly mudstone. The deposits are mainly burrowed with diminutive *Chondrites* and indistinct sub-mm scale burrow mottling. Subordinate trace fossils include abundant overprinted *Zoophycos* and larger (up to 1.5 mm in diameter) mud-filled *Chondrites.* Disseminated pyrite is pervasive.

Interpretation: Low diversity to monospecific occurrences of *Chondrites*-dominated trace fossil assemblages may point to a stressed, possibly oxygen restricted environment (e.g., Martin 2004). Alternatively, *Chondrites* dominated ichnofabric may reflect dominance of deep tier trace fossils. Indeed, the observed high bioturbation intensity and compound ichnofabric (cross cutting, reburrowing) indicate very low sedimentation rates and ambient depositional energy. The very low clastic sediment input is interpreted to be due to the late syn-rift – early post-rift paleogeographic configuration (compartmentalizated basin) and eustatic sea level rise (Surlyk, 1978). Consequently, F4A is interpreted as sediment-starved basinal deposits.

F4B: Bioturbated, light grey sandy mudstone (Figs. 4.6CD)

Description: F4B is the dominant facies type in the studied Albrechts Bugt Member interval. It consists of variably bioturbated sandy mudstone forming m-scale trendless intervals. Typically, the GR log is relatively non-serrated (~90-120 API). The sandstone content is commonly 20-40%, but locally, the facies may grade into muddy very fine to fine grained sandstone. The matrix carbonate-content is also variable and locally it is concentrated in irregular cemented patches.

F4B is moderately to intensively bioturbated (BI 2-6) with a low diversity assemblage consisting of very common *Zoophycos* and *Chondrites*, and subordinate *Thalassinoides* and *Planolites.* In addition, *Helminthopsis*-like, horizontally-oriented dark mud-filled burrows occur locally. At least some of the *Helminthopsis*-like burrows, if not all, are diminutive *Zoophycos,* where the causative burrow is barely visible due to its sub-mm scale size. In contrast to F4A, cross-cutting and re-burrowing is less well developed. Minerological accessories include abundant pyrite that occurs either disseminated or as large clusters. Pyrite-filled fractures are also common. Shell fragments and reworked molluscs are pervasive.

Interpretation: Variable bioturbation intensity coupled with common shell fragments, reworked molluscs and high-matrix sandstone content suggest variable depositional rate and presence of bottom currents. Furthermore, the compound ichnofabric is less developed than in F4A also pointing to increased sedimentation rate. This is either due to the influence of distal gravity flow currents from the contemporary fan deltas or to approaching wave-base. Nevertheless, the *Zoophycos*-dominated low diversity trace fossil assemblage indicates the environment remained dominantly of low-ambient energy with a low event deposition frequency. The presence of pyritized fractures shows that pyrite formation, at least in part, is late. Similarly, the observed patchy distribution of matrix carbonate may suggest that part of the matrix carbonate is post depositional and may relate to dissolution of fossil material.

4.2 Discussion and conclusions

The Rødryggen core penetrates three major lithological units: 1) Kimmeridgian – Lower Volgian Bernbjerg Formation, 2) Middle Volgian – Lower Ryazanian Lindemans Bugt Formation and 3) Upper Ryazanian – Upper Valanginian Palnatokes Bjerg

Formation (Albrechts Bugt Member). In the following, the sedimentary facies described above are discussed in the context of chronostratigraphic zonation and the tectonic evolution of the area in order to get a wider insight into the paleoenviromental development and source rock controlling factors in these deposits.

The black shale succession described reflects an overall transgressive setting from a wave-influenced, shallow deltaic shelf (Bernbjerg Formation; cf. Surlyk and Clemmensen, 1983; Surlyk, 1990) to a restricted basinal environment below maximum storm wave base (Lindemans Bugt Formation; Fig. 4.1). This overall transgressive trend is punctuated by a subtly prograding to aggrading interval between ~172–124 m, which contains local 3–8 m-thick, poorly defined upward coarsening parasequences, which ideally consist of F1C-F2A-F2B-(F3) successions. Most commonly, however, facies successions show subtle F2A-F2B alternation. This unbioturbated interval hosts elevated coarse siltstone content (20-40%), shows common soft sedimentary deformation and signs of wave-reworking, features which in concert suggest increased depositional rate. This zone also correlates with decreasing source rock quality (Chapter 8).

In general, trace fossil content suggests that the Bernbjerg Formation is a somewhat atypical shelf environment: it is only sparsely bioturbated and there is a complete lack of grazing structures (*Phycosiphon, Helminthopsis*) and many other typical elements of the distal *Cruziana* Ichnofacies, which are commonly present in storm-influenced proximal offshore settings (e.g., MacEachern et al., 2007). Instead, the deposits are mainly unbioturbated and contain only thin intervals of monospecific to very low-diversity trace fossil assemblages comprising generally diminutive burrow mottling. This, coupled with widespread occurrence of micro-slumps and wave-generated sedimentary structures, is interpreted to result from combination of moderate depositional rate, locally low substrate consistency, and possibly dysoxic setting (but no anoxia). The soft sedimentary deformation structures are nearly exclusively horizontally oriented (no loading structures) consisting of Z-shaped contorted lamination. This may further suggest that the shelf was of relatively high gradient, and probably prone to mud-dominated gravity flow currents.

The change from the Bernbjerg Formation to the Lindemans Bugt Formation is gradational, and probably corresponds to increased tectonic activity in the Wollaston Forland area during the Middle Volgian (Surlyk, 1978; 1990; 2003; Fig. 4.1). This rift climax resulted in accelerated tilted fault block development and basin segmentation and lasted until the Early Ryazanian. As a result, the basin geometry changed from the Kimmeridgian – Early Volgian regionally continuous shelfal setting to narrow, 10–30 km wide, S-N oriented basins that were strongly tilted westwards (Surlyk, 1978; Figs. 4.7, 4.8). The Rødryggen core penetrates the Permpas fault block, and is situated ~20 km east of the main fault zone (the Dombjerg fault; Fig. 4.8). During the Middle Volgian, major conglomeratic fan deltas developed east of the Dombjerg fault (Surlyk, 1978). The eastern limit of the fan delta deposits was controlled by the Kuppel Fault, which delineated the western margin of the Permpas block. Due to the basin segmentation and changes in sediment source areas, the Permpas block became isolated from the main deltaic sedimentation and received progressively less terrestrial clastic sediment input during the ongoing rifting. This is directly reflected in the sedimentary facies, which suggest transformation into a deeper, oxygen restricted basin below storm wave base (F1AB) during the Middle Volgian. The Early – Late Ryazanian interval appears to be most condensed, and records the first appearance of well-developed *Zoophycos* (Fig. 4.1).

The observed facies change at the Bernbjerg Formation – Lindemans Bugt Formation boundary is strongly reflected in source rock characteristics: the Lindemans Bugt Formation interval contains a markedly more marine source rock than the Bernbjerg Formation interval (e.g., Fig. 8.2.7). Finally, any estimations of source rock volumes should take account of the change in basin geometry during the deposition of these strata. In this regard, future lithocorrelation with the Brorson Halv Ø core situated at the footwall crest is expected to give a further insight to the timeing of faulting and geometry of these units.

The change from the Lindemans Bugt Formation to the Albrechts Bugt Member (Palnatokes Bjerg Formation) is also partly gradational and associated with relatively abrupt decrease in clastic sediment input into the basin. Albrechts Bugt Member accumulation coincided with the late syn-rift – early post-rift phase, when the basin was fully segmented and affected by eustatic sea level rise (Surlyk, 1978; Fig. 4.6). The interpretation of limited clastic input and sedimentation rate is supported by the high fossil content, increased bioturbation intensity, strongly composite ichnofabric (cross-cutting, reburrowing), and the nature of the ichnofauna. In particular, the most common trace fossil in the studied section, *Zoophycos*, is a typical trace fossil of non-tempestitic/turbiditic settings. The monospecific and very low diversity assemblages consisting of *Zoophycos* and *Chondrites* reflect a very stressed environment with prolonged periods of non-deposition. The locally fluctuating bioturbation intensity reflects episodes of increased depositional rate.

4.3 References

MacEachern, J.A, Bann, K.L., Pemberton, S.G., and Gingras, M.K., 2007: The Ichnofacies Paradigm: High-Resolution Paleoenvironmental Interpretation of the Rock Record. In: MacEachern, J.A et al., (eds.): Applied Ichnology: SEPM, Short Course Notes 52, 27–64.

Macquaker, J., Bentley, S., and Bohacs, K., 2010: Wave-enhanced sediment-gravity flows and mud dispersal across continental shelves: Reappraising sediment transport processes operating in ancient mudstone successions. Geology,, **38**, 947–950.

Martin, K.D., 2004: A re-evaluation of the relationship between trace fossils and dysoxia. In: McIlroy, D., (ed.): The Application of Ichnology to Palaeoenvironmental and Stratigraphic Analysis. Geological Society, London, Special Publication, no. 228, 141–156.

Myrow, P., Fischer, W., and Goodge, J., 2002: Wave-modified turbidites: combined-flow shoreline and shelf deposits, Cambrian, Antarctica. Journal of Sedimentary Research, **72**, 641–656.

Schieber, J., Southard, J., And Thaisen, K., 2007: Accretion of mudstone beds from migrating floccule ripples. Science, **318**, 1760–1763.

Surlyk, F. 1978: Submarine fan sedimentation along fault scarps on tilted fault blocks (Jurassic–Cretaceous boundary, East Greenland). Bulletin Grønlands Geologiske Undersøgelse, **128**, 108 pp.

Surlyk, F. 2003: The Jurassic of East Greenland: a sedimentary record of thermal subsidence, onset and culmination of rifting. In: Ineson, J.R. & Surlyk, F. (eds): The Jurassic of Denmark and Greenland. Geological Survey of Denmark and Greenland Bulletin, **1**, 659–722

Surlyk, F. & Clemmensen, L.B. 1983: Rift propagation and eustacy as controlling factors during Jurassic inshore and shelf sedimentation in northern East Greenland. Sedimentary Geology, **34**, 119–143.

Taylor, A.M., and R. Goldring, 1993: Description and analysis of bioturbation and ichnofabric. Journal of the Geological Survey, London, **150**, 141–148.

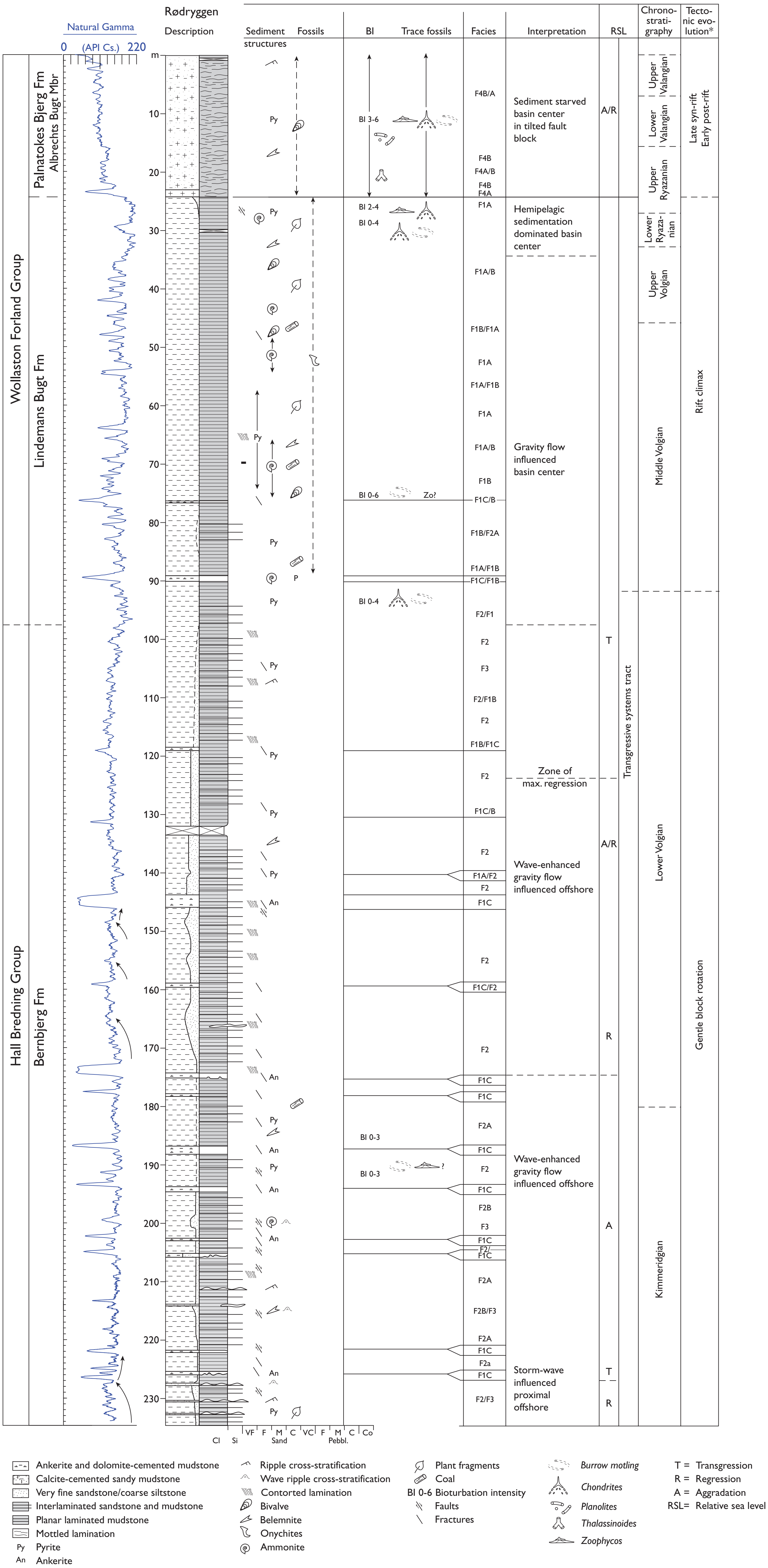

Figure 4.1 Sedimentary log of the Rødryggen-1 core. Tectonic evolution of the Wollaston Forland area is adapted from Surlyk (2003).

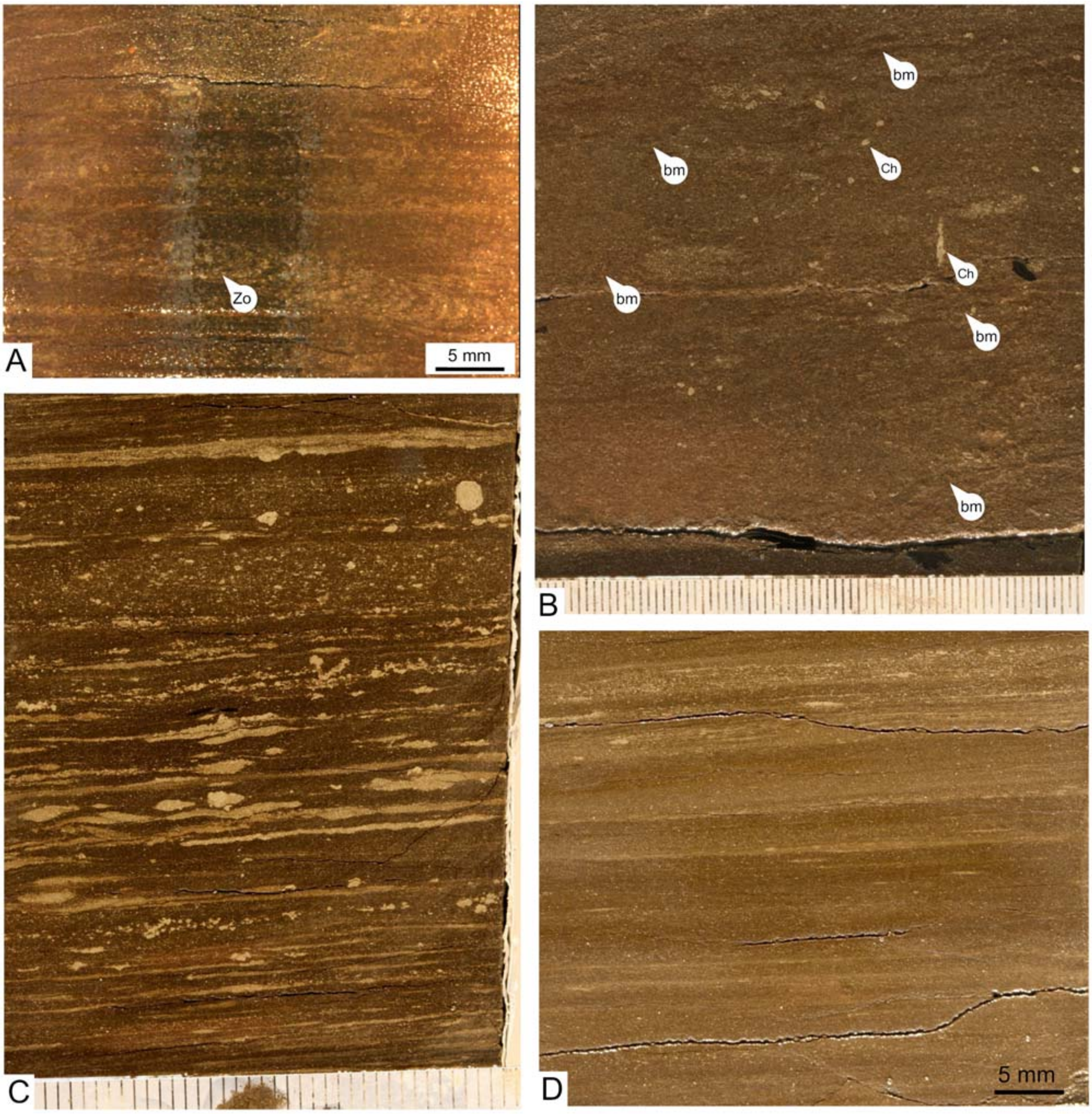

Figure 4.2. A-B) Bioturbated black mudstone (F1A). A) Colour-enhanced view of black, laminated to bioturbated mudstone. Zo–*Zoophycos.* Background trace fossils include small *Chondrites*. B) Intensively bioturbated black mudstone. bm–burrow mottling, Ch–*Chondrites.* C, D) Colour banded mudstone (F1B). C) Laminated mud and pyrite. D) Laminated mud, pyrite and ankerite-rich mud.

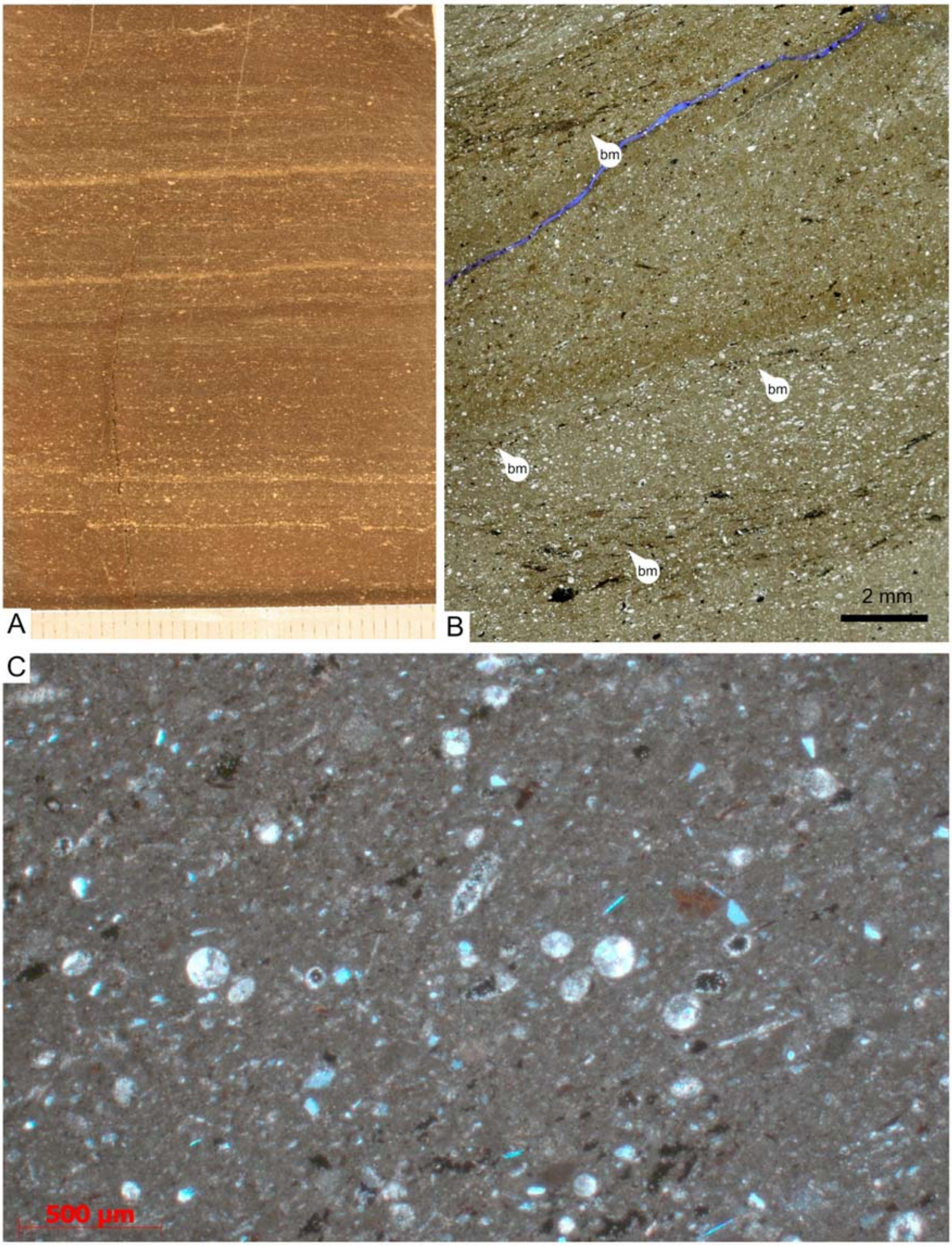

Figure 4.3. A-C) Examples of ankerite- and dolomite-cemented mudstone intervals (F1C). A) Laminated mudstone and bioclasts. B) Burrow-mottled interval showing enrichment in bioclastic material. C) Photomicrograph show moulds of microfossils now filled with pyrite and ankerite cement. Most microfossil cross-sections are sub-circular (i.e. resemble calcispheres) but rare examples show cup or vase-shaped cross-section comparable to calpionellids.

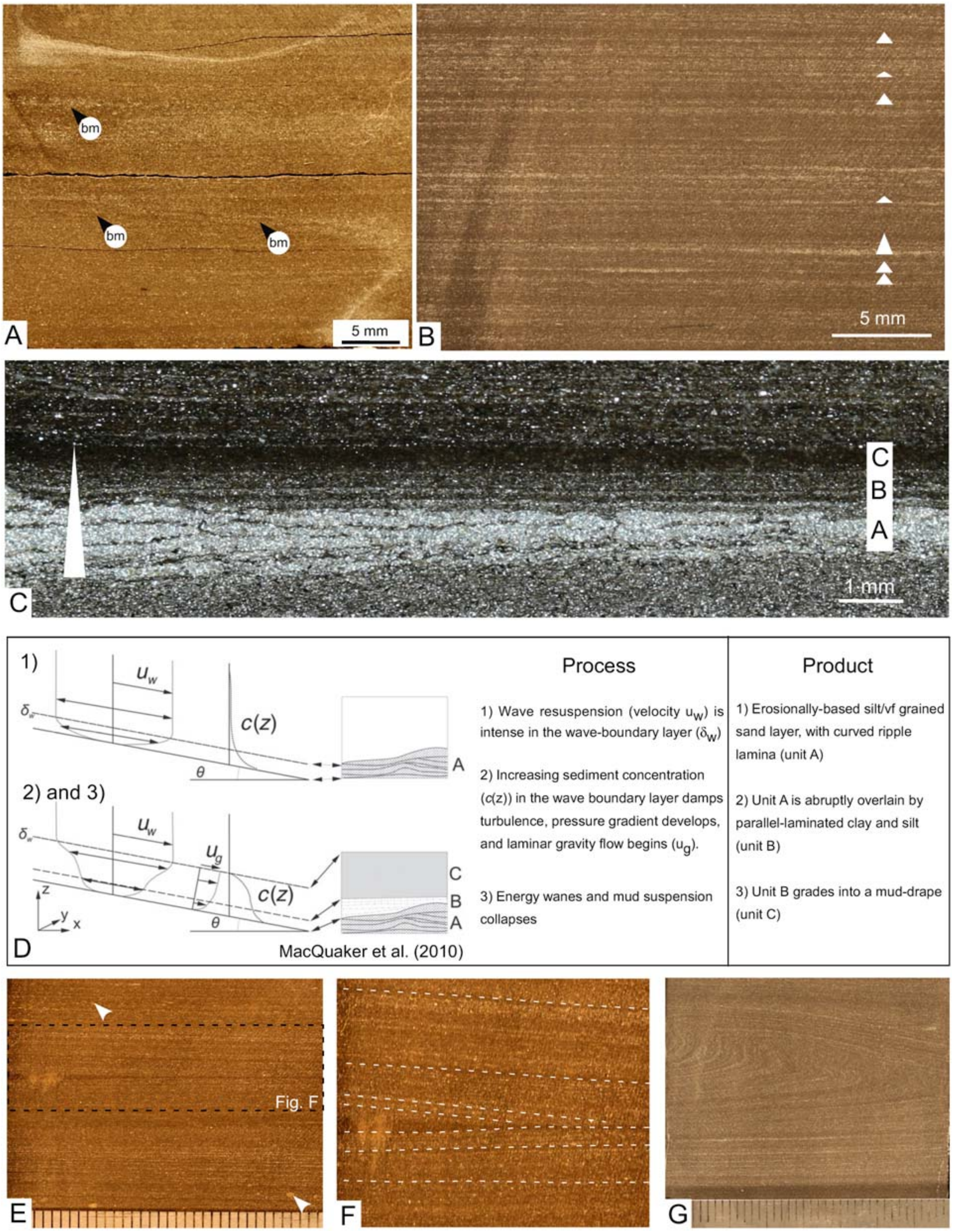

Figure 4.4. Examples of interlaminated mud and sand (F2). A) Parallel laminated mud with burrow-mottled intervals (F2A). B) Interlaminated very fine-grained sand, silt and clay. Note the presence of subtle normally graded lamina sets, indicated by white arrows (F2B). C) Photomicrograph of an upward fining lamina set showing characteristic tripartite

microstratigraphy: Basal, erosionally-based sand/coarse silt lamina (unit A), parallel laminated silt and clay (unit B), and mud-drape (unit C). D) Hydrodynamic interpretation of the lamina set fromMacquaker et al. (2010). See text for further discussion. E) Quasi-parallel heterolithic interlamination (F2B). Black dash-lined box shows the location of Figure F. White arrows indicate pyrite patches. F) 2.5 x vertical exaggeration of the previous figure. Note changes in lamina angle and onlapping/downlapping lamina contacts in the middle of the figure. G) Example of micro-slump interval consisting of contorted lamination.

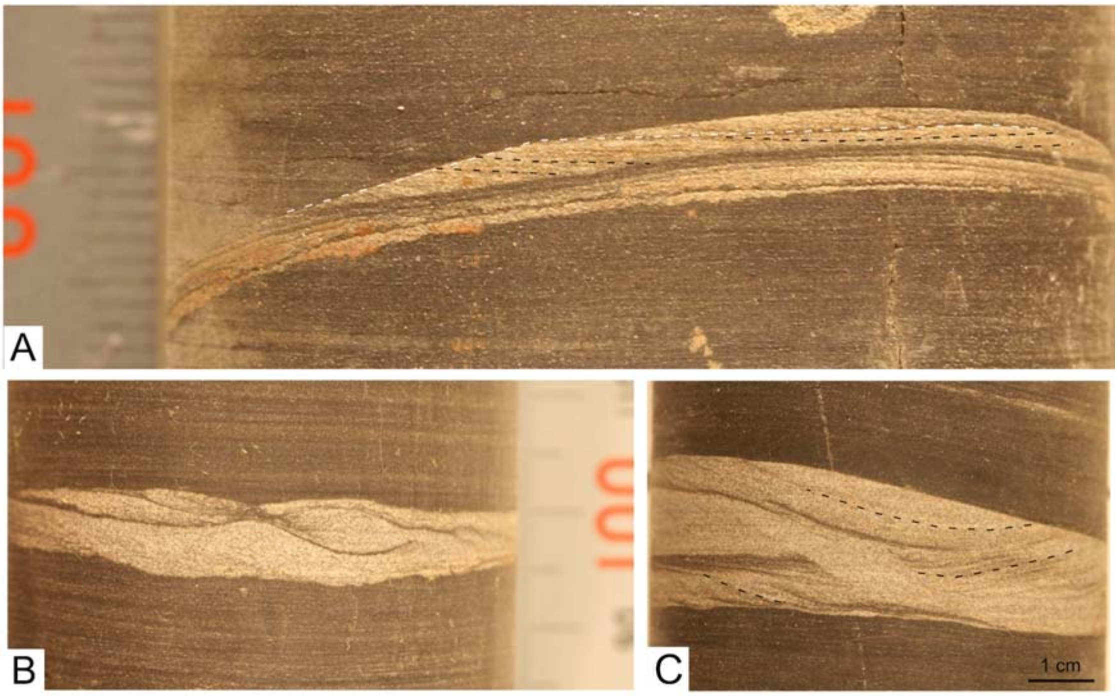

Figure 4.5. A-C) Examples of wave-ripple cross-stratification (F3) interbedded with F2. A) Low-relief ripples showing bidirectional foresets (black dashed line). B) Symmetrical ripple profile characteristic of wave ripples. C) Ripple cross-stratification.

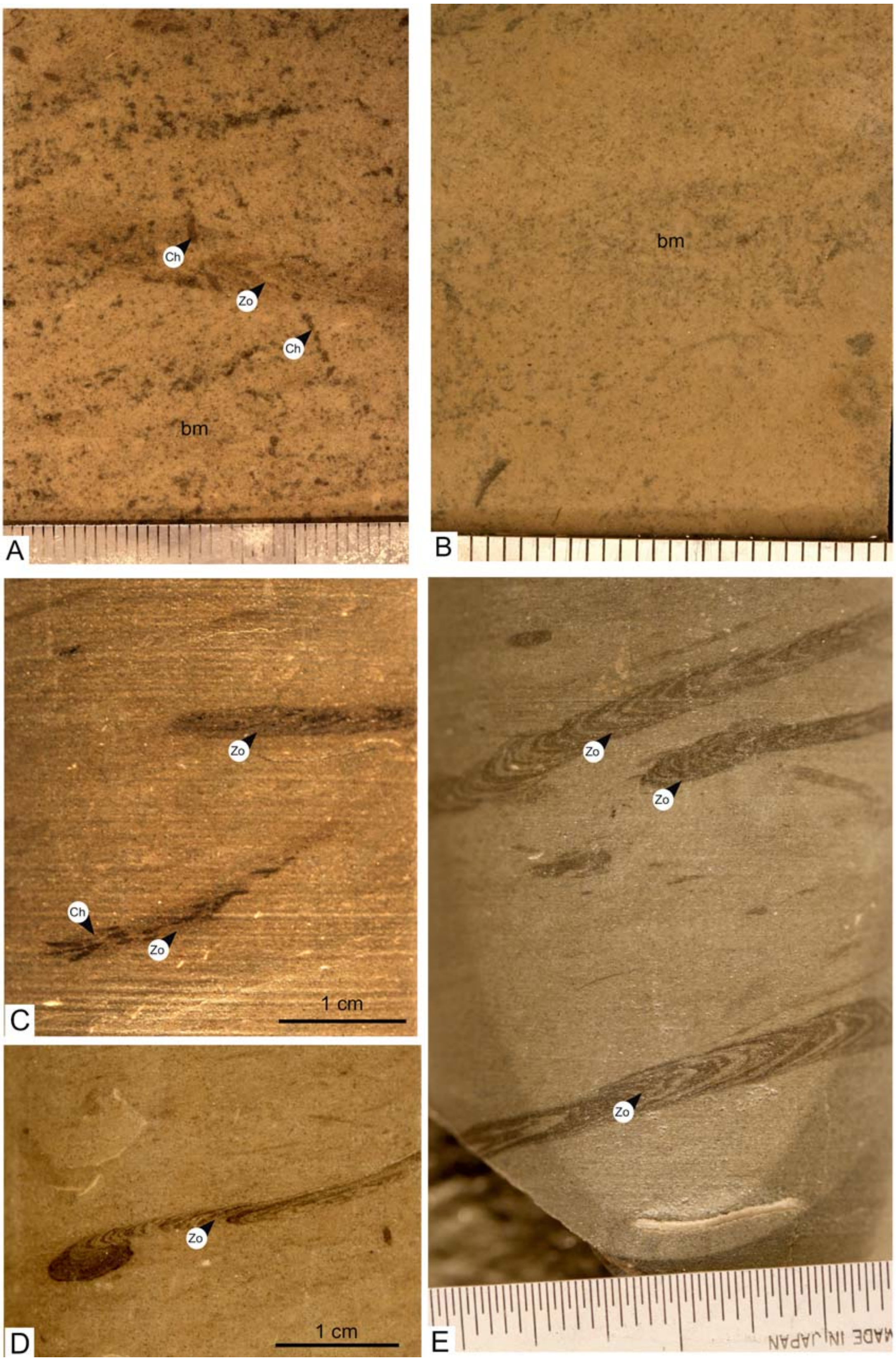

Figure 4.6. Sedimentary facies of the Albrechts Bugt Member. A, B) Fully bioturbated limestone/marly mudstone (F4A). C-E) Bioturbated sandy calcareous mudstone (F4B). Note that the apparent lamina in (C) is an artefact (drill-marks on core surface).

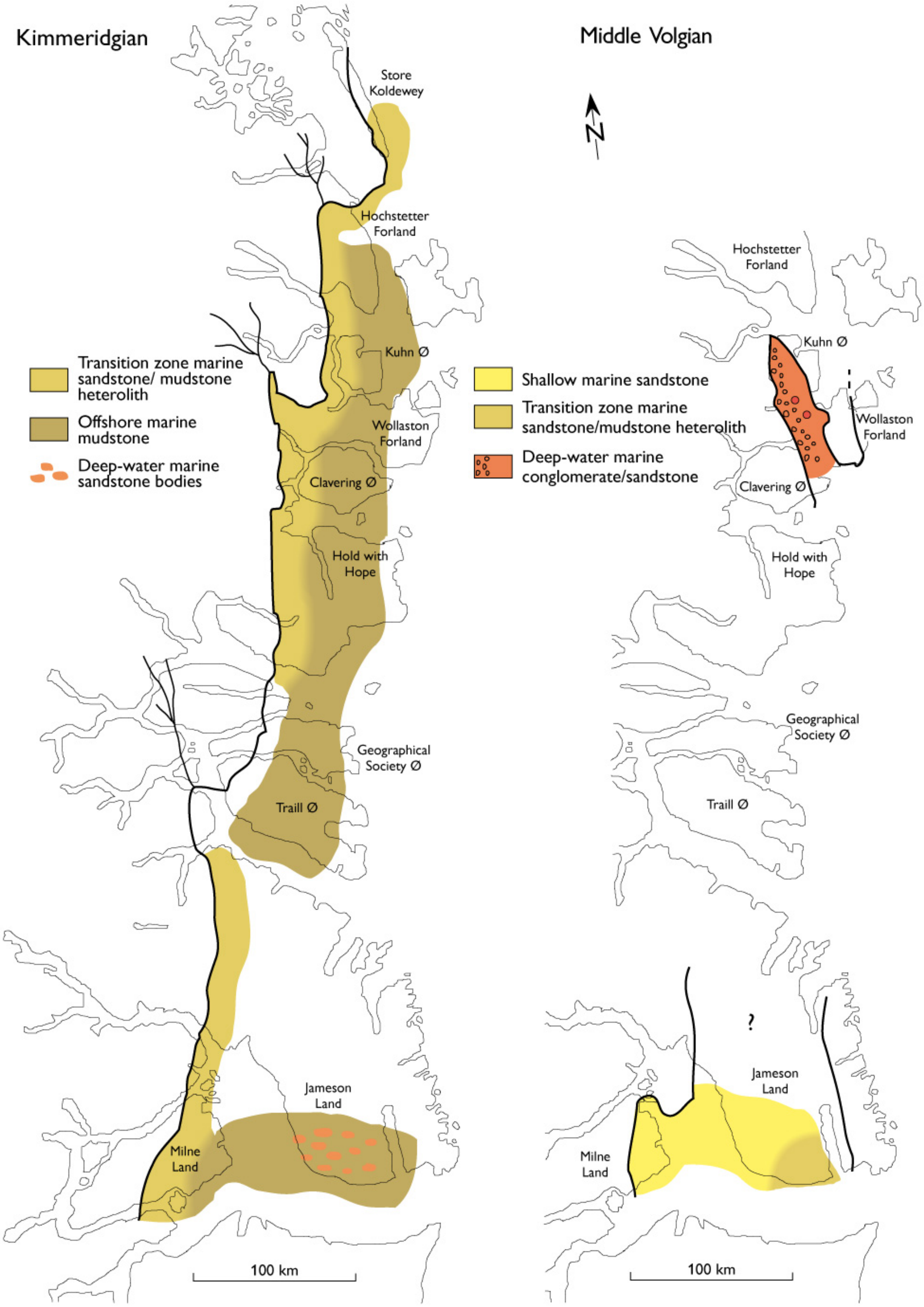

Figure 4.7. Paleogeographic maps showing regional paleoenvironmental settings during the Kimmeridgian – Early Volgian (Bernbjerg Fm) and the Middle Volgian – Early Ryazanian (Lindemans Bugt Fm.) times. From Surlyk (2003).

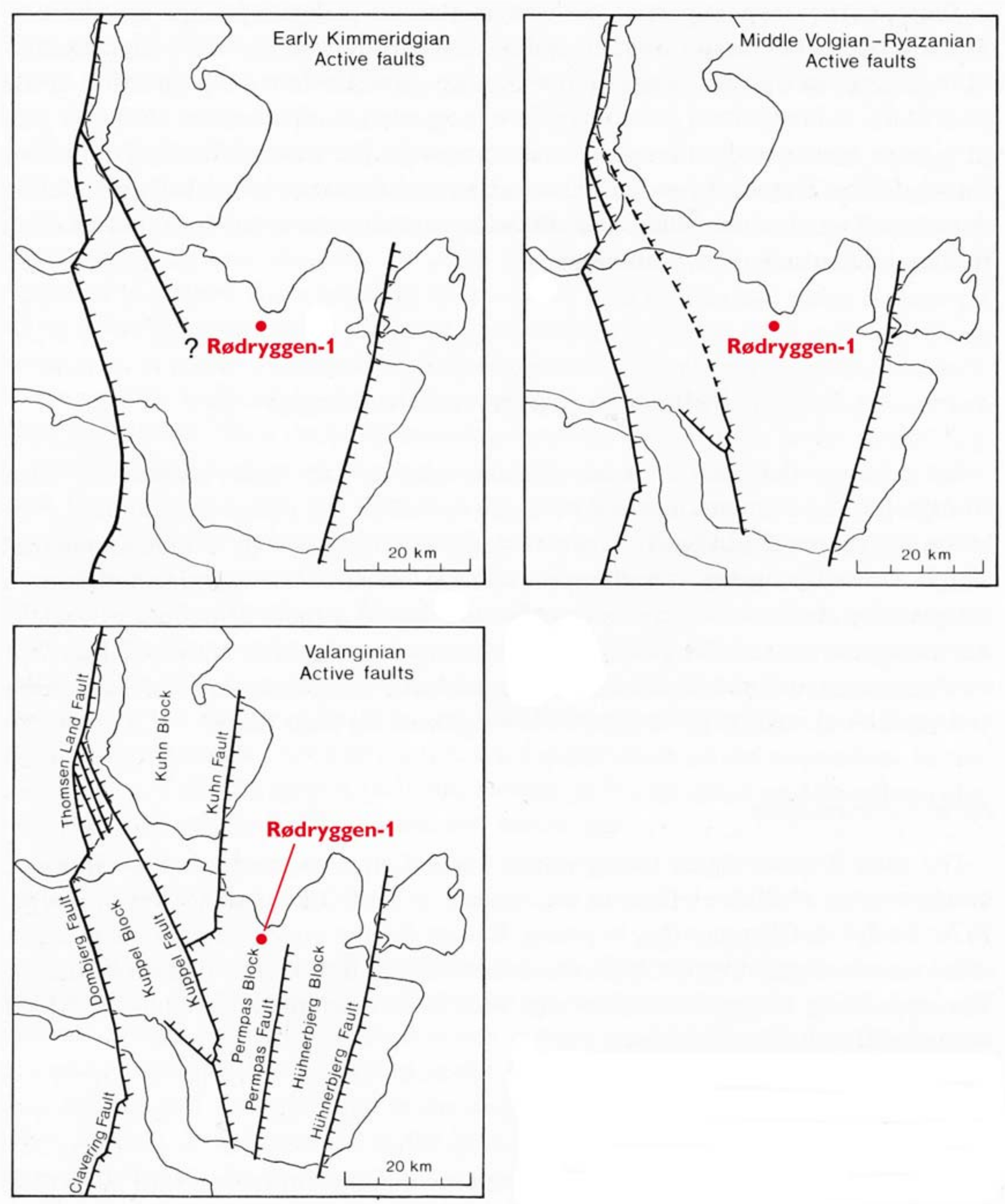

Figure 4.8. Tectonic evolution of Wollaston Forland during the late Jurassic – Early Cretaceous (modified after Surlyk, 1978). A) During the Kimmeridgian – Early Volgian (Bernbjerg Fm) the area was influenced by gentle block rotation. B) During the Middle Volgian – Early Ryazanian (Lindemans Bugt Fm) the area experienced strong tectonic activity. As a result, the previously laterally continuous platform was dissected into narrow, N–S oriented basins that were tilted westwards. The studied Permpas block became effectively isolated from the main deltaic sedimentation and received progressively less terrestrial clastic sediment input during the ongoing rifting (see Fig. 4.1.). C) During the Valanginian (Albrechts Bugt Mbr.) the late syn-rift – early post -rift basin was fully segmented and was drowned by a eustatic sea level rise.

5. Mineralogy and Diagenesis

The relationship between cemented and uncemented mudstone in the Rødryggen-1 core was evaluated through mineralogical and diagenetic examinations. Intervals of both mudstone and cemented mudstone were chosen from each formation covering all facies, whereas the rarity of sandstone only made a few analyses possible. A single interval of pore-filling cement was also included. The large content of authigenic minerals affecting the porosity and permeability were evaluated by including several methods to determine the diagenetic sequence of mineral reactions. However, the fine-grained nature of the sediments has prevented point counting in thin sections.

5.1 Methods

5.1.1 X-Ray Diffraction

The bulk and clay mineralogy was measured by X-Ray Diffraction (XRD) on 21 samples by GEUS, Copenhagen. The edge of the core was removed to avoid contamination. The samples were gently hand ground to pass a 250 µm sieve. XRD was carried out on randomly oriented specimens using a Philips 1050 goniometer with fixed divergence, anti-scatter slits and Co-K α-radiation (pulse-high selection and Fe-filter). Organic matter was removed in the chemical pre-treatment using NaOCl of pH 9.0. The samples were dispersed ultrasonically in distilled water in order to obtain the clay fraction <2 µm for analysis. The fraction >30 µm was removed by sedimentation and the 2-30 µm by centrifugation in a centrifugal particle size analyser (Slater and Cohen, 1962). The suspensions were flocculated in 1 M NaCl. Excess salt was removed by centrifugation and washing with water and ethanol. The fraction was then air-dried. Three oriented specimens were prepared for each sample by the pipette method as follows: Mg-saturated air-dry, Mg-saturated with glycerol added to the suspension and K-saturated air-dry heated for 1 hour at 300°C. The clay fractions were investigated by XRD producing a diffractogram for each of the three saturated specimens for each sample. The discrete minerals were identified from peak positions on the XRD diffractograms and semi-quantified by application of correction factors obtained for another instrument.

5.1.2 Thin sections

Thin sections were produced from 14 samples by GeoTech Labs, Canada, of intervals with diagenetic features characterizing the core. Polished thin sections were prepared from 3.6*2.4*0.5 cm sandstone samples using blue epoxy for the impregnation to help the identification of free pore space. Half of each thin section was etched and stained with sodium cobaltinitrite for K-feldspar identification.

5.1.3 Scanning Electron Microscopy

Scanning Electron Microscopy (SEM) analyses were made on 13 samples and 6 thin sections by GEUS, Copenhagen, on a Philips XL40 SEM equipped with a ThermoNoran Energy Dispersive X-ray spectrometry (EDX) detector. EDX was used for making elemental analyses of the grains to give a qualitative identification of the minerals. The SEM analyses were performed on carbon-coated thin sections and gold-coated samples fixed on stubs with glue. The carbon coating was produced in Ar vacuum of 0.02 mbar. At first the thin sections were exposed to 3 V in 1 min. and then they were coated at 8 V in 5 sec. The gold coating was made in Ar vacuum of 0.3 mbar by exposing the samples to 25 kV in 12 min.

5.2 Results and Discussion

5.2.1 Detrital mineralogy

Most of the clay minerals in the mudstones are likely to be detrital. The detrital mineralogy is besides clay minerals dominated by quartz (Fig. 5.2), which is present as silt and sand sized grains in the mudstones. The content of K-feldspar and plagioclase is approximately equal, whereas the apatite content is a bit lower, except for a few intervals primarily in the Lindemans Bugt Formation (Fig. 5.1 A). Mica is not differentiated from the clay minerals, but observations from thin sections indicate a fairly high content. Some calcite is present as detrital clasts and bioclasts in the Palnatokes Bjerg Formation.

The clay minerals are presumably largely detrital, as seen by their lack of growth structures and by their tangential orientation around the other detrital minerals. However, at least some of the kaolinite is found to be authigenic (Fig. 5.5 A). Far most of the quartz content is detrital, but some macroquartz have precipitated in particular in the coarser-grained intervals (Fig. 5.5 C). The K-feldspars are generally well-preserved, whereas the albite and plagioclase have been more susceptible to dissolution (Fig. 5.5 D), so the original mineralogy was richer in feldspar. Secondary porosity has been created by the feldspar dissolution and has been preserved because of the lateness of this process. The mica consists both of muscovite and biotite, and it is generally oriented parallel to the layering and sometimes bend abound grains because of the compaction. Apatite is found as detrital clasts (Fig. 5.6 A-C) with high concentration in a few intervals (Fig. 5.2). A phosphorite conglomerate might be present near the base of Lindemans Bugt Formation, as a P content of 5.6 wt% is found in the mudstone at 89.7 m depth (Fig. 3.3.1). If this surface is present it would indicate a transgressive lag, where P containing shells and shark teeth could concentrate. Calcite is the only carbonate mineral that is not entirely authigenic, as it occurs in primary fossils (Fig. 5.7 A-F) and as clasts (Fig. 5.6 A) in Palnatokes Bjerg Formation. The dilution of the detrital minerals in the cemented intervals is most obvious for quartz (Fig. 5.2), whereas the dolomitic fracture-fill dilutes all other phases.

5.2.2 Clay mineralogy

The highest content of clay minerals in the clay-sized fraction is present in the Palnatokes Bjerg Formation (Fig. 5.3), whereas quartz is more dominating in the other formations (Fig. 5.1 B). Kaolinite is present in the matrix of all samples, but the largest content is found in the Palnatokes Bjerg Formation (Fig. 5.3). Kaolinite has moreover precipitated in some of the fractures (Fig. 5.8 B). The illite content is fairly constant up through the formations. Mixed-layer clay minerals (Fig. 5.6 D) are present in all formations and are found in highest amounts in the Palnatokes Bjerg Formation, whereas they are missing in the sandstone in the Bernbjerg Formation and in several samples of the Lindemans Bugt Formation. The Bernbjerg Formation is characterized by neither containing chlorite nor vermiculite. The Lindemans Bugt Formation does not contain chlorite either, but it has unambiguous vermiculite content in all samples. The Palnatokes Bjerg Formation contains both vermiculite and chlorite.

The clay mineral assemblage does not vary with the lithology, and this consistency indicates that that no additional authigenic clay minerals, or only minor amounts of kaolinite, have been favored in the cemented intervals. The proximity to the cemented intervals does not influence the mudstone mineralogy either. Kaolinite is the only clay mineral that is clearly authigenic in numerous places in the formations (Fig. 5.5 A) and it occurs often around or within mica (Fig. 5.7 F), where the mica occasionally has become completely kaolinized. Kaolinite must therefore have precipitated before most of the mechanical compaction happened (Fig. 5.4). This coincides with the necessity of meteoric water for the kaolinite formation (Bjørlykke, 1998), which must have taken place quite early after deposition. The climate was humid subtropical at the time of deposition (Surlyk, 2003), so kaolinite is the most likely clay mineral to precipitate (Rateev et al., 2008). It is unlikely that no detrital smectite was deposited with the rest of the sediment, so it might have been present and transformed during burial. Transformation and dehydration of smectite into mixed-layer clay minerals and illite would have released cations usable for the formation of dolomite and ankerite. However, apart from kaolinite the clay minerals are so small and compact that it is difficult to see if some of them are authigenic, but at least a few unambiguous examples of precipitated mixed-layer clays have been found.

5.2.3 Authigenic heavy minerals

Pyrite is present as an authigenic phase in all sampled intervals (Fig. 5.2), and it is enveloped by all other authigenic minerals. The highest contents are found in the Lindemans Bugt Formation (Fig. 5.1 A), as also visible in the screening data (Chapter 8.1). Framboidal pyrite is often overgrown by euhedral pyrite in this formation (Fig. 5.5 B). Pyrite has moreover precipitated in some of the fractures (Fig. 5.8 B). Baryte has formed in so small amounts that it has not been included in the mineralogical estimates (Fig. 5.1 A). It is found in some of the examined intervals, where it has overgrown all other mineral phases (Fig. 5.5 E-F).

Pyrite framboids have precipitated early in the sediments with simultaneous bacterial degradation of organic matter (Fig. 5.4). The pyrite is therefore often present near clay minerals, where organic matter was concentrated. The exhumation caused splitting around clay minerals have then given a false impression of pyrite precipitating late in open pore space (Fig. 5.6 D). The membrane of organic matter on shells may also have promoted early pyrite formation, which precipitated within many of the bioclasts around the rim (Fig. 5.7 H-I) or occupying the whole cavity (Fig. 5.7 K-L). Ankerite could not take over the precipitation as long as the S reducing bacteria prevailed (Burns et al., 2005), so the pyrite euhedra succeeding the framboids in Lindemans Bugt Formation delayed the ankerite formation (Fig. 5.4). Baryte is typically a late authigenic phase because the pore fluids need to be very concentrated before the residue contains enough Ba for baryte formation. This is also the case here as seen by the euhedral overgrowing crystal habit (Fig. 5.5 F), where the string-like precipitation identifies the transport route of the last pore fluid (Fig. 5.5 E).

5.2.4 Bioclasts

The mudstones of the Bernbjerg and Lindemans Bugt Formations contain at least probable calpionellids (Jon Ineson, pers. comm., 2010) (Fig. 5.7 G-L, 4.3 A-C), which are present in largest amounts in the cemented mudstones. The calpionellids are hollow calcareous nannofossils having an oblong shell with a pointed end and a hole in the other. A wide range of cross-section outlines is therefore found from spherical (Fig. 5.7 J) to oblong (Fig. 5.7 L). The calpionellids are filled with either dolomite (Fig. 5.7 G) or micrite (Fig. 5.7 H). Ankerite and pyrite are often present in variable amounts (Fig. 5.7 H-L). The Palnatokes Bjerg Formation contains many thoracosphaera (Chapter 3.2.4) (Fig. 5.7 A-F) especially in the cemented intervals. They are calcareous nannofossils with a spherical outline of the shell. Large calcite crystals are present within the thoracosphaera (Fig. 5.7 E), and small euhedral ankerite crystals are sometimes found in the calcite (Fig. 5.7 F). Of other fossils in the Palnatokes Bjerg Formation is found e.g. ostracods, brachiopods, foraminifers and inocerams. The Bernbjerg and Lindemans Bugt Formations are rich in organic matter including some coal fragments, as described by Alsgaard et al. (2003) for the Bernbjerg Formation, which has the highest TOC values of the three formations (Chapter 8.1). The Palnatokes Bjerg Formation has a low content of C (Fig. 3.3.6) in the mudstones and is heavily bioturbated in contrast to the other formations (Chapter 4).

The calpionellids are all recrystallized along with all other shell material in the Bernbjerg and Lindemans Bugt Formations, but imprints of mollusks and ammonites have been found (Chapter 3.2.2). Pyrite was the first mineral to precipitate, as seen by its presence along the rim of many shells (Fig. 5.7 H) or filling most of the cavity (Fig. 5.7 I). Afterwards ankerite took over and formed small euhedral crystals, of which most were precipitated outside the bioclasts (Fig. 5.7 J-K). Poikilotopic dolomite crystals precipitated in most of the remaining cavity (Fig. 5.7 G), but some porosity is often preserved (Fig. 5.7 J-K). The original fossils are preserved in the Palnatokes Bjerg Formation, as seen by the characteristic shell pattern of the thoracosphaera (Fig. 5.7 B) and by the extinction pattern following the growth structure in other fossils. Limited amounts of ankerite precipitated in this formation.

The organic matter in the Bernbjerg and Lindemans Bugt Formations must have created reducing conditions with recrystallization of all bioclasts. The low C content in the Palnatokes Bjerg Formation implies that the content of organic matter must be very small. However, the rich bioturbation in this formation shows that the organic matter is not missing due to almost total degradation, as this would not have been possible during these oxygenated conditions. Bacterial degradation of organic matter was thus not able to establish a reducing environment for mineral reactions, so the original bioclasts are generally preserved.

The proportional increase in Ca and C (Fig. 3.3.6) in the profoundly cemented intervals occurring in all formations (Fig. 3.3.3) shows that $CaCO_3$ must have been added to these layers. This can in the case of the Bernbjerg and Lindemans Bugt Formation be explained by dissolution of calpionellids resulting in precipitation of carbonate cement in layers with large bioclast content. These layers possibly represent events of minor transgressions with reworking causing the high bioclast concentration (Burns et al., 2005; Chapter 4). The Palnatokes Bjerg Formation is sediment starved (Chapter 4), so carbonate ooze had time to accumulate at the sea floor. The deposition must have been extra slow in the cemented intervals, which has provided time for additional carbonate ooze supply. Some of the ooze became micrite matrix via recrystallization during burial, whereas some resulted in calcite cementation.

5.2.5 Authigenic carbonate minerals

The marine clastics are carbonate cemented in intervals with large initial concentration of bioclasts or carbonate ooze. The intervals of carbonate cementation are clearly visible from low gamma-ray values in the screening data (Fig. 8.1.1). Calcitic clasts and bioclasts in the Palnatokes Bjerg Formation (Fig. 5.6 A) contain the only detrital carbonate found in the core. Dolomite is the predominant cement type in the Bernbjerg and Lindemans Bugt Formations, whereas poikilotopic and micritic calcite dominates the Palnatokes Bjerg Formation by far. The growth form of ankerite is euhedral as rhombs (Fig. 5.6 E), while calcite and dolomite are poikilotopic (Fig. 5.6 B, F). Dolomite and calcite often encloses the ankerite crystals. Both ankerite rhombs and dolomite crystals increase in Fe content outwards. Dolomite has in some places precipitated as radiating large crystals around muscovite.

Ankerite was the first carbonate mineral that began precipitating and was in the Bernbjerg and Lindemans Bugt Formations followed by dolomite (Fig. 5.6 C), whereas it was followed by calcite in the Palnatokes Bjerg Formation (Fig. 5.6 B). The formation of ankerite stopped when the pore fluids had been sufficiently drained of Fe. The presence of bioclasts is important for the precipitation of ankerite (e.g. Hendry et al., 2000; Burns et al., 2005), where the bioclasts act both as nucleation sites for the ankerite and dolomite crystals and as a source of carbonate constituents.

5.2.6 Fracture generations

Small fractures can be found in most of the core, but are especially abundant in the cemented intervals. These fractures always cut through the carbonate cemented fabrics. Opal is found at the rim of the first fracture generation (Fig. 5.8 G-I), where it is radiating in spherical layers around protruding matrix. The remaining parts of these fractures are occupied by dolomite, where the darkening towards the middle of the fractures (Fig. 5.8 J) represents an increase in Mg with simultaneous decrease in Fe. The dolomite is generally euhedral (Fig. 5.8 E-F) with occasional grading in crystal size (Fig. 5.8 K). The second fracture generation consists of calcite lamellas (Fig. 5.8 D) with occasional euhedral pyrite (Fig. 5.8 B-C). Both these phases are enveloped by kaolinite (Fig. 5.8 B). The third generation of fractures has not been filled by any minerals.

The fracturing must have happened late, as the fractures cut all authigenic phases in the sediments. The exhumation must have been the triggering mechanism of the fracture formation, as the sediments needed to be cooled in order to lose sufficient of their elastic properties. The fractures formed mainly in the cemented intervals because they had lost most of their elasticity through the cementation. The analyzed fracture with fill of dolomite has a geochemistry that resembles the cemented intervals of the mudstones well, as it comprise the end-member chemical composition of the Bernbjerg Formation (Fig. 3.3.6) where it was sampled. The fracturing has happened in several phases with increasing size of the fractures, as seen by the cross-cutting relationships (Fig. 5.8 L).

The pore fluids have in the beginning been oversaturated in silica, so opal was formed. All other minerals of the fracture-fill are late phases of authigenic minerals already present in the sediments, wherefore the pore fluids and the fysiochemical conditions favored their formation. Some of the opal was replaced by dolomite when the dolomite precipitation began (Fig. 5.8 G). There was overlap between the growth periods of opal and dolomite (Fig. 5.8 G-I), but it was very brief (Fig. 5.4). The pore fluids were firstly depleted in Fe during the dolomite precipitation, as it included only small amounts of Fe. The remaining pore fluids then used the enrichment in Mg for continued dolomite formation. Calcite took over when Mg ran out after additional exhumation, and the Fe in these later fractures was used to form pyrite. Kaolinite then resumed when meteoric water was supplied and Ca and Fe had ceased. The latest fracturing episode happened so late that no mineral phases were able to precipitate, thus forming minor amounts of secondary porosity. However, some of the fractures without fill are artifacts from the drilling and drying created in the mudstone due to the cleavage.

5.2.7 Diagenetic causes and effects

Textural relationships have been used to determine the diagenetic sequence (Fig. 5.4). Major phases comprise kaolinite, pyrite, ankerite, dolomite and calcite. The precipitation of these minerals has been controlled by organic matter degradation and bioclast dissolution. Minor phases include macroquartz and baryte in the mudstones and sandstones, whereas the fracture-fill consists of opal, dolomite, calcite, pyrite and kaolinite. The formation of secondary porosity as a consequence of bioclast dissolution, feldspar dissolution and fracture formation does not have a major influence on the sediments either. Small amounts of gypsum have been identified on core surfaces and by XRD, but they are artifacts formed during the dry up of the core.

On the basis of the chemostratigraphy in section 3.3 it was concluded that each formation has a characteristic mudstone component that is similar in all intervals of the formation including both the cemented and uncemented successions. The mudstone components of the Bernbjerg and Palnatokes Bjerg Formations are especially well-defined by their geochemistry (Fig. 3.3.6). However, this component is diluted by authigenic carbonate minerals in the cemented mudstone, where the concentration of bioclasts has controlled the amount of dilution. The bioclasts might very well be tracers of flooding surfaces (e.g. Burns et al., 2005), where transgressive reworking has concentrated them. This is in accordance with the fact that the cemented mudstone typically occurs in the top of a few metres thick upward-coarsening successions or at the finest grain size intervals in the base of upward-coarsening cycles (Chapter 4). The decreasing concentration of carbonate minerals in the cemented intervals up through the core (Fig. 3.3.5) could be explained by decreasing dissolution of bioclasts or diminishing input of bioclasts to supply ions for carbonate precipitation. The latter could imply a progressive deepening of the setting, where the influence of transgressions decreased steadily. The nature of the tectonic regime confirms this assumption, as described below.

The marine shelf setting of the Bernbjerg Formation with sediment supply from the delta system to the west is reflected in the sandy nature of the mudstone with storm-wave influence in the lower part of the core (Fig. 4.1) and with much quartz in the clay-sized fraction (Fig. 5.2). The faulting was only minor (Fig. 4.8) but growing (Surlyk, 2003). It was greatly increased when the Lindemans Bugt Formation began deposit and soon reached its culmination of rotational block faulting, where a fault was created west of the study area with westwards tilting of the resulting basin. The sub-aerial fault scarp west of this half-graben blocked sediment input from the main land, but some sediment was supplied by gravity flows originating at the fault scarp. The fairly short distance to the fault scarp resulted in input of detrital grains the size of silt in spite of the relatively sediment starved environment. Clasts of quartz, feldspar, apatite and mica (Fig. 5.2) were supplied by the gravity flows, in addition to the detrital clay minerals (Fig. 5.3). The high gamma-ray values of the Lindemans Bugt Formation (Fig. 4.1) reveal the finer-grained nature of these deposits. The appearance of vermiculite in this formation confirms the changed setting, as calm conditions are needed in order for the mineral to deposit. The second episode of pyrite precipitation only found in Lindemans Bugt Formation (Fig. 5.4) could indicate that S gasses were released as a consequence of the intense rifting. The Palnatokes Bjerg Formation is more sediment starved than the Lindemans Bugt Formation probably due to the fully segmented late synrift - early postrift basin that was influenced by eustatic sea level rise (Surlyk, 2003). This is in accordance with the continued presence of vermiculite and with the large calcareous content revealing slow clastic deposition. However, occasional muddy sandstones imply that gravity flows still happened. Chlorite is introduced in this formation, which could have been supplied from another marine sediment source or have formed within the sediment. The high content of kaolinite in the Palnatokes Bjerg Formation must on the contrary have a non-marine source. This could imply renewed uplift in the source area which is unlikely (Fig. 4.8), so the part of the kaolinite that is additional to the content of the Lindemans Bugt Formation is assumed to be authigenic.

5.2.8 Maximum burial depth

Burial temperatures of mineral reactions are much better evaluated in the literature than burial depths, so temperatures are used here to estimate maximum burial. The carbonate minerals can precipitate at very variable temperatures, so they are of no use in estimating maximum burial. Macroquartz has only precipitated in small amounts, so the sediments cannot have been buried farther than the onset temperature of the macroquartz precipitation (e.g. 80-100°C, Bjørlykke et al., 2009). This correlates well with the temperature of baryte formation (e.g. 83-105°C, Burley et al., 1989), which precipitated after quartz as the deepest mineral phase. Smectite illitization is supposed to have occurred in order to provide cations for the formation of carbonate minerals, and the precipitation temperatures of quartz and baryte confirms that the sediments have been buried deep enough for this mineral reaction to happen (e.g. I-S >74°C, Weibel, 1999). The fracturing of the sediments must have happened relatively late during the exhumation, as low temperatures are required for the precipitation of opal (e.g. <65°C, Weibel et al., 2010) and kaolinite (e.g. <60°C, Glasmann et al., 1989). Based on diagenetic mineral associations, the maximum burial depth is thus interpreted as 2-3 km, depending on the geothermal gradient.

5.3 Conclusions

The sedimentary succession of the Rødryggen-1 core has poor reservoir properties. The few sandstone intervals are thin and muddy, and the porosities and permeabilities of all intervals are low. The detrital and authigenic mineralogy and grain size are results of the tectonic regime of the depositional setting, where rotational block faulting caused increasing basin depth and sediment starvation up through the succession. The reservoir properties have especially been reduced in the thin intervals with major carbonate cementation. The processes controlling the formation of secondary porosity have only had a minor influence. The sediments have gradually been buried to depths of about 2-3 km triggering the precipitation of first kaolinite and pyrite followed by ankerite and then dolomite or calcite depending on the formation. Macroquartz and baryte are only minor phases along with those precipitated in the fractures created during the exhumation in the cemented intervals mainly. The three formations can besides for the geochemistry also be unambiguously separated by the clay mineralogy.

5.4 References

Alsgaard, P.C., Felt, V.L., Vosgerau, H. and Surlyk, F., 2003: The Jurassic of Kuhn Ø, North-East Greenland. In: Ineson, J.R. and Surlyk, F (eds.): The Jurassic of Denmark and Greenland. Geological Survey of Denmark and Greenland Bulletin, 659–723.

Bjørlykke, K., Jahren, J., Mondol, N.H., Marcussen, Ø., Croize, D., Peltonen, C. and Thyberg, B., 2009: Sediment compaction and rock properties. Search and Discovery Article 50192.

Burley, S.D., Mullis, J. and Matter, A., 1989: Timing diagenesis in the Tartan reservoir (UK North Sea): constraints from combined cathodoluminescence microscopy and fluid inclusion studies. Marine and Petroleum Geology, **6**, 98–120.

Burns, F.E., Burley, S.D., Gawthorpe, R.L. and Pollard, J.E., 2005: Diagenetic signatures of stratal surfaces in the Upper Jurassic Fulmar Formation, Central North Sea, UKCS. Sedimentology, **52**, 1155–1185.

Glasmann, J.R., Clark, R.A., Larter, S., Briedis, N.A. and Lundegård, P.D., 1989: Diagenesis and hydrocarbon accumulation, Brent sandstone (Jurassic), Bergen High Area, North Sea. AAPG Bulletin, **73**, 1341–1360.

Hendry, J.P., Wilkinson, M., Fallick, A.E. and Haszeldine, R.S., 2000: Ankerite cementation in deeply buried Jurassic sandstone reservoirs of the Central North Sea. Journal of Sedimentary Research, **70**, 227–239.

Rateev, M.A., Sadchikova, T.A. and Shabrova, V.P., 2008: Clay minerals in recent sediments of the world ocean and their relation to types of lithogenesis. Lithology and Mineral Resources, **43**, 125–135.

Slater, C. and Cohen, L., 1962: A centrifugal particle size analyser. Journal of Scientific Instrumentation, **39**, 614–617.

Surlyk, F., 2003. The Jurassic of East Greenland: a sedimentary record of thermal subsidence, onset and culmination of rifting. In: Ineson, J.R. and Surlyk, F (eds.): The Jurassic of Denmark and Greenland. Geological Survey of Denmark and Greenland Bulletin, 659–723.

Weibel, R., 1999. Effects of burial on the clay assemblages in the Triassic Skagerrak Formation, Denmark. Clay Minerals 34, 619–635.

Weibel, R., Friis, H., Kazerouni, A.M., Svendsen, J.B., Stokkendal, J. and Poulsen, M.L.K., 2010. Development of early diagenetic silica and quartz morphologies. Sedimentary Geology 228, 151–170.

.

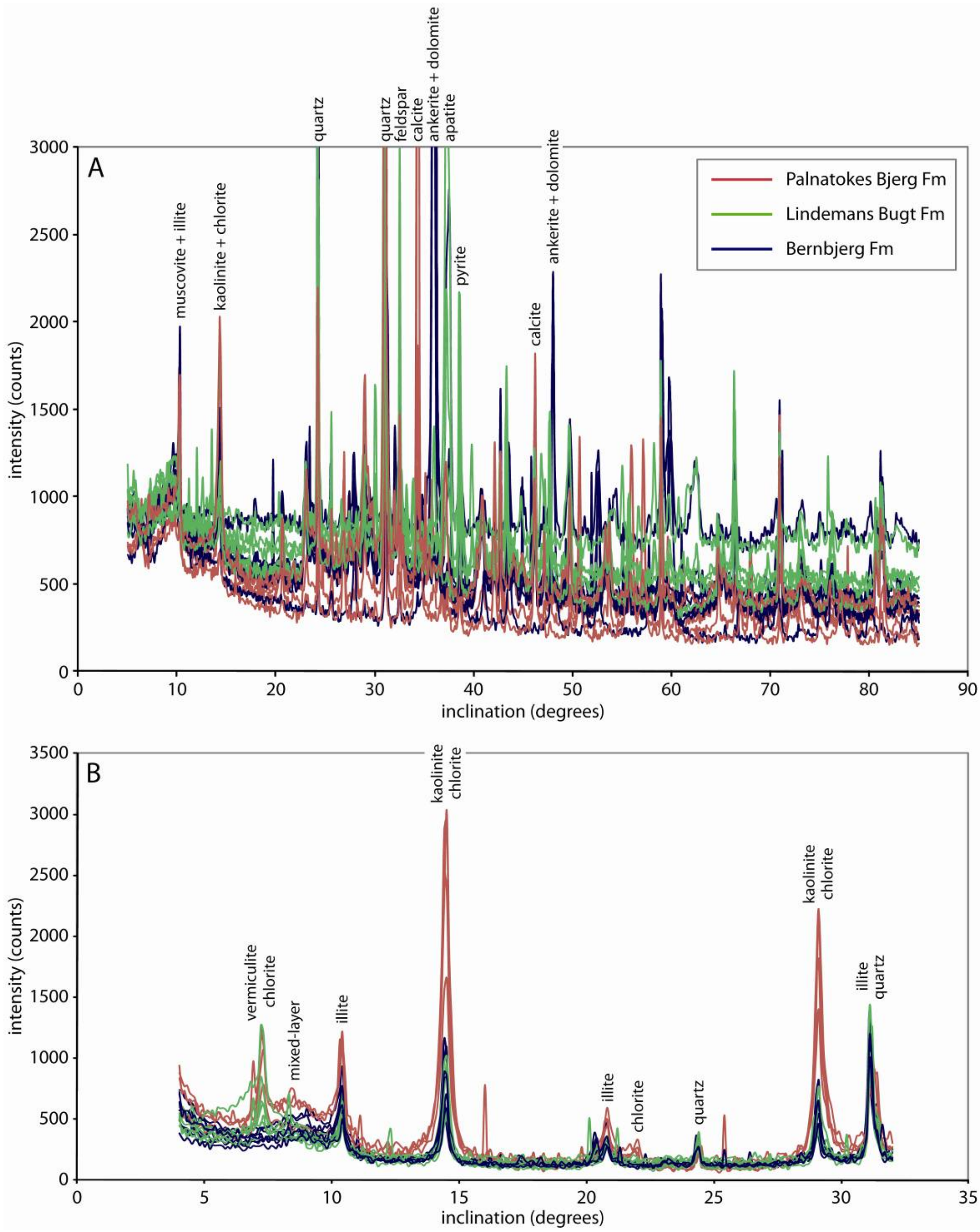

Figure 5.1. A) XRD peaks of the bulk mineralogy of the < 250 µm fraction with labels on the most important peaks. Four samples with much noise have been excluded. B: XRD peaks of the clay mineralogy based on Mg air-dry treatment. The sharp peaks without label are spikes caused by instrument noise. Three samples with much noise have been excluded.

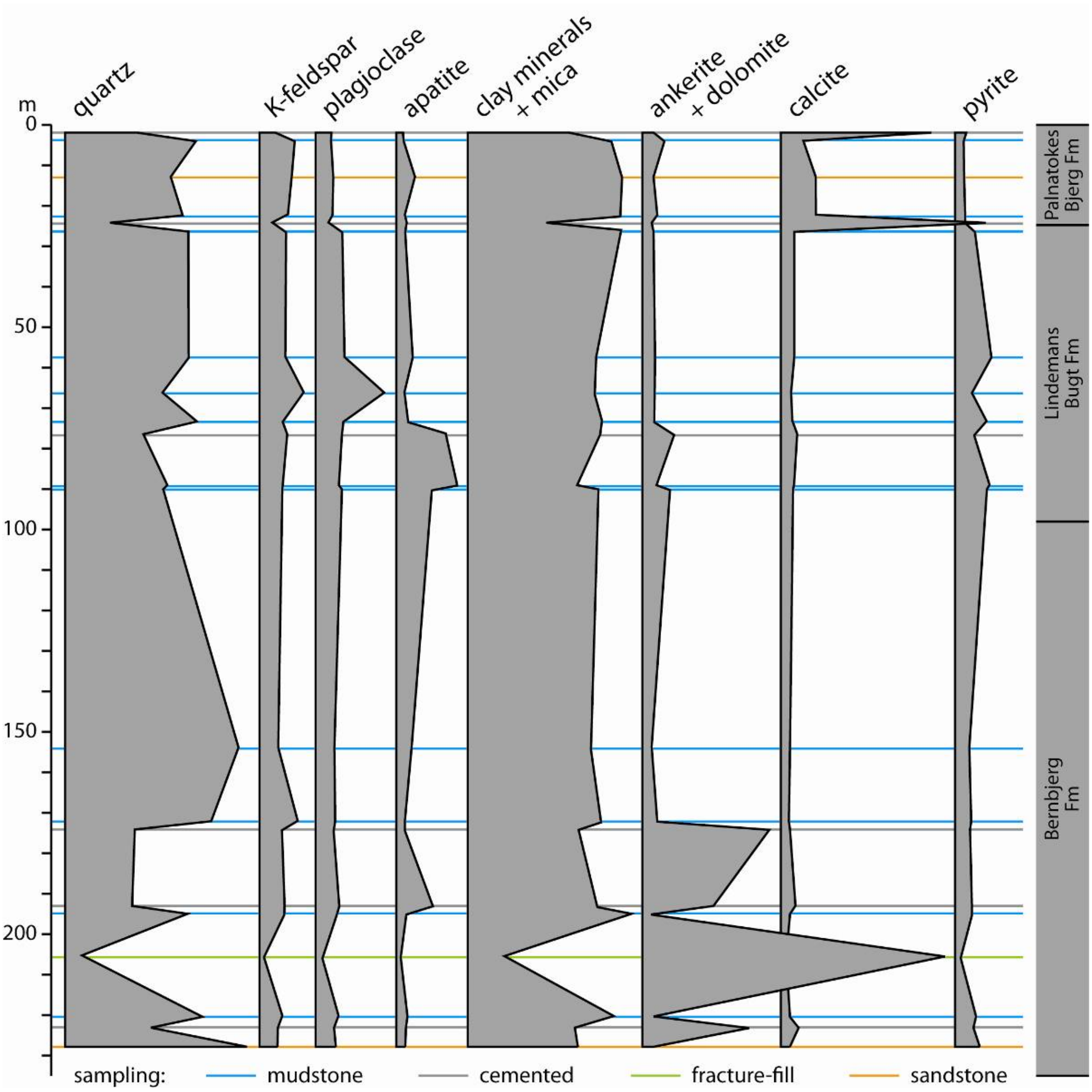

Figure 5.2. Bulk mineralogy of the < 250 µm fraction of 12 mudstones, 6 cemented mudstones, 1 cemented fracture and 2 sandstones from the Rødryggen-1 core. Relative contents estimated on the basis of XRD data.

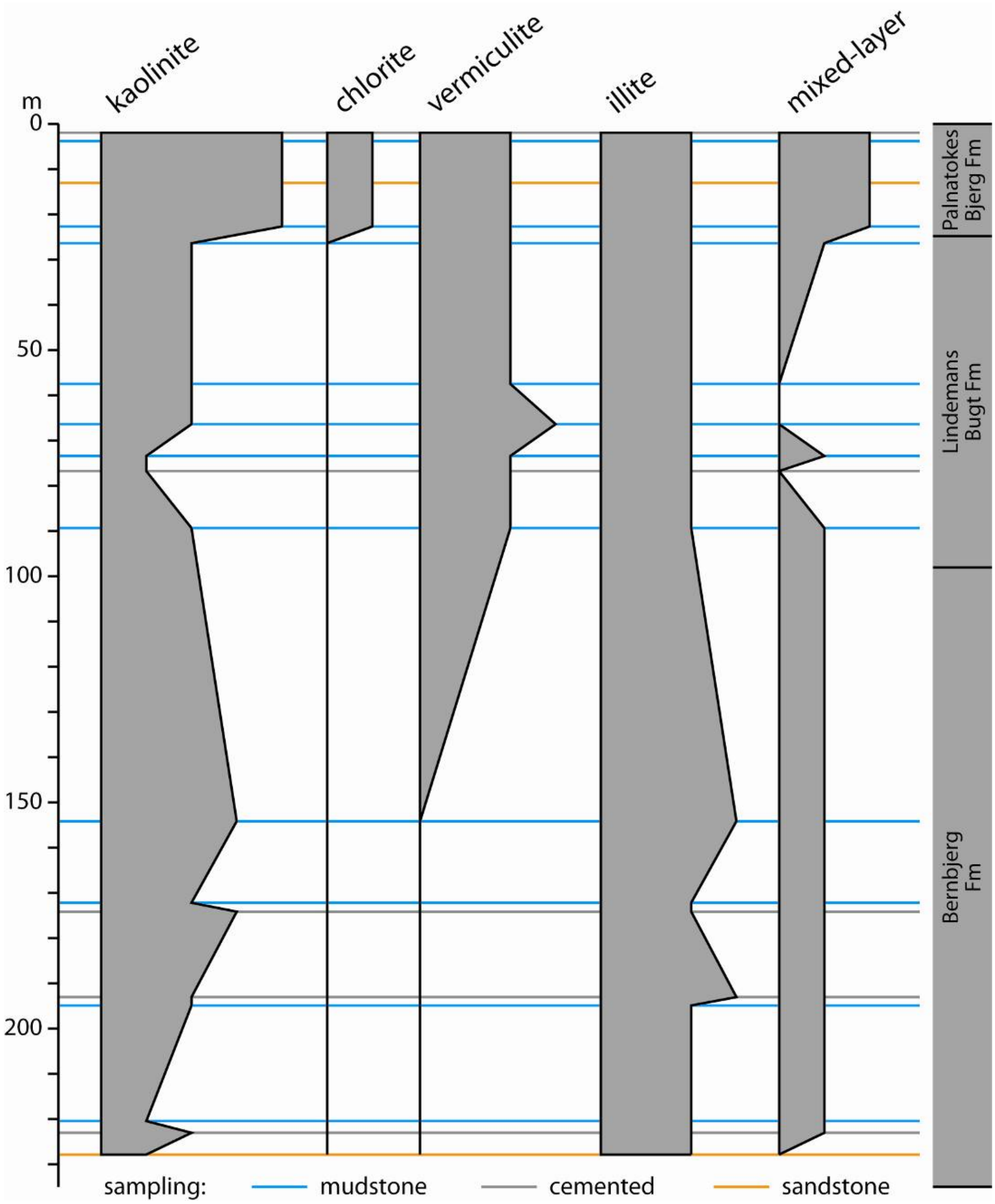

Figure 5.3. Mineralogy of the clay-sized fraction of 11 mudstones, 5 cemented mudstones and 2 sandstones from the Rødryggen-1 core. Relative contents estimated from XRD data. The rest of the clay-sized fraction is occupied by other mineral phases, mostly quartz.

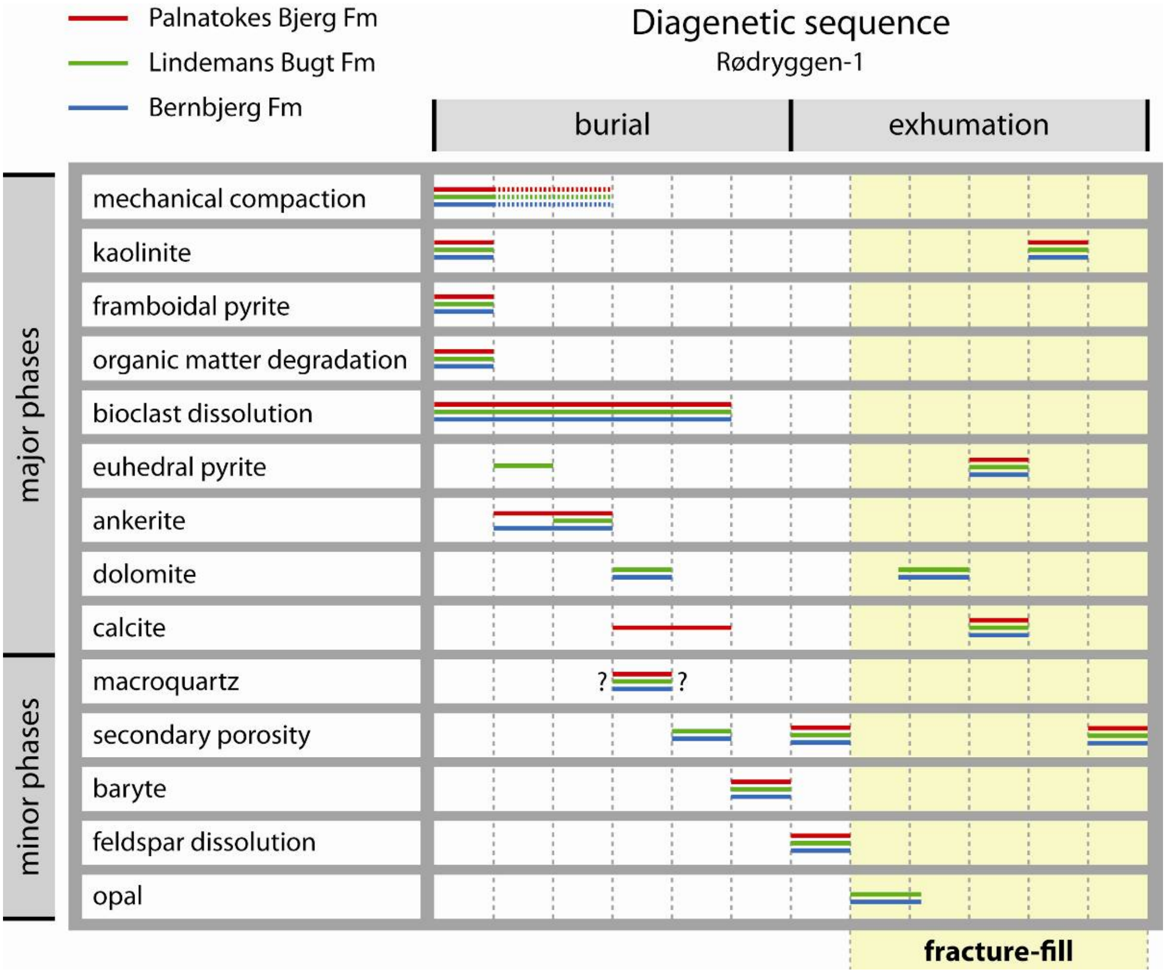

Figure 5.4. Diagenetic sequence of the Rødryggen-1 core showing events of precipitation, recrystallization, dissolution and degradation. Variation between the three formations occurs primarily in the carbonate minerals and in the growth phases of pyrite. The mineral precipitations from opal and onwards are filling fractures mainly in the cemented intervals.

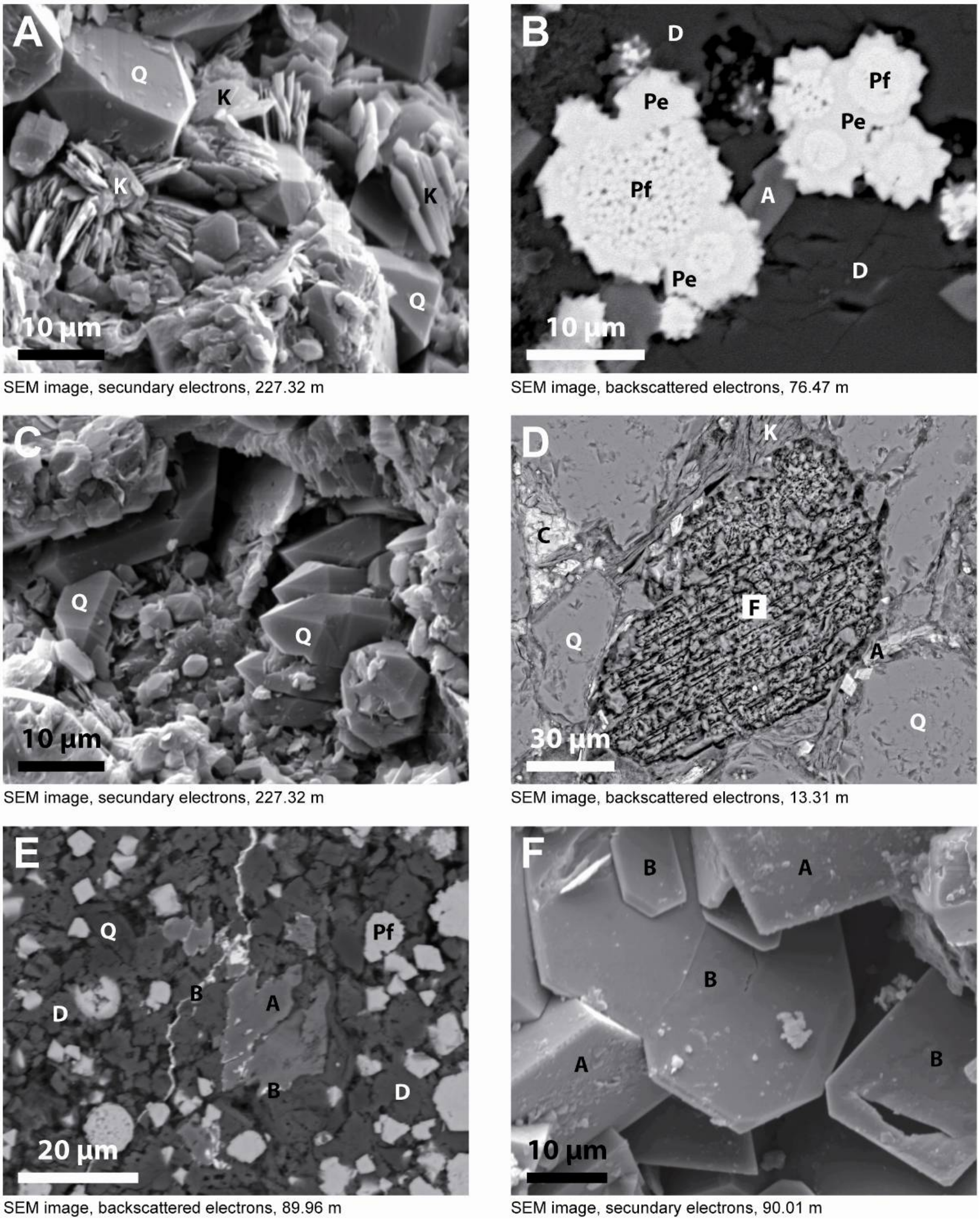

Figure 5.5. Important mineral reactions beside carbonate minerals. A) Kaolinite precipitation and later quartz formation. B) Framboidal pyrite is often overgrown by euhedral pyrite in the Lindemans Bugt Formation. C) Macroquartz is found in the most coarse-grained intervals. D) Dissolution of albite has formed secondary porosity. E) Baryte has precipitated from the most concentrated pore fluids. F) Euhedral baryte has grown later than ankerite. See mineral abbreviations in Fig. 5.7.

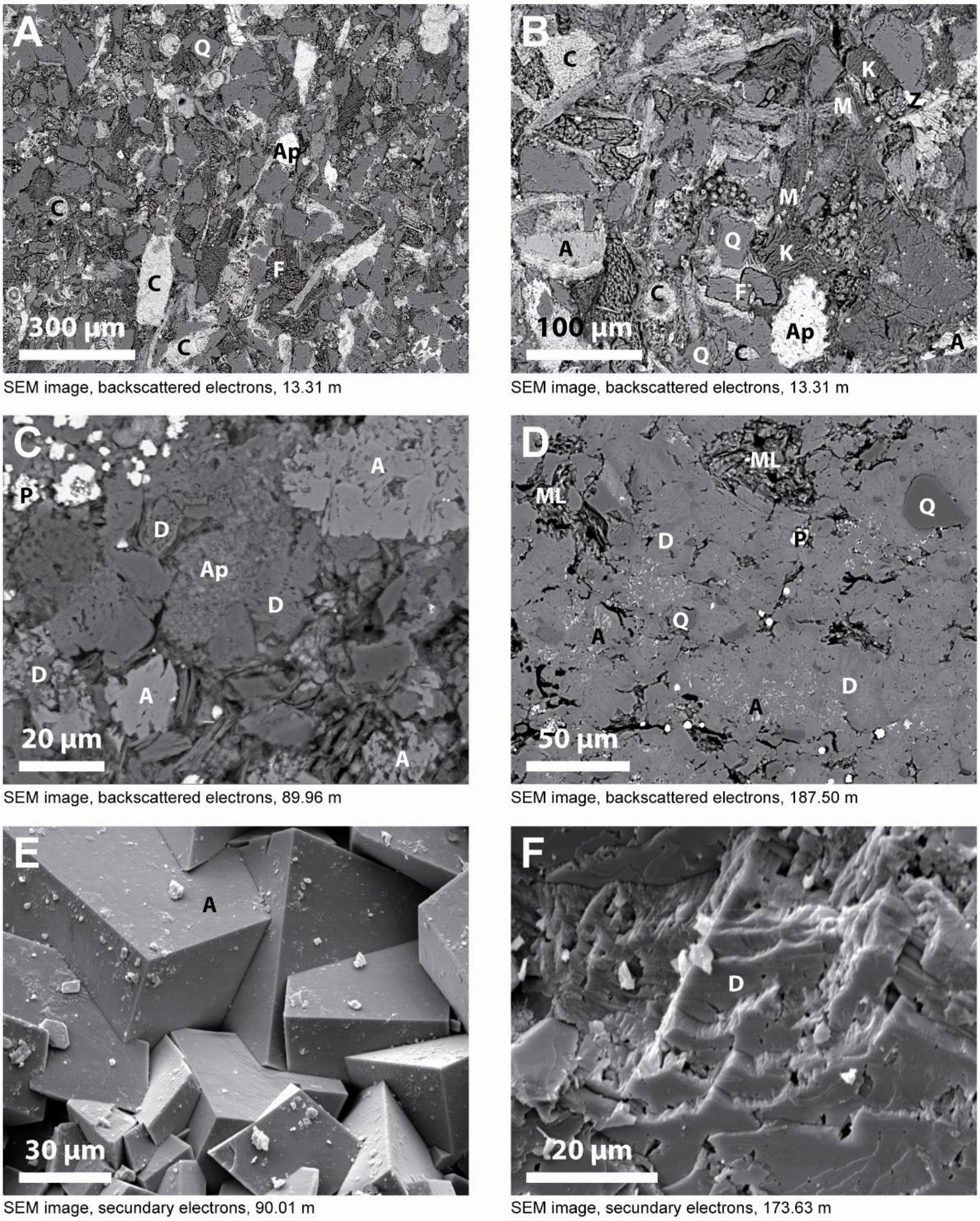

Figure 5.6. Behavior of the carbonate minerals. A) Detrital clasts of calcite, apatite, quartz, feldspar and thoracosphaera. B) Authigen calcite and detrital apatite etc. C) Authigen dolomite, ankerite and pyrite, besides detrital apatite etc. D) Authigen dolomite, ankerite and pyrite. E) Growth form of ankerite. F) Growth form of dolomite. See mineral abbreviations in Fig. 5.7.

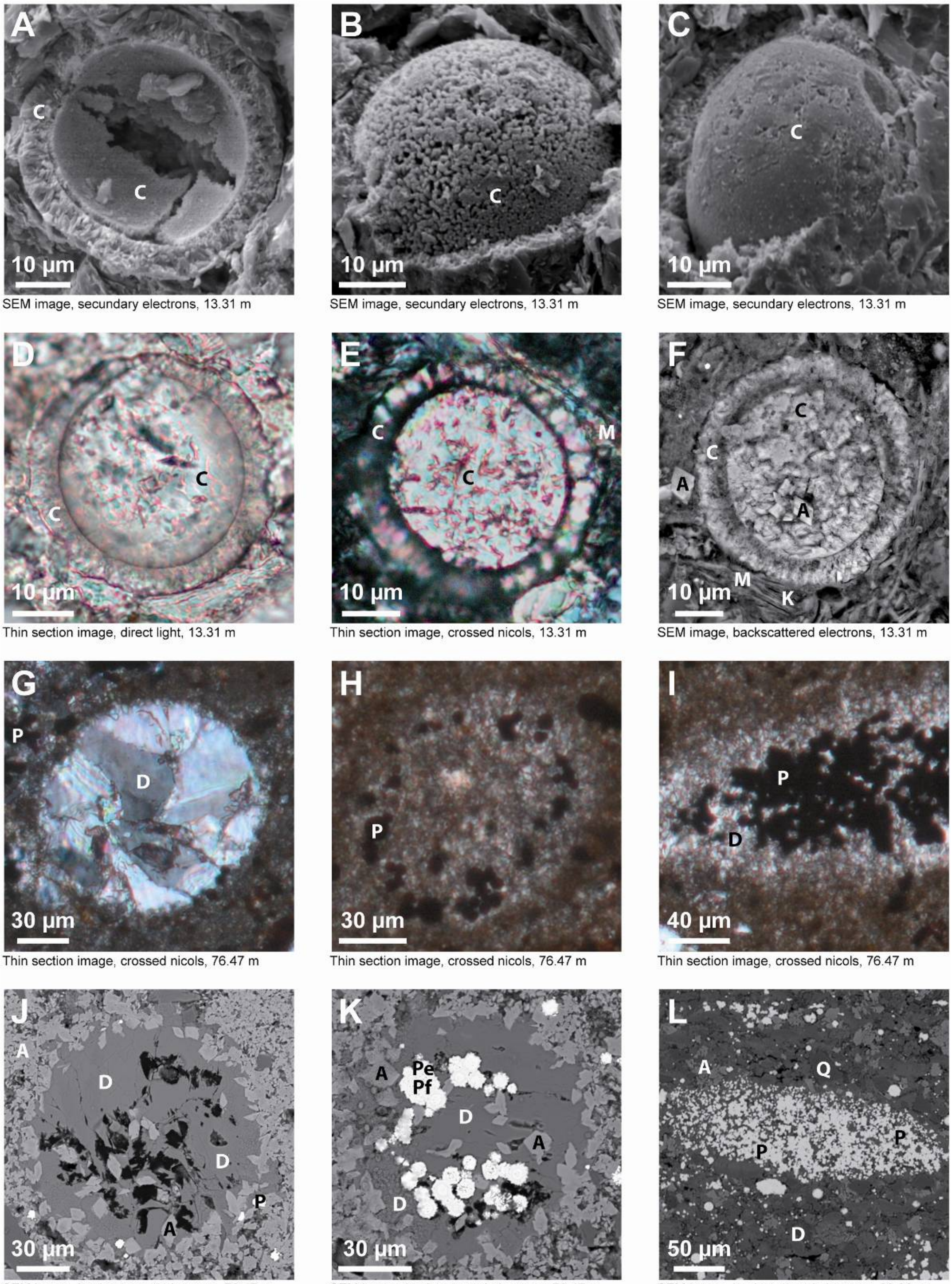

SEM image, secundary electrons, 13.31 m

SEM image, secundary electrons, 13.31 m

SEM image, secundary electrons, 13.31 m

Thin section image, direct light, 13.31 m

Thin section image, crossed nicols, 13.31 m

SEM image, backscattered electrons, 13.31 m

Thin section image, crossed nicols, 76.47 m

Thin section image, crossed nicols, 76.47 m

Thin section image, crossed nicols, 76.47 m

SEM image, backscattered electrons, 76.47 m

SEM image, backscattered electrons, 76.47 m

SEM image, backscattered electrons, 89.96 m

Figure 5.7 (previous page). Calcareous nannofossils. A-F: Thoracosphaera from Palnatokes Bjerg Fm. G-L: Remnant outlines of replaced calpionellids from Lindemans Bugt Fm. The thoracosphaera are well-preserved and sometimes partly recrystallized by calcite and small amounts of ankerite crystals (F). The calpionellids have in some cases been filled by micrite (H), but generally they are filled with some ankerite and much dolomite cement (G,J,K). Secondary porosity is found in some of them (J,K). Pyrite has commonly precipitated within the rim of the replaced shell (H, K) and sometimes fills the whole cavity (I, L).

Minerals in the images are abbreviated as:

A = ankerite	$Ca(Fe,Mg,Mn)(CO_3)_2$
Ap = apatite	$Ca_5(PO_4)_3(F,Cl,OH)$
B = baryte	$BaSO_4$
C = calcite	$CaCO_3$
D = dolomite	$CaMg(CO_3)_2$
F = feldspar (albite)	$NaAlSi_3O_8$
K = kaolinite	$Al_2Si_2O_5(OH)_4$
M = mica	$KAl_{0-2}(Mg,Fe)_{0-3}AlSi_3O_{10}(F,OH)_2$
ML = mixed-layer clays	variable
O = opal	SiO_2*nH_2O
P = pyrite	FeS_2
Pe = pyrite (euhedral)	FeS_2
Pf = pyrite (framboidal)	FeS_2
Q = quartz	SiO_2
Z = zircon	$ZrSiO_4$

Figure 5.8 (following page). Fracture fill in the Lindemans Bugt Fm (A-D) and the Bernbjerg Fm (E-L). A-C: Calcitic fracture fill in different orientations, where pyrite has precipitated simultaneous and kaolinite afterwards. The atypical interference colors in A and C are caused by an optical phenomenon of the lens. D-F: The fracture growth forms of calcite (D) and dolomite (E-F) are distinct. G: Opal has begun precipitating before dolomite, and dolomite has afterwards replaced some opal near the rim. H: The opal growth is radiating in spherical layers. I: The intergrowth of opal and dolomite indicates an overlapping formation phase before dolomite took over. J: The dolomite cement in the center of the fracture contains more Mg and less Fe than the earlier dolomite. K: Progressive carbonate growth. L: A thin fracture is cut by a younger and much broader fracture. See mineral abbreviations in Fig. 5.7.

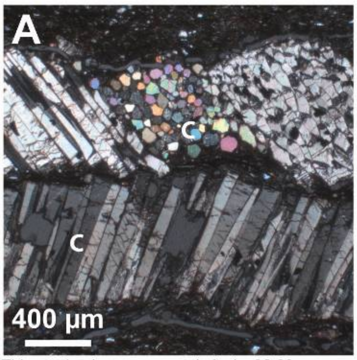

Thin section image, crossed nicols, 26.60 m

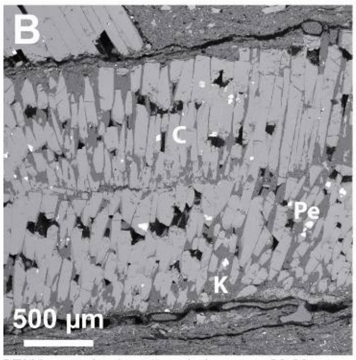

SEM image, backscattered electrons, 26.60 m

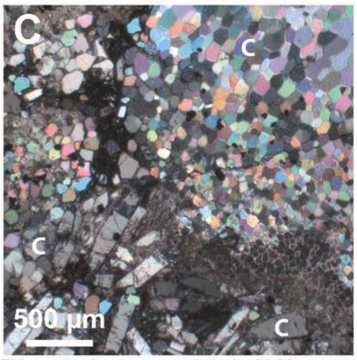

Thin section image, crossed nicols, 26.60 m

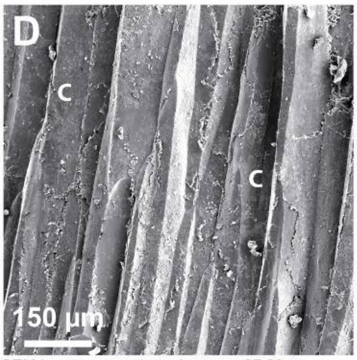

SEM image, secundary electrons, 27.33 m

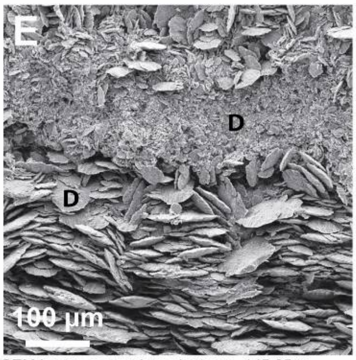

SEM image, secundary electrons, 145.65 m

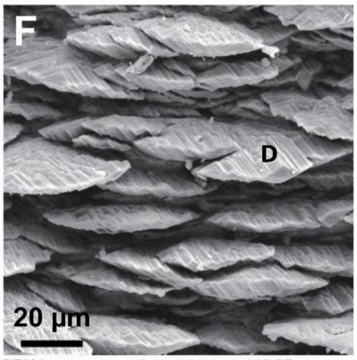

SEM image, secundary electrons, 145.65 m

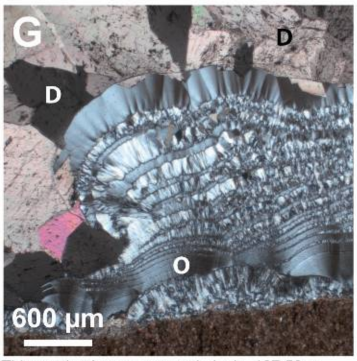

Thin section image, crossed nicols, 187.50 m

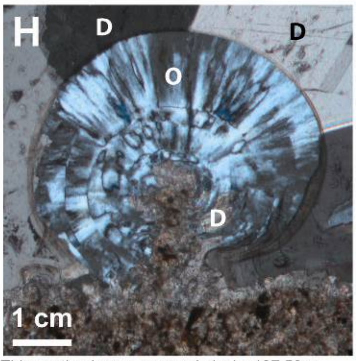

Thin section image, crossed nicols, 187.50 m

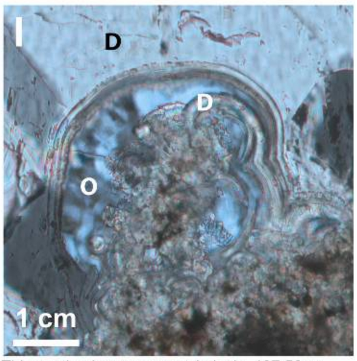

Thin section image, crossed nicols, 187.50 m

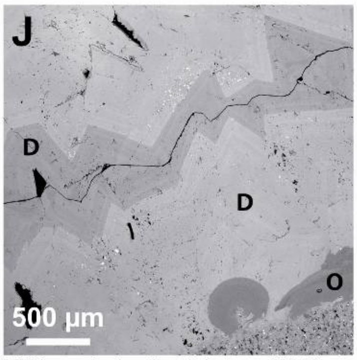

SEM image, backscattered electrons, 187.50 m

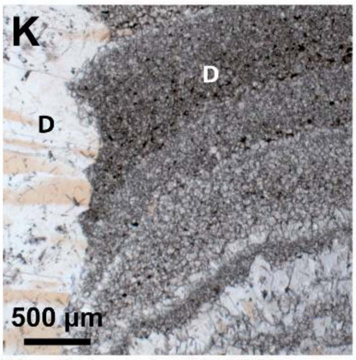

Thin section image, direct light, 205.73 m

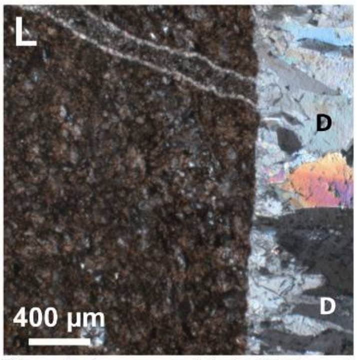

Thin section image, crossed nicols, 205.73 m

6. Porosity, Permeability and Grain Density

Conventional core analysis was conducted on 11 plugs of mudstone with varying degree of sand lamina.

6.1 Methods

The conventional core analysis (CCAL) of the Rødryggen core was carried out at GEUS Core Laboratory. For a more detailed description of methods, instrumentation and principles of calculation, the reader is referred to American Petroleum Institute (API) recommended practice for core-analysis procedure (API 1998).

The present description only encounters CCAL of plugs taken from the well core.

Plugging

The location of the plugs is presented in Table 6.2.

Plugging of the core was carried out from selected mudstone at irregular intervals. Plugs were taken as 1" vertical (i.e. normal to bedding) plugs using an air-stream as coolant. Though the plugging was carried out as careful as possible, some plugs were fractured or broken during plugging due to the interlaminar nature and high clay content of the plugs. Plugs broken during plugging were not analysed for permeability (cf. table 6.2)

Cleaning and drying

The plugs did not contain hydrocarbons and showed no visible signs of salt precipitates. Therefore, due to the high clay content of the plugs and the associated risk of damaging the plugs further by conventional cleaning with methanol, the plugs were not cleaned.

Thus, following plugging, the samples were dried at 40 °C for 24 h and left in an exicator until analysed.

Gas permeability, uncorrected (GEUS steady state instrument)

Each non-broken plug was mounted in a Hassler core holder, and a confining pressure of 400 psi (27.6 bar) was applied to the sleeve. The uncorrected permeability to gas was measured by flowing nitrogen gas through a plug of known dimensions at differential pressures between 0 and 14.5 psi (0 and 1 bar). No back pressure was applied and due to the low permeability of the plugs, the gas flow was registered by bubble pipe readings. The performance of the gas permeameter is checked regularly by routine measurement of permeable steel reference plugs (Core Laboratories™ gas permeability reference plug set).

He-porosity and grain density

The porosity of each plug was determined by subtraction of the measured grain volume from the measured bulk volume. The Helium technique, employing Boyle's Law, was used for grain volume determination, applying a double chambered Helium porosimeter with digital readout. The sample bulk volume was measured by submersion of the plug in a mercury bath using Archimedes principle. Grain density was calculated from the grain volume measurement and the weight of the cleaned and dried sample.

Due to the low porosity and permeability of the plugs, the measurements on the Helium porosimeter were carried out by saturating each plug with Helium for 15 minutes prior to analysis. Subsequently, readings where taken at regular intervals for up to 30 minutes until stable results were obtained.

Before measurements, the Helium porosimeter was calibrated using a set of steel plugs (Core Laboratories™ volume reference plug set). The bulk volume apparatus is checked frequently as a laboratory routine using a steel plug with known volume.

Precision of analytical data

Table 6.1 shows the precision (= reproducibility) at the 68% level of confidence (+/- 1 standard deviation) for routine core analysis measurements performed at the GEUS Core Laboratory.

6.2 Results

Results of the conventional core analyses are presented in Table 6.2 and Figure 6.1.

The porosity of the selected plugs varies between 1.55 and 9.68 % with an average of 6.62%. Although based on relatively few samples, there is a tendency of a generally decreasing porosity with increasing depth (Figure 6.1).

Permeability measurements were possible on only five of the 11 selected plugs (cf. table 6.2). The remaining six plugs were broken or severely fractured during the plugging and drying proces. Among the five permeability measurements, four represent matrix permeability and one represents a fracture permeability (cf. table 6.2). The measured matrix permeabilities are rather low and ranges between 0.011 and 0.015 mD.

No correlation between porosity and permeability was found, presumably due to the low number of analyses.

The grain density of the samples ranges from 2.520–2.876 g/cc, with an average of 2.736 g/cc. No correlation between grain density and depth or porosity was found.

6.3 Discussion and conclusions

The Rødryggen-1 core is throughout of low permeability and porosity, and lack reservoir intervals. One of the nearest reservoir rocks are the Middle Volgian – Valanginian coarse grained fan delta deposits (Rigi and Yound Sund Members of the Lindemans Bugt and Palnatokes Bjerg Formations, respectively), occurring in the westernmost tilted fault block. Moreover, the lowermost part of the Bernbjerg Formation (the Ugpik Ravine Member), which was not reached by the Rødryggen-1 core, reportedly bears thin sandy layers may be of limited reservoir significance. Finally, the Bernbjerg Formation overlies either the Pelion Formation, the Payer Dal Formation or the Jakobsstigen Formation of the Vardekløft Group (Surlyk, 2003), all of which contain sandstone-dominated intervals (Fig. 3.1.1).

6.4 References

American Petroleum Institute (API) 1998: Recommended Practices For Core Analysis. Exploration and Production Department, American Petroleum Institute, Second edition.

Measurement	Range	Precision
Grain density		0.003 g/cc
Porosity		0.1 porosity-%
Permeability: (Conventional)	0.05-0.1 mD > 0.1 mD	15% 4%

Table 6.1 Precision of analytical data.

Plug ID	Plug H/V	Depth [m]	$Porosity_{(He)}$ [%]	Grain density [g/cc]	Permeability [mD]
80	V	9,85	9,22	2,851	#I/T
81	V	20,82	6,30	2,818	#I/T
82	V	42,51	9,68	2,866	#I/T
83	V	62,53	8,33	2,564	#I/T
84	V	76,83	7,83	2,876	0,015
85	V	120,01	7,11	2,619	1.477*
86	V	155,75	6,18	2,631	#I/T
87	V	174,54	1,55	2,799	0,014
88	V	222,39	3,20	2,796	0,011
89	V	233,49	6,74	2,520	0,011
90	V	16,92	6,67	2,756	#I/T

#I/T = not analysed due to broken plug *) Fracture permeability

Table 6.2 Porosity, permeability and grain density of plugs.

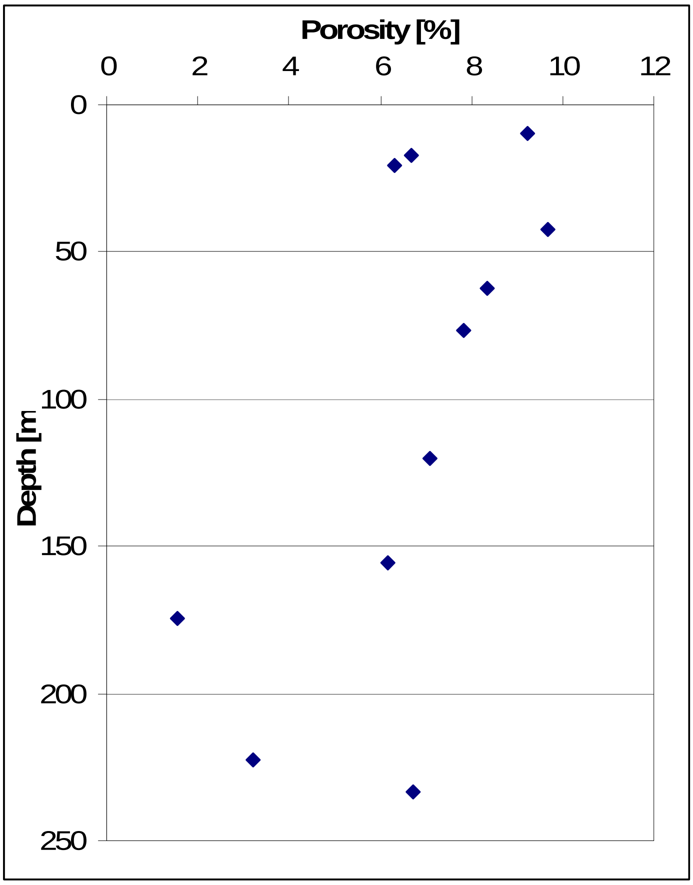

Figure. 6.3 Porosity variation with sample depth of 11 selected mudstone samples

7. Sonic Velocity

Sonic velocity was measured on 9 vertical plugs from the drill core at Denmark's Technical University (DTU) (Table 7.1). Prior to that, porosity and grain density were measured for the plugs at GEUS' core laboratory (Table 7.2). Bulk density (wet) was calculated for the plugs assuming that the pore space was fully water saturated.

7.1 Methods

P-wave velocity was measured using a V-Meter MKII/Tektronix TDS 1012 Oscilloscope. The reported precision of the apparatus is 0.98%. The equipment can measure plugs that are 2.0 –7.0 cm long. This criteria was met in 8/9 samples, but one of the plugs broke into two pieces, each less than 2 cm long (plugs 386 ad 386.1; Table7.1). For the measurements to represent the sampled rock under uniform conditions, the samples should not be cracked, fractured or contain hydrocarbons. Prior to analyses, the samples were kept dry in an oven at 50^{0}C for 2 days.

In brief the procedure was as follows: the sample was placed between two piezoelectric P-wave transducers that were connected to a V-Meter and an Oscilloscope. The V-Meter generates an electric pulse, which is transmitted through the sample between the two transducers. From reading of arrival time for the transmitted P-wave combined with the length of sample, P-wave velocity was calculated. The calculation included subtraction of the system delay.

Each sample was measured twice and the results were found to be reproducible.

7.2 Results

Results are presented in Tables 7.1 and 7.2. Figure 7.1 shows cross-plots of the different parametres (porosity, grain and bulk densities and sonic velocity).

7.3 Discussion

The results show considerable velocity variability ranging from 1729 to 5310 m/s. However, most of the samples from the Bernbjerg Formation and the Lindemans Bugt Formation have sonic velocities between ~3000-4000 m/s. The extreme values are considered unreliable: the highest value (Plug No. 388, 5310 m/s) probably reflects the shortness of the plug, which is on the lower limit of the measurement range (2–7 cm) of the apparatus. The plug in question contained also another piece (Plug No. 388.1, ~3.5 cm long), which gave a velocity of 3492 m/s. Similarly, another plug that broke into two short pieces (Plug No. 386, ~19 and ~18 mm) recorded extreme velocities > 5600 m/s (Table 1).

The plug with the lowest recorded velocity value (Plug No 389, 1729 m/s) had somewhat elevated porosity (9.71%), which may point to the presence of fractures/cracks in the sample. Indeed, a close examination of the plug revealed the presence of a micro-crack in the sample. This velocity value is thus unreliable.

As a conclusion, the small data set analysed indicates that sonic velocity of the mudstones of the Bernbjerg Formation and the Lindemans Bugt Formation most commonly have velocities between 2900 and 4000 m/s. Non-cemented mudstone and heterolithic interlamination (Facies 1AB–3, n=3), which constitutes the bulk of these deposits, have velocity values of ~3300-3600 m/s, whereas locally occurring ankerite and dolomite cemented mudstone (Facies 1C, n=3), have a larger range of measured velocities with values ranging from 2973 to 3928 m/s.

Two samples from the Albrechts Bugt member had high velocities and this probably reflects the presence of matrix cement: one sample with bioturbated limestone (Facies 4A) had a velocity of ~4600 m/s whereas a sample of calcareous sandy mudstone (Facies 4B) had a velocity of ~3800 m/s.

7.4 References

P-wave Velocity by V-Meter MKII/Tektronix TDS 1012 Oscilloscope. 2009. Users manual used at DTU.

Subnr	Dybde (m)	Length (mm)	Dia meter (mm)	Arrival Time (µs)	Velocity (m/s)	Facies
383	234,19	34,57	25	12,8	3604	F2
383.1	234,19	38,66	25	14,4	3275	F2/F3
384	222,45	60,18	25	14	3928	F1C
385	146,20	60,32	25	15,4	3549	F1C
386	142,04	19,22	25	7,6	5674	F2
386.1	142,04	17,94	25	7,4	5784	F2
387	89,72	60,41	25	17,9	2973	F1C/B
388	82,90	20,02	25	8,1	5310	F1
388.1	82,90	34,79	25	13,2	3492	F1
389	24,81	58,58	25	29,6	1729	F1
390	24,03	52,03	25	11,6	4563	F4A
391	17,19	36,48	25	12,4	3787	F4B

Table 7.1. Sonic velocity data. The data in red are considered unreliable due to shortness of the analysed plugs (Plugs 386, 386.1 and 388) or due to presence of a crack (Plug 389). These values are omitted from Figure 1.

Plug ID #1	Plug H/V	Porosity$_{(He)}$ [%]	Grain density [g/cc]	Bulk density [g/cc]
383	V	6,30	2,533	2,436
383,1	V	6,14	2,555	2,460
384	V	1,99	2,793	2,757
385	V	9,11	2,799	2,635
386	V	6,77	2,617	2,508
386,1	V	6,82	2,623	2,512
387	V	5,38	2,880	2,779
388	V	7,64	2,612	2,489
388,1	V	6,69	2,604	2,497
389	V	9,71	2,753	2,583
390	V	3,74	2,748	2,683
391	V	6,93	2,744	2,623

Table 7.2. Porosity, grain density and bulk density of the measured plugs. See Table 7.1 for the Facies division.

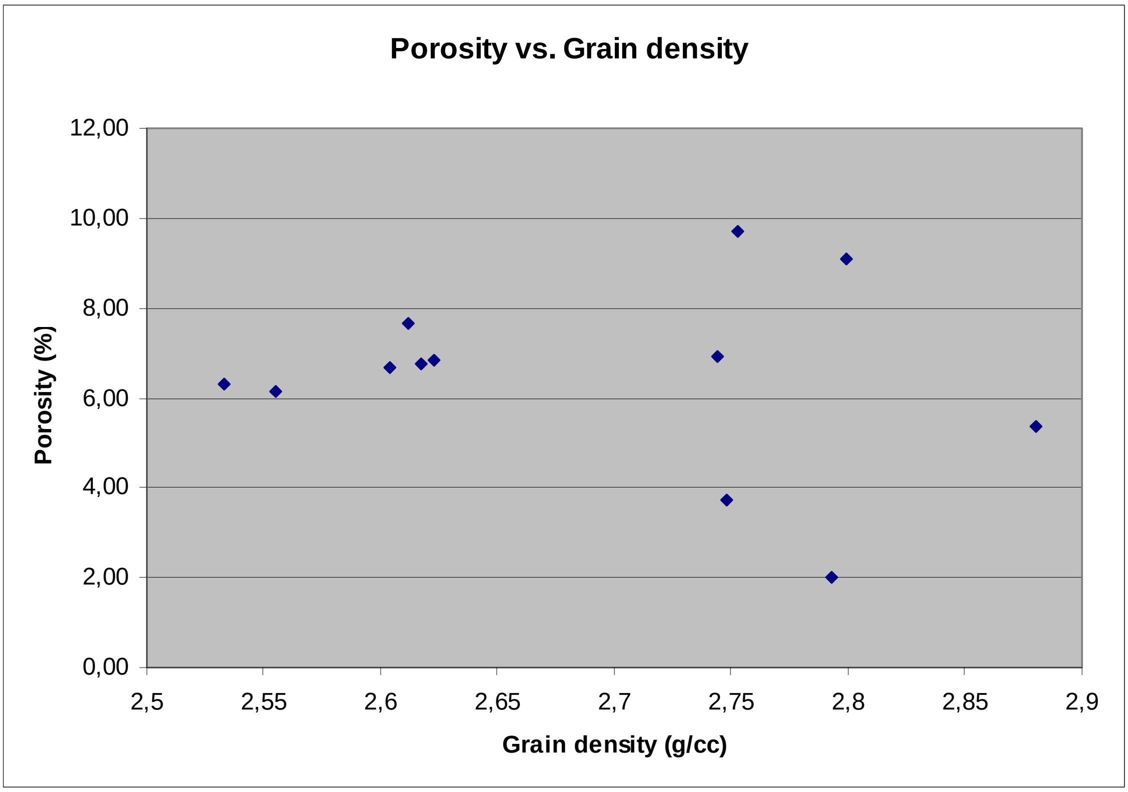

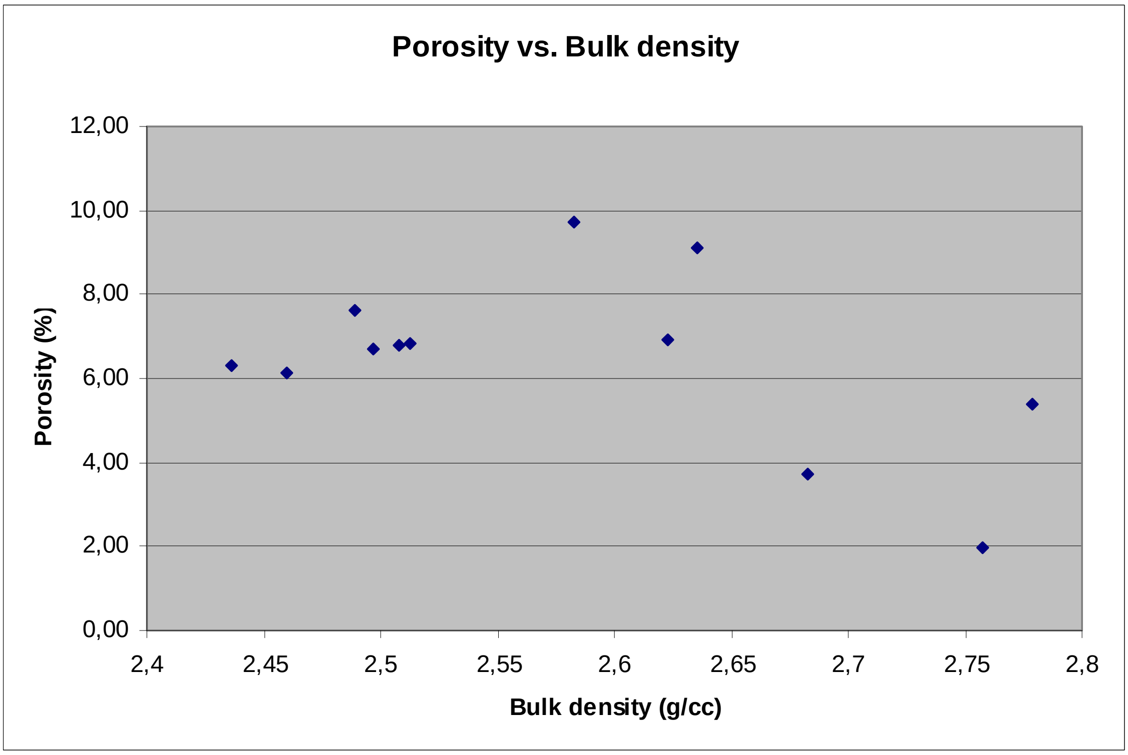

Figure 7.1. Relationships between porosity and grain density, and porosity and bulk density.

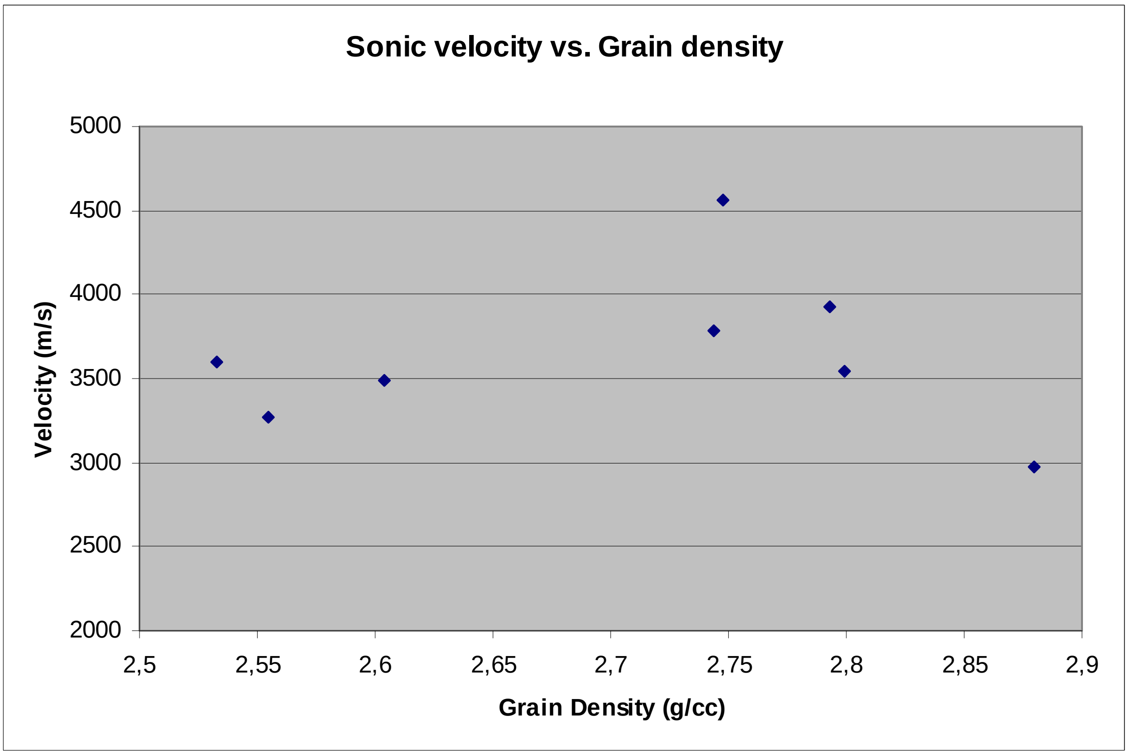

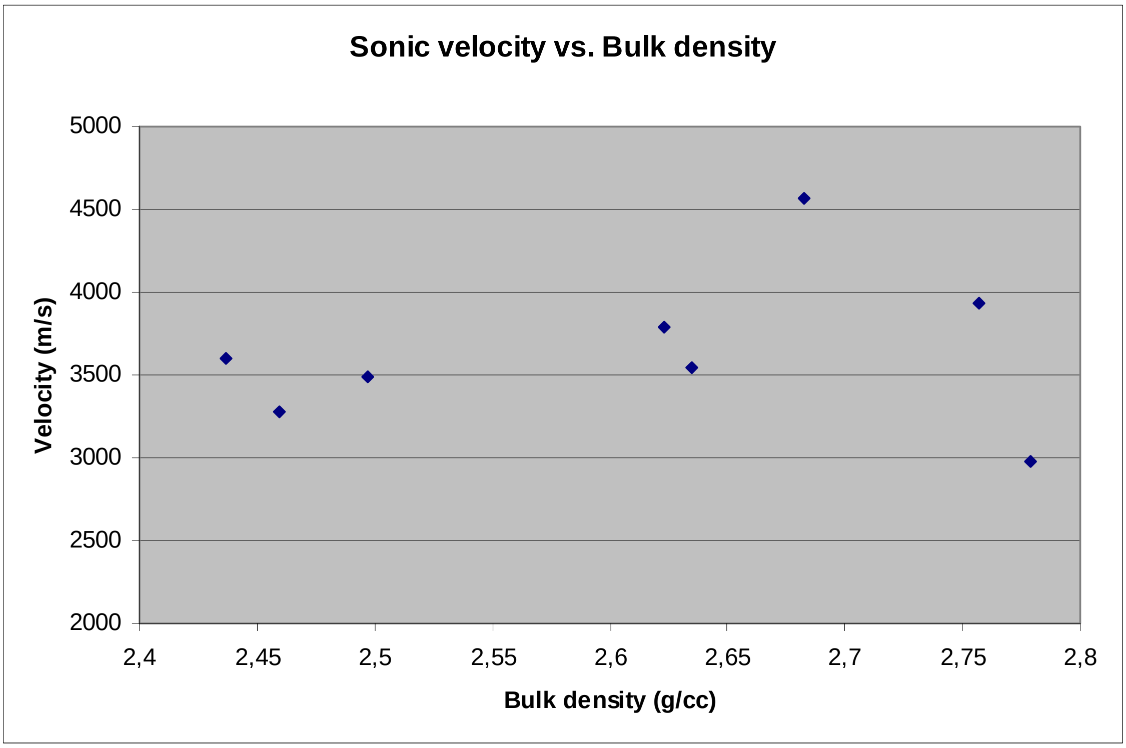

Figure 7.1., continued. Relationships between sonic velocity and grain density, and sonic velocity and bulk density.

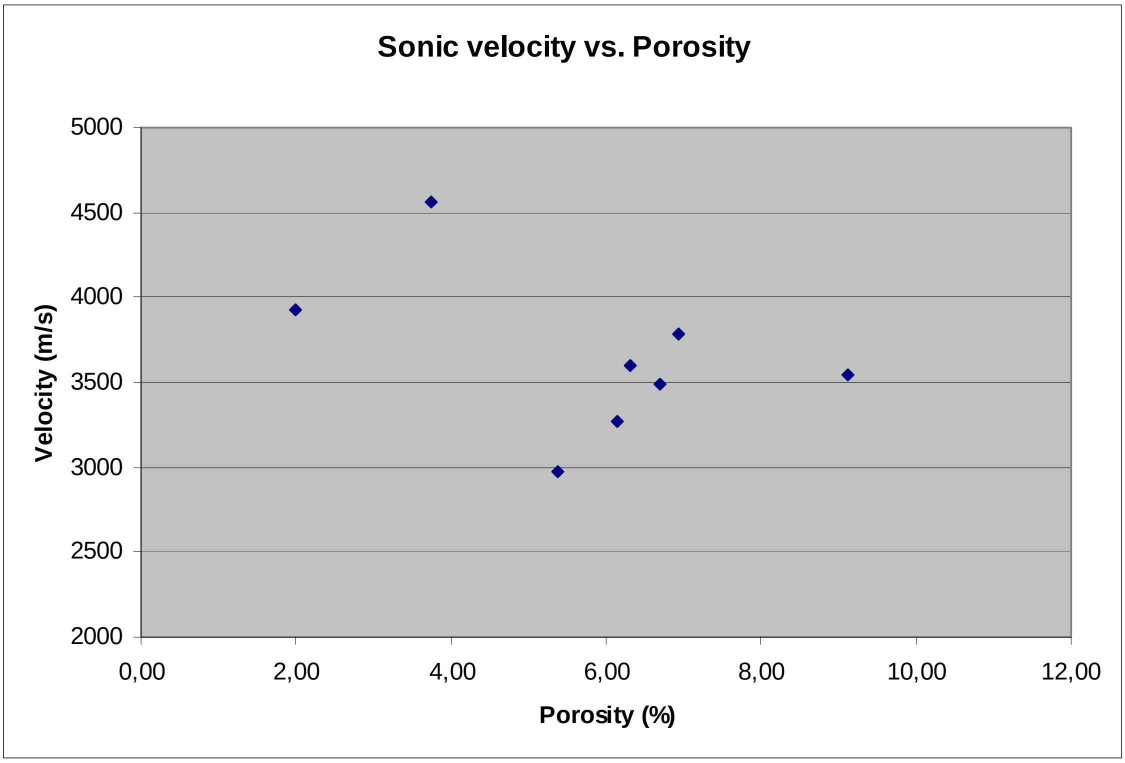

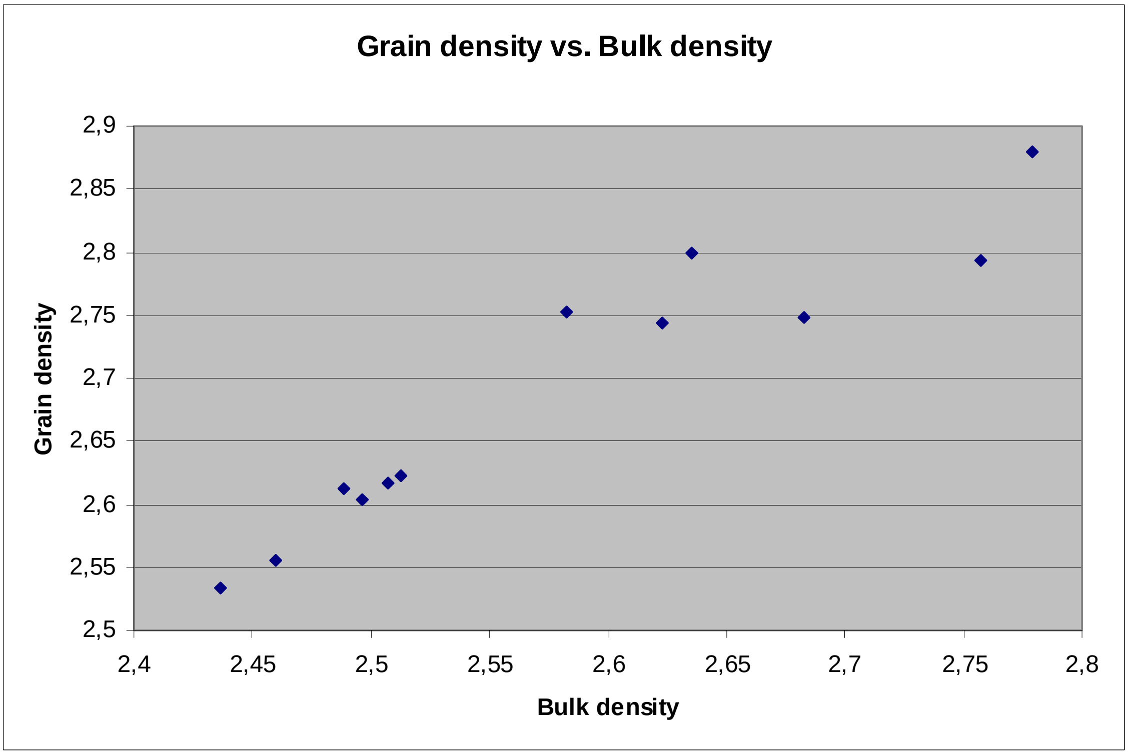

Figure 7.1., continued. Relationships between sonic velocity and porosity, and grain density and bulk density.

8. Petroleum Geology

8.1 Petroleum source potential and thermal maturity

This section reports on the results of TC/TOC/TS/Rock-Eval screening analysis, vitrinite reflectance analysis, kerogen composition analysis and kerogen acttivation energy distribution analysis of samples from the Rødryggen corewell.

8.1.1 Methods

A total of 258 samples covering the entire succession penetrated by the Rødryggen corewell were analysed for total Carbon (TC), total Sulphur (TS), total organic Carbon (TOC), and subjected to Rock-Eval type screening pyrolysis.

Total Carbon (TC) and total Sulphur (TS) were determined by combustion of sample aliquots in a LECO CS-200 induction furnace. Total organic carbon (TOC) was determined by combustion in a LECO CS-200 induction furnace after treatment of sample aliquots by hydrocloric acid in order to remove mineral-bound carbon, and recalculation based on loss of weight.

Rock-Eval-type screening pyrolysis was carried out using a Source Rock Analyser instrument (SRA) manufactured by Humble Instruments and Services (presently Weatherford Laboratories), calibrated using the IFP55000 pyrolysis standard in order to ensure full comparability with standard Rock-Eval data. An in-house standard (Marl Slate, Sunderland Quarry, UK) was used for stability control, with sets of one standard and one blank being run for every 10 samples.

Particulate blocks suited for reflected light microscopy were prepared from 12 samples covering the depth range 25 m to 234.66 m. The samples were lightly crushed and sieved between 63 µm and 1 mm. The analysis fraction from each sample was embedded in epoxy resin, and the blocks were ground and polished to obtain a smooth surface for microscopy. The preparation procedure follows international standards (Taylor et al., 1998).

VR measurements (random, oil immersion) were conducted using a Leitz Orthoplan reflected light microscope equipped with a 32x objective and the Diskus Fossil system

(Hilgers Technisches Buero). The VR readings were taken at 546 nm (monochromatic light). Before measurement the microscope was calibrated against a YAG 0.903%R_o standard with integrated optical zero standard. The average VR for each depth was calculated from a population selected from the total reflectance histogram (Appendices 1 and 2).

A number of samples were also qualitatively inspected for their kerogen content in reflected white light and fluorescing-inducing blue light using a Zeiss microscope.

Activation energy distributions were analysed by means of an SRA bulk-flow pyrolysis system manufactured by Humble Instruments and Services (presently Weatherford Laboratories). A total of seven subsamples of each sample were analysed, using 5 different heating rates: 50°C/minute (run in duplo); 30°C/minute; 10°C/minute; 3°C/Minute; 1°C/minute (run in duplo). The Green River 99901 kinetics standard supplied by Humble Instruments and Services (presently Weatherford Laboratories) was used for calibration. Kinetic parameters were calculated using the Kinetics-2000 software package, developed by Lawrence Livermore National Laboratories (USA) and Humble Instruments and Services (presently Weatherford Laboratories).

8.1.2 Petroleum Potential

TC/TOC/TS/Rock-Eval type screening data are tabulated in Table 8.1.1. Analytical results are plottet versus depth in Fig. 8.1.1., and as 10-sample moving average versus depth in Fig. 8.1.2. The uppermost c. 25 metres of the penetrated succession belongs to the Lower Cretaceous Albrecths Bugt Member of the Palnatokes Bjerg Formation. Lithologically, this is a marly shale, with negligible organic carbon content and thus without any petroleum source potential whatsoever (Table 8.1.1, Figs. 8.1.1. and 8.1.2.).

The remainder of the drilled succession consists of Kimmeridgian – Lower Volgian-Bernbjerg Formation (234.5–97 m) and Middle Volgian – Upper Ryazanian Lindemans Bugt Formation (97–24.4 m). These deposits consist of a black laminated organic-rich shale with a generally rather low content of mineral-bound carbon. These Upper Jurassic–Lower Cretaceous shales form the local equivalent of the Kimmeridge Clay Formation *s.l.* that in the North Atlantic region is known under a variety of names, among these the Hareelv, Kap Leslie, Farsund, Mandal, Draupne, Spekk and Bazhenov formations.

The total Carbon content shown by the black shale succession is generally only slightly higher than the organic Carbon content, indicating a low content of carbonate minerals, although a few “stringers” of carbonate can be observed in the GR-log as well as in the geochemical data (Chapter 3.3). Such thin intervals of carbonate are common in equivalent formations in the North Atlantic region.

The black shale succession penetrated by the Rødryggen corewell is generally characterised by high organic carbon contents. However, notable variation in organic Carbon content is observed with depth (Table 1). The Lindemans Bugt Formation shows an average TOC of 3.5%, ranging from 0.12 to 5.37.% Downwards from c. 80 metres, TOC shows an irregularly decreasing trend until c. 100 metres, where TOC stabilises at approximately 3% until 125 metres. This transitional zone between the Bernbjerg and Lindemans Bugt Formations is interpreted to reflect gradational drowning due to accelerated block rotation (onset of Rift climax, Surlyk, 1978; see Chapter 4 for discussion). The interval c. 173–125 m represents a regressive to aggrading interval (Chapter 4), which is directly reflected in TOC content, which shows an irregularly increasing trend with depth. In the lowermost, transgressive parts of the the Bernbjerg Formation, TOC reach values exceeding 6%.

A major break in organic matter characteristics at c. 125 metres is also evident in other parameters such as TS, S1, S2 and the Hydrogen Index.

The total Sulphur content (TS) is very high in the Lindemans Bugt Formation, commonly 3-4%, occasionally reaching extreme values exceeding 12%. Over the transitional interval interval c. 90 to c. 135 metres, TS passes through a minimum of approximately 2%, whereas in the deeper Bernbjerg Formation portion, TS stabilises at 2.5 – 3%.

The S1 yield is generally low throughout the entire succession, but passes through a minimum close to the zone of maximum regression at 125 metres with average values close to 0.5 mg/g above and average values close to 1.0 mg/g below.

The S2 yield is generally high throughout the entire succession with an average yield close to 12 mg/g and maximum yield close to 20 mg/g. S2 shows an overall decreasing trend from the top of the Lindemans Bugt Formation to a depth of 120 – 125 metres followed by an overall increasing trend with depth. Hence, S2 show near-identical values near the top and near the base of the penetrated succession.

The Hydrogen Index is consistently high, close to 400 on average from the top of the Lindemans Bugt Formation to a depth of c. 90 metres, from which point the Hydrogen Index shows a fairly regular decrease to a depth of 120 – 125 metres. In the deeper parts of the Bernbjerg Formation, the Hydrogen index remains fairly stable at values of 200 – 300.

To conclude, the Lindemans Bugt Formation – to depth of approximately 97 metres – is a rich, oil-prone marine petroleum source rock, containing predominantly type II kerogen. A transition zone between Lindemans Bugt and Bernbjerg formations is present from c. 90 metres to c. 125 metres, where a major shift in organic facies is seen. The Bernbjerg Formation succession generally shows higher proportions of terrestrial organic matter, as indicated by somewhat lower Hydrogen Indices, and the kerogen type may be described at type II/III. However, the generation potential in absolute terms, *i.e.* S2, remains essentially identical to that of the uppermost part of the succession (Figs. 8.1.3. and 8.1.4.).

The interpreted shift in organic facies in the transitional boundary of Bernberg and Lindemans Bugt formations is corroborated by several other independant types of data such as biological marker analysis, stable Carbon isotopic analysis and microscopy, and palynological studies, cfr. relevant sections. The change corresponds to increased tectonic activity in the Wollaston Forland area during the Middle Volgian (Surlyk, 1978; 1990; 2003; Figs. 4.1). This rift climax resulted in accelerated tilted fault block development and basin segmentation and lasted until the Early Ryazanian (Chapter 4).

The petroleum potential of the studied Upper Jurassic–Lower Cretaceous shales as indicated by the analyses carried out on samples collected from the Rødryggen corewell is significantly higher than expected from analyses of outcrop samples collected in the nearby area. Essentially, the petroleum potential as given by the average Hydrogen Index of the core samples is two to three times higher than that observed in outcrop samples. This is very similar to observations made in the Blokelv corewell (Jameson Land). The phenomenon may probably be attributed to the very high proportions of pyritic sulphur present in the samples. Upon weathering, pyrite will generate sulphuric acid that will destroy organic matter in the rock and reduce the apparent petroleum potential. This effect is prominent in outcrop samples, whereas it is not present in core samples.

8.1.3 Thermal maturity

As demonstrated above, samples of the uppermost c. 25 metres of the penetrated succession, which belongs to the Lower Cretaceous Albrecths Bugt Member of the Palnatokes Bjerg Formation, possess essentially nil petroleum potential, and thus yield nonsens Tmax data.

Conversely, samples of the Lindemans Bugt and Bernbjerg formations that make up the remainder of the penetrated succession, show values of Tmax ranging from 419°C to 432°C, steadily increasing with depth (Table 8.1.1, Figs. 8.1.1 and 8.1.2.). Defining the oil window for Type II kerogen as T_{max} = 435–460°C (Espitalié et al. 1985, 1986; Bordenave et al, 1993; Peters and Cassa, 1994), Tmax data suggest that the succession as a whole is immature with respect to petroleum generation. However, the level of thermal maturity clearly increases relatively fast with depth. This is further corroborated by the Production Index, showing values ranging from 0.03 to 0.13, and a steadily increasing trend with depth (Table 8.1.1, Figs. 8.1.1 and 8.1.2.).

Total reflectance histograms (Appendix 10.4) have been measured for all of the twelve selected samples. The mudstones contain relatively abundant huminitic material and it was therefore possible to take from 89 to 174 readings in each of the samples. The average VR values calculated for each depth from a selected VR population considered to represent the indigenous huminite are shown in Table 8.1.2. Despite the short section drilled by Rødryggen-1, the average VR values display an increasing trend with depth that on a semi-log plot defines a relatively well-constrained straight line with a correlation coefficient of r^2 = 0.86 (Figs. 8.1.5 and 8.1.6). The VR gradient intercepts the surface at a VR just above 0.40%R_o, which is too high a value for peaty organic matter (*e.g.* Cohen et al., 1987). This shows that the succession at the well-site has been exhumed and parts of the strata have been removed by erosion.

The mudstones reach a VR of about 0.60%R_o in the lowermost part of the well, and if the start of the oil window is set at a maturity level corresponding to c. 0.60%R_o the mudstones are thermally immature with regard to petroleum generation.

All available maturity indicators are in perfect agreement both with respect to the overall level of thermal maturity relative to petroleum generation and with respect to the slight change in maturity with depth. Hence, in addition to the parameters Tmax, PI and R_o discussed above, biological marker-based maturity indicators such as homohopane and regular sterane isomerisation ratios point to the same results: overall pre-oil window maturity and increasing level of thermal maturity with depth, see section on biological markers (Chapter 8.2).

Assessment of the uplift history of the drilled succession is difficult based on the available data since simple "backwards" extrapolation based on maturity data from only approximately 200 metres of section must be deemed reckless.

Japsen et al. (2009), based on apatite fission track analysis (AFTA) of a Jurassic sandstone sample collected west of the drilling position and data from nearby regions, estimate that 1-2 kilometres of basalts and Eocene sediments have been removed from the area. Maturity modelling (Petromod) using a very simple approach, i.e. simple subsidence followed by exhumation from the start of the Neogene, using only VR data from the terrestrially influenced Bernbjerg Formation (in order to avoid possible suppression in the marine-dominated Lindemans Bugt Fm.) yield approximately 1.5 kilometres of uplift (A. Mathiesen, 2010, pers. comm.).Despite the overall agreement between the two figures, it must be emphazised that both represent estimates that may at best serve as rough guides to the order of magnitude of uplift in the area.

8.1.4 Kerogen composition

Two samples (17097, 25.0 m; 17916, 56.88 m) from the Lindemans Bugt Formation were qualitatively analysed under the microscope. The samples are characterised by abundant framboidal pyrite and a slightly fluorescing groundmass, which suggests the presence of amorphous organic matter (AOM) intimately associated with the mineral matrix (Figs 8.1.7 and 8.1.8). The structured liptinitic kerogen consists of alginite, liptodetrinite and possibly some sporinite. Some of the alginite appears to have a morphology similar to the marine algae *Tasmanites* and *Leiosphaeridae* (Figs 8.1.7 and 8.1.8). Scattered small huminite and inertinite particles are also present. The kerogen composition of samples 17097 and 17916 is thus predominantly marine with a minor terrigenous contribution. They are rich source rocks with HI values of 379 mg HC/g TOC and 316 mg HC/g TOC, respectively. The predominantly marine character of these two samples is further corroborated by biological marker data. Both samples show high proportions of C_{30} desmethyl steranes that are recognised as indicators contributions from marine algae to the kerogen.

Two samples (18012, 148.46 m; 18086, 216.55 m) from the Bernbjerg Formation were likewise investigated. The samples are characterised by less framboidal pyrite than the two Lindemans Bugt Formation samples and a weakly fluorescing groundmass (Figs. 8.1.9. and 8.1.10.). Overall algal-derived organic matter appears to be less abundant. In contrast, terrigenous organic matter constitutes a considerably larger proportion of the kerogen, and larger huminite and inertinite particles are relatively abundant (Figs. 8.1.9. and 8.1.10.). Samples 18012 and 18086 have HI values of 256 mg HC/g TOC and 224 mg HC/g TOC, respectively, and the immaturity of the mudstones adds credibility to the assumption that the lower HI values (compared to the mudstones of the overlying Lindemans Bugt Formation) are not due to generation and exhaustion of the source rock potential, but rather to a change towards a more terrigenous kerogen composition. Again, biological marker data corroborate this interpretation. Both samples show only minor proportions of marine-derived C_{30} desmethyl steranes, whereas C_{29} steranes that are generally abundant in terrestrial organic matter and coals, constitute more than 50% of the regular steranes in both samples

8.1.5 Activation energy distribution

Activation energy distributions and Arrhenius factors were computed for two samples 2010008-17895 (37.88m) and 2010008-18054 (187.85m), representing the Lindemans Bugt Formation and the Bernbjerg Formation, respectively. Both samples show relative broad Ea-distributions, sample 18054 however somewhat broader than sample 17895 (Table 8.1.3, Figs. 8.1.11: and 8.1.12.). The distributions suggest mixed kerogen, and the slightly broader distribution observed for sample 18054, a relatively higher proportion of terrestrial organic matter. This is in perfect accordance with other data types.

8.1.6 Conclusions

- The Albrechts Bugt Member of the Palnatokes Bjerg Formation penetrated by the Rødryggen-1 corewell is devoid of petroleum source potential.
- The Rødryggen-1 corewell penetrated more than 200 metres of Kimmeridgian – Ryazanian Lindemans Bugt and Bernbjerg Formation organic-rich mudrocks classified as oilprone petroleum source rocks.
- The Lindemans Bugt Formation shales show an average TOC of 3.50% and an average S2 yield of app. 12.7 mg/g. The Hydorgen Index ranges between 9 and 445 with an average of 333.
- The Bernbjerg Formation shales show an average TOC of 4.84% and an average S2 yield of app. 11,5 mg/g. The Hydrogen Index ranges between 136 and 342 with an average of 235.
- The Lindemans Bugt Formation contains predominantly marine Type II kerogen, whereas the Bernbjerg Formation shows higher proportions of terrestrial organic matter and contains mixed Type II/III kerogen. This diffrence is consistently indicated by data from a number of independant types of analyses such TC/TOC/TC/Rock-Eval screening, organic petrology, biological marker analysis, stable Carbon isotope analysis, palynology and sedimentary facies. The change is interpreted to correspond to increased

tectonic activity, which resulted in accelerated tilted fault block development and basin segmentation (Chapter 4).

- The succession as a whole is immature with respect to petroleum generation, but a clearly increasing trend in the level of thermal maturity with depth is consistently indicated by a number of different independent analysis types.

8.1.7 References

Bordenave, M. L., Espitalié, J., Leplat, P., Oudin, J. L. & Vandenbrouke, M., 1993: Chapter II-2: Screening techniques for source rock evaluation. In: Bordenave, M.L. (ed.): Applied petroleum geochemistry. Paris, Éditions Technip, 219–278.

Cohen, A. D., Raymond, R. Jr., Archuleta, L. M. & Mann, D. A., 1987: Preliminary study of the reflectance of huminite macerals in recent surface peat. Organic Geochemistry, **11**, 429–430.

Espitalié, J., Deroo, G. & Marquis, F., 1985 : La pyrolyse Rock-Eval et ses applications. Part II. Revue de l'Institut Francais du Pétrole, **40**, 755–784.

Espitalié, J., Deroo, G. & Marquis, F., 1986 : La pyrolyse Rock-Eval et ses applications. Part III. Revue de l'Institut Francais du Pétrole, **41**, 73–89.

Peters, K. E. & Cassa, M. R., 1994 : Applied source rock geochemisry. In: Magoon, L. B. & Dow, W. G. (eds.): The petroleum system – from source to trap. American Association of Petroleum Geologists Memoir, **60**, 93–120.

Taylor, G. H., Teichmüller, M., Davis, A., Diessel, C. F. K., Littke, R. & Robert, P., 1998: Organic Petrology. Berlin, Stuttgart, Gebrüder Borntraeger, 704 pp.

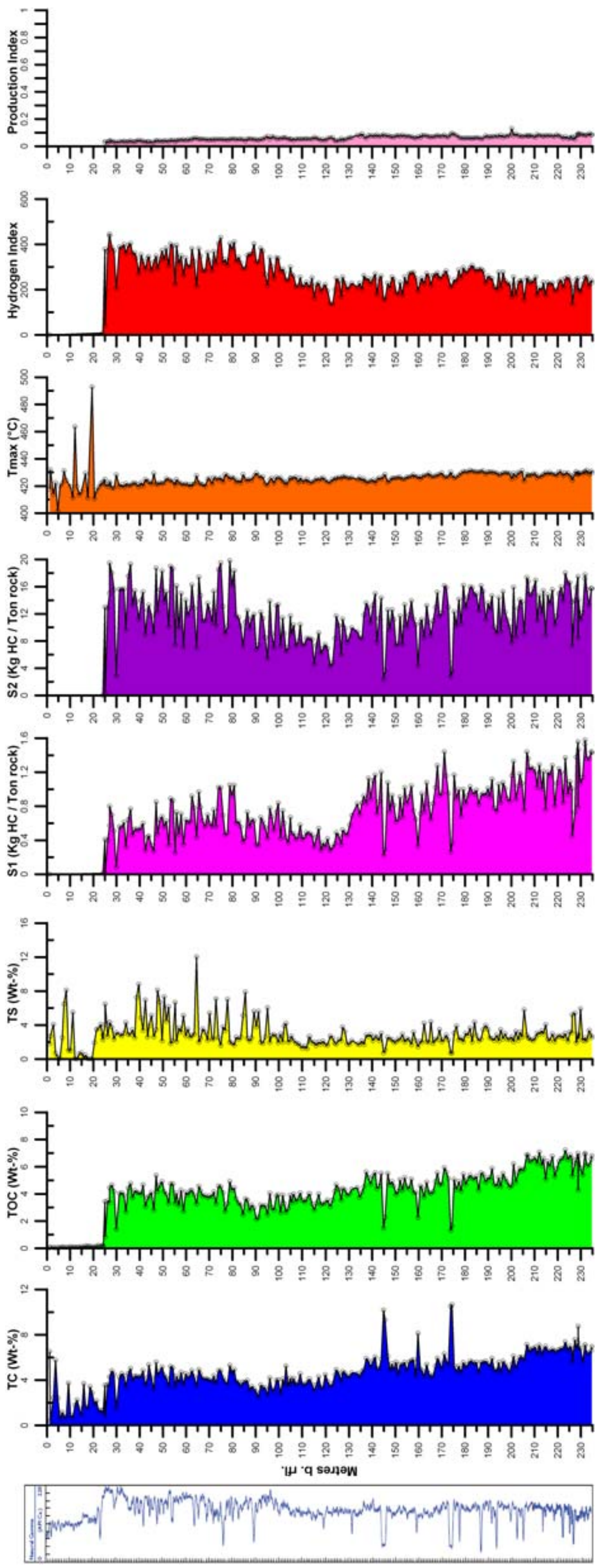

Figure 8.1.1. Organic geochemical screening data plottet versus depth. GR-log shown on the left.

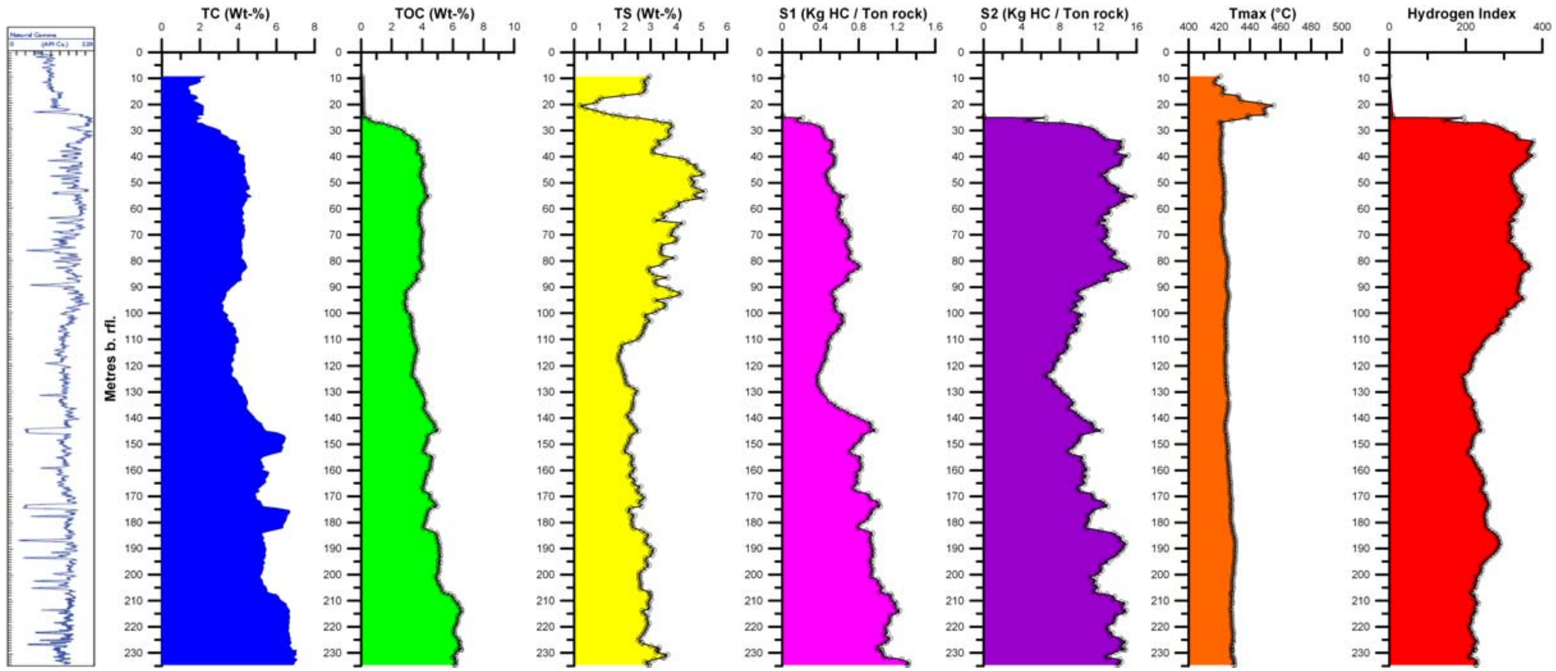

Figure 8.1.2. Organic geochemical screening data, 10-sample moving average plottet versus depth. GR-log shown on the left.

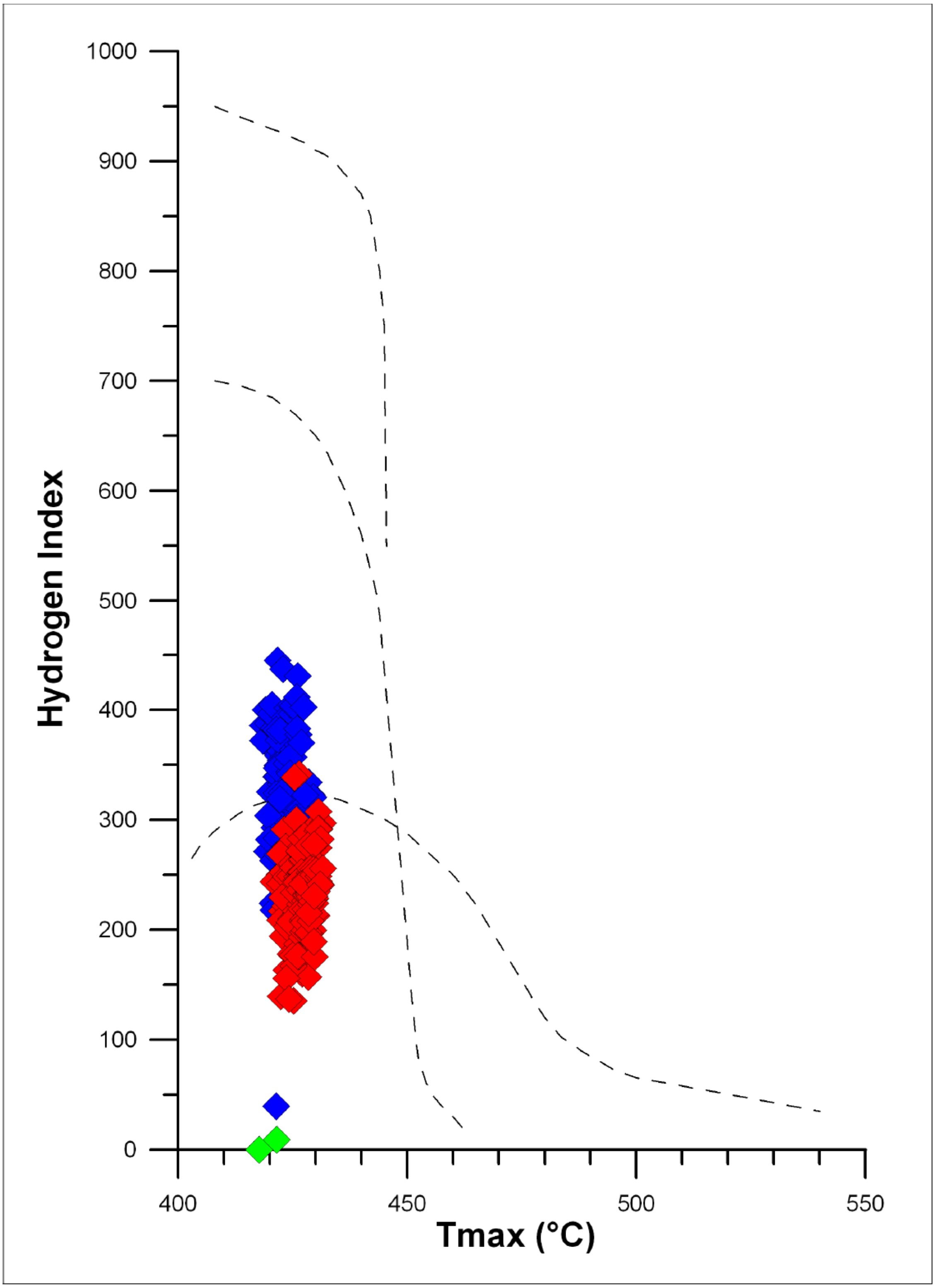

Figure. 8.1.3. Tmax *versus* Hydrogen Index for samples from the Rødryggen corewell. Green symbols: Albrechts Bugt Member (Palnatokes Bjerg Formation); blue symbols: Lindemans Bugt Formation; red symbols: Bernbjerg Formation

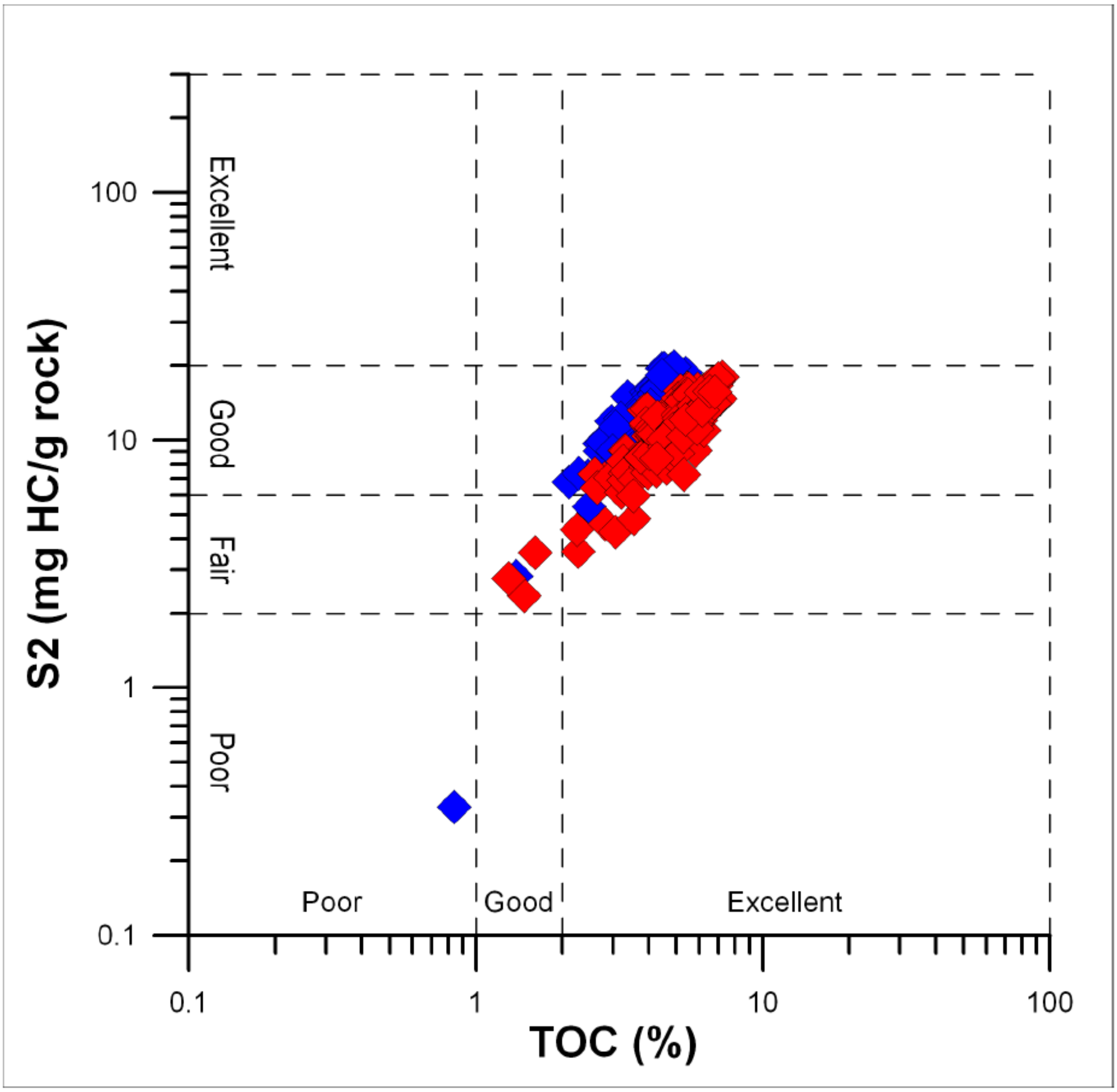

Figure 8.1.4. TOC versus S2 for samples from the Rødryggen corewell. Blue symbols: Lindemans Bugt Formation; red symbols: Bernbjerg Formation.

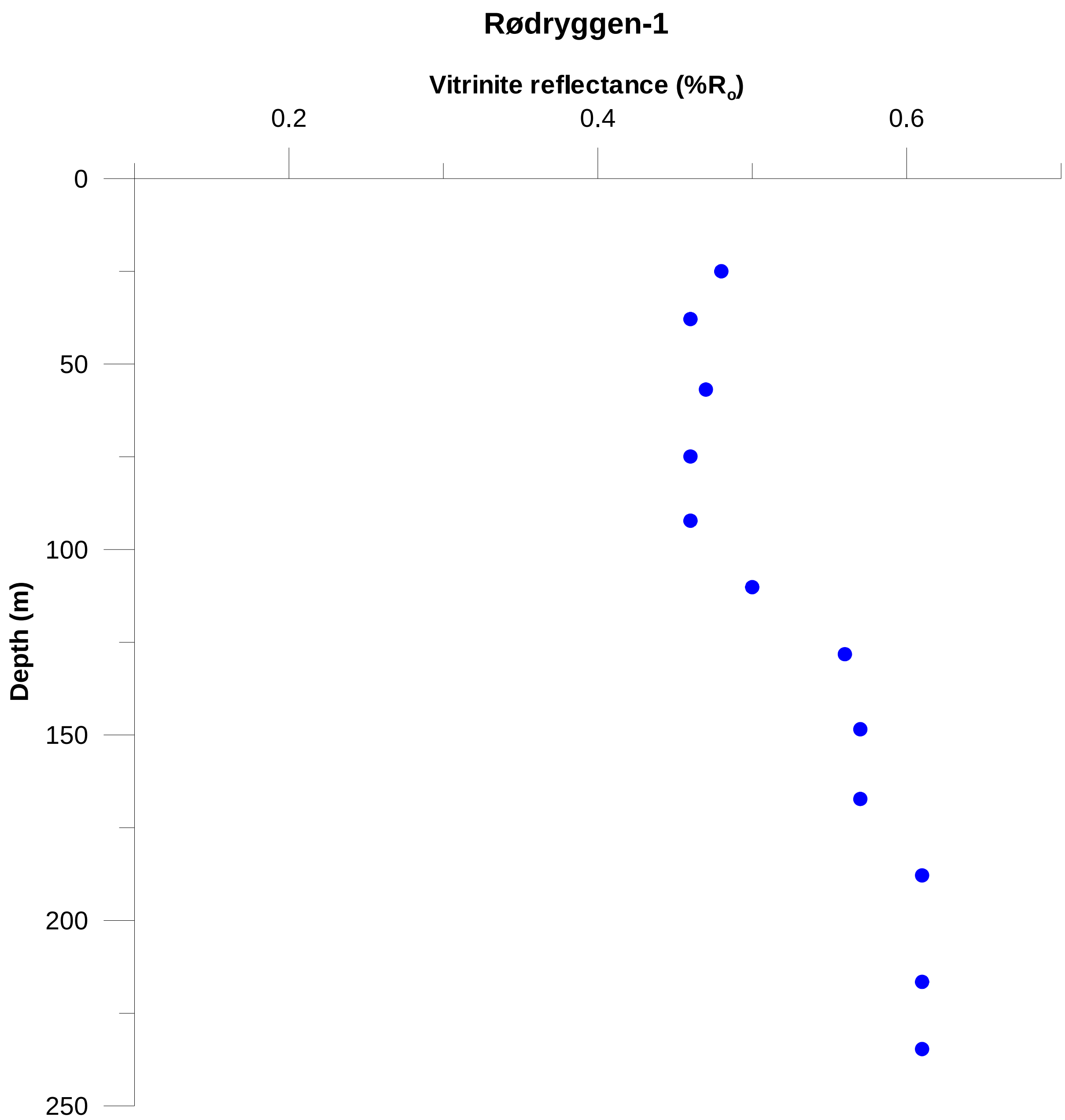

Figure 8.1.5. VR gradient of the Rødryggen-1 well.

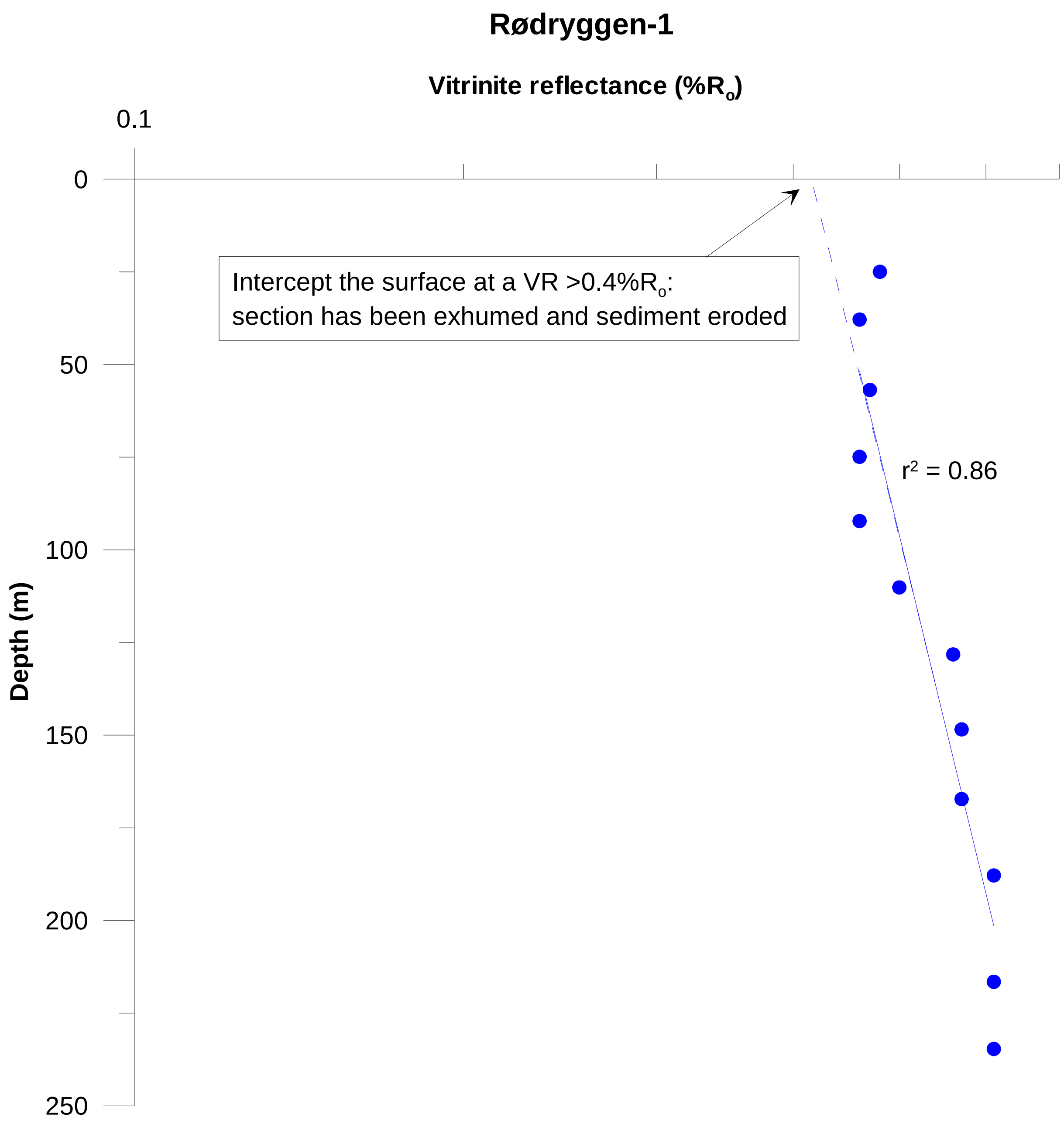

Figure 8.1.6. Semi-log plot showing a well-defined straight VR gradient intercepting the surface at a VR just above 0.40%R_o. The gradient shows a gradual increase in VR reaching approximately 0.60%R_o in the deepest part of the well. The mudstones are thermally immature with regard to petroleum generation.

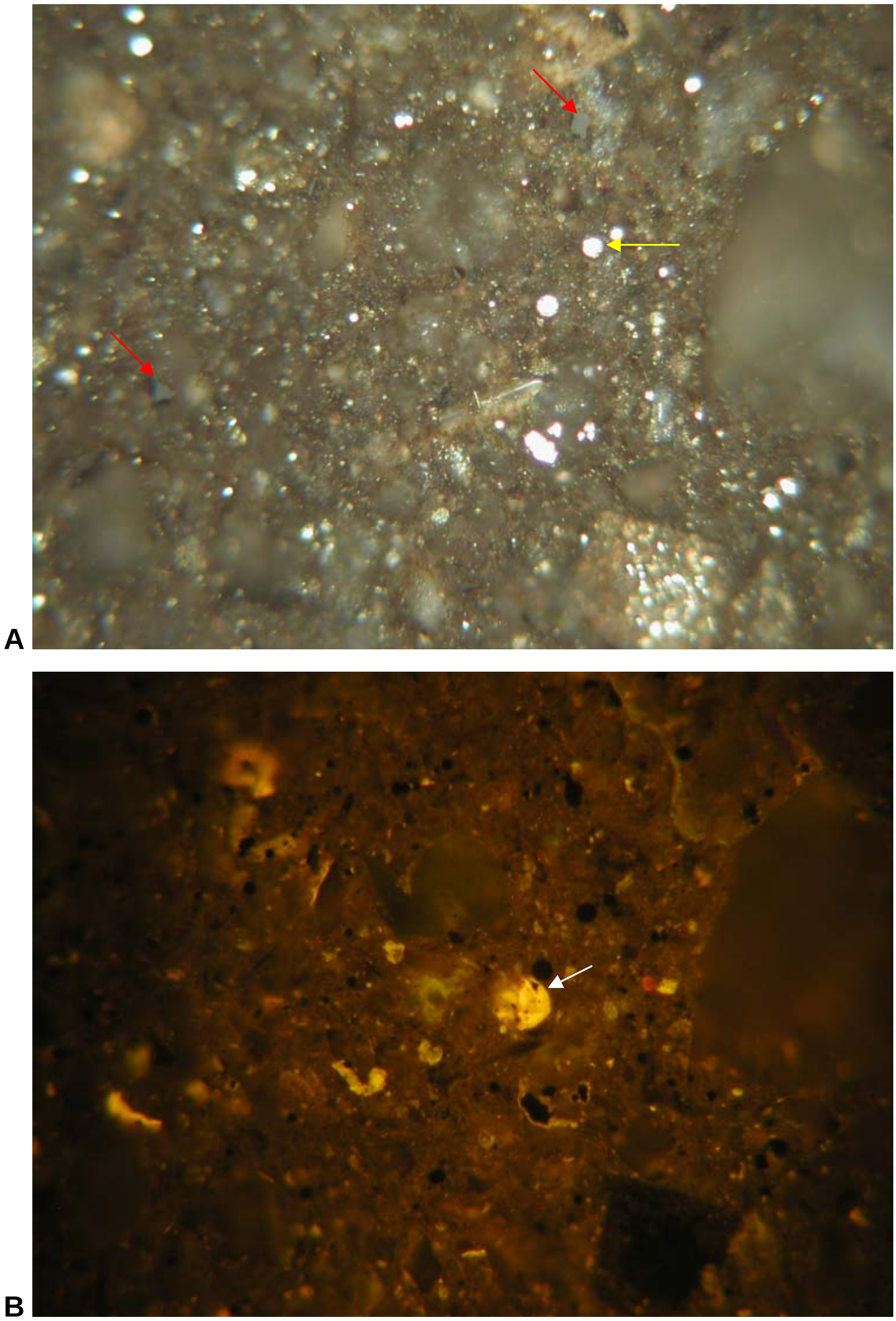

Figure 8.1.7. Photomicrographs (incident light, oil immersion) of the kerogen in sample 17097, 25.0 m. A and B show same area, but A in white reflected light and B in fluorescing-inducing blue light. Scale: 1 cm = ~25 µm. **A**. Few and small huminite and inertinite particles (red arrows) and abundant framboidal pyrite (yellow arrow) in the mineral matrix. **B**. Slightly fluorescing groundmass, detrital liptinite and alginite, some with the morphology similar to *Leiospaerida* algae (seen parallel to bedding; white arrow).

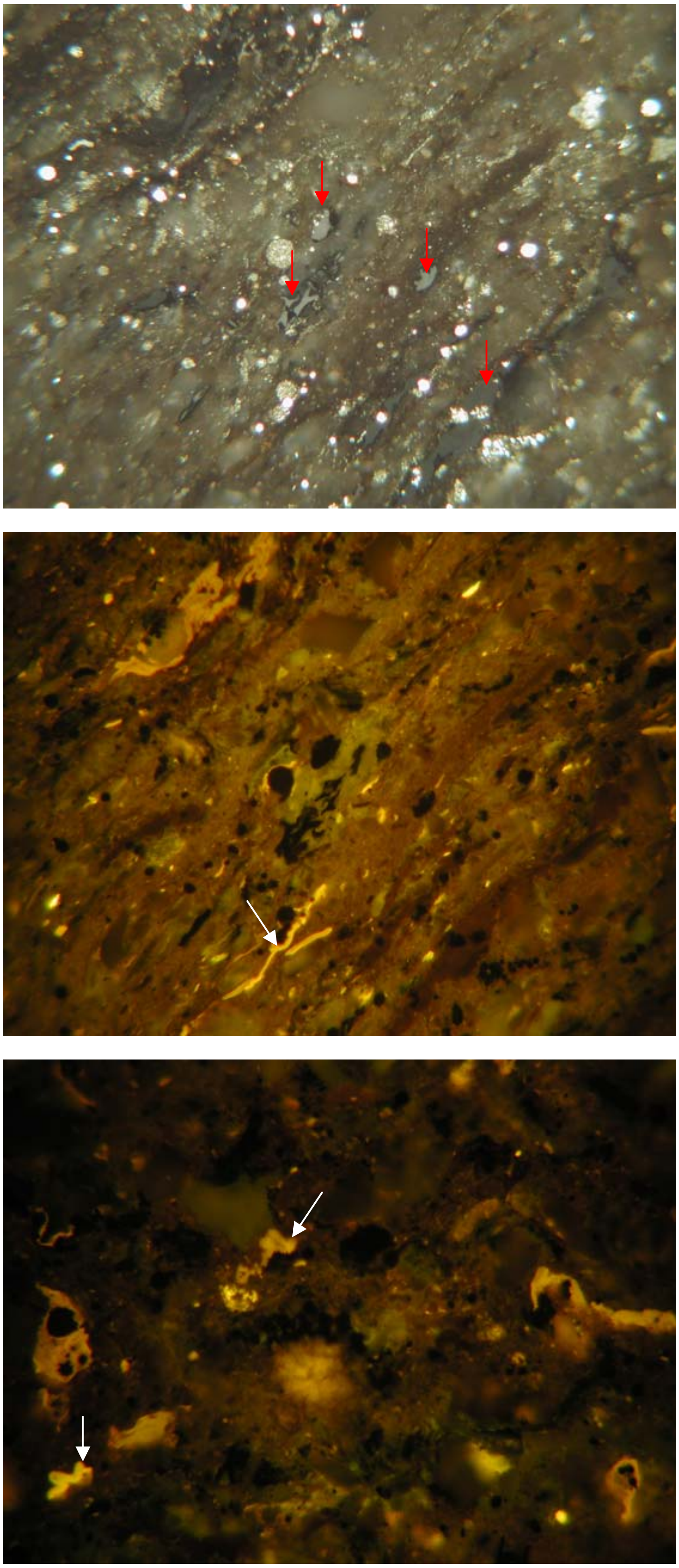

A

B

C

Figure 8.1.8. Photomicrographs (incident light, oil immersion) of the kerogen in sample 17916, 56.88 m. A in white reflected light, B and C in fluorescing-inducing blue light. Scale: 1 cm = ~30 µm. **A**. Few and

small huminite and inertinite particles (red arrows) and framboidal pyrite in the mineral matrix. **B**. Same area as A. Slightly fluorescing groundmass, detrital liptinite and alginite, some with the morphology similar to *Leiospaerida* algae (white arrow). **C**. Slightly fluorescing groundmass, detrital liptinite and alginite, some with the morphology similar to *Tasminites* algae (white arrows).

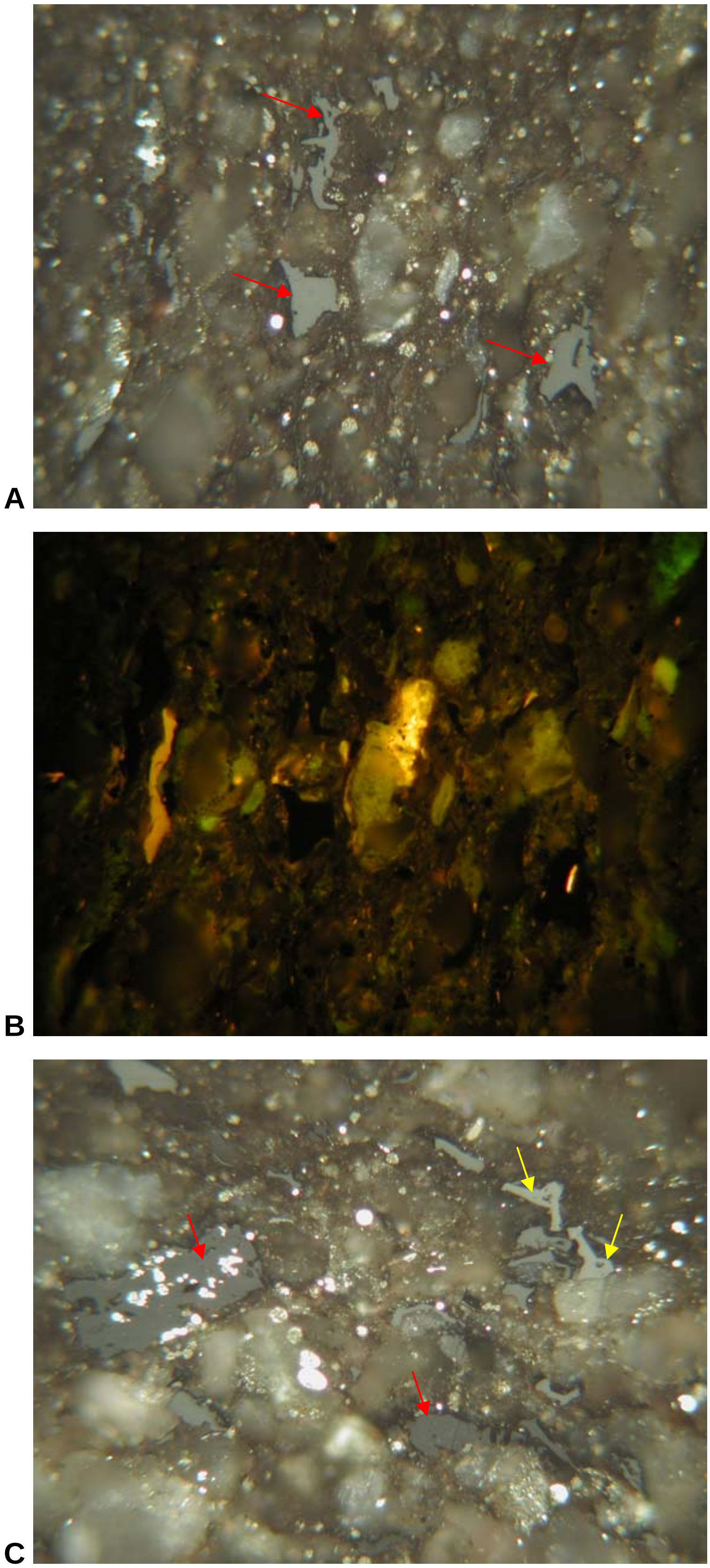

Figure 8.1.9. Photomicrographs (incident light, oil immersion) of the kerogen in sample 18012, 148.46 m. A and C in white reflected light, B in fluorescing-inducing blue light. Scale: 1 cm = ~30 µm. **A**.

Abundant larger huminite and inertinite particles (red arrows) and minor framboidal pyrite in the mineral matrix. **B**. Same area as A. Weakly fluorescing groundmass. **C**. Abundant larger huminite (red arrows) and inertinite (yellow arrows) particles. The huminite is associated with framboidal pyrite.

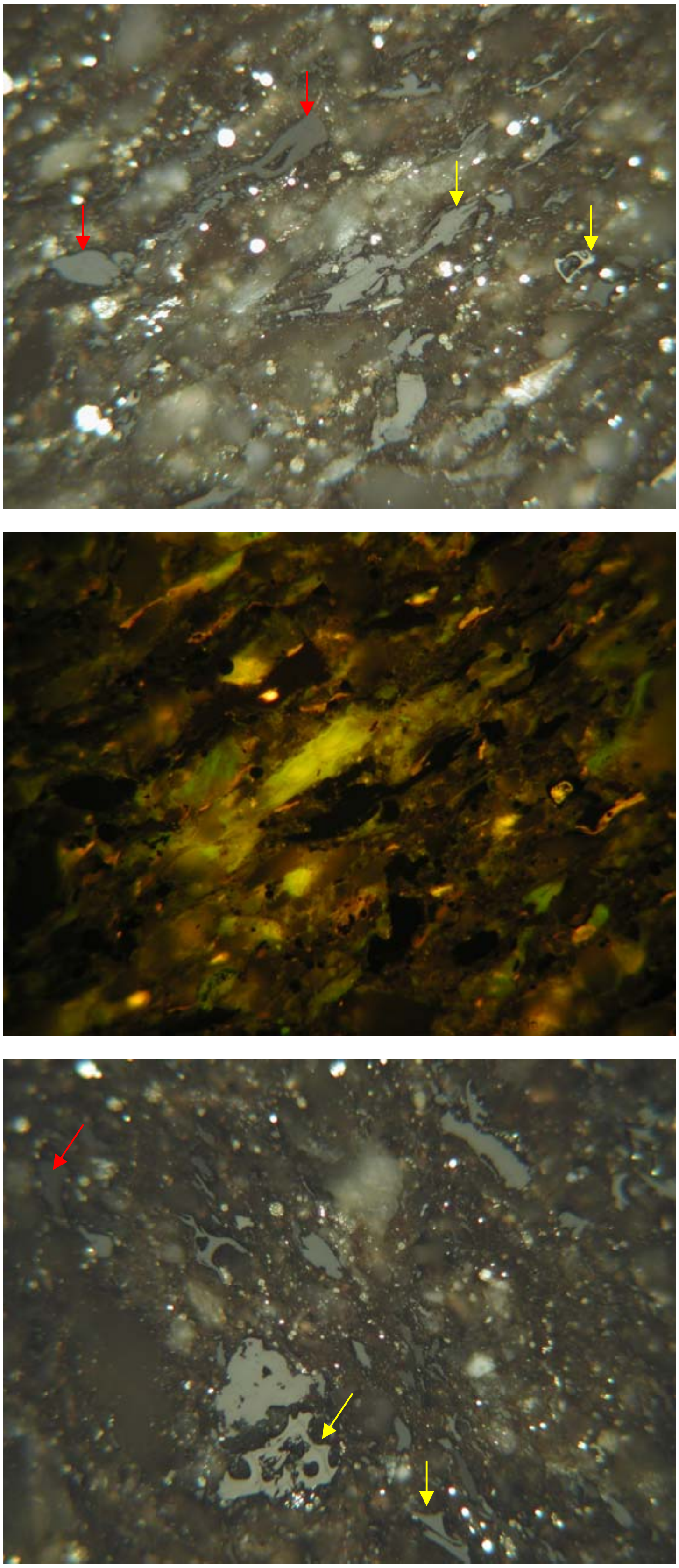

A

B

C

Figure 8.1.10. Photomicrographs (incident light, oil immersion) of the kerogen in sample 18086, 216.55 m. A and C in white reflected light, B in fluorescing-inducing blue light. Scale: 1 cm = ~30 µm. **A**.

Abundant larger huminite (red arrows) and inertinite (yellow arrows) particles and minor framboidal pyrite in the mineral matrix. **B**. Same area as A. Weakly fluorescing groundmass. **C**. Abundant larger huminite (red arrow) and inertinite (yellow arrows) particles. Minor amounts of framboidal pyrite are present.

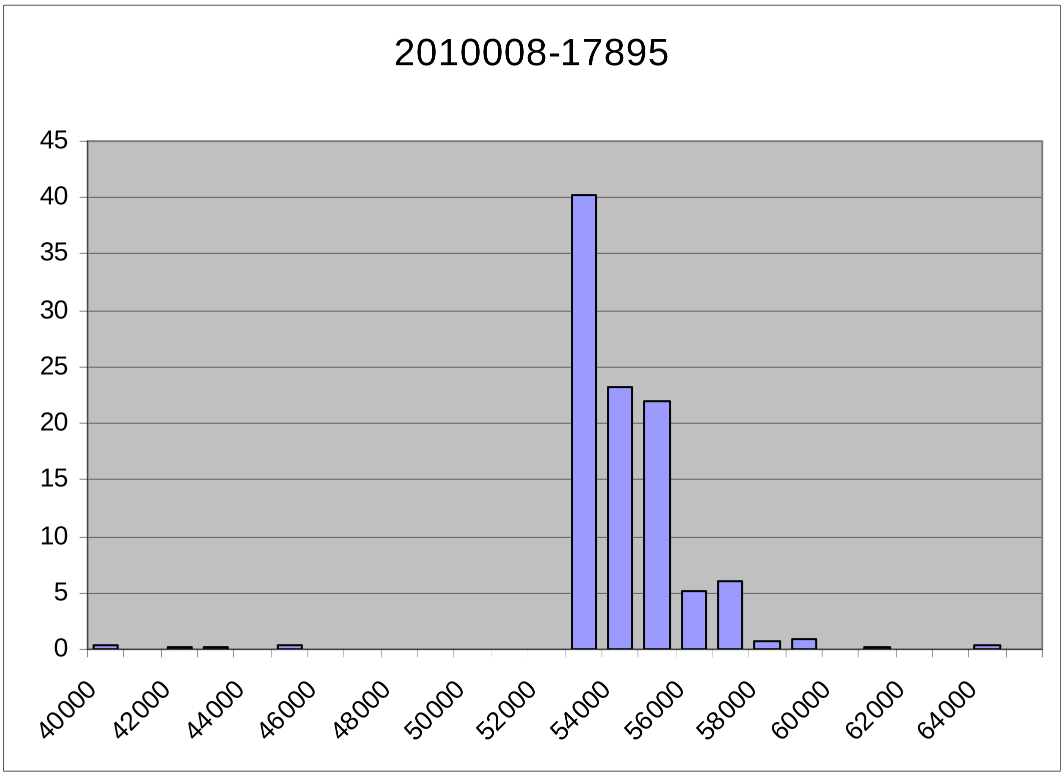

Figure 8.1.11. Activation energy distribution, sample 2010008-17895 (37.88 m).

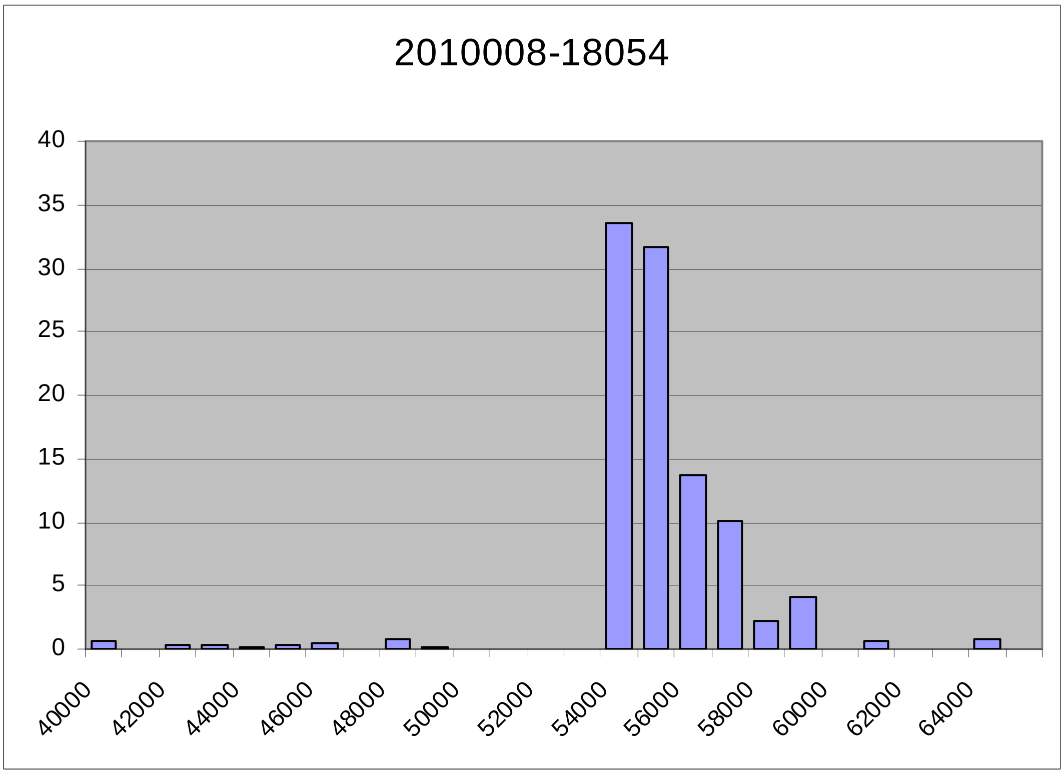

Figure 8.1.12. Activation energy distribution, sample 2010008-18054 (187.85m).

Table 8.1.1. Organic geochemical screening data

Lab.no.	Sample	Depth (m)	TOC (%)	TC (%)	TS (%)	Tmax (°C)	S1 (mg/g)	S2 (mg/g)	HI	PI	PC
17095	517001-1	1,1	0,05	6,53	1,80	418	0,00		0	0,00	0,00
17857	517001-339	1,46	0,07	0,40	2,68	432					
17858	517001-338	2,78	0,06	2,40	4,09	414					
17859	517001-337	3,73	0,04	5,77	0,68	423					
17860	517001-336	4,65	0,04	2,41	0,22	402					
17861	517001-335	5,57	0,07	0,57	0,06	420					
17862	517001-334	6,59	0,10	1,18	2,50	422					
17863	517001-333	7,35	0,07	0,79	6,48	431					
17864	517001-332	8,35	0,07	0,77	8,12	424					
17865	517001-331	9,22	0,07	3,74	1,02	399					
17866	517001-330	10,17	0,11	0,91	1,00	420					
17867	517001-329	11,14	0,10	0,71	5,51	411					
17868	517001-328	12,05	0,08	1,79	0,02	464					
17869	517001-327	13,02	0,11	2,25	0,02	420					
17870	517001-326	13,90	0,09	1,52	0,61	413					
17871	517001-325	14,84	0,13	0,92	0,73	416					
17872	517001-324	15,85	0,08	3,70	0,14	526					
17873	517001-323	16,63	0,17	1,70	0,47	429					
17874	517001-322	17,60	0,17	1,53	0,03	411					
17875	517001-321	18,52	0,13	3,43	0,03	527					
17876	517001-320	19,44	0,12	2,87	0,02	493					
17877	517001-319	20,44	0,10	1,86	1,92	411					
17878	517001-318	21,38	0,15	2,17	3,47	417					
17879	517001-317	22,24	0,21	1,25	3,59	419					
17880	517001-316	23,25	0,16	1,35	4,09	422					
17096	517001-3	24,1	0,22	1,13	2,26	422	0,01	0,02	9	0,33	0,00
17881	517001-315	24,26	0,12	1,35	2,77	423					
17097	517001-5	25,0	3,43	3,54	4,05	425	0,41	12,97	379	0,03	1,11
17882	517001-314	25,13	0,84	0,81	6,49	421	0,01	0,33	39	0,03	0,03
17883	517001-313	26,13	3,48	3,61	2,64	420	0,40	12,83	368	0,03	1,10
17884	517001-312	26,97	3,37	3,61	4,31	422	0,57	15,00	445	0,04	1,29
17098	517001-7	27,0	4,45	4,30	4,29	423	0,80	19,46	437	0,04	1,68

Lab.no.	Sample	Depth (m)	TOC (%)	TC (%)	TS (%)	Tmax (°C)	S1 (mg/g)	S2 (mg/g)	HI	PI	PC
17885	517001-311	27,96	4,66	4,83	3,76	419	0,70	17,99	386	0,04	1,55
17886	517001-310	28,89	4,19	4,52	2,34	419	0,51	15,59	372	0,03	1,34
17887	517001-309	29,89	1,38	1,47	3,11	428	0,08	2,82	204	0,03	0,24
17888	517001-308	31,25	4,02	4,25	2,91	420	0,56	15,61	388	0,03	1,34
17889	517001-307	32,22	4,08	4,58	2,71	421	0,55	15,63	384	0,03	1,34
17890	517001-306	33,18	3,92	4,38	3,05	419	0,61	15,70	400	0,04	1,35
17891	517001-305	34,02	2,69	3,40	4,30	422	0,32	9,67	360	0,03	0,83
17892	517001-304	35,02	4,42	4,60	2,90	420	0,64	17,53	396	0,04	1,51
17893	517001-303	36,03	4,77	5,03	2,87	421	0,77	19,32	405	0,04	1,67
17894	517001-302	36,89	3,69	4,01	3,45	422	0,46	13,24	358	0,03	1,14
17895	517001-301	37,88	4,25	4,35	2,52	422	0,53	15,41	363	0,03	1,32
17896	517001-300	38,60	4,07	4,36	7,24	421	0,53	13,79	339	0,04	1,19
17897	517001-299	39,61	4,12	4,26	8,80	419	0,52	11,17	271	0,04	0,97
17898	517001-298	40,62	3,95	4,36	4,84	422	0,55	13,99	354	0,04	1,21
17899	517001-297	41,45	4,68	4,84	3,37	420	0,60	15,23	326	0,04	1,31
17900	517001-296	42,44	3,07	3,55	6,96	425	0,28	8,93	291	0,03	0,76
17901	517001-295	43,43	3,70	4,25	2,59	424	0,44	12,52	339	0,03	1,08
17902	517001-294	43,91	3,84	5,36	3,87	423	0,45	13,29	347	0,03	1,14
17903	517001-293	45,08	4,13	4,21	5,15	421	0,34	11,70	283	0,03	1,00
17904	517001-292	46,09	2,80	3,14	2,61	429	0,27	9,05	323	0,03	0,77
17905	517001-291	47,06	5,37	5,60	3,47	422	0,85	18,75	349	0,04	1,63
17906	517001-290	47,67	4,16	4,45	8,13	421	0,47	12,19	293	0,04	1,05
17907	517001-289	48,67	4,66	4,80	6,71	423	0,64	15,53	334	0,04	1,34
17908	517001-288	49,66	4,91	5,17	2,14	422	0,68	18,31	373	0,04	1,58
17909	517001-287	50,53	4,16	4,43	7,35	423	0,56	13,83	332	0,04	1,19
17910	517001-286	51,48	3,99	4,21	4,45	425	0,63	15,27	383	0,04	1,32
17911	517001-285	52,48	3,31	3,46	6,16	425	0,34	10,11	306	0,03	0,87
17912	517001-284	53,33	4,74	5,21	1,82	424	0,89	19,03	402	0,04	1,65
17913	517001-283	54,31	4,75	5,09	2,15	423	0,87	18,66	393	0,04	1,62
17914	517001-282	55,30	3,31	3,40	6,66	421	0,25	7,42	224	0,03	0,64
17915	517001-281	55,88	4,07	4,38	2,05	425	0,73	16,13	396	0,04	1,40

Lab.no.	Sample	Depth (m)	TOC (%)	TC (%)	TS (%)	Tmax (°C)	S1 (mg/g)	S2 (mg/g)	HI	PI	PC
17916	517001-280	56,88	3,13	3,80	3,69	423	0,47	9,89	316	0,05	0,86
17917	517001-279	57,84	4,29	4,69	3,14	422	0,71	15,01	350	0,05	1,30
17918	517001-278	58,83	2,70	3,64	5,13	421	0,35	7,11	263	0,05	0,62
17919	517001-277	59,85	4,13	4,58	2,68	422	0,64	14,03	340	0,04	1,22
17920	517001-276	60,80	3,91	4,13	3,56	421	0,61	11,78	301	0,05	1,03
17921	517001-275	61,80	4,24	4,47	2,52	420	0,62	12,89	304	0,05	1,12
17922	517001-274	62,47	4,26	4,86	2,81	421	0,92	16,26	382	0,05	1,43
17923	517001-273	63,47	3,95	4,29	2,90	422	0,78	12,80	324	0,06	1,13
17924	517001-272	64,47	3,25	3,48	12,05	428	0,43	6,98	214	0,06	0,62
17925	517001-271	65,47	4,57	4,93	1,96	422	0,97	17,41	381	0,05	1,53
17926	517001-270	66,21	4,24	4,56	2,45	422	0,79	14,71	347	0,05	1,29
17927	517001-269	67,19	3,84	4,10	3,57	421	0,63	10,95	285	0,05	0,96
17928	517001-268	68,26	3,90	4,15	3,17	420	0,56	11,00	282	0,05	0,96
17929	517001-267	69,26	3,72	4,08	2,20	425	0,70	13,53	364	0,05	1,18
17930	517001-266	70,15	3,86	4,01	5,42	426	0,60	12,59	326	0,05	1,09
17931	517001-265	71,18	3,80	3,91	2,37	422	0,56	10,76	283	0,05	0,94
17932	517001-264	71,97	4,17	4,40	2,38	426	0,76	15,35	368	0,05	1,34
17933	517001-263	72,90	3,28	3,70	7,09	426	0,56	10,28	314	0,05	0,90
17934	517001-262	73,94	4,57	4,83	2,54	425	1,02	18,50	405	0,05	1,62
17935	517001-261	74,92	4,53	4,86	1,58	426	1,02	19,51	431	0,05	1,70
17936	517001-260	75,94	4,09	4,19	3,82	423	0,69	13,05	319	0,05	1,14
17937	517001-259	76,88	2,70	3,87	3,31	429	0,46	9,04	334	0,05	0,79
17938	517001-258	77,87	3,29	3,66	7,06	428	0,49	10,13	308	0,05	0,88
17939	517001-257	78,82	4,91	5,31	1,97	425	1,05	19,83	404	0,05	1,73
17940	517001-256	79,74	4,27	4,62	1,89	426	0,92	16,11	377	0,05	1,41
17941	517001-255	80,74	4,45	4,96	1,62	426	1,05	18,33	412	0,05	1,61
17942	517001-254	81,62	3,64	3,87	2,59	423	0,60	11,83	325	0,05	1,03
17943	517001-253	82,64	3,33	3,84	2,30	424	0,62	11,44	344	0,05	1,00
17944	517001-252	83,57	3,19	3,46	2,56	422	0,56	10,18	319	0,05	0,89
17945	517001-251	84,60	2,46	3,84	5,13	429	0,38	7,19	293	0,05	0,63
17946	517001-250	85,59	3,65	3,84	7,89	425	0,43	10,79	296	0,04	0,93
17947	517001-249	86,37	3,56	3,97	2,42	424	0,73	12,51	351	0,06	1,10
17948	517001-248	87,39	2,75	3,09	2,11	425	0,56	9,82	357	0,05	0,86
17949	517001-247	88,25	3,20	3,45	2,49	424	0,64	11,40	357	0,05	1,00

Lab.no.	Sample	Depth (m)	TOC (%)	TC (%)	TS (%)	Tmax (°C)	S1 (mg/g)	S2 (mg/g)	HI	PI	PC
17950	517001-246	89,27	2,97	3,24	5,63	427	0,63	11,94	402	0,05	1,04
17951	517001-245	90,27	2,11	2,99	3,76	430	0,35	6,77	320	0,05	0,59
17952	517001-244	91,21	2,28	2,49	5,62	428	0,34	7,35	322	0,04	0,64
17953	517001-243	92,23	3,20	3,59	1,98	426	0,67	12,24	383	0,05	1,07
17954	517001-242	93,07	3,06	3,30	1,86	427	0,62	11,33	370	0,05	0,99
17955	517001-241	94,08	3,17	3,33	2,60	422	0,55	8,50	268	0,06	0,75
17956	517001-240	95,06	2,47	2,67	6,05	421	0,42	5,39	218	0,07	0,48
17957	517001-239	96,06	4,06	4,18	1,95	424	0,78	13,87	342	0,05	1,22
17958	517001-238	96,92	3,00	3,23	2,78	426	0,68	9,06	302	0,07	0,81
17959	517001-237	97,92	2,81	3,07	2,89	422	0,51	7,01	250	0,07	0,62
17960	517001-236	98,88	3,86	3,99	2,67	426	0,73	13,19	342	0,05	1,16
17961	517001-235	99,72	3,94	4,02	1,92	425	0,84	13,36	339	0,06	1,18
17962	517001-234	100,73	2,60	2,80	2,95	426	0,42	7,32	282	0,05	0,64
17963	517001-233	101,66	3,92	4,08	1,99	423	0,75	11,43	291	0,06	1,01
17964	517001-232	102,30	3,29	3,50	3,89	424	0,60	9,08	276	0,06	0,80
17965	517001-231	103,08	2,64	5,26	4,21	421	0,43	6,44	244	0,06	0,57
17966	517001-230	104,07	2,94	3,48	1,97	424	0,37	7,08	241	0,05	0,62
17967	517001-229	104,98	3,91	4,18	2,33	426	0,67	11,71	300	0,05	1,03
17968	517001-228	105,39	3,33	3,67	2,70	426	0,48	9,03	271	0,05	0,79
17969	517001-227	106,39	3,99	4,16	2,17	426	0,48	10,39	260	0,04	0,90
17970	517001-226	107,41	3,43	3,57	1,85	427	0,41	7,29	213	0,05	0,64
17971	517001-225	108,38	3,68	3,76	1,81	423	0,45	7,98	217	0,05	0,70
17972	517001-224	109,16	4,08	4,56	1,57	426	0,58	10,44	256	0,05	0,91
17973	517001-223	110,15	3,51	3,63	1,27	423	0,41	7,43	212	0,05	0,65
17974	517001-222	111,17	3,41	3,59	1,54	423	0,44	7,55	222	0,06	0,66
17975	517001-221	111,96	3,61	3,75	1,20	425	0,49	8,42	233	0,05	0,74
17976	517001-220	112,99	4,02	4,10	2,67	422	0,48	8,40	209	0,05	0,74
17977	517001-219	113,99	3,25	3,63	1,91	423	0,46	8,21	253	0,05	0,72
17978	517001-218	115,01	2,81	3,07	2,01	424	0,32	4,60	163	0,07	0,41

Lab.no.	Sample	Depth (m)	TOC (%)	TC (%)	TS (%)	Tmax (°C)	S1 (mg/g)	S2 (mg/g)	HI	PI	PC
17979	517001-217	115,86	3,30	3,56	1,55	425	0,43	7,33	222	0,06	0,64
17980	517001-216	116,87	4,00	4,30	2,04	424	0,54	9,20	230	0,06	0,81
17981	517001-215	117,82	3,20	3,36	1,74	425	0,28	6,16	192	0,04	0,53
17982	517001-214	118,76	3,27	3,30	2,13	426	0,37	6,90	211	0,05	0,60
17983	517001-213	119,77	3,35	4,49	1,68	424	0,32	7,49	223	0,04	0,65
17984	517001-212	120,77	3,56	3,90	1,62	423	0,42	6,91	194	0,06	0,61
17985	517001-211	121,87	3,06	3,41	2,72	422	0,28	4,27	140	0,06	0,38
17986	517001-210	122,86	3,55	3,68	2,49	425	0,32	4,81	136	0,06	0,43
17987	517001-209	123,86	4,19	4,43	1,88	425	0,36	8,38	200	0,04	0,73
17988	517001-208	124,46	4,69	4,94	1,77	426	0,49	11,72	250	0,04	1,01
17989	517001-207	125,66	4,33	4,54	2,34	426	0,45	10,28	237	0,04	0,89
17990	517001-206	126,62	3,53	3,89	2,14	426	0,35	5,95	168	0,06	0,52
17991	517001-205	127,23	4,39	4,74	3,76	427	0,52	11,25	256	0,04	0,98
17992	517001-204	128,22	4,30	4,64	3,25	427	0,49	9,90	230	0,05	0,86
17993	517001-203	129,16	3,90	4,34	1,75	426	0,46	7,82	201	0,06	0,69
17994	517001-202	130,26	4,00	4,29	1,76	426	0,58	8,62	215	0,06	0,76
17995	517001-201	131,21	4,34	4,64	2,20	426	0,69	9,96	229	0,06	0,88
17996	517001-200	133,57	4,46	4,61	1,79	425	0,83	9,37	210	0,08	0,85
17997	517001-199	134,57	3,73	4,30	1,68	426	0,70	8,53	229	0,08	0,77
17998	517001-198	135,58	4,13	4,76	2,15	424	0,84	8,37	203	0,09	0,76
17999	517001-197	136,41	4,52	4,92	1,69	425	0,92	11,83	262	0,07	1,06
18000	517001-196	137,42	5,61	5,91	2,83	422	0,83	13,59	242	0,06	1,20
18001	517001-195	138,41	5,19	5,68	2,63	424	1,13	12,90	248	0,08	1,16
18002	517001-194	139,26	4,71	5,14	2,90	423	0,88	10,67	227	0,08	0,96
18003	517001-193	140,25	5,33	5,70	2,16	424	1,10	13,28	249	0,08	1,19
18004	517001-192	141,27	5,57	6,06	2,65	422	1,17	14,98	269	0,07	1,34
18005	517001-191	141,94	4,39	5,00	2,58	425	0,71	7,81	178	0,08	0,71
18006	517001-190	142,93	4,57	5,00	2,16	426	0,86	11,37	249	0,07	1,02
18007	517001-189	143,89	5,52	5,85	3,06	425	1,20	14,36	260	0,08	1,29
18008	517001-188	144,88	1,48	10,19	0,73	427	0,22	2,36	160	0,09	0,21
18009	517001-187	145,56	2,27	9,30	1,07	428	0,29	3,56	157	0,08	0,32
18010	517001-186	146,66	5,50	6,12	2,58	423	1,08	12,62	229	0,08	1,14
18011	517001-185	147,56	4,67	4,86	2,31	424	0,74	9,66	207	0,07	0,86
18012	517001-184	148,46	4,92	5,44	2,31	426	0,93	12,60	256	0,07	1,12

Lab.no.	Sample	Depth (m)	TOC (%)	TC (%)	TS (%)	Tmax (°C)	S1 (mg/g)	S2 (mg/g)	HI	PI	PC
18013	517001-183	149,31	4,56	4,92	1,94	426	0,81	11,18	245	0,07	1,00
18014	517001-182	150,25	3,96	5,59	2,01	426	0,62	7,40	187	0,08	0,67
18015	517001-181	151,24	4,21	4,53	2,37	426	0,65	7,65	182	0,08	0,69
18016	517001-180	152,01	5,06	5,37	2,25	426	0,91	11,72	232	0,07	1,05
18017	517001-179	152,99	4,24	5,35	2,95	425	0,67	7,50	177	0,08	0,68
18018	517001-178	153,98	5,20	5,58	2,00	425	1,02	13,36	257	0,07	1,19
18019	517001-177	154,90	4,51	4,84	2,39	427	0,83	10,08	223	0,08	0,91
18020	517001-176	155,87	4,38	5,59	2,28	427	0,91	11,83	270	0,07	1,06
18021	517001-175	156,91	5,10	5,73	1,68	427	1,04	13,95	274	0,07	1,24
18022	517001-174	157,78	4,08	5,80	3,19	428	0,75	11,23	275	0,06	0,99
18023	517001-173	158,77	4,13	4,38	2,18	427	0,65	10,41	252	0,06	0,92
18024	517001-172	159,69	2,24	8,14	1,41	427	0,33	4,34	193	0,07	0,39
18025	517001-171	160,71	4,59	4,99	2,11	425	0,71	10,73	234	0,06	0,95
18026	517001-170	161,39	4,45	4,87	1,96	427	0,95	11,21	252	0,08	1,01
18027	517001-169	162,38	3,76	4,34	4,23	428	0,73	8,51	226	0,08	0,77
18028	517001-168	163,41	4,88	5,38	2,06	428	1,08	13,24	271	0,08	1,19
18029	517001-167	164,41	4,11	4,58	1,94	429	0,82	10,70	260	0,07	0,96
18030	517001-166	165,24	4,03	4,28	4,38	427	0,64	8,81	219	0,07	0,78
18031	517001-165	166,24	4,17	4,41	1,84	427	0,83	10,97	263	0,07	0,98
18032	517001-164	167,24	4,89	5,23	2,34	427	1,02	12,94	264	0,07	1,16
18033	517001-163	168,06	5,54	5,96	2,28	428	1,28	15,18	274	0,08	1,37
18034	517001-162	169,02	4,67	5,56	3,48	428	0,93	11,65	249	0,07	1,04
18035	517001-161	170,01	4,71	4,98	2,02	430	0,95	12,10	257	0,07	1,08
18036	517001-160	171,02	5,93	6,33	2,35	426	1,44	16,13	272	0,08	1,46
18037	517001-159	171,89	5,61	5,73	2,82	427	1,16	15,86	283	0,07	1,41
18038	517001-158	172,80	5,15	5,39	2,27	427	0,95	12,99	252	0,07	1,16
18039	517001-157	173,82	1,30	10,49	0,70	430	0,26	2,77	213	0,09	0,25
18040	517001-156	174,36	1,61	10,66	0,72	428	0,37	3,51	219	0,10	0,32
18041	517001-155	175,34	5,06	5,28	3,08	426	1,17	12,33	243	0,09	1,12

Lab.no.	Sample	Depth (m)	TOC (%)	TC (%)	TS (%)	Tmax (°C)	S1 (mg/g)	S2 (mg/g)	HI	PI	PC
18042	517001-154	176,33	4,31	4,75	3,91	427	0,89	10,20	237	0,08	0,92
18043	517001-153	177,37	4,93	5,25	2,23	428	1,00	14,17	287	0,07	1,26
18044	517001-152	178,31	4,19	4,67	2,52	429	0,68	10,54	252	0,06	0,93
18045	517001-151	179,26	5,44	5,55	2,02	431	1,00	16,20	298	0,06	1,43
18046	517001-150	180,26	4,69	5,12	3,06	431	0,83	12,87	274	0,06	1,14
18047	517001-149	181,19	5,09	5,38	2,76	430	0,93	14,38	282	0,06	1,27
18048	517001-148	182,15	5,37	5,68	3,65	432	1,03	15,95	297	0,06	1,41
18049	517001-147	183,12	5,15	5,62	1,99	431	0,97	15,85	308	0,06	1,40
18050	517001-146	184,10	5,07	5,43	4,36	431	0,94	14,80	292	0,06	1,31
18051	517001-145	184,96	5,30	5,59	2,75	430	0,99	14,96	282	0,06	1,32
18052	517001-144	185,94	4,28	4,66	2,15	430	0,82	12,41	290	0,06	1,10
18053	517001-143	186,95	5,53	5,59	2,33	431	0,93	16,13	292	0,05	1,42
18054	517001-142	187,85	5,44	5,53	3,49	431	0,95	15,35	282	0,06	1,35
18055	517001-141	188,88	4,85	5,68	3,97	429	0,93	11,11	229	0,08	1,00
18056	517001-140	189,86	5,23	5,46	3,51	430	1,01	13,61	260	0,07	1,21
18057	517001-139	190,73	5,07	5,22	2,47	430	0,91	12,65	249	0,07	1,13
18058	517001-138	191,60	5,88	5,94	2,44	430	1,12	14,67	249	0,07	1,31
18059	517001-137	192,56	4,70	4,93	2,17	430	0,78	10,08	214	0,07	0,90
18060	517001-136	193,68	4,58	4,80	2,83	430	0,74	9,14	200	0,07	0,82
18061	517001-135	194,51	5,21	5,58	2,10	428	1,06	14,40	277	0,07	1,28
18062	517001-134	195,41	4,52	4,71	3,46	428	0,84	9,38	207	0,08	0,85
18063	517001-133	196,39	5,50	5,66	2,35	430	1,08	15,26	278	0,07	1,36
18064	517001-132	197,24	5,12	5,41	3,00	430	1,01	12,28	240	0,08	1,10
18065	517001-131	198,25	4,86	5,06	2,30	430	0,89	11,09	228	0,07	0,99
18066	517001-130	199,27	4,50	4,69	2,34	429	0,86	10,06	224	0,08	0,91
18067	517001-129	200,19	4,62	5,40	2,62	425	1,16	7,71	167	0,13	0,74
18068	517001-128	200,93	6,22	6,12	2,02	429	1,33	15,93	256	0,08	1,43
18069	517001-127	201,91	4,85	5,07	3,27	426	0,88	8,55	176	0,09	0,78
18070	517001-126	202,88	5,57	5,69	2,22	430	1,04	12,74	229	0,08	1,14
18071	517001-125	203,64	5,88	6,03	3,19	429	1,18	14,05	239	0,08	1,26
18072	517001-124	204,56	5,72	6,06	2,56	431	1,07	13,78	241	0,07	1,23
18073	517001-123	205,47	5,82	5,74	5,81	424	0,75	9,07	156	0,08	0,82
18074	517001-122	206,68	6,89	7,16	2,85	429	1,44	17,36	252	0,08	1,56
18075	517001-121	207,21	6,83	6,84	2,51	428	1,36	16,79	246	0,07	1,51

Lab.no.	Sample	Depth (m)	TOC (%)	TC (%)	TS (%)	Tmax (°C)	S1 (mg/g)	S2 (mg/g)	HI	PI	PC
18076	517001-120	207,55	6,43	6,48	2,41	428	1,23	14,94	232	0,08	1,34
18077	517001-119	208,35	6,38	6,67	2,29	428	1,26	14,78	232	0,08	1,33
18078	517001-118	209,48	6,58	6,81	2,16	429	1,24	15,71	239	0,07	1,41
18079	517001-117	210,44	6,64	6,87	2,56	429	1,20	16,97	256	0,07	1,51
18080	517001-116	211,03	6,22	6,28	3,08	426	1,02	10,96	176	0,09	0,99
18081	517001-115	212,02	7,09	7,08	2,94	427	1,29	14,73	208	0,08	1,33
18082	517001-114	213,19	6,07	6,26	3,35	427	1,00	12,01	198	0,08	1,08
18083	517001-113	213,78	6,62	6,74	2,94	429	1,21	15,42	233	0,07	1,38
18084	517001-112	214,76	5,05	6,98	4,08	430	0,76	8,86	175	0,08	0,80
18085	517001-111	215,59	6,40	6,61	2,34	429	1,20	14,79	231	0,08	1,33
18086	517001-110	216,55	5,99	6,51	2,14	430	1,16	13,45	224	0,08	1,21
18087	517001-109	217,69	6,77	6,75	2,98	429	1,28	15,59	230	0,08	1,40
18088	517001-108	218,66	5,27	6,58	2,05	429	0,80	10,37	197	0,07	0,93
18089	517001-107	219,63	5,86	6,49	2,66	428	1,07	11,68	199	0,08	1,06
18090	517001-106	220,51	6,38	6,72	2,63	430	1,24	14,98	235	0,08	1,35
18091	517001-105	221,52	6,60	6,79	2,78	430	1,20	15,98	242	0,07	1,43
18092	517001-104	222,40	6,63	6,78	2,43	427	0,84	13,89	210	0,06	1,22
18093	517001-103	223,23	7,22	7,38	3,04	430	1,37	17,99	249	0,07	1,61
18094	517001-102	224,44	6,50	6,61	2,08	430	0,94	16,57	255	0,05	1,45
18095	517001-101	225,21	6,86	7,00	3,22	427	1,09	16,60	242	0,06	1,47
18096	517001-100	226,05	6,64	6,73	3,10	427	1,01	13,73	207	0,07	1,22
18097	517001-77	226,23	5,30	5,60	5,21	424	0,45	7,25	137	0,06	0,64
18098	517001-99	227,38	6,25	7,57	5,43	429	0,73	13,96	223	0,05	1,22
18099	517001-98	227,95	6,50	6,79	1,90	431	1,38	15,85	244	0,08	1,43
18100	517001-340	228,68	6,99	7,30	2,94	430	1,56	17,49	250	0,08	1,58
18101	517001-97	228,77	4,28	8,74	2,78	428	0,79	8,44	197	0,09	0,77
18102	517001-78	228,95	6,77	6,95	2,37	429	1,47	14,07	208	0,09	1,29
18103	517001-96	229,81	5,89	6,80	5,91	430	1,07	11,13	189	0,09	1,01
18104	517001-95	230,73	5,38	5,58	2,19	429	1,14	12,16	226	0,09	1,10

Lab.no.	Sample	Depth (m)	TOC (%)	TC (%)	TS (%)	Tmax (°C)	S1 (mg/g)	S2 (mg/g)	HI	PI	PC
18105	517001-94	231,70	6,90	7,11	2,52	431	1,53	17,18	249	0,08	1,55
18106	517001-79	231,74	6,99	7,10	2,13	430	1,58	17,74	254	0,08	1,60
18107	517001-93	232,53	6,07	6,32	2,28	432	1,36	15,55	256	0,08	1,40
18108	517001-92	233,56	6,14	6,43	3,40	429	1,36	13,21	215	0,09	1,21
17099	517001-75	234,4	6,53	6,59	2,76	431	1,44	15,76	241	0,08	1,43
18109	517001-91	234,66	6,81	6,94	2,54	430	1,43	15,72	231	0,08	1,42

Mean (Lindemanns Bugt Fm)			3,50	3,90	3,82	423	0,58	12,67	333	0,05	1,10
Max (Lindemanns Bugt Fm)			5,37	5,60	12,05	430	1,05	19,83	445	0,33	1,73
Min (Lindemanns Bugt Fm)			0,12	0,81	1,58	417	0,01	0,02	9	0,03	0,00

Mean (Bernbjerg Fm)	4,84	5,48	2,54	427	0,86	11,45	235	0,07	1,02
Max (Bernbjerg Fm)	7,22	10,66	5,91	432	1,58	17,99	342	0,13	1,61
Min (Bernbjerg Fm)	1,30	2,80	0,70	421	0,22	2,36	136	0,04	0,21

Table 8.1.1, continued

Average VR (random) values derived from selected VR populations

Lab. no.	Sample	Depth (m)	Material	VR (%Ro)	Std.	n
17097	517001-5	25	core	0,48	0,042	73
17895	517001-301	37,88	core	0,46	0,046	76
17916	517001-280	56,88	core	0,47	0,054	84
17935	517001-261	74,92	core	0,46	0,048	92
17953	517001-243	92,23	core	0,46	0,041	67
17973	517001-223	110,15	core	0,50	0,037	76
17992	517001-204	128,22	core	0,56	0,044	80
18012	517001-184	148,46	core	0,57	0,041	132
18032	517001-164	167,24	core	0,57	0,045	96
18054	517001-142	187,85	core	0,61	0,046	121
18086	517001-110	216,55	core	0,61	0,054	165
18109	517001-91	234,66	core	0,61	0,052	140

Table 8.1.2. Average VR (random) values derived from selected VR populations

	Sample	
Ea kCal/mole	17895 37,88m	18054 187,85m
40000	0,42	0,65
41000	0	0
42000	0,09	0,29
43000	0,21	0,32
44000	0	0,21
45000	0,35	0,27
46000	0	0,44
47000	0	0
48000	0	0,78
49000	0	0,19
50000	0	0
51000	0	0
52000	0	0
53000	40,16	0
54000	23,23	33,62
55000	21,94	31,73
56000	5,19	13,65
57000	6,06	10,14
58000	0,72	2,15
59000	0,96	4,14
60000	0,05	0,01
61000	0,2	0,66
62000	0	0
63000	0	0
64000	0,43	0,76
65000	0	0

Arrhenius Factor	1,7795E+14	2,2698E+14

Table 8.1.3. Activation energy distributions and Arrhenius factors for samples 2010008-17895 (37.88 m) and 2010008-18054 (187.85 m).

8.2 Biomarker analysis – Extraction, MPLC-separation, GC, GC-MS and GC-MS-MS

The Rødryggen core-well drilled c. 210 m of marine black shales. 24 shale samples were selected for solvent extraction, MPLC-separation, gas chromatography (GC) and gas chromatography-mass spectrometry (GC-MS and GC-MS-MS) of the saturated fraction. The aromatic fraction from all samples was analysed in SIM-mode and four fractions were analysed in full scan mode.

8.2.1 Methods

Extraction and separation

Crushed shale samples were extracted with methanol/dichloromethane 7:93 vol/vol using a Soxtec equipment (extraction yield: Table 1; Fig. 8.2.1). The asphaltenes (Fig. 8.2.2) were removed from the extracts by precipitation in *n*-pentane. Medium pressure liquid chromatography (MPLC) fractionation of the maltenes yielded a saturated hydrocarbon, an aromatic hydrocarbon and a polar fraction (composition: Table 1; Fig. 8.2.3). The saturated fraction was analysed by GC, GC-MS and GC-MS-MS. The aromatic fraction was analysed using GC-MS.

Gas chromatography (GC) of saturated hydrocarbons

Gas chromatography was performed using a Shimadzu GC-2010 instrument equipped with a splitless injector and a ZB-1 capillary column (25 m x 0.25 mm i.d., film thickness 0.10 µm). The temperature program was 5^{o}C/min from 80 to 300^{o}C, followed by 15 min at 300^{o}C. The concentration for GC analyses was 5 mg / ml isooctane. Pristane/phytane ratios (Fig. 8.2.4) and relative concentrations of isoprenoids (Fig. 8.2.5) were obtained from peak areas in the gas chromatograms.

Gas chromatography-mass spectrometry (GC-MS and GC-MS-MS) of saturated hydrocarbons

Gas chromatography-mass spectrometry was carried out using an Agilent 6890N gas chromatograph connected to a Waters (Micromass) Quattro Micro GC tandem quadrupole mass spectrometer. A Phenomenex ZB-5 column (30 m x 0.25 mm i.d., film thickness 0.10 µm) was used. The injection temperature was 70^{o}C (2 min hold). The temperature program was 30^{o}C/min from 70 to 100^{o}C and 4^{o}C/min from 100 to 308^{o}C followed by 8 min at 308^{o}C. Argon was used as collision gas for MS-MS experiments. The saturated hydrocarbons were analysed by GC-MS in SIM-mode and by GC-MS-MS using relevant transitions for C_{26}-C_{30} steranes and C_{27}-C_{35} hopanes. Four separate GC-MS and GC-MS-MS methods were used. Samples were dissolved in isooctane. The concentration for GC-MS and GC-MS-MS was 3 mg / ml isooctane. One sample (216.55 m) was analysed in full scan mode.

GC-MS, SIM

71.10	*n*-alkanes
177.16	25-norhopanes
191.18	hopanes
205.20	methylhopanes
217.20	steranes
218.20	steranes
231.21	methylsteranes
253.20	monoaromatic steranes (should be absent in sat. fraction)
355.35	25- and 28-norhopanes
369.35	hopanes

GC-MS-MS, Steranes

358.36 → 217.20	C_{26} steranes
372.38 → 217.20	C_{27} steranes
386.39 → 217.20	C_{28} steranes
400.41 → 217.20	C_{29} steranes
414.42 → 217.20	C_{30} steranes
412.41 → 191.18	C_{30} hopanes
414.42 → 259.24	TPP

GC-MS-MS, Hopanes

370.36 → 191.18	C_{27} hopanes
384.38 → 191.18	C_{28} hopanes
398.39 → 191.18	C_{29} hopanes
412.41 → 191.18	C_{30} hopanes

412.41 → 369.35 C_{30} hopanes
426.42 → 191.18 C_{31} hopanes
440.44 → 191.18 C_{32} hopanes
454.45 → 191.18 C_{33} hopanes
468.47 → 191.18 C_{34} hopanes
482.49 → 191.18 C_{35} hopanes

GC-MS-MS, C_{33} + C_{34} hopanes and isohopanes (only two transitions for better signal/noise ratio)

454.45 → 191.18 C_{33} hopanes
468.47 → 191.18 C_{34} hopanes

Hopanes and steranes were quantified using peak areas from the relevant MS-MS transitions. GC-MS-MS allows quantification of C_{27}-C_{30} steranes (Table 2, Fig. 8.2.6 – Fig. 8.2.10) with little interference from co-eluting gas chromatographic peaks which is not possible using only GC-MS. Biomarker ratios obtained using GC-MS-MS will, in some cases, be slightly different to those obtained from the usual *m/z* 191, 217 and 218 fragmentograms because of different response factors.

GC-MS and GC-MS-MS chromatograms showing the most important biomarkers have been included as pdf-files in the appendix 10.6.

Biomarker ratios and other data can be found in four tables.

Table 1: extraction, MPLC-separation and GC
Table 2: sterane data
Table 3: hopane data
Table 4: 28-norhopanes and aromatic compounds

Gas chromatography-mass spectrometry (GC-MS) of aromatic hydrocarbons

The same instrument, GC-column and temperature program was used for GC-MS analysis of aromatic hydrocarbons. Four samples (25.00, 139.26, 148.46 and 216.55 m) were analysed in full scan mode and all 24 samples were analysed in SIM-mode.

GC-MS, SIM

170.04 C3-naphthalenes
178.08 phenanthrene
184.03 C4-naphthalenes, dibenzothiophene
191.18 benzohopanes
192.09 methylphenanthrenes
198.05 C5-naphthalenes, methyldibenzothiophenes
206.11 dimethylphenanthrenes
212.07 C6-naphthalenes, dimethyldibenzothiophenes
219.12 retene
228.09 chrysene
231.12 triaromatic steranes
234.14 retene
253.20 monoaromatic steranes
351.31 demethylated monoaromatic 8,14-secohopanes
365.32 monoaromatic 8,14-secohopanes

8.2.2 Organic matter

The composition of biomarkers in extracts from Rødryggen shales shows a mixture of marine and terrigenous organic matter with an increasing proportion of terrigenous matter below ~ 110 m (*i.e.*, the Bernbjerg Formation). The relative abundances of C_{27}, C_{28}, and C_{29} steranes are almost equal above 100 m whereas C_{29} steranes dominate below 100 m (Fig. 8.2.6). C_{30} steranes (24-*n*-propylcholestanes) is the most powerful means in order to identify input of marine organic matter to the source rock (Peters et al., 2005). The relative proportion of C_{30} steranes is high (8-13 %, C_{27}+C_{28}+C_{29}+C_{30} = 100 %, Fig. 8.2.7) in the top half of the core (Lindemans Bugt Formation) and generally below 8 % in the lower half (Bernbjerg Formation).

Various markers for gymnosperms are abundant in the aromatic fraction – especially in the lower half of the core. The major compound is retene which accounts for 7% of all aromatic compounds (Fig. 8.2.20, GC-MS, full scan) in the aromatic fraction from 216.55 m. Fig. 8.2.22 shows the abundance of retene versus methylphenanthrenes and methyldibenzothiophenes which have a more diverse origin. Other aromatic markers for gymnosperms such as cadalene, simonellite and dihydro-*ar*-curcumene were also identified but compared to retene their concentrations were at least ten times lower. Saturated higher plant markers (pimaranes, phyllocladanes, eudesmane and cadinane) were identified in the only saturated fraction (216.55 m) analysed in full scan mode.

The relative content of sulphur-containing compounds in the aromatic fraction (e.g. the dibenzothiophene / phenanthrene ratio; Hughes et al., 1995) decreases from top to bottom (Fig. 8.2.21). The methyldibenzothiophene / methylphenanthrene ratio behaves in a similar way (Fig. 8.2.21).

28,30-Bisnorhopane (BNH, C_{28}, Seifert et al., 1978; Moldowan and Seifert 1984; Schoell et al., 1992) was identified in all samples. Below 100 m it is often the most abundant hopane (Figs. 8.2.12). 28,30-bisnorhopane is typical of petroleum source rocks deposited under anoxic conditions and high BNH correlates with high benzothiophene and low pristane/phytane for oils and extracts from the Monterey Formation and equivalents, where BNH was first identified (Peters et al., 2005 and references therein). The Rødryggen core samples appear entirely different. The abundance of BNH is high in samples having a low C_{35} homohopane index (Fig. 8.2.11), high pristane/phytane (Fig. 8.2.4) and a high content of terrigenous compounds (Fig. 8.2.22). Clearly, other explanations for a high content of BNH must exist. BNH can sometimes be detected in coal (Bojesen-Koefoed et al., 2001 and GEUS unpublished) and some of the highest concentrations have been found in coals from Sibiria (Vladimir Kashirtsev, personal communication).

28,30-Bisnorhopane is often the only 28-norhopane (*e.g.* in the Monterey formation, California). However, a complete series complete series of 28-norhopanes (C_{28}-C_{34}) has been identified in West Greenland and the North Sea (Bojesen-Koefoed et al., 1999; Nytoft et al., 2000) and several other places (GEUS unpublished). The complete series of 28-norhopanes (Nytoft et al., 2000) is also present in the Rødryggen core, but the abundance of C_{33} and C_{34} compounds is very low in most samples. Fig. 8.2.13 shows *m/z* 355 mass chromatograms for two samples having different distributions of 28-norhopanes and Fig. 8.2.14 shows the distribution of C_{28}-C_{32} 28-norhopanes in all samples. All 28-norhopanes could not be reliably quantified in samples above 50m. The relative abundance of the higher carbon number 28-norhopanes is low in samples with a high concentration of BNH and vice versa indicating that BNH and the complete series of 28-norhopanes may have different origins (Nytoft et al., 2000). Demethylated monoaromatic 8.14-secohopanes were were relatively abundant in the aromatic fraction from most samples.

Most samples have 17α,21β(H)-norhopane/17α,21β(H)-hopane ratios (H29/H30) between 0.6 and 0.8 (Fig. 8.2.15) which is typical of marine shales (Peters et al., 2005). One sample (216.55 m) has a very high H29/H30 ratio (1.354). Ratios above 1 are normal for oils from carbonate source rocks but this sample lacks all the other characteristics of carbonate source rocks such as the presence 30-norhopanes, a high C_{35} homohopane index and a low diasterane/sterane ratio (Fig. 8.2.10). It should, however, be noted that it has unusually low Ts/(Ts+Tm) and 29Ts/(29Ts + H29) ratios (Fig. 8.2.17).

Extended hopanes (C_{31}-C_{35}) show little odd-over-even-predominance (HOEP, Bishop and Farrimond 1995, Table 3). More of the higher homohopanes are preserved under anoxic depositional conditions and the C_{35} homohopane index (HHI, Table 3, Fig. 8.2.11) can thus be used as an indicator of redox potential in marine sediments during diagenesis (Peters et al., 2005). The C_{35} homohopane index is relatively low (0.03-0.08) and decreasing from top to bottom (Fig. 8.2.11). Typical values for oils from the Danish North Sea are around 0.08. Isohopanes (Fig. 8.2.11) can be used in a similar way. Isohopanes are “novel" extended hopanes having a side chain with an additional methyl branch (C_{33} and higher). All C_{33} and C_{34} isohopanes have recently been identified by comparison with synthetic standards (Nytoft 2007, 2009). Details concerning the identification and use of isohopanes will be reported elsewhere (Organic Geochemistry, submitted). The relative abundance of isohopanes is low in oils sourced from marine organic matter deposited under anoxic conditions and very high in oils having a coaly source. Gammacerane is almost absent in all samples. Gammacerane is highly specific for water-column stratification (commonly due to hypersalinity) during source rock deposition (Sinninghe Damsté et al., 1995). A ring-A demythylated gammacerane (Nytoft et al., 2006, not tabulated, no figures shown) is fairly abundant in all samples and its concentration relative to H29 is almost constant. It is probably not derived from gammacerane or its precursors but may be formed by enlargement of ring E in hopanoids during diageneseis (Nytoft et al., 2006). It coelutes with the C_{30} neohopane (30Ts). The two compounds can be quantified separately using GC-MS-MS (398 $\rightarrow$ 191 and 412 $\rightarrow$ 191).

Two series of rearranged hopanes are moderately abundant in the Rødryggen samples. They are 17α-diahopanes and the so-called “early eluting rearranged hopanes” (Moldowan et al., 1991; Farrimond et al., 1996). The relative abundance of the C_{30} members of the two series (30D and 30E) can be found in Table 3. 30E is more abundant than 30D in all samples (Fig. 8.2.18) whereas 30D is usually the major rearranged C_{30} hopane in oils and source rocks from other locations.

Tricyclic terpanes can be seen in the *m/z* 191 fragmentograms. They are, however, minor compounds in all samples and they were not quantified.

The C_{26} 24/(24 + 27) nordiacholestane ratio (Holba et al., 1998a,b, not tabulated, no chromatograms shown) is low (0.19 to 0.29) in accordance with the age of the shale (Jurassic).

Tetracyclic polyprenoids (TPP, Holba et al., 2000, 2003) are markers for lacustrine matter input. They were were tentatively identified in the Rødryggen shales where they partly coelute with C_{30} steranes. The TPP ratio (not tabulated) was very low in all samples.

8.2.3 Maturity

The 22S/(22S + 22R) ratio for C_{32} and C_{33} hopanes is below equilibrium at the top of the well (Table 3; Fig. 8.2.19). Equilibrium (0.60) is reached around 170 m. The 22S/(22S + 22R) ratio for C_{31} hopanes is close to equilibrium in all samples.

The 20S/(20S + 20R) ratio of C_{29} steranes (ethylcholestanes) shows a gradual increase with depth from 0.30 at the top to 0.50 at the bottom of the well (Table 2, Fig. 8.2.8), indicating that the shales at the bottom are within the oil window. The 20S/(20S + 20R) ratio for steranes decreases in the order $C_{27} > C_{28} > C_{29} > C_{30}$ (Table 2).

Isomerization at C-14 and C-17 in steranes causes a slight increase in the $\beta\beta/(\alpha\alpha + \beta\beta)$ ratio with depth/maturity (Fig. 8.2.9). The C_{27} steranes show a lower $\beta\beta/(\alpha\alpha + \beta\beta)$ ratio than the C_{28}-C_{30} steranes in all samples.

The relative proportion of C_{27} diasteranes is influenced both by thermal maturity and the depositional environment. The diasteranes/(diasteranes + regular steranes) ratios are relatively high (~ 0.7) from top to bottom except in three samples at 128.22, 139.26 and 148.46 m (Table 2; Fig. 8.2.10).

8.2.4 Conclusions

Extracts of the Rødryggen shales show the typical characteristics of a marine source rock but with an increasing proportion of terrestrially-influenced kerogen below ~110 m (i.e., the Bernbjerg Formation). The deeper parts of the core are within the oil window.

8.2.5 References

Bishop, A.N. & Farrimond, P., 1995: A new method of comparing extended hopane distributions. Organic Geochemistry **23**, 987–990.

Bojesen-Koefoed, J.A., Christiansen, F.G., Nytoft, H.P. & Pedersen, A.K., 1999: Oil seepage onshore West Greenland: evidence of multiple source rocks and oil mixing. In Fleet, A.S. & Boldy, S. (eds.) Petroleum Geology of NW-Europe, proceedings of the 5th Conference, 305–314.

Bojesen-Koefoed, J. A., Dam, G., Nytoft, H. P., Pedersen, G. K. & Petersen , H. I., 2001: Drowning of a nearshore peatforming environment, Atane Formation (Cretaceous) at Asuk, West Greenland: sedimentology, organic petrography and geochemistry. Organic Geochemistry, **32**, 841–856

Farrimond, P. & Telnaes, N., 1996: Three series of rearranged hopanes in Toarcian sediments (northern Italy). Organic Geochemistry, **25**, 165–177.

Holba, A.G., Tegelaar, E.W., Huizinga, B.J., Moldowan, J.M., Singletary, M.S., McCaffrey, M.A., & Dzou, L.I.P., 1998a: 24-norcholestanes as age-sensitive molecular fossils. Geology **26**, 783–786.

Holba, A.G., Dzou, L.I.P., Masterson, W.D., Hughes, W.B., Huizinga, B.J., Singletary, M.S., Moldowan, J.M., Mello, M.R., & Tegelaar, E., 1998b: Application of 24-norcholestanes for constraining source age of petroleum. Organic Geochemistry, **29**, 1269–1283.

Holba, A.G., Tegelaar, E., Ellis, L., Singletary, M.S. & Albrechts, P., 2000: Tetracyclic polyprenoids: indicators of freshwater (lacustrine) algal input. Geology, **28**, 251–254.

Hughes, W.B., Holba, A.G & DZOU, L.I.P., 1995: The ratios of dibenzothiophene to phenanthrene and pristane to phytane as indicators of depositional environment and lithology of petroleum source rocks. Geochim. Cosmochim. Acta, **59**, 3581–3598.

Holba, A.G., Dzou, L.I., Wood, G.D., Ellis, L., Adam, P., Schaeffer, P., Albrechts, P., Greene, T. & Hughes, W.B., 2003: Application of tetracyclic polyprenoids as indicators of input from fresh-brackish water environments. Organic Geochemistry, **34**, 441–469.

Moldowan, J.M. & Seifert, W.K., 1984: Structure proof and significance of stereoisomeric 28,30-bisnorhopanes in petroleum and petroleum source rocks. Geochimica et Cosmochimica Acta, **48**, 1651–1661.

Moldowan, J.M., Fago, F.J., Carlson, R.M.K., Young, D.V., Van Duyne, G., Clardy, J., Schoell, M., Pillinger, C.T. & Watt, D.S., 1991: Rearranged hopanes in sediments and petroleum. Geochimica et Cosmochimica Acta, **55**, 3333–3353.

Nytoft, H.P., Lutnæs, B.F., Johansen, J.E., 2006: 28-*Nor*-spergulanes, a novel series of rearranged hopanes. Organic Geochemistry, **37**, 772–786.

Nytoft, H.P. 2009: Novel isohopanes II. The 24rd International Meeting on Organic Geochemistry. 6-11 September, 2009-12-03. Bremen, Germany. European Association of Organic Geochemists. Book of Abstracts, p–172.

Nytoft, H.P. 2007: Novel "isohopanes" and their use as source markers. The 23rd International Meeting on Organic Geochemistry. 9-14 September, 2007. Torquay, England. European Association of Organic Geochemists. Book of Abstracts, 273–274.

Nytoft, H.P., Bojesen-Koefoed, J.A. & Christiansen, F.G., 2000: C_{26} and C_{28}-C_{34} 28-norhopanes in sediments and petroleum. Organic Geochemistry, **31**, 25–39.

Peters, K.E., Walters, C.C. & Moldowan, J.M., 2005: The Biomarker Guide Second Edition Volume 2: Biomarkers and Isotopes in Petroleum Exploration and Earth History. Cambridge University Press.

Schoell, M., McCaffrey, M.A., Fago, F.J. & Moldowan, J.M., 1992: Carbon isotopic compositions of 28,30-bisnorhopanes and other biological markers in a Monterey crude oil. Geochimica et Cosmochimica Acta, **56**, 1391–1399.

Seifert, W.K., Moldowan, J.M., Smith, G.W. & Whitehead, E.W., 1978: First proof of structure of a C_{28}-pentacyclic triterpane in petroleum. Nature, **271**, 436–437.

Sinninghe Damsté, J.S., Kenig, F., Koopmans, M.P., Köster, J., Schouten, S., Hayes, J.M. & de Leeuw, J.W. 1995: Evidence for gammacerane as an indicator of water column stratification. Geochimica et Cosmochimica Acta, **59**, 1895–1900.

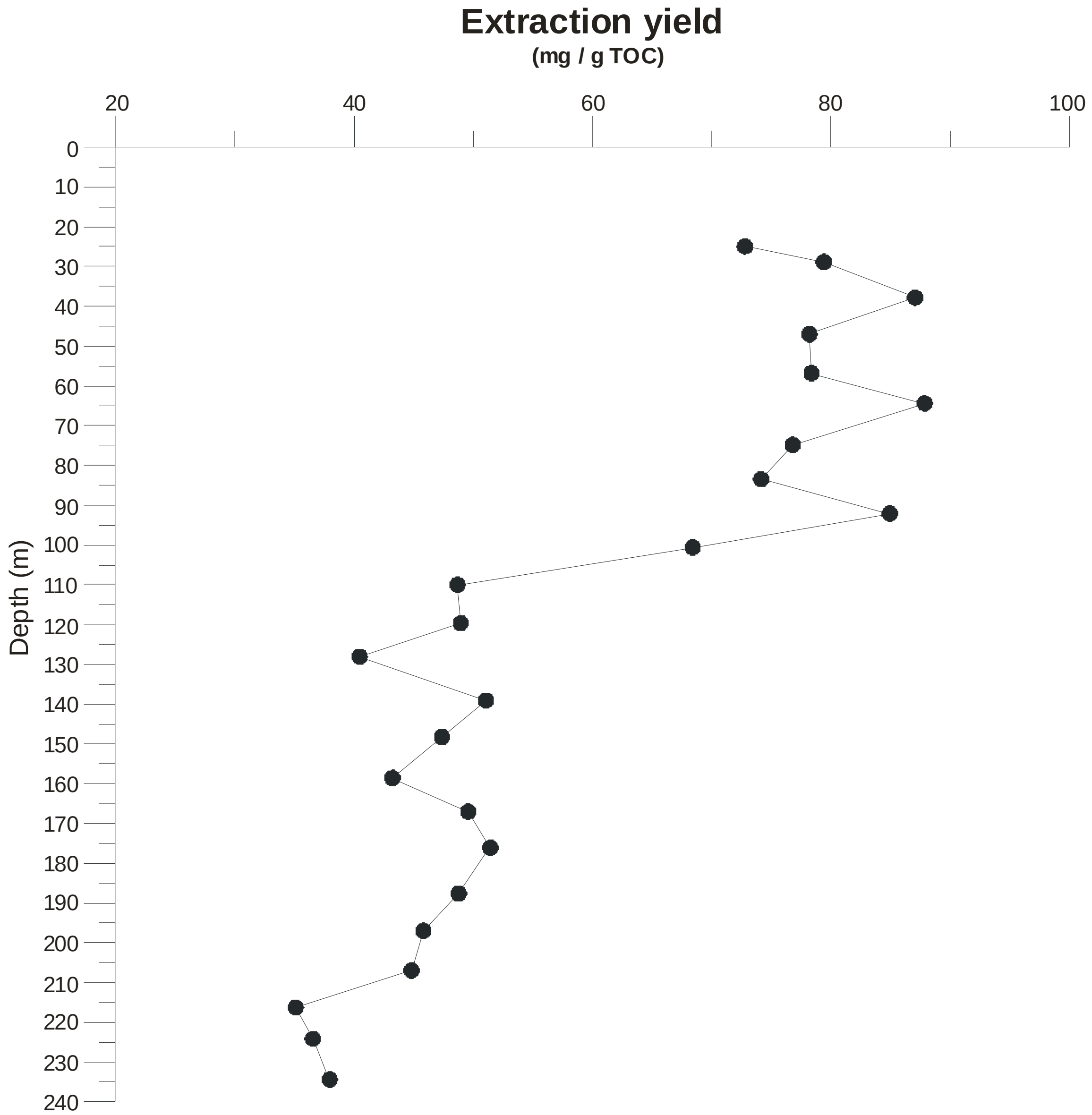

Figure 8.2.1. Variation in extract yield through the Rødryggen well.

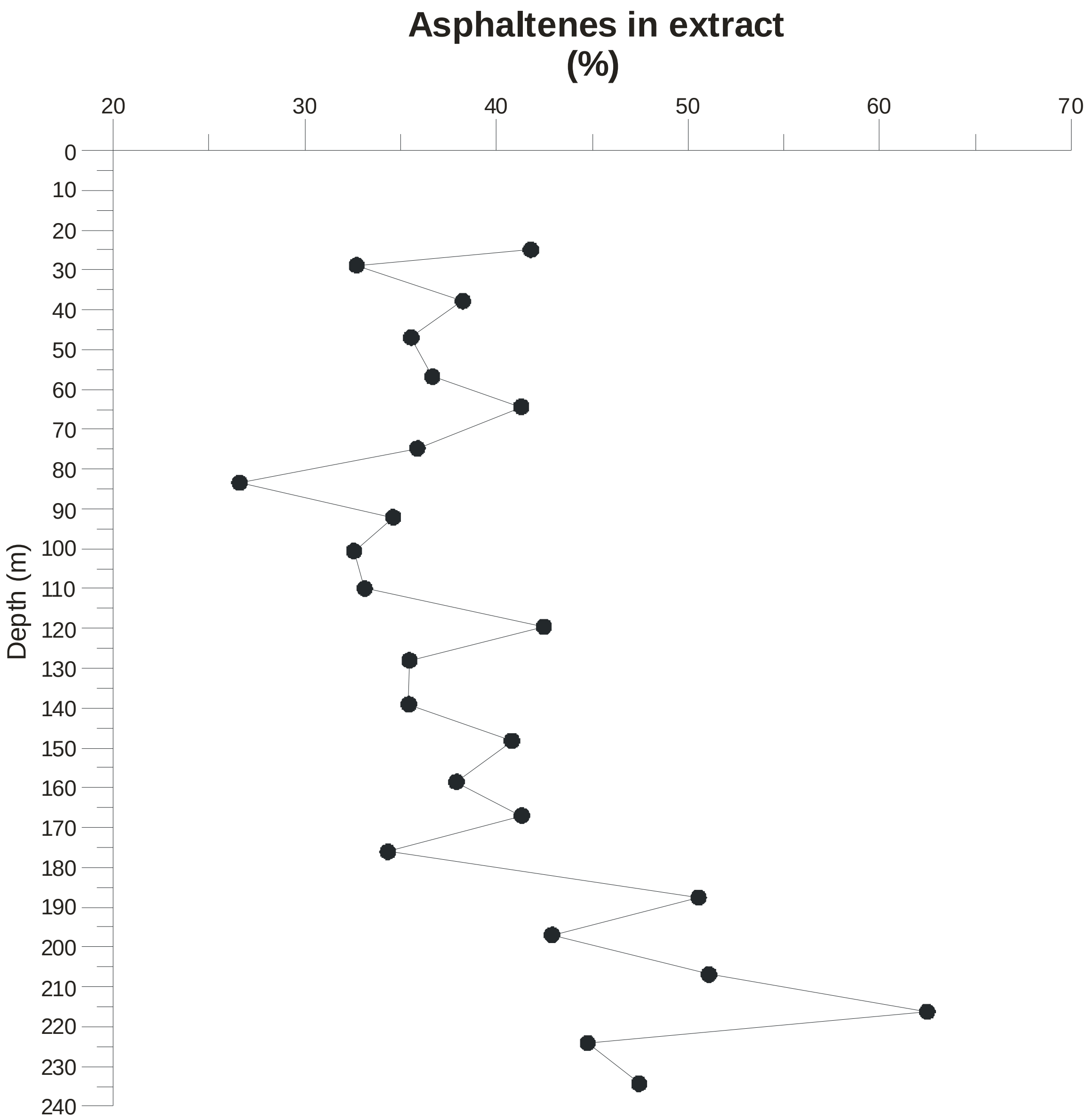

Figure 8.2.2. Asphaltene-content in extracts through the Rødryggen well.

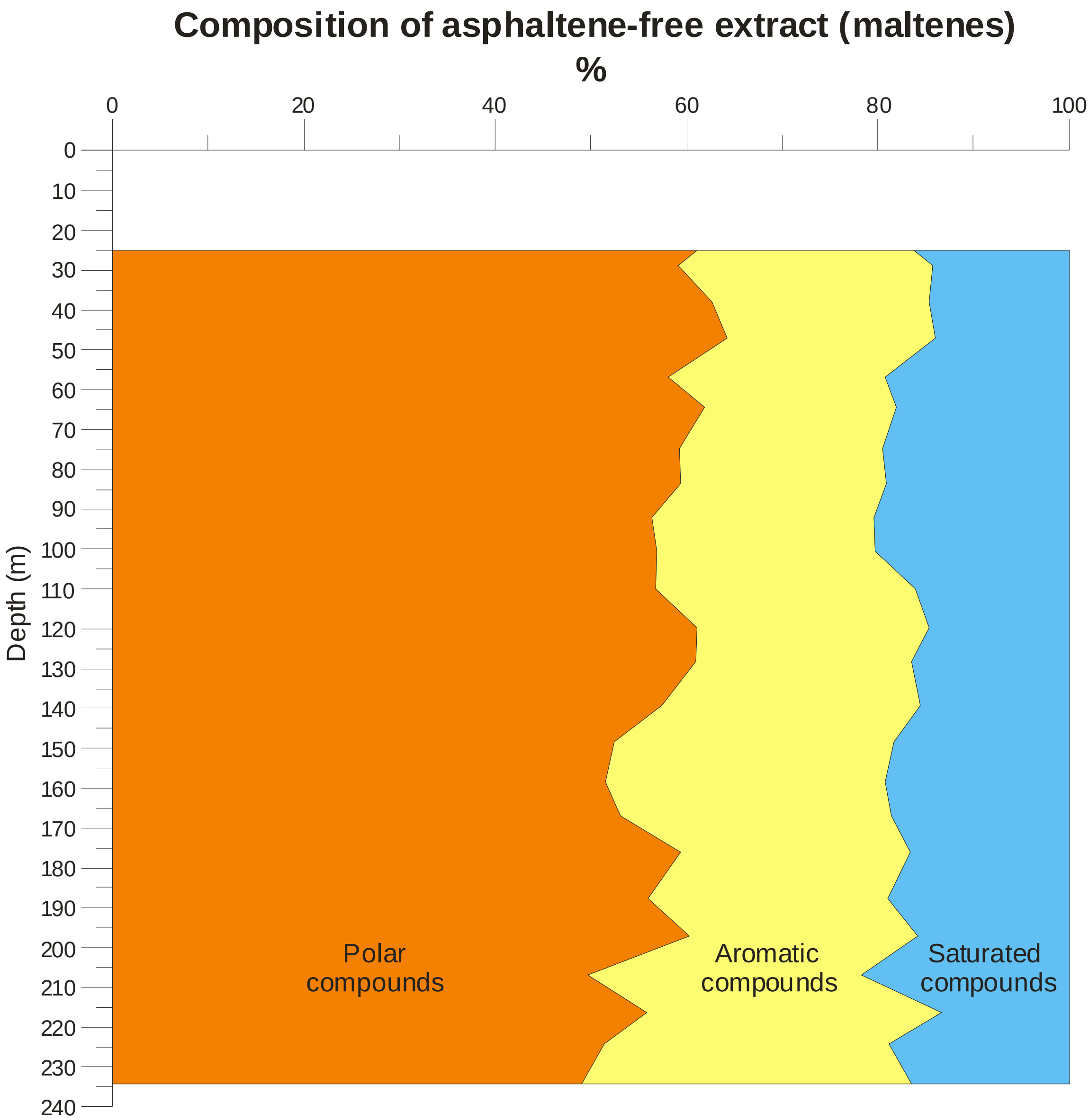

Figure 8.2.3. Composition of asphaltene-free extract (maltenes) in extracts through the Rødryggen well. The relative content of saturated hydrocarbons is constant. Polar compounds decrease slightly with depth.

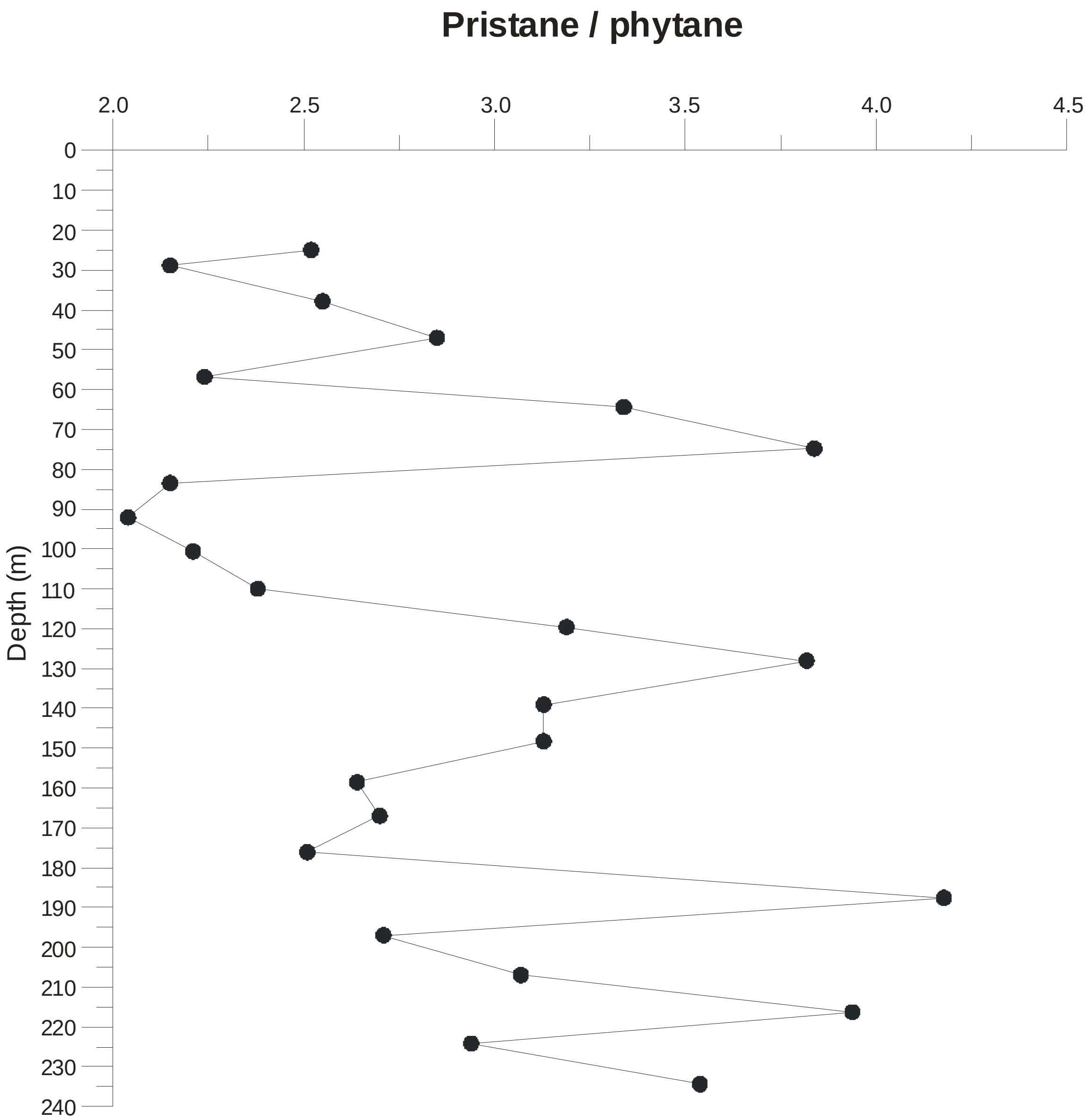

Figure 8.2.4. Pristane/phytane ratios (Pr/Ph) measured using gas chromatography.

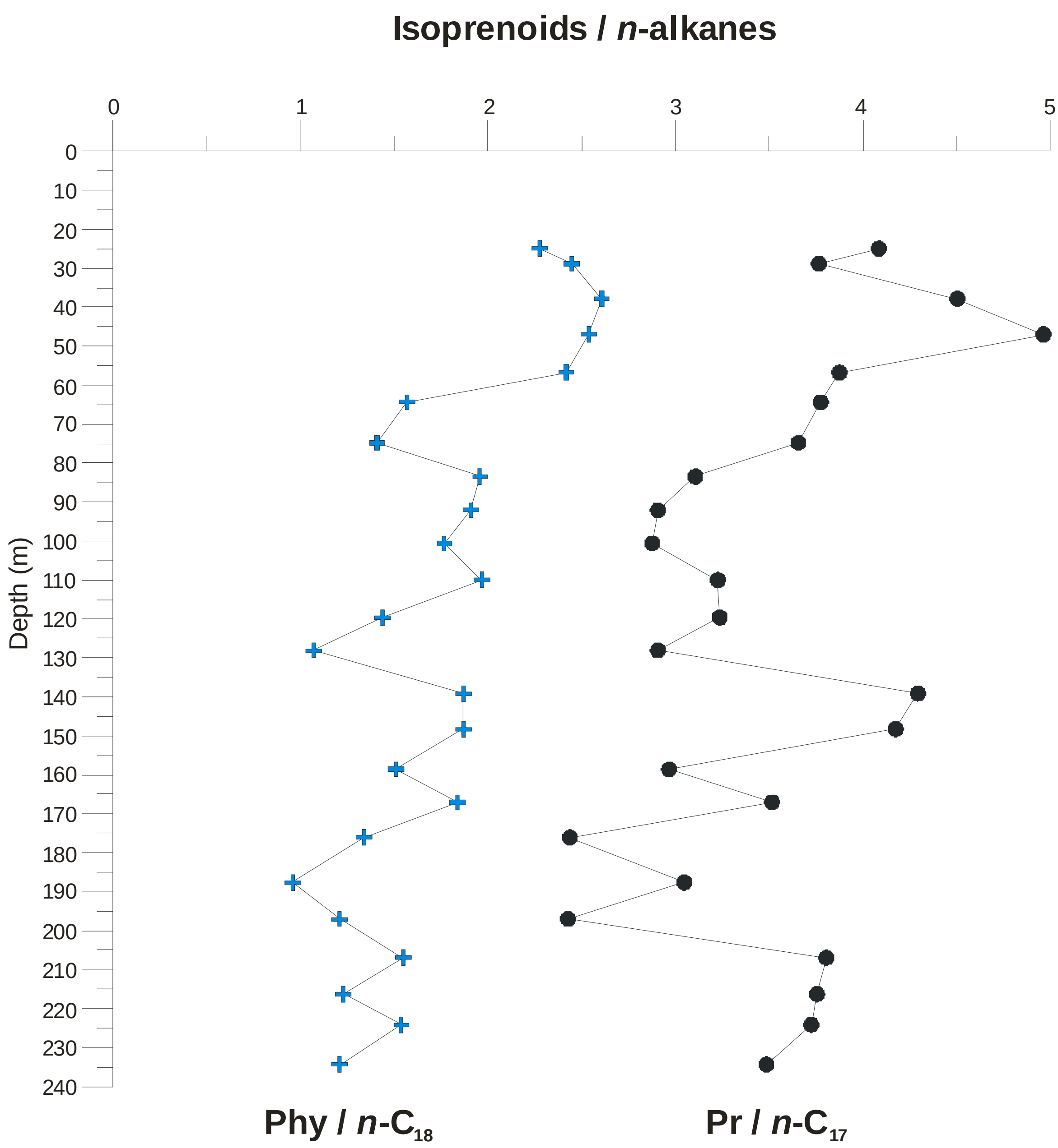

Figure 8.2.5. Pristane/*n*-C_{17} and Phytane/*n*-C_{18} ratios

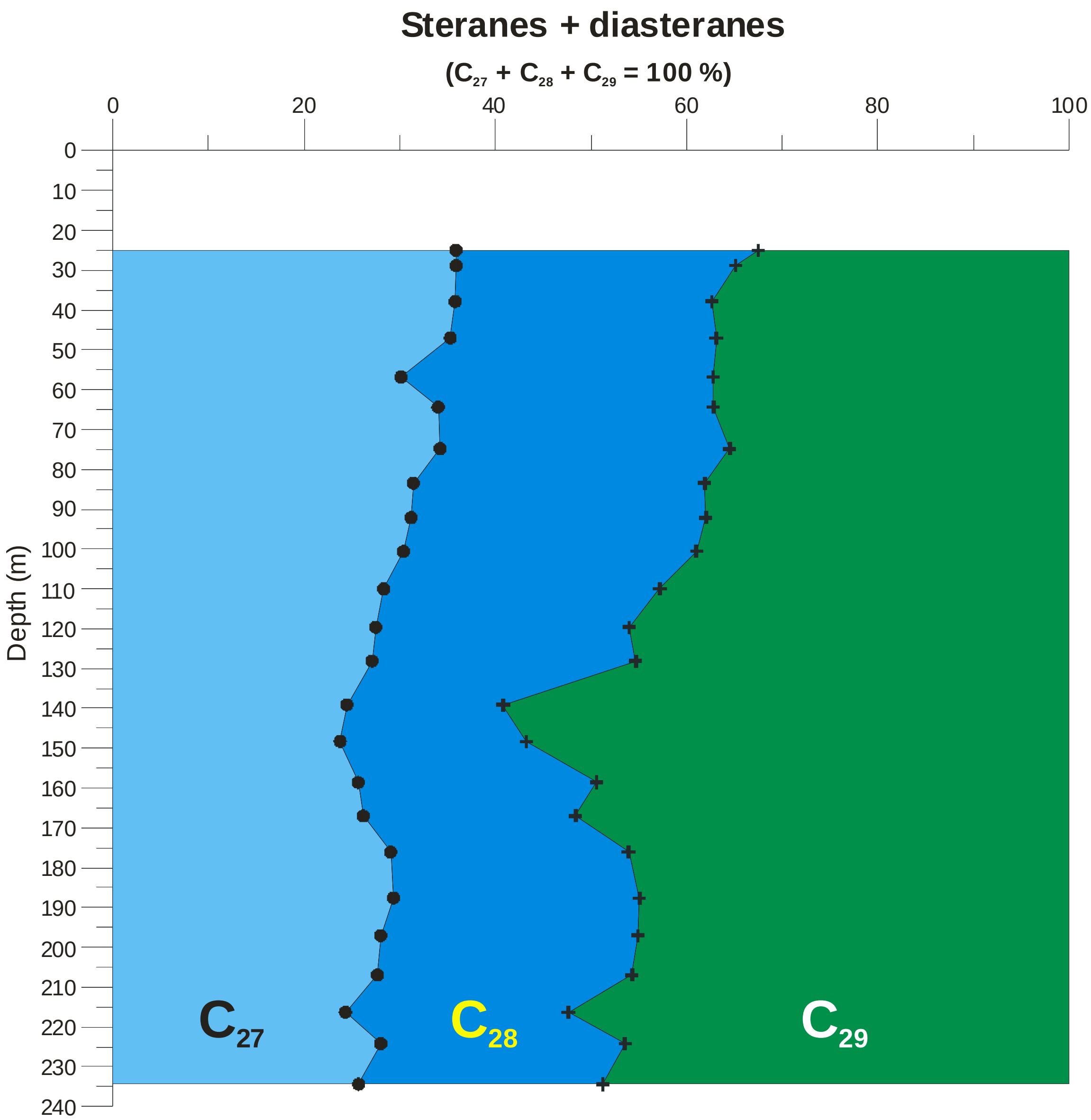

Figure 8.2.6. Distribution of C_{27}, C_{28} and C_{29} diasteranes + steranes. The proportion of C_{29} steranes increases below 120 m indicating a more terrestrial-influenced kerogen.

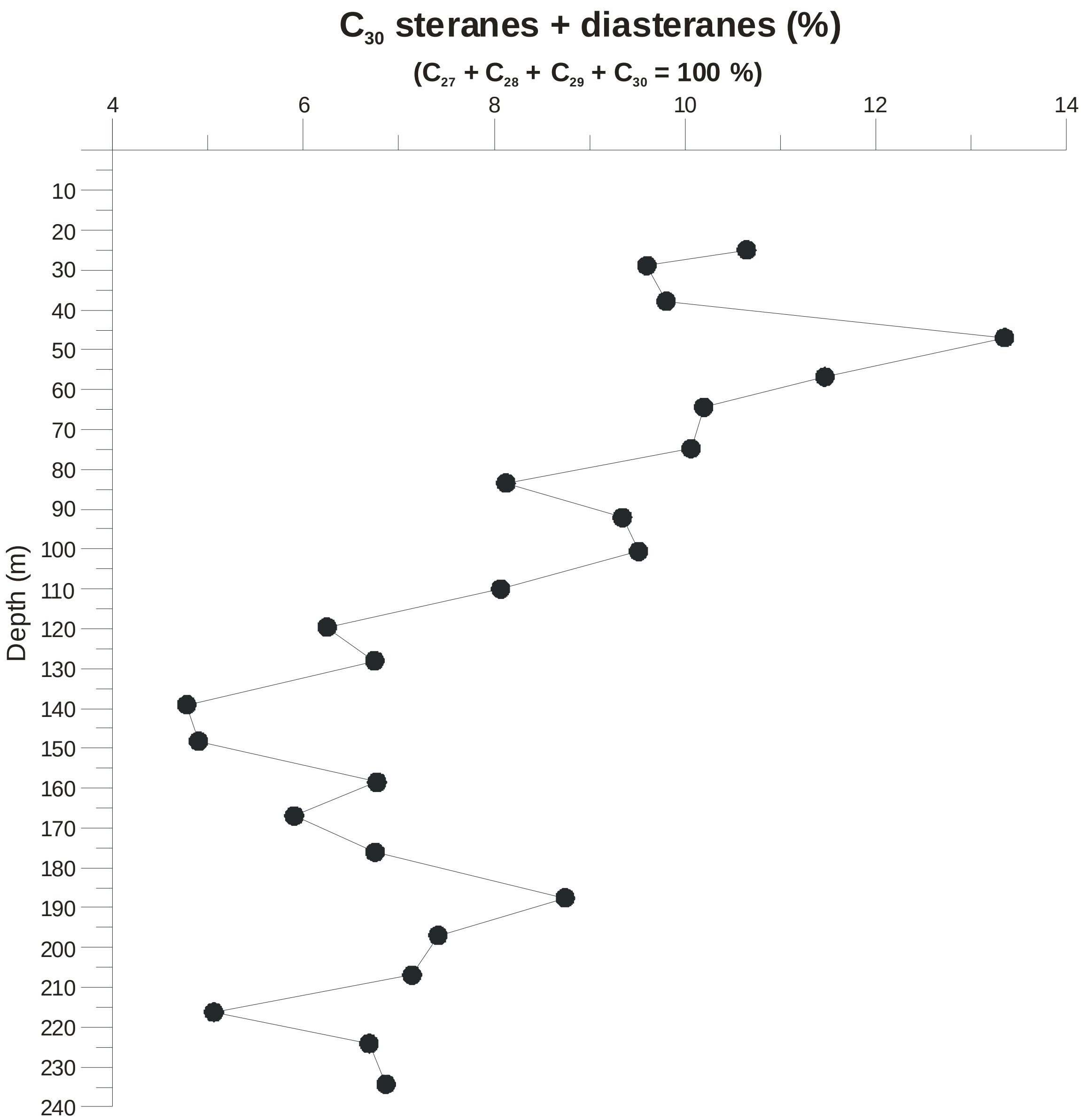

Figure 8.2.7. The relative proportion of C_{30} steranes decreases below ~100m = less marine input. C_{30} steranes (24-*n*-propylcholestanes) is the most powerful means in order to identify input of marine organic matter to the source rock (Peters et al., 2005).

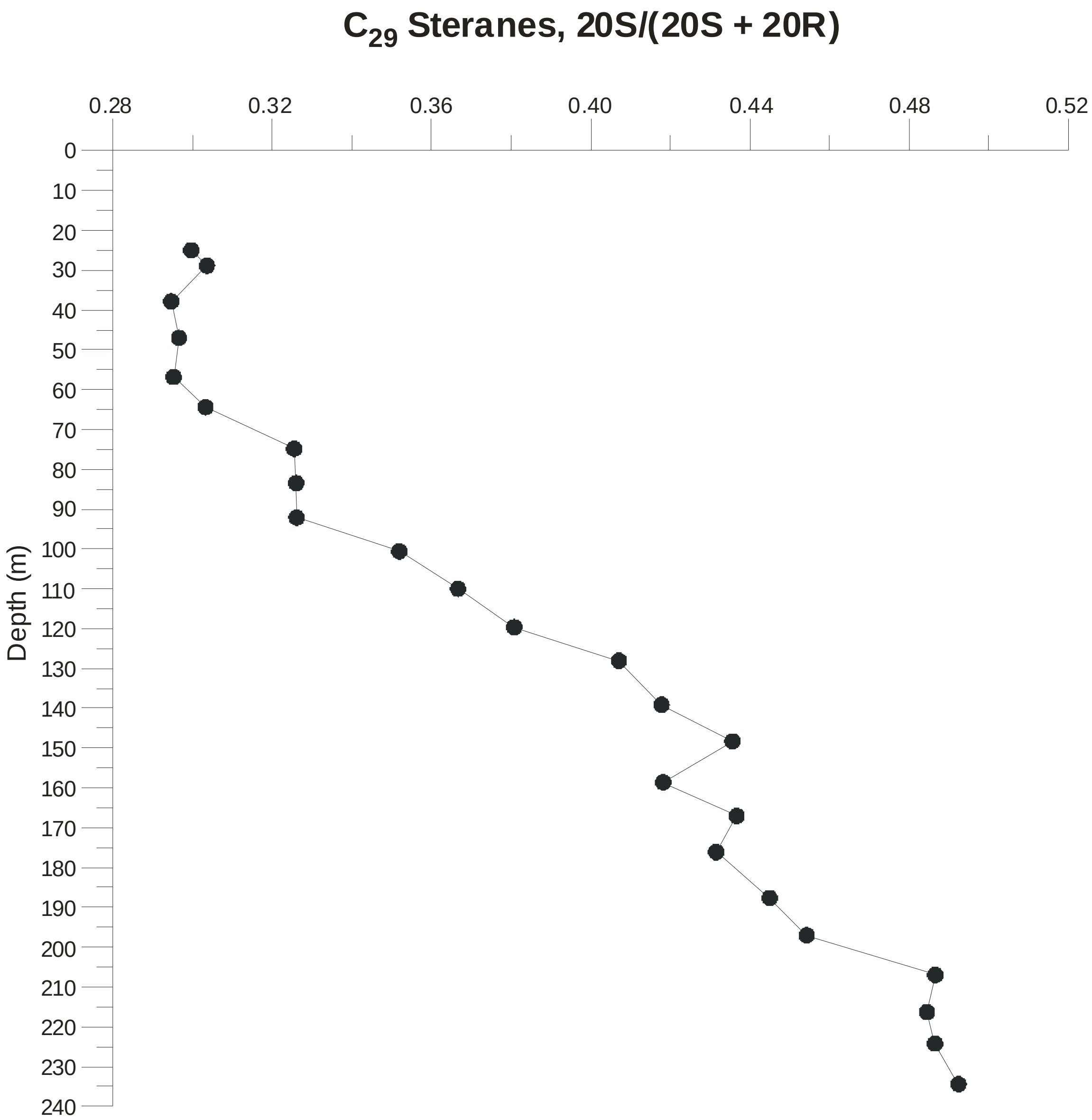

Figure 8.2.8. 20S/(20S + 20R) ratio for C_{29} steranes (400 → 217). The steranes are approaching equilibrium at the bottom.

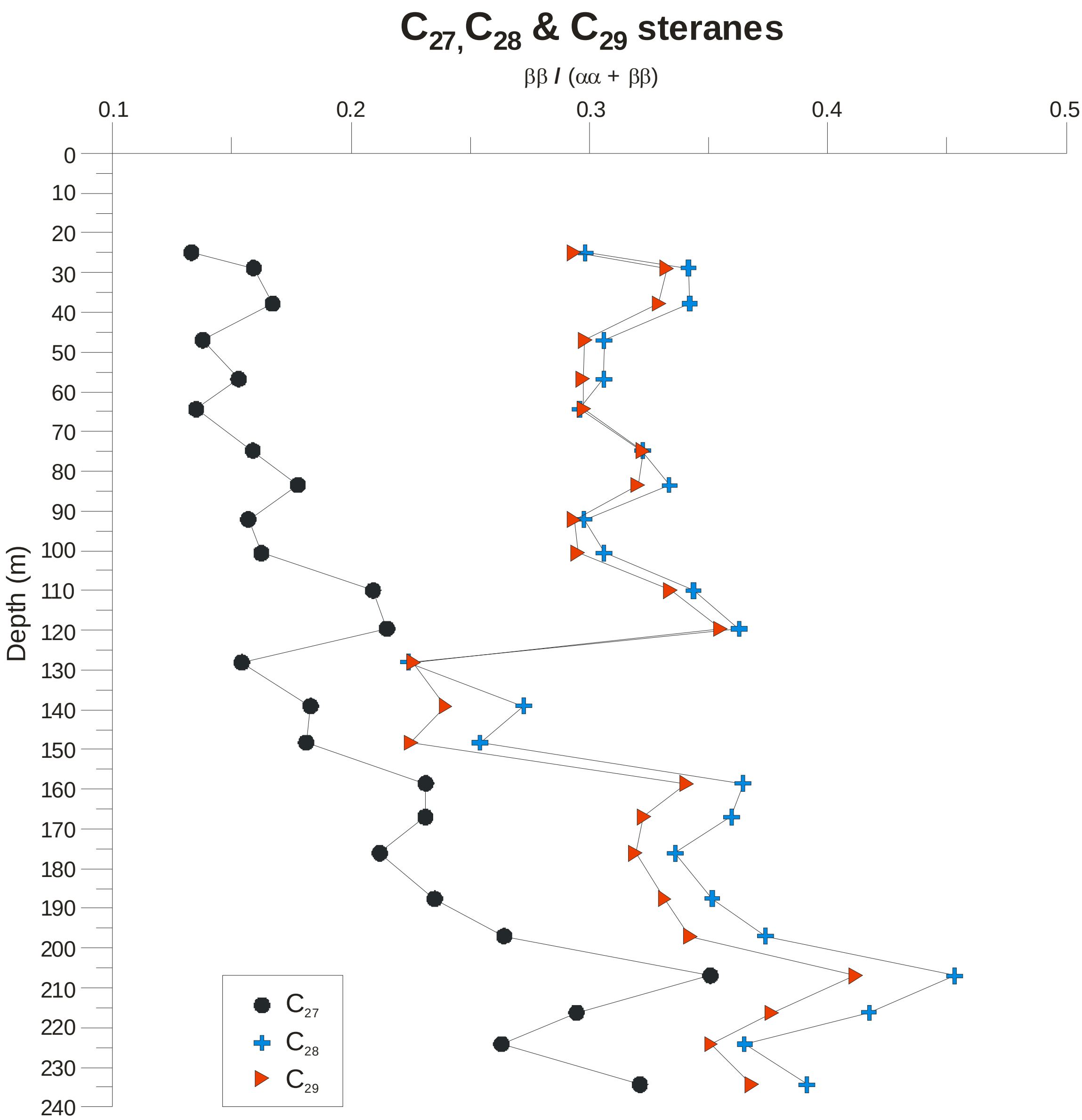

Figure 8.2.9. Variation in the relative proportions of C_{27}, C_{28} and C_{29} ββ steranes through the Rødryggen well.

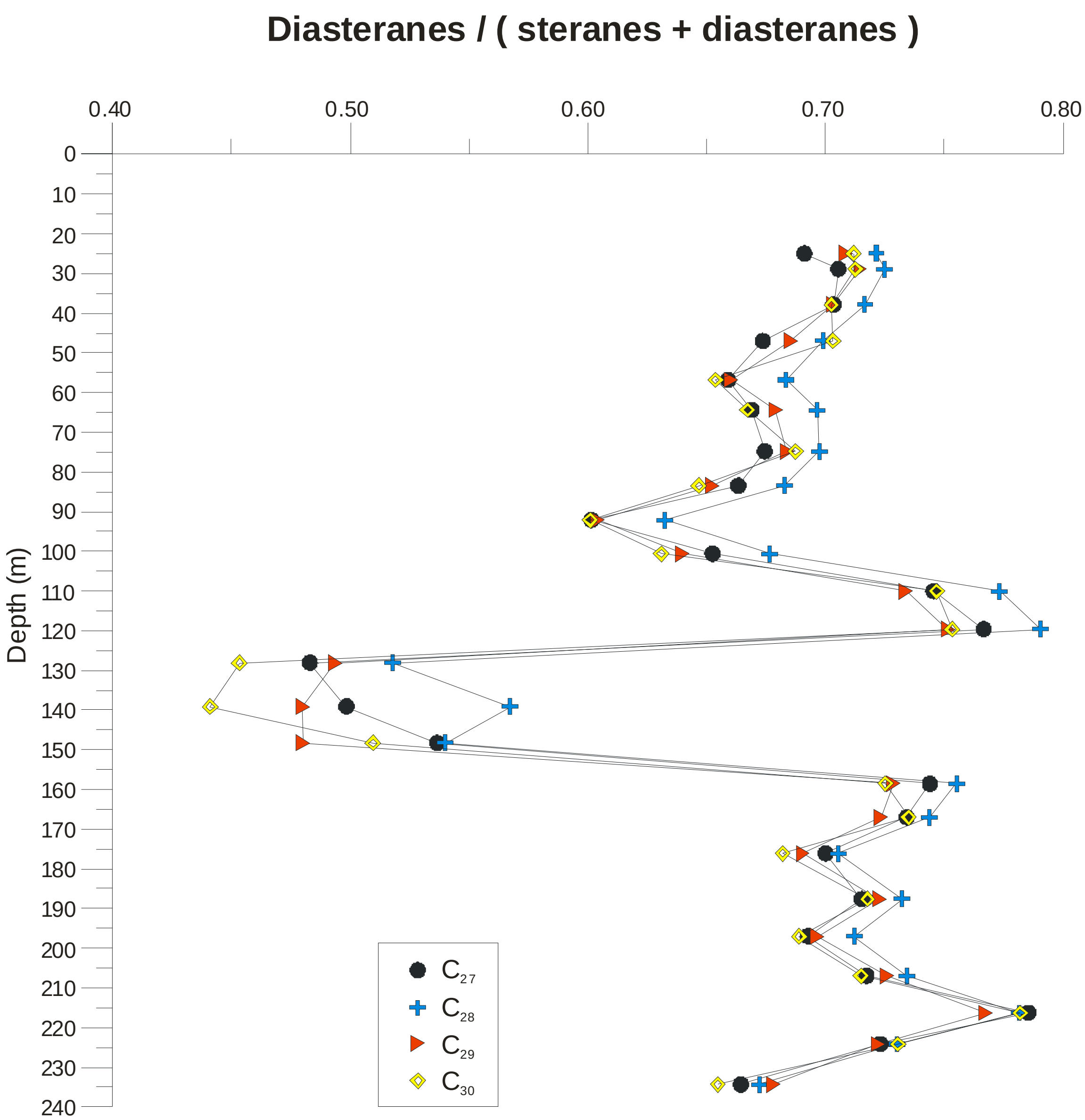

Figure 8.2.10. Variation in the diasteranes/(diasteranes + regular steranes) ratio through the Rødryggen well. Low ratios are found from 125 m to 150 m.

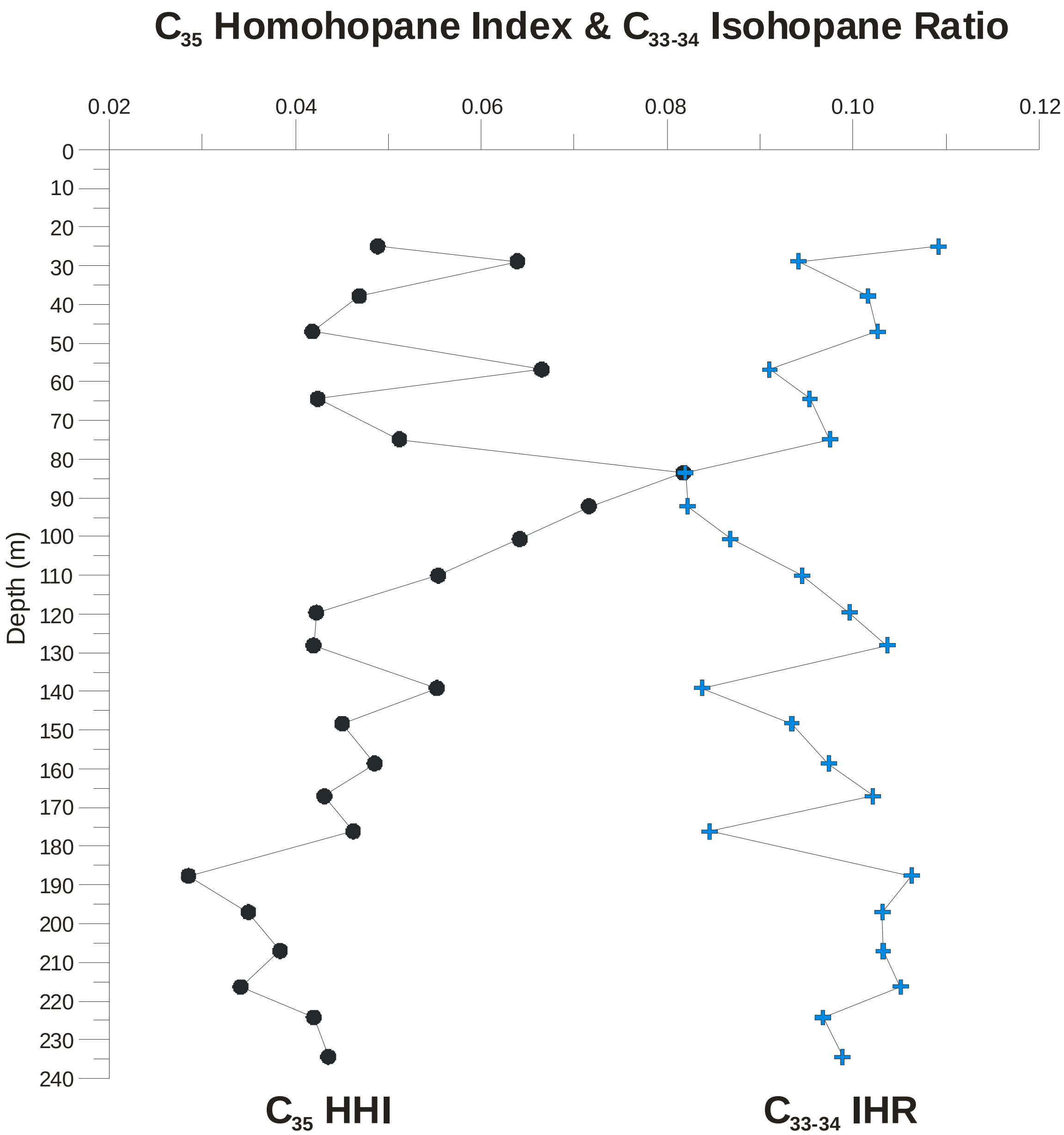

Figure 8.2.11. Variation in the C_{35} homohopane index = $C_{35}/(C_{31}-C_{35})$ and C_{33-34} isohopane ratio through the Rødryggen well. The C_{35} homohopane index is an indicator of redox potential in marine sediments. High values indicate anoxia. Isohopanes are extended hopanes having a side chain with an additional methyl branch (C_{33} and higher, Nytoft 2007, 2009). Their relative abundance is low in oils sourced from marine organic matter deposited under anoxic condition and high in oils having a coaly source.

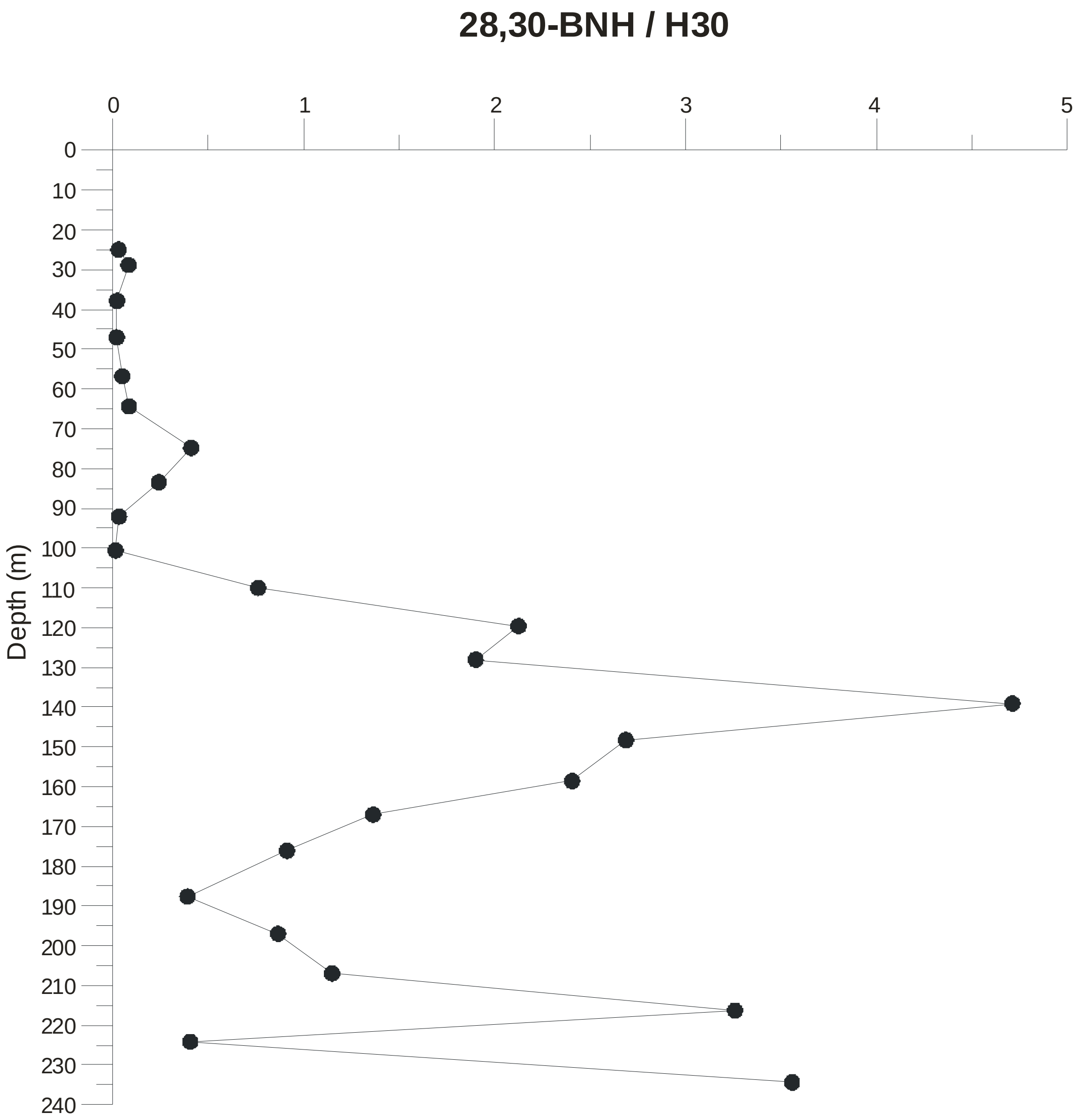

Figure 8.2.12. Variation in the 28,30-bisnorhopane/17α,21β(H)-hopane ratio (BNH/H30, 412 > 191) through the Rødryggen well.

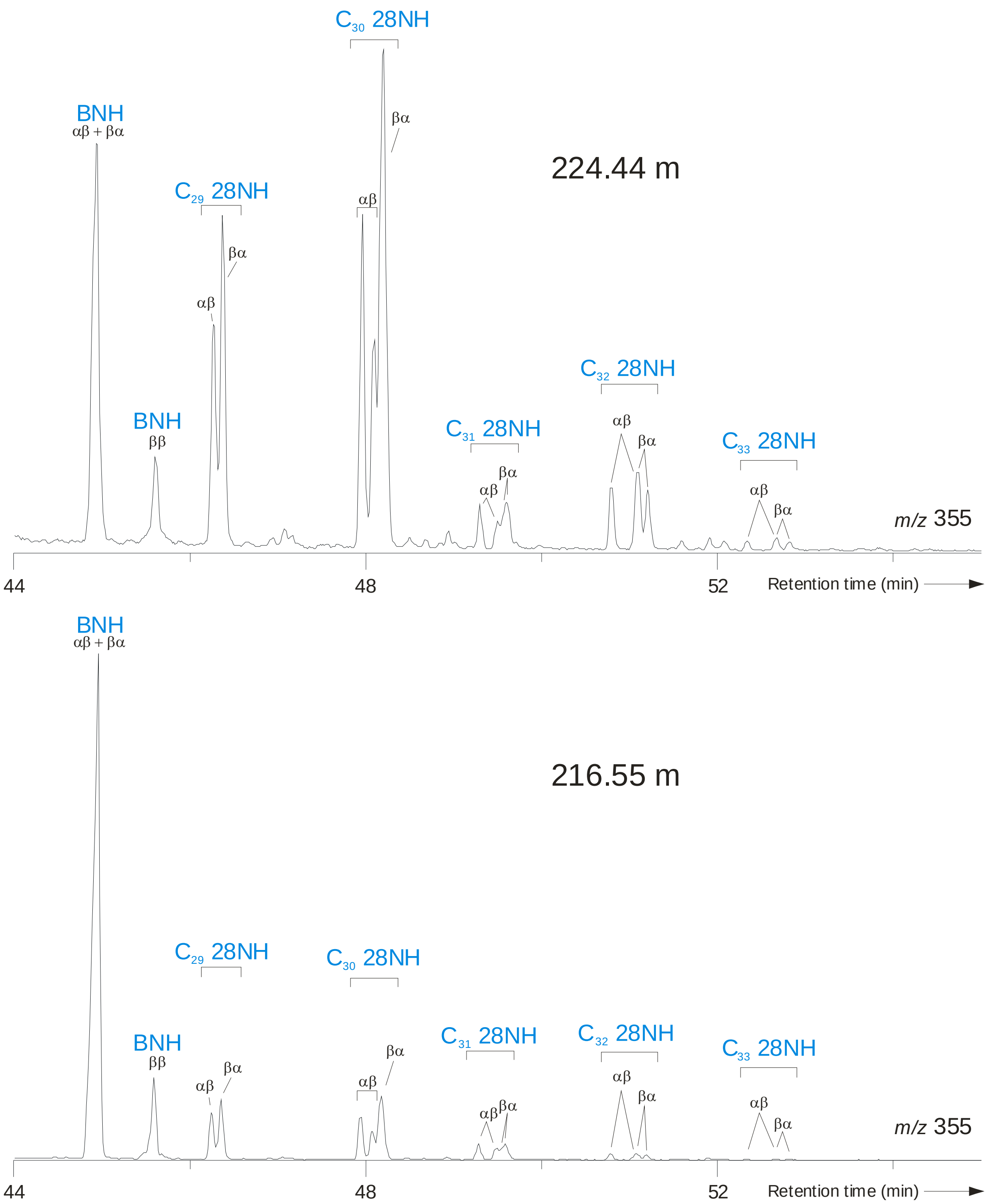

Figure 8.2.13. 28,30-Bisnorhopane (BNH, C_{28}) and other 28-norhopanes (NH, *m/z* 355) in two Rødryggen extracts.

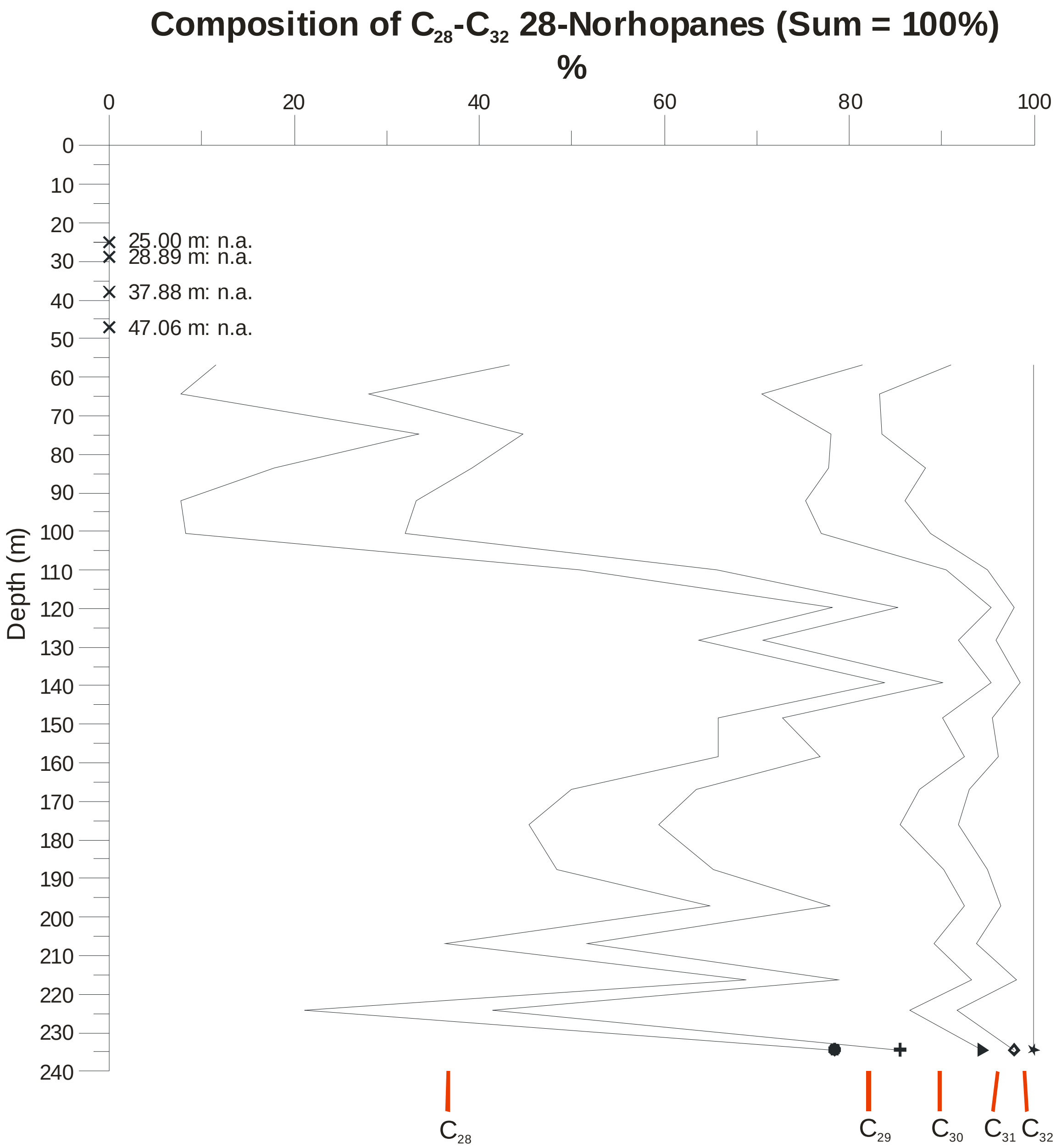

Figure 8.2.14. Composition of C_{28} – C_{32} 28-norhopanes (*m/z* 355) in extracts from the Rødryggen well.

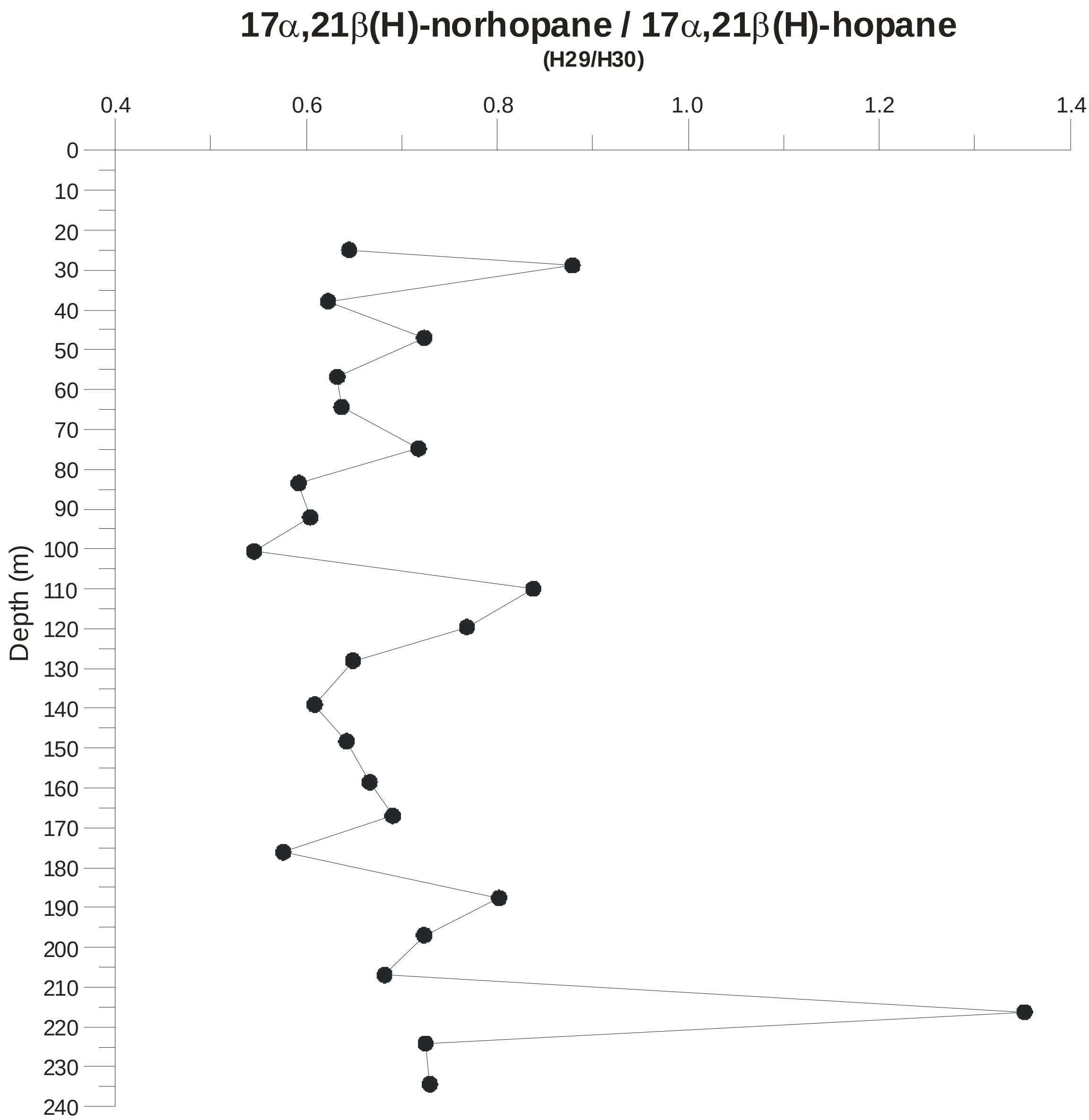

Figure 8.2.15. Variation in the 17α,21β(H)-norhopane/17α,21β(H)-hopane ratio through the Rødryggen well.

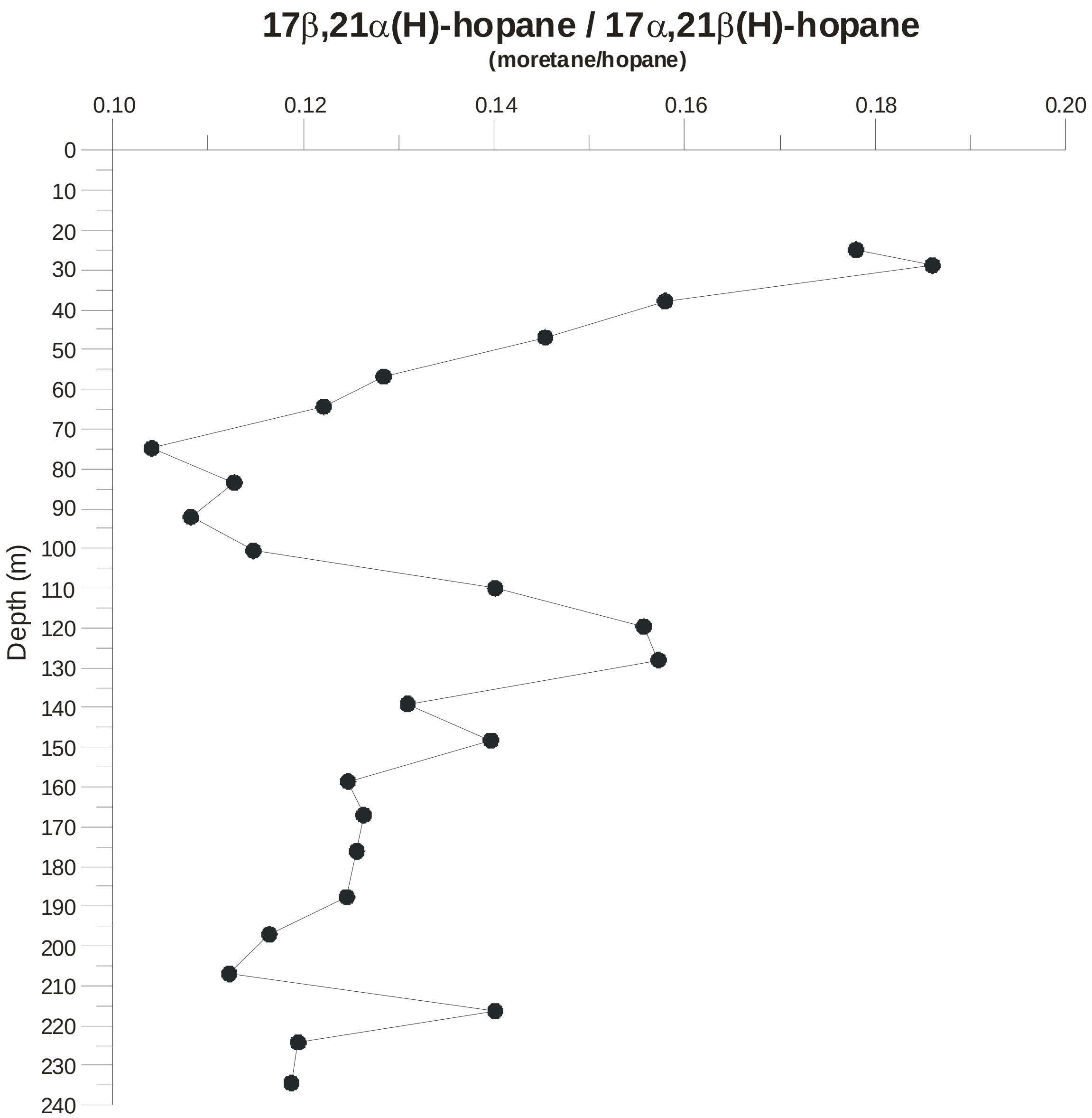

Figure 8.2.16. Variation in the 17β,21α(H)-hopane/17α,21β(H)-hopane ratio through the Rødryggen well.

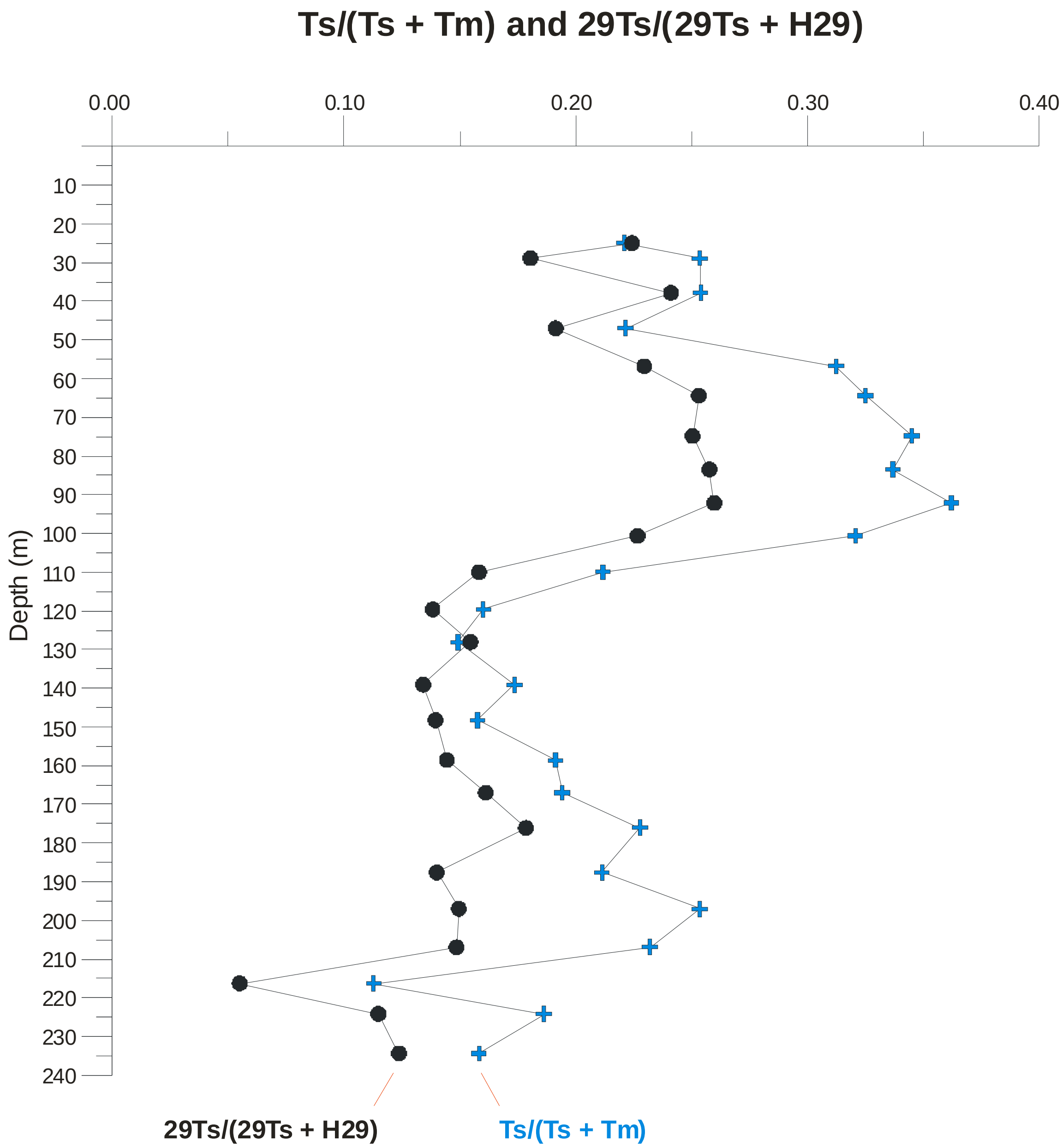

Figure 8.2.17. Variation in the relative proportion of C_{27} and C_{29} 18α-neohopanes (Ts/(Ts+Tm) & 29Ts/(29Ts+H29)) through the Rødryggen well.

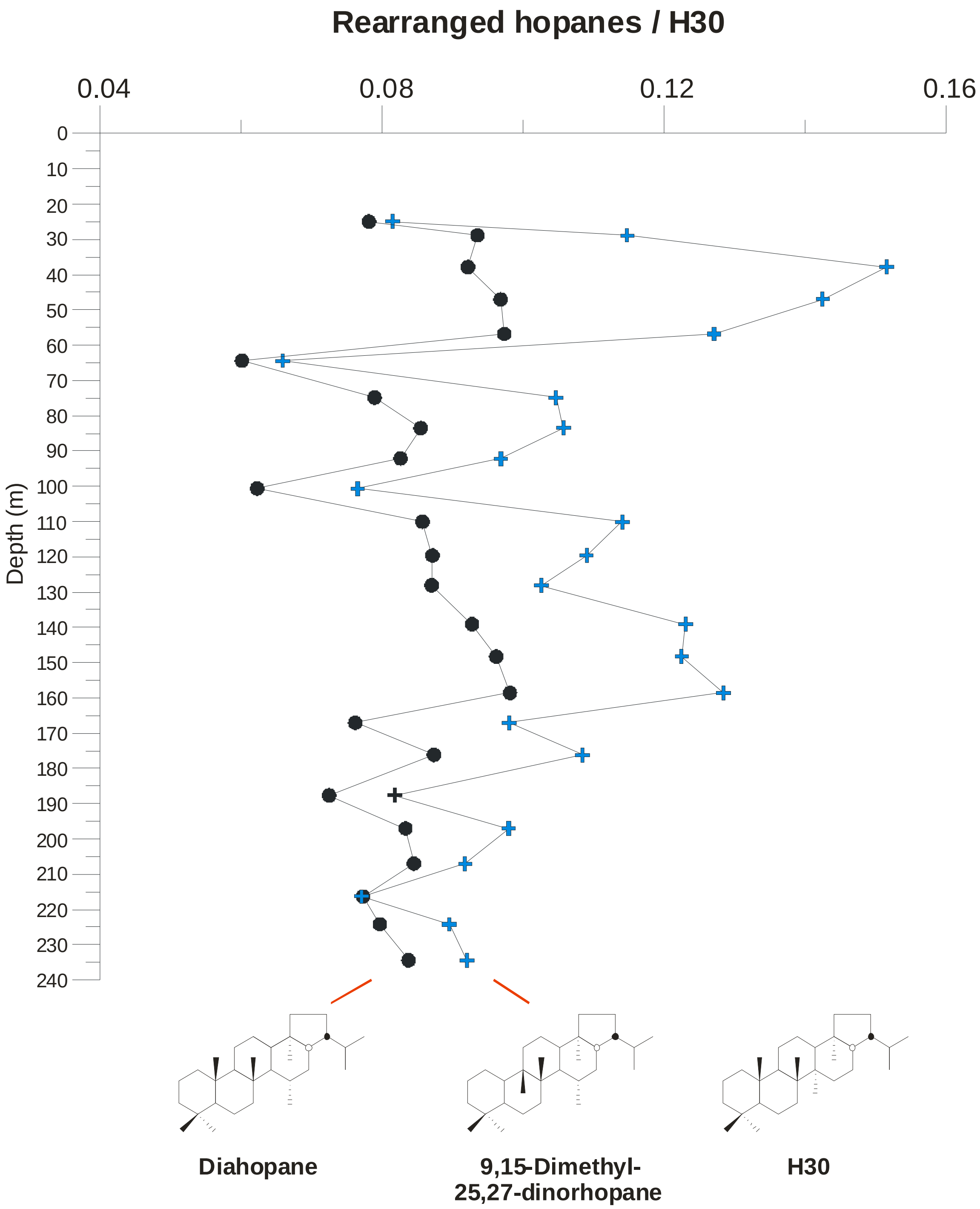

Figure 8.2.18. Relative proportion of two rearranged C_{30} hopanes.

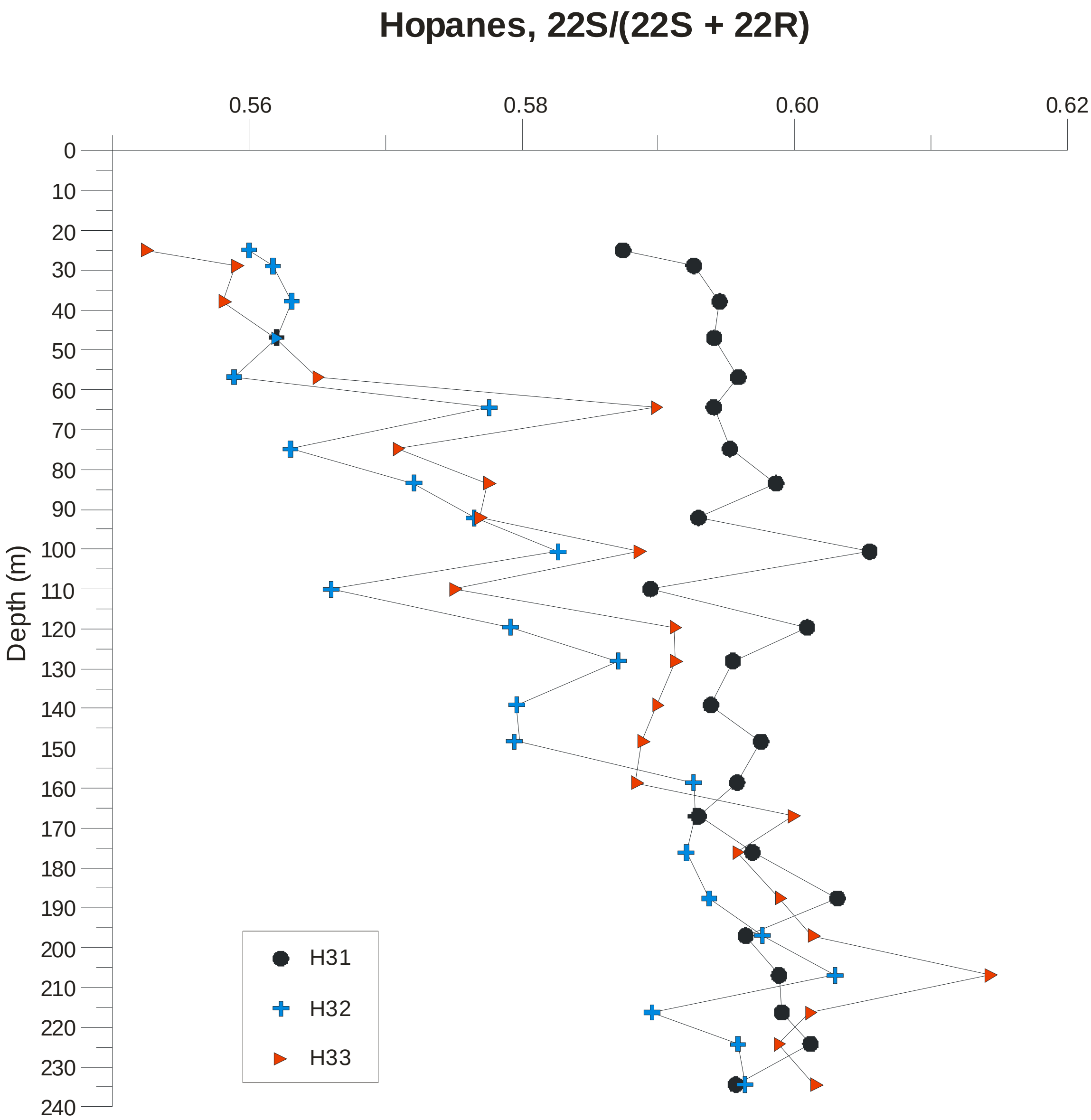

Figure 8.2.19. Isomerization of C_{31}, C_{32} and C_{33} hopanes

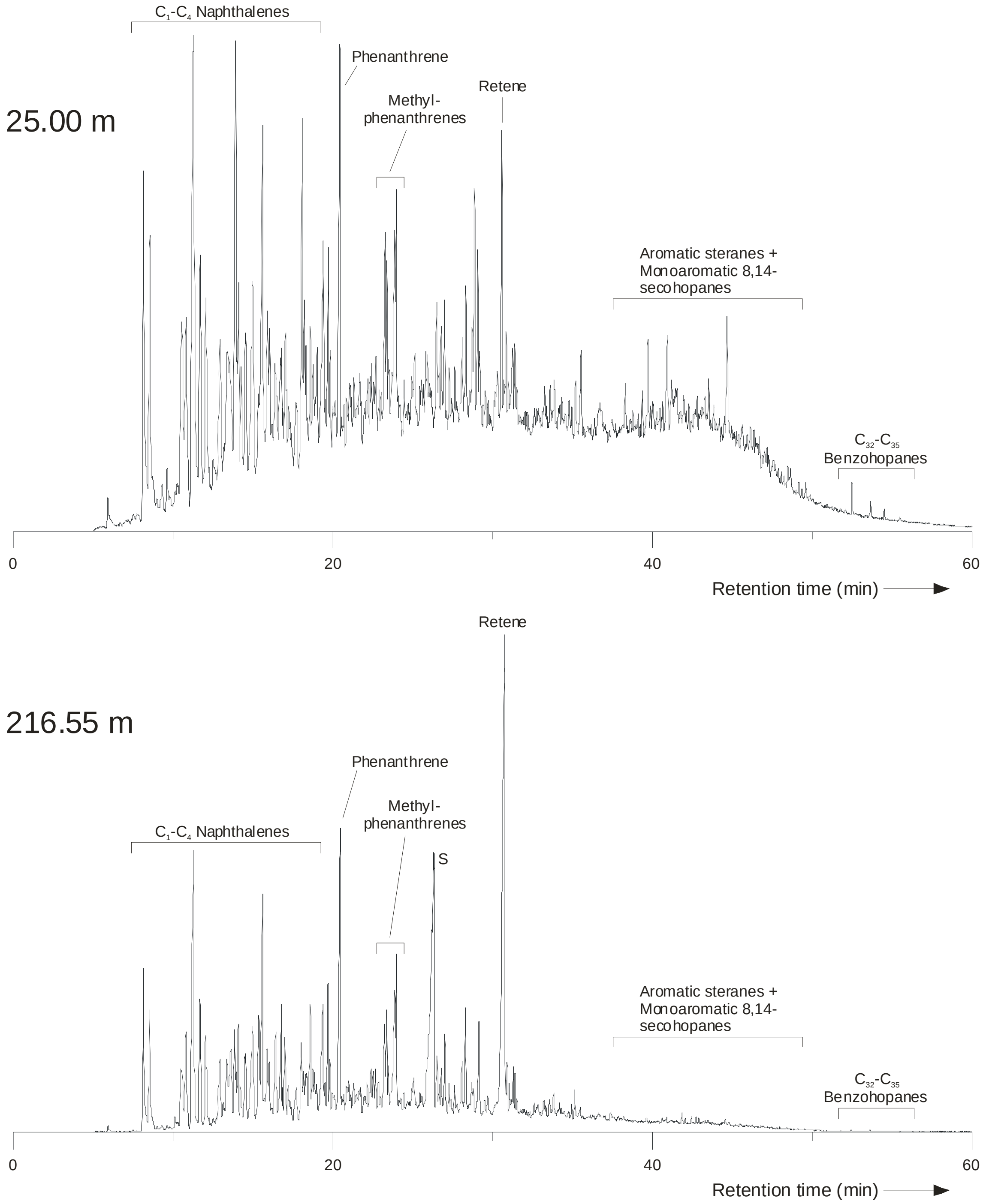

Figure 8.2.20. Aromatic hydrocarbons (GC-MS, full scan)

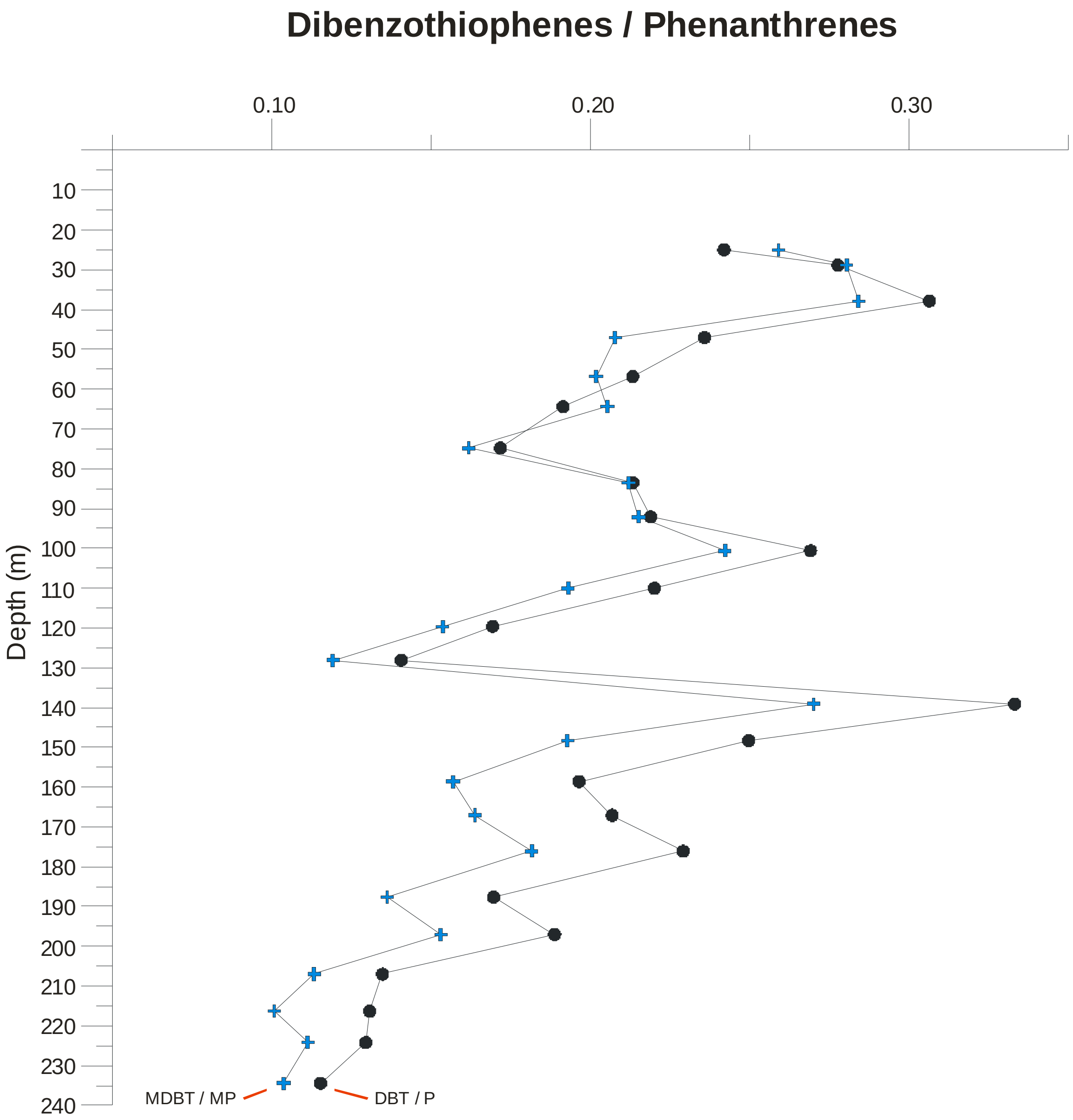

Figure 8.2.21. Relative content of sulphur-containing compounds in the aromatic hydrocarbon fraction: Dibenzothiophene, *m/z* 184 / phenanthrene *m/z* 178 (DBT/P) and methyldibenzothiophenes *m/z* 198 / methylphenanthrenes, *m/z* 192 (MDBT/MP).

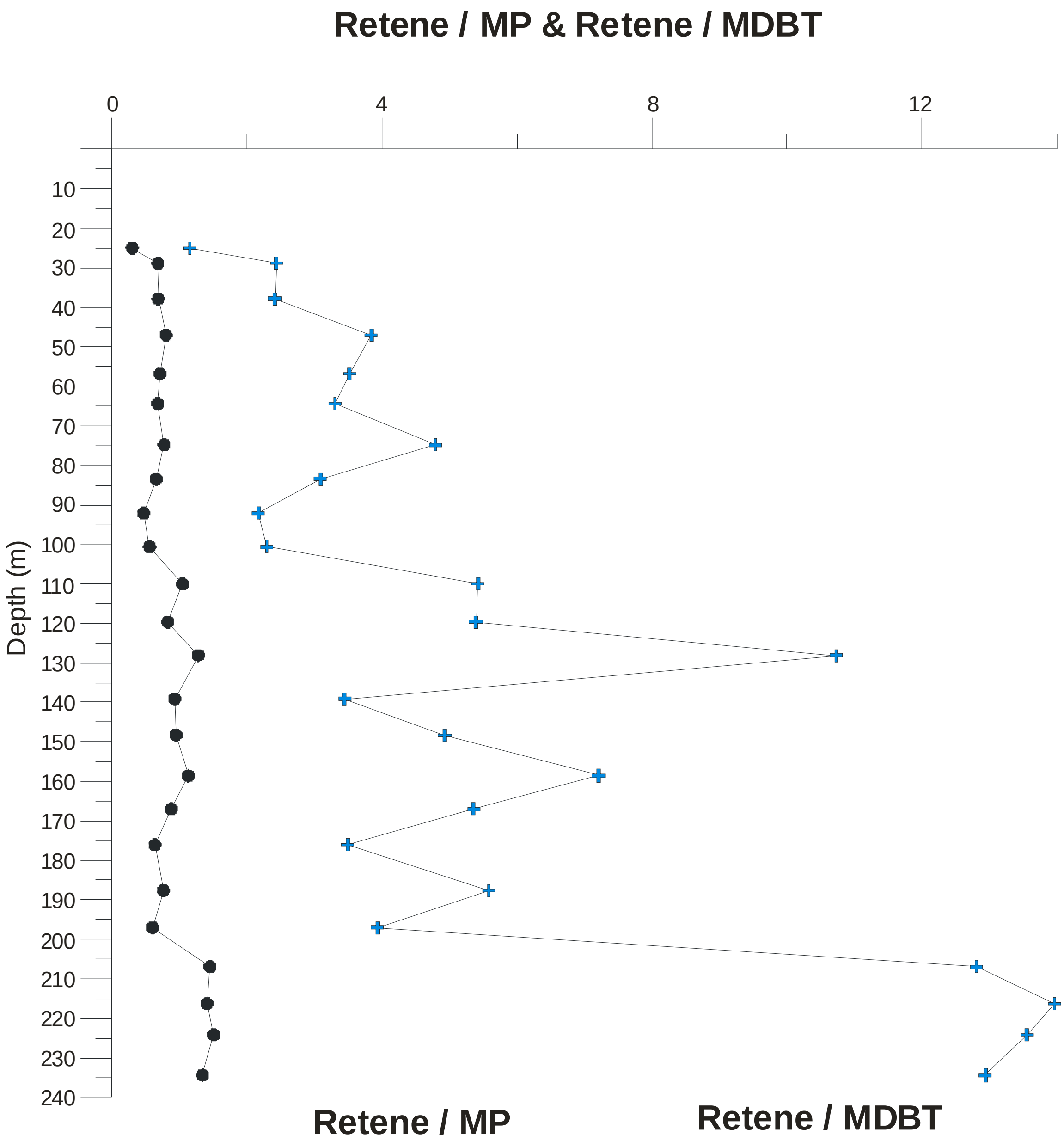

Figure 8.2.22. Aromatic hydrocarbons, relative proportion of retene (marker for gymnosperms, *m/z* 234, 198 & 192).

Table 1 Extraction, MPLC-separation and GC

Lab no.	Sample no.	Depth Bottom	Yield mg/g TOC	% Asph.	% Sat.	% Aro.	% Polars	Pristane/ phytane	Pristane/ *n*C17	Phytane *n*C18
2010008-17097	517001-005	25.00	72.78	41.82	16.04	22.76	61.19	2.52	4.09	2.28
2010008-17886	517001-310	28.89	79.40	32.72	14.16	26.61	59.23	2.15	3.77	2.45
2010008-17895	517001-301	37.88	87.06	38.27	14.49	22.71	62.80	2.55	4.51	2.61
2010008-17905	517001-291	47.06	78.20	35.57	13.81	21.90	64.29	2.85	4.97	2.54
2010008-17916	517001-280	56.88	78.38	36.67	19.18	22.60	58.22	2.24	3.88	2.42
2010008-17924	517001-272	64.47	87.86	41.32	17.92	20.13	61.95	3.34	3.78	1.57
2010008-17935	517001-261	74.92	76.80	35.89	19.33	21.33	59.33	3.84	3.66	1.41
2010008-17944	517001-252	83.57	74.15	26.60	19.00	21.50	59.50	2.15	3.11	1.96
2010008-17953	517001-243	92.23	84.94	34.63	20.35	23.26	56.40	2.04	2.91	1.91
2010008-17962	517001-234	100.73	68.41	32.58	20.18	22.87	56.95	2.21	2.88	1.77
2010008-17973	517001-223	110.15	48.69	33.14	16.02	27.18	56.80	2.38	3.23	1.97
2010008-17983	517001-213	119.77	48.96	42.50	14.51	24.35	61.14	3.19	3.24	1.44
2010008-17992	517001-204	128.22	40.49	35.48	16.37	22.57	61.06	3.82	2.91	1.07
2010008-18002	517001-194	139.26	51.07	35.44	15.42	27.08	57.50	3.13	4.30	1.87
2010008-18012	517001-184	148.46	47.39	40.83	18.22	29.24	52.54	3.13	4.18	1.87
2010008-18023	517001-173	158.77	43.23	37.93	19.07	29.38	51.55	2.64	2.97	1.51
2010008-18032	517001-164	167.24	49.59	41.35	18.50	28.32	53.18	2.70	3.52	1.84
2010008-18042	517001-154	176.33	51.44	34.35	16.56	23.93	59.51	2.51	2.44	1.34
2010008-18054	517001-142	187.85	48.79	50.59	18.89	25.00	56.11	4.18	3.05	0.96
2010008-18064	517001-132	197.24	45.83	42.93	15.72	23.90	60.38	2.71	2.43	1.21
2010008-18075	517001-121	207.21	44.83	51.13	21.65	28.57	49.78	3.07	3.81	1.55
2010008-18086	517001-110	216.55	35.13	62.54	13.24	30.88	55.88	3.94	3.76	1.23
2010008-18094	517001-102	224.44	36.56	44.79	18.79	29.70	51.52	2.94	3.73	1.54
2010008-18109	517001-091	234.66	37.97	47.48	16.36	34.55	49.09	3.54	3.49	1.21

Table 2

			Diasteranes/ (diasteranes + reg. steranes)				ββ steranes/ (ββ steranes + αα steranes)				Steranes 20S/(20S + 20R)				% C27, 28 & 29 Sum = 100 % Regular steranes only			% C27, 28 & 29 Sum = 100 % Diasteranes only			% C27, 28 & 29 Sum = 100 % Diasteranes + reg. steranes			% C30
		Depth	C27	C28	C29	C30	C27	C28	C29	C30	C27	C28	C29	C30	C27	C28	C29	C27	C28	C29	C27	C28	C29	C30
Lab no.	Sample no.	Bottom	D/(R+D)	D/(R+D)	D/(R+D)	D/(R+D)	B/(B+A)	B/(B+A)	B/(B+A)	B/(B+A)	S/(S+R)	S/(S+R)	S/(S+R)	S/(S+R)	R-st	R-st	R-st	Dia	Dia	Dia	D+R	D+R	D+R	D+R
2010008-17097	517001-005	25.00	0.691	0.721	0.708	0.712	0.133	0.298	0.294	0.257	0.445	0.329	0.300	0.287	37.78	30.01	32.21	35.15	32.32	32.54	35.92	31.64	32.44	10.65
2010008-17886	517001-310	28.89	0.705	0.725	0.715	0.713	0.159	0.342	0.333	0.282	0.451	0.345	0.304	0.281	37.05	28.18	34.77	35.49	29.69	34.82	35.94	29.26	34.80	9.60
2010008-17895	517001-301	37.88	0.703	0.717	0.703	0.703	0.167	0.342	0.329	0.268	0.443	0.355	0.295	0.280	36.25	25.98	37.77	35.66	27.25	37.10	35.83	26.87	37.30	9.80
2010008-17905	517001-291	47.06	0.674	0.699	0.685	0.703	0.138	0.306	0.298	0.252	0.434	0.338	0.297	0.281	36.61	26.62	36.77	34.75	28.41	36.84	35.33	27.85	36.82	13.35
2010008-17916	517001-280	56.88	0.659	0.683	0.660	0.654	0.153	0.306	0.297	0.246	0.430	0.340	0.295	0.279	30.93	31.12	37.95	29.78	33.45	36.77	30.16	32.68	37.16	11.47
2010008-17924	517001-272	64.47	0.669	0.696	0.679	0.667	0.135	0.296	0.298	0.257	0.435	0.341	0.303	0.280	35.29	27.40	37.30	33.46	29.51	37.03	34.05	28.84	37.12	10.20
2010008-17935	517001-261	74.92	0.674	0.697	0.684	0.687	0.159	0.322	0.322	0.267	0.451	0.360	0.326	0.293	35.36	29.13	35.50	33.74	30.90	35.36	34.25	30.34	35.41	10.06
2010008-17944	517001-252	83.57	0.663	0.683	0.652	0.647	0.178	0.334	0.320	0.263	0.446	0.371	0.326	0.297	31.62	28.91	39.47	31.37	31.34	37.29	31.46	30.53	38.02	8.12
2010008-17953	517001-243	92.23	0.601	0.632	0.604	0.601	0.157	0.298	0.294	0.257	0.443	0.364	0.326	0.300	32.06	29.27	38.67	30.68	31.93	37.39	31.22	30.90	37.89	9.34
2010008-17962	517001-234	100.73	0.652	0.677	0.640	0.631	0.162	0.306	0.295	0.260	0.467	0.380	0.352	0.322	30.64	28.76	40.60	30.30	31.69	38.01	30.42	30.68	38.90	9.51
2010008-17973	517001-223	110.15	0.745	0.773	0.734	0.747	0.209	0.344	0.334	0.279	0.495	0.406	0.367	0.329	28.70	26.07	45.23	28.24	29.86	41.90	28.35	28.91	42.74	8.07
2010008-17983	517001-213	119.77	0.767	0.791	0.751	0.753	0.215	0.363	0.355	0.304	0.511	0.425	0.381	0.333	27.45	23.76	48.79	27.54	27.40	45.06	27.52	26.55	45.94	6.25
2010008-17992	517001-204	128.22	0.483	0.518	0.493	0.453	0.154	0.224	0.226	0.196	0.487	0.456	0.407	0.364	27.91	26.49	45.60	26.35	28.76	44.89	27.13	27.62	45.25	6.75
2010008-18002	517001-194	139.26	0.498	0.567	0.480	0.441	0.183	0.272	0.240	0.236	0.493	0.516	0.418	0.366	24.50	14.14	61.36	24.47	18.63	56.90	24.48	16.38	59.14	4.78
2010008-18012	517001-184	148.46	0.537	0.540	0.480	0.509	0.181	0.254	0.225	0.237	0.506	0.469	0.436	0.382	22.29	18.11	59.60	25.27	20.82	53.91	23.80	19.48	56.72	4.90
2010008-18023	517001-173	158.77	0.744	0.755	0.729	0.725	0.231	0.365	0.341	0.313	0.516	0.462	0.418	0.389	25.21	23.42	51.38	25.85	25.48	48.68	25.68	24.94	49.38	6.77
2010008-18032	517001-164	167.24	0.734	0.744	0.723	0.735	0.231	0.360	0.323	0.300	0.521	0.462	0.437	0.378	25.88	21.19	52.93	26.33	22.66	51.01	26.21	22.26	51.53	5.90
2010008-18042	517001-154	176.33	0.700	0.705	0.690	0.682	0.212	0.336	0.319	0.300	0.531	0.465	0.432	0.388	28.76	24.26	46.98	29.19	25.24	45.57	29.06	24.94	45.99	6.75
2010008-18054	517001-142	187.85	0.715	0.732	0.723	0.718	0.235	0.352	0.332	0.296	0.534	0.480	0.445	0.415	30.19	24.90	44.91	29.07	26.11	44.83	29.38	25.77	44.85	8.74
2010008-18064	517001-132	197.24	0.693	0.712	0.696	0.689	0.264	0.374	0.342	0.326	0.539	0.486	0.454	0.432	28.68	25.82	45.50	27.75	27.43	44.82	28.03	26.94	45.02	7.41
2010008-18075	517001-121	207.21	0.717	0.734	0.726	0.715	0.351	0.453	0.412	0.415	0.553	0.511	0.487	0.460	28.53	25.85	45.62	27.37	26.99	45.65	27.69	26.67	45.64	7.14
2010008-18086	517001-110	216.55	0.785	0.781	0.767	0.782	0.295	0.417	0.377	0.340	0.563	0.492	0.485	0.418	23.22	22.71	54.07	24.66	23.55	51.79	24.34	23.36	52.30	5.06
2010008-18094	517001-102	224.44	0.723	0.730	0.722	0.731	0.263	0.365	0.351	0.327	0.548	0.493	0.487	0.438	28.17	25.07	46.76	27.99	25.79	46.22	28.04	25.59	46.37	6.69
2010008-18109	517001-091	234.66	0.664	0.672	0.678	0.655	0.321	0.391	0.368	0.344	0.564	0.521	0.493	0.462	26.41	25.67	47.92	25.39	25.55	49.06	25.72	25.59	48.69	6.87

Table 3

			Hopanes, relative abundance, 17α,21β(H)-HOPANE = 1																				Hopane ratios					
Lab no.	Sample no.	Depth Bottom	C27 27Ts	C27 27Tm	C28 BNH	C29 29αβ	C29 29Ts	C30 30E	C30 30D	C30 30αβ	C30 30Ts	C30 30βα	C31 αβ-22S	C31 αβ-22R	C32 αβ-22S	C32 αβ-22R	C33 αβ-22S	C33 αβ-22R	C34 αβ-22S	C34 αβ-22R	C35 αβ-22S	C35 αβ-22R	Ts/(Ts + Tm)	29Ts/(H29 + 29Ts)	C32 (S/S+R)	C31-35 HOEP	C35 HHI	C33,34 IHR
2010008-17097	517001-005	25.00	0.140	0.494	0.030	0.645	0.187	0.089	0.085	1.000	0.056	0.178	0.463	0.325	0.151	0.119	0.112	0.091	0.056	0.043	0.040	0.030	0.22	0.22	0.56	1.41	0.049	0.109
2010008-17886	517001-310	28.89	0.133	0.390	0.082	0.879	0.194	0.130	0.103	1.000	0.067	0.186	0.428	0.294	0.165	0.129	0.125	0.099	0.072	0.057	0.053	0.040	0.25	0.18	0.56	1.28	0.064	0.094
2010008-17895	517001-301	37.88	0.159	0.467	0.022	0.623	0.198	0.179	0.102	1.000	0.067	0.158	0.452	0.308	0.149	0.116	0.118	0.094	0.064	0.049	0.037	0.029	0.25	0.24	0.56	1.39	0.047	0.102
2010008-17905	517001-291	47.06	0.140	0.492	0.020	0.724	0.171	0.166	0.107	1.000	0.062	0.145	0.471	0.322	0.150	0.117	0.119	0.092	0.067	0.054	0.033	0.027	0.22	0.19	0.56	1.37	0.042	0.103
2010008-17916	517001-280	56.88	0.159	0.350	0.049	0.633	0.188	0.146	0.108	1.000	0.078	0.128	0.394	0.267	0.154	0.121	0.115	0.089	0.072	0.055	0.051	0.040	0.31	0.23	0.56	1.23	0.067	0.091
2010008-17924	517001-272	64.47	0.184	0.382	0.084	0.637	0.216	0.071	0.064	1.000	0.067	0.122	0.403	0.275	0.157	0.115	0.115	0.080	0.070	0.048	0.032	0.024	0.33	0.25	0.58	1.22	0.042	0.095
2010008-17935	517001-261	74.92	0.196	0.371	0.410	0.718	0.240	0.117	0.086	1.000	0.076	0.104	0.314	0.213	0.125	0.097	0.098	0.074	0.056	0.040	0.031	0.023	0.35	0.25	0.56	1.27	0.051	0.098
2010008-17944	517001-252	83.57	0.168	0.332	0.241	0.592	0.206	0.118	0.093	1.000	0.080	0.113	0.371	0.249	0.169	0.126	0.118	0.086	0.082	0.059	0.065	0.048	0.34	0.26	0.57	1.13	0.082	0.082
2010008-17953	517001-243	92.23	0.177	0.312	0.032	0.604	0.212	0.107	0.090	1.000	0.077	0.108	0.389	0.267	0.165	0.121	0.124	0.091	0.082	0.062	0.058	0.042	0.36	0.26	0.58	1.19	0.072	0.082
2010008-17962	517001-234	100.73	0.145	0.308	0.014	0.546	0.160	0.083	0.066	1.000	0.062	0.115	0.404	0.263	0.182	0.130	0.126	0.088	0.085	0.060	0.054	0.038	0.32	0.23	0.58	1.12	0.064	0.087
2010008-17973	517001-223	110.15	0.117	0.435	0.763	0.838	0.158	0.129	0.094	1.000	0.058	0.140	0.381	0.266	0.162	0.124	0.104	0.077	0.065	0.043	0.043	0.028	0.21	0.16	0.57	1.15	0.055	0.095
2010008-17983	517001-213	119.77	0.094	0.493	2.128	0.769	0.123	0.122	0.095	1.000	0.051	0.156	0.458	0.304	0.193	0.140	0.122	0.085	0.076	0.053	0.038	0.025	0.16	0.14	0.58	1.12	0.042	0.100
2010008-17992	517001-204	128.22	0.087	0.495	1.903	0.649	0.119	0.114	0.095	1.000	0.051	0.157	0.453	0.308	0.197	0.139	0.119	0.082	0.074	0.048	0.038	0.025	0.15	0.15	0.59	1.11	0.042	0.104
2010008-18002	517001-194	139.26	0.098	0.466	4.718	0.609	0.094	0.140	0.102	1.000	0.056	0.131	0.344	0.235	0.164	0.119	0.124	0.086	0.069	0.049	0.041	0.029	0.17	0.13	0.58	1.19	0.055	0.084
2010008-18012	517001-184	148.46	0.102	0.545	2.691	0.642	0.104	0.140	0.106	1.000	0.054	0.140	0.425	0.287	0.190	0.138	0.137	0.096	0.072	0.049	0.039	0.027	0.16	0.14	0.58	1.21	0.045	0.093
2010008-18023	517001-173	158.77	0.101	0.427	2.409	0.667	0.112	0.147	0.109	1.000	0.061	0.125	0.381	0.258	0.180	0.124	0.113	0.079	0.064	0.044	0.039	0.024	0.19	0.14	0.59	1.12	0.049	0.097
2010008-18032	517001-164	167.24	0.115	0.477	1.365	0.691	0.133	0.109	0.082	1.000	0.055	0.126	0.420	0.288	0.200	0.137	0.137	0.091	0.070	0.045	0.038	0.025	0.19	0.16	0.59	1.18	0.043	0.102
2010008-18042	517001-154	176.33	0.113	0.383	0.913	0.576	0.125	0.122	0.096	1.000	0.057	0.126	0.370	0.250	0.180	0.124	0.128	0.087	0.062	0.041	0.037	0.024	0.23	0.18	0.59	1.21	0.046	0.085
2010008-18054	517001-142	187.85	0.114	0.426	0.391	0.802	0.131	0.089	0.078	1.000	0.051	0.125	0.440	0.289	0.182	0.124	0.105	0.070	0.055	0.035	0.023	0.015	0.21	0.14	0.59	1.15	0.028	0.106
2010008-18064	517001-132	197.24	0.124	0.365	0.866	0.724	0.127	0.109	0.091	1.000	0.056	0.116	0.411	0.278	0.185	0.125	0.118	0.078	0.054	0.035	0.028	0.018	0.25	0.15	0.60	1.20	0.035	0.103
2010008-18075	517001-121	207.21	0.135	0.446	1.149	0.682	0.119	0.101	0.092	1.000	0.049	0.112	0.430	0.288	0.185	0.122	0.106	0.067	0.053	0.033	0.031	0.020	0.23	0.15	0.60	1.15	0.038	0.103
2010008-18086	517001-110	216.55	0.072	0.563	3.263	1.354	0.079	0.084	0.084	1.000	0.039	0.140	0.500	0.334	0.204	0.142	0.109	0.072	0.056	0.038	0.033	0.019	0.11	0.05	0.59	1.12	0.034	0.105
2010008-18094	517001-102	224.44	0.100	0.435	0.406	0.725	0.094	0.098	0.087	1.000	0.052	0.119	0.430	0.285	0.179	0.121	0.108	0.072	0.058	0.035	0.036	0.021	0.19	0.11	0.60	1.18	0.042	0.097
2010008-18109	517001-091	234.66	0.089	0.472	3.563	0.730	0.103	0.101	0.091	1.000	0.052	0.119	0.453	0.308	0.209	0.141	0.125	0.083	0.067	0.043	0.041	0.024	0.16	0.12	0.60	1.13	0.044	0.099

Table 4 28-Norhopanes (*m/z* 355) and aromatic compounds (*m/z* 178, 184, 192, 198 & 234)

Lab no.	Sample no.	Depth Bottom	% C_{28} (BNH) *m/z* 355	% C_{29} *m/z* 355	% C_{30} *m/z* 355	% C_{31} *m/z* 355	% C_{32} *m/z* 355	DBT *m/z* 184 / P *m/z* 178	MDBT *m/z* 198 / MP *m/z* 192	Retene m/z 234 / MP *m/z* 192	Retene m/z 234 / MDBT *m/z* 198
2010008-17097	17001-005	25.00	n.a.	n.a.	n.a.	n.a.	n.a.	0,24	0.26	0.30	1.16
2010008-17886	517001-310	28.89	n.a.	n.a.	n.a.	n.a.	n.a.	0,28	0.28	0.68	2.43
2010008-17895	517001-301	37.88	n.a.	n.a.	n.a.	n.a.	n.a.	0,31	0.28	0.69	2.41
2010008-17905	517001-291	47.06	n.a.	n.a.	n.a.	n.a.	n.a.	0,24	0.21	0.80	3.84
2010008-17916	517001-280	56.88	11.5	31.8	38.2	9.6	8.9	0,21	0.20	0.71	3.52
2010008-17924	517001-272	64.47	7.8	20.3	42.6	12.7	16.6	0,19	0.21	0.68	3.31
2010008-17935	517001-261	74.92	33.5	11.2	33.4	5.5	16.3	0,17	0.16	0.78	4.79
2010008-17944	517001-252	83.57	17.8	21.4	38.7	10.4	11.7	0,21	0.21	0.65	3.09
2010008-17953	517001-243	92.23	7.7	25.5	42.1	10.7	13.9	0,22	0.22	0.47	2.17
2010008-17962	517001-234	100.73	8.3	23.7	45.1	11.8	11.1	0,27	0.24	0.56	2.29
2010008-17973	517001-223	110.15	50.9	14.9	24.8	4.5	4.9	0,22	0.19	1.05	5.42
2010008-17983	517001-213	119.77	78.2	7.2	10.0	2.5	2.1	0,17	0.15	0.83	5.39
2010008-17992	517001-204	128.22	63.8	7.0	21.1	4.0	4.0	0,14	0.12	1.28	10.73
2010008-18002	517001-194	139.26	83.8	6.3	5.3	3.2	1.3	0,33	0.27	0.93	3.44
2010008-18012	517001-184	148.46	65.9	6.9	17.3	5.3	4.5	0,25	0.19	0.95	4.93
2010008-18023	517001-173	158.77	65.9	11.0	15.7	3.6	3.8	0,20	0.16	1.13	7.21
2010008-18032	517001-164	167.24	50.0	13.5	24.2	5.4	6.9	0,21	0.16	0.88	5.35
2010008-18042	517001-154	176.33	45.4	14.0	26.2	6.4	8.1	0,23	0.18	0.63	3.49
2010008-18054	517001-142	187.85	48.4	17.1	24.9	4.7	5.0	0,17	0.14	0.76	5.58
2010008-18064	517001-132	197.24	64.9	13.0	14.5	4.0	3.5	0,19	0.15	0.60	3.93
2010008-18075	517001-121	207.21	36.3	15.4	37.5	4.5	6.2	0,13	0.11	1.45	12.80
2010008-18086	517001-110	216.55	68.9	10.0	14.6	4.7	1.9	0,13	0.10	1.41	13.96
2010008-18094	517001-102	224.44	21.2	20.3	45.1	5.1	8.3	0,13	0.11	1.51	13.55
2010008-18109	517001-091	234.66	78.5	7.1	9.0	3.3	2.1	0,12	0.10	1.34	12.94

8.3 Stable Carbon isotope analyses

Stable carbon isotope analyses of saturated, aromatic, polar and asphaltene fractions of 20 solvent extracts from the Rødryggen corewell were carried out by APT, Kjeller, Norway. Results are reported in Table 8.3.1.

Galimov-type plots of data from all samples are shown in Fig. 8.3.1. All samples show very similar trends with respect to the relative δ^{13}C-values of saturated, aromatic, polar, and asphaltene fractions. With few and very marginal exceptions the relative δ^{13}C values show:

$\boldsymbol{\delta^{13}C_{(saturates)} \leq \delta^{13}C_{(aromatics)} \leq \delta^{13}C_{(polars)} \leq \delta^{13}C_{(asphalthenes)}}$

Variation among neighbouring samples is very limited, but over a transition zone the mid-point of which lies approximately at a depth of 125 metres, a notable shift in overall isotopic composition is observed. Thus, deeper samples seem generally less depleted in ^{13}C (i.e. less negative δ^{13}C values), which is manifest in an overall shift in isotopic composition of approximately 2 permil. This shift affects all analysed fractions, whereas the internal isotopic relationships among the analysed fractions remain constant. This phenomenon may be attributed to an overall more terrestrial nature of the organic matter in the lower portion of the drilled succession (Bernbjerg Formation) compared to the uppermost portion (Lindemans Bugt Formation), and the shift corresponds well to similar indications provided by other datasets such as Rock-Eval/TOC screening and biomarker analyses (See sections 8.1 and 8.2).

A crossplot of $\delta^{13}C_{(saturates)}$ versus $\delta^{13}C_{(aromatics)}$ is shown in Fig. 8.3.2. Extract samples generally plot very close to the broken line that indicates the empirically defined (by Sofer 1984) best separation between "waxy" (*i.e.* terrestrially dominated, above line) and "non-waxy" (*i.e.* marine, below line) oils or extracts.

A crossplot of the "canonical variable", as defined by Sofer (1984) versus pristane/phytane ratio for solvent extracts from the Rødryggen corewell is shown in Fig. 8.3.3. The broken line indicates the empirically defined (by Sofer 1984) best separation between "waxy" (*i.e.* "terrestrial", above line) and non-waxy (*i.e.* marine, below line) oils/extracts. Blue symbols indicate samples collected from the Lindemans Bugt Formation, whereas red symbols indicate samples collected from the Bernbjerg Formation. A tentative separation is noted, however primarily defined by the pristane/phytane ratio rather than by the canonical variable.

Plotting the isotopic composition of the total extracts (calculated from the isotopic compositions of the individual extract fractions and the proportions of the same fractions in the total extract, since the total extract composition was not measured) versus the pristane/phytane ratio provides a very clear separation between the upper “marine-dominated” and the lower more “terrestrial/deltaic” portions of the succesion emerges (Fig. 8.3.4), after Chung et al., 1992).

In summary, stable Carbon isotopic data show little sample-to-sample variation, but consistently indicate that the succession is generally dominated by marine organic matter, however with a higher proportion of terrestrial organic matter in the lower part of the succession (*i.e.* deeper than approximately 125 metres). This corresponds well to indication provided by other types of data, among which are Rock-Eval /TOC screening analyses and biological marker analyses.

8.3.1 References:

Chung, H. M., Rooney, M. A., Toon, M. B. & Claypool, G. E., 1992: Carbon isotope composition of marine crude oils. AAPG Bulletin, **76**, 1000–1007

Galimov, E. M. & Ivlev, A. A.1973: Thermodynamic isotope effects in organic compounds. I. Carbon isotope effects in straight-chain alkanes. Russian Journal of Physics, **47**, 1564–1566

Japsen, P. Bonow, J. & Green, P. F. 2009: Uplift history. Special study of the East and Northeast Greenland GIS project. Burial, uplift and exhumation history of East Greenland (70° to 75° N) based on AFTA data, the geological recod and preliminary landscape analysis. GEUS rapport 2009/53

Sofer, Z. 1984: Stable carbon isotope compositions of crude oils; application to source depositional environments and petroleum alteration. AAPG Bulletin, **68**, 31–49

Sample	Depth metres	$\delta^{13}C$ Saturates	$\delta^{13}C$ Aromatics	$\delta^{13}C$ NSO	$\delta^{13}C$ Asphaltenes	CV	$\delta^{13}C$ (calculated) Total extract
517001-310	28,89	-31,6	-30,4	-29	-27,8	0,8	-29,1
517001-301	37,88	-31,4	-30	-29,1	-28	1,2	-29,0
517001-291	47,06	-31,7	-30,3	-29,2	-28,1	1,3	-29,2
517001-280	56,88	-31,9	-30,3	-29,2	-27,8	1,8	-29,2
517001-261	74,92	-32,2	-30,9	-29,9	-28,7	1,2	-29,9
517001-252	83,57	-31,9	-30,7	-29,5	-28,4	0,9	-29,7
517001-243	92,23	-32,2	-30,8	-29,8	-28,7	1,4	-29,9
517001-234	100,73	-31,6	-30,2	-29,3	-28,1	1,3	-29,4
517001-223	110,15	-30,7	-29,4	-28,4	-27,1	0,8	-28,4
517001-213	119,77	-30,9	-29,2	-28,3	-27,1	1,7	-28,1
517001-202	128,22	-30,6	-29,1	-28,3	-27	1,2	-28,2
517001-194	139,26	-29,2	-27,9	-27,5	-26,4	0,3	-27,3
517001-184	148,46	-29,2	-27,8	-27,1	-26,4	0,5	-27,2
517001-173	158,77	-30,1	-28,4	-27,9	-26,7	1,5	-27,8
517001-164	167,24	-29,1	-27,9	-27,3	-26,6	0,0	-27,3
517001-142	187,85	-29,1	-28,4	-27,5	-26,6	-1,1	-27,3
517001-132	197,24	-29,8	-28,2	-27,6	-26,4	1,1	-27,4
517001-121	207,21	-28,9	-27,3	-27,4	-25,7	0,9	-26,7
517001-102	224,44	-29,3	-27,4	-27,4	-26,1	1,7	-27,0
517001-91	234,66	-28,7	-26,8	-27	-26	1,5	-26,6

Table 8.3.1, Stable Carbon isotope data on solvent extracts from the Rødryggen corewell. Canonical variable (CV) according to Sofer (1984). Total extract isotopic composition was calculated from the isotopic signatures of the individual extract fractions (asphaltenes, saturates, aromatics, NSO's) and the proportions of the same fractions in the total extract.

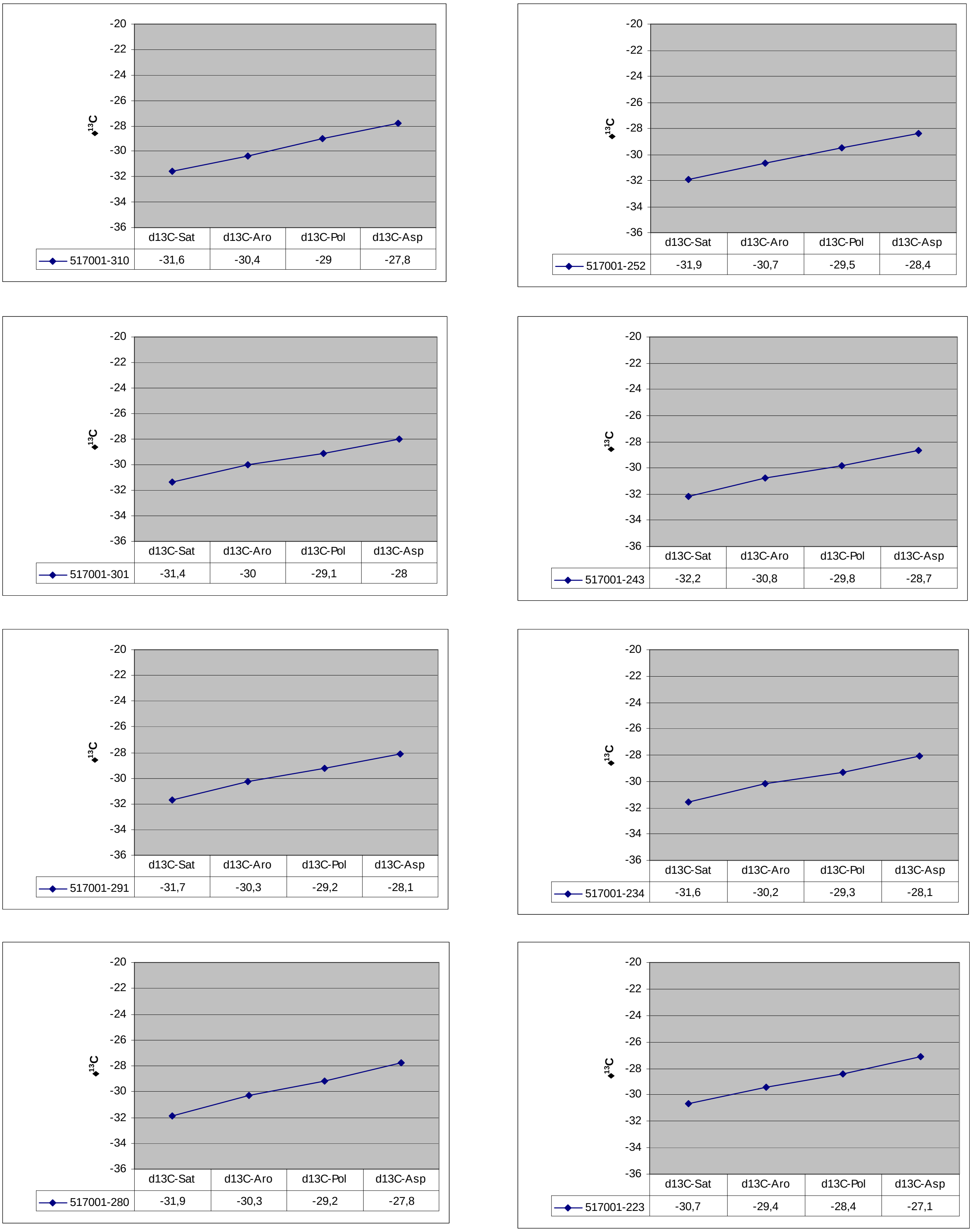

Figure 8.3.1 Galimov-type plots of stable carbon isotope data from the Rødryggen corewell. Horizontal axis: extract fraction, vertical axis $\delta^{13}C$. Sample identification: lower left corner of each plot. Plot modified from Galimov & Ivlev (1973).

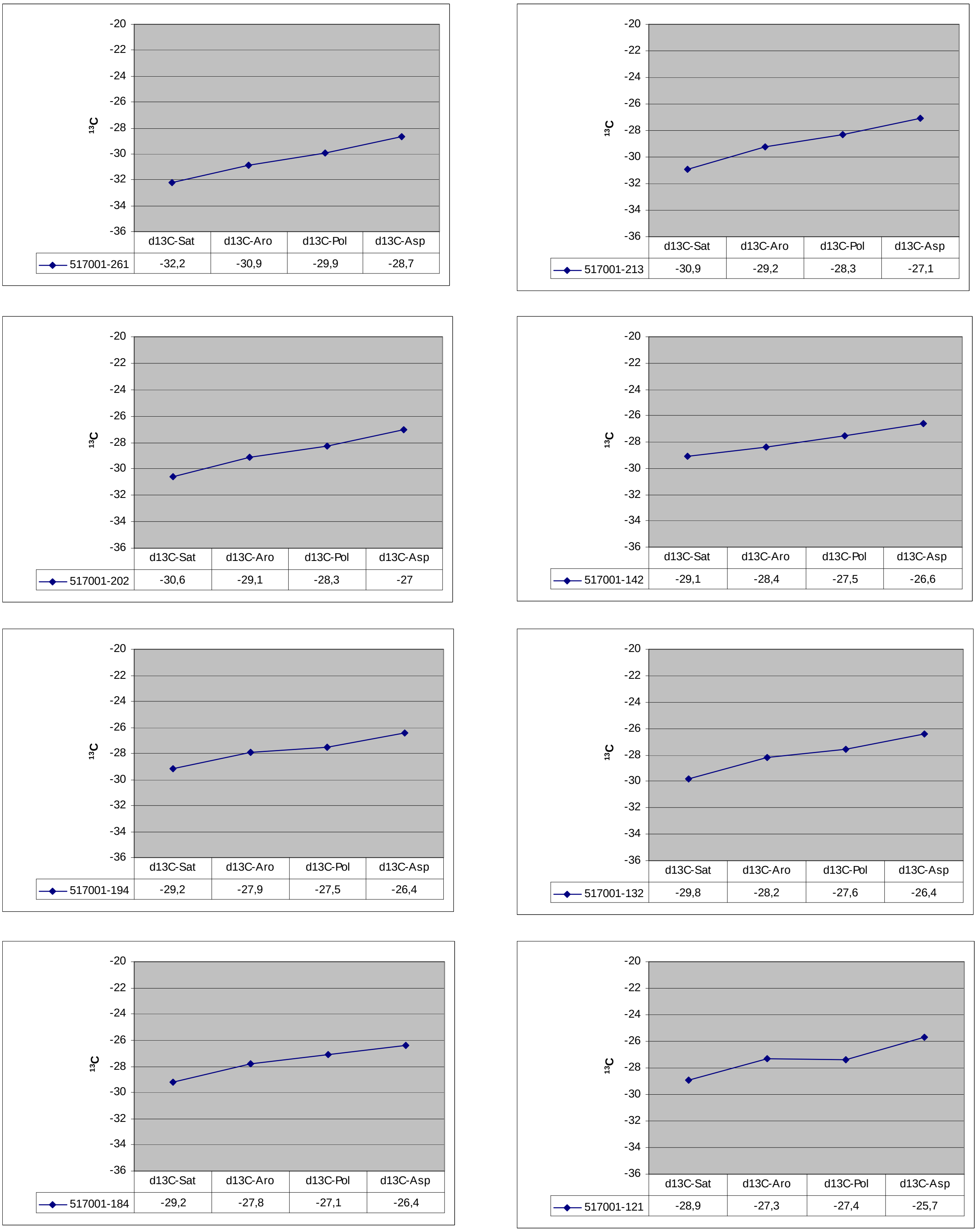

Figure 8.3.1, continued. Galimov-type plots of stable carbon isotope data from the Rødryggen corewell. Horizontal axis: extract fraction, vertical axis $\delta^{13}C$. Sample identification: lower left corner of each plot. Plot modified from Galimov & Ivlev (1973).

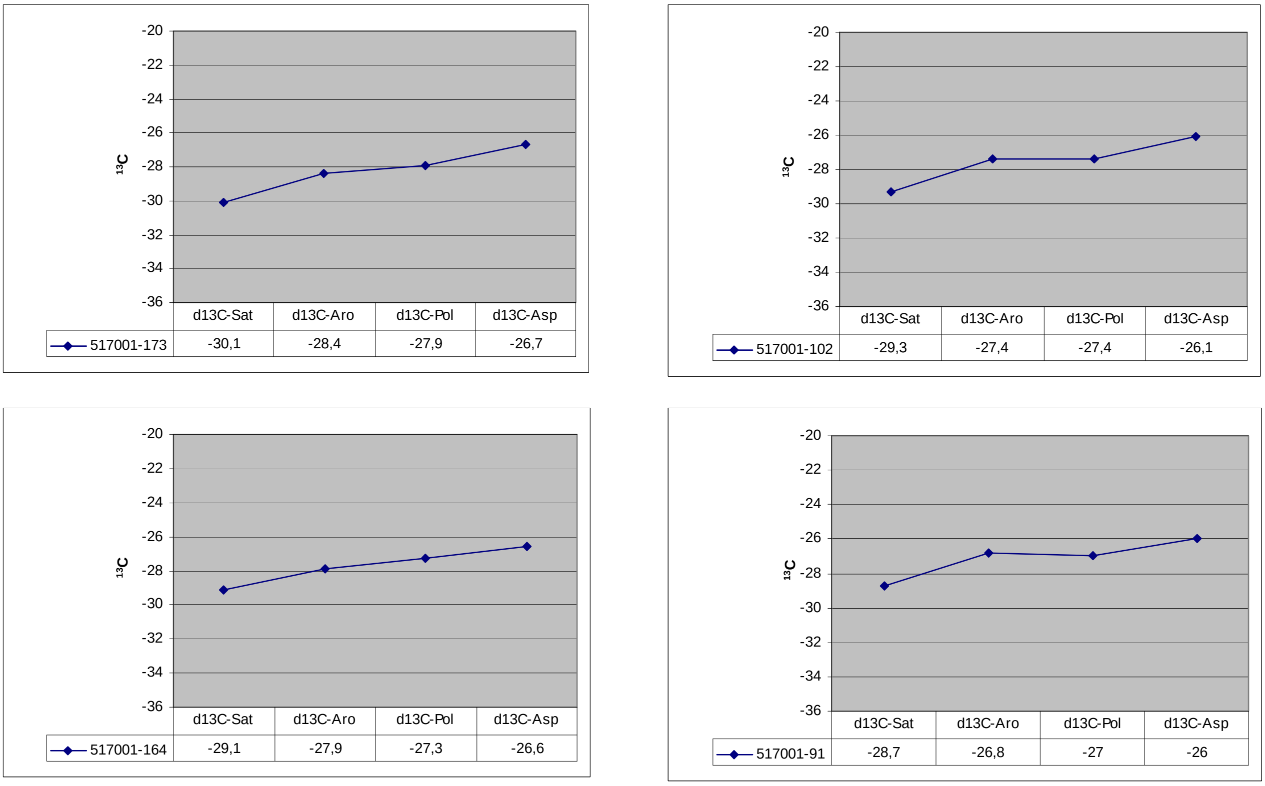

Figure 8.3.1., continued. Galimov-type plots of stable carbon isotope data from the Rødryggen corewell. Horizontal axis: extract fraction, vertical axis $\delta^{13}C$. Sample identification: lower left corner of each plot. Plot modified from Galimov & Ivlev (1973).

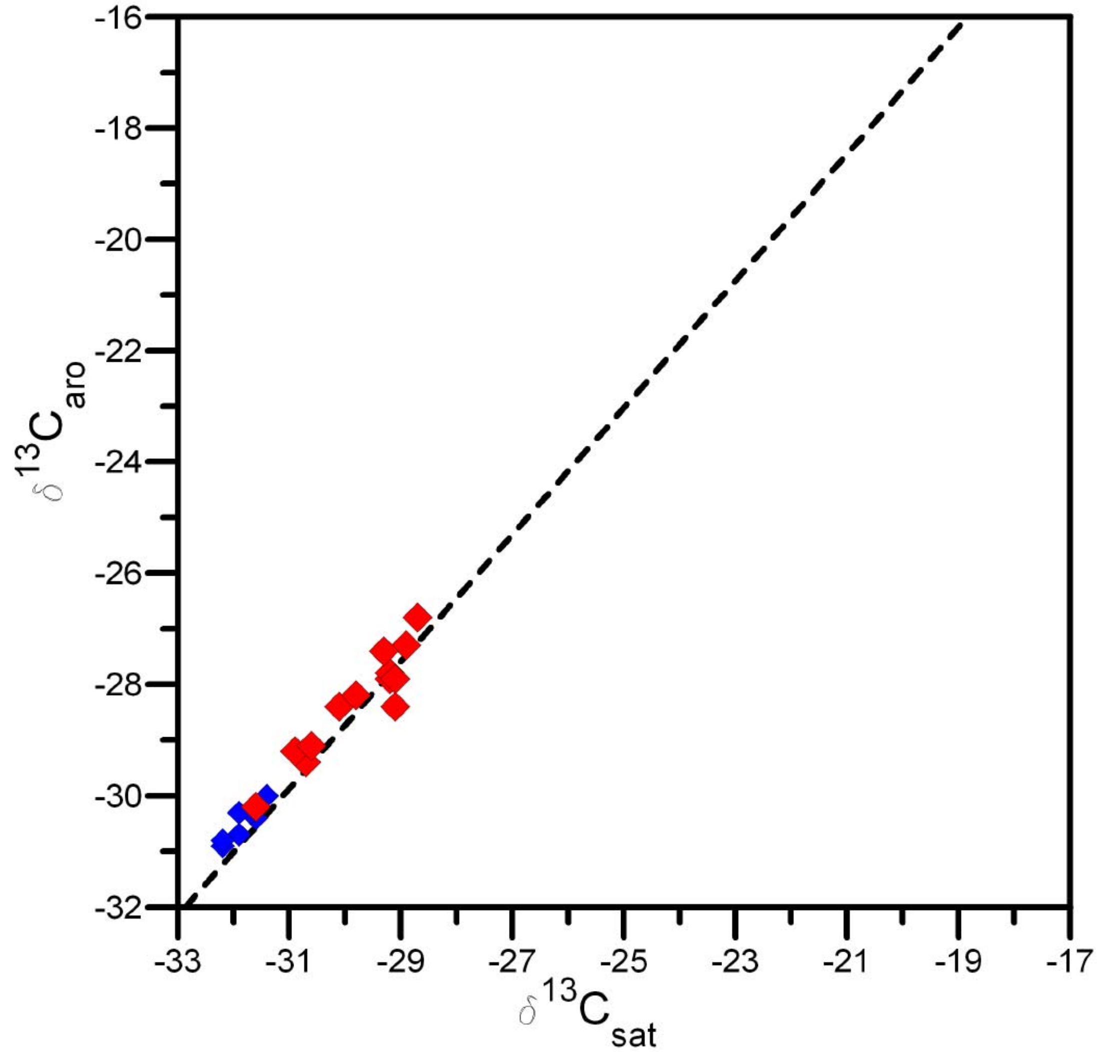

Figure 8.3.2. $\delta^{13}C_{(saturates)}$ *versus* $\delta^{13}C_{(aromatics)}$ for solvent extracts from the Rødryggen corewell. Broken line indicates the empirically defined best separation between "waxy" (above line) and non-waxy (below line) oils/extracts. From Sofer (1984). Red symbols–Bernbjerg Formation, Blue symbols–Lindemans Bugt Formation.

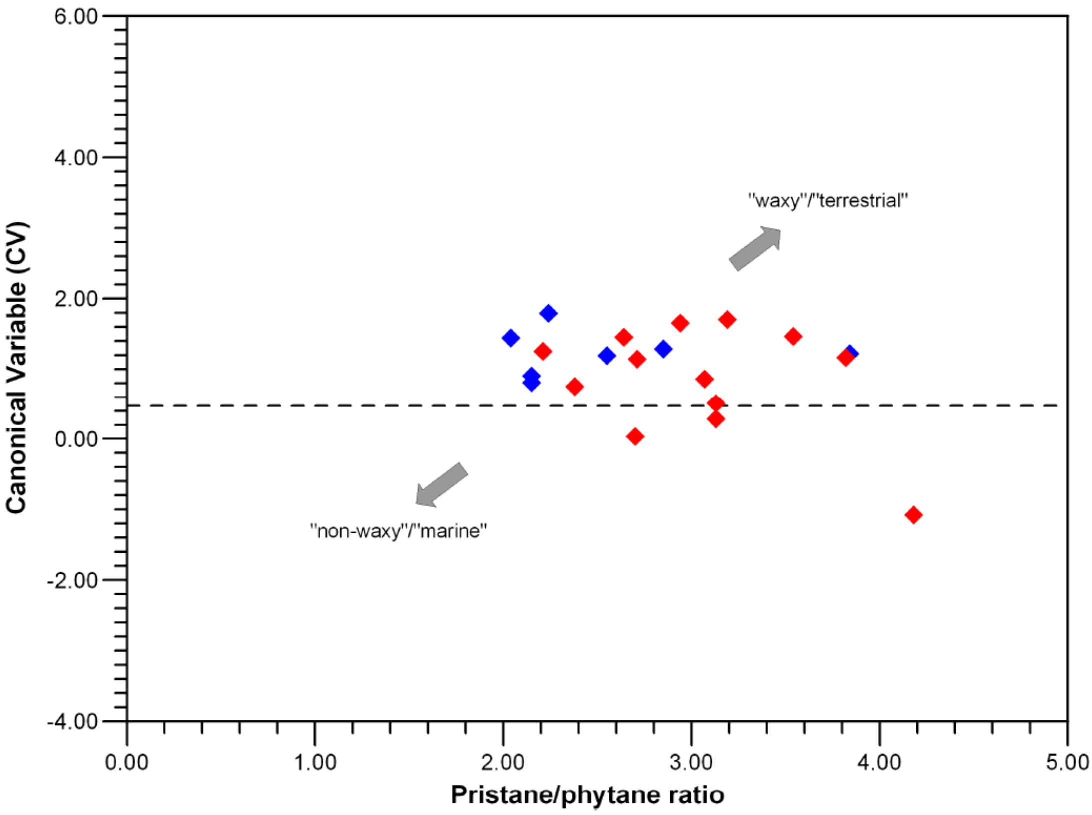

Figure 8.3.3. Canonical variable, as defined by Sofer (1984) *versus* pristane/phytane ratio for solvent extracts from the Rødryggen corewell. Blue symbols: samples shallower than 125 metres, red symbols: samples deeper than 125 metres. Broken line indicates the empirically defined best separation between "waxy" (above line) and non-waxy (below line) oils/extracts. Modified from Sofer (1984). Red symbols–Bernbjerg Formation, Blue symbols–Lindemans Bugt Formation.

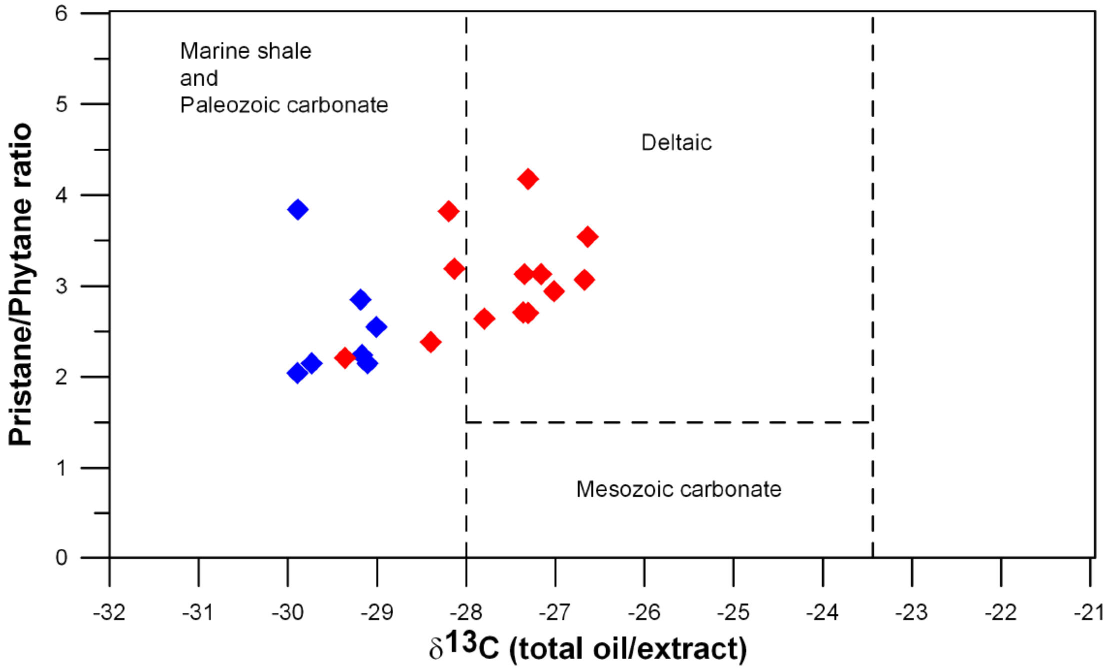

Figure 8.3.4. Carbon isotopic composition versus pristane/phytane ratio for extracts from the Rødryggen corewell. Note that the δ^{13}C values are calculated based on the isotopic signatures of individual solvent fractions (asphaltenes, saturates, aromatics and NSO's) and the proportions of the same fractions in the total extracts. Red symbols–Bernbjerg Formation, Blue symbols–Lindemans Bugt Formation. Note the very clear separation of the upper and lower parts of the drilled succession. Plot modified from Chung et al. (1992).

8.4 Headspace gas analysis

Samples for headspace gas analysis include 8 core-pieces evenly spaced throughout the drilled succession. Core pieces were placed in airtight containers at the wellsite immediately after retrieval of each core-section. Compositional and isotopic data on headspace gas from the containers were produced by APT, Kjeller, Norway (Appendix 10.5).

Data are listed in Tables 8.4.1 and 8.4.2.

The gas composition is dominated by Nitrogen that constitutes from app. 70 vol-% to more than 90 vol-% of the total headspace gas. Hydrocarbon gas (C1-C5) concentrations are variable, ranging from near-zero over the uppermost c. 100 m drilled section to values exceeding 8 vol-% in the deeper part (Fig. 8.4.1).

Except for the uppermost sample, which shows near-zero HC-gas concentration, the gas composition is very dry. The anomalous result obtained for the uppermost sample may be attributed to the low overall concentration of HC-gases combined with evaporative losses that affect methane to a larger extent than heavier HC-gases.

Due to low concentration of HC-gases in some samples the analytical dataset is not complete, and isotopic data are not available for samples from the upper part of the succession. Based on combined compositional and isotopic data (Fig. 8.4.2), the gases seem to have a mixed origin comprising both biogenic and thermogenic contributions. However, bearing in mind the fact that microbial oxydation of microbially generated methane through for instance sulphate reduction (which is conceivable due to weathering pyrite, which will generate sulphate ions) will lead to an apparent increasingly "thermogenic" signature of the remaining methane (Whiticar et al., 1999), the gases are probably predominantly microbial, although perhaps with a minor contribution of thermogenic methane in the deeper part of the well. The microbial nature of the methane is also evident form the Carbon versus Hydrogen isotopic crossplot (Fig. 8.4.3).

The stable isotopic composition of carbon dioxide leaps from values in the range from -11 to -18 in the upper half of the well section to strongly positive values of +6 to +15 in the deeper part (Fig. 8.4.4). The isotopic signature in the upper part of the well may represent a mixture of CO_2 from microbial oxydation of methane and atmospheric CO_2, whereas the very positive values in the deeper part are enigmatic, but could possibly represent CO_2 from groundwater bicarbonate. This would imply that the permafrost zone terminates at around 100 metres below the surface.

8.4.1 References

Bernard, B. B., Brooks, J. M. & Sackett, W. M. 1978: Light hydrocarbons in recent Texas continental slope sediments. Journal of Geophysical Research, **83**, 4053–4061

Schoell, M. 1983: Genetic classification of natural gases. AAPG bulletin, **67**, 2225–2238

Peters, K. E., Walters, C. C. and Moldowan, J. M., 2005: The Biomarker Guide, volumes 1+2, Cambridge University Press, 1155pp.

Whiticar, M. J. 1999: Carbon and hydrogen isotope systematics of bacterial formation and oxidation of methane. Chemical Geology, **161**, 291–314

Sample	Depth (m)	C1	C2	C3	iC4	nC4	iC5	nC5	C6+
517001-6	26,5	0,011	0,0009	0,0014	0,0048	0,0083	0,0077	0,0047	0,0088
517001-19	68,0	0,5			0,0018	0,002	0,0089	0,0026	0,011
517001-31	99,1	0,013							0,0023
517001-41	128,8	8,08	0,0014			0,0004	0,0038	0,0035	0,0051
517001-50	157,8	7,2	0,0036	0,022	0,015	0,022	0,01	0,0061	0,0071
517001-59	181,0	7,27	0,24	0,2	0,0092	0,039	0,0057	0,0057	0,0061
517001-65	203,5	4,17	0,0015	0,0086	0,0033	0,0072	0,0023	0,0019	0,0033
517001-74	231,3	11	0,03	0,099	0,0077	0,033	0,0049	0,0048	0,0053

Sample	Depth (m)	CO2	Sum C1-C5	Wetness	iC4/nC4	H2	O2/Ar	N2	ppm
517001-6	26,5	7,32	0,039	57,9	0,58	0,88	2,04	89,7	940615
517001-19	68,0	3,5	0,52	0,75	0,9	0,68	4,13	91,2	938772
517001-31	99,1	9,82	0,013	0		1,19	1,81	87,2	943192
517001-41	128,8	4,83	8,08	0,022		0,57	1,7	84,8	943404
517001-50	157,8	14,1	7,28	0,88	0,69	1,1	2,81	74,7	954454
517001-59	181,0	5,66	7,77	6,36	0,23	7,26	3,72	75,6	938037
517001-65	203,5	5,59	4,19	0,49	0,46	2,66	10,3	77,3	946863
517001-74	231,3	14,6	11,2	1,52	0,23	3,16	0,73	70,3	956642

Table 8.4.1 (parts A and B). Compositional data on headspace gases from 8 core pieces. Gas composition in vol-% of total.

Sam-ple	Depth (m)	C1 δ13C	C2 δ13C	C3 δ13C	i-C4 δ13C	n-C4 δ13C	i-C5 δ13C	n-C5 δ13C	CO2 δ13C	C1 δD
517001-6	26,5								-15,2	
517001-19	68,0	-54,7							-17,8	
517001-31	99,1								-16,5	
517001-41	128,8	-74,1							-11,1	-304,5
517001-50	157,8	-58,9							15	-278,1
517001-59	181,0	-61,8		-34,2					6,1	-245,4
517001-65	203,5	-62,1							11,7	-248,2
517001-74	231,3	-63,8							7,7	-249,2

Table 8.4.2. Headspace gas isotopic data

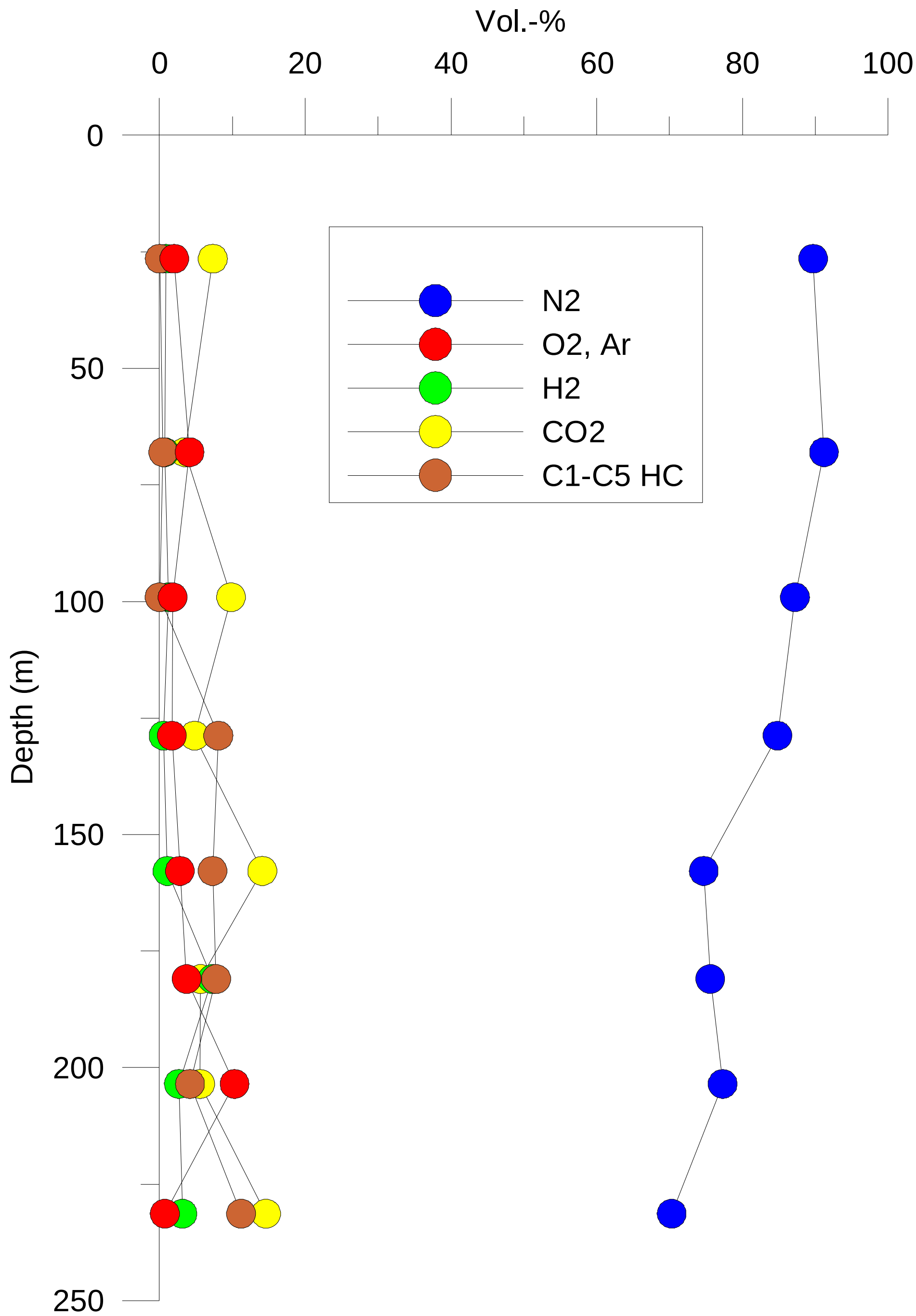

Figure 8.4.1. Total headspace gas composition. Note predominance of Nitrogen and near-zero concentration of HC-gases in the uppermost part of the section.

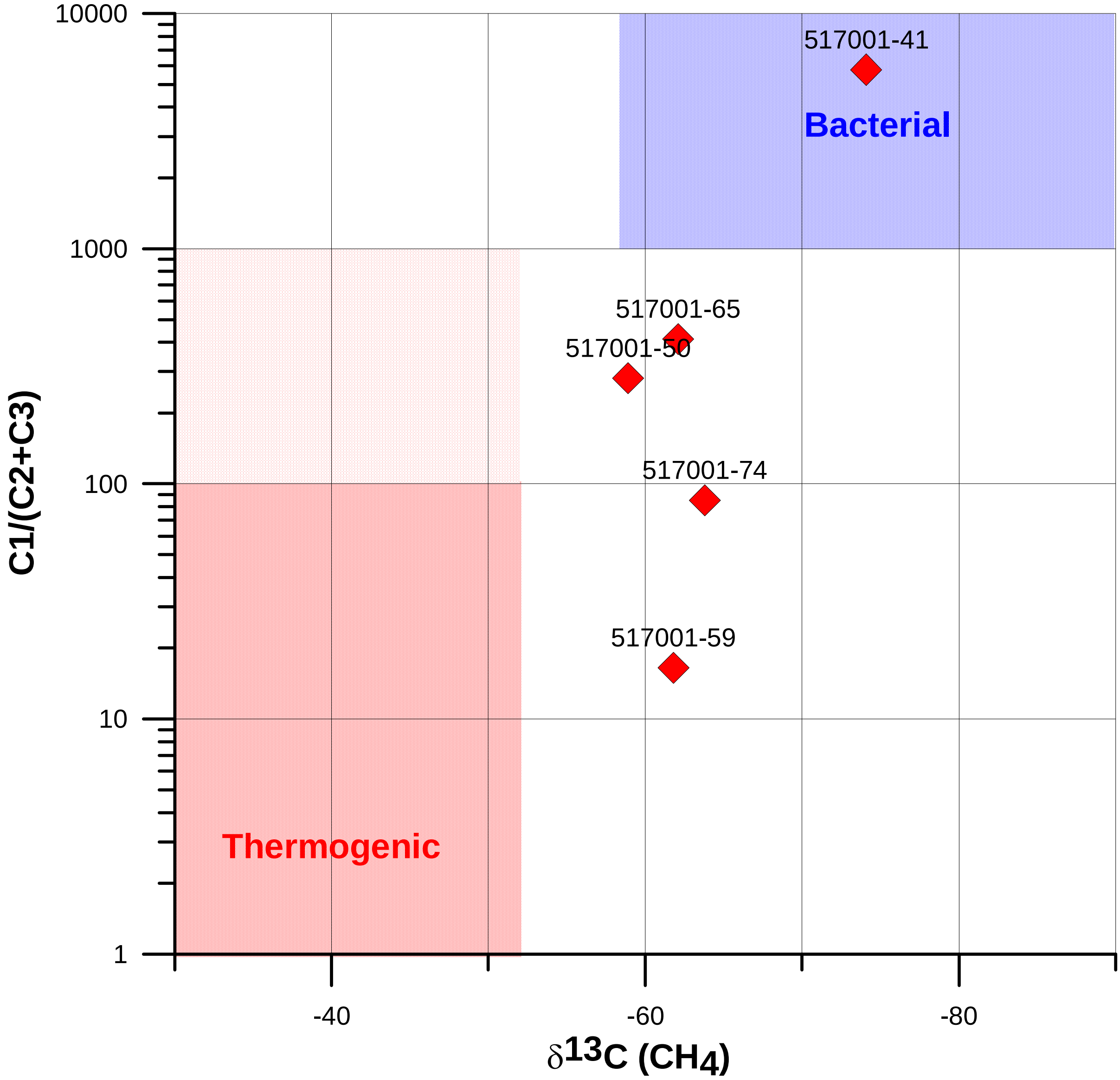

Figure 8.4.2. Bernard-plot. Only data from the deeper portion of the drilled succession are available. Based on combined isotopic and compositional data, the origin of the gas is probably mixed, comprising both biogenic as well as thermogenic contributions. Plot adapted from Bernard et al. (1978)

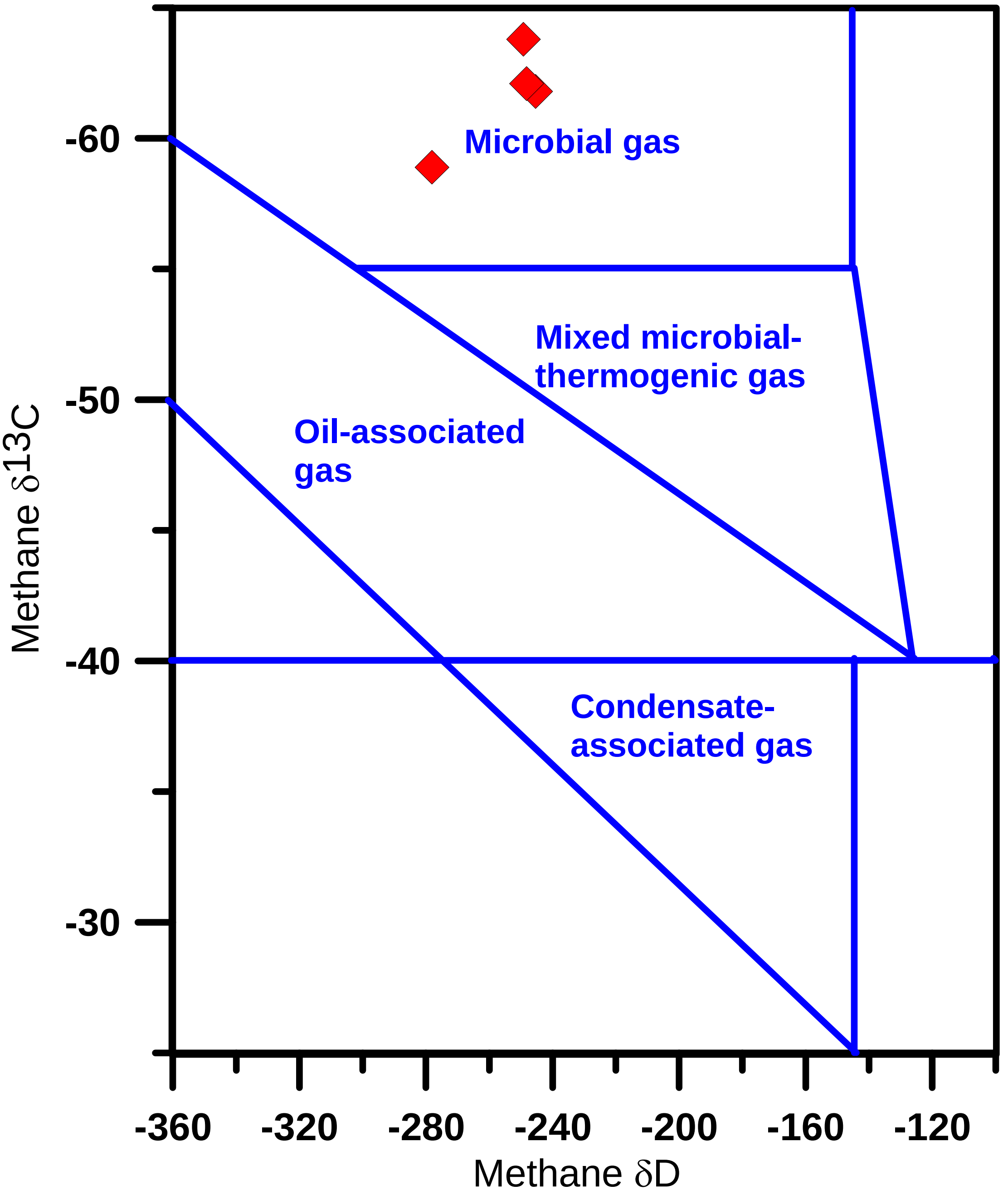

Figure 8.4.3. Methane Hydrogen versus Carbon isotopic composition. The predominantly microbial origin of the hydrocarbon gases found in the headspace of canned core samples from the Rødryggen corewell is evident. Plot adapted from Schoell (1983) and Peters et al. (2005).

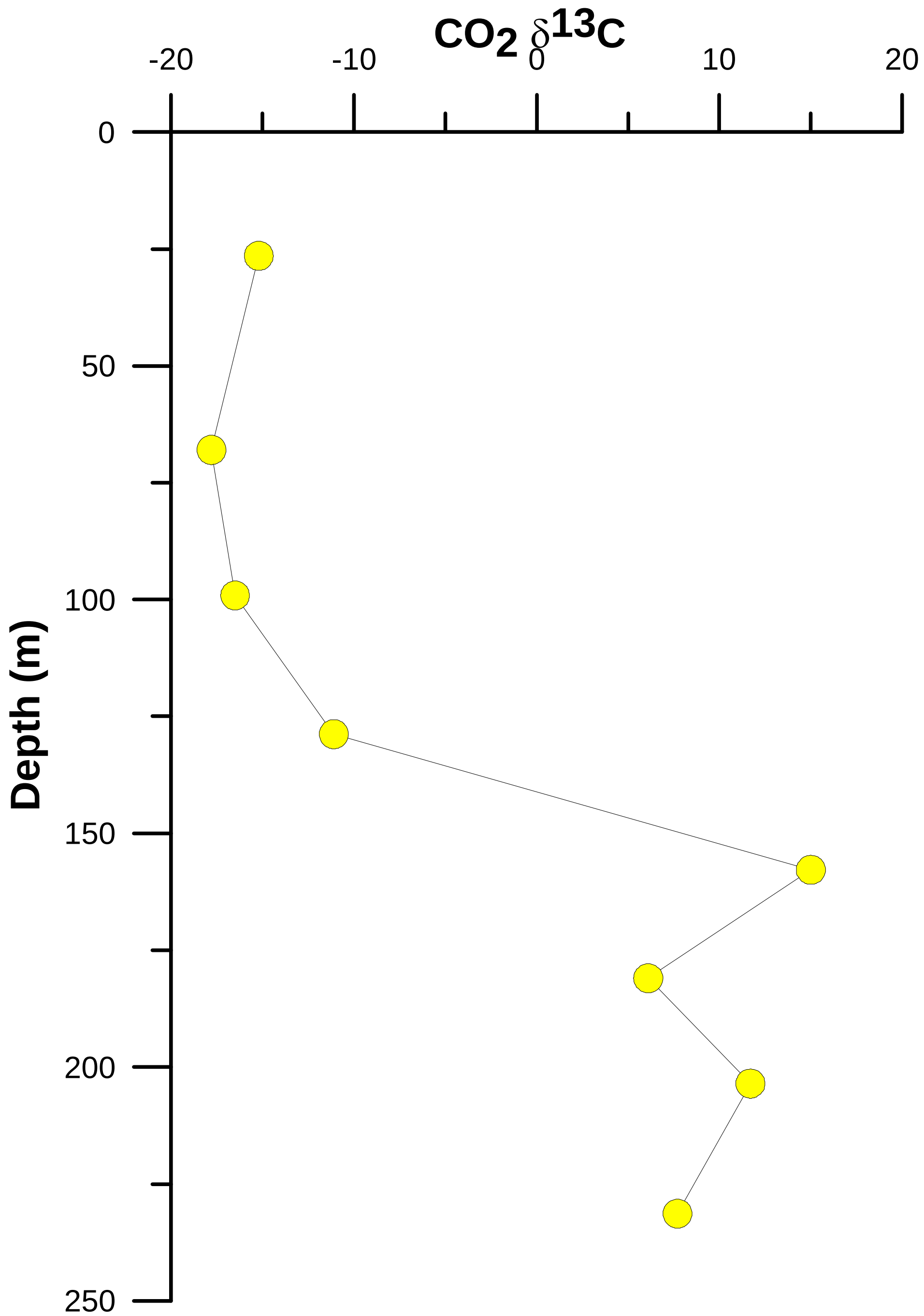

Figure 8.4.4. Stable carbon isotope composition of CO_2. Note marked shift in isotopic composition at approximately 125 metres.

9. Sandstone Provenance

The Rødryggen-1 core does not contain enough sandstone for provenance analysis. Outcrop samples collected in august 2009 from three locations in the relative vicinity of the drill site are therefore used for the provenance analysis (Fig. 9.1). The altitudes of the sampling locations 1, 2 and 3 are 188, 150 and 38 metres above sea level, respectively. The samples consist of silty sandstone to sandy siltstone with a light-grey to grey appearance. Samples 2 and 3 are well-cemented. Sample 3 is a thin bed in a mudstone succession. The sampling was done east of the Rødryggen-1 drill site (Fig. 9.1) and the layers dip towards west. Sample 1 is stratigraphically youngest and sample 3 is oldest, assuming a general dip of the Upper Jurassic succession of 5 degrees towards the west, which is supported by field observations. Samples 1 and 2 correlate approximately with depths of 190 and 200 metres in the Rødryggen-1 well. Sample 3 correlates with a stratigraphic level of 280 metres below the drilling site. The samples are thus all from the Bernbjerg Fm, as the succession below the base of the Rødryggen-1 well is expected to be part of the Bernbjerg Fm for at least the upper hundred metres.

9.1 Methods

9.1.1 Heavy mineral analysis

Heavy mineral concentrates were produced from the grain size interval 45-500 µm by crushing and sieving the samples. Heavy liquid separation was made by bromoform with a specific density of 2.82 g/cm2. The modal abundances of heavy minerals were determined at the laboratory at GEUS by Computer Controlled Scanning Electron Microscopy (CCSEM) on a Philips XL40SEM (Keulen et al., 2008), where about 900-1200 grains were analysed per sample. The method integrates Back-Scattered Electron (BSE) micrographs with Energy Dispersive X-ray spectrometry (EDX) to measure the element composition of each grain. The major element weight percentages (wt%) of the minerals were measured as oxides, along with the trace elements Cr, Ni, Cu, Y, Zr, Nb, Sn and Ce. The grain-size and grain-shape parameters were measured at the cut surface in the polished section.

9.1.2 Zircon age dating

Heavy mineral concentrates with discharge of grains below 45 µm were produced on a Wilfley water shaking table after crushing the samples to below 500 µm. About 100-150 zircon grains per sample were handpicked randomly. U-Pb ages were obtained by Laser Ablation Inductively Coupled Plasma Mass Spectroscopy (LA-ICP-MS) at the laboratory at GEUS (Frei and Gerdes, 2009). The method uses a focused laser to ablate minute quantities of a sample with an approximate spot diameter of 30 µm and ablation time of 30 seconds. An uncertainty on the 2σ level was used for the crystallization ages of zircon. 207Pb/206Pb ages were used for the ages above 600 Ma, and 206Pb/238U were used for those with a 207Pb/206Pb age below 600 Ma, as the 206Pb/238U ages are more accurate below this age. Kolmogorov-Smirnoff (K-S) tests have been made for the age probability distributions by extracting the p-values. This was done by calculating the distance between the curves to discover if significant differences exist. Uncertainty was included as the 2σ errors of the measured ages in the construction of the Cumulative Distribution Function (CDF).

9.2 Results and Discussion

9.2.1 Heavy mineral assemblage

Carbonate grains dominate the heavy mineral assemblage of provenance samples 1 and 2, and also constitute a large part of sample 3 (Fig. 9.2). The relative contents of Ca, Mg, Fe and Mn in the carbonate grains (Fig. 9.3) reveal that far most of the grains consist of ankerite, as seen by the high amounts of both Mg and Fe and the presence of Mn. Element scatter plots have been used to decipher that a few calcite grains are present and possibly some Fe-rich dolomite, but ankerite dominate the carbonate fraction. The cemented intervals of Bernbjerg Fm in the Rødryggen-1 core are heavily cemented with ankerite and dolomite (Fig. 5.2), so the similarity in mineralogy of samples 1 and 2 is in agreement with their stratigraphic correspondence to the core. Sample 3 reveals that the lower part of the Bernbjerg Fm also exhibits ankerite cementation, although in a lesser degree. The CCSEM method does not include detection of Ba, but a very high S content in many unclassified grains in sample 3 points to additional cementation by baryte, indicating that this interval constituted a transport route for the last pore fluids during burial (Chapter 5.2.3).

Only a small amount of pyrite is present in the heavy mineral assemblage according to the CCSEM results (Fig. 9.2). However, the actual pyrite content is much larger, as pyrite is only present as framboids in Bernbjerg Fm (Chapter 5.2.3), which are largely too small to be measured by CCSEM. Some Ti-minerals are present in all samples, but there are too few grains to give a reliable indication of the Ti-mineral maturity. Few garnets are present in the samples (Fig. 9.2), and the composition is typical crustal with domination of almandine (Fig. 9.5). The zircon content is also low (Fig. 9.2), but large enough for zircon age dating (Fig. 9.7). The sediments have not been entirely split in to single grains because of their well-cemented nature, so the measured content of amphiboles and pyroxenes has been subtracted from the results, because the intermediary composition between ankerite and quartz has the same chemistry. However, no amphiboles or pyroxenes have been observed in thin section or SEM (Chapter 5). The relative contents of K, Na and Ca in the feldspars (Fig. 9.4) reveal that the proportion between K-feldspar and plagioclase is around equal, as it was also concluded from the XRD measurements (Fig. 5.2).

The large muscovite content of the provenance samples (Fig. 9.2) correlates with the rather high amount of muscovite found in the Rødryggen-1 core (Fig. 5.1 A). It points to short transport distance from source areas to place of deposition, as the mica would otherwise not have been preserved. This is in agreement with the proximity to the deltaic coast of Northeast Greenland to the west (Chapter 5.2.7) with high mountains consisting of readily erodible material in the immediate hinterland (Henriksen and Higgins, 2008).

9.2.2 Age distribution

About half of the zircon grains have discordant ages, but they are shown in the age distributions (Fig. 9.7) as they do not vary much from the concordant ages, and because they contain Cenozoic ages in all three age distributions, which are not detected by the concordant grains. The CDF sums the probabilities with increasing age, and the K-S test made on this basis is used to check if the age distributions came from the same parent population (Fig. 9.6). The p-values show that the three age distributions are not significantly different, and that age distributions 1 and 2 are the most likely to have the same parent population. Age distribution 3 contains a predominance of slightly older ages than the other populations, especially in the 2.0-1.1 Ga interval.

The broad age spectrum (Fig. 9.7) is in agreement with the stratigraphic correlation of the samples to Bernbjerg Fm, where the deltaic depositional setting could supply zircon grains from a wide range of sources (Chapter 5.2.7). The age distributions contain Archean peaks in the interval 2.89-2.55 Ga, and they are dominated by Paleoproterozoic ages with two large shared peaks at 1.98-1.97 Ga and 1.65-1.62 Ga. There are also many Mesoproterozoic ages present, whereas Neoproterozoic ages are scarce. A single shared Caledonian age peak is present around 411 Ma.

The basement geology of Northeastern Greenland has been mapped by the Geological Survey of Denmark and Greenland (e.g. Henriksen, 2003; Henriksen and Higgins, 2008). The most important and widespread rock units of the basement have been age dated radiometrically, so these ages can be compared with the age distributions of the three provenance samples. Minor age peaks that cannot be correlated to any source areas are thus likely to stem from the smaller undated units. These include among others a wide range of Neoproterozoic sediments, which are likely to have a broad age spectrum dominated by Mesoproterozoic ages (Watt et al., 2000).

Orthogneisses with Caledonian granulite facies overprint are present to the west of the study area on Payer Land in the Niggli Spids Thrust Sheet of the Caledonian Orogen (Elvevold et al. 2003). They have protolith ages that approximate 2.6 Ga, so they probably account for most of the Archean ages found in the samples. Relatively homogeneous orthogneisses with ages of 2.0-1.6 Ga are present in large amounts to the north, northwest, west and southwest of the study area in the Caledonian Orogen (Kalsbeek et al., 1993). These gneisses are very likely sources of the Paleoproterozoic ages of the samples, possibly together with foliated metagranitoids with ages of 2.0-1.75 Ga emplaced into homogeneous orthogneisses with ages of 2.0-1.8 Ga in the basement complexes of the Caledonian Orogen north of Bessel Fjord shear zone at ca. 76ºN. However, this would imply that the deltas had large upland areas that extended far to the north, or that south-directed coast-parallel sediment transport happened at the time of deposition.

The Neoproterozoic and Cenozoic zircon grains are possibly sourced by migmatitic-pelitic, semi-pelitic and psammitic metasediments derived by partial melding at ca. 930 or 420 Ma (Higgins et al., 2004). They are found in large amounts to the northwest, west and southwest of the study area in the Hagar Bjerg Thrust Sheet of the Caledonian Orogen and form part of the Krummedal Supracrustal Sequence. However, three granite populations have matching ages, but they are only locally important. Granites with ages of ca. 930 Ma are present to the west-southwest of the study area in the Hagar Bjerg Thrust Sheet. Granites with screens of metasediments with ages of ca. 930 or 430 Ma are present in the Niggli Spids Thrust Sheet to the west-southwest of the study area. Granites with screens of metasediments with ages of ca. 430 Ma are present in smaller areas of the Hagar Bjerg Thrust Sheet to the northwest, west and southwest of the study area.

9.3 Conclusions

The outcrop samples used for provenance analysis have likely source areas along the immediate paleo-coast of Northeast Greenland. The large amounts of ankerite and the broadness of the zircon age spectra are in accordance with the stratigraphic relationship between the provenance samples and the cemented intervals of Bernbjerg Fm in the Rødryggen-1 core and below. The preservation of a large amount of muscovite indicates short transport distance from the source areas to the place of deposition. All major peaks and populations in the zircon age distributions can be referred to source areas along the present coast of Northeast Greenland in the relative vicinity of the study area.

9.4 References

Elvevold, S., Thrane, K. and Gilotti, J.A., 2003: Metamorphic history of high-pressure granulites in Payer Land, Greenland Caledonides. Journal of Metamorphic Geology, **21**, 49–63.

Kalsbeek, F., Nutman, A.P. and Taylor, P.N., 1993: Palaeoproterozoic basement province in the Caledonian fold belt of North-East Greenland. Precambrian Research, **63**, 163–178.

Frei, D. and Gerdes, A., 2009: Precise and accurate in situ U-Pb dating of zircon with high sample throughput by automated LA-SF-ICP-MS. Chemical Geology, **261**, 261–270.

Henriksen, N., 2003: Caledonian orogen of East Greenland 70°N–82°N. Geological map at 1: 1.000.000. Geological Survey of Denmark and Greenland.

Henriksen, N. and Higgins, A.K., 2008: Geological research and mapping in the Caledonian orogen of East Greenland, 70°N–82°N. In: Higgins, A.K., Gilotti, J.A. and Smith, M.P. (eds): The Greenland Caledonides: Evolution of the Northeast Margin of Laurentia. Geological Society of America Memoirs 202, 1–27.

Higgins, A.K., Elvevold, S., Escher, J.C., Frederiksen, K.S., Gilotti, J.A., Henriksen, N., Jepsen, H.F., Jones, K.A., Kalsbeek, F., Kinny, P.D., Leslie, A.G., Smith, M.P., Thrane, K. and Watt, G.R., 2004: The foreland-propagating thrust architecture of the East Greenland Caledonides 72°–75°N. Journal of the Geological Society, **161**, 1009–1026.

Keulen, N., Frei, D., Bernstein, S., Hutchison, M.T., Knudsen, C. and Jensen, L., 2008: Fully automated analysis of grain chemistry, size and morphology by CCSEM: examples from cement production and diamond exploration. Geological Survey of Denmark and Greenland Bulletin, **15**, 93–96.

Watt, G.R., Kinny, P.D. and Friderichsen, J.D., 2000: U–Pb geochronology of Neoproterozoic and Caledonian tectonothermal events in the East Greenland Caledonides. Journal of the Geological Society, **157**, 1031–1048.

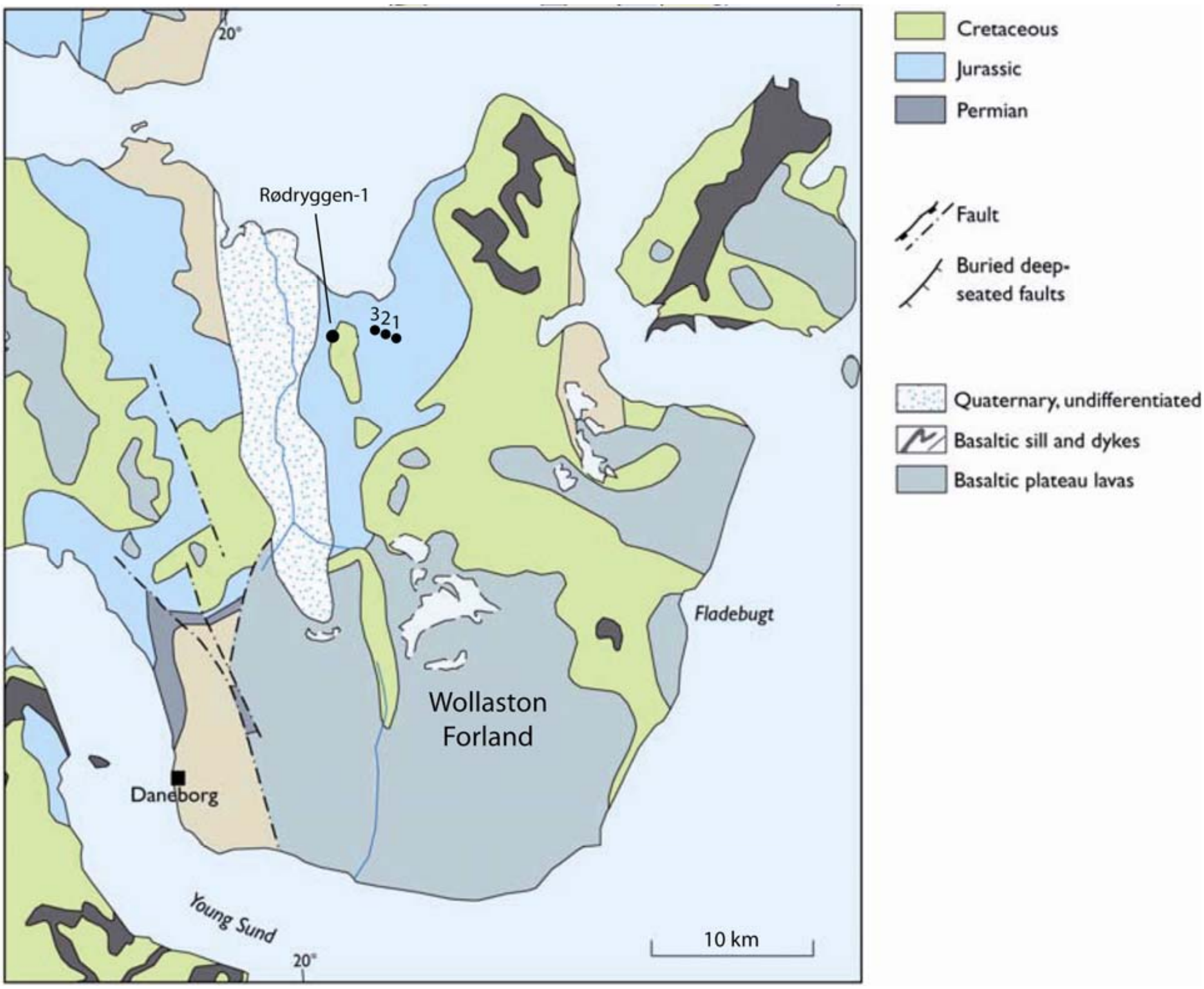

Figure 9.1. Location on Wollaston Forland of the outcrop samples used for provenance analysis. Regional dip suggests that the samples correlate with the Bjernberg Fm.

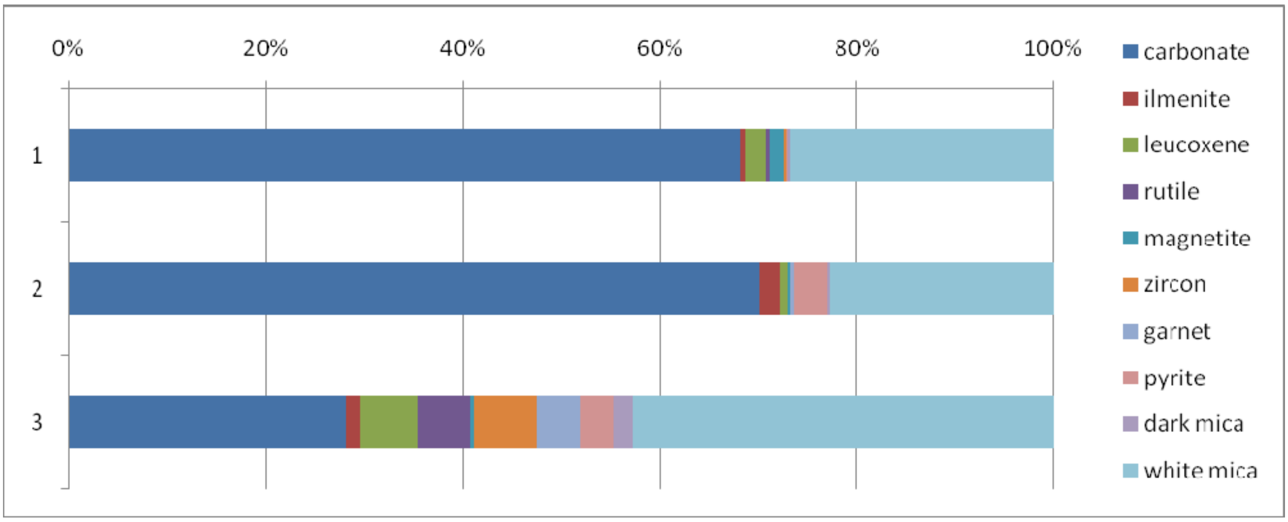

Figure 9.2. Heavy mineral content measured by CCSEM in the three provenance samples. Minerals present in amounts < 1 wt% in all samples have been omitted.

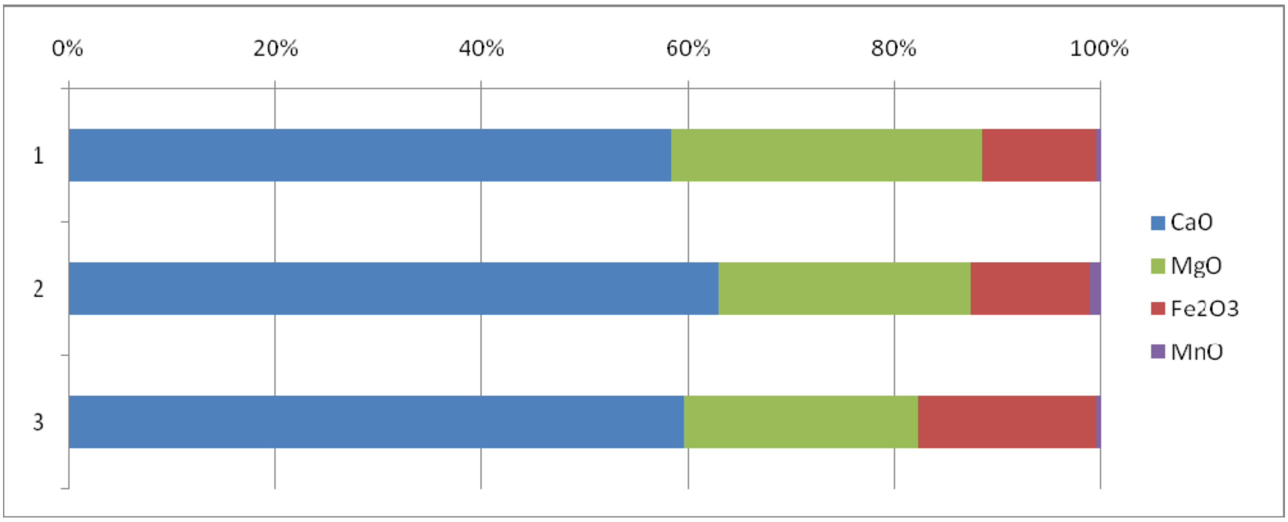

Figure 9.3. Relative contents of Ca, Mg, Fe and Mn in the carbonate grains measured by CCSEM in the three provenance samples. Ankerite dominates the carbonate grains, as revealed by the high amounts of both Mg and Fe and the presence of Mn.

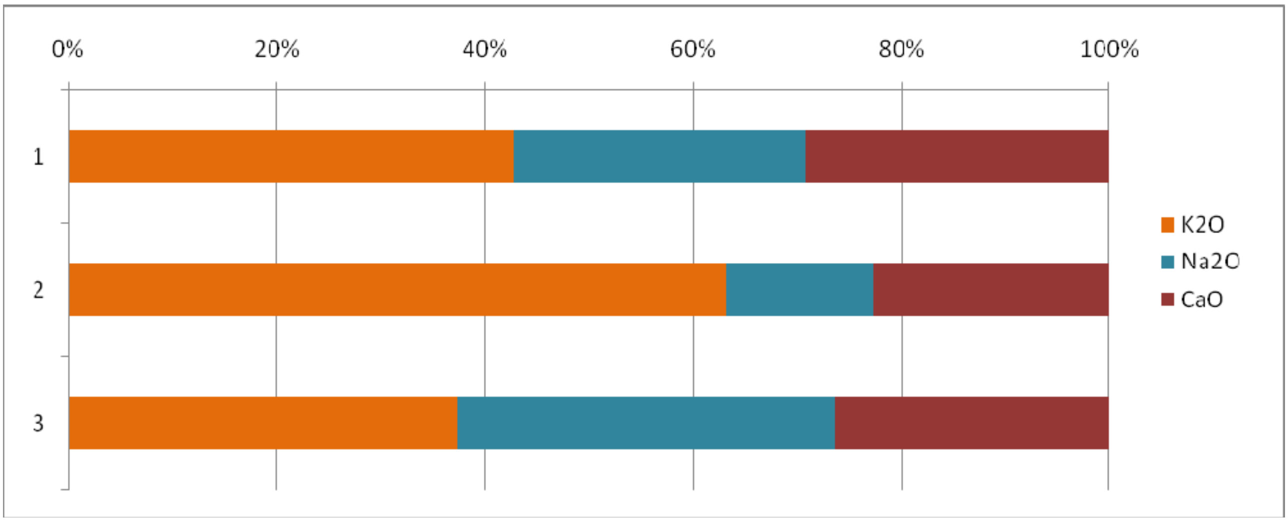

Figure 9.4. Relative contents of K, Na and Ca in the feldspars measured by CCSEM in the three provenance samples. There have been measured 13-15 feldspar grains per sample.

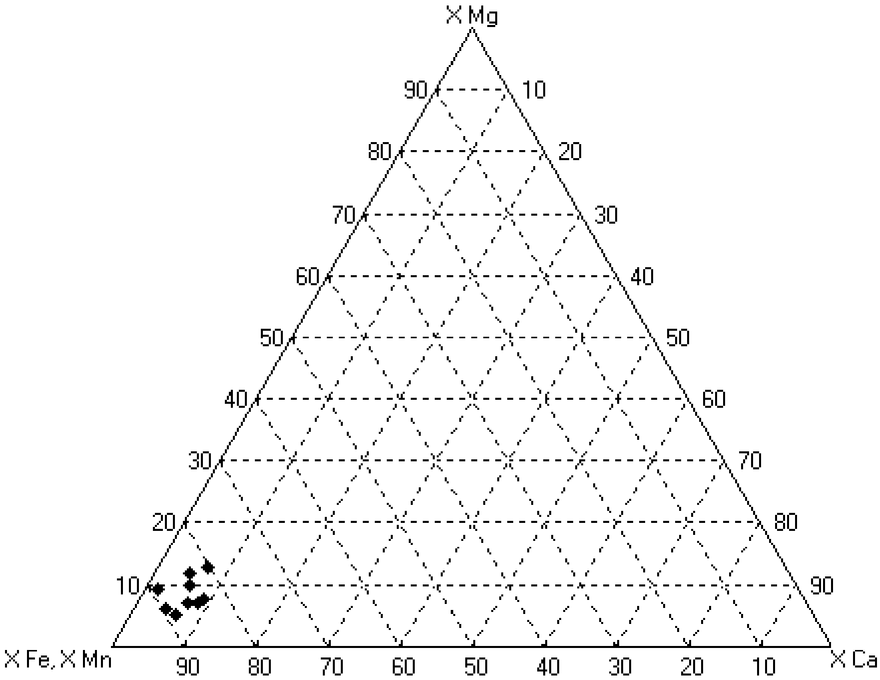

Figure 9.5. Garnet composition of provenance sample 3 measured by CCSEM.

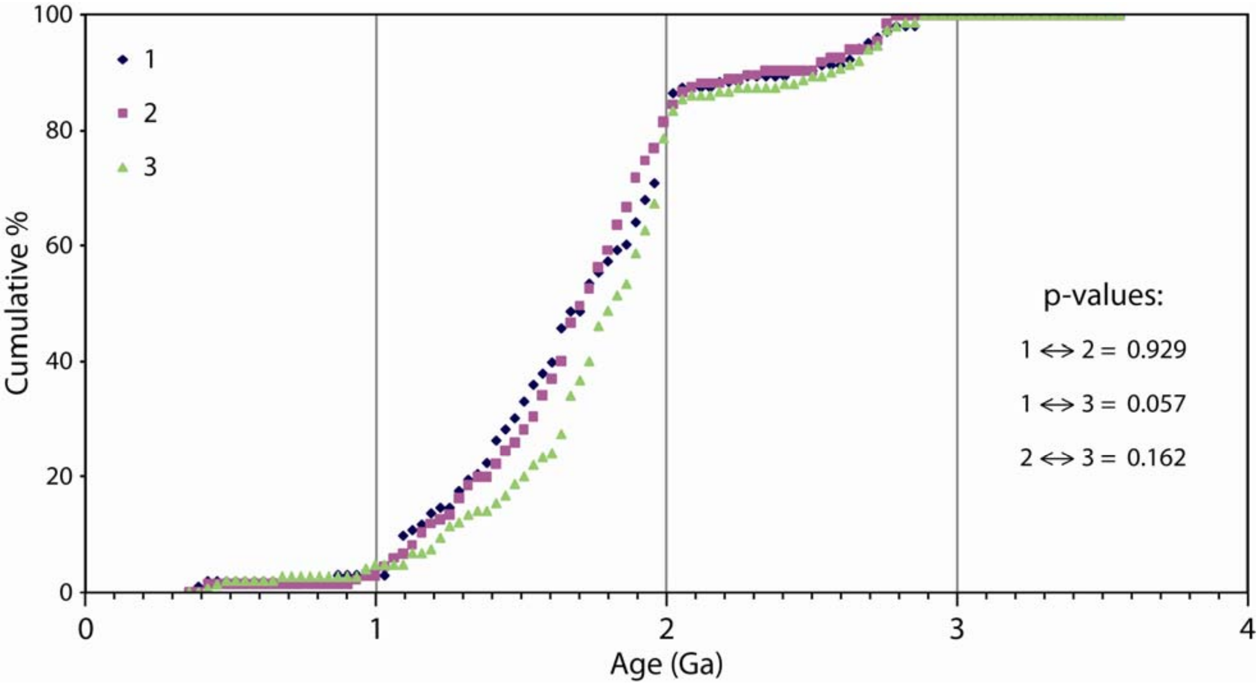

Figure 9.6. Cumulative percentage of the U-Pb zircon ages of the three age distributions made by CDF. K-S p-values are made using error in the CDF. The p-values show that the age distributions are not significantly different from each other.

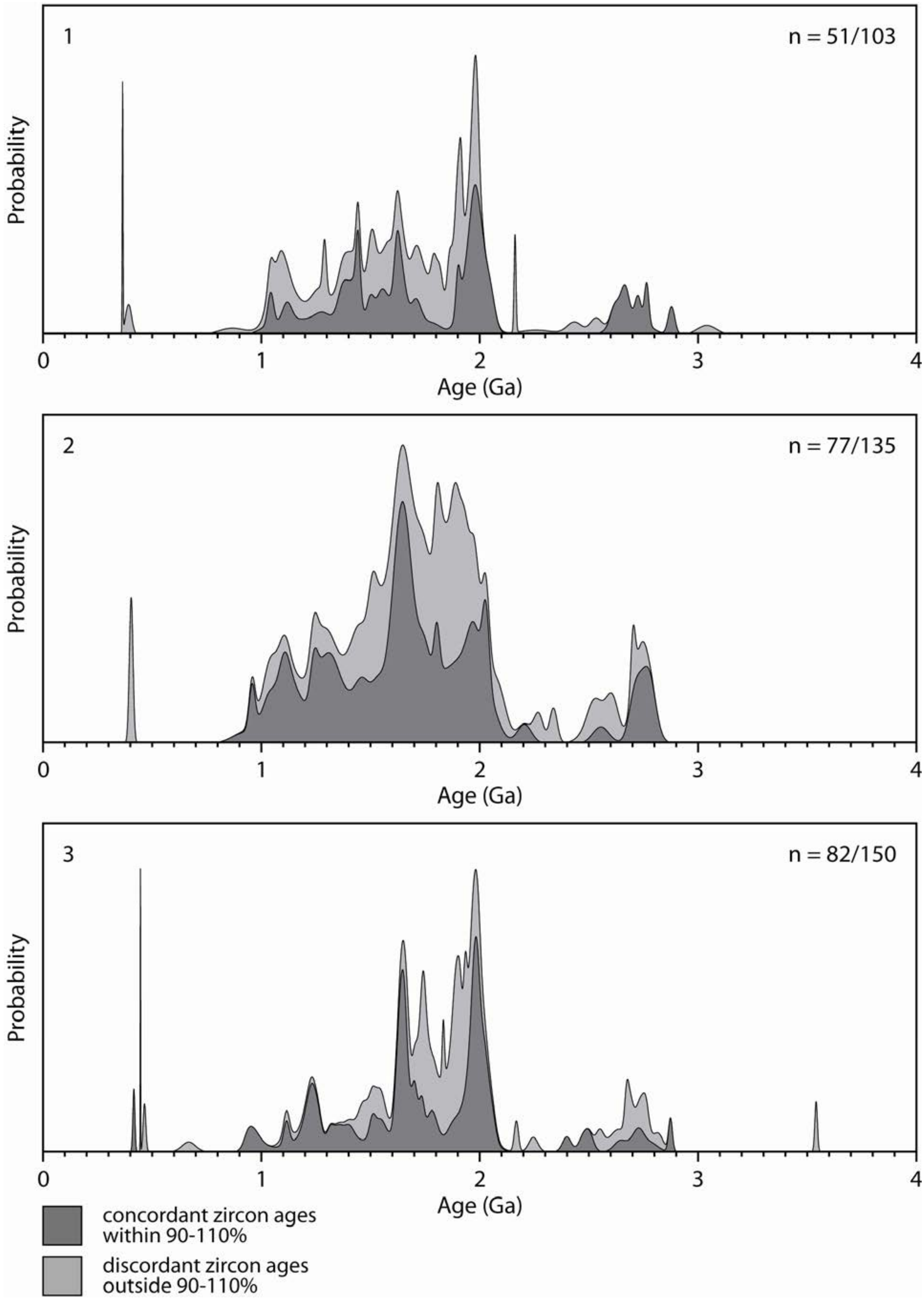

Figure 9.7. Zircon age distributions of the three provenance samples.

10. Appendix

10.1 Core photographs

Contents:

Dry, wet and UV-light photos of the core boxes. Base of the core boxes in the lower left, top in the upper right corner.


GEUS RØDRYGGEN-1 231,55 - 234,54 m
KODAK Color Control Patches
cm 10 20 30 40 50 60 70 80 100
234.54
BUNDEN ER NÅET 13/8 - 2009 John Boserup ANDREAS H. FRANDSEN
KODAK Gray Scale


GEUS RØDRYGGEN-1 231,55 - 234,54 m
KODAK Color Control Patches
cm 10 20 30 40 50 60 70 80 100
234.54
BUNDEN ER NÅET 13/8 - 2009
ANDREAS H. FRANDSEN
KODAK Gray Scale

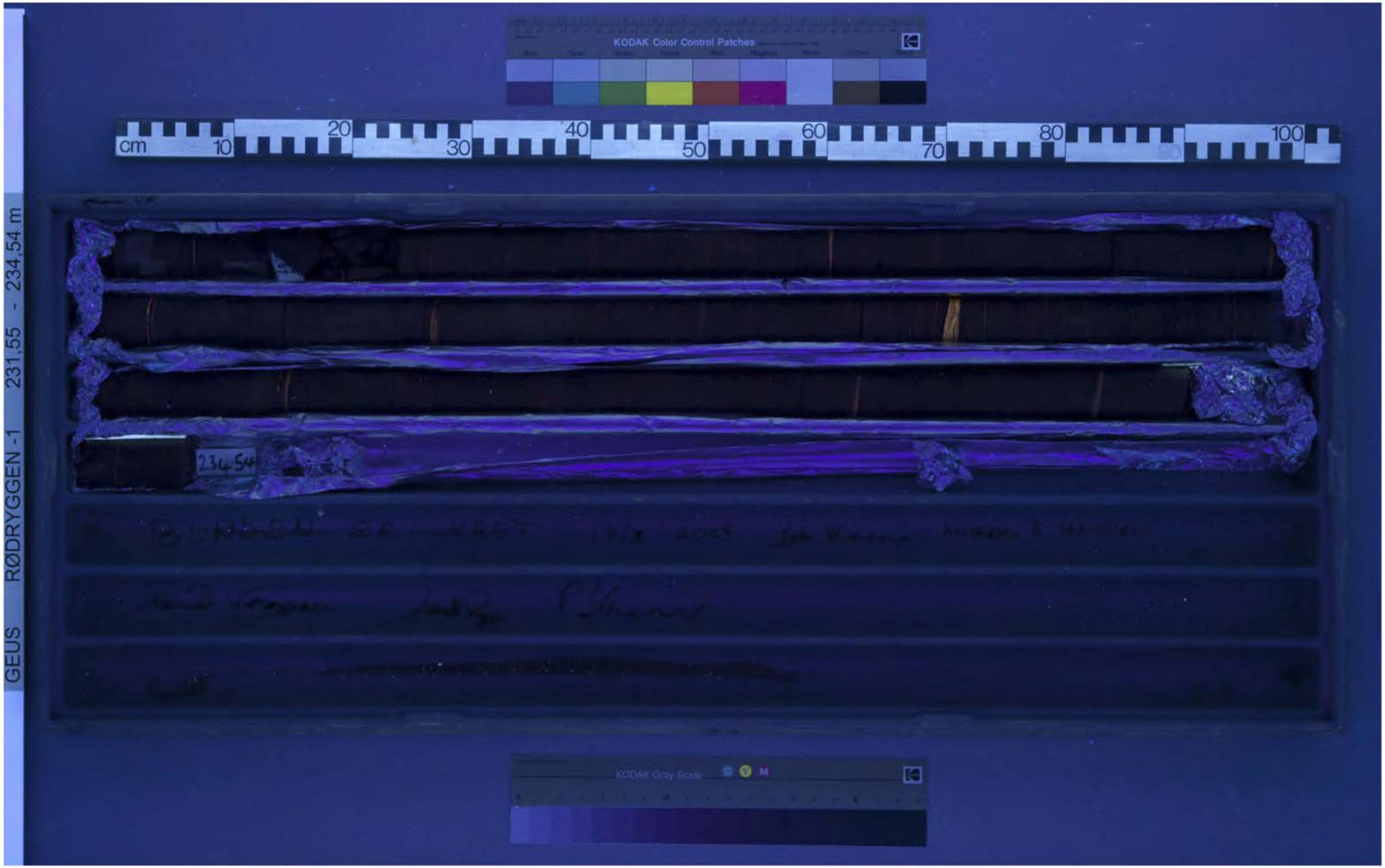
GEUS RØDRYGGEN -1 231,55 - 234,54 m
KODAK Color Control Patches
cm 10 20 30 40 50 60 70 80 100
234.54
KODAK Gray Scale


GEUS RØDRYGGEN-1 225,00 - 231,55 m
KODAK Color Control Patches
KODAK Gray Scale


GEUS RØDRYGGEN-1 225,00 - 231,55 m
KODAK Color Control Patches
cm 10 20 30 40 50 60 70 80 100
KODAK Gray Scale


GEUS RØDRYGGEN-1 225,00 - 231,55 m
KODAK Color Control Patches
cm 10 20 30 40 50 60 70 80 90 100
KODAK Gray Scale


GEUS RØDRYGGEN-1 218,59 - 225,00 m
KODAK Color Control Patches
KODAK Gray Scale


GEUS RØDRYGGEN-1 218,59 - 225,00 m
KODAK Color Control Patches
KODAK Gray Scale
cm

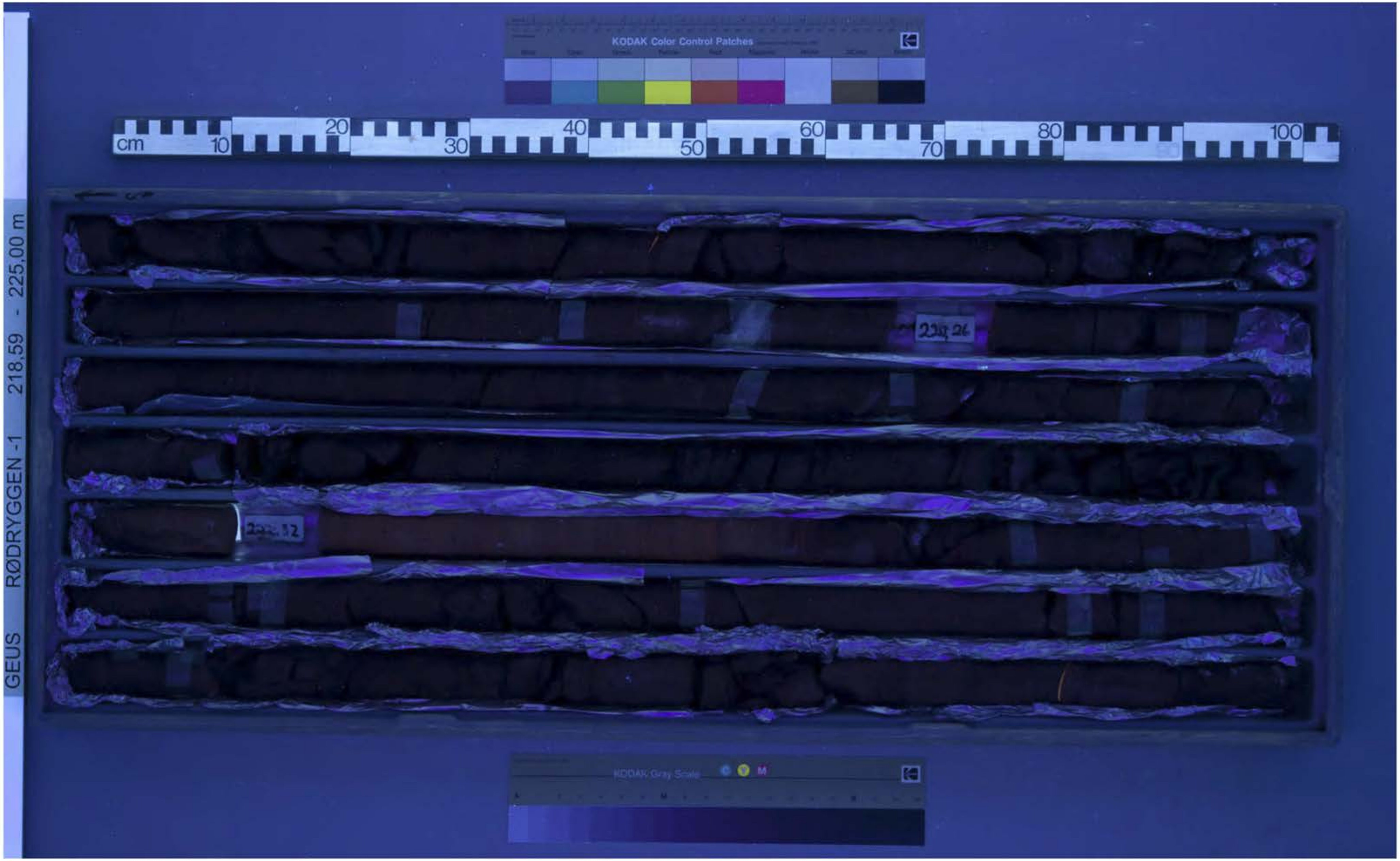
GEUS RØDRYGGEN-1 218,59 - 225,00 m
KODAK Color Control Patches
cm
KODAK Gray Scale


GEUS RØDRYGGEN-1 211,97 - 218,59 m
KODAK Color Control Patches
cm 10 20 30 40 50 60 70 80 100
213,62
KODAK Gray Scale


GEUS RØDRYGGEN-1 211,97 - 218,59 m
KODAK Color Control Patches
KODAK Gray Scale
213,62

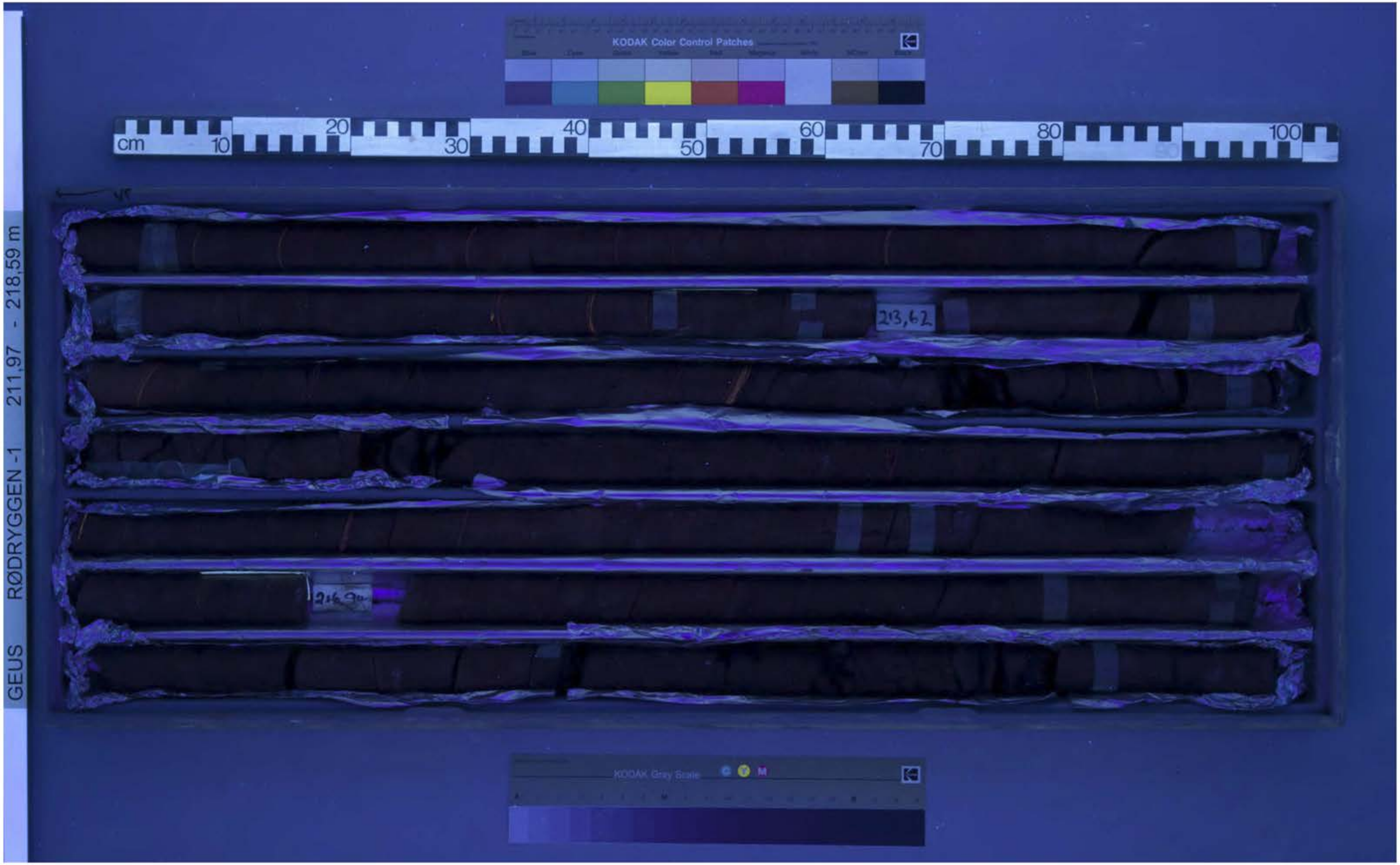
GEUS RØDRYGGEN-1 211,97 - 218,59 m
KODAK Color Control Patches
KODAK Gray Scale
cm
213,62


GEUS RØDRYGGEN-1 205,46 - 211,97 m
KODAK Color Control Patches
KODAK Gray Scale


GEUS RØDRYGGEN -1 205,46 - 211,97 m
KODAK Color Control Patches
cm 10 20 30 40 50 60 70 80 100
KODAK Gray Scale

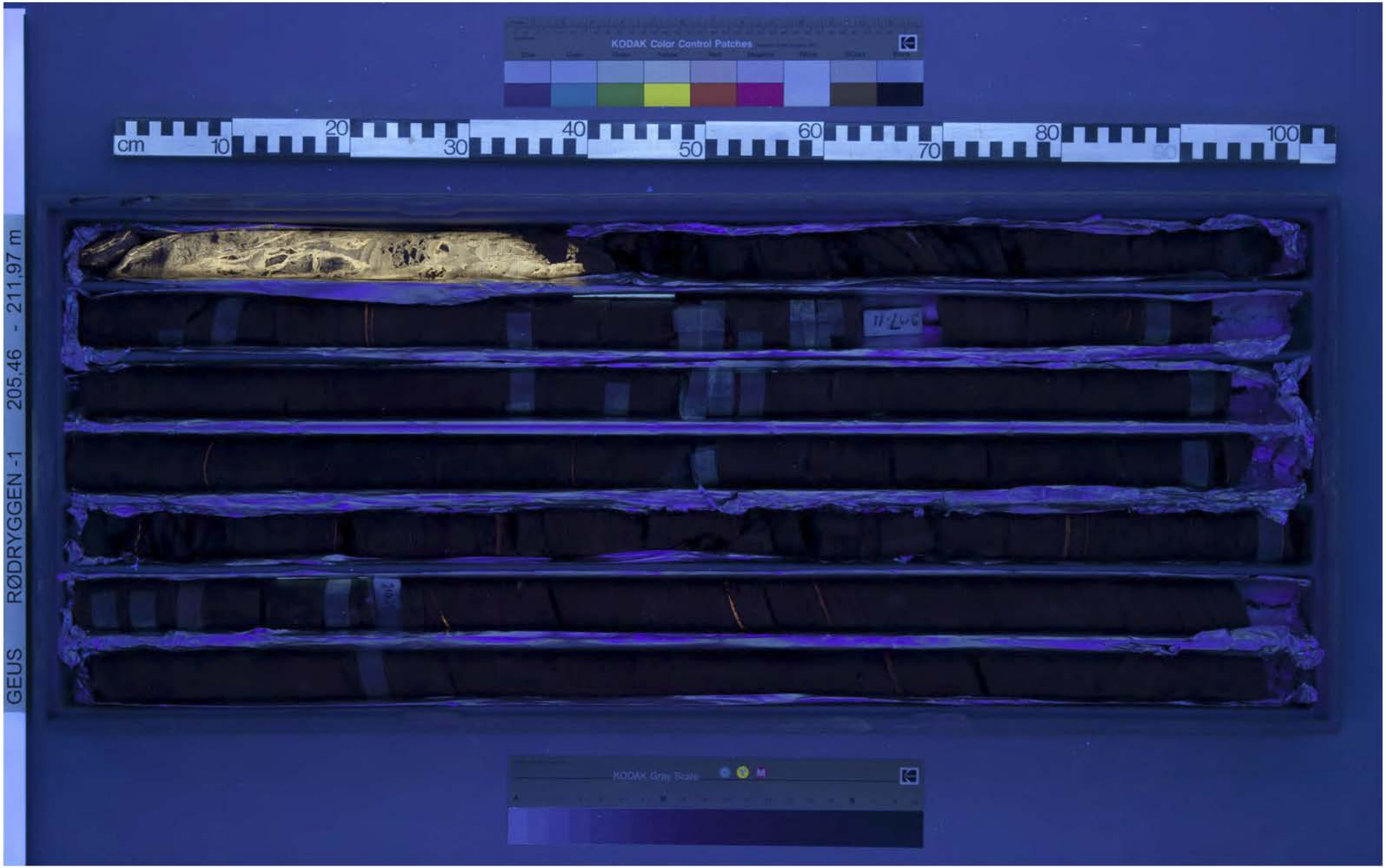
GEUS RØDRYGGEN -1 205,46 - 211,97 m
KODAK Color Control Patches
KODAK Gray Scale


GEUS RØDRYGGEN-1 199,18 - 205,46 m
KODAK Color Control Patches
KODAK Gray Scale
cm 10 20 30 40 50 60 70 80 100


GEUS RØDRYGGEN-1 199,18 - 205,46 m

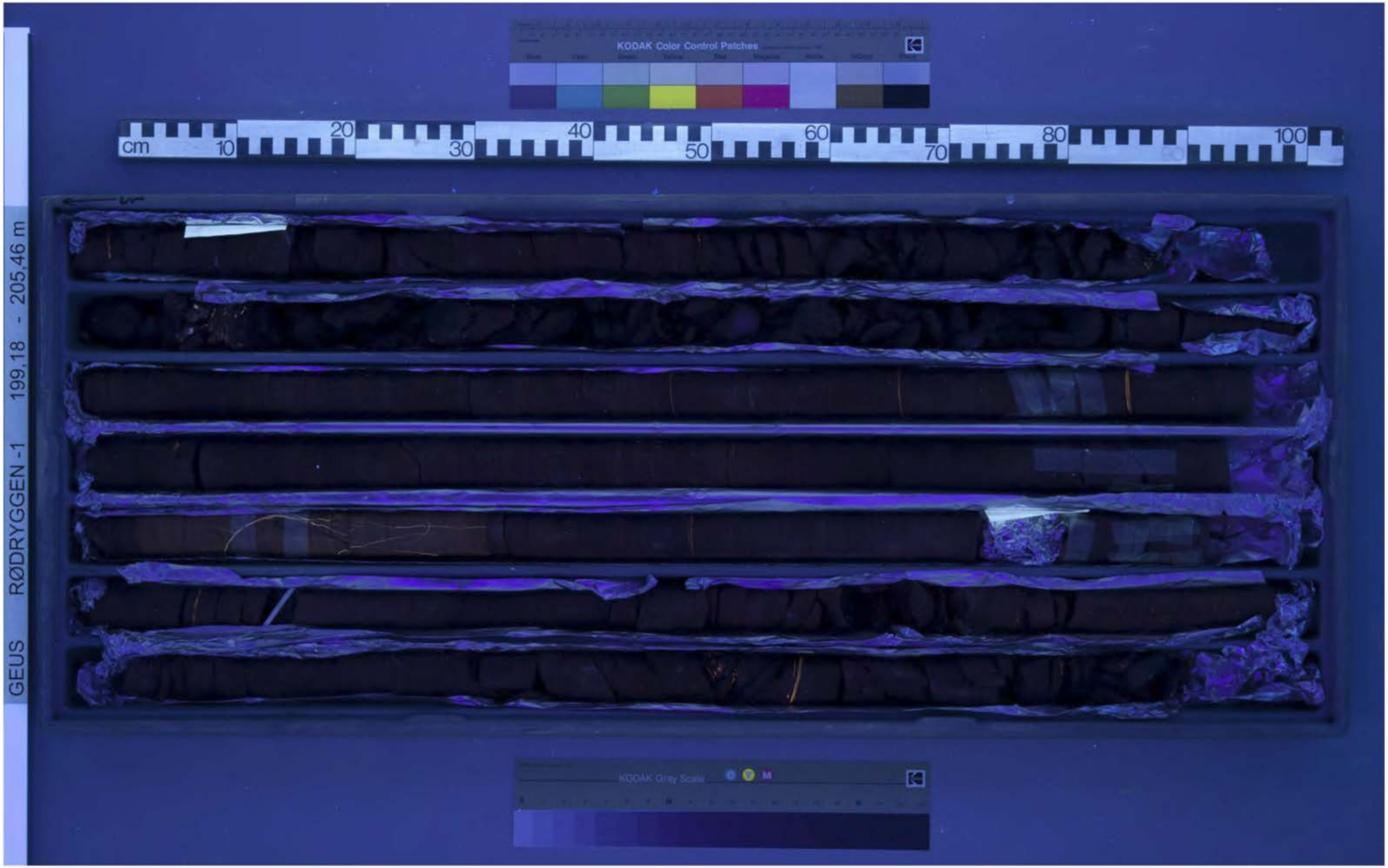
GEUS RØDRYGGEN -1 199,18 - 205,46 m
KODAK Color Control Patches
KODAK Gray Scale
cm 10 20 30 40 50 60 70 80 100


GEUS RØDRYGGEN -1 192,56 - 199,18 m
KODAK Color Control Patches
cm
193.97
197,22
KODAK Gray Scale


GEUS RØDRYGGEN-1 192,56 - 199,18 m
KODAK Color Control Patches
cm 10 20 30 40 50 60 70 80 100
193.97
197,22
KODAK Gray Scale

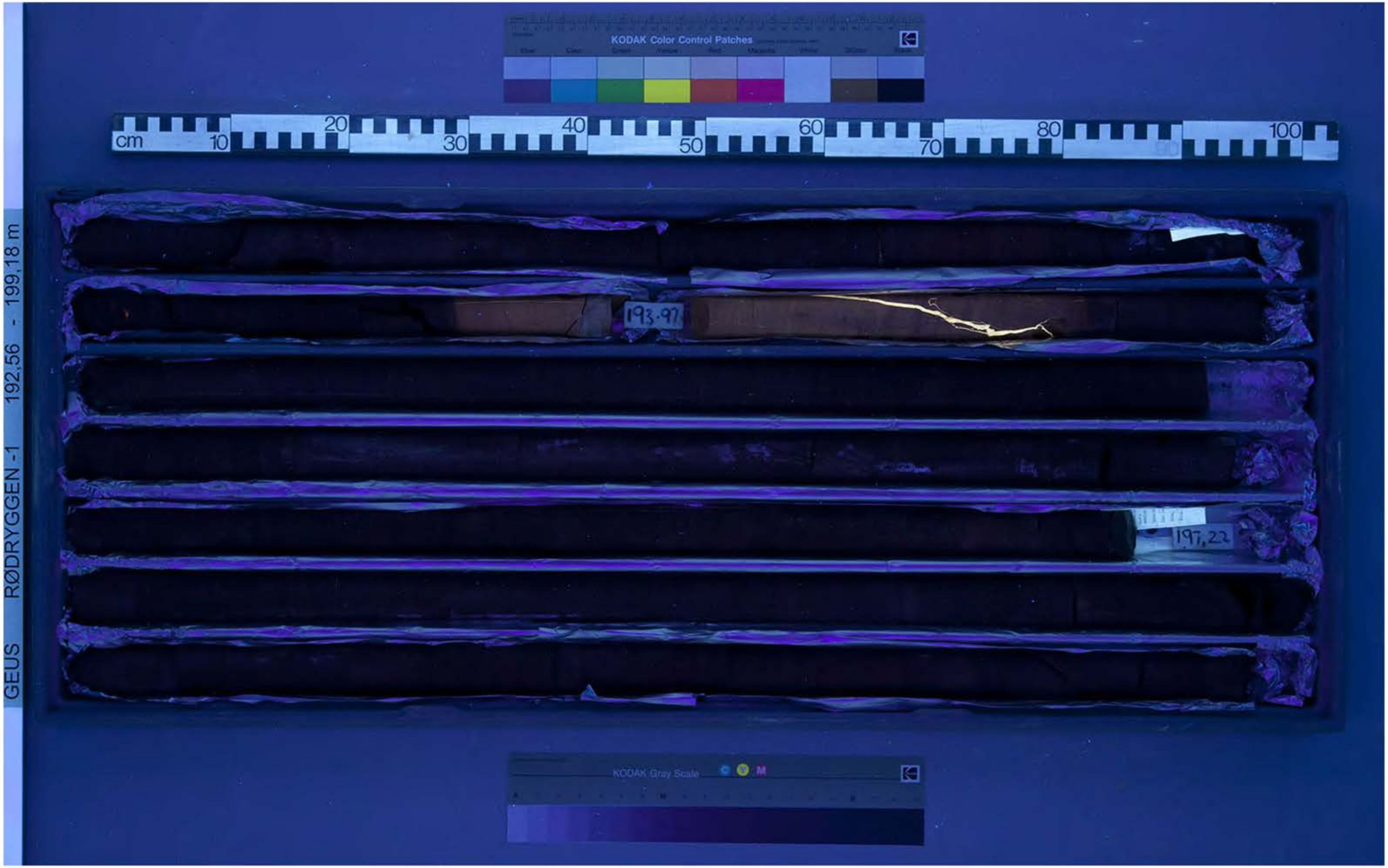
GEUS RØDRYGGEN-1 192,56 - 199,18 m
KODAK Color Control Patches
cm 10 20 30 40 50 60 70 80 100
193.97
197,22
KODAK Gray Scale


GEUS
RØDRYGGEN -1
185,91 - 192,56 m
KODAK Color Control Patches
Blue Cyan Green Yellow Red Magenta White 3/Color Black
cm 10 20 30 40 50 60 70 80 100
KODAK Gray Scale
A M B


GEUS RØDRYGGEN-1 185,91 - 192,56 m
KODAK Color Control Patches
KODAK Gray Scale
cm

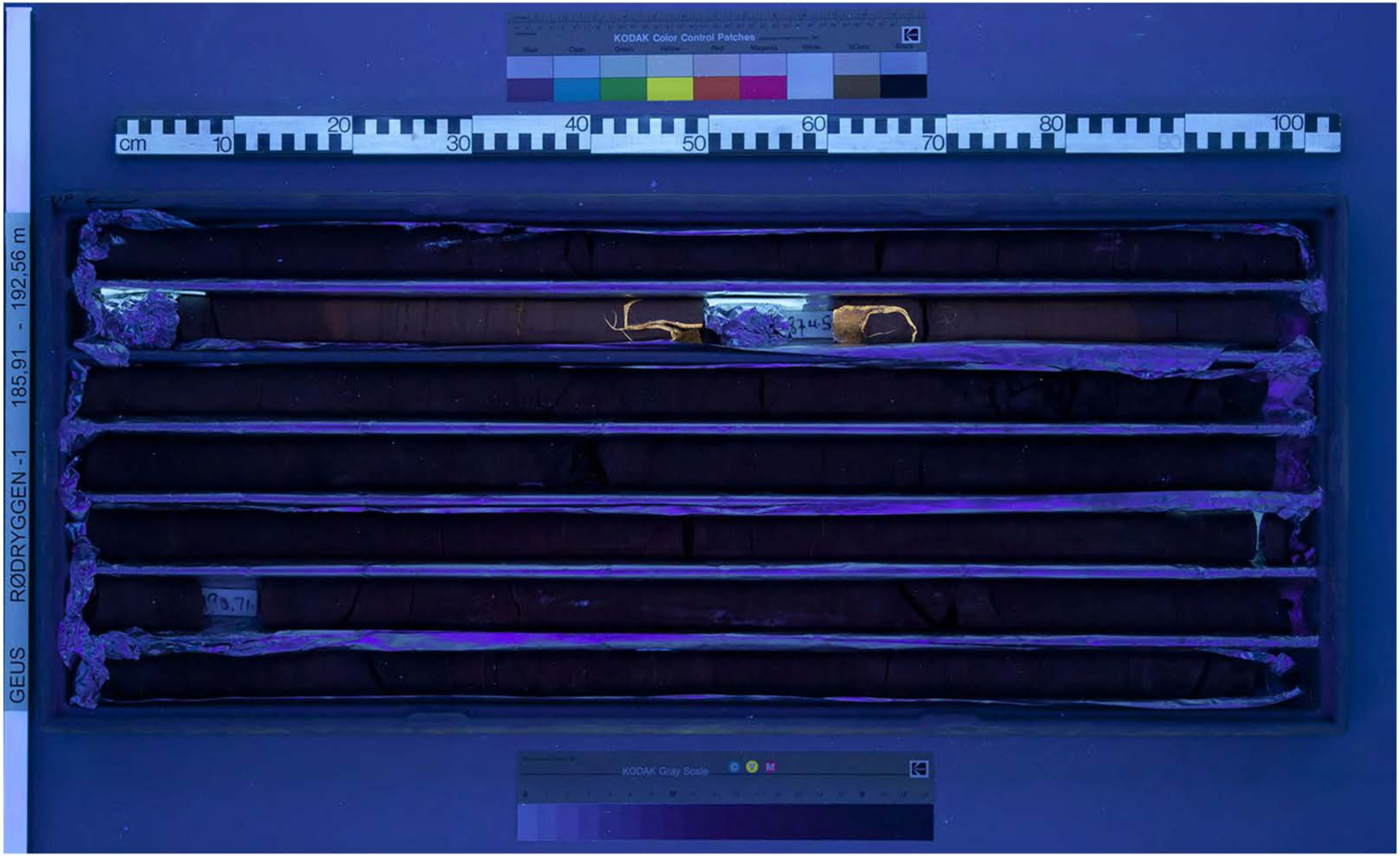
GEUS RØDRYGGEN-1 185,91 - 192,56 m
KODAK Color Control Patches
KODAK Gray Scale

GEUS RØDRYGGEN -1 179,26 - 185,91 m


GEUS RØDRYGGEN-1 179,26 - 185,91 m
KODAK Color Control Patches
cm
181,04
184,13
KODAK Gray Scale

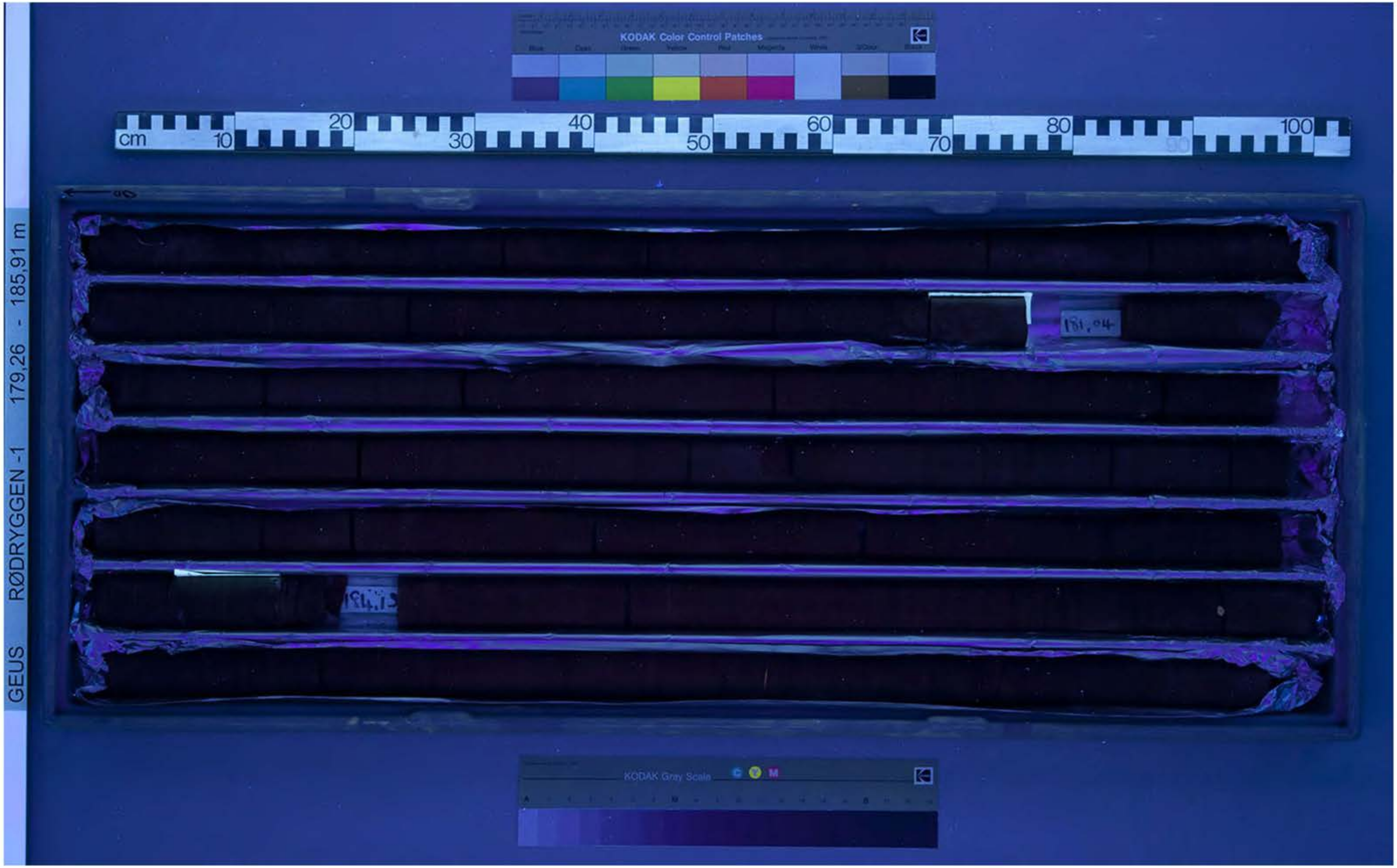
GEUS RØDRYGGEN -1 179,26 - 185,91 m
KODAK Color Control Patches
cm 10 20 30 40 50 60 70 80 90 100
181,04
KODAK Gray Scale


GEUS RØDRYGGEN-1 172,74 - 179,26 m
KODAK Color Control Patches
Blue
Cyan
Green
Yellow
Red
Magenta
White
3/Color
Black
cm
10
20
30
40
50
60
70
80
100
177.69
KODAK Gray Scale
C
Y
M
A
M
B


GEUS RØDRYGGEN -1 172,74 - 179,26 m
KODAK Color Control Patches
cm 10 20 30 40 50 60 70 80 100
177.69
KODAK Gray Scale

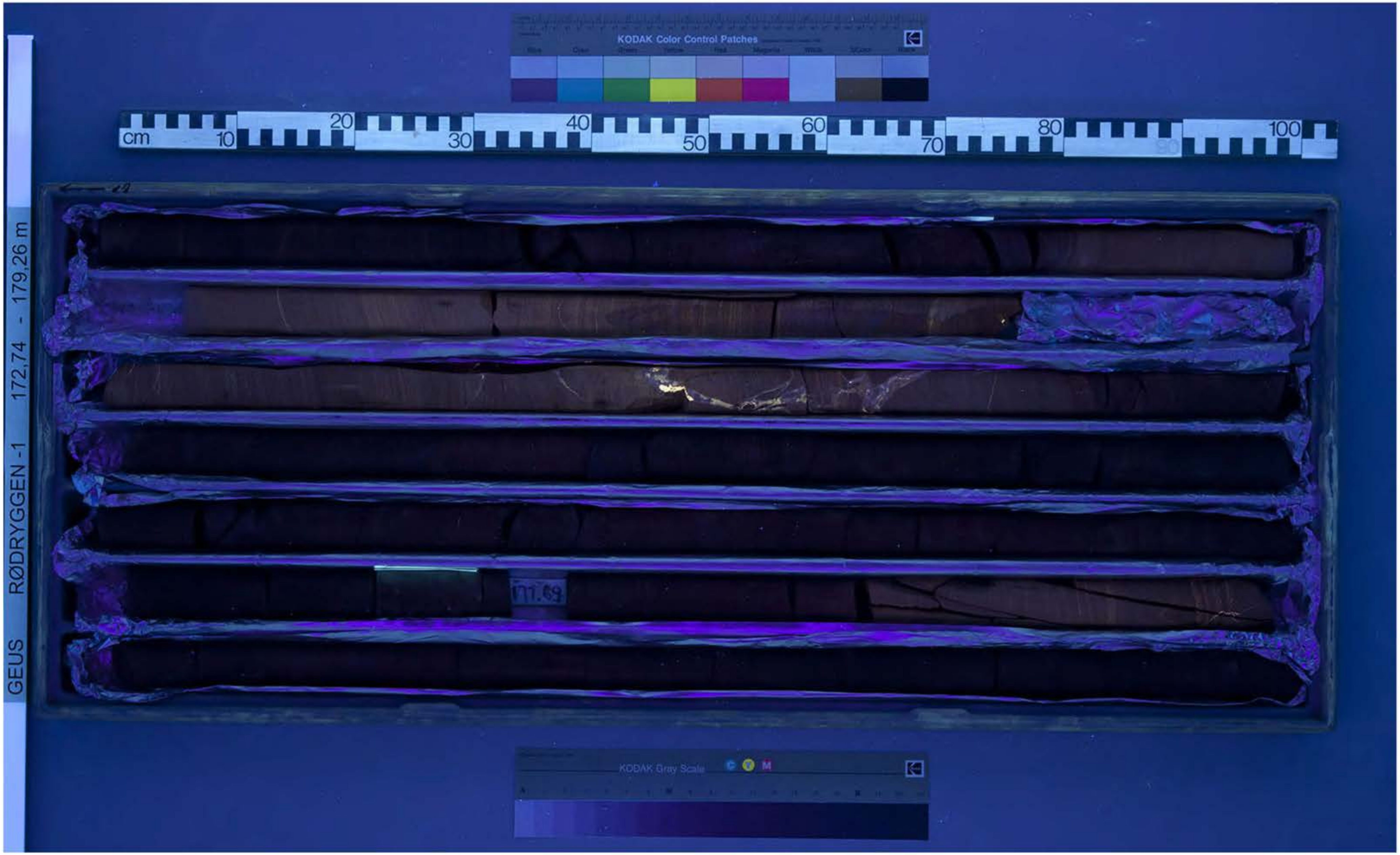
GEUS RØDRYGGEN-1 172,74 - 179,26 m
KODAK Color Control Patches
cm 10 20 30 40 50 60 70 80 90 100
171.69
KODAK Gray Scale


GEUS RØDRYGGEN-1 166,16 - 172,74 m
KODAK Color Control Patches
Blue Cyan Green Yellow Red Magenta White 3/Color Black
cm 10 20 30 40 50 60 70 80 90 100
167.74
KODAK Gray Scale
C Y M


GEUS RØDRYGGEN-1 166,16 - 172,74 m
KODAK Color Control Patches
cm
167.74
KODAK Gray Scale

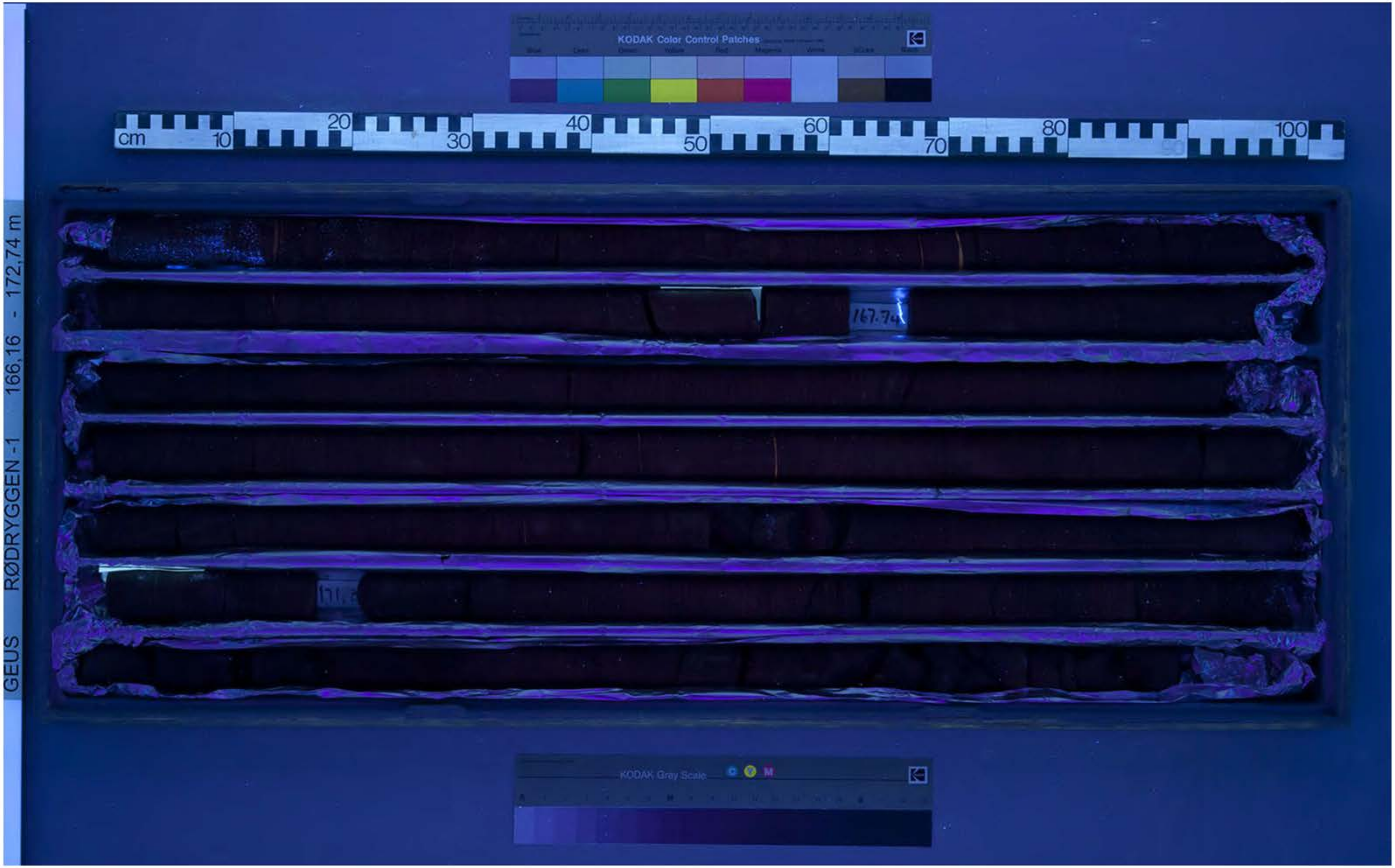
GEUS RØDRYGGEN-1 166,16 - 172,74 m
KODAK Color Control Patches
167.74
KODAK Gray Scale


GEUS RØDRYGGEN-1 159,62 - 166,16 m
KODAK Color Control Patches
Blue Cyan Green Yellow Red Magenta White 3/Color Black
cm 10 20 30 40 50 60 70 80 100
KODAK Gray Scale
A M B


GEUS
RØDRYGGEN -1 159,62 - 166,16 m
KODAK Color Control Patches
Blue Cyan Green Yellow Red Magenta White 3/Color Black
cm 10 20 30 40 50 60 70 80 100
161·14
164·14
KODAK Gray Scale
C Y M
A M B


GEUS RØDRYGGEN-1 159,62 - 166,16 m
KODAK Color Control Patches
cm 10 20 30 40 50 60 70 80 90 100
KODAK Gray Scale
C Y M


GEUS RØDRYGGEN-1 152,97 - 159,62 m
KODAK Color Control Patches
cm 10 20 30 40 50 60 70 80 100
154,54
157,84
KODAK Gray Scale

GEUS RØDRYGGEN -1 152,97 - 159,62 m

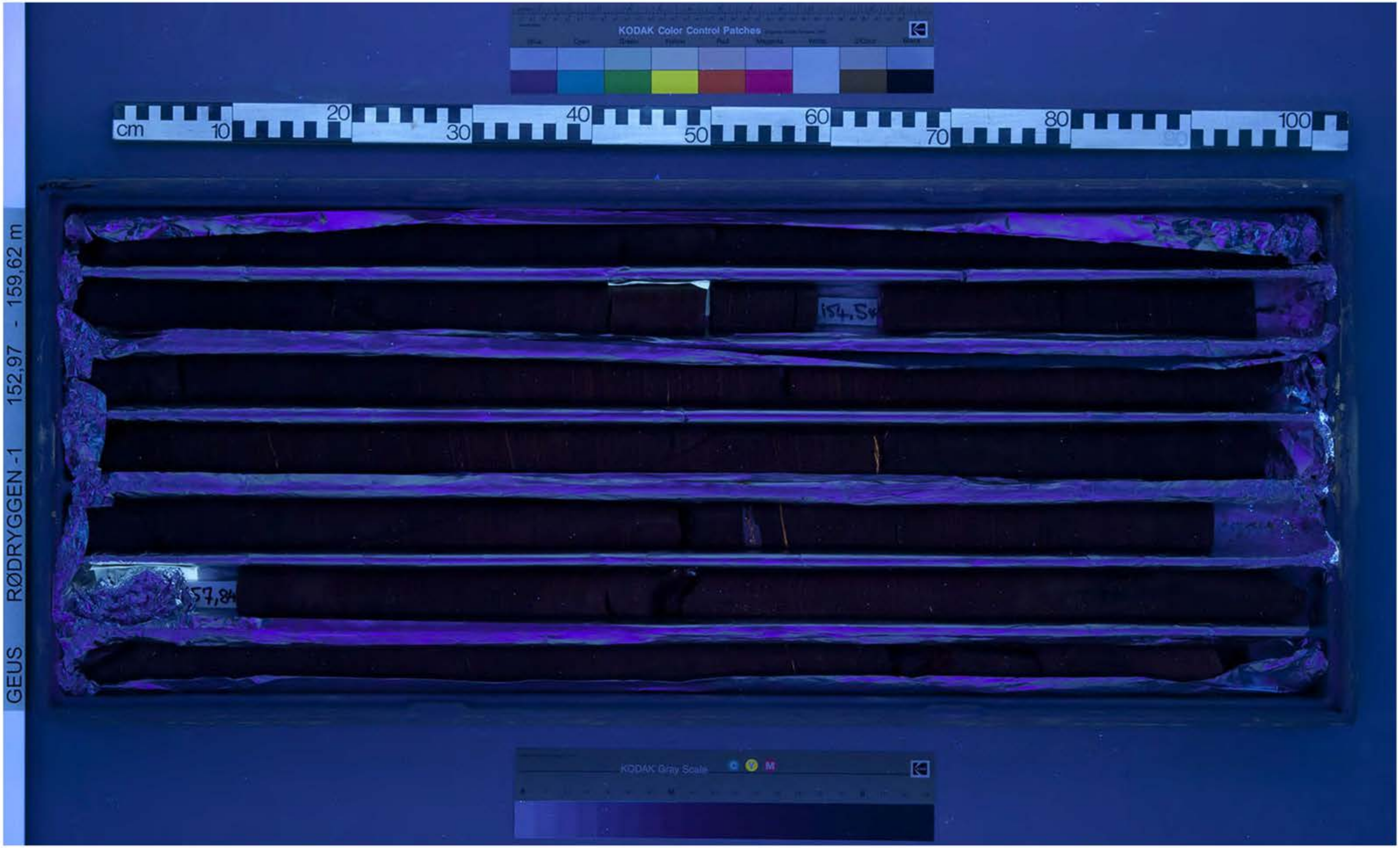
GEUS RØDRYGGEN -1 152,97 - 159,62 m
KODAK Color Control Patches
cm 10 20 30 40 50 60 70 80 100
157,84
KODAK Gray Scale


GEUS RØDRYGGEN-1 146,53 - 152,97 m
KODAK Color Control Patches
KODAK Gray Scale


GEUS RØDRYGGEN-1 146,53 - 152,97 m
KODAK Color Control Patches
KODAK Gray Scale
cm

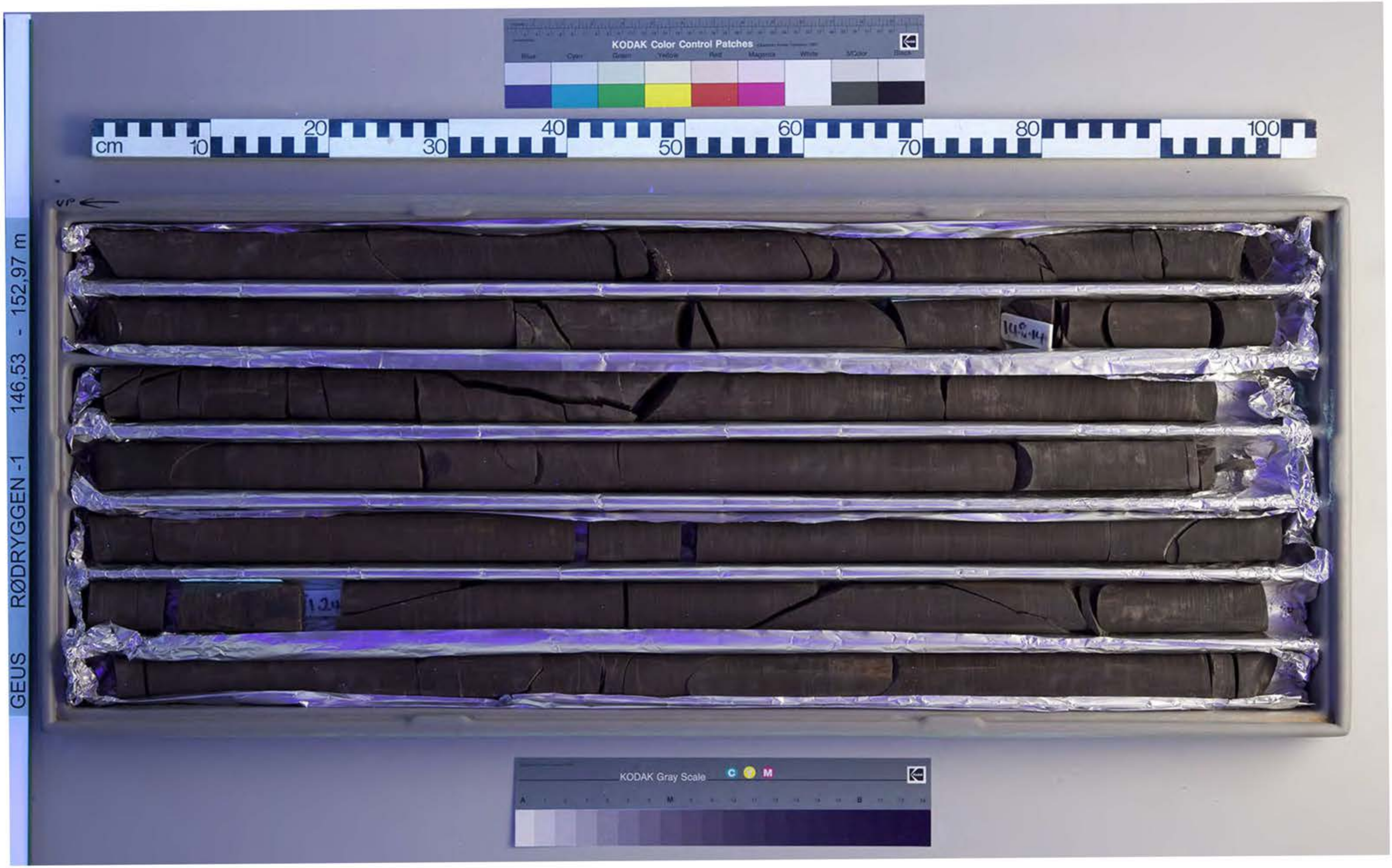
GEUS RØDRYGGEN -1 146,53 - 152,97 m
KODAK Color Control Patches
cm 10 20 30 40 50 60 70 80 100
KODAK Gray Scale


GEUS RØDRYGGEN -1 140,20 - 146,53 m
KODAK Color Control Patches
Blue Cyan Green Yellow Red Magenta White 3/Color Black
cm 10 20 30 40 50 60 70 80 100
UP
141,59
144.84
KODAK Gray Scale
A M B

GEUS RØDRYGGEN-1 140,20 - 146,53 m

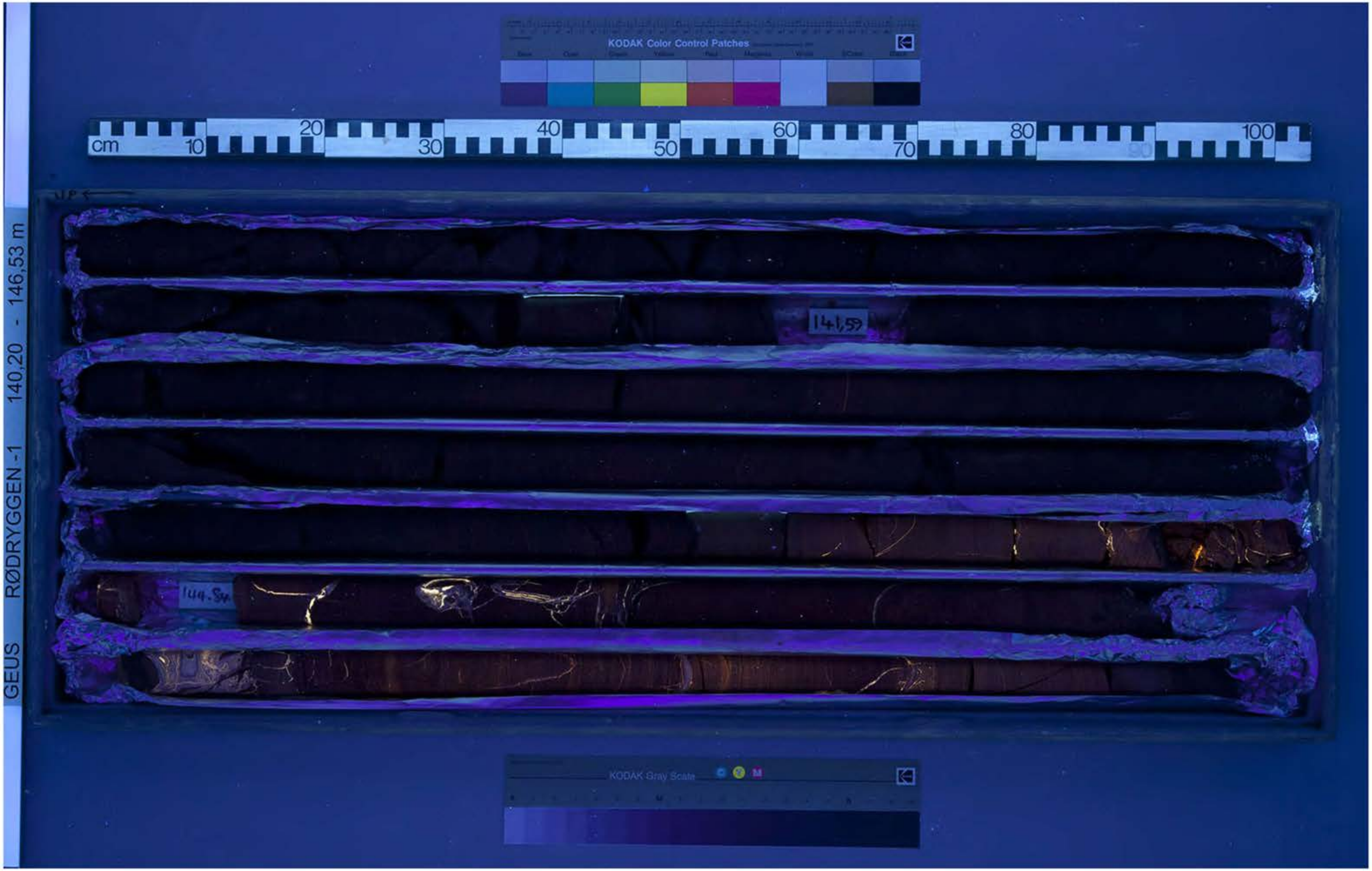
GEUS RØDRYGGEN-1 140,20 - 146,53 m
KODAK Color Control Patches
cm 10 20 30 40 50 60 70 80 90 100
141,57
144.54
KODAK Gray Scale


GEUS RØDRYGGEN-1 133,54 - 140,20 m
KODAK Color Control Patches
cm 10 20 30 40 50 60 70 80 100
UP
138.49
KODAK Gray Scale


GEUS RØDRYGGEN-1 133,54 - 140,20 m
KODAK Color Control Patches
Blue
Cyan
Green
Yellow
Red
Magenta
White
3/Color
Black
cm
10
20
30
40
50
60
70
80
100
138.49
KODAK Gray Scale
C
Y
M
A
M
B

GEUS RØDRYGGEN-1 133,54 - 140,20 m

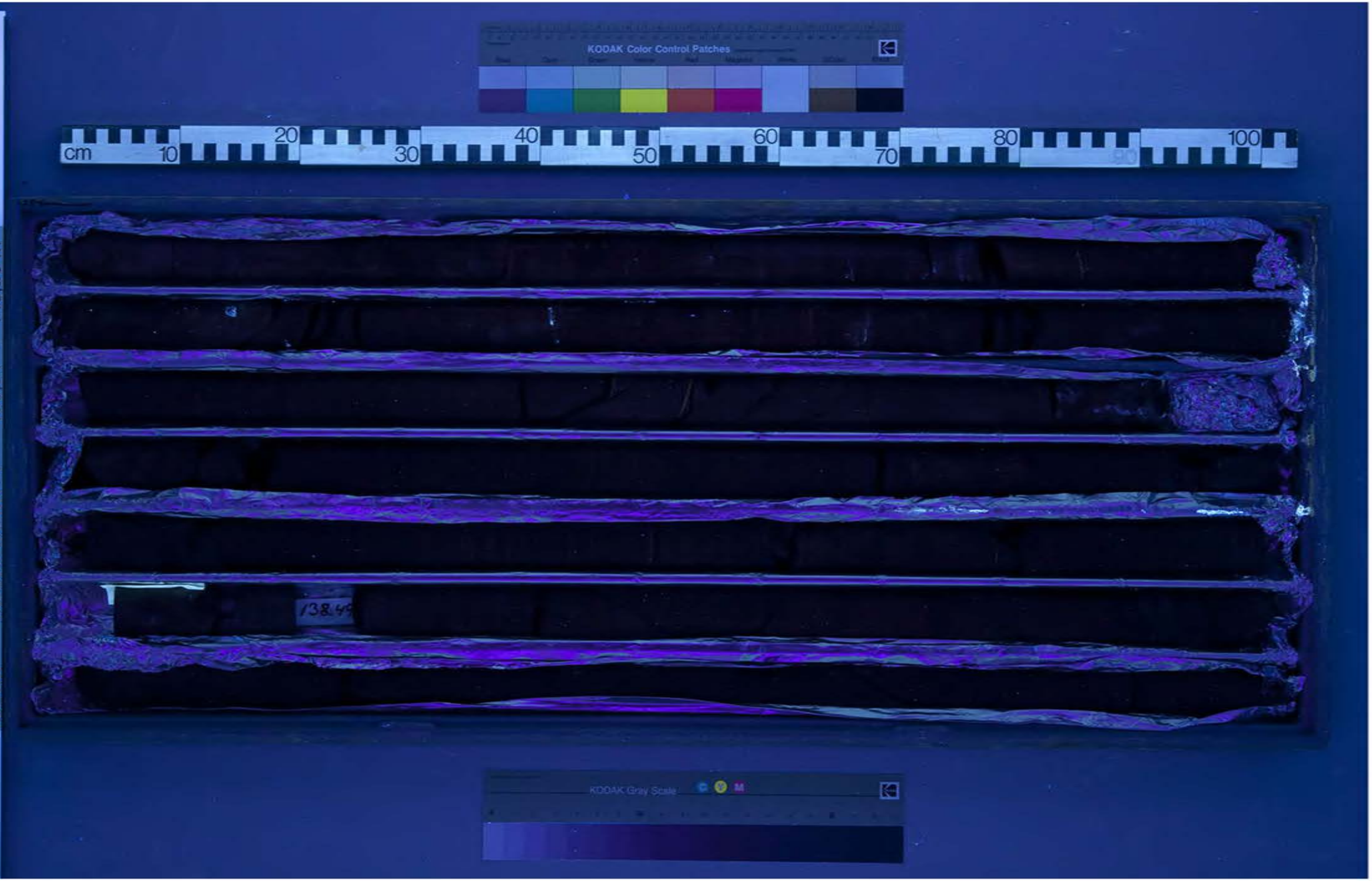


GEUS RØDRYGGEN-1 125,40 - 133,54 m
KODAK Color Control Patches
Blue Cyan Green Yellow Red Magenta White 3/Color Black
cm 10 20 30 40 50 60 70 80 100
125.64
126.90
130.24
133.54
KODAK Gray Scale
A M B


GEUS RØDRYGGEN-1 125,40 - 133,54 m
KODAK Color Control Patches
cm
125.64
126.90
130.29
133.54
KODAK Gray Scale

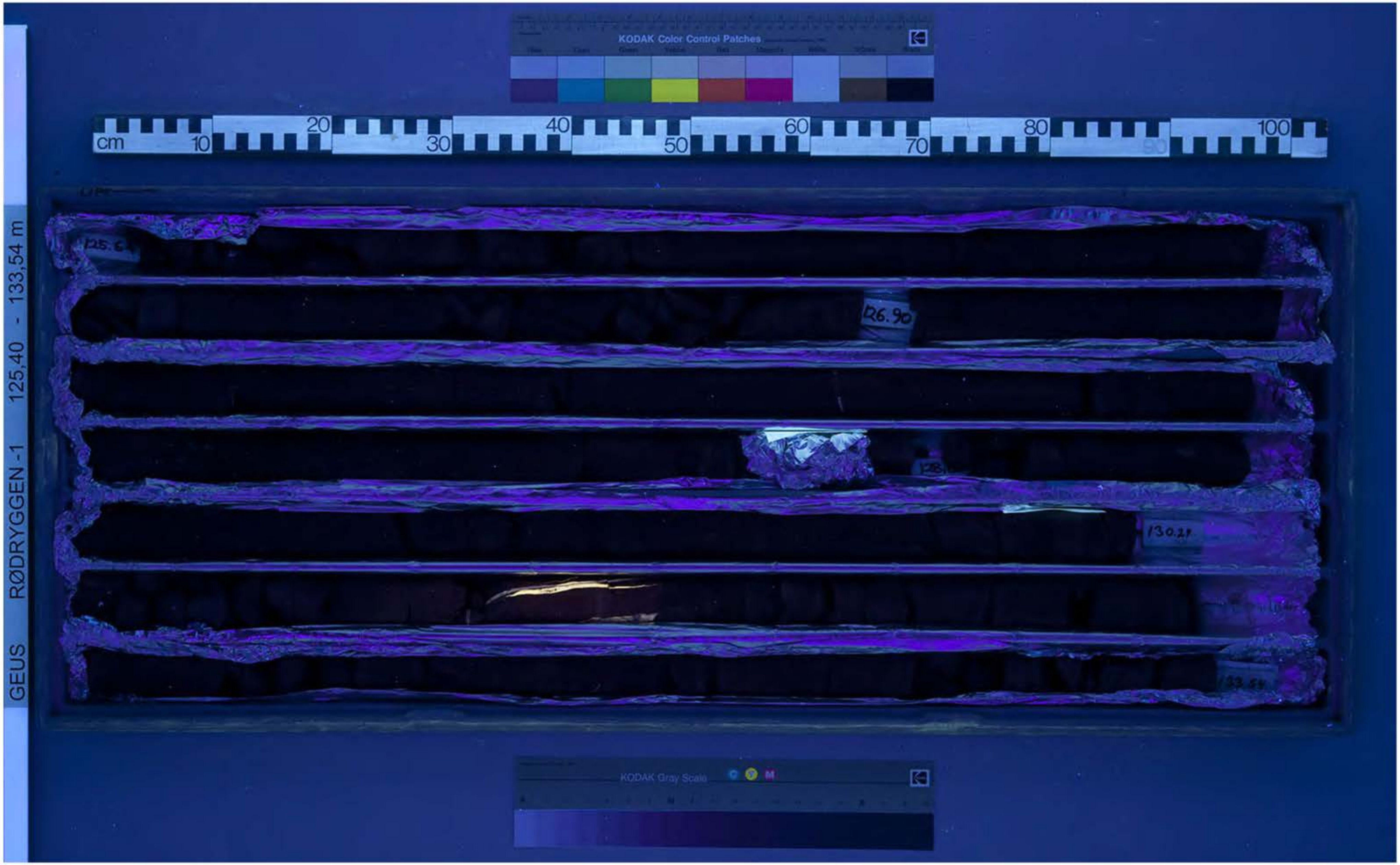
GEUS RØDRYGGEN-1 125,40 - 133,54 m
KODAK Color Control Patches
cm 10 20 30 40 50 60 70 80 90 100
126.90
KODAK Gray Scale


GEUS RØDRYGGEN-1 118,73 - 125,40 m
KODAK Color Control Patches
Blue Cyan Green Yellow Red Magenta White 3/Color Black
cm 10 20 30 40 50 60 70 80 100
121,44
123,69
KODAK Gray Scale
C Y M
A M B


GEUS RØDRYGGEN-1 118,73 - 125,40 m
KODAK Color Control Patches
cm
121,44
123,69
KODAK Gray Scale

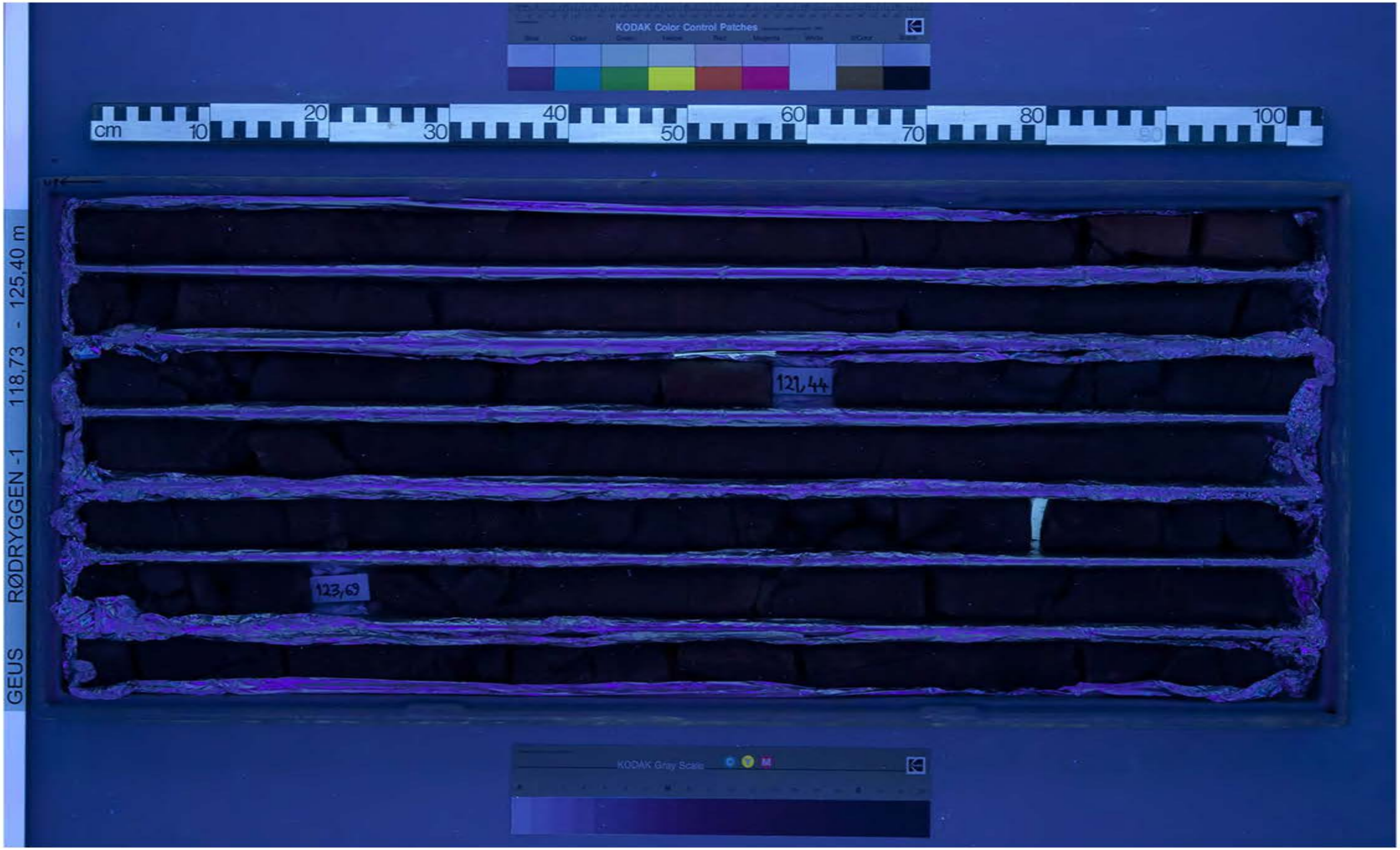
KODAK Color Control Patches
cm
10
20
30
40
50
60
70
80
100
121,44
123,69
KODAK Gray Scale
GEUS RØDRYGGEN -1 118,73 - 125,40 m


GEUS RØDRYGGEN-1 111,94 - 118,73 m
KODAK Color Control Patches
cm
10
20
30
40
50
60
70
80
100
115.2
118,54
KODAK Gray Scale


GEUS RØDRYGGEN-1 111,94 - 118,73 m
KODAK Color Control Patches
KODAK Gray Scale
cm
118,54

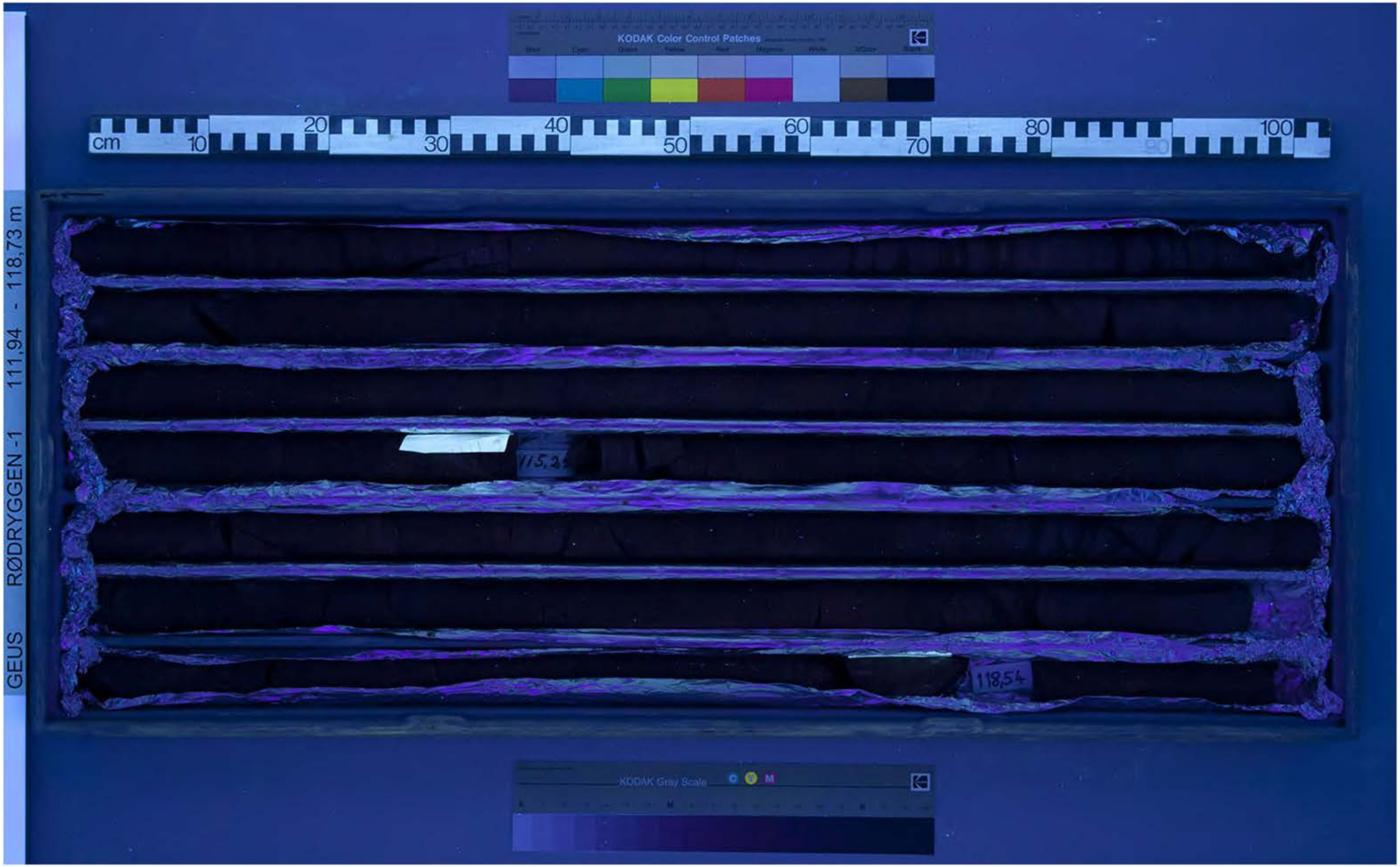
GEUS RØDRYGGEN-1 111,94 - 118,73 m
KODAK Color Control Patches
cm 10 20 30 40 50 60 70 80 90 100
115,24
118,54
KODAK Gray Scale


GEUS RØDRYGGEN-1 105,37 - 111,94 m
KODAK Color Control Patches
KODAK Gray Scale
108.66
111.94


GEUS RØDRYGGEN -1 105,37 - 111,94 m
KODAK Color Control Patches
Blue
Cyan
Green
Yellow
Red
Magenta
White
3/Color
Black
cm
10
20
30
40
50
60
70
80
100
108.66
111.94
KODAK Gray Scale
C
Y
M
A
M
B

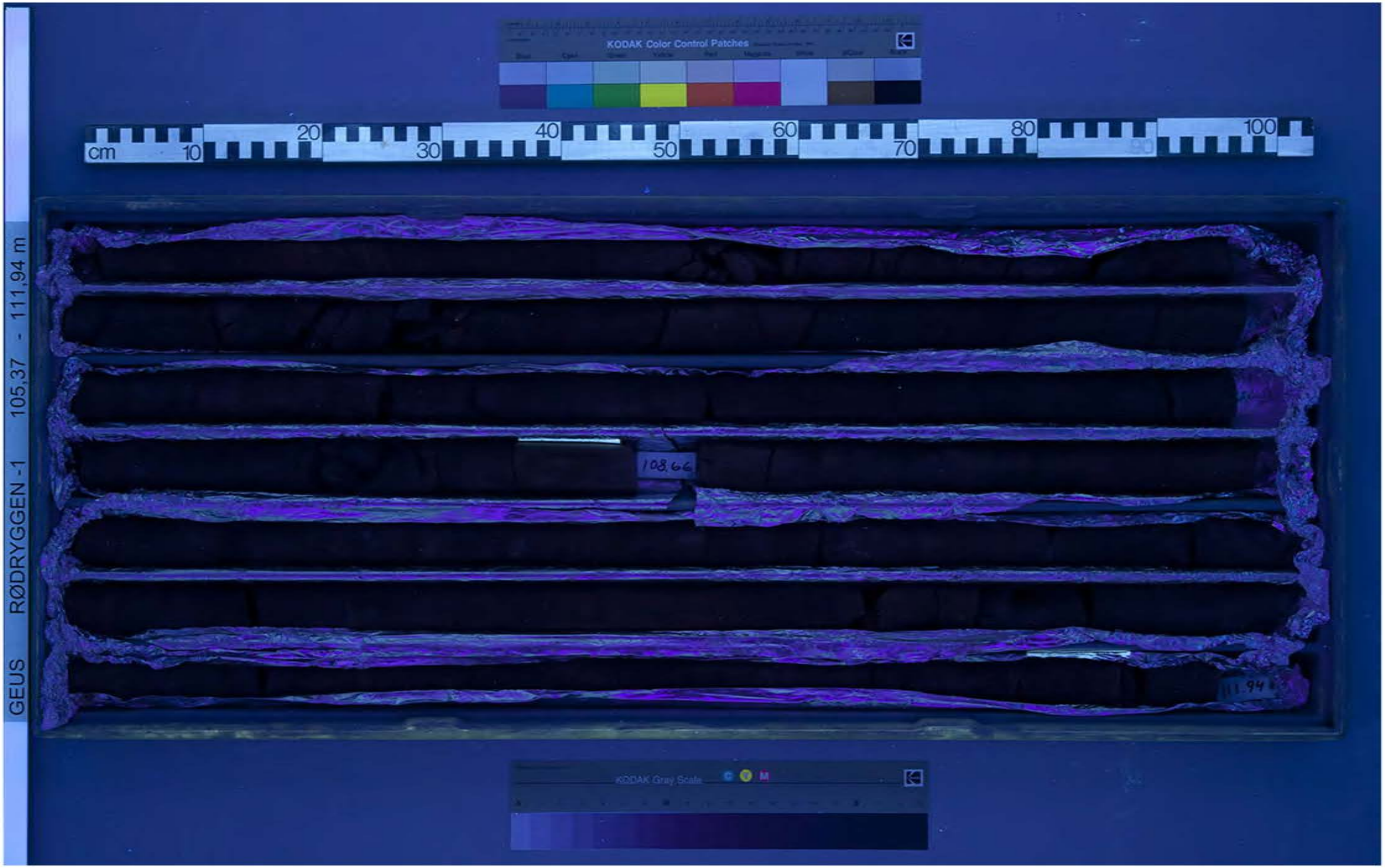

GEUS RØDRYGGEN -1 105,37 - 111,94 m
KODAK Color Control Patches
cm 10 20 30 40 50 60 70 80 90 100
108.66
111.94
KODAK Gray Scale


GEUS RØDRYGGEN-1 99,69 - 105,37 m
KODAK Color Control Patches
Blue
Cyan
Green
Yellow
Red
Magenta
White
3/Color
Black
cm 10 20 30 40 50 60 70 80 100
102.54
105,37
KODAK Gray Scale
A
M
B


GEUS RØDRYGGEN -1 99,69 - 105,37 m
KODAK Color Control Patches
Blue Cyan Green Yellow Red Magenta White 3/Color Black
cm 10 20 30 40 50 60 70 80 100
102.54
105,37
KODAK Gray Scale
C Y M
A M B

GEUS RØDRYGGEN -1 99,69 - 105,37 m

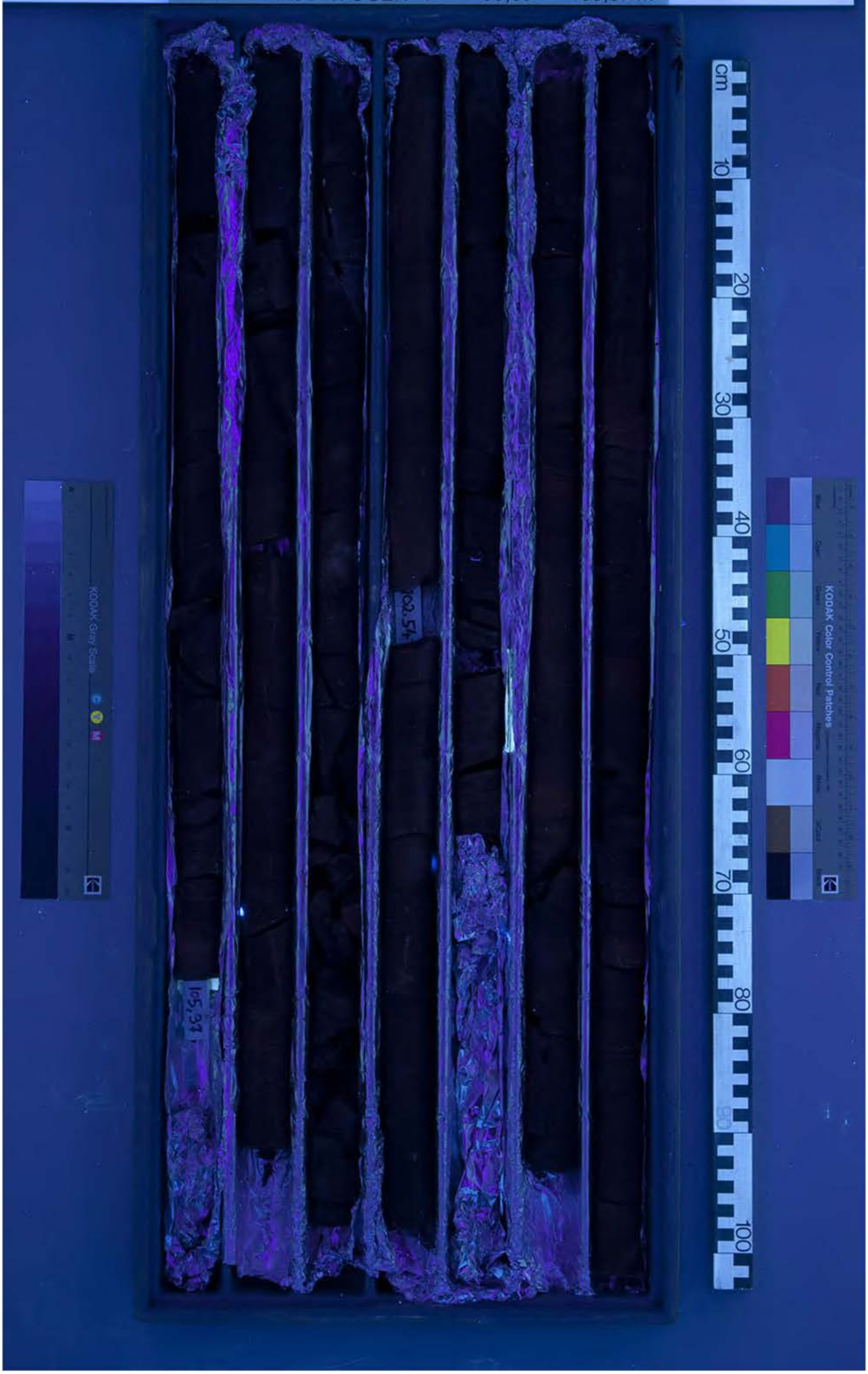


GEUS RØDRYGGEN-1 93,04 - 99,69 m
KODAK Color Control Patches
Blue Cyan Green Yellow Red Magenta White 3/Color Black
cm 10 20 30 40 50 60 70 80 100
99.34
KODAK Gray Scale
C Y M
A M B

GEUS RØDRYGGEN-1 93,04 - 99,69 m
KODAK Color Control Patches
cm 10 20 30 40 50 60 70 80 100
99.34
KODAK Gray Scale

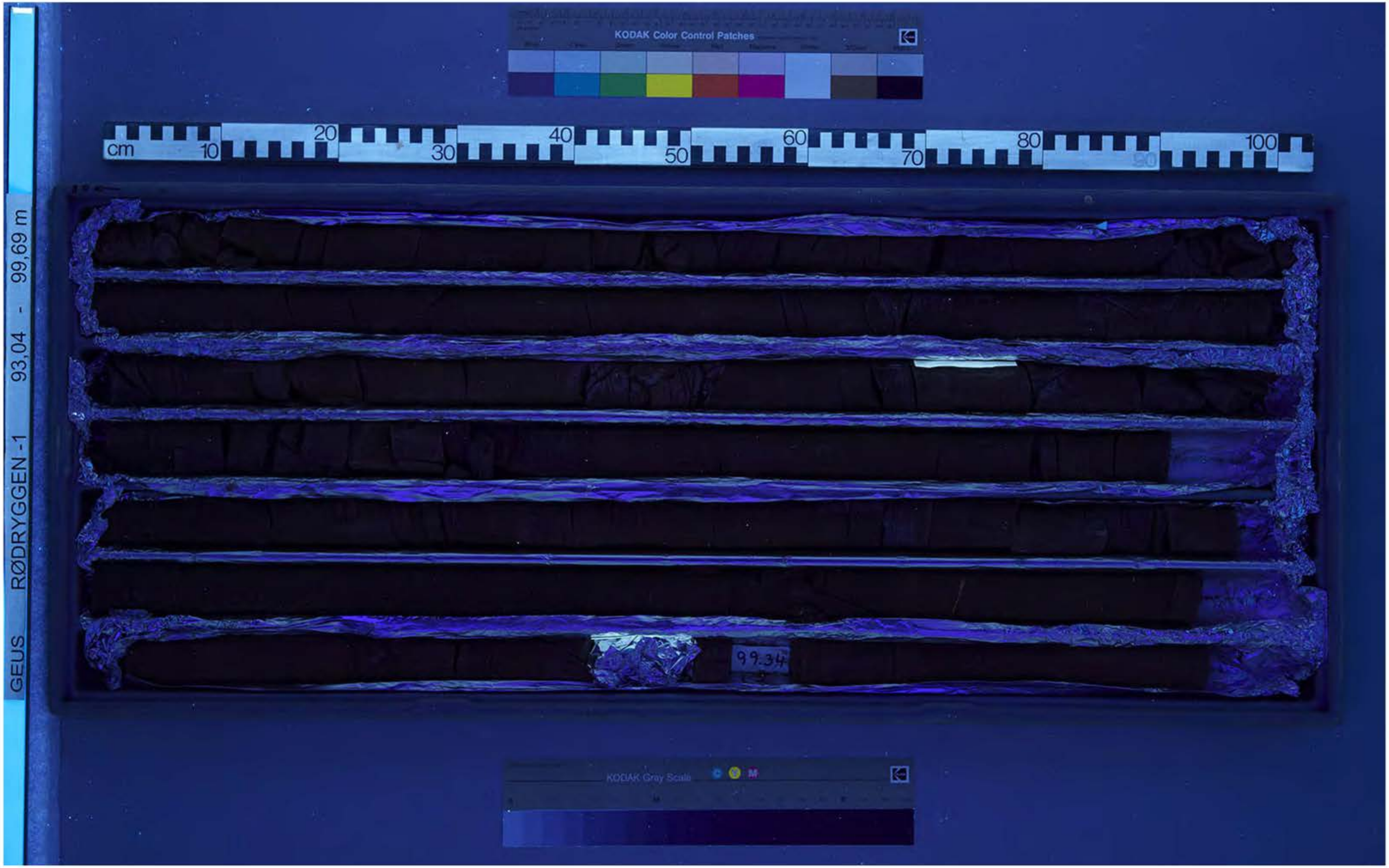
GEUS RØDRYGGEN-1 93,04 - 99,69 m
KODAK Color Control Patches
cm 10 20 30 40 50 60 70 80 90 100
99.34
KODAK Gray Scale


GEUS RØDRYGGEN -1 86,35 - 93,04 m
KODAK Color Control Patches
cm 10 20 30 40 50 60 70 80 100
87,60
90.79
93,04
KODAK Gray Scale


GEUS RØDRYGGEN-1 86,35 - 93,04 m
KODAK Color Control Patches
cm 10 20 30 40 50 60 70 80 100
87,60
90·79
93,04
KODAK Gray Scale

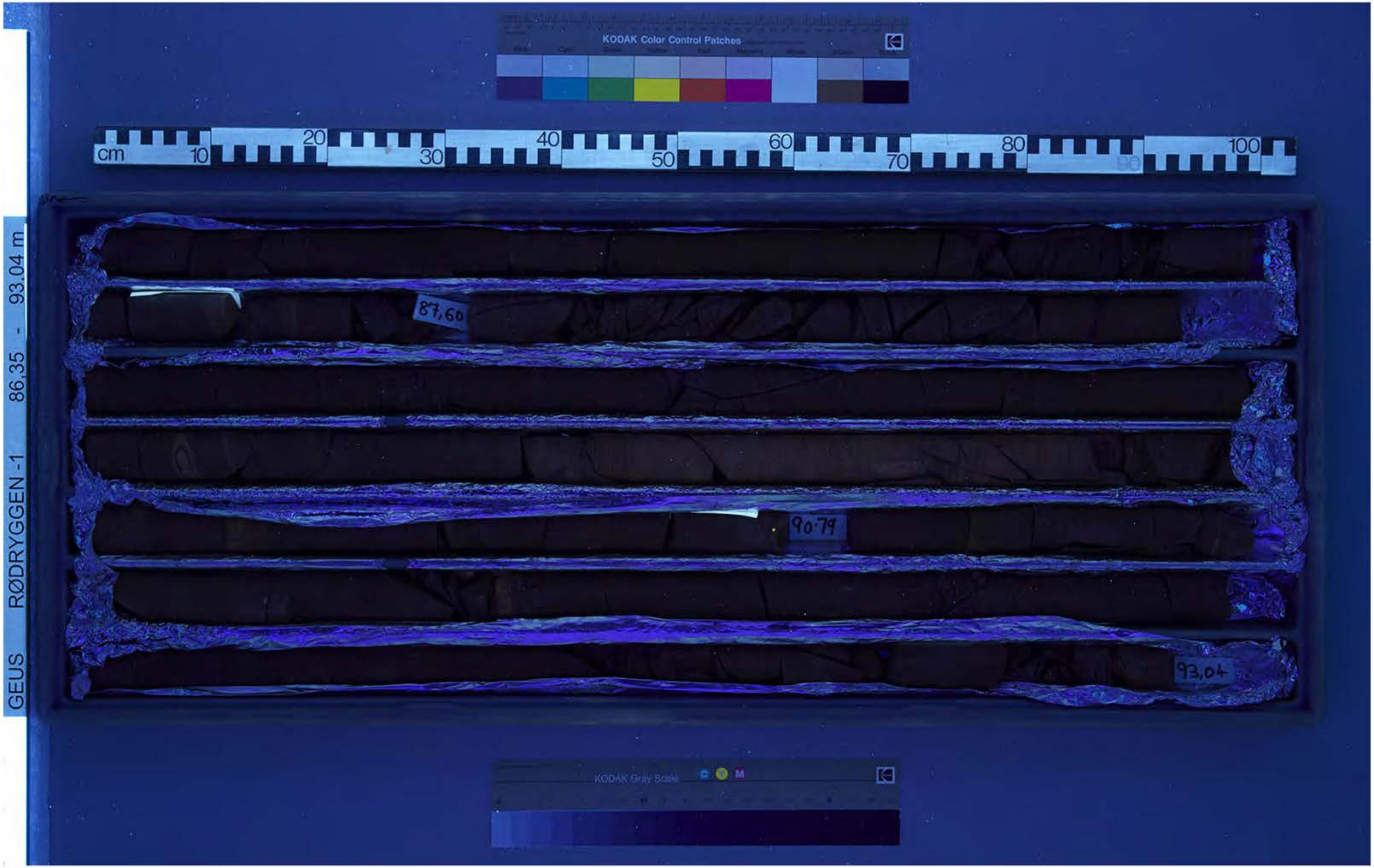
GEUS RØDRYGGEN-1 86,35 - 93,04 m
KODAK Color Control Patches
KODAK Gray Scale
87,60
90·79
93,04


GEUS RØDRYGGEN-1 79,68 - 86,35 m
KODAK Color Control Patches
Blue Cyan Green Yellow Red Magenta White 3/Color Black
cm 10 20 30 40 50 60 70 80 100
80.90
85.89
KODAK Gray Scale
C Y M
A M B


GEUS RØDRYGGEN-1 79,68 - 86,35 m
KODAK Color Control Patches
KODAK Gray Scale
80.90
85.89

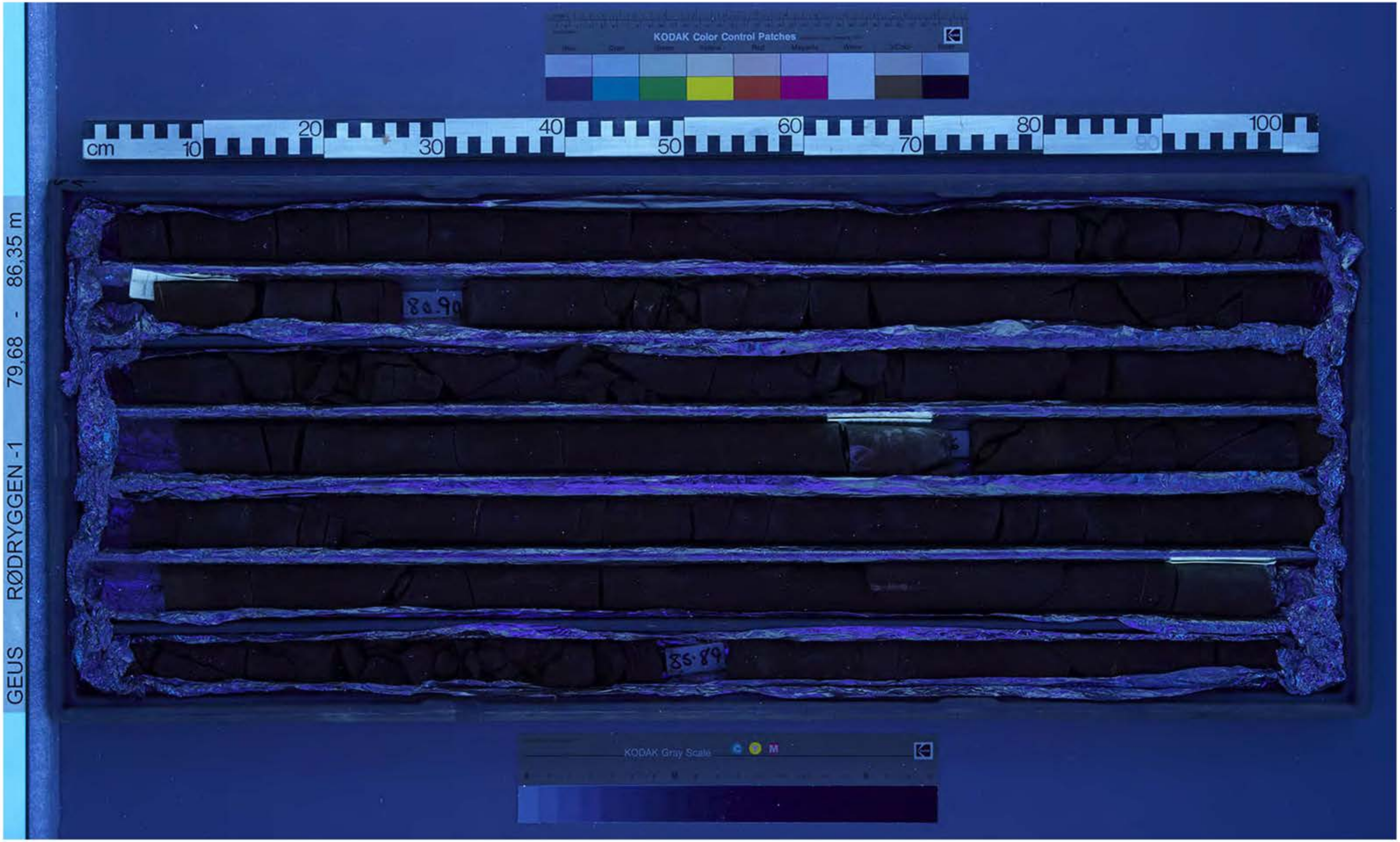
GEUS RØDRYGGEN -1 79,68 - 86,35 m
KODAK Color Control Patches
cm 10 20 30 40 50 60 70 80 90 100
80.90
85.89
KODAK Gray Scale


GEUS RØDRYGGEN-1 72,95 - 79,68 m
KODAK Color Control Patches
Blue Cyan Green Yellow Red Magenta White 3/Color Black
cm 10 20 30 40 50 60 70 80 100
74.90
KODAK Gray Scale
C Y M


GEUS RØDRYGGEN-1 72,95 - 79,68 m
KODAK Color Control Patches
Blue Cyan Green Yellow Red Magenta White 3/Color Black
cm 10 20 30 40 50 60 70 80 100
74.90
KODAK Gray Scale
C Y M
A M B

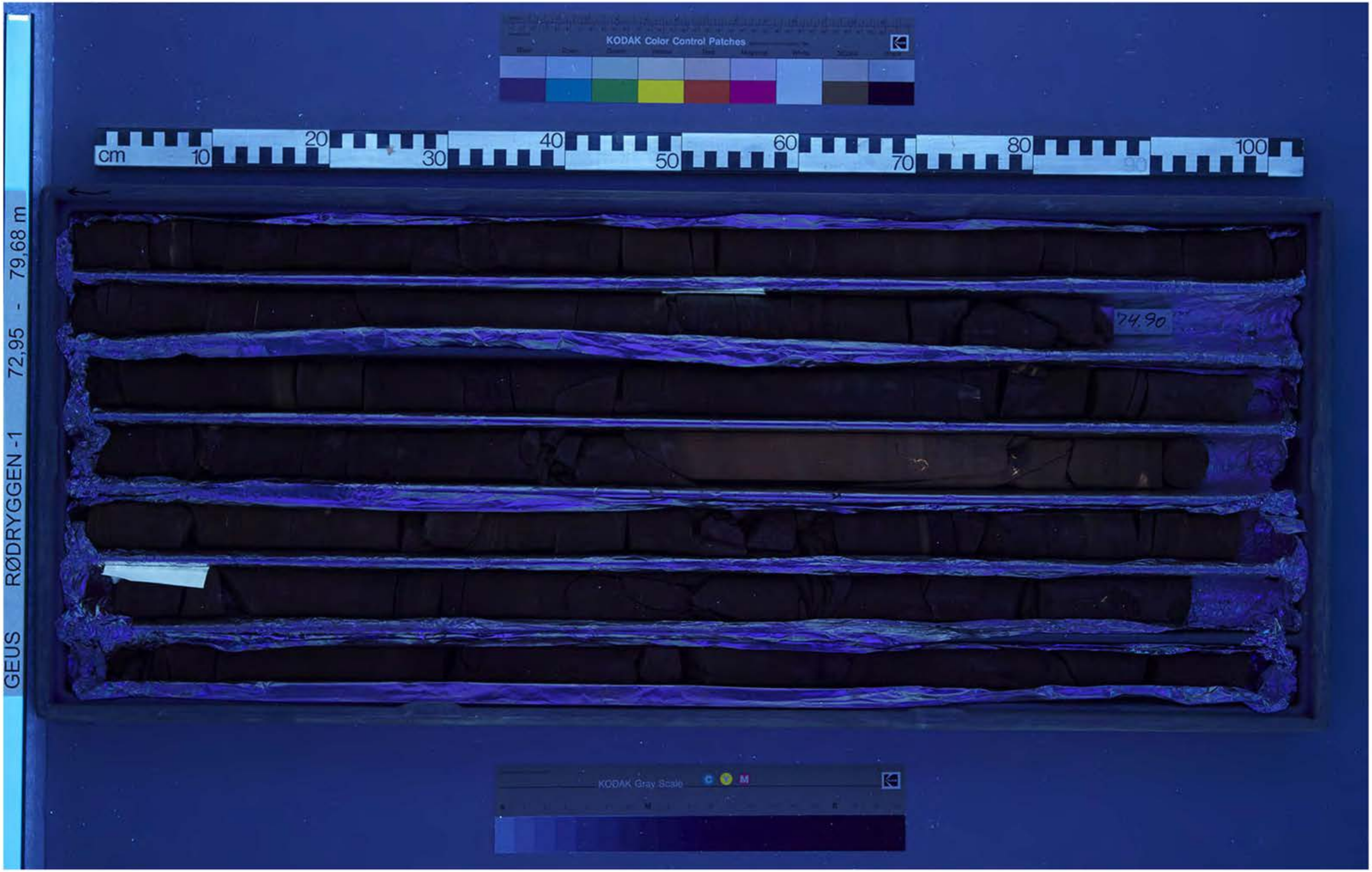
GEUS RØDRYGGEN -1 72,95 - 79,68 m
KODAK Color Control Patches
cm 10 20 30 40 50 60 70 80 90 100
74,90
KODAK Gray Scale


GEUS RØDRYGGEN-1 66,16 - 72,95 m
KODAK Color Control Patches
KODAK Gray Scale
68.07
69.56
71.99


GEUS RØDRYGGEN-1 66,16 - 72,95 m
KODAK Color Control Patches
cm 10 20 30 40 50 60 70 80 100
69.56
KODAK Gray Scale

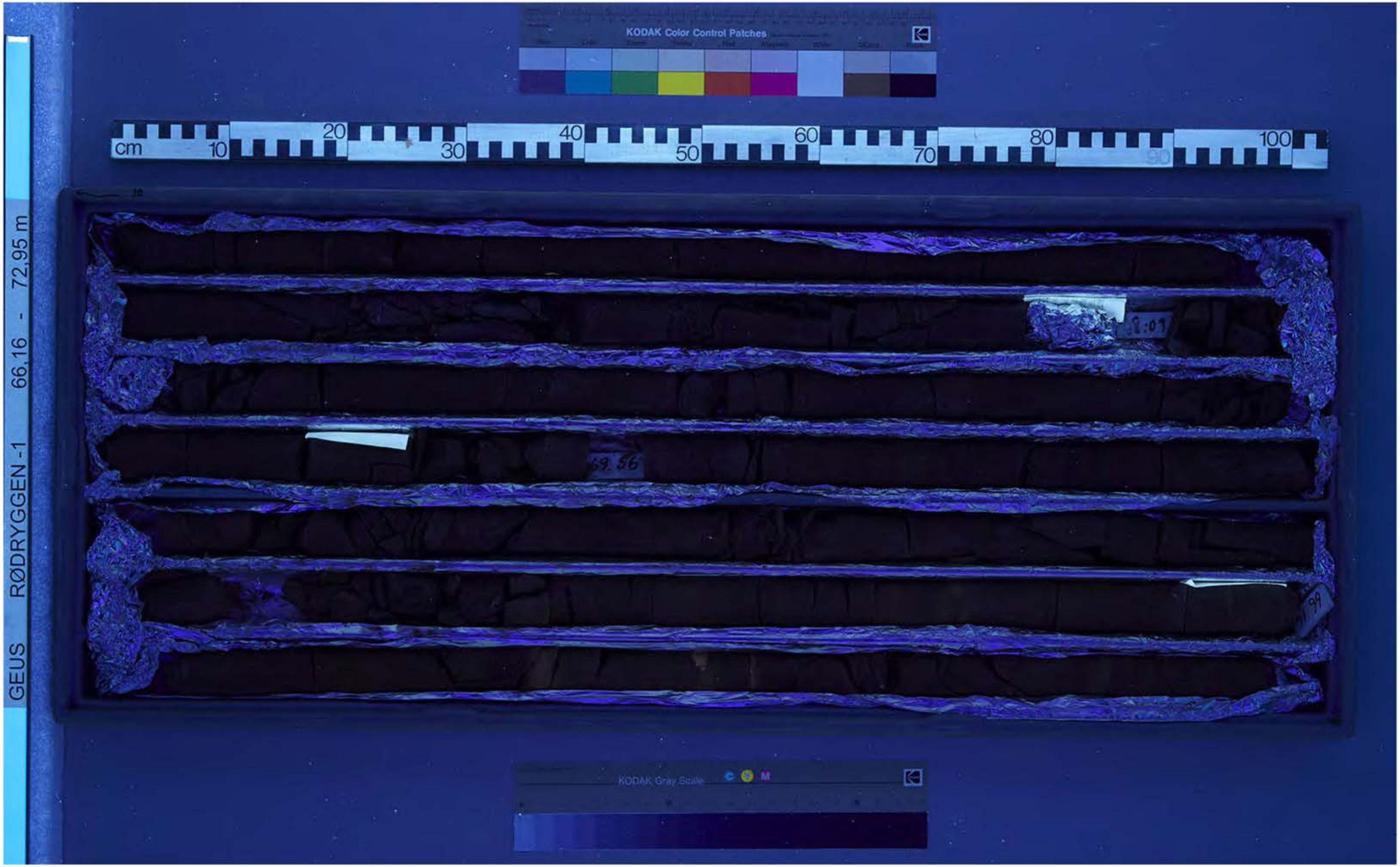
GEUS RØDRYGGEN-1 66,16 - 72,95 m
KODAK Color Control Patches
cm 10 20 30 40 50 60 70 80 90 100
69.56
KODAK Gray Scale

GEUS RØDRYGGEN-1 59,81 - 66,16 m


GEUS RØDRYGGEN-1 59,81 - 66,16 m
KODAK Color Control Patches
Blue
Cyan
Green
Yellow
Red
Magenta
White
3/Color
Black
cm 10 20 30 40 50 60 70 80 100
2,29
65.44
KODAK Gray Scale
C Y M
A
M
B

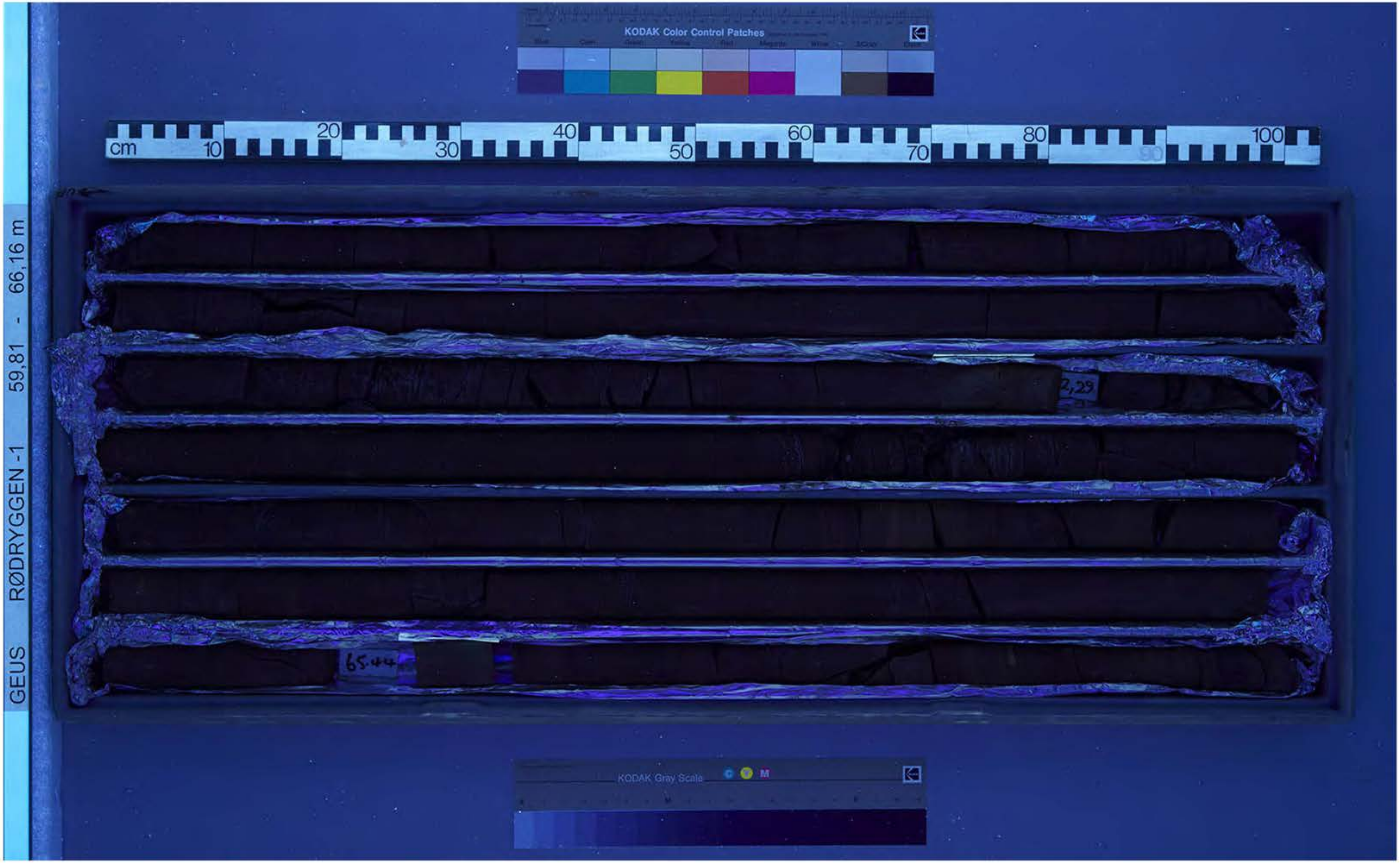
GEUS RØDRYGGEN -1 59,81 - 66,16 m
KODAK Color Control Patches
cm 10 20 30 40 50 60 70 80 90 100
2,29
65.44
KODAK Gray Scale


GEUS RØDRYGGEN-1 53,28 - 59,81 m
KODAK Color Control Patches
cm 10 20 30 40 50 60 70 80 100
59,40
KODAK Gray Scale


GEUS RØDRYGGEN-1 53,28 - 59,81 m
KODAK Color Control Patches
Blue
Cyan
Green
Yellow
Red
Magenta
White
3/Color
Black
cm
10
20
30
40
50
60
70
80
100
59,40
KODAK Gray Scale
C
Y
M
A
M
B

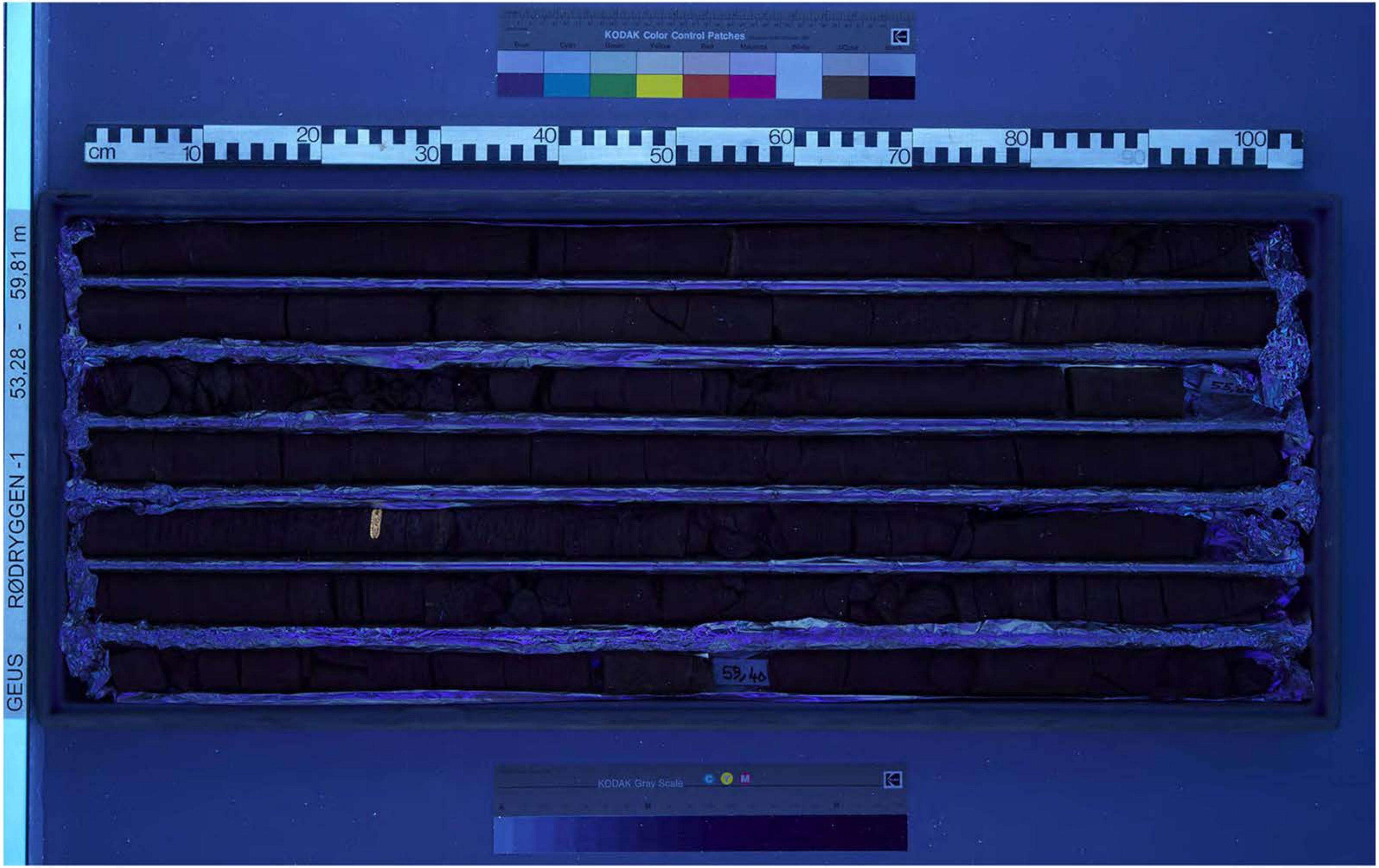
GEUS RØDRYGGEN-1 53,28 - 59,81 m
KODAK Color Control Patches
cm 10 20 30 40 50 60 70 80 90 100
59,40
KODAK Gray Scale


GEUS RØDRYGGEN -1 46,80 - 53,28 m
KODAK Color Control Patches
Blue
Cyan
Green
Yellow
Red
Magenta
White
3/Color
Black
cm
10
20
30
40
50
60
70
80
100
47,0
48,94
52,99
KODAK Gray Scale
C
Y
M
A
M
B

GEUS RØDRYGGEN-1 46,80 - 53,28 m
KODAK Color Control Patches
Blue
Cyan
Green
Yellow
Red
Magenta
White
3/Color
Black
cm 10 20 30 40 50 60 70 80 100
47,0
48,94
52,99
KODAK Gray Scale
C Y M
A M B

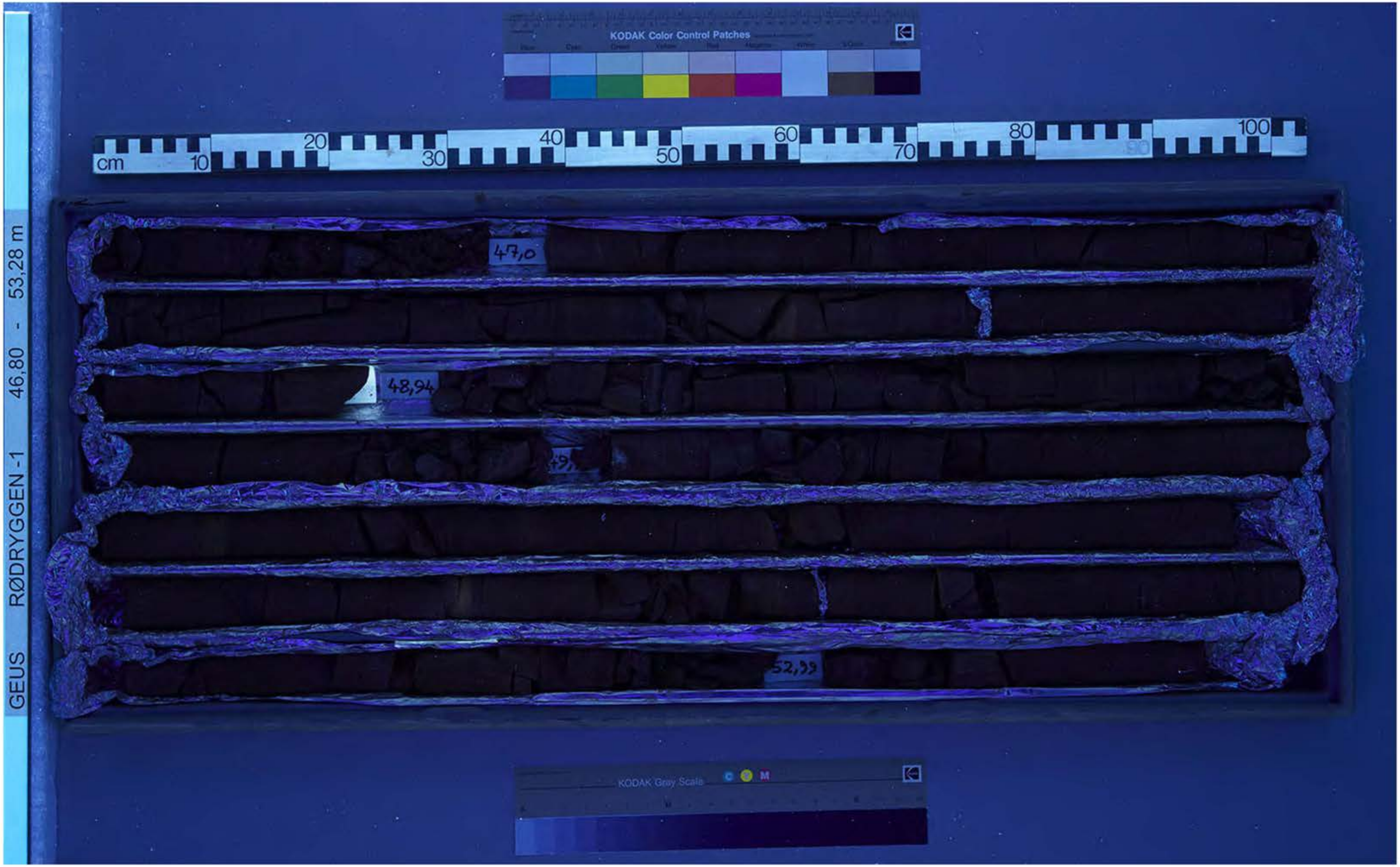
GEUS RØDRYGGEN-1 46,80 - 53,28 m
KODAK Color Control Patches
cm 10 20 30 40 50 60 70 80 90 100
47,0
48,94
52,99
KODAK Gray Scale


GEUS RØDRYGGEN-1 40,56 - 46,80 m
KODAK Color Control Patches
cm 10 20 30 40 50 60 70 80 100
43,50
KODAK Gray Scale


GEUS RØDRYGGEN-1 40,56 - 46,80 m
KODAK Color Control Patches
Blue
Cyan
Green
Yellow
Red
Magenta
White
3/Color
Black
cm
10
20
30
40
50
60
70
80
100
43,50
KODAK Gray Scale
C
Y
M

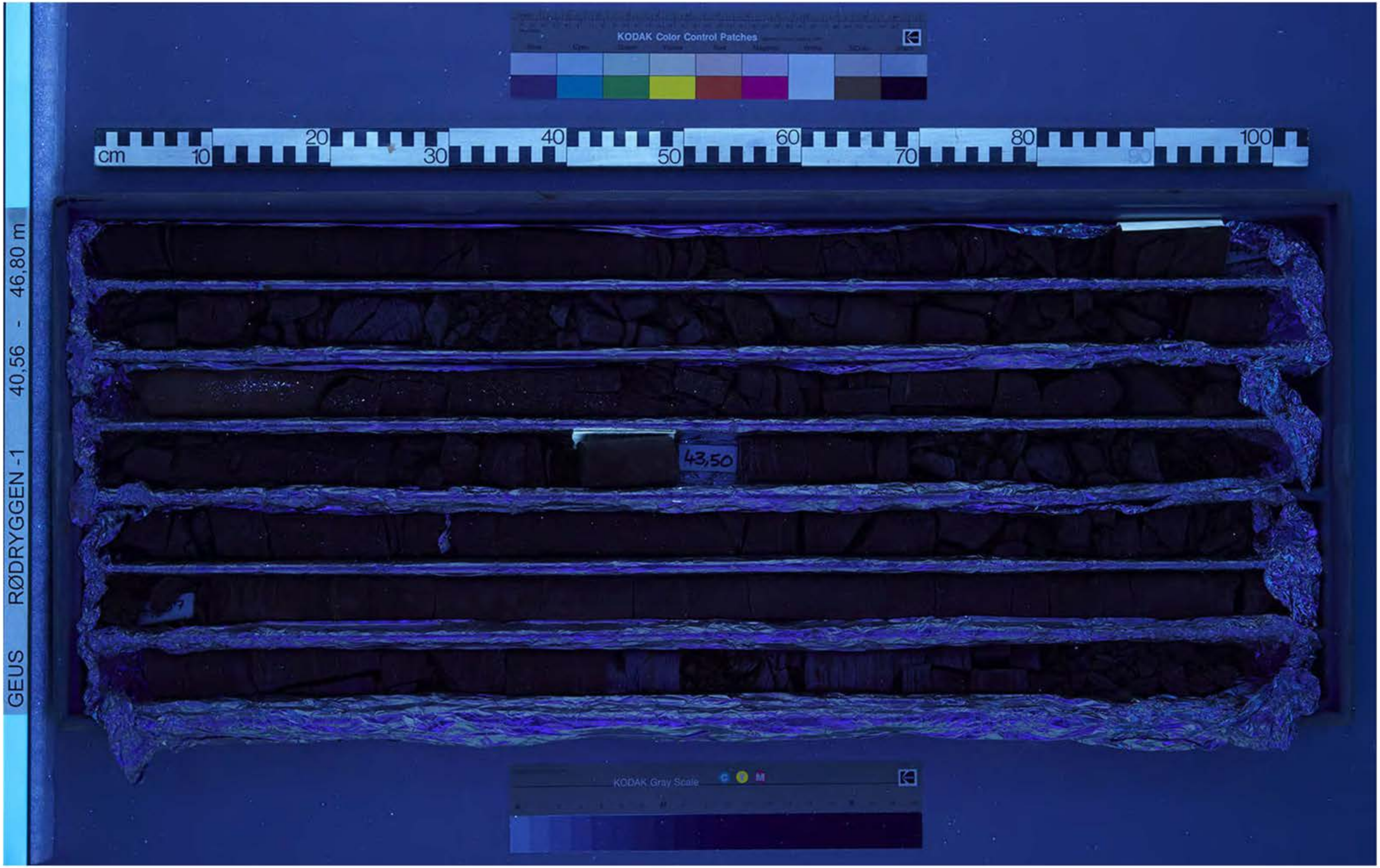
GEUS RØDRYGGEN -1 40,56 - 46,80 m
KODAK Color Control Patches
cm 10 20 30 40 50 60 70 80 90 100
43,50
KODAK Gray Scale


GEUS RØDRYGGEN-1 33,94 - 40,56 m
KODAK Color Control Patches
Blue Cyan Green Yellow Red Magenta White 3/Color Black
cm 10 20 30 40 50 60 70 80 100
KODAK Gray Scale
C Y M
A M B


GEUS RØDRYGGEN-1 33,94 - 40,56 m
KODAK Color Control Patches
Blue
Cyan
Green
Yellow
Red
Magenta
White
3/Color
Black
cm 10 20 30 40 50 60 70 80 100
KODAK Gray Scale
C Y M

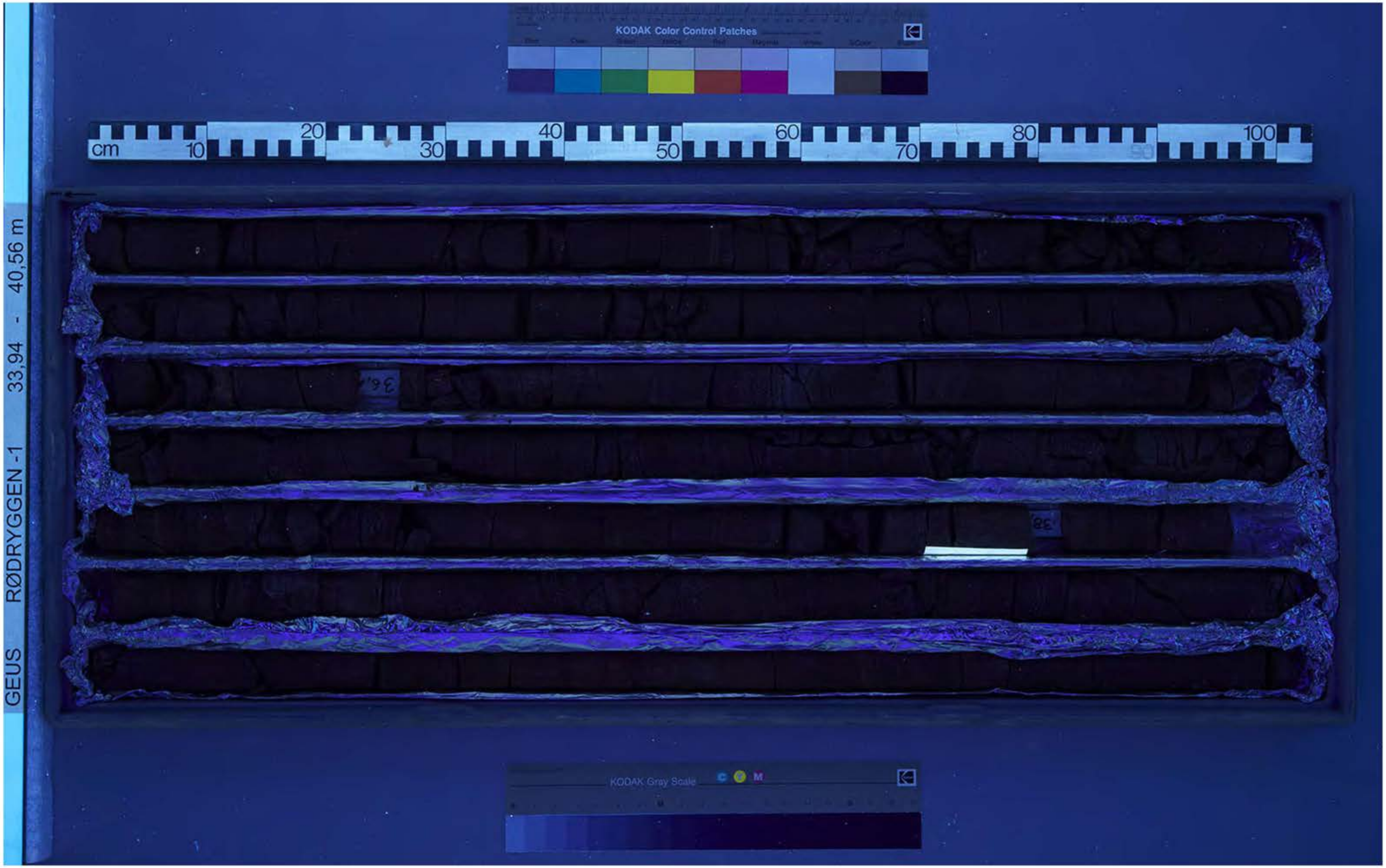
GEUS RØDRYGGEN -1 33,94 - 40,56 m
KODAK Color Control Patches
cm 10 20 30 40 50 60 70 80 100
KODAK Gray Scale
C Y M


GEUS RØDRYGGEN -1 26,94 - 33,94 m
KODAK Color Control Patches
Blue
Cyan
Green
Yellow
Red
Magenta
White
3/Color
Black
cm 10 20 30 40 50 60 70 80 100
30
32,44
33,41
KODAK Gray Scale
A
M
B

GEUS RØDRYGGEN-1 26,94 - 33,94 m

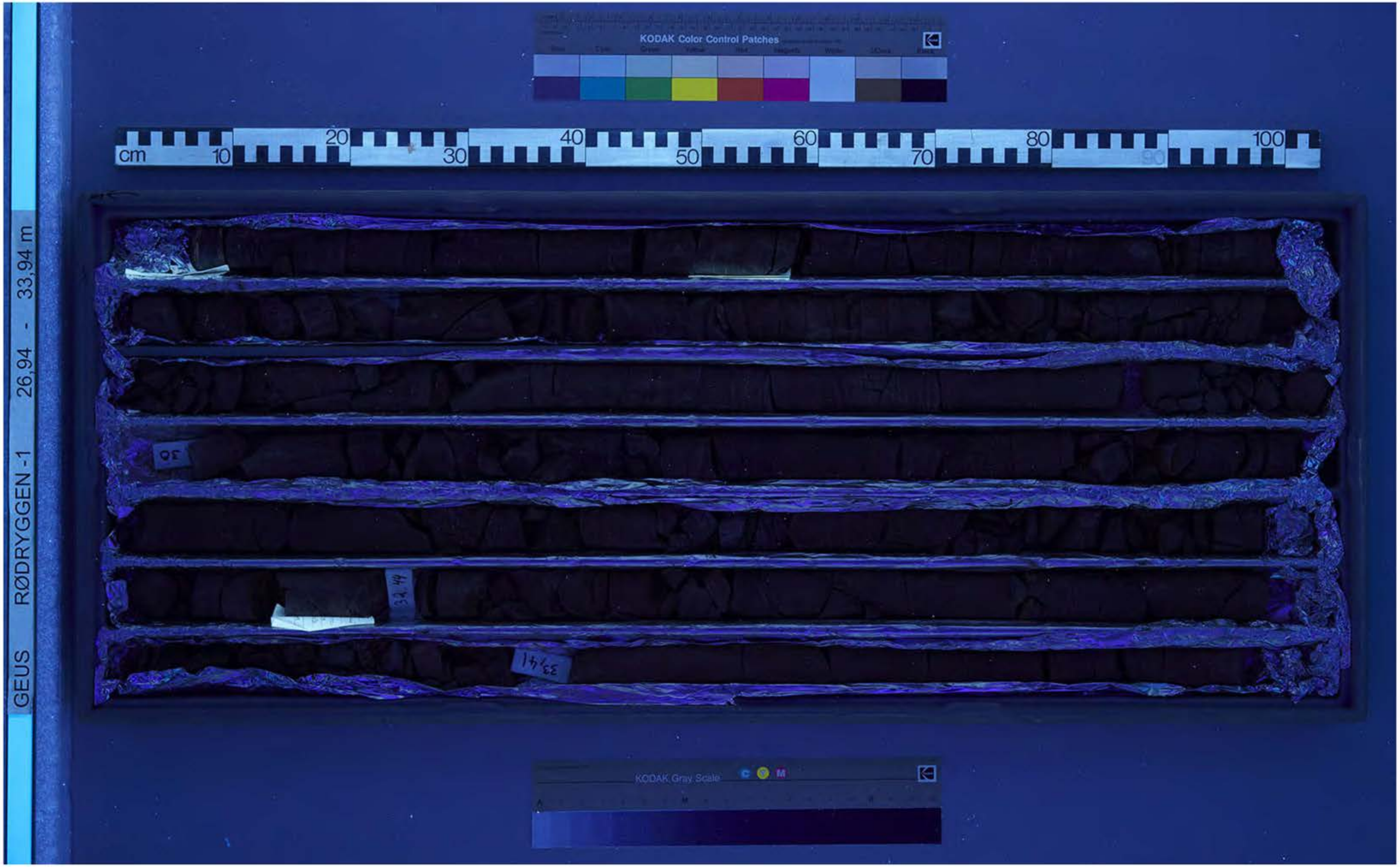
GEUS RØDRYGGEN-1 26,94 - 33,94 m
KODAK Color Control Patches
KODAK Gray Scale
cm
10
20
30
40
50
60
70
80
90
100


GEUS RØDRYGGEN-1 20,44 - 26,94 m
KODAK Color Control Patches
Blue Cyan Green Yellow Red Magenta White 3/Color Black
cm 10 20 30 40 50 60 70 80 100
KODAK Gray Scale
C Y M
A M B

GEUS RØDRYGGEN-1 20,44 - 26,94 m
KODAK Color Control Patches
Blue Cyan Green Yellow Red Magenta White 3/Color Black
cm 10 20 30 40 50 60 70 80 100
KODAK Gray Scale
C Y M
A M B

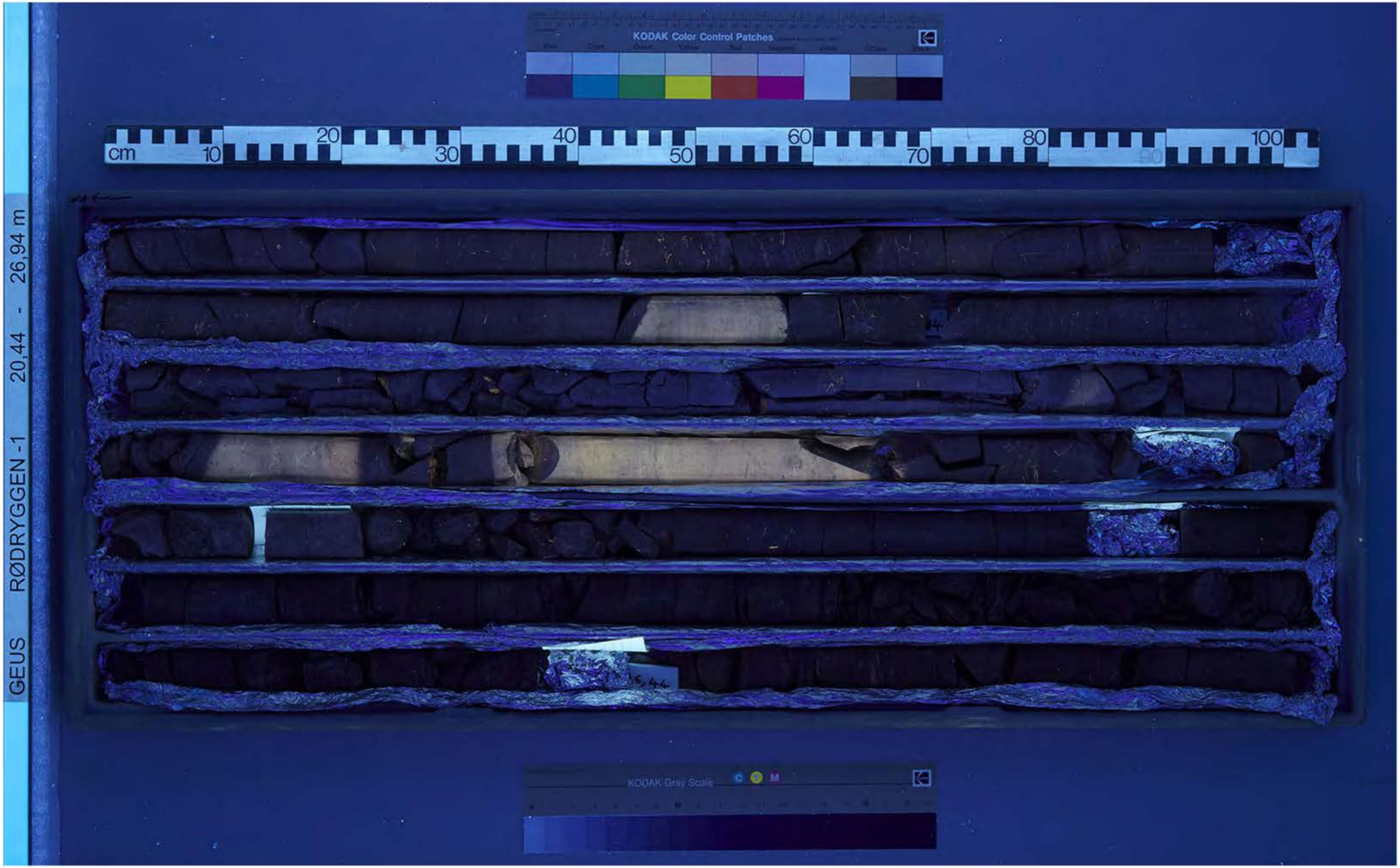
GEUS
RØDRYGGEN -1
20,44 - 26,94 m
KODAK Color Control Patches
KODAK Gray Scale
cm 10 20 30 40 50 60 70 80 90 100

GEUS RØDRYGGEN -1 13,82 - 20,44 m
KODAK Color Control Patches
Blue
Cyan
Green
Yellow
Red
Magenta
White
3/Color
Black
cm 10 20 30 40 50 60 70 80 100
UP
14
KODAK Gray Scale
C
Y
M
A
M
B


GEUS RØDRYGGEN -1 13,82 - 20,44 m
KODAK Color Control Patches
KODAK Gray Scale

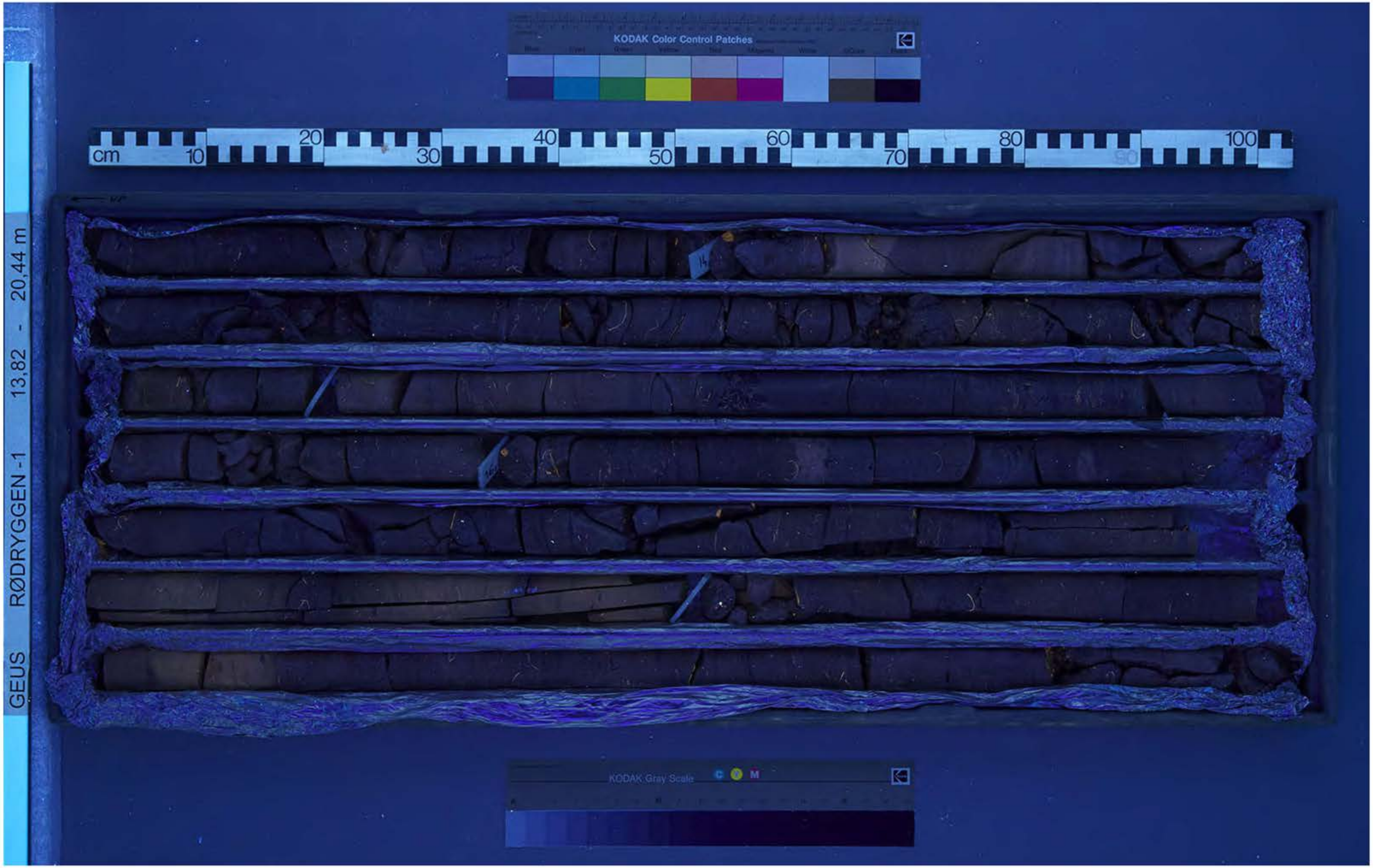
GEUS RØDRYGGEN -1 13,82 - 20,44 m
KODAK Color Control Patches
cm 10 20 30 40 50 60 70 80 90 100
KODAK Gray Scale
C Y M


GEUS RØDRYGGEN-1 7,30 - 13,82 m
KODAK Color Control Patches
Blue Cyan Green Yellow Red Magenta White 3/Color Black
cm 10 20 30 40 50 60 70 80 100
8.32
9.82
KODAK Gray Scale
C Y M
A M B


GEUS RØDRYGGEN-1 7.30 - 13,82 m
KODAK Color Control Patches
Blue
Cyan
Green
Yellow
Red
Magenta
White
3/Color
Black
cm 10 20 30 40 50 60 70 80 100
8.32
9.82
KODAK Gray Scale
C Y M
A M B

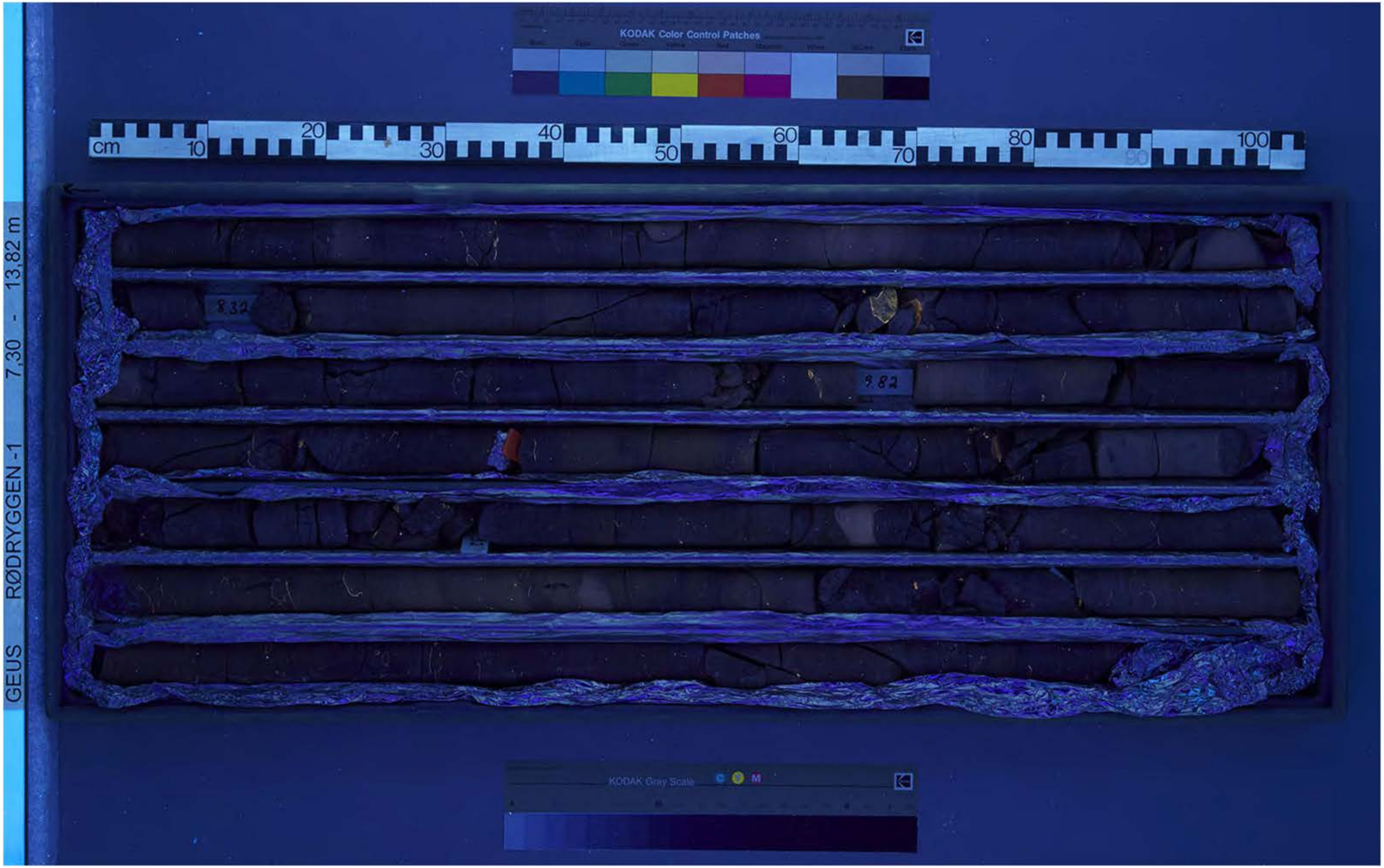
GEUS RØDRYGGEN-1 7,30 - 13,82 m
KODAK Color Control Patches
cm 10 20 30 40 50 60 70 80 90 100
8.32
9.82
KODAK Gray Scale


GEUS RØDRYGGEN-1 0,00 - 7,30 m
KODAK Color Control Patches
KODAK Gray Scale
TOP BORING
0.82
2.32
3.82
5.32
6.82


GEUS RØDRYGGEN -1 0,00 - 7,30 m
KODAK Color Control Patches
KODAK Gray Scale
TOP BORING
0.62
2.32
3.82
5.32
6.82

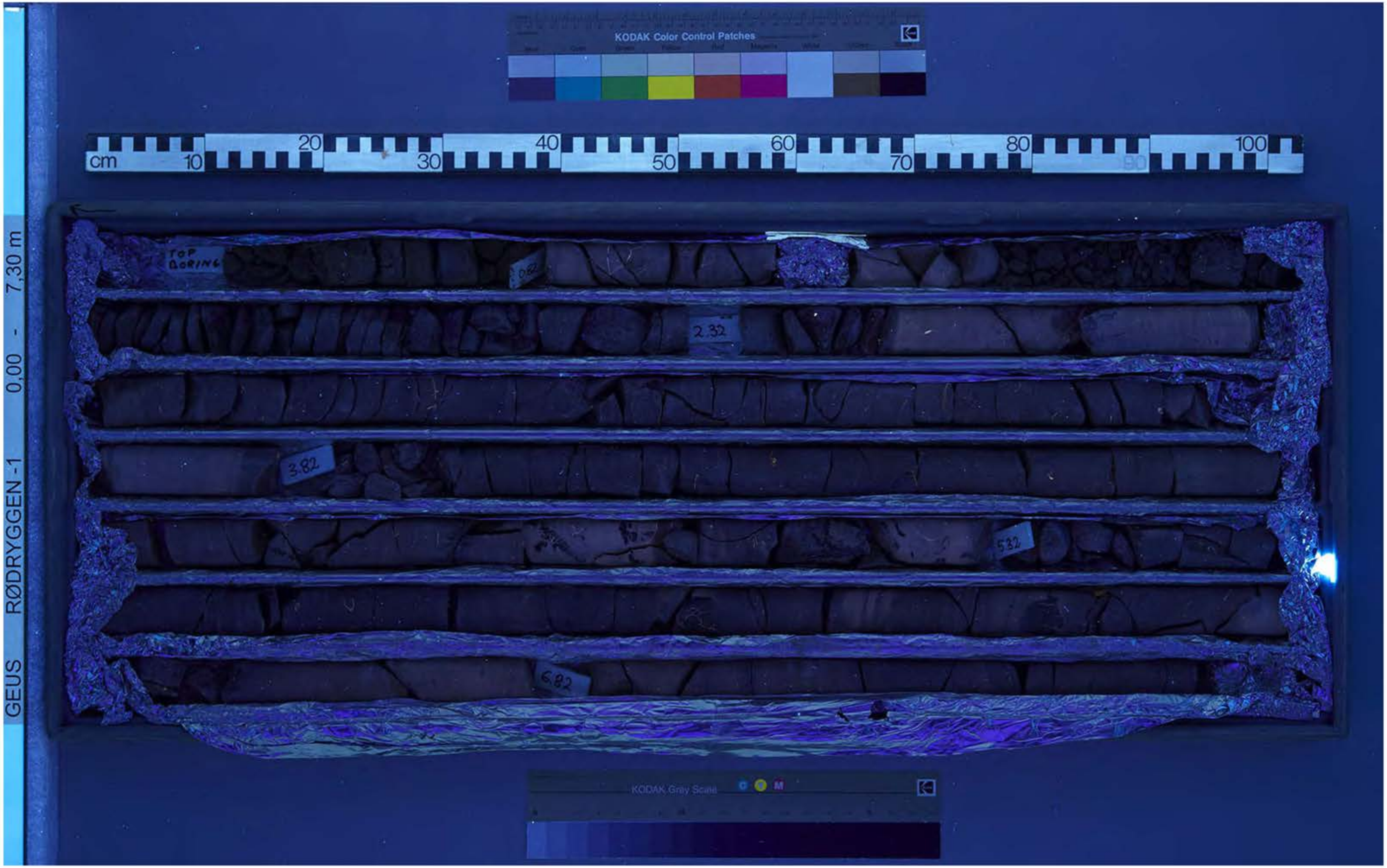
GEUS RØDRYGGEN-1 0.00 - 7,30 m
KODAK Color Control Patches
TOP BORING
0.82
2.32
3.82
5.82
6.82
KODAK Gray Scale

10.2 Thin sections

Contents: Thin section photographs without and with crossed nicoles. Depth and orientation indicated in the slides. Width of the thin sections is 28 mm and the length is 48 mm.

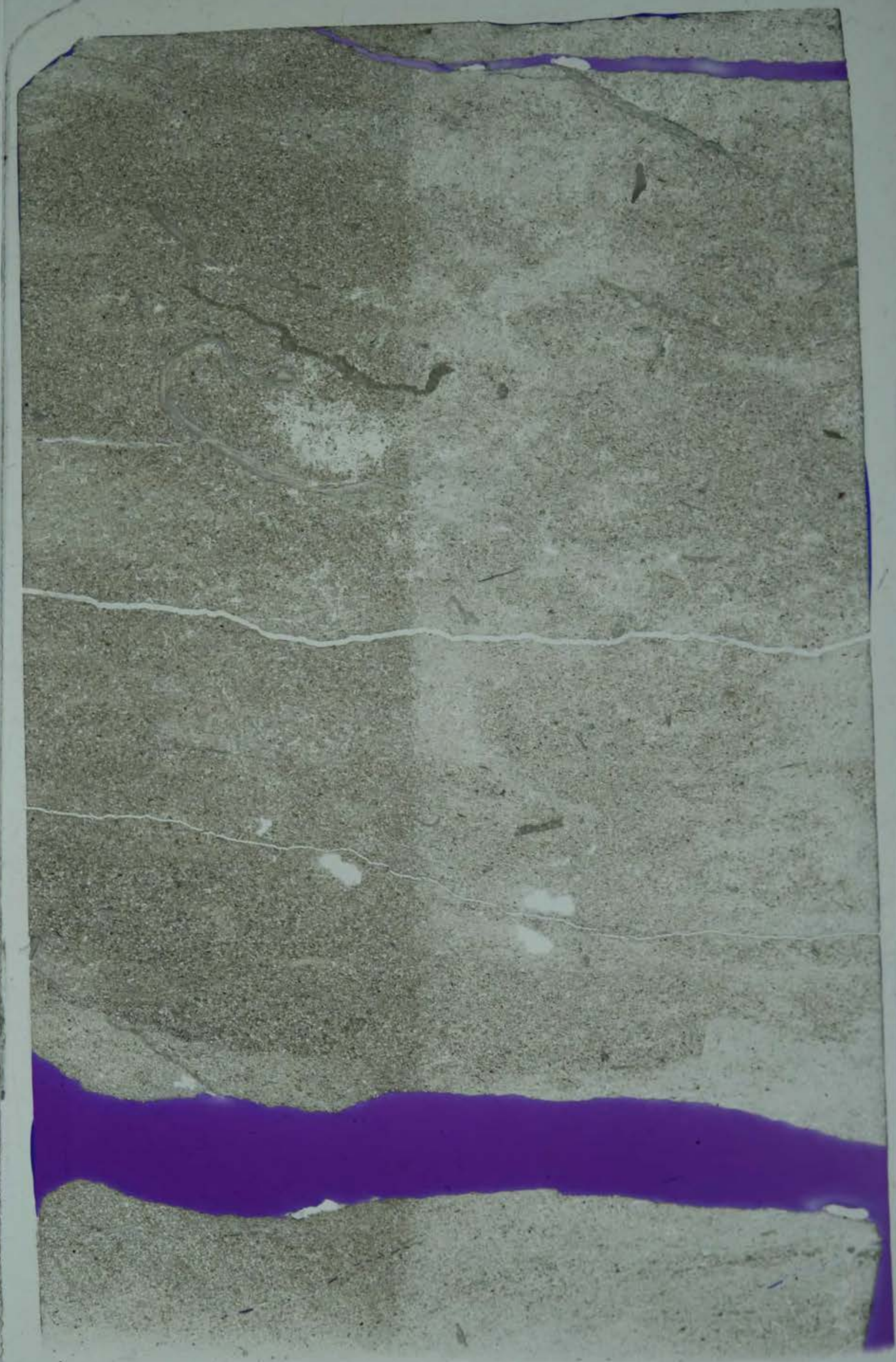

↑ R-013.31

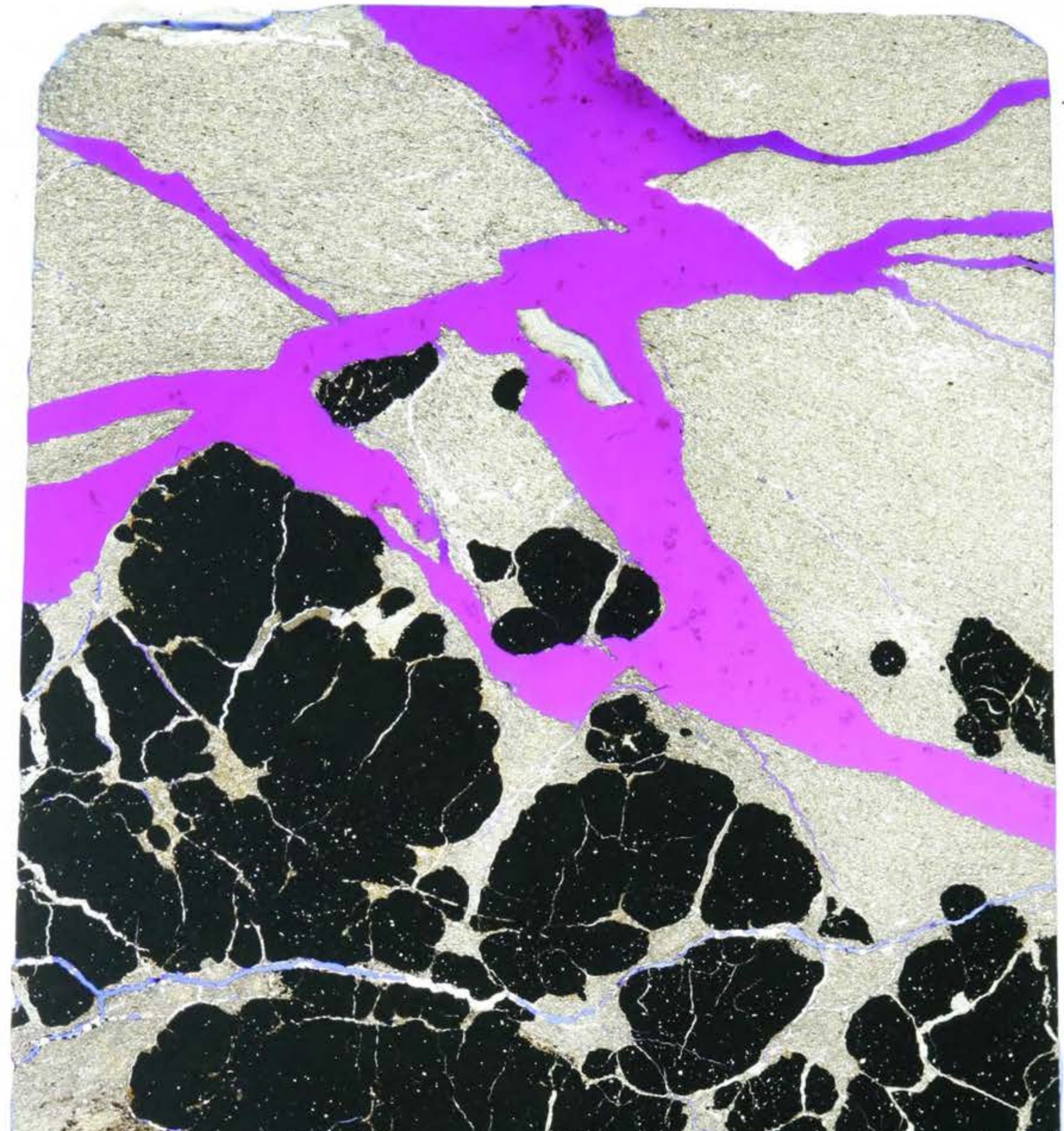

R-016.15


R-016.15

R·022.36 →

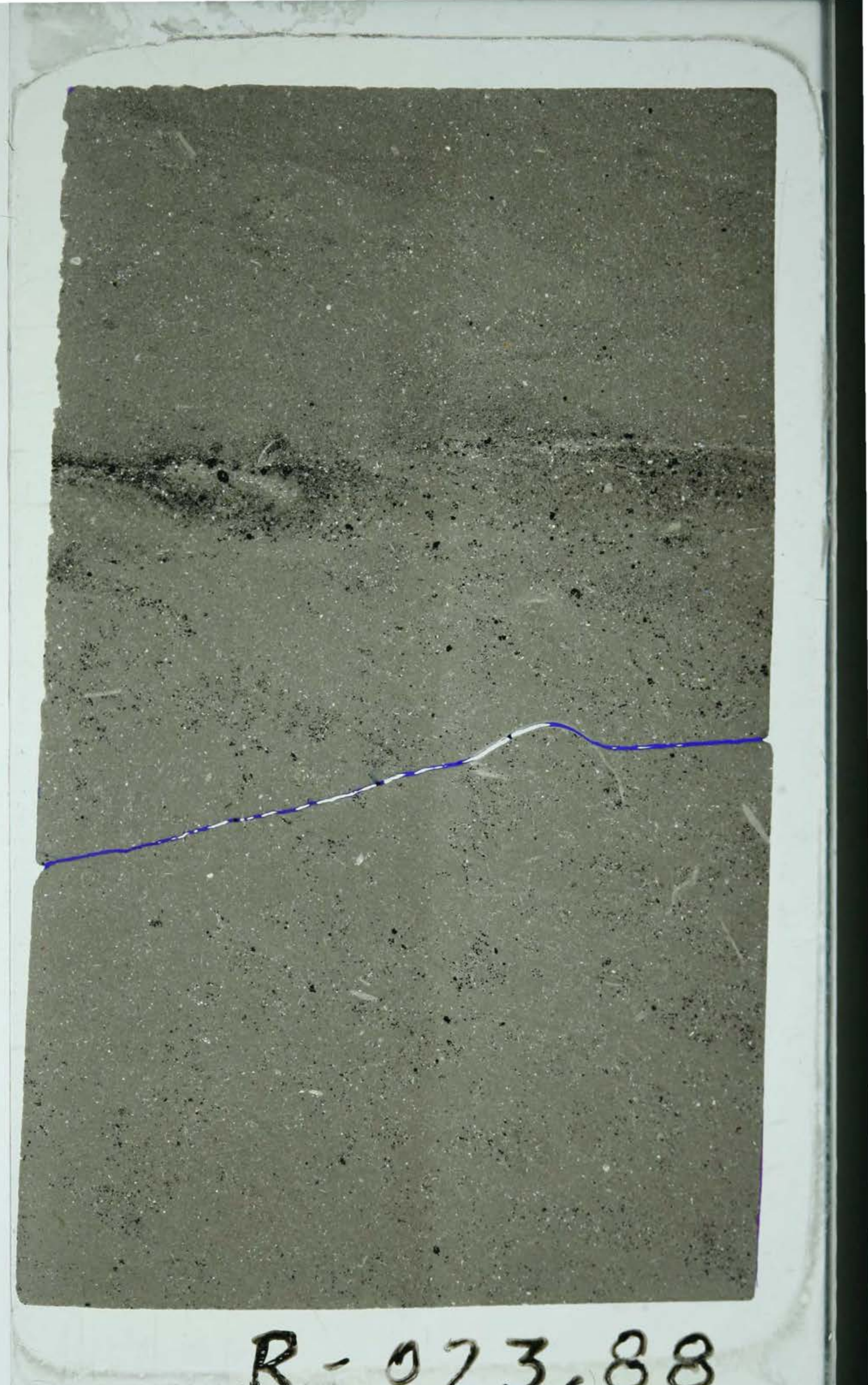
R-023.88


R-022.36

R-026.60

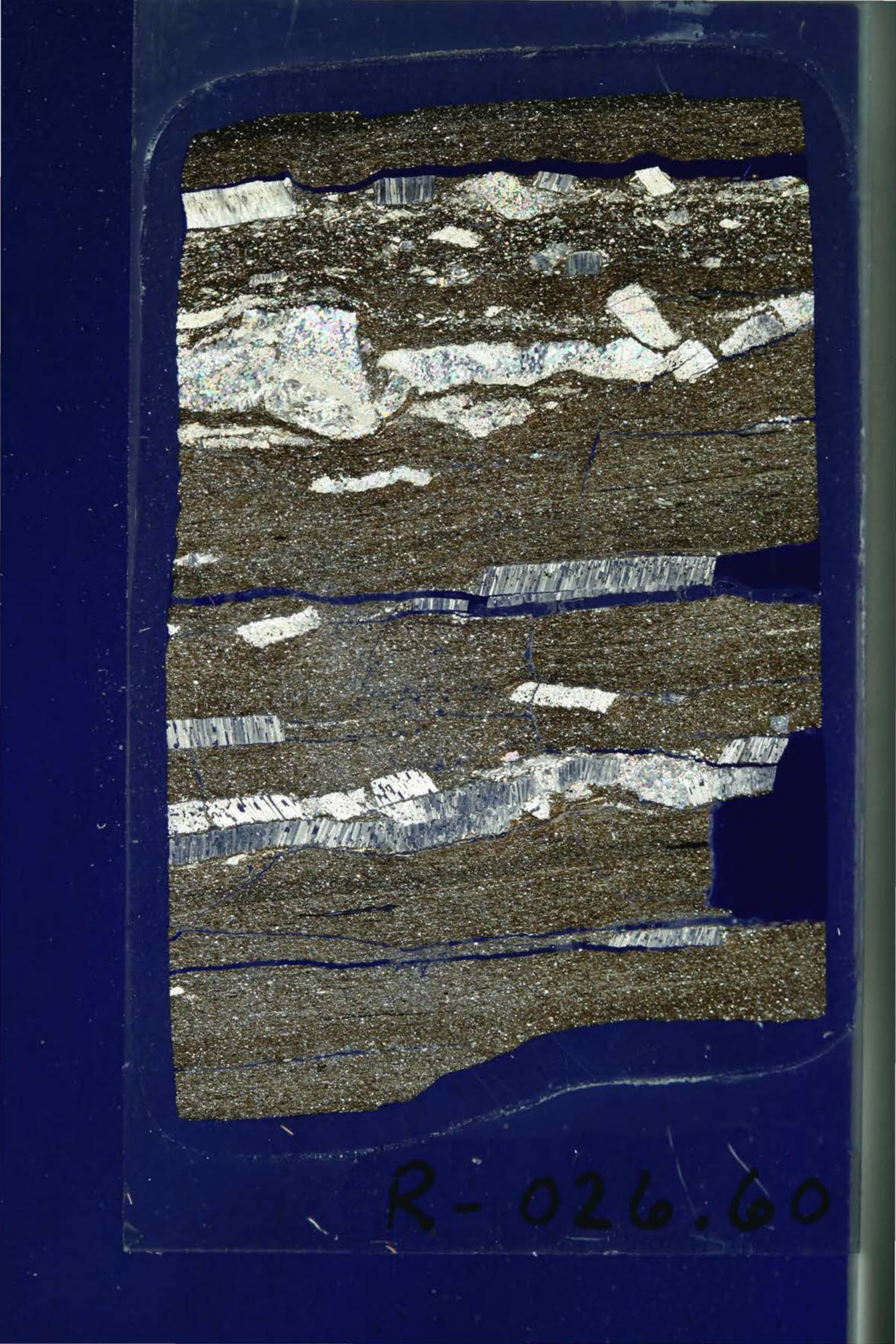
R-026.60

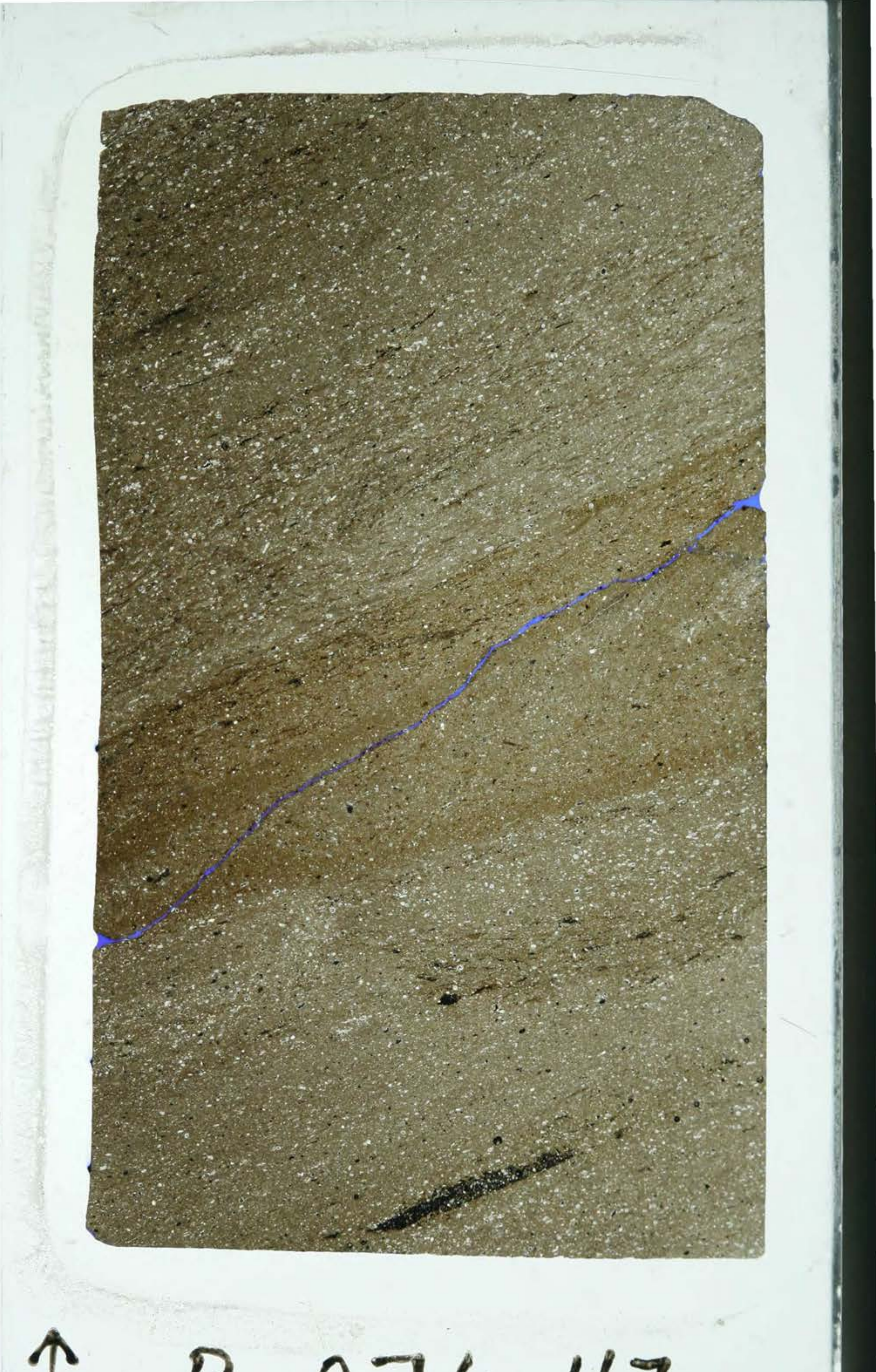

↑ R-076.47

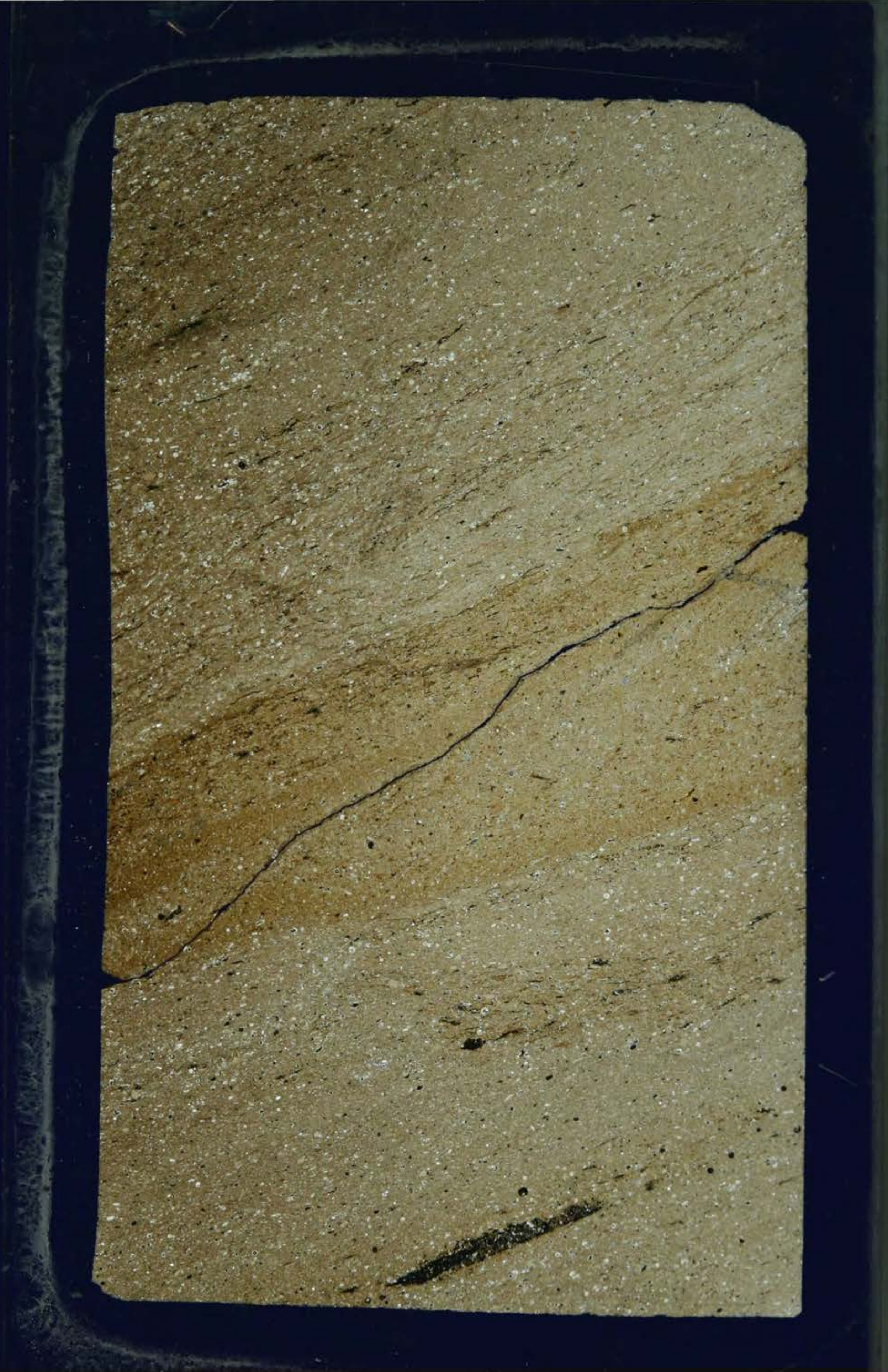


R-089.96

R-089.96


R-173.63


R-173.63

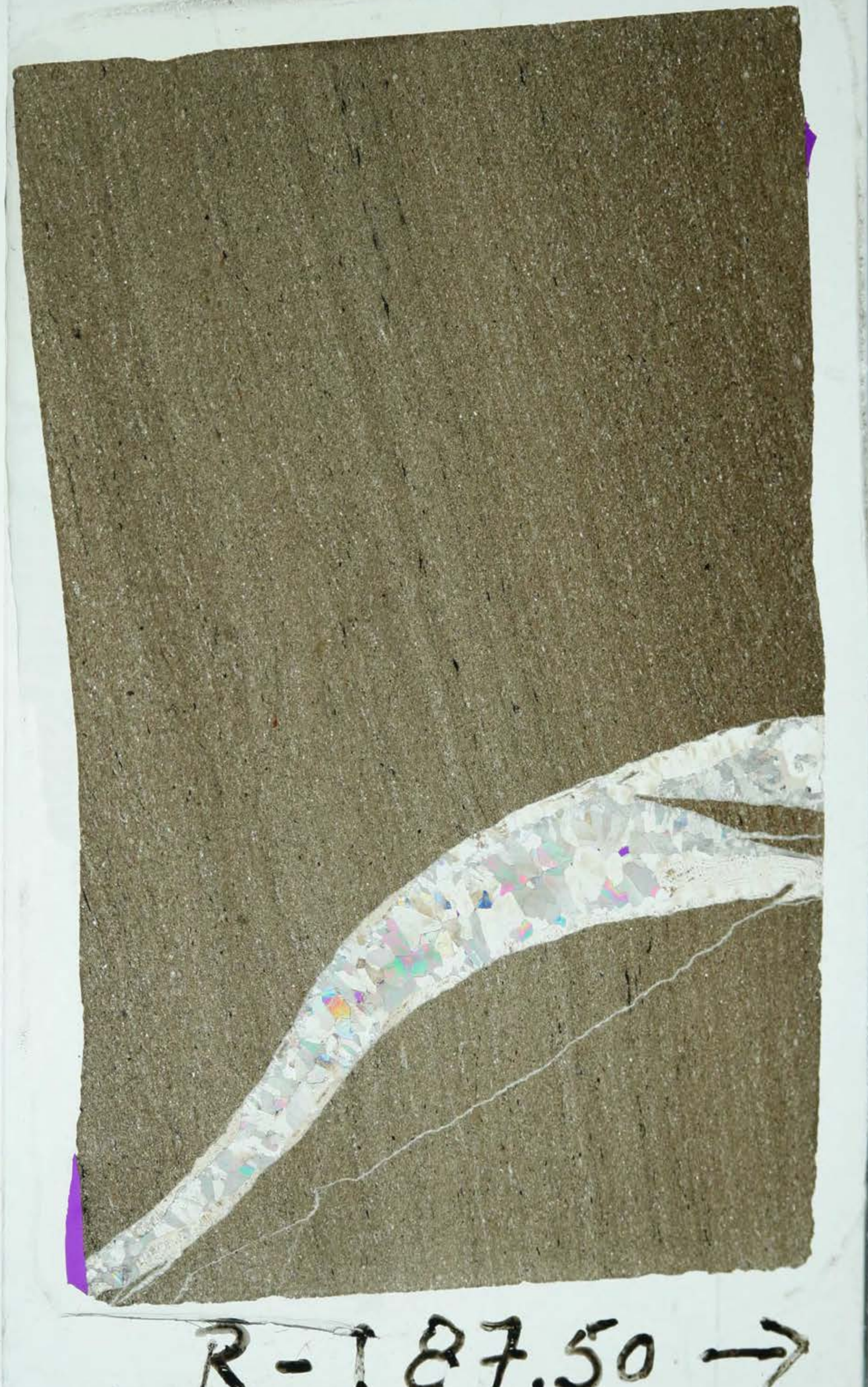

R-187.50 →


R-1 87.50 →


← R-201.81

← R-201.81


R-205.73

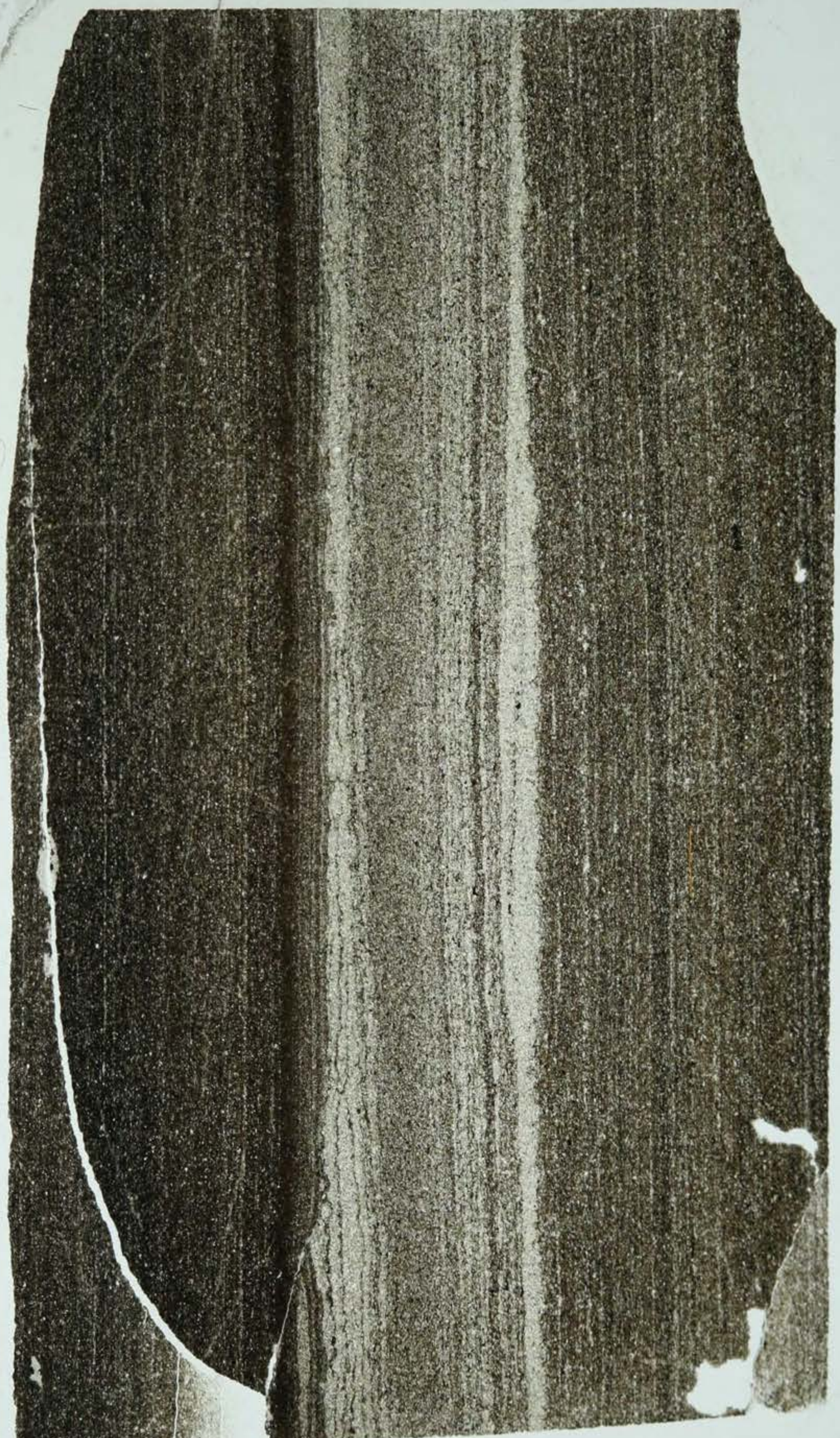

← R-206.76

← R-206.76

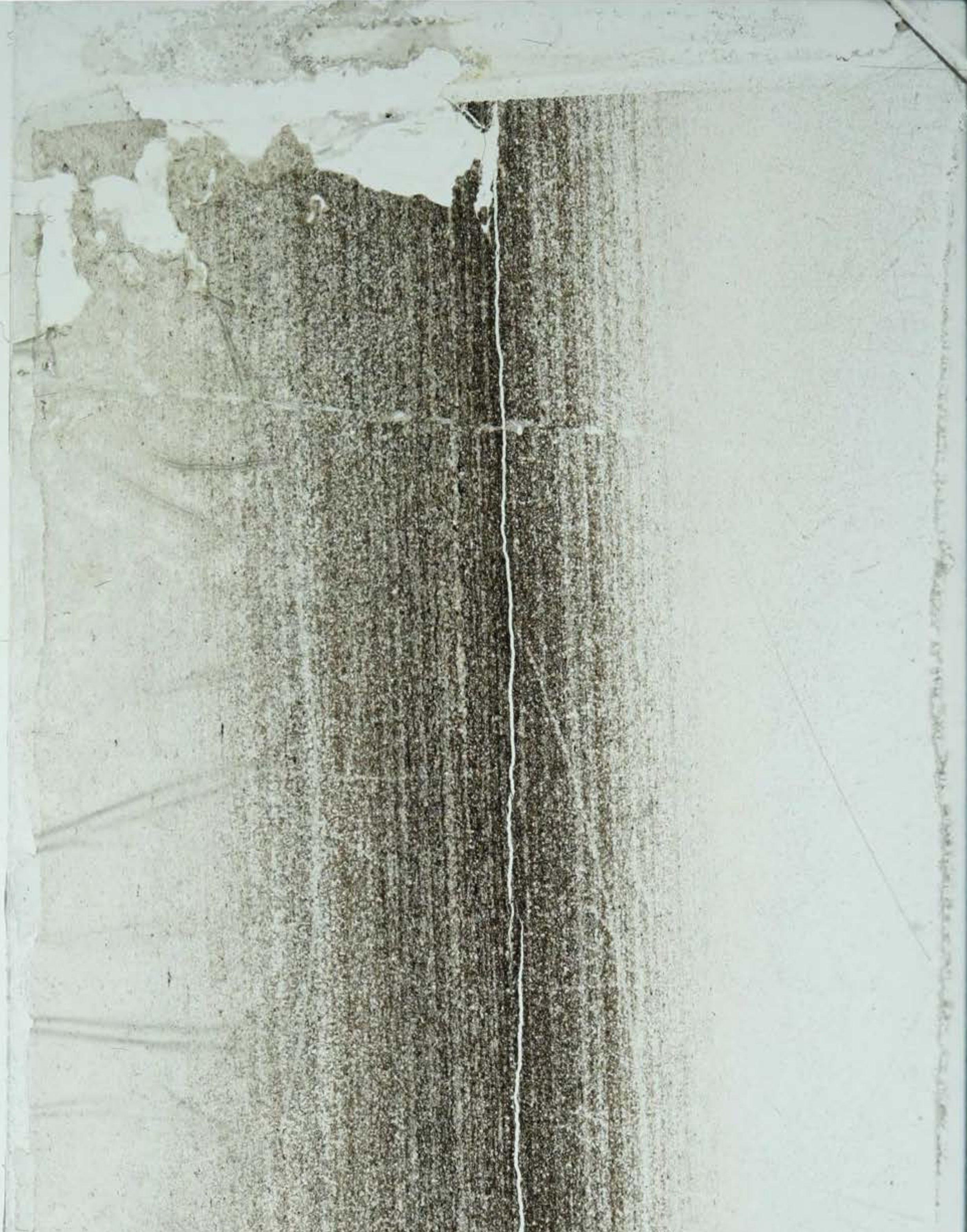

R-231.77 →

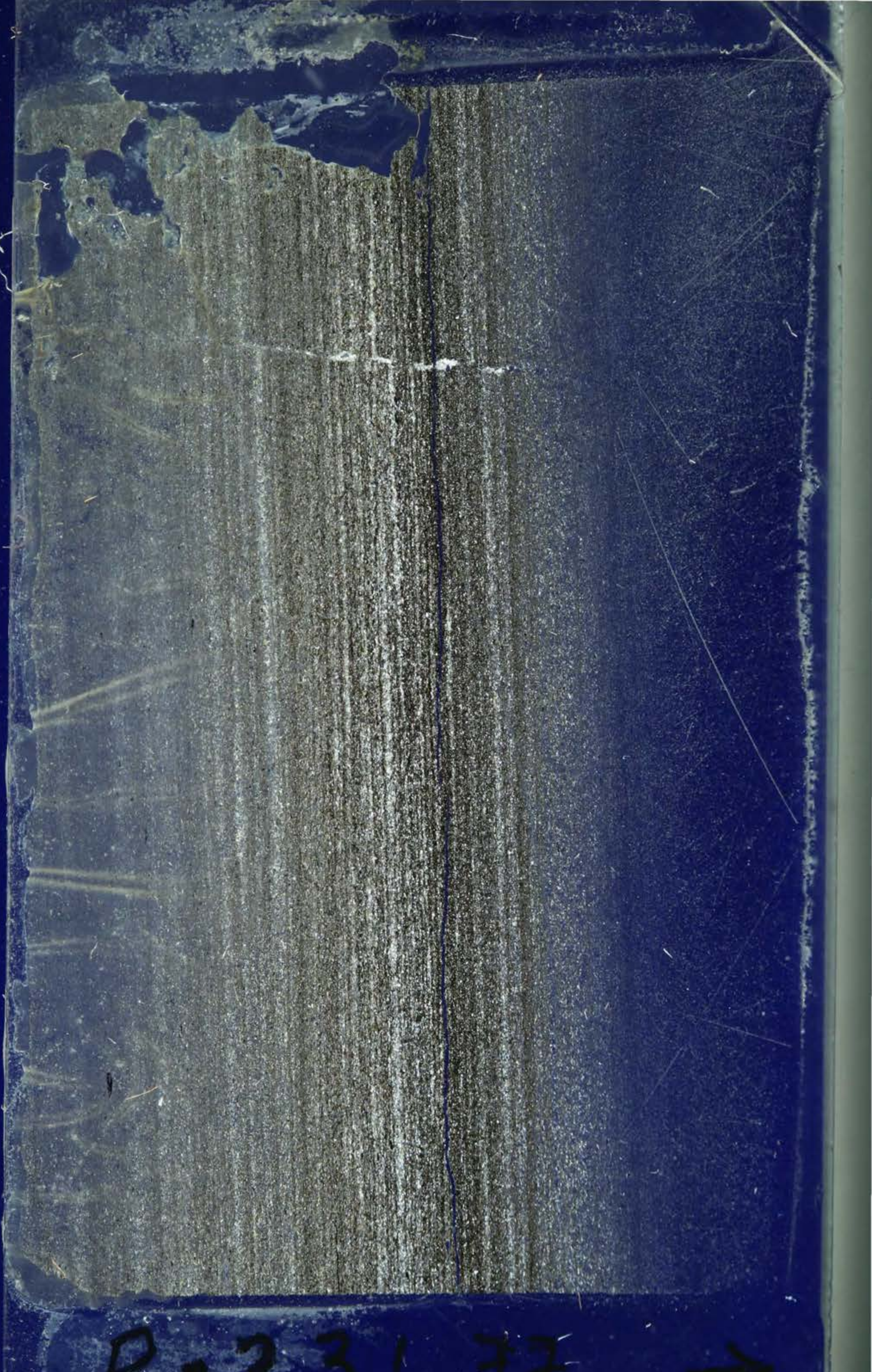
R·231.77

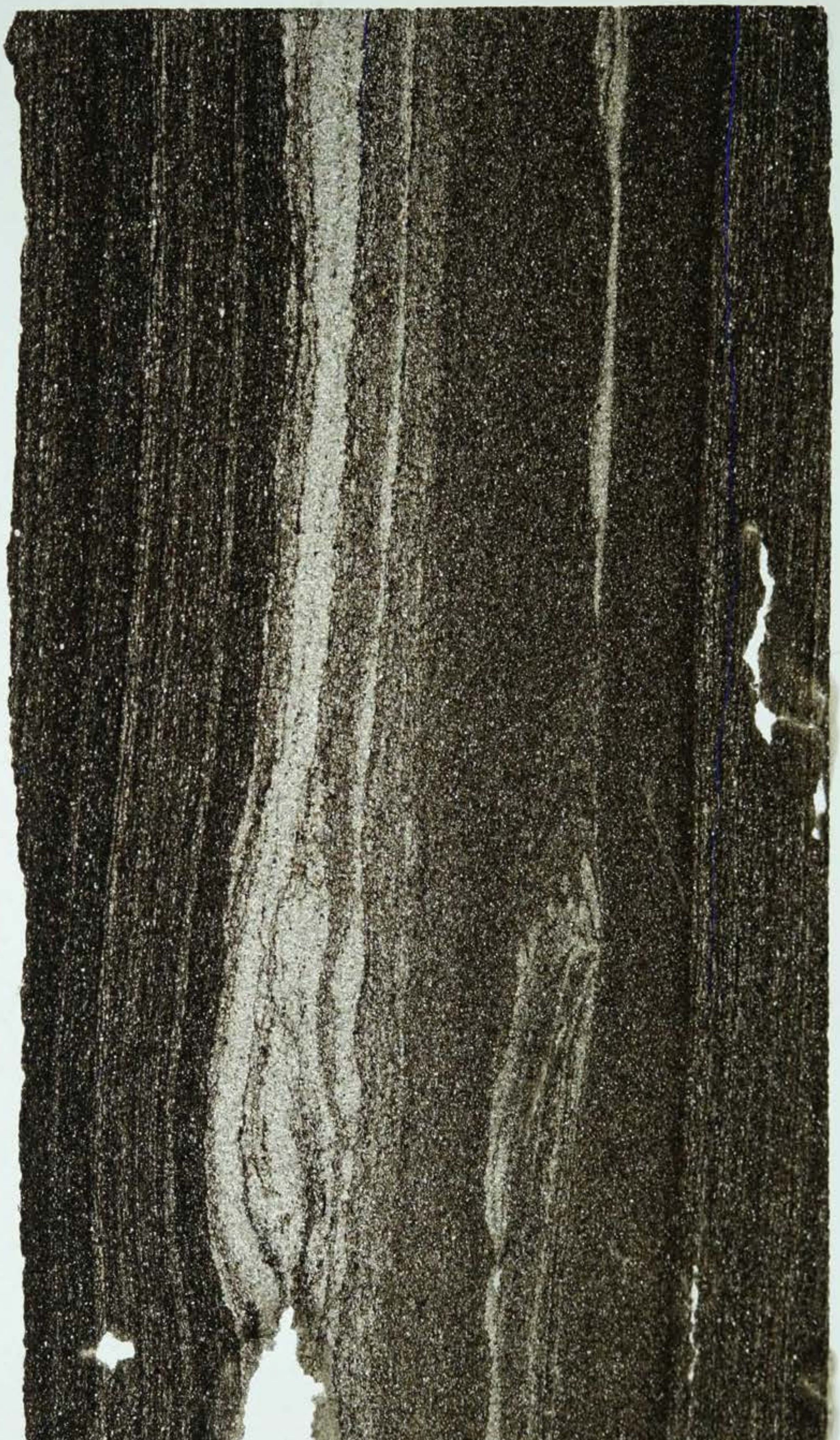

R-233.69 →7


R-233.69 -7

10.3 Geochemistry data

Analyte	SiO2	Al2O3	Fe2O3	MgO	CaO	Na2O	K2O	TiO2	P2O5	MnO	Cr2O3
Unit	%	%	%	%	%	%	%	%	%	%	%
Minimum	0.01	0.01	0.04	0.01	0.01	0.01	0.01	0.01	0.01	0.01	0.002
R-002.70	26.33	8.37	4.43	1.48	29.66	0.56	1.39	0.37	0.07	0.49	0.006
R-003.30	57.26	18.03	3.89	1.94	3.54	0.90	2.94	0.83	0.16	0.13	0.012
R-013.31	55.62	16.48	5.64	1.65	5.08	0.91	2.69	0.75	0.11	0.15	0.013
R-022.27	53.14	17.43	6.74	1.49	4.73	0.89	2.72	0.76	0.12	0.07	0.012
R-023.88	17.45	5.91	2.80	1.28	36.98	0.47	0.83	0.26	0.23	0.19	0.004
R-026.60	46.05	16.44	4.97	1.22	8.07	0.84	2.31	0.66	0.13	0.03	0.017
R-027.33	53.45	17.93	5.04	1.42	2.53	1.07	2.74	0.73	0.14	0.03	0.017
R-057.43	50.01	13.51	12.48	1.22	0.52	0.87	2.27	0.58	0.13	0.20	0.021
R-066.45	57.86	15.10	5.25	1.65	1.21	1.09	2.53	0.65	0.10	0.08	0.022
R-074.60	52.70	13.22	10.49	1.40	1.85	0.96	2.50	0.58	1.20	0.30	0.021
R-076.67	15.03	3.63	30.85	6.99	7.89	0.31	0.65	0.16	1.06	3.12	0.006
R-089.66	36.71	9.39	12.35	3.38	11.95	0.73	1.70	0.42	5.60	0.29	0.016
R-090.01	24.25	6.99	14.29	8.34	16.09	0.47	1.17	0.32	0.76	0.53	0.011
R-119.62	19.56	5.55	15.79	10.13	16.26	0.46	1.02	0.27	0.94	0.36	0.009
R-145.48	24.51	6.15	5.61	10.55	19.10	0.68	1.20	0.28	0.22	0.22	0.006
R-154.54	56.32	14.21	6.62	1.79	0.93	1.13	2.68	0.69	0.17	0.06	0.015
R-173.51	57.31	16.72	4.39	1.23	0.81	1.17	3.02	0.77	0.14	0.02	0.017
R-173.63	16.95	4.87	8.39	11.18	22.78	0.45	0.83	0.23	0.07	0.19	0.005
R-194.29	11.17	3.71	9.87	12.07	25.28	0.29	0.67	0.18	0.44	0.55	0.005
R-194.41	58.12	16.52	4.33	1.19	0.74	1.05	2.96	0.72	0.22	0.03	0.018
R-196.70	56.39	16.36	5.79	1.14	0.31	0.95	3.07	0.73	0.15	0.02	0.017
R-205.73	11.67	3.53	3.46	14.74	26.17	0.26	0.63	0.16	0.07	0.06	0.004
R-221.00	55.12	15.87	5.79	0.99	0.54	1.03	2.84	0.73	0.13	0.03	0.019
R-222.67	15.60	5.38	10.76	11.30	22.46	0.35	0.94	0.25	1.01	0.17	0.008
R-233.40	56.20	13.65	7.41	0.93	0.84	0.95	2.61	0.64	0.65	0.09	0.015

Analyte	LOI	Ni	Sc	Ba	Be	Co	Cs	Ga	Hf	Nb	Rb
Unit	%	PPM	PPM	PPM	PPM	PPM	PPM	PPM	PPM	PPM	PPM
Minimum	-5.1	20	1	1	1	0.2	0.1	0.5	0.1	0.1	0.1
R-002.70	26.7	23	12	256	2	7.1	2.6	10.3	2.9	6.7	46.9
R-003.30	10.1	42	16	553	2	12.5	5.6	20.8	7.8	14.7	101.9
R-013.31	10.7	48	14	499	3	7.7	5.3	19.3	8.2	13.1	111.4
R-022.27	11.7	54	14	493	3	18.0	5.1	20.3	6.7	13.8	105.3
R-023.88	33.5	<20	6	207	1	6.1	1.9	7.2	2.1	4.8	35.2
R-026.60	18.8	101	17	399	2	12.9	5.6	18.5	4.2	11.6	95.0
R-027.33	14.5	95	18	496	3	14.0	6.1	21.5	4.8	12.8	112.5
R-057.43	18.0	76	17	417	2	26.5	5.2	14.5	4.2	10.5	89.8
R-066.45	14.0	91	15	488	2	13.3	5.6	18.2	4.6	11.9	102.1
R-074.60	14.4	62	12	1653	2	44.8	4.6	15.3	3.7	10.9	94.2
R-076.67	30.1	<20	7	512	2	13.3	1.1	6.5	1.2	3.1	25.2
R-089.66	17.2	39	19	636	3	12.9	3.2	11.6	4.0	7.2	65.8
R-090.01	26.5	<20	9	455	<1	13.3	2.6	8.0	2.2	6.1	45.5
R-119.62	29.2	<20	32	1230	2	10.8	1.9	7.0	2.6	4.9	37.2
R-145.48	31.1	34	6	1169	1	5.9	1.8	7.6	2.7	4.8	44.2
R-154.54	15.1	79	17	883	3	13.7	4.7	18.8	5.2	12.6	104.3
R-173.51	14.0	86	13	755	2	15.3	6.5	20.0	5.2	14.1	118.4
R-173.63	33.7	31	11	564	2	5.3	1.7	6.2	2.1	6.2	32.9
R-194.29	35.4	<20	23	1147	3	13.4	1.5	4.6	1.3	3.3	26.6
R-194.41	13.7	79	12	1091	2	13.9	6.8	19.7	4.6	13.2	119.7
R-196.70	14.7	108	16	793	3	17.2	7.5	20.5	5.1	12.9	128.4
R-205.73	38.8	<20	2	604	<1	4.1	1.4	4.5	1.3	3.0	23.8
R-221.00	16.7	78	16	534	2	15.5	6.0	19.3	5.0	13.5	113.5
R-222.67	31.3	23	19	1301	2	17.9	2.0	5.6	1.9	4.5	34.9
R-233.40	15.6	48	13	2550	2	24.5	5.5	16.7	5.1	12.3	105.4

Analyte	Sn	Sr	Ta	Th	U	V	W	Zr	Y	La	Ce
Unit	PPM	PPM	PPM	PPM	PPM	PPM	PPM	PPM	PPM	PPM	PPM
Minimum	1	0.5	0.1	0.2	0.1	8	0.5	0.1	0.1	0.1	0.1
R-002.70	1	273.5	0.5	8.9	2.3	66	0.7	130.3	22.0	22.0	69.7
R-003.30	3	402.3	1.0	19.6	2.9	129	1.6	242.6	23.7	51.7	152.3
R-013.31	3	176.9	1.0	16.9	2.6	97	1.6	259.4	25.7	36.2	83.1
R-022.27	3	213.9	1.0	19.2	3.9	142	1.5	215.6	23.7	46.8	128.1
R-023.88	<1	228.4	0.2	6.4	1.1	60	0.5	74.9	11.7	16.3	46.1
R-026.60	3	239.3	0.8	15.5	10.0	752	1.1	143.4	30.2	35.2	84.2
R-027.33	3	160.8	0.9	17.6	9.9	701	1.0	153.2	31.5	39.4	93.0
R-057.43	2	136.9	0.7	13.9	4.3	643	0.9	129.8	14.2	28.5	64.1
R-066.45	2	154.8	0.8	14.3	5.4	660	1.2	139.3	16.4	32.9	72.4
R-074.60	2	724.0	0.8	12.9	3.0	440	1.3	131.6	44.9	40.5	131.9
R-076.67	<1	159.2	0.2	3.5	0.8	418	0.7	53.2	16.6	12.0	36.8
R-089.66	2	388.4	0.5	8.9	2.9	269	0.8	210.2	44.3	36.9	94.1
R-090.01	1	193.5	0.4	6.3	1.9	195	0.7	105.0	24.7	26.6	71.8
R-119.62	<1	474.5	0.2	5.1	2.9	220	<0.5	93.6	75.3	25.8	71.1
R-145.48	<1	187.4	0.3	5.4	2.7	105	<0.5	105.1	13.3	14.0	34.5
R-154.54	2	269.8	0.9	13.5	5.6	327	1.0	178.1	32.7	36.3	84.1
R-173.51	3	233.3	1.0	15.8	6.8	371	1.3	179.8	29.9	39.7	93.9
R-173.63	<1	222.7	0.4	4.5	2.2	156	<0.5	81.5	25.7	12.1	31.4
R-194.29	<1	256.3	0.2	3.6	1.2	327	<0.5	72.9	53.5	10.9	27.2
R-194.41	2	288.3	1.0	18.6	4.8	367	1.2	154.4	21.9	38.4	88.6
R-196.70	3	250.5	1.0	16.1	7.5	412	1.2	155.7	34.0	40.9	98.9
R-205.73	<1	632.1	0.2	3.8	1.3	65	<0.5	48.0	6.4	9.4	23.9
R-221.00	3	171.9	1.0	17.7	3.9	416	1.3	169.9	33.0	34.3	76.7
R-222.67	<1	637.8	0.3	7.6	4.2	168	<0.5	84.6	67.9	41.8	122.3
R-233.40	2	605.3	0.9	12.5	3.9	289	1.3	164.5	44.4	47.8	109.8

Analyte	Pr	Nd	Sm	Eu	Gd	Tb	Dy	Ho	Er	Tm	Yb
Unit	PPM	PPM	PPM	PPM	PPM	PPM	PPM	PPM	PPM	PPM	PPM
Minimum	0.02	0.3	0.05	0.02	0.05	0.01	0.05	0.02	0.03	0.01	0.05
R-002.70	6.13	24.4	5.01	1.09	4.83	0.81	4.55	0.86	2.46	0.37	2.49
R-003.30	12.69	46.0	7.54	1.39	5.96	0.99	5.53	1.05	3.07	0.48	3.21
R-013.31	8.72	31.5	6.17	1.10	5.52	0.96	4.95	1.00	3.11	0.47	2.99
R-022.27	11.99	42.7	7.67	1.34	5.39	0.90	4.55	0.89	2.70	0.43	2.75
R-023.88	4.23	16.0	3.13	0.63	2.57	0.42	2.18	0.41	1.20	0.20	1.20
R-026.60	9.46	36.0	6.92	1.49	5.99	0.99	5.36	1.06	3.02	0.48	3.06
R-027.33	10.67	40.1	8.03	1.68	6.64	1.11	5.85	1.13	3.48	0.50	3.30
R-057.43	6.47	22.2	3.74	0.69	2.69	0.44	2.45	0.48	1.56	0.28	2.04
R-066.45	7.71	27.8	4.39	0.80	3.03	0.50	2.70	0.58	1.86	0.32	2.25
R-074.60	10.22	38.5	7.40	1.62	6.93	1.15	6.56	1.41	4.16	0.61	3.63
R-076.67	3.16	12.2	2.31	0.52	2.20	0.37	1.96	0.44	1.47	0.22	1.47
R-089.66	8.36	31.1	5.74	1.23	5.37	0.88	5.07	1.13	3.62	0.56	3.72
R-090.01	6.14	23.0	4.15	0.89	3.91	0.65	3.36	0.73	2.05	0.29	1.89
R-119.62	6.45	25.8	5.28	1.26	6.36	1.13	7.15	1.77	5.67	0.85	5.56
R-145.48	3.54	13.4	2.53	0.52	2.07	0.33	1.87	0.37	1.08	0.18	1.14
R-154.54	9.24	33.4	6.44	1.30	5.50	0.90	4.96	1.03	3.13	0.48	3.03
R-173.51	10.32	37.9	6.95	1.38	5.62	0.92	4.95	0.98	2.90	0.42	2.74
R-173.63	3.20	12.2	2.45	0.53	2.43	0.44	2.78	0.64	2.11	0.31	2.01
R-194.29	2.69	10.1	2.30	0.57	2.99	0.58	4.23	1.15	4.03	0.65	4.28
R-194.41	9.35	33.4	5.67	1.07	3.89	0.64	3.44	0.70	2.15	0.35	2.38
R-196.70	10.80	40.4	7.61	1.62	6.53	1.06	5.83	1.14	3.39	0.50	3.24
R-205.73	2.44	8.6	1.67	0.30	1.23	0.20	1.06	0.20	0.63	0.08	0.60
R-221.00	8.22	28.7	4.35	0.79	3.09	0.58	3.68	0.90	3.33	0.58	4.02
R-222.67	11.23	45.7	9.18	2.14	9.24	1.51	8.24	1.72	5.18	0.76	5.00
R-233.40	11.44	44.2	8.05	1.74	7.19	1.20	6.75	1.41	4.18	0.59	3.66

Analyte	Lu	TOT/C	TOT/S	Mo	Cu	Pb	Zn	Ni	As	Cd	Sb
Unit	PPM	%	%	PPM	PPM	PPM	PPM	PPM	PPM	PPM	PPM
Minimum	0.01	0.02	0.02	0.1	0.1	0.1	1	0.1	0.5	0.1	0.1
R-002.70	0.37	6.61	1.56	0.9	20.0	5.8	38	17.6	20.1	<0.1	<0.1
R-003.30	0.45	1.00	0.37	0.4	40.4	16.2	71	35.0	6.7	<0.1	<0.1
R-013.31	0.45	1.52	<0.02	3.2	57.0	26.0	58	40.6	1.3	<0.1	<0.1
R-022.27	0.42	1.24	3.14	2.1	57.8	22.1	80	41.9	34.5	<0.1	0.1
R-023.88	0.19	8.83	1.41	1.0	13.4	6.3	28	15.6	20.0	<0.1	<0.1
R-026.60	0.47	6.37	2.39	43.0	124.1	22.0	2195	99.9	56.9	55.5	2.4
R-027.33	0.49	4.25	2.32	46.2	111.4	23.8	1709	98.1	70.1	40.6	2.8
R-057.43	0.35	3.86	8.64	16.6	82.6	23.9	174	70.9	323.2	2.4	2.7
R-066.45	0.36	4.50	2.16	29.4	120.8	19.5	2221	88.5	64.7	56.5	2.1
R-074.60	0.50	3.94	5.61	3.6	64.1	18.2	132	54.9	88.7	0.4	1.1
R-076.67	0.23	9.48	1.52	2.7	21.5	6.0	60	21.3	22.8	0.8	0.9
R-089.66	0.61	4.55	4.81	7.2	63.0	12.7	134	37.8	52.8	1.3	4.7
R-090.01	0.30	8.43	2.70	3.9	25.5	9.2	65	19.1	32.0	0.6	1.0
R-119.62	0.87	9.65	1.93	1.8	16.8	6.2	70	14.5	18.1	0.8	1.3
R-145.48	0.17	10.06	1.02	9.4	17.8	6.9	62	29.8	9.7	1.0	0.1
R-154.54	0.47	5.88	2.08	15.6	52.2	14.2	615	74.3	29.3	9.5	0.6
R-173.51	0.43	5.73	2.09	16.6	76.2	17.8	1288	81.5	39.0	23.2	0.9
R-173.63	0.31	10.97	0.84	6.3	18.9	5.0	199	22.1	27.7	3.0	1.1
R-194.29	0.68	11.22	1.36	3.6	11.8	4.6	56	11.7	20.6	0.6	1.3
R-194.41	0.35	5.48	2.04	17.8	87.5	20.8	1022	67.5	32.1	21.2	0.9
R-196.70	0.47	5.90	3.15	32.5	70.1	20.6	1009	104.9	53.6	13.6	1.0
R-205.73	0.08	12.12	0.61	3.9	12.8	4.4	172	15.0	11.1	2.9	0.6
R-221.00	0.64	7.37	3.50	10.7	98.5	22.1	743	72.5	52.0	14.5	0.9
R-222.67	0.77	11.30	3.12	3.8	28.2	7.7	128	20.0	34.1	1.5	1.4
R-233.40	0.52	6.24	4.95	3.7	57.7	19.3	185	45.9	63.1	1.0	0.7

Analyte	Bi	Ag	Au	Hg	Tl	Se
Unit	PPM	PPM	PPB	PPM	PPM	PPM
Minimum	0.1	0.1	0.5	0.01	0.1	0.5
R-002.70	0.2	<0.1	<0.5	<0.01	<0.1	0.6
R-003.30	0.4	<0.1	<0.5	<0.01	0.2	<0.5
R-013.31	0.4	<0.1	0.5	<0.01	0.2	0.5
R-022.27	0.4	<0.1	<0.5	0.03	0.1	0.7
R-023.88	0.1	<0.1	<0.5	<0.01	<0.1	<0.5
R-026.60	0.4	2.3	<0.5	0.10	0.7	18.8
R-027.33	0.4	1.5	<0.5	0.09	1.0	18.0
R-057.43	0.4	3.8	<0.5	0.48	0.3	46.9
R-066.45	0.3	4.9	<0.5	0.05	0.2	30.5
R-074.60	0.3	0.9	<0.5	0.16	<0.1	13.1
R-076.67	<0.1	0.2	<0.5	0.05	<0.1	4.3
R-089.66	0.2	2.2	<0.5	0.07	<0.1	11.3
R-090.01	0.1	0.6	<0.5	0.04	<0.1	5.0
R-119.62	<0.1	0.4	<0.5	0.09	<0.1	5.0
R-145.48	<0.1	<0.1	<0.5	0.02	<0.1	3.3
R-154.54	0.2	0.4	<0.5	0.04	0.2	10.1
R-173.51	0.2	1.0	<0.5	0.05	0.3	18.4
R-173.63	<0.1	0.1	<0.5	0.02	0.1	5.0
R-194.29	<0.1	<0.1	1.6	0.12	0.1	2.0
R-194.41	0.3	1.9	<0.5	0.05	0.2	13.4
R-196.70	0.3	1.0	<0.5	0.09	0.3	22.7
R-205.73	<0.1	0.2	<0.5	0.02	0.1	2.4
R-221.00	0.3	2.6	<0.5	0.11	0.2	13.4
R-222.67	0.1	0.5	<0.5	0.24	0.1	6.1
R-233.40	0.3	0.6	<0.5	0.35	<0.1	8.7

10.4 Total reflectance histograms (Appendix 1) and Selected VR populations (Appendix 2)

Appendix 1

Total reflectance histograms

Sample : 17097

Activity no: 2009012; Standard: 0.903%
Locality: Roedryggen-1 (East Greenland)
Depth: 25 m; Material: core
Sample: 517001-5

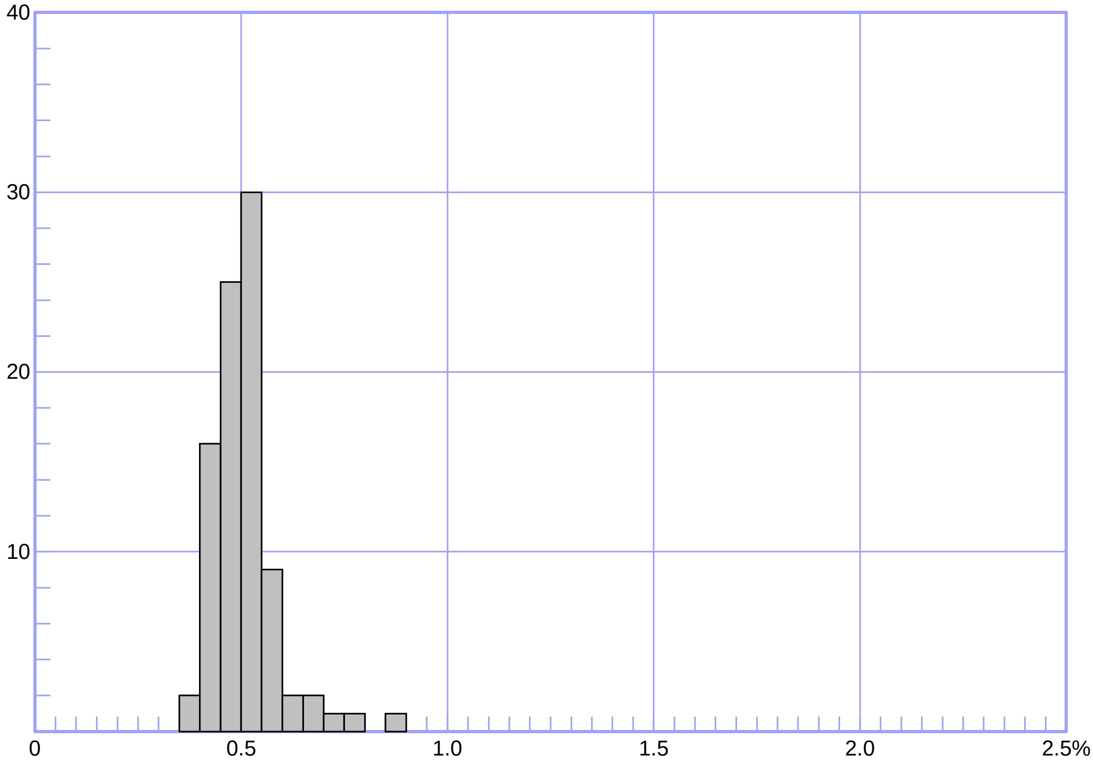

Measure count =	89		Date	9/20/2010	09:06
Reflectance Rr =	0.511	%	Operator	cgu	
s =	0.079	%	Printed	9/20/2010	

0.35 - 0.40	% R	2	0.60 - 0.65	% R	2
0.40 - 0.45	% R	16	0.65 - 0.70	% R	2
0.45 - 0.50	% R	25	0.70 - 0.75	% R	1
0.50 - 0.55	% R	30	0.75 - 0.80	% R	1
0.55 - 0.60	% R	9	0.85 - 0.90	% R	1

F=3.0.3194 D=4.80.6392

Sample : 17895

Activity no: 2010008; Standard: 0.903% Ro
Locality: Roedryggen-1(East Greenland)
Depth: 37.88 m; Material: core
Sample: 517001-301

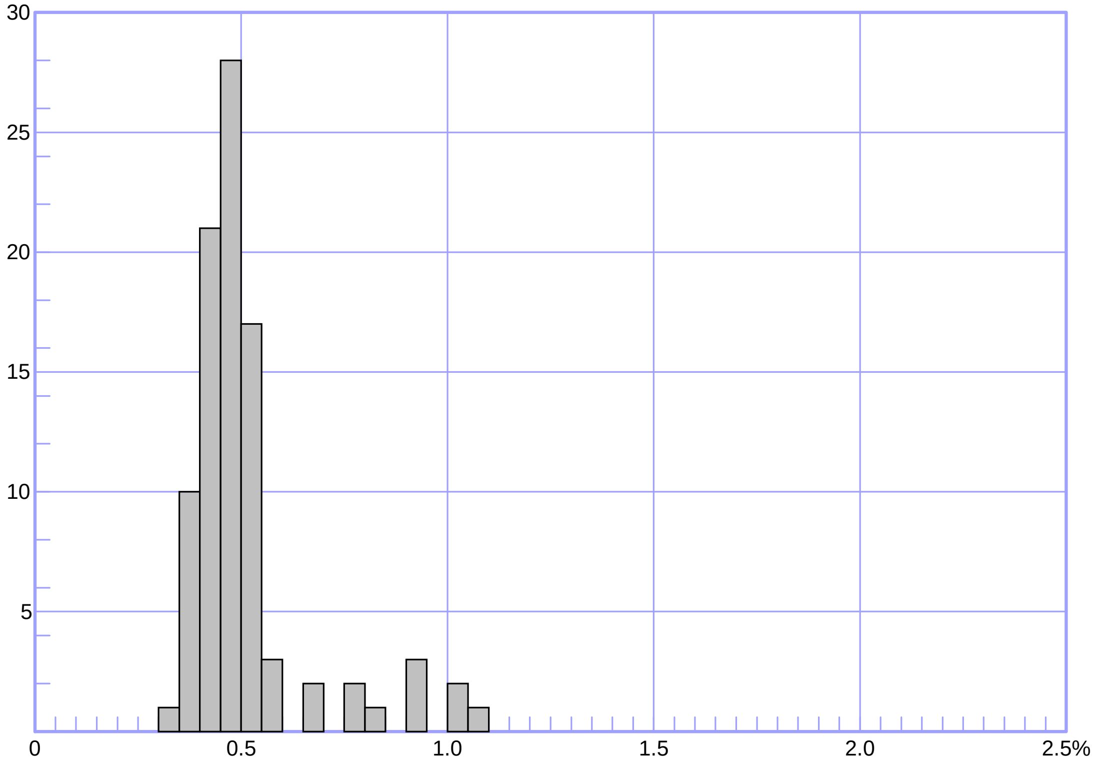

Measure count	=	91		Date	6/22/2010 10:58
Reflectance Rr	=	0.511	%	Operator	cgu
s	=	0.148	%	Printed	6/22/2010

0.30 - 0.35 % R	1		0.65 - 0.70 % R	2
0.35 - 0.40 % R	10		0.75 - 0.80 % R	2
0.40 - 0.45 % R	21		0.80 - 0.85 % R	1
0.45 - 0.50 % R	28		0.90 - 0.95 % R	3
0.50 - 0.55 % R	17		1.00 - 1.05 % R	2
0.55 - 0.60 % R	3		1.05 - 1.10 % R	1

F=3.0.3194 D=4.80.6392

Sample : 17916

Activity no: 2010008; Standard: 0.903% Ro
Locality: Roedryggen-1 (East Greenland)
Depth: 56.88 m; Material: core
Sample: 517001-280

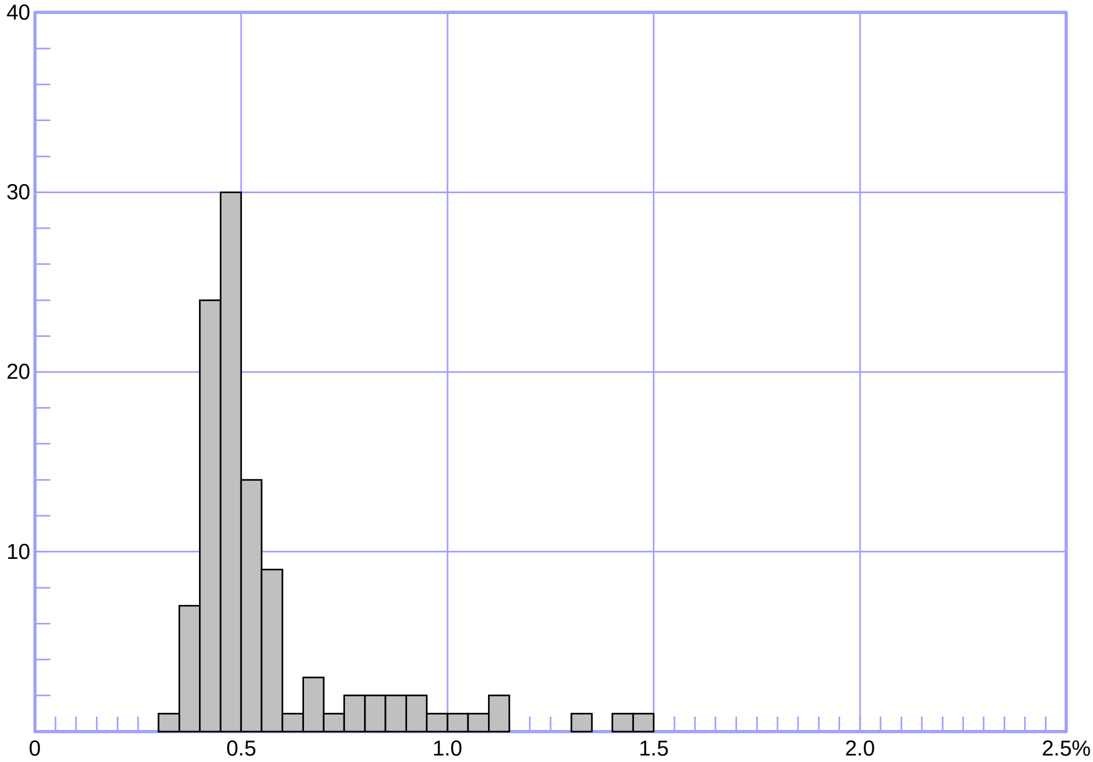

Measure count =	106		Date	6/22/2010	13:18
Reflectance Rr =	0.564	%	Operator	cgu	
s =	0.222	%	Printed	6/22/2010	

0.30	-	0.35	%	R	1		0.80	-	0.85	%	R	2
0.35	-	0.40	%	R	7		0.85	-	0.90	%	R	2
0.40	-	0.45	%	R	24		0.90	-	0.95	%	R	2
0.45	-	0.50	%	R	30		0.95	-	1.00	%	R	1
0.50	-	0.55	%	R	14		1.00	-	1.05	%	R	1
0.55	-	0.60	%	R	9		1.05	-	1.10	%	R	1
0.60	-	0.65	%	R	1		1.10	-	1.15	%	R	2
0.65	-	0.70	%	R	3		1.30	-	1.35	%	R	1
0.70	-	0.75	%	R	1		1.40	-	1.45	%	R	1
0.75	-	0.80	%	R	2		1.45	-	1.50	%	R	1

F=3.0.3194 D=4.80.6392

Sample : 17935

Activity no: 2010008; Standard: 0.903% Ro
Locality: Roedryggen-1 (East Greenland)
Depth: 74.92 m; Material: core
Sample: 517001-261

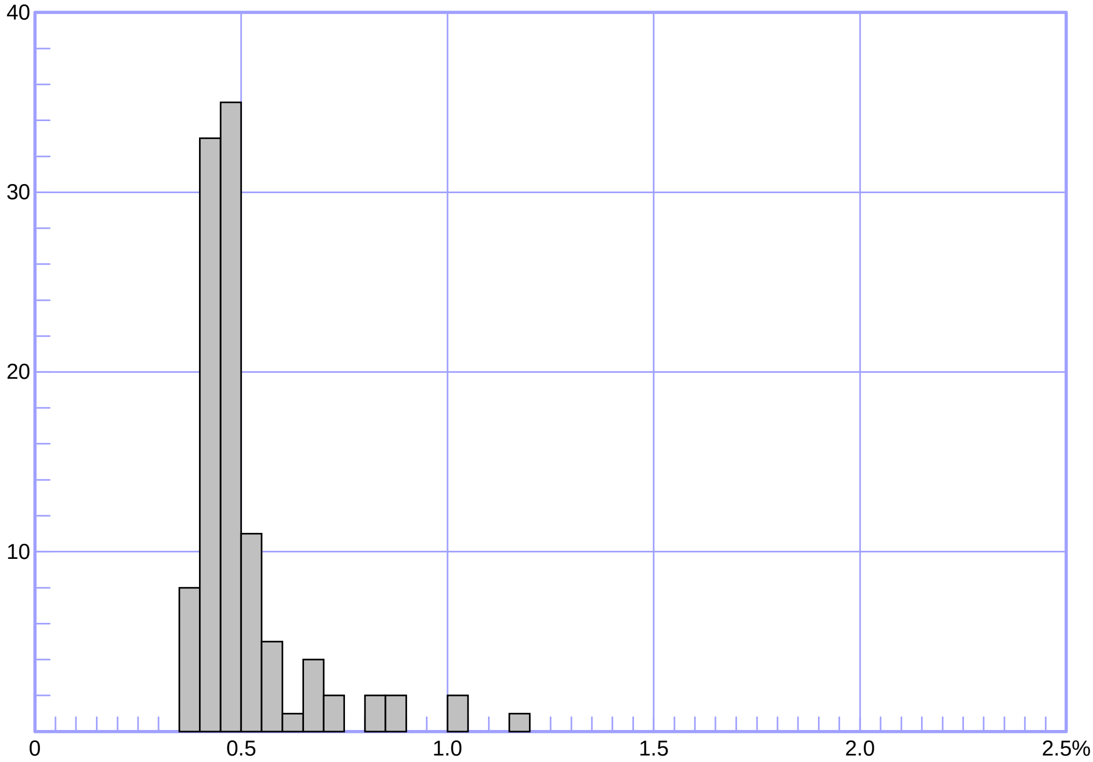

Measure count =	106	Date	6/22/2010 14:35
Reflectance Rr =	0.506 %	Operator	cgu
s =	0.139 %	Printed	6/25/2010

0.35 - 0.40 % R	8	0.65 - 0.70 % R	4
0.40 - 0.45 % R	33	0.70 - 0.75 % R	2
0.45 - 0.50 % R	35	0.80 - 0.85 % R	2
0.50 - 0.55 % R	11	0.85 - 0.90 % R	2
0.55 - 0.60 % R	5	1.00 - 1.05 % R	2
0.60 - 0.65 % R	1	1.15 - 1.20 % R	1

F=3.0.3194 D=4.80.6392

Sample : 17953

Activity no: 2010008; Standard: 0.903% Ro
Locality: Roedryggen-1 (East Greenland)
Depth: 92.23 m; Material: Core
Sample: 517001-243

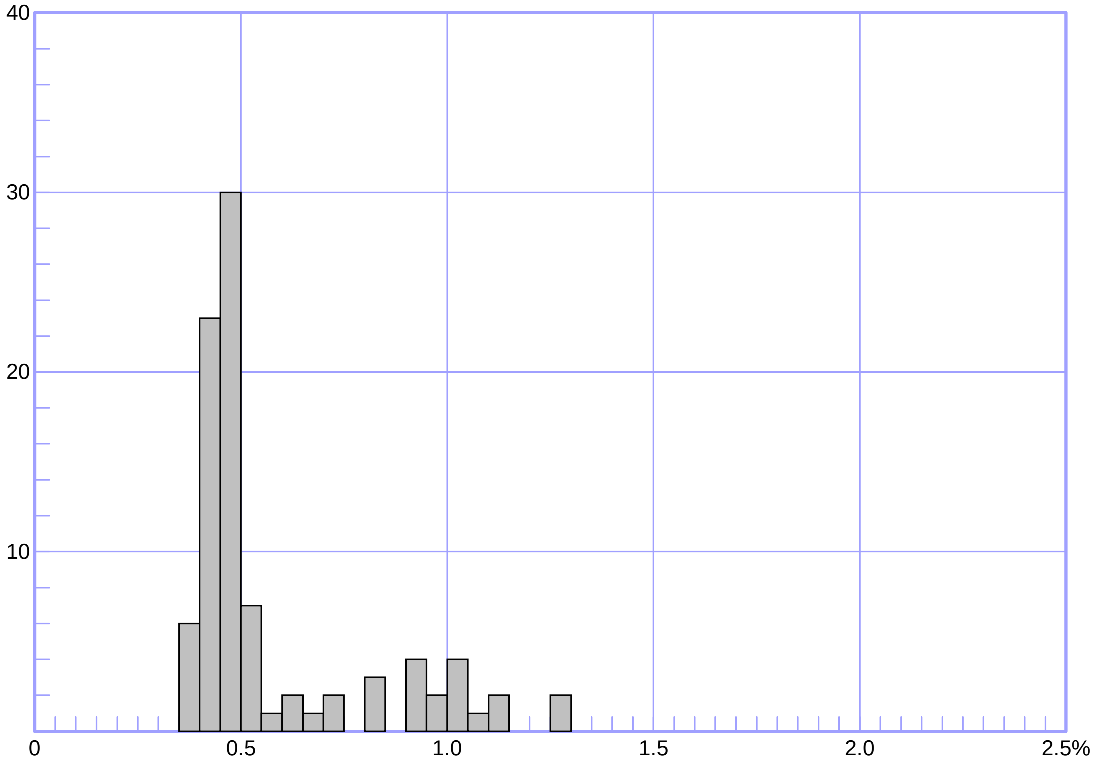

Measure count	=	90	Date	6/23/2010	11:20
Reflectance Rr	=	0.580 %	Operator	cgu	
s	=	0.231 %	Printed	6/23/2010	

0.35 - 0.40 % R	6	0.80 - 0.85 % R	3
0.40 - 0.45 % R	23	0.90 - 0.95 % R	4
0.45 - 0.50 % R	30	0.95 - 1.00 % R	2
0.50 - 0.55 % R	7	1.00 - 1.05 % R	4
0.55 - 0.60 % R	1	1.05 - 1.10 % R	1
0.60 - 0.65 % R	2	1.10 - 1.15 % R	2
0.65 - 0.70 % R	1	1.25 - 1.30 % R	2
0.70 - 0.75 % R	2		

F=3.0.3194 D=4.80.6392

Sample : 17973

Activity no: 2010008; Standard: 0.903% Ro
Locality: Roedryggen-1 (East Greenland)
Depth: 110.15 m; Material: core
Sample: 517001-223

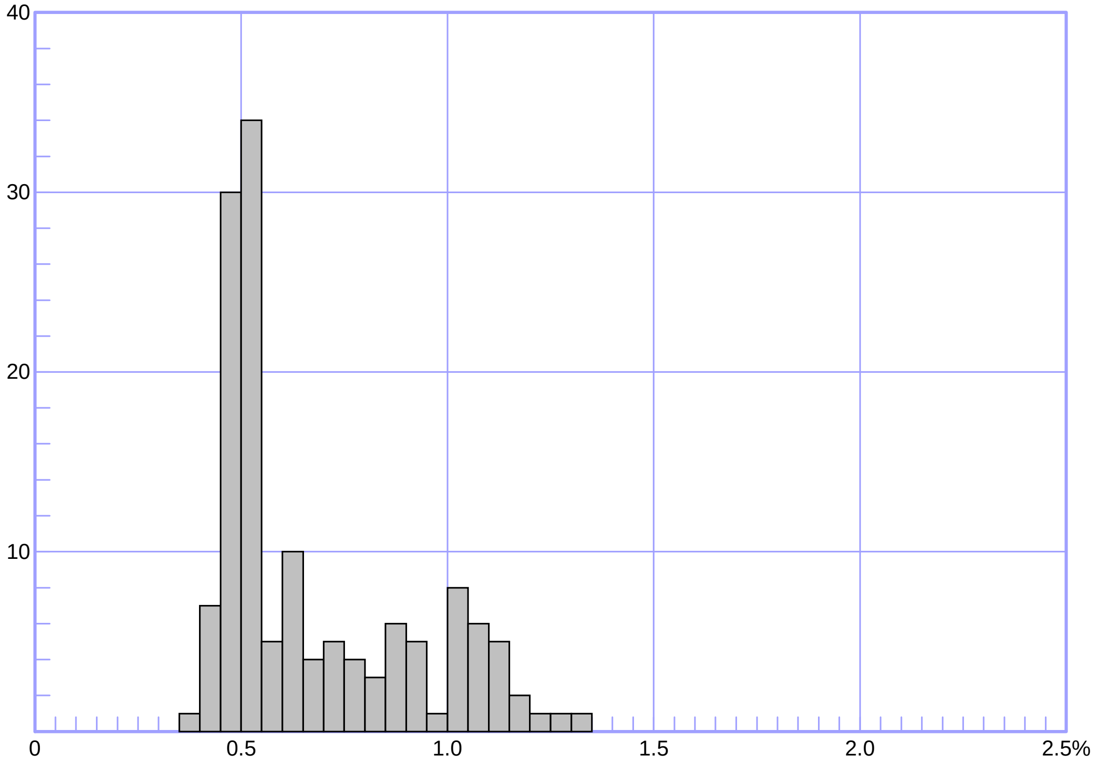

Measure count =	139		Date	6/23/2010	14:09
Reflectance Rr =	0.676	%	Operator	cgu	
s =	0.239	%	Printed	6/23/2010	

0.35 - 0.40 % R	1		0.85 - 0.90 % R	6
0.40 - 0.45 % R	7		0.90 - 0.95 % R	5
0.45 - 0.50 % R	30		0.95 - 1.00 % R	1
0.50 - 0.55 % R	34		1.00 - 1.05 % R	8
0.55 - 0.60 % R	5		1.05 - 1.10 % R	6
0.60 - 0.65 % R	10		1.10 - 1.15 % R	5
0.65 - 0.70 % R	4		1.15 - 1.20 % R	2
0.70 - 0.75 % R	5		1.20 - 1.25 % R	1
0.75 - 0.80 % R	4		1.25 - 1.30 % R	1
0.80 - 0.85 % R	3		1.30 - 1.35 % R	1

F=3.0.3194 D=4.80.6392

Sample : 17992

Activity no: 2010008; Standard: 0.903% Ro
Locality: Roedryggen-1 (East Greenland)
Depth: 128.22 m; Material: core
Sample: 517001-204

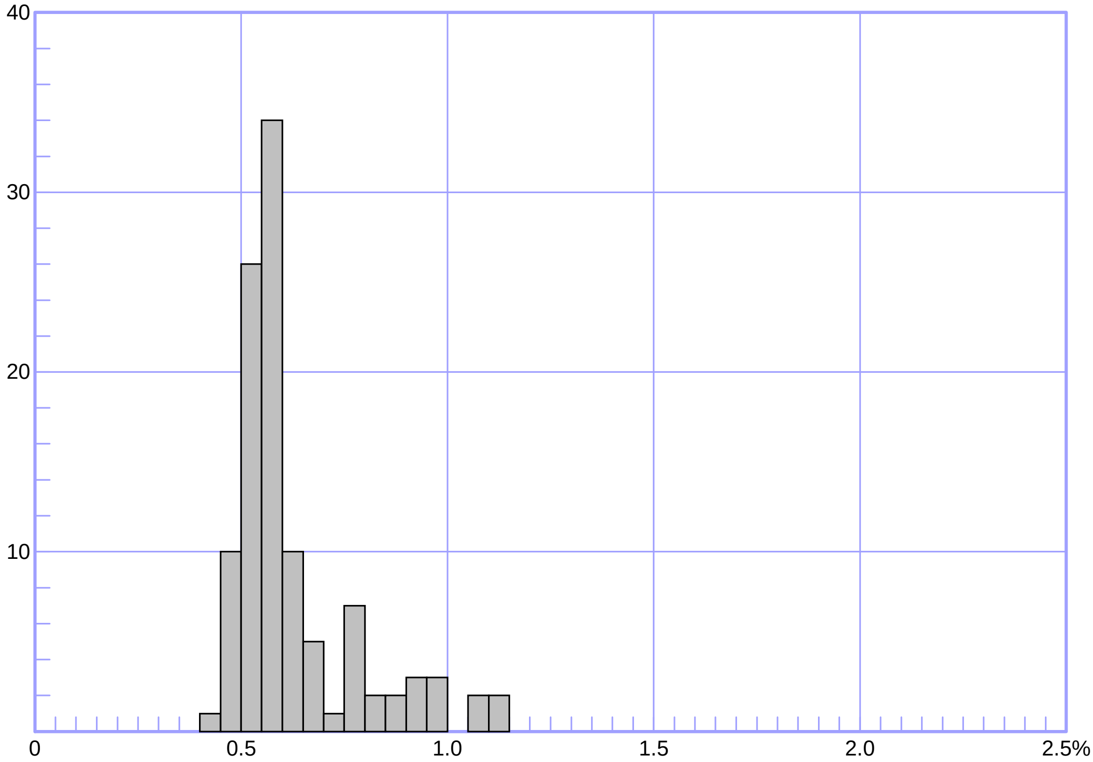

Measure count =	108	Date	6/24/2010 09:24
Reflectance Rr =	0.629 %	Operator	cgu
s =	0.154 %	Printed	10/18/2010

0.40 - 0.45 % R	1	0.75 - 0.80 % R	7
0.45 - 0.50 % R	10	0.80 - 0.85 % R	2
0.50 - 0.55 % R	26	0.85 - 0.90 % R	2
0.55 - 0.60 % R	34	0.90 - 0.95 % R	3
0.60 - 0.65 % R	10	0.95 - 1.00 % R	3
0.65 - 0.70 % R	5	1.05 - 1.10 % R	2
0.70 - 0.75 % R	1	1.10 - 1.15 % R	2

F=3.0.3194 D=4.80.6392

Sample : 18012

Activity no: 2010008; Standard: 0.903% Ro
Locality: Roedryggen-1 (East Greenland)
Depth: 148.46 m; Material: core
Sample: 517001-184

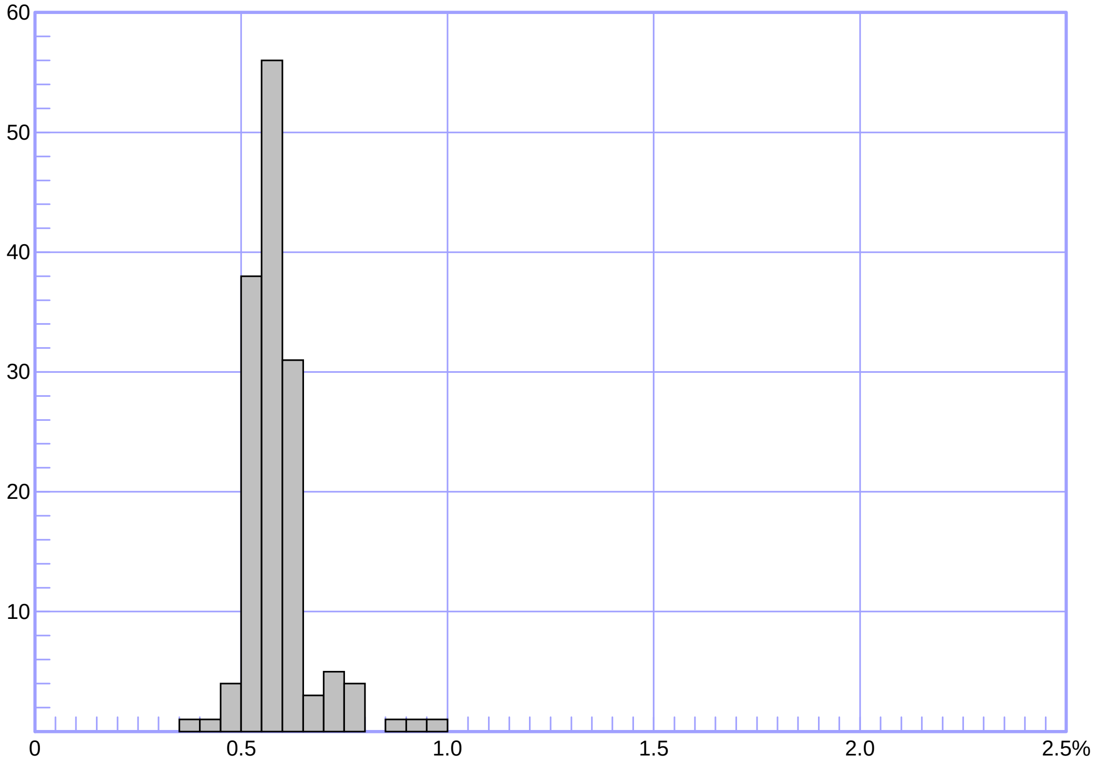

Measure count =	146		Date	6/24/2010	10:16
Reflectance Rr =	0.588	%	Operator	cgu	
s =	0.078	%	Printed	6/24/2010	

0.35 - 0.40 % R	1		0.65 - 0.70 % R	3
0.40 - 0.45 % R	1		0.70 - 0.75 % R	5
0.45 - 0.50 % R	4		0.75 - 0.80 % R	4
0.50 - 0.55 % R	38		0.85 - 0.90 % R	1
0.55 - 0.60 % R	56		0.90 - 0.95 % R	1
0.60 - 0.65 % R	31		0.95 - 1.00 % R	1

F=3.0.3194 D=4.80.6392

Sample : 18032

Activitry no: 2010008; Standard: 0.903% Ro
Locality: Roedryggen-1 (East Greenland)
Depth: 167.24 m; Material: core
Sample: 517001-164

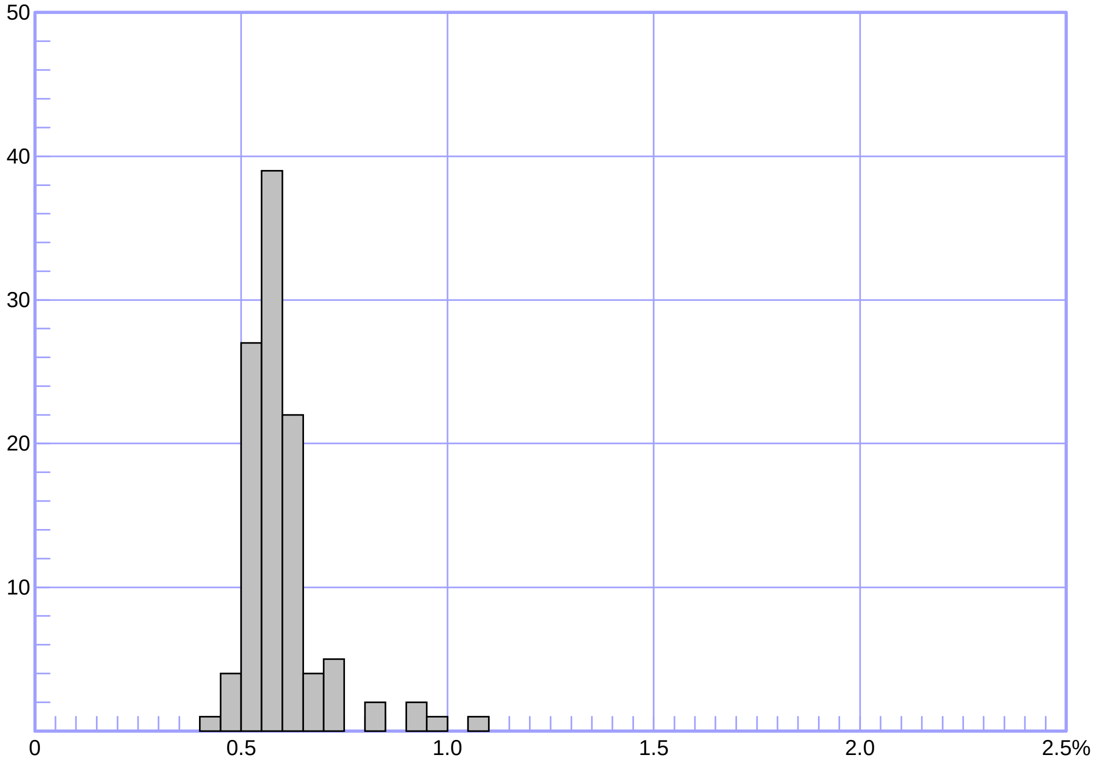

Measure count =	108		Date	6/24/2010	12:30
Reflectance Rr =	0.597	%	Operator	cgu	
s =	0.097	%	Printed	6/24/2010	

0.40 - 0.45	%	R	1		0.70 - 0.75	%	R	5
0.45 - 0.50	%	R	4		0.80 - 0.85	%	R	2
0.50 - 0.55	%	R	27		0.90 - 0.95	%	R	2
0.55 - 0.60	%	R	39		0.95 - 1.00	%	R	1
0.60 - 0.65	%	R	22		1.05 - 1.10	%	R	1
0.65 - 0.70	%	R	4					

F=3.0.3194 D=4.80.6392

Sample : 18054

Activity no: 2010008; Standard: 0.903% Ro
Locality: Roedryggen-1 (East Greenland)
Depth: 187.85 m; Material: core
Sample: 517001-142

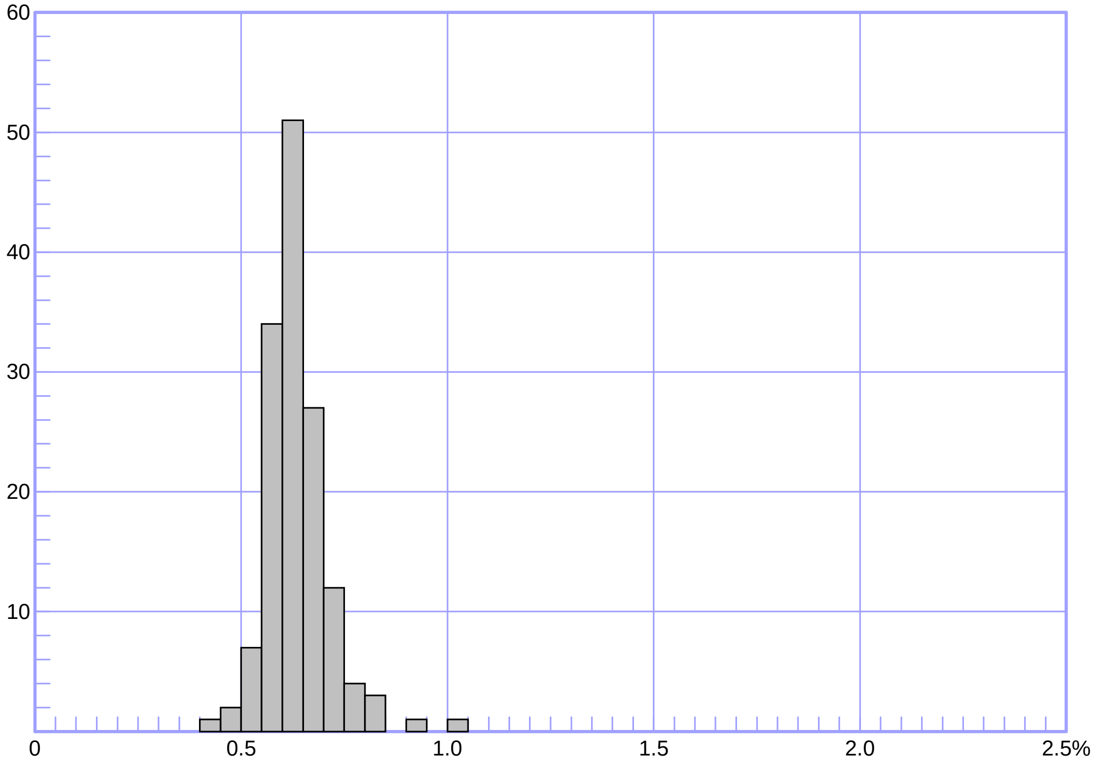

Measure count	=	143	Date	6/24/2010	14:27
Reflectance Rr	=	0.635 %	Operator	cgu	
s	=	0.077 %	Printed	6/24/2010	

0.40 - 0.45	%	R	1		0.70 - 0.75	%	R	12
0.45 - 0.50	%	R	2		0.75 - 0.80	%	R	4
0.50 - 0.55	%	R	7		0.80 - 0.85	%	R	3
0.55 - 0.60	%	R	34		0.90 - 0.95	%	R	1
0.60 - 0.65	%	R	51		1.00 - 1.05	%	R	1
0.65 - 0.70	%	R	27					

F=3.0.3194 D=4.80.6392

Sample : 18086

Activity no: 2010008; Standard: 0.903% Ro
Locality: Roedryggen-1 (East Greenland)
Depth: 216.55 m; Material: core
Sample: 517001-110

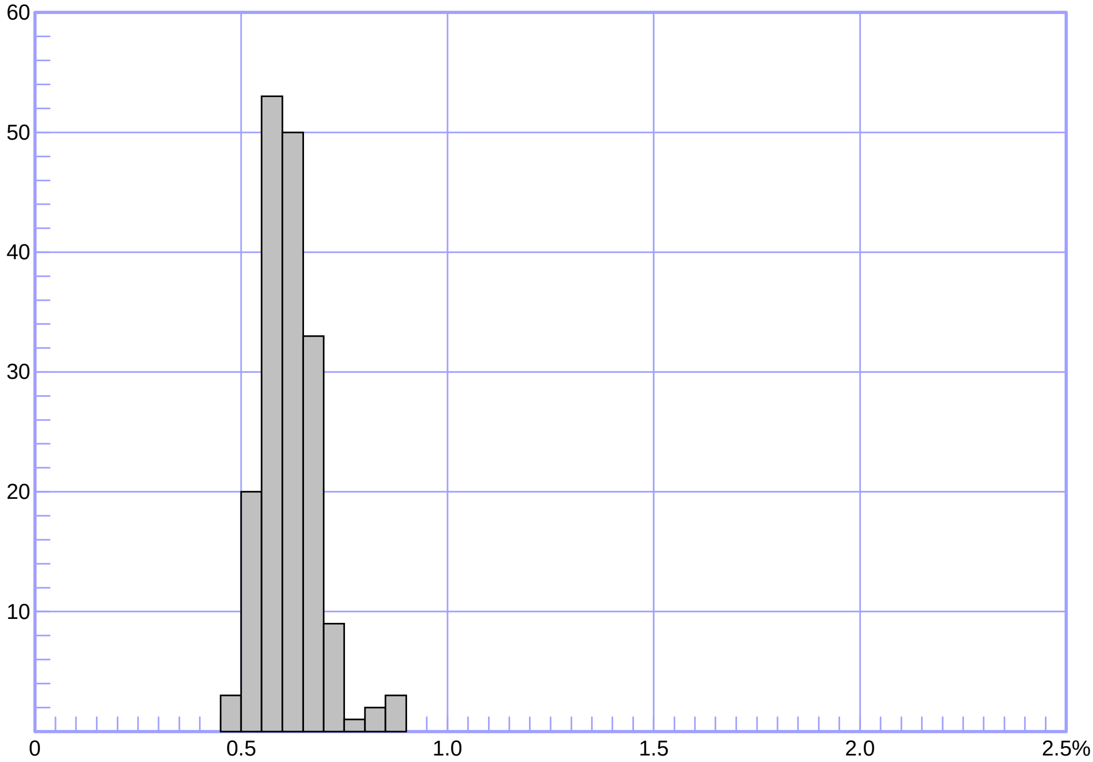

Measure count =	174		Date	6/25/2010	10:55
Reflectance Rr =	0.619	%	Operator	cgu	
s =	0.069	%	Printed	6/25/2010	

0.45 - 0.50	%	R	3		0.70 - 0.75	%	R	9
0.50 - 0.55	%	R	20		0.75 - 0.80	%	R	1
0.55 - 0.60	%	R	53		0.80 - 0.85	%	R	2
0.60 - 0.65	%	R	50		0.85 - 0.90	%	R	3
0.65 - 0.70	%	R	33					

F=3.0.3194 D=4.80.6392

Sample : 18109

Activity no: 2010008; Standard 0.903% Ro
Locality: Roedryggen-1 (East Greenland)
Depth: 234.66 m; Material: core
Sample: 517001-91

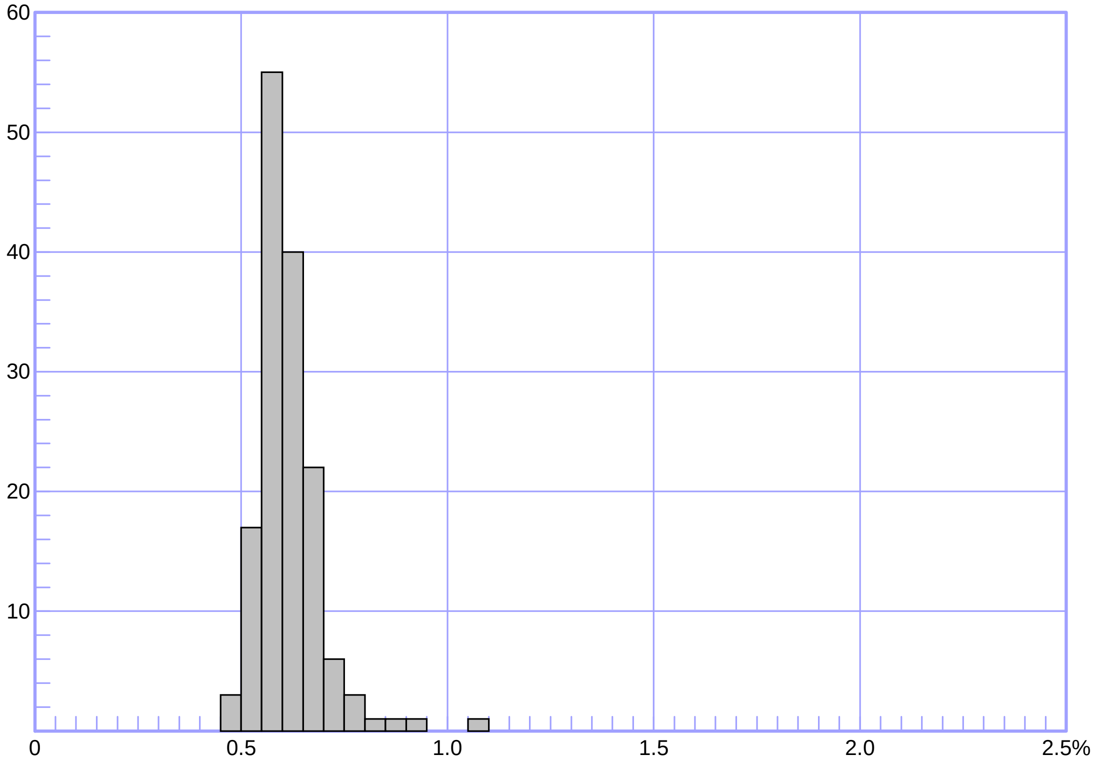

Measure count	=	150	Date	6/25/2010	13:04
Reflectance Rr	=	0.615 %	Operator	cgu	
s	=	0.079 %	Printed	6/25/2010	

0.45 - 0.50	% R	3	0.75 - 0.80	% R	3
0.50 - 0.55	% R	17	0.80 - 0.85	% R	1
0.55 - 0.60	% R	55	0.85 - 0.90	% R	1
0.60 - 0.65	% R	40	0.90 - 0.95	% R	1
0.65 - 0.70	% R	22	1.05 - 1.10	% R	1
0.70 - 0.75	% R	6			

F=3.0.3194 D=4.80.6392

Appendix 2

Selected VR populations

Sample : 17097

Activity no: 2009012; Standard: 0.903%
Locality: Roedryggen-1 (East Greenland)
Depth: 25 m; Material: core
Sample: 517001-5

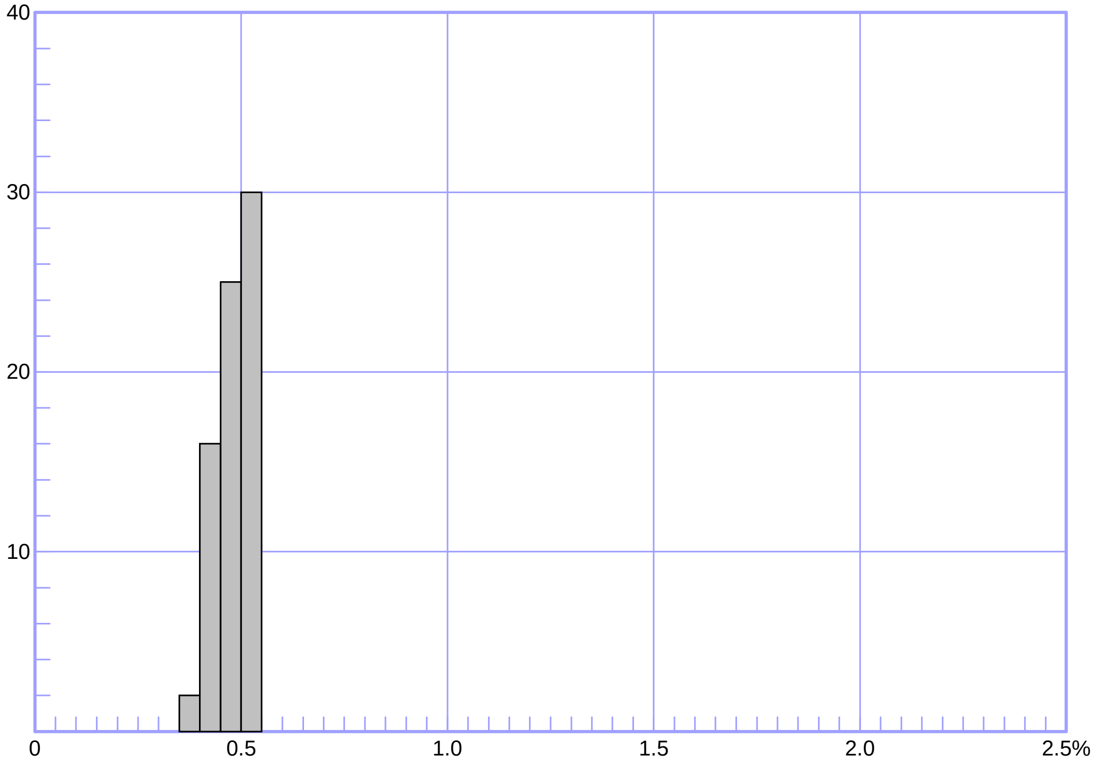

Measure count =	73		Date	9/20/2010 09:06
Reflectance Rr =	0.484 %		Operator	cgu
s =	0.042 %		Printed	9/22/2010

0.35 - 0.40 % R	2	0.45 - 0.50 % R	25
0.40 - 0.45 % R	16	0.50 - 0.55 % R	30

F=3.0.3194 D=4.80.6392

Sample : 17895

Activity no: 2010008; Standard: 0.903% Ro
Locality: Roedryggen-1(East Greenland)
Depth: 37.88 m; Material: core
Sample: 517001-301

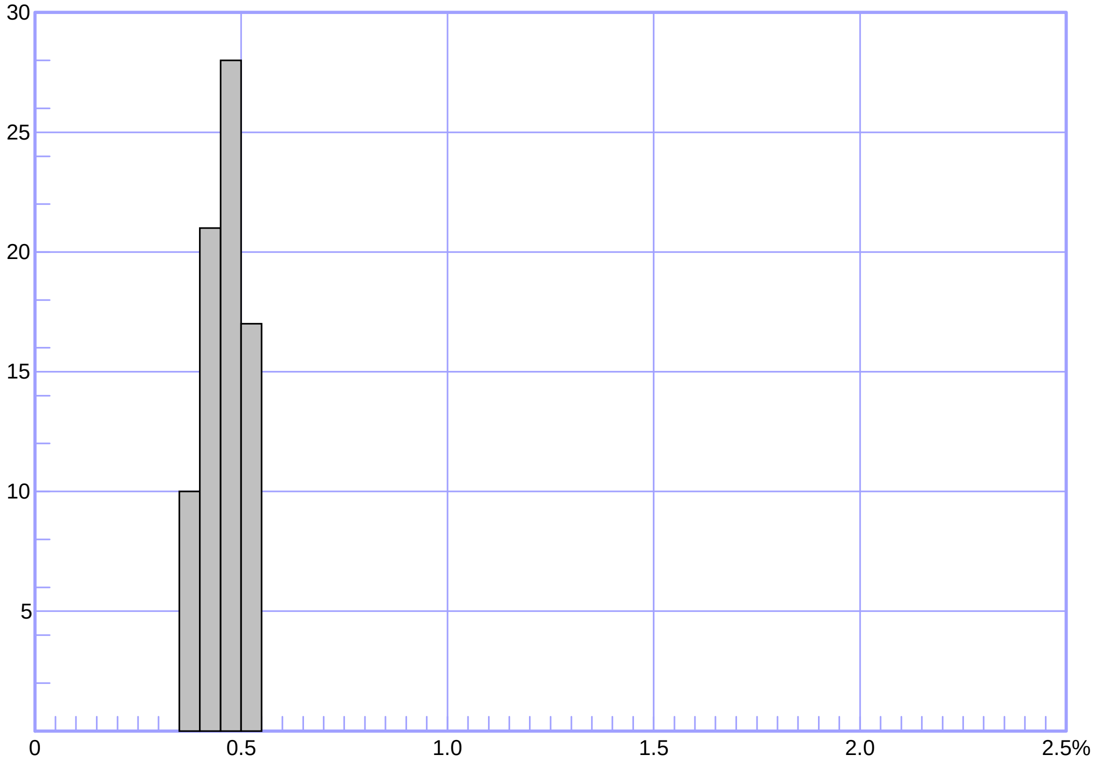

Measure count	=	76	Date	6/22/2010	10:58
Reflectance Rr	=	0.459 %	Operator	cgu	
s	=	0.046 %	Printed	9/22/2010	

0.35 - 0.40	%	R	10	0.45 - 0.50	%	R	28
0.40 - 0.45	%	R	21	0.50 - 0.55	%	R	17

F=3.0.3194 D=4.80.6392

Sample : 17916

Activity no: 2010008; Standard: 0.903% Ro
Locality: Roedryggen-1 (East Greenland)
Depth: 56.88 m; Material: core
Sample: 517001-280

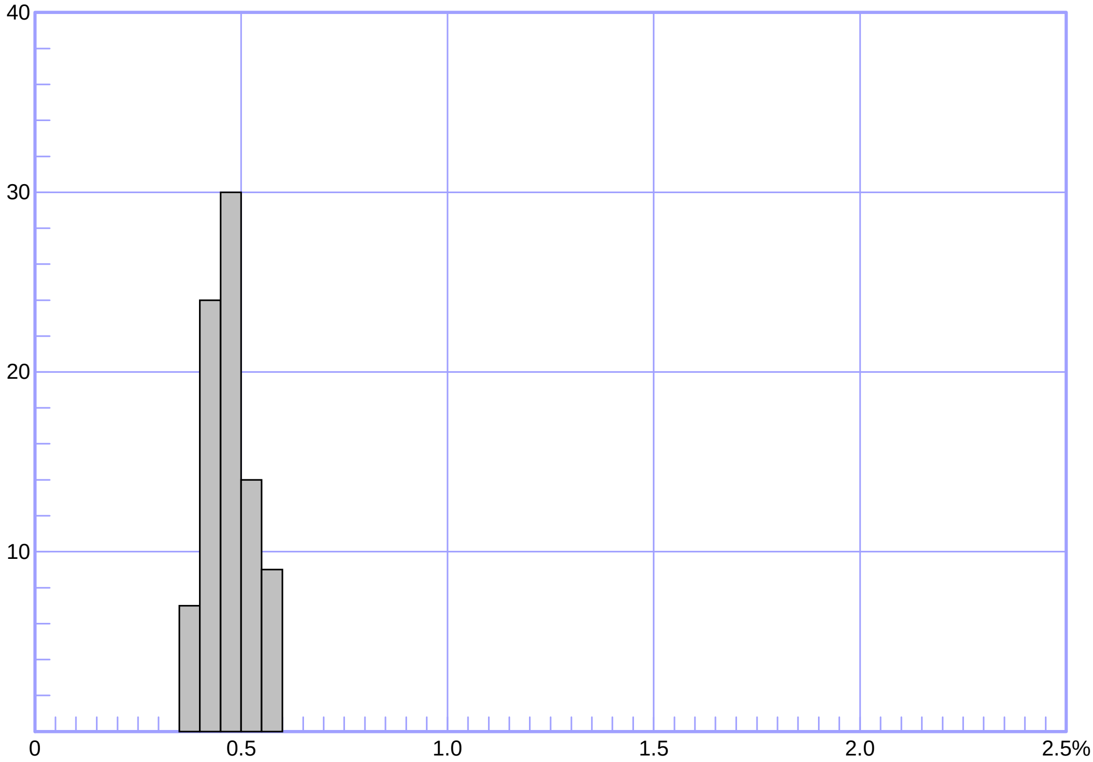

Measure count	=	84	Date	6/22/2010	13:18
Reflectance Rr	=	0.472 %	Operator	cgu	
s	=	0.054 %	Printed	9/22/2010	

0.35 - 0.40	% R	7	0.50 - 0.55	% R	14
0.40 - 0.45	% R	24	0.55 - 0.60	% R	9
0.45 - 0.50	% R	30			

F=3.0.3194 D=4.80.6392

Sample : 17935

Activity no: 2010008; Standard: 0.903% Ro
Locality: Roedryggen-1 (East Greenland)
Depth: 74.92 m; Material: core
Sample: 517001-261

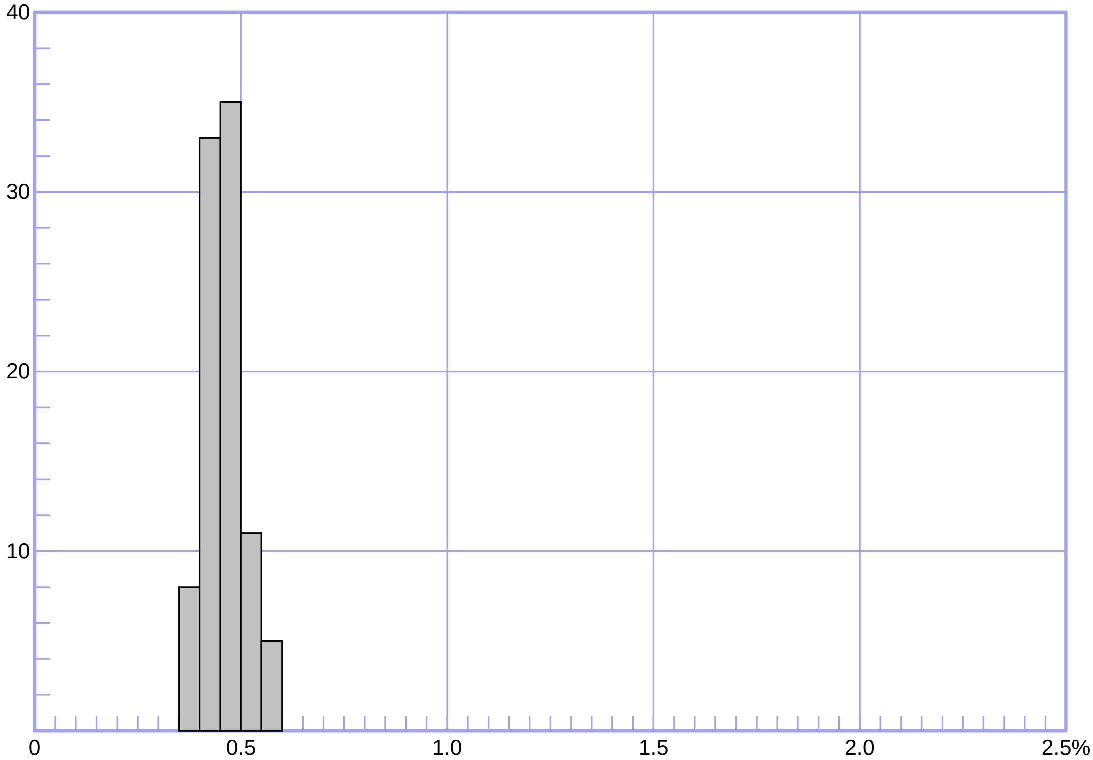

Measure count	=	92		Date	6/22/2010	14:35
Reflectance Rr	=	0.460	%	Operator	cgu	
s	=	0.048	%	Printed	9/22/2010	

0.35 - 0.40	%	R	8	0.50 - 0.55	% R	11
0.40 - 0.45	%	R	33	0.55 - 0.60	% R	5
0.45 - 0.50	%	R	35			

F=3.0.3194 D=4.80.6392

Sample : 17953

Activity no: 2010008; Standard: 0.903% Ro
Locality: Roedryggen-1 (East Greenland)
Depth: 92.23 m; Material: Core
Sample: 517001-243

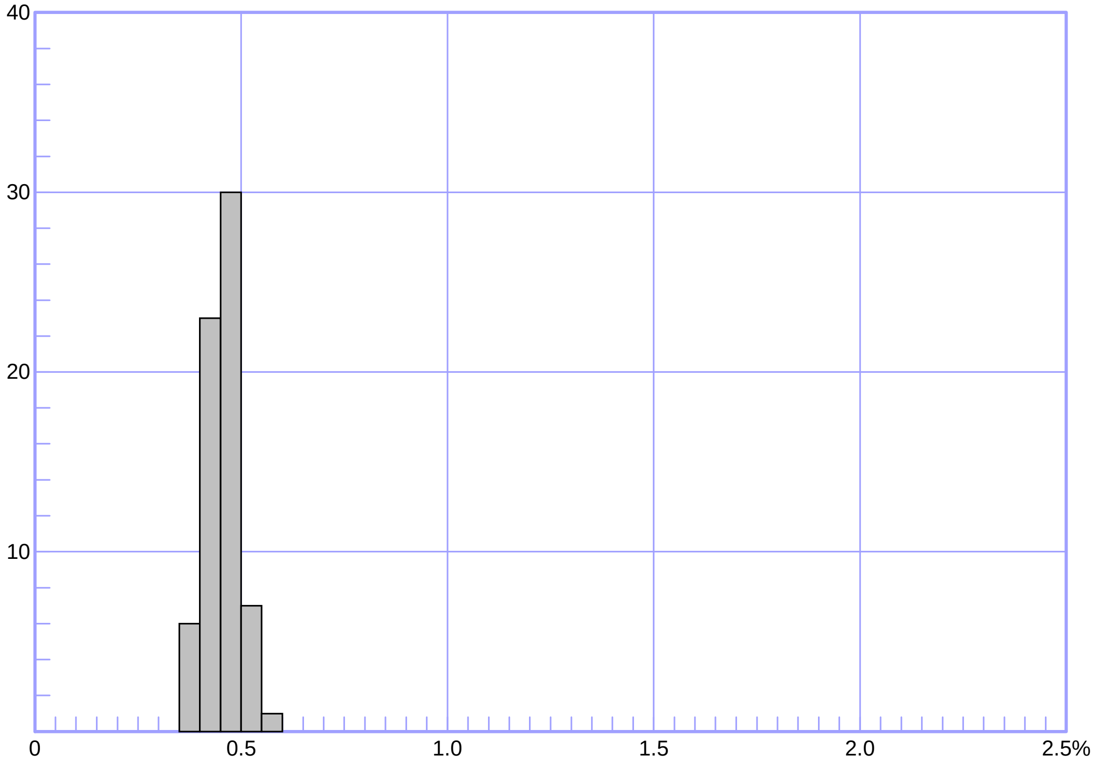

Measure count	=	67	Date	6/23/2010	11:20
Reflectance Rr	=	0.457 %	Operator	cgu	
s	=	0.041 %	Printed	6/23/2010	

0.35 - 0.40 % R	6	0.50 - 0.55 % R	7
0.40 - 0.45 % R	23	0.55 - 0.60 % R	1
0.45 - 0.50 % R	30		

F=3.0.3194 D=4.80.6392

Sample : 17973

Activity no: 2010008; Standard: 0.903% Ro
Locality: Roedryggen-1 (East Greenland)
Depth: 110.15 m; Material: core
Sample: 517001-223

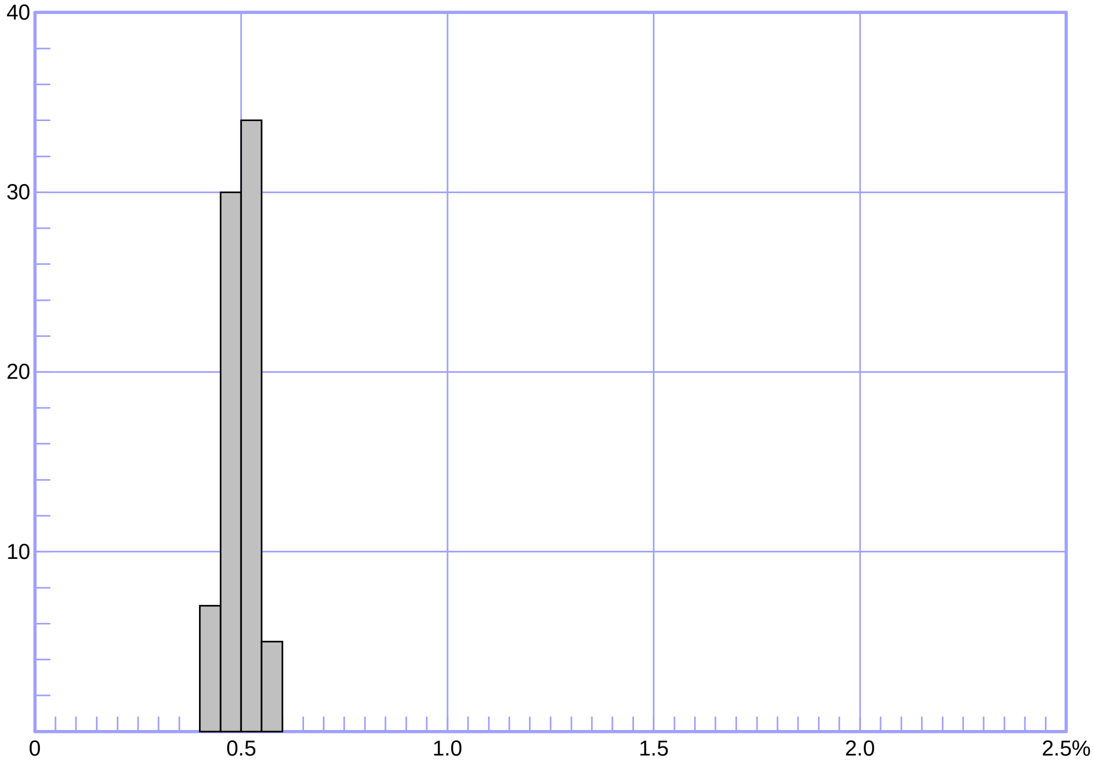

Measure count	=	76	Date	6/23/2010	14:09
Reflectance Rr	=	0.499 %	Operator	cgu	
s	=	0.037 %	Printed	9/22/2010	

0.40 - 0.45 % R	7	0.50 - 0.55 % R	34
0.45 - 0.50 % R	30	0.55 - 0.60 % R	5

F=3.0.3194 D=4.80.6392

Sample : 17992

Activity no: 2010008; Standard: 0.903% Ro
Locality: Roedryggen-1 (East Greenland)
Depth: 128.22 m; Material: core
Sample: 517001-204

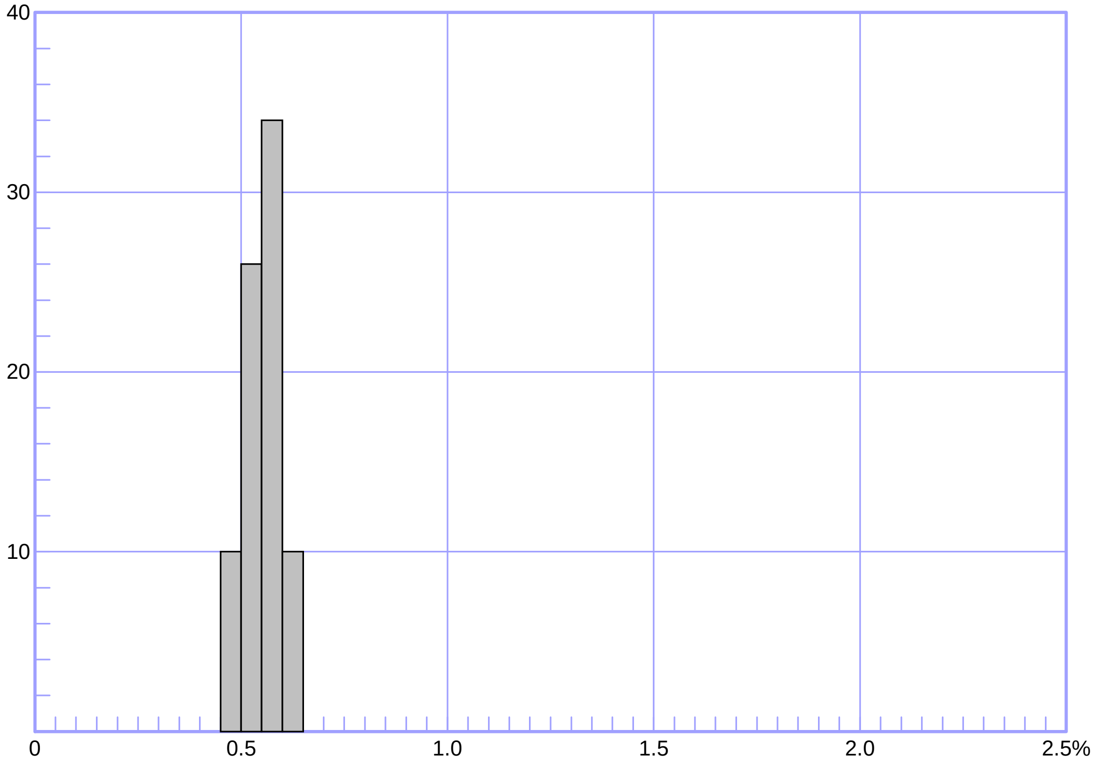

Measure count	=	80		Date	6/24/2010 09:24
Reflectance Rr	=	0.556	%	Operator	cgu
s	=	0.044	%	Printed	9/22/2010

0.45	-	0.50	%	R	10	0.55	-	0.60	%	R	34
0.50	-	0.55	%	R	26	0.60	-	0.65	%	R	10

F=3.0.3194 D=4.80.6392

Sample : 18012

Activity no: 2010008; Standard: 0.903% Ro
Locality: Roedryggen-1 (East Greenland)
Depth: 148.46 m; Material: core
Sample: 517001-184

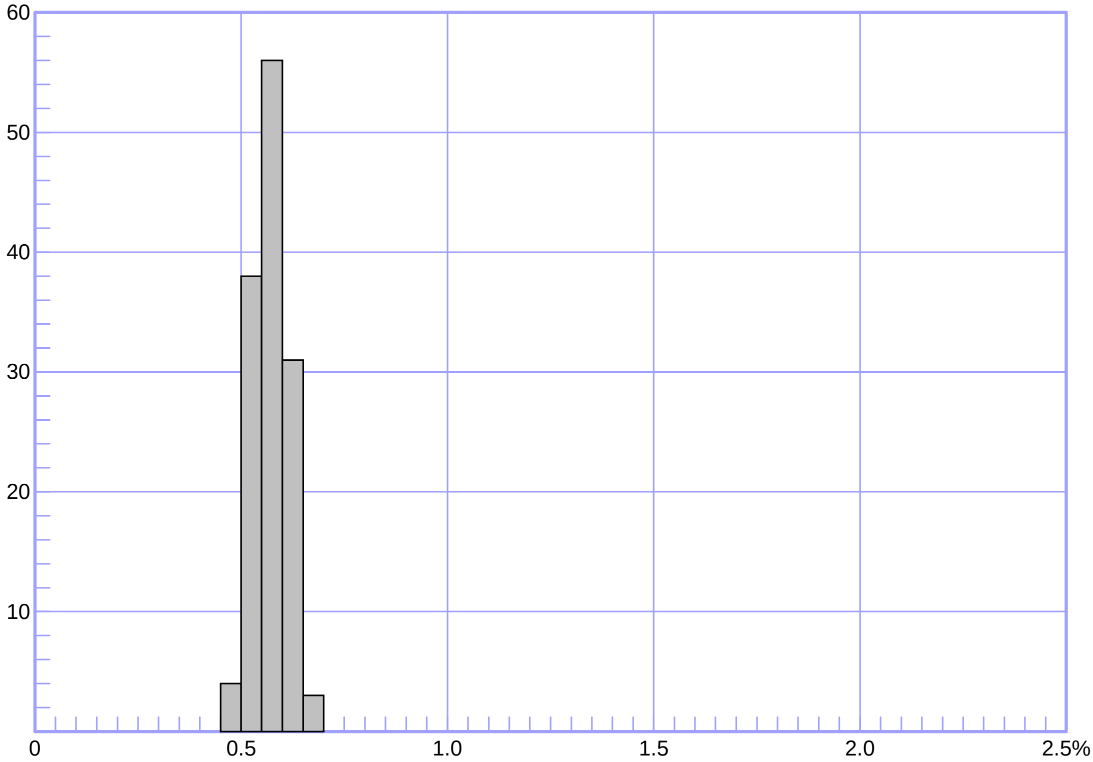

Measure count =	132		Date	6/24/2010	10:16
Reflectance Rr =	0.572	%	Operator	cgu	
s =	0.041	%	Printed	9/22/2010	

0.45 - 0.50 % R	4		0.60 - 0.65 % R	31
0.50 - 0.55 % R	38		0.65 - 0.70 % R	3
0.55 - 0.60 % R	56			

F=3.0.3194 D=4.80.6392

Sample : 18032

Activitry no: 2010008; Standard: 0.903% Ro
Locality: Roedryggen-1 (East Greenland)
Depth: 167.24 m; Material: core
Sample: 517001-164

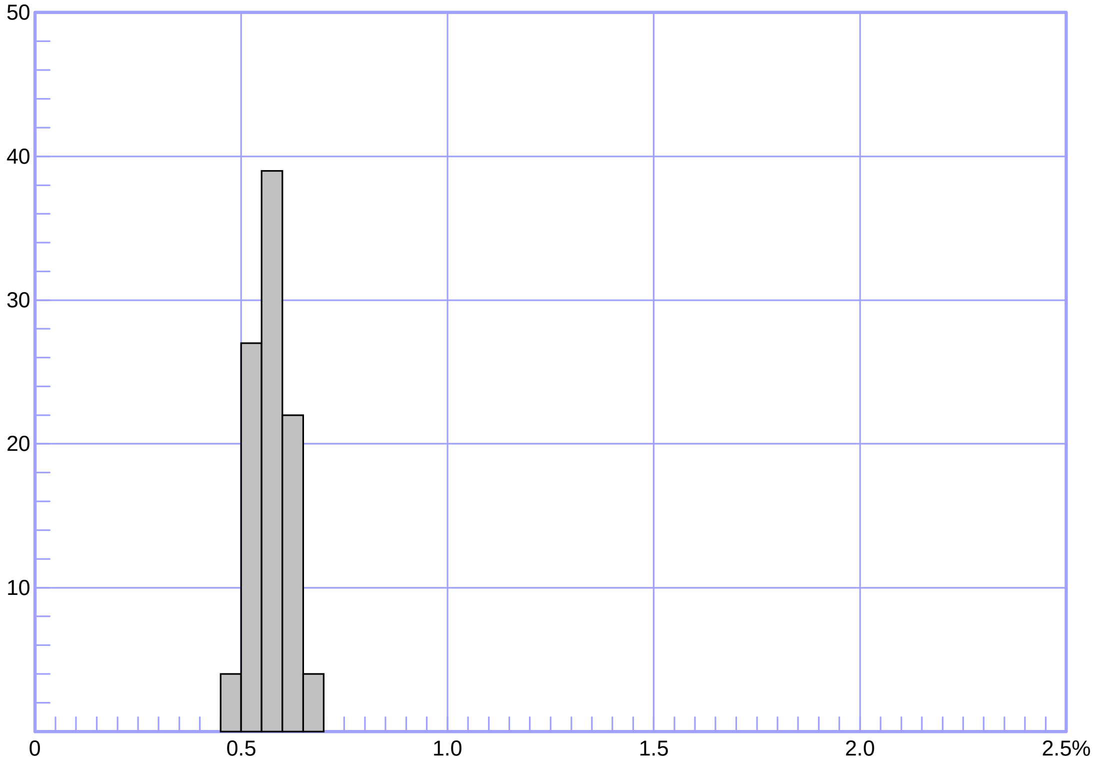

Measure count =	96		Date	6/24/2010	12:30
Reflectance Rr =	0.572	%	Operator	cgu	
s =	0.045	%	Printed	9/22/2010	

0.45 - 0.50 % R	4
0.50 - 0.55 % R	27
0.55 - 0.60 % R	39
0.60 - 0.65 % R	22
0.65 - 0.70 % R	4

F=3.0.3194 D=4.80.6392

Sample : 18054

Activity no: 2010008; Standard: 0.903% Ro
Locality: Roedryggen-1 (East Greenland)
Depth: 187.85 m; Material: core
Sample: 517001-142

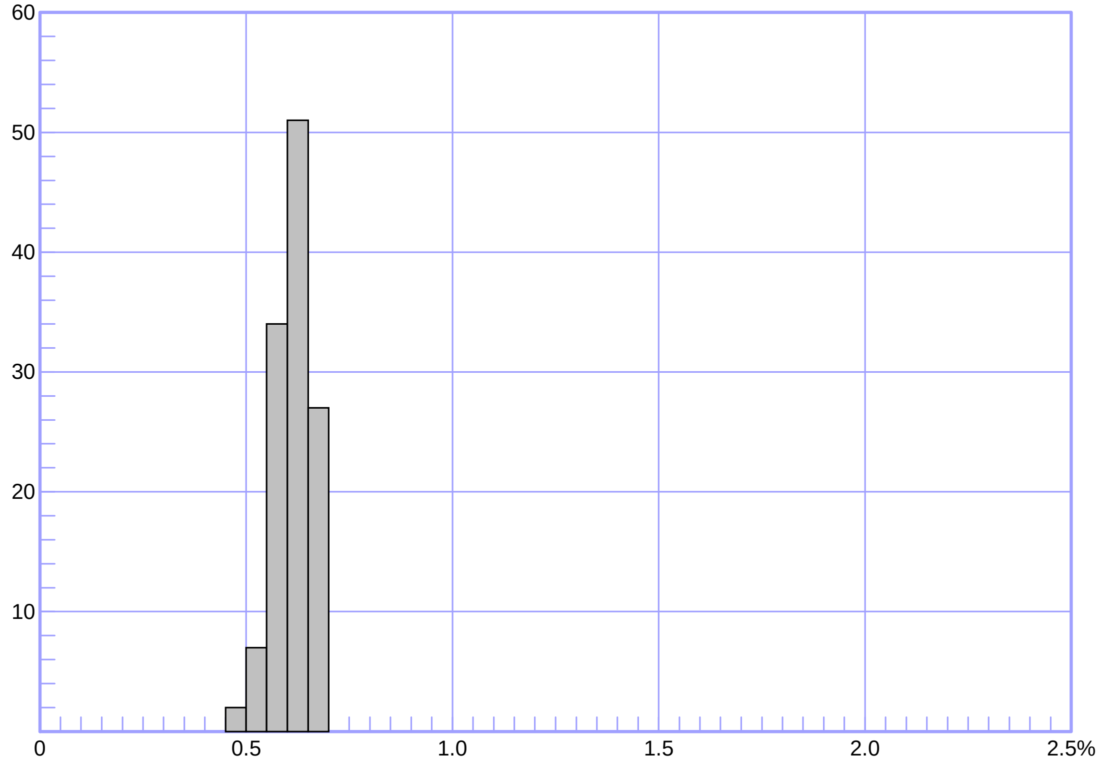

Measure count =	121	Date	6/24/2010 14:27
Reflectance Rr =	0.614 %	Operator	cgu
s =	0.046 %	Printed	9/22/2010

0.45 - 0.50 % R	2	0.60 - 0.65 % R	51
0.50 - 0.55 % R	7	0.65 - 0.70 % R	27
0.55 - 0.60 % R	34		

F=3.0.3194 D=4.80.6392

Sample : 18086

Activity no: 2010008; Standard: 0.903% Ro
Locality: Roedryggen-1 (East Greenland)
Depth: 216.55 m; Material: core
Sample: 517001-110

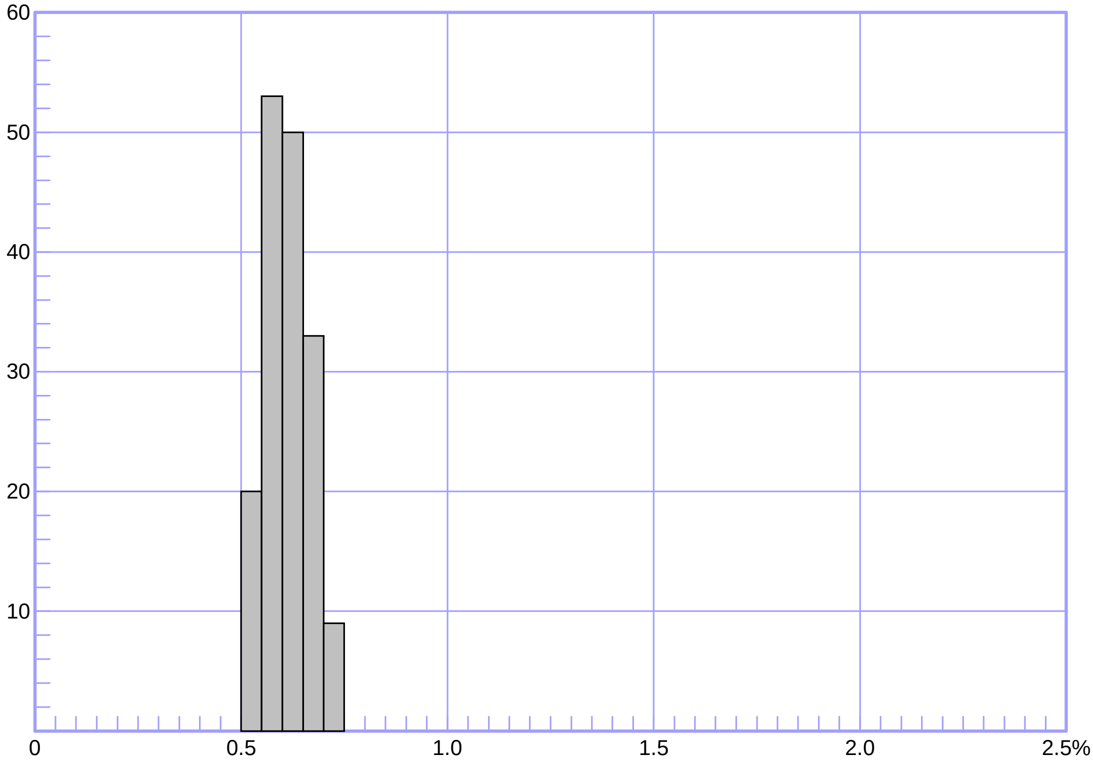

Measure count =	165	Date	6/25/2010 10:55
Reflectance Rr =	0.613 %	Operator	cgu
s =	0.054 %	Printed	9/22/2010

0.50 - 0.55 % R	20	0.65 - 0.70 % R	33
0.55 - 0.60 % R	53	0.70 - 0.75 % R	9
0.60 - 0.65 % R	50		

F=3.0.3194 D=4.80.6392

Sample : 18109

Activity no: 2010008; Standard 0.903% Ro
Locality: Roedryggen-1 (East Greenland)
Depth: 234.66 m; Material: core
Sample: 517001-91

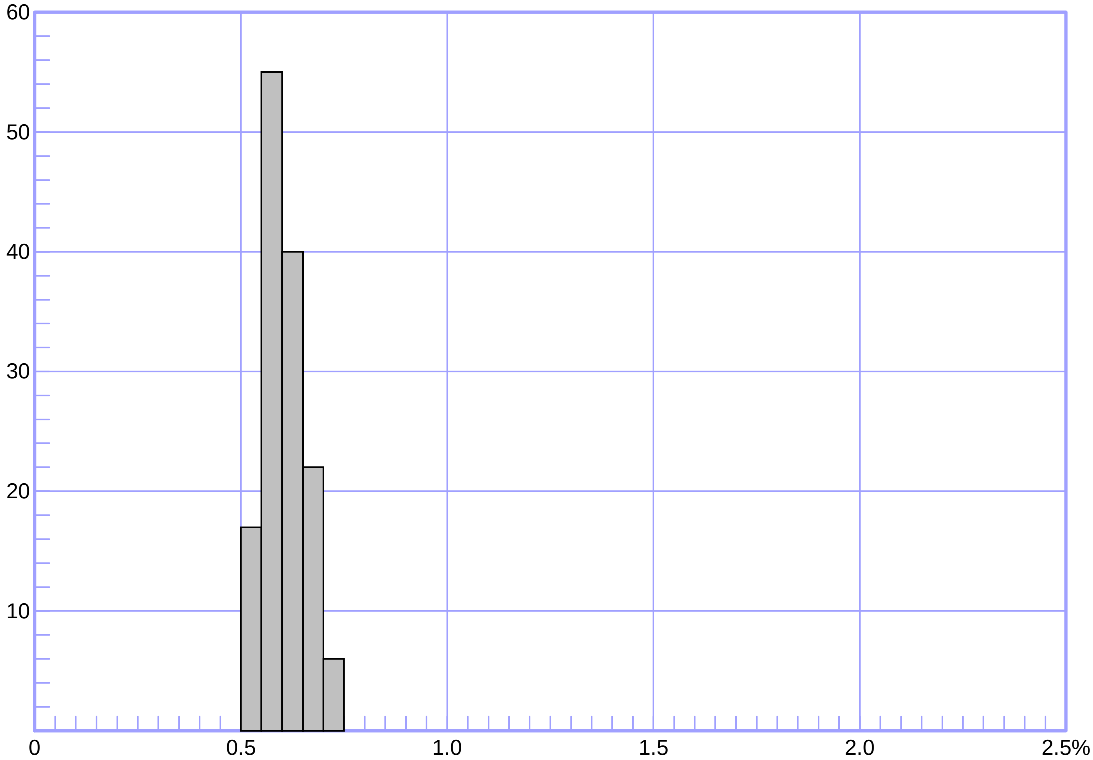

Measure count	=	140	Date	6/25/2010	13:04
Reflectance Rr	=	0.606 %	Operator	cgu	
s	=	0.052 %	Printed	9/22/2010	

0.50 - 0.55 % R	17
0.55 - 0.60 % R	55
0.60 - 0.65 % R	40
0.65 - 0.70 % R	22
0.70 - 0.75 % R	6

F=3.0.3194 D=4.80.6392

10.5 Headspace gas analysis

Geochemistry Data Report –
Gas Analysis of 8 COPL Samples

Applied Petroleum Technology AS
P. O. Box 123
2027 Kjeller
Norway

Address:	**Applied Petroleum Technology AS** **P.O.Box 123** **2027 Kjeller**
Telephone:	**+47 63 80 60 00**
Telefax:	**+47 63 80 11 38**

Report number APT09-2164	**Classification** Confidential
Report Title Geochemistry Data Report - Gas Analysis of 8 COPL Samples	**Submitted** December 09
Client GEUS	**Service Order**
Client Reference Jørgen Bojesen-Koefoed	**Number of pages** 5
Distribution GEUS (digital) APT (digital)	

Author
Ingar Johansen

	Name	Date	Signature
Reviewed by	Geir Hansen	2009-12-21	
Approved by	Tore Haaland	2009-12-21	

CONTENTS

Table 1. Number of analyses performed

Analysis	Core	Total
Headspace	8	8
Stable isotopes of gas	8	8

Figure 1. Gas composition (volume based)

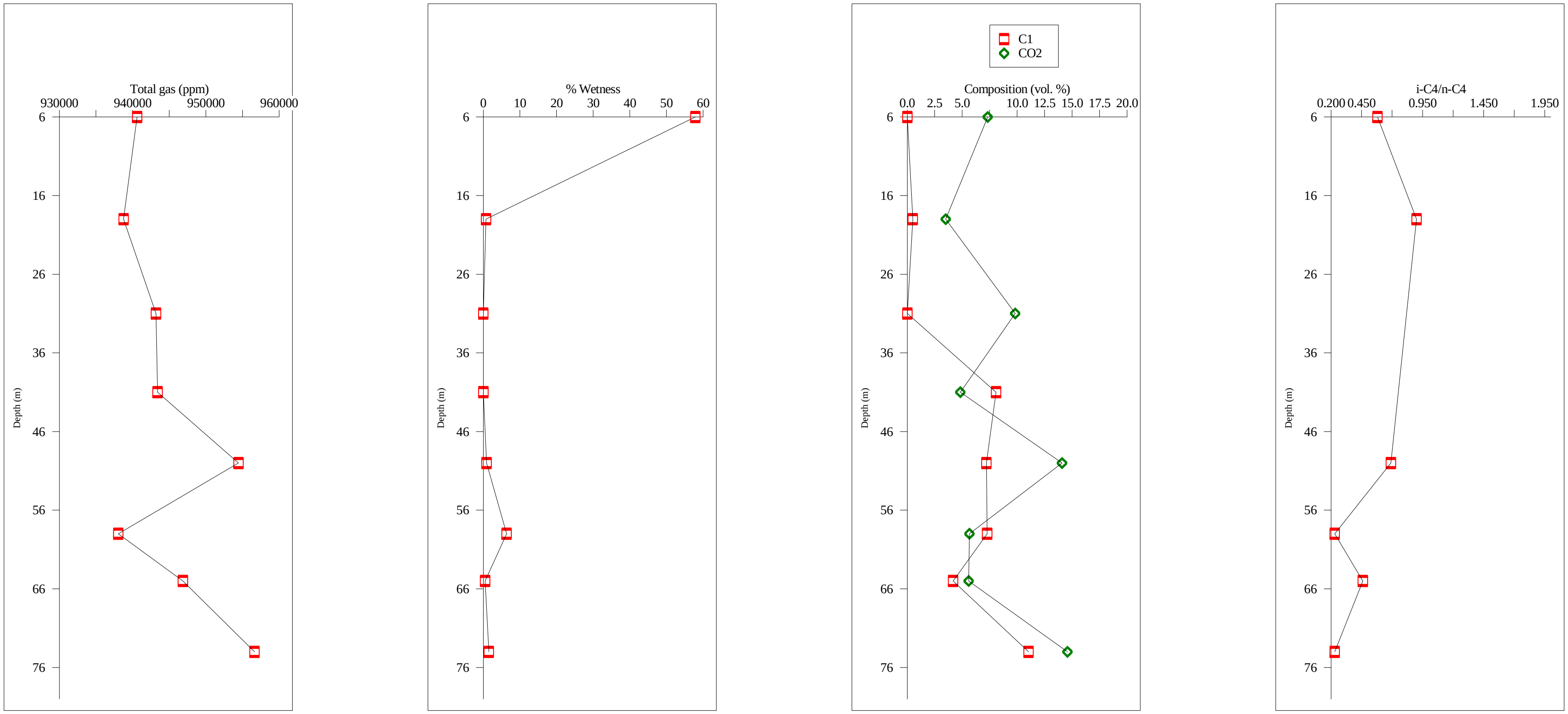

Figure 2. Isotopic composition

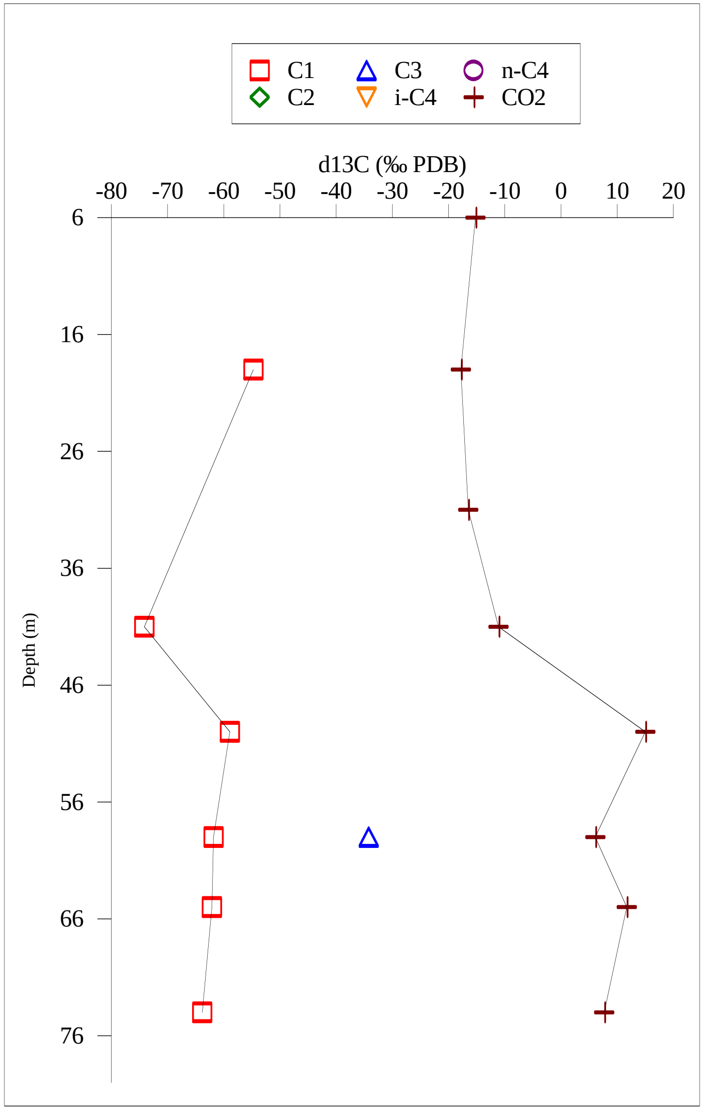

Table 2. Gas Composition (volume-%)

Well	Sample type	Sample info	Lower Depth (m)	APT ID	C1	C2	C3	iC4	nC4	iC5	nC5	C6+	CO2	Sum C1-C5	Wetness	iC4/nC4	H2	O2/Ar	N2	ppm
GEUS	Canned COPL	517001	6	66024	0.011	0.0009	0.0014	0.0048	0.0083	0.0077	0.0047	0.0088	7.32	0.039	57.9	0.58	0.88	2.04	89.7	940615
GEUS	Canned COPL	517001	19	66025	0.50			0.0018	0.0020	0.0089	0.0026	0.011	3.50	0.52	0.75	0.90	0.68	4.13	91.2	938772
GEUS	Canned COPL	517001	31	66026	0.013							0.0023	9.82	0.013	0.0000		1.19	1.81	87.2	943192
GEUS	Canned COPL	517001	41	66027	8.08	0.0014			0.0004	0.0038	0.0035	0.0051	4.83	8.08	0.022		0.57	1.70	84.8	943404
GEUS	Canned COPL	517001	50	66028	7.20	0.0036	0.022	0.015	0.022	0.010	0.0061	0.0071	14.1	7.28	0.88	0.69	1.10	2.81	74.7	954454
GEUS	Canned COPL	517001	59	66029	7.27	0.24	0.20	0.0092	0.039	0.0057	0.0057	0.0061	5.66	7.77	6.36	0.23	7.26	3.72	75.6	938037
GEUS	Canned COPL	517001	65	66030	4.17	0.0015	0.0086	0.0033	0.0072	0.0023	0.0019	0.0033	5.59	4.19	0.49	0.46	2.66	10.3	77.3	946863
GEUS	Canned COPL	517001	74	66031	11.0	0.030	0.099	0.0077	0.033	0.0049	0.0048	0.0053	14.6	11.2	1.52	0.23	3.16	0.73	70.3	956642

Table 3. Gas Isotopes (δ13C (‰ PDB) & δD (‰ SMOW))

Well	Sample type	Sample info	Lower Depth (m)	APT ID	C1 δ13C	C2 δ13C	C3 δ13C	i-C4 δ13C	n-C4 δ13C	i-C5 δ13C	n-C5 d13C	CO2 d13C	C1 δD
GEUS	Canned COPL	517001	6	66024								-15.2	*
GEUS	Canned COPL	517001	19	66025	-54.7							-17.8	*
GEUS	Canned COPL	517001	31	66026								-16.5	*
GEUS	Canned COPL	517001	41	66027	-74.1							-11.1	-304.5
GEUS	Canned COPL	517001	50	66028	-58.9							15.0	-278.1
GEUS	Canned COPL	517001	59	66029	-61.8		-34.2					6.1	-245.4
GEUS	Canned COPL	517001	65	66030	-62.1							11.7	-248.2
GEUS	Canned COPL	517001	74	66031	-63.8							7.7	-249.2

**: Too low amounts for δD measurements*

Experimental Procedures

All procedures follow NIGOGA, 4th Edition. Below are brief descriptions of procedures/analytical conditions.

GC analysis of gas components
Aliquots of the samples were transferred to exetainers. 0.1-1ml were sampled using a Gerstel MPS2 autosampler and injected into a Agilent 7890 RGA GC equipped with Molsieve and Poraplot Q columns, a flame ionisation detector (FID) and 2 thermal conductivity detector (TCD). Hydrocarbons were measured by FID. H_2, CO_2, N_2 and O_2/Ar by TCD.

Carbon isotope analysis of hydrocarbon compounds and CO2
The carbon isotopic composition of the hydrocarbon gas components was determined by a GC-C-IRMS system. Aliquots were sampled with a syringe and analysed on a Trace GC2000, equipped with a Poraplot Q column, connected to a Delta plus XP IRMS. The components were burnt to CO_2 and water in a 1000 ºC furnace over Cu/Ni/Pt. The water was removed by Nafion membrane separation. Repeated analyses of standards indicate that the reproducibility of $\delta^{13}C$ values is better than 1 ‰ PDB (2 sigma).

Hydrogen isotope analysis of methane
The hydrogen isotopic composition of methane was determined by a GC-C-IRMS system. Aliquots were sampled with a GCPal and analysed on a Trace GC2000, equipped with a Poraplot Q column, connected to a Delta plus XP IRMS. The components were decomposed to H_2 and coke in a 1400 ºC furnace. The international standard NGS-2 and an in-house standard (Std A) were used for testing accuracy and precision. The “true” value of NGS-2 is given to –172.5 ‰ V-SMOW (http://deuterium.nist.gov/standards.html). Repeated analyses of standards indicate that the reproducibility of δD values is better than 10 ‰ PDB (2 sigma).

10.6 Biomarker data

Contents:

CHROMATOGRAMS

Hopanes